Analysis of the role of Krebs cycle rewiring in macrophage cytokine production

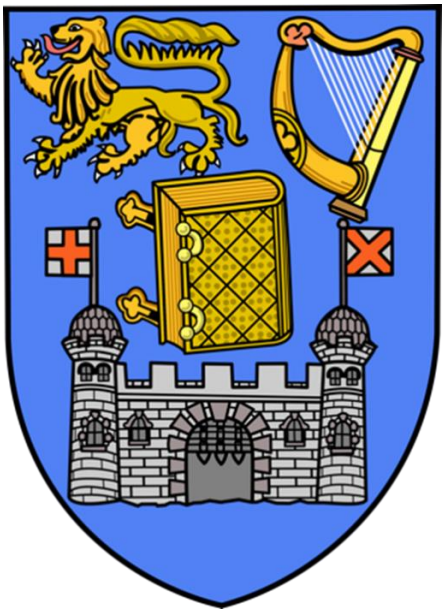

Thesis submitted to the University of Dublin

for the

Degree of Doctor of Philosophy

by

Dylan Gerard Ryan

School of Biochemistry and Immunology
Trinity Biomedical Sciences Institute
Trinity College Dublin
Ireland

August 2019

Declaration

I declare that this thesis has not been submitted as an exercise for a degree at this or any other university and is entirely my own work with the exception of the following figures:

- Figure 3.3b
- Figure 3.10c
- Figure 4.2
- Figure 4.18
- Figure 4.31
- Figure 4.32
- Figure 4.33
- Figure 4.34

This work was carried out in collaboration with Evanna Mills, Harvard University.

- Figure 4.13
- Figure 4.17b, c

This work was performed by Hiran Prag, University of Cambridge.

- Figure 4.27

This work was performed by Lee M. Booty, University of Cambridge.

- Figure 4.29

This work was performed by Dina Dikovskaya, University of Dundee.

Where any of the content presented is the result of specialist input from a collaborative research programme this is duly acknowledged in the text.

Dylan Ryan

This PhD thesis is dedicated to the memory of my uncle Padraic Ryan

Acknowledgements

The 4 years are complete. A sentence that felt a world away not so very long ago. If doing a PhD has taught me anything it's that there's a lot of life to live in 4 years, jam-packed with an incredible amount of highs but also an incredible amount of lows. Success and failure, happiness and sadness, life and death. For those of you who've been on this journey with me I just want to thank you for all your support and guidance. For those of you who are no longer with us you will be sorely missed.

Thank you, Luke, for taking me on when you did. If you hadn't have hired me, I may have been living a very different life with very different people in a very different scientific discipline. Let's just say I'm glad that didn't happen as I can't imagine myself with a 'neuroimaging' PhD. Thanks for all the advice and the guidance over the years and all the best in the future. I'm sure this won't be the last we see of each other. I'd also like to thank all the valuable input and assistance from my colleagues and collaborators who made this project possible.

Note to the reader: *most of you can stop reading here as this captures everything I have to say but for fear of disappointing those who expect more, the next sections for you.*

To the rest of the LON lab, I really wish I could go through you all one by one but I wouldn't be able to keep this to one page if I did (but I can sense the disappointment in this sentence so I'll extend it to two).

To the lads:

Richie and Jamie for the endless and varied debates and discussions, Mark for taking me under your wing, our cigarette breaks during lab nights out and that dirty humour that gave me some laughs, Z for our shared love of MMA, bench-pressing me and robbing that bottle of Jameson, Alex for a Bradley Cooper look-a-like (bet you'll be delighted with this) Chelski supporter you're alright so lets organise a Stamford bridge trip after I move, Jay in so little time you gave us some laughs (and nicknames), Danny you were always a gentleman and a few more lab games of croquet would have been nice and Moritz my go-to for technical advice (even long after you left).

To the lasses:

Kathy you were the greatest support and my very own personal life coach throughout the 4 years. It means more to me than you will ever know having had someone like you to confide in when times were tough. To Niamh who started this journey with me we're nearly there, we just have to keep swimming (or running in our case)! Sarah who probably hit-up more festivals than me speaks volumes, Anne the ever-present and ever lovely that ensured the lab didn't descend into chaos and anarchy, Eva another key member of the former cigarette crew during lab nights out, Big serve Cianabon it's all in the name, Deepthi for genuinely just wanting the best for me and finally to all the rest Beth, Silvia and Evanna that I only worked with for a short while but learned a lot.

A big thank you is owed to my parents for always putting education first (without my mam forcing me into school in the early morning due to my night owl tendencies I'd not be here), and my nana and grandad Corrigan who always had a place for me to do my work on their computer, sleep when required and kept me well fed and fuelled for completing my undergraduate degree and my brother Shane for the lifts to and from college when we were the studying late in the library. I hope I've made you proud.

A big thank you to my partner Lisa who has been with me from the very beginning of the journey and was a big source of inspiration. She came through so much adversity to get to where she is now and that deserves to be acknowledged. I love you and am looking forward to starting the next chapter of our lives.

I most definitely wouldn't have got here if it wasn't for the most wonderful group of friends you all know who you are. From Friday night board games with the lads to hot tub parties in the forest of Body & Soul we've had one hell of a ride. I love you all.

Last but not least, I'd like to thank Has Adolf Krebs for discovering the Krebs cycle, Alan Turing for inventing the computer, Bill Gates for inventing Microsoft office and Clarivate analytics for designing endnote. You've made writing and citing this PhD possible and a whole lot easier.

Table of Contents

List of Figures

Chapter 1 - Introduction

Chapter 2 – Materials and Methods

Chapter 3 – Potential role for an inflammatory aspartate-argininosuccinate shunt and fumarate in the regulation of cytokine production

Chapter 4 – Itaconate is an anti-inflammatory metabolite that inhibits SDH and activates Nrf2

List of Tables

Abbreviations

2DG - 2-deoxyglucose

2SC - (S)-2-succinocysteine

Acetyl-CoA – Acetyl coenzyme A

ACLY - ATP-citrate lyase

ACN - Acetonitrile

ACO2 - Aconitase 2

ADPR - ADP-ribose

AOAA - Aminooxyacetic acid

AOX - Alternative oxidase

ARE - AU-rich element also anti-oxidant response element

Ass1 - Argininosuccinate synthase

BMDMs - Bone-marrow derived macrophages

BTA - 1,2,3-benzentricarboxylic acid

CAC - Citric acid cycle

CAD - *cis*-Aconitate decarboxylase

cAMP - 3’-5’-cyclic adenosine monophosphate

CD14 – Cluster of differentiation 14

CIC - Mitochondrial citrate carrier

CNC - Cap’n’collar

CoQ - Coenzyme Q

CORM2 - CO releasing molecule 2

COX2 - Cyclooxygenase 2

CS - Citrate synthase

DAMP - Danger-associated molecular pattern

DC - Dendritic cell

DMEM - Dulbecco's Modified Eagle Medium

DMF - Dimethyl fumarate

DMI - Dimethyl itaconate

DMM - Dimethyl malonate

ECAR - Extracellular acidification rates

EDTA - Ethylenediaminetetraacetic acid

ER - Endoplasmic reticulum

ETC - Electron transport chain

F-2,6-BP - Fructose-2,6-bisphosphate

FASN - Fatty acid synthase

FCCP - Carbonyl cyanide-4-(trifluoromethoxy) phenylhydrazone

FCS - Fetal calf serum

FH - Fumarate hydratase

G3P - glyceraldehyde 3-phosphate

GABA - γ-gamma-aminobutyric acid

GAPDH - Glyceraldehyde 3-phosphate dehydrogenase

GCLC - Glutamate-cysteine ligase catalytic

GCLM - Glutamate-cysteine ligase modifier

GLUT1 - Glucose transporter 1

GPCR - G-protein coupled receptor

GSH - Glutathione

GSR - Glutathione reductase

GSSG - Glutathione disulphide

HAT - Histone acetyltransferase

HCA2 - Hydroxycarboxylic acid receptor 2

HDAC - Histone deacetylase

HEK - Human embryonic kidney

HIF1α - Hypoxia-inducible factor 1 alpha

HK2 - Hexokinase 2

HLRCC - Hereditary leiomyomatosis and renal cell carcinoma

HO-1/HMOX1 - Heme oxygenase 1

HRE - Hypoxia-inducible response element

HsAAC1 - H. sapiens ADP/ATP carrier

HsCTP - H. sapiens citrate carrier

HsODC - H. sapiens 2-oxidicarboxylate carrier

HsOGC - H. sapiens 2-oxoglutarate carrier

IAA - Iodoacetamide

ICL - Isocitrate lyase

IDH - Isocitrate dehydrogenase

IkB - Inhibitor of k light chain gene enhancer in B cells

IKK - IkB kinase

IMM - Inner mitochondrial membrane

IRAK1 - IL-1 receptor-associated kinase 1

IRAK4 - IL-1 receptor-associated kinase 4

IRF3 - Interferon regulatory factor 3

IRF5 - Interferon regulatory factor 5

IRG1 - Immunoresponsive gene 1

JMJDs - Jumonji C-domain-containing histone demethylases

KEAP1 - Kelch like-ECH-associated protein 1

LBP - LPS-binding protein

LC-MS - Liquid chromatography- mass spectrometry

LDHA - Lactate dehydrogenase A subunit (LDHA)

LPS - Lipopolysaccharide

Maf - Musculoaponeurotic fibrosarcoma

MAL - MyD88-adaptor like

MAPK - mitogen-activated protein kinase

MDH - Malate dehydrogenase

ME - Malic enzyme

MI - 4-methyl itaconate

MMF - Monomethyl fumarate

moDC - monocyte-derived DC

mtROS - mitochondrial ROS

MUT - Methylmalonyl-CoA mutase

MyD88 - Myeloid differentiation primary response gene 88

NF-kB - nuclear factor kappa-light-chain-enhancer of activated B cells

NQO1 - NADPH:quinone-oxidoreductase-1

Nrf2 - Nuclear factor-erythroid 2 p45-related factor 2

OCR - Oxygen consumption rates

OGDH - a-ketoglutarate dehydrogenase

OI - 4-octyl itaconate

OMS - 4-octyl-2-methylsucinnate

OS - 4-octyl succinate

OXPHOS - Oxidative phosphorylation

PAMP - Pathogen-associated molecular pattern

PDH - Pyruvate dehydrogenase complex

PEP - Phosphoenolpyruvic acid

PFK2 - Phosphofructokinase 2

PGE2 - Prostaglandin E2

PHD - prolyl hydroxylases

PKA - Protein kinase A

PKM2 - Pyruvate kinase M2

PPP - Pentose phosphate pathway

PRR - Pathogen recognition receptor

PTM - Post-translational modification

PTX - Pertussis toxin

PVDF - Polyvinylidene difluoride

R5P - Ribose 5-phosphate

RA - Rheumatoid arthritis

RET - Reverse electron transport

RHIM - Rip homotypic interaction motif

RING - Really interesting new gene

RIP1 - Serine/threonine kinase receptor interacting protein 1

SAM - S-adenosyl methionine

SARM - Sterile α and HEAT-Armadillo motifs-containing protein

ScAAC2 - S. cerevisiae ADP/ATP carrier

ScDIC - S. cerevisiae dicarboxylate carrier

SDH - Succinate dehydrogenase

SDS-PAGE - Sodium dodecyl sulphate-polyacrylamide gel electrophoresis

SFN - Sulphoraphane

SLC25a1 - Solute carrier family 25 member 1

SNP - Single nucleotide polymorphism

TAK1 - Transforming growth factor-b-activated kinase 1

TANK - TRAF family member-associated NF-kB

TBK1 - TANK-binding kinase 1

TCA - Tricarboxylic acid

TET - Ten-eleven translocation

TLR - Toll-like receptor

TMT - Tandem mass tag

TRAF3 - TNF receptor-associated factor 3

TRAF6 - TNF receptor-associated factor 6

TRAM - TRIF-related adaptor molecule

TRIF - TIR-domain containing adaptor protein inducing IFNb

UBC13 - Ubiquitin-conjugating enzyme 13

UEV1A - Ubiquitin-conjugating enzyme E2 variant 1 isoform A

VHL - Von Hippel-Lindau

Abstract

A striking change has happened in the field of immunology whereby specific metabolic processes have been shown to be a critical determinant of immune cell activation. Multiple immune receptor types rewire metabolic pathways as a key part of how they promote effector functions. Perhaps surprisingly for immunologists, the Krebs cycle has emerged as the central immunometabolic hub of the macrophage. During pro-inflammatory macrophage activation, there is an accumulation of the Krebs cycle intermediates succinate, succinyl-CoA, fumarate and citrate, and the Krebs cycle-derived metabolite itaconate.

The first aspect of this project investigated the role of the aspartate-argininosuccinate shunt and fumarate accumulation in regulating cytokine production in macrophages. Lipopolysaccharide (LPS) was shown to increase argininosuccinate synthethase (Ass1) expression and boost the production of argininosuccinate and fumarate, while decreasing fumarate hydratase (Fh) and aspartate levels. Using the aspartate aminotransferase inhibitor aminooxyacetic acid (AOAA), the argininosuccinate shunt was shown to regulate fumarate accumulation in the macrophage. Furthermore, AOAA was also shown to inhibit LPS-induced TNF, IL-6 and IL-1β production. Using two pharmacological agents, dimethyl fumarate (DMF) and monomethyl fumarate (MMF), and one genetic approach, *Fh*-deficiency, fumarate was shown to modulate LPS-induced cytokine production. Interestingly, elevated fumarate levels also resulted in an increase in the non-enzymatic and covalent modification of protein cysteine residues by fumarate, a process termed succination, as well as an increase in the metabolite S-(2)-succinocysteine (2SC), a biomarker of succination. This represents the first

report of this metabolite and the understudied post-translational modification (PTM) in LPS-activated macrophages.

The second aspect of this project examined the immunomodulatory role of itaconate, which is derived from *cis*-aconitate, in LPS-activated macrophages. Here it's shown that LPS induces immunoresponsive gene 1 (IRG1), also known as *cis*-aconitate decarboxylase (CAD), expression and modulates glycolysis and glutaminolysis to support itaconate synthesis. Using a new cell-permeable itaconate derivative 4-octyl itaconate (4-OI), itaconic acid (ITA) and *Irg1/Acod1*-deficient macrophages, itaconate was found to be required for LPS-induced succinate accumulation, inhibition of complex II of the ETC and activation of the anti-inflammatory transcription factor nuclear factor-erythroid 2 p45-related factor 2 (Nrf2). Interestingly, itaconate directly modifies proteins via alkylation of cysteine residues, a novel post-translational modification (PTM) termed 2, 3-dicarboxypropylation not previously known. This also results in an increase in the itaconate-cysteine adduct, 2, 3-dicarboxypropyl cysteine, akin to 2SC. Itaconate was exported from the mitochondria where it is proposed to alkylate cysteine residues 151, 257, 273, 288 and 297 on the anti-oxidant protein kelch like-ECH-associated protein 1 (KEAP1), as determined by direct alkylation of KEAP1 by 4-OI, enabling Nrf2 to increase the expression of downstream genes with anti-oxidant and anti-inflammatory capacities. Furthermore, the activation of Nrf2 was impaired in *Irg1* -/- BMDMs and was essential for the inhibition of LPS-induced IL-1β by 4-OI. Overall, immunomodulatory roles for fumarate, itaconate and their derivatives have been characterised, whilst new insights into the anti-inflammatory effect of itaconate have been uncovered that may have therapeutic potential for the treatment of inflammatory diseases.

Chapter 1:

Introduction

1.1 – Innate immune signalling and metabolism

1.1.1 – General introduction

Recently, the role of intracellular metabolic changes in governing the inflammatory response has become a major focus for research in the field of immunology. Intriguingly, distinct metabolic adaptations have been reported in macrophages, T cells and dendritic cells (DCs), which are providing new insights into the complexity of immunometabolism. Specifically, this project concerns the role of Krebs cycle rewiring in innate immunity, with a focus on the metabolites fumarate and itaconate and their role in cytokine production.

The innate immune system itself is an evolutionarily ancient form of host defence against pathogenic microbes and infection (1). Innate immune recognition of invading microbes relies on a limited number of germline-encoded receptors, termed pathogen recognition receptors (PRRs), designed to recognise pathogen-associated molecular patterns (PAMPs), expressed by bacteria, viruses and fungi (1). Macrophages constitute a major component of innate immunity responsible for sensing microbial PAMPs via multiple families of so-called PRRs, such as Toll-like receptors (TLRs) (2). Importantly, macrophages are myeloid-derived immune cells ubiquitously distributed throughout the human body and are essential for the maintenance of biological homeostasis in the face of infection or tissue damage. As macrophages represent the first line of defence against infection, they also play a critical role in bridging the innate and adaptive immune systems through phagocytosis, bactericidal killing, inflammatory cytokine production and antigen presentation (2). In addition to PAMPs, macrophages can bind to endogenous molecular motifs associated with cellular

damage, termed danger-associated molecular patterns (DAMPs), to mediate the sterile inflammatory response (3). Ligation of PAMPs and/or DAMPs to PRRs leads to an induction of intracellular signalling cascades that result in cellular activation and pronounced alterations in inflammatory gene expression (3). The sensing of these products also activates downstream signalling cascades that we now know reprogram cellular metabolism in a manner dependent on the nature of the stimulus. While engagement of PRRs induces a 'classical' pro-inflammatory polarisation state, macrophages can also undergo 'alternative' activation to a more anti-inflammatory state (4). This alternatively-activated state is usually induced by IL-4 stimulation (M[IL-4]) *in vitro* and is also essential in maintaining homeostasis *in vivo* through tissue remodelling, wound repair and the resolution of inflammation (4). Importantly, metabolic reprogramming of alternatively-activated macrophages also underlies their ability to execute their specific functions.

1.1.2 – Toll-like receptor 4 (TLR4) signalling

TLR4 represents a critical member of the TLR family responsible for the detection of several PAMPs, notably, lipopolysaccharide (LPS), a key component of gram-negative bacterial cell membranes (1). LPS is one of the best studied immunostimulatory molecules and is known to induce systemic inflammation culminating in septic shock, if excessive signalling occurs (5). TLR4 binds LPS in conjunction with Lymphocyte antigen 96 (also known as MD2) (6). The efficiency of LPS extraction from bacterial outer membranes and sensitivity of detection by the TLR4-MD2 complex is further supported by two key accessory molecules known as LPS-binding protein (LBP) and cluster of differentiation 14 (CD14) (6). Following recognition of LPS, TLR4 undergoes oligomerisation and recruits

downstream adaptor proteins, namely myeloid differentiation primary response gene 88 (MyD88), MyD88-adapter like (MAL, also known as TIRAP, TIR-domain containing adaptor protein), TIR-domain containing adaptor protein inducing IFNβ (TRIF), TRIF-related adaptor molecule (TRAM), and sterile α and HEAT-Armadillo motifs-containing protein (SARM) (5).

TLR4 signal transduction itself can be divided into two pathways, the MyD88-dependent pathway, responsible for the induction of pro-inflammatory cytokine production, and the MyD88-independent pathway, responsible for the induction of Type 1 interferons and interferon-inducible genes (5). Activation of the MyD88-dependent pathway results in the recruitment of IL-1 receptor-associated kinase 4 (IRAK4), which is required for the subsequent recruitment, activation and degradation of IRAK1 (5). TNF receptor-associated factor 6 (TRAF6) is recruited downstream of IRAK1/4, and in complex with ubiquitin-conjugating enzyme 13 (UBC13) and ubiquitin-conjugating enzyme E2 variant 1 isoform A (UEV1A), activates transforming growth factor-β-activated kinase 1 (TAK1) (5). TAK1 can then go on to phosphorylate and activate both the IκB kinase (IKK) and mitogen-activated protein kinase (MAPK) pathways (5). IKK forms a complex composed of IKKα, IKKβ and IKKγ that phosphorylates and inhibits inhibitor of k light chain gene enhancer in B cells (IκB), which results in IκB degradation, translocation of nuclear factor kappa-light-chain-enhancer of activated B cells (NF-κB) to the nucleus and induction of pro-inflammatory cytokine production (5). MAPK signalling also results in the induction of another transcription factor AP-1, which also plays an important role in the induction of pro-inflammatory cytokines (7). Additionally, IκBζ, which is essential for IL-6

expression, and interferon regulatory factor 5 (IRF5) are two important downstream mediators of the MyD88-dependent pathway (5).

The MyD88-independent pathway is primarily mediated by the adaptor TRIF (5). TRIF plays an essential role in the induction of IRF3 and late-phase activation of the NF-κB and MAPK signalling pathways (8). TRIF interacts with the serine/threonine kinase receptor interacting protein 1 (RIP1) via a Rip homotypic interaction motif (RHIM), which is essential for TRIF-mediated NF-κB activation (9). The induction of IRF3 is mediated by TRAF3 recruitment and occurs independently of RIP1 (10, 11). TRAF3 associates with TRAF family member-associated NF-κB (TANK), TANK-binding kinase 1 (TBK1) and IKKi, essential mediators of IRF3 dimerisation and its translocation to the nucleus to induce Type I interferons (10, 12). As TLR4 is highly expressed on macrophages, the binding of LPS to TLR4-MD2 results in the potent activation of quiescent macrophages via initiation of these downstream signalling pathways (5).

Interestingly, a recent report by Essuman *et al* (2018) have shown that ancestral prokaryotic TIR domains constitute a new family of NADase enzymes, which cleave NAD^+ into nicotinamide and ADP-ribose (ADPR) (13). The TIR domain is the critical signalling domain used by all TLRs and their adapters as well as receptors for the IL-1 family of cytokines, which include IL-12, IL-1β, and IL-18 and IL-33.These findings suggest that the ancestral function of this domain was as a key metabolic regulatory enzyme (13). As such, it could be speculated that during evolutionary history the TIR domain was co-opted to function as a scaffold for protein complexes for innate immune signalling. Furthermore, this ancient link with the TIR domain and metabolism is even more intriguing given

the recent developments in the field of immunometabolism and TLR-driven metabolic reprogramming.

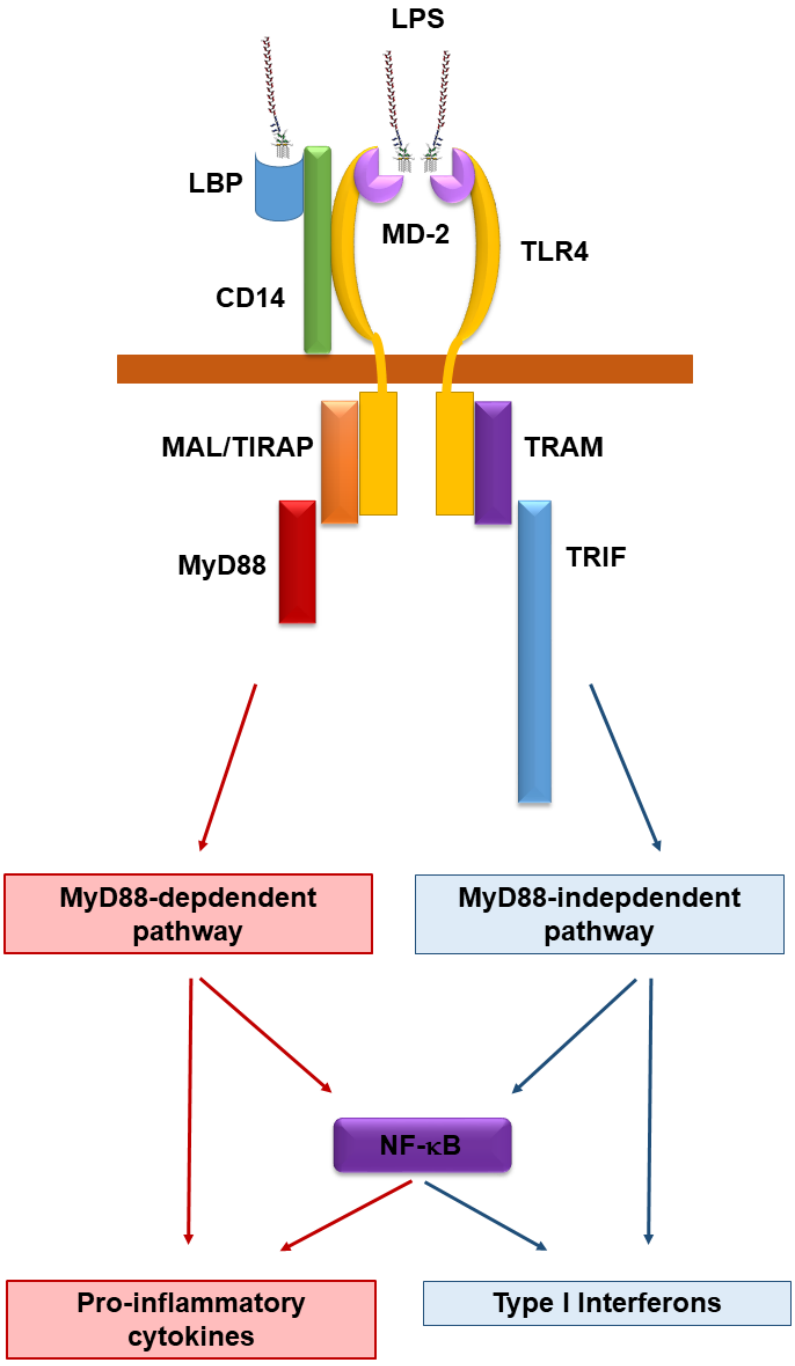

Figure 1.1 – Overview of LPS/TLR4 signal transduction pathway (5)

Recognition of LPS is facilitated by LBP and CD14, and is mediated by TLR4/MD-2 receptor complex. LPS/TLR4 signalling can be further subdivided into MyD88-dependent and MyD88-independent pathways, which mediate the activation of the transcription factor NF-kB and the induction of both pro-inflammatory cytokines and Type I interferons.

1.1.3 – Overview of TLR4-induced metabolic rewiring

Several recent studies have implicated the global rewiring of metabolic pathways, elicited during the transition from a resting to an activated state, in response to LPS ligation of TLR4 (2, 14, 15). Of importance, is the shift away from the use of oxidative phosphorylation (OXPHOS) toward a glycolytic phenotype, termed aerobic glycolysis or the Warburg effect, thus tailoring cellular metabolism to suit the bioenergetic and biosynthetic demands of the cell (14, 15). This metabolic switch also supports the diversion of glucose and glycolytic intermediates into the pentose phosphate pathway (PPP) (16, 17). The PPP is an anabolic pathway that runs parallel to glycolysis and is essential to produce NADPH, an important cofactor in lipid biosynthesis, antioxidant defence and NO/ROS production, and ribose 5-phosphate (R5P), the precursor for nucleotide biosynthesis (17). The very first observation of increased glycolysis and decreased OXPHOS in activated macrophages occurred in 1969 (18), and since then we have garnered important molecular insights into the signalling pathways that govern glycolytic reprogramming during macrophage activation.

1.1.4 – TLR4-induced glycolytic reprogramming

One of the central regulators of glycolysis identified in macrophages is the transcription factor hypoxia-inducible factor 1 alpha (HIF1α) (19, 20). Under both normoxic and hypoxic conditions, HIF1α was found to be induced by LPS and regulate the induction of several enzymes involved in glycolysis, such as the glucose transporter GLUT1 (19, 20). Furthermore, inhibition of glycolysis with 2-deoxyglucose (2DG), a competitive inhibitor of hexokinase, blocked induction of HIF1α and the pro-inflammatory cytokine IL-1β (20). In macrophages, another

key mechanism for inducing aerobic glycolysis is through the induction of pyruvate kinase M2 (PKM2) (21). PKM2 is an enzymatically inactive isoform of pyruvate kinase, the enzyme responsible for catalysing the rate-limiting conversion of phosphoenolpyruvic acid (PEP) to pyruvate (21). It was found that PKM2, in its dimeric form, translocates to the nucleus to form a complex with HIF1α on hypoxia-inducible response elements (HREs), thus promoting the expression of HIF1α -target genes involved in aerobic glycolysis, including Lactate dehydrogenase A subunit (LDHA) (21). Using two compounds, TEPP-46 and DASA-58, which promote tetramerisation and enzymatic activation of PKM2, it was found that induction of HIF1α-target genes and glycolysis were inhibited by preventing translocation of PKM2 to the nucleus and its interaction with HIF1α (21). Interestingly, TEPP-46 and DASA-58 also inhibited LPS-induced activation of bone-marrow derived macrophages (BMDMs), as observed by the blocking of classically induced pro-inflammatory genes, *IL1B*, *IL12p40* and *CXCL10*, whilst promoting the induction of classical anti-inflammatory markers, such as *ARG1* (21).

Insights into glycolytic reprogramming independent of HIF1α have also been garnered in macrophages. For example, LPS induction of the *PFKFB3* gene that encodes u-PFK2 (PFKB3), a ubiquitous isoform of phosphofructokinase 2 (PFK2), still occurs in HIF1α-deficient macrophages (15). PFKB3 activity is essential for flux through glycolysis as it is a dual kinase: bisphosphatase that regulates levels of the glycolytic intermediate fructose-2, 6-bisphosphate (F-2, 6-BP), an allosteric activator of phosphofructokinase 1 (PFK1) (2, 15). Additionally, early glycolytic reprogramming by LPS and other TLR agonists were found to be dependent on the kinases TBK1, IKKε and protein kinase B (Akt), which

promoted association of hexokinase 2 (HK2) with the outer mitochondrial membrane (16). Furthermore, glyceraldehyde 3-phosphate dehydrogenase (GAPDH), a glycolytic enzyme that converts glyceraldehyde 3-phosphate (G3P) into 1, 3-bisphosphoglycerate, has been demonstrated to regulate TNF production in mouse and human macrophages (22). GAPDH achieves this by utilising its lesser known capacity as an RNA binding protein (22). Specifically, GAPDH binds to an AU-rich element (ARE) in the 3'UTR of TNF resulting in its post-transcriptional repression, an event sensitive to the alterations in the glycolytic state of the cell (22).

1.2 – Krebs cycle rewiring in macrophages

1.2.1 – Overview of the Krebs cycle

Most of the energy rich adenosine triphosphate (ATP) generated in metabolism is provided by the aerobic processing of key fuel molecules and starts with the complete oxidation of their derivatives to CO_2 (23-25). This oxidation takes place in a series of chemical reactions first described by Hans Adolf Krebs in 1937, a metabolic cycle that now bears his name (23). In eukaryotic organisms, the reactions of the Krebs cycle take place inside the mitochondrial matrix whereby its primary function is the harvesting of high energy electrons from carbon fuel sources (25). It is a truly remarkable process that begins with the energy in sunlight in the form of photons being captured in carbohydrates in plants during photosynthesis (26). Electrons from carbohydrates are then captured in the Krebs cycle, which then create a proton gradient used to drive ATP production. Photons to electrons to protons to ATP. Indeed, the Krebs cycle is the final common pathway for the oxidation of not only carbohydrates but also fatty acids

and amino acids, with most entering the cycle as acetyl coenzyme A (acetyl-CoA) (25). As such, it is the gateway to the aerobic metabolism of any molecule that can be transformed into an acetyl group or an intermediate of the cycle itself. Importantly, the Krebs cycle is also a source of precursors for the building blocks of many other biological molecules, such as nonessential amino acids, nucleotide bases and porphyrin (25). For example, oxaloacetate is an intermediate for the synthesis of glucose from non-carbohydrate precursors, a process termed gluconeogenesis. Likewise, citrate provides essential carbon units for the synthesis of fatty acids, a process termed lipogenesis. As such, the Krebs cycle is the central metabolic hub of the cell acting as an important nexus for the integration of many anabolic (gluconeogenesis and lipid synthesis) and catabolic (glycolysis and β-oxidation) pathways. It is in fact the central biochemical process in eukaryotic life.

The oxidation of acetyl-CoA to CO_2 by the Krebs cycle is the central process in energy metabolism because it is essential for the generation of the high-transfer-potential electron carriers' nicotinamide adenine dinucleotide (NADH) and flavin adenine dinucleotide ($FADH_2$). These redox metabolites once generated then act as shuttles for the transfer of high energy electrons to O_2, the terminal electron acceptor in the oxidation of carbon, via a series of electron carriers collectively termed the ETC (27, 28). The famous Albert Szent-Gyorgyi, who is credited with co-discovering the Krebs cycle, once defined life as being 'nothing but an electron looking for a place to rest' (29). He would be amazed that this process has been co-opted for signalling in an immune system. In one turn, the Krebs cycle oxidises two-carbon units transferring three hydride ions to three molecules of NAD^+ and one pair of hydrogen atoms to one molecule of FAD, thus producing two

molecules of CO_2 and one molecule of GTP (or ATP). The net reaction of the Krebs cycle is:

Acetyl-CoA + 3 NAD^+ + FAD + GDP + Pi + 2 H_2O → 2 CO_2 + 3 NADH + $FADH_2$ + GTP + 2 H^+ + CoA

In total eight reactions are required to give this stoichiometry (Fig. 1.2). The Krebs cycle begins with the condensation of oxaloacetate and acetyl-CoA to form citryl-CoA, an aldol condensation, followed by the hydrolysis of citryl-CoA with H_2O to yield citrate and CoA (30). The hydrolysis of the citryl-CoA thioester drives the overall direction of the reaction in the direction of citrate synthesis (30). This first reaction is catalysed by citrate synthase (CS). As the hydroxyl group of citrate is not properly located for the oxidative decarboxylation that follows, the second reaction of the Krebs cycle is the stereospecific isomerisation citrate to isocitrate (31). The isomerisation of citrate is catalysed by aconitase (ACO) and is accomplished by a dehydration step followed by a hydration step (31). In the first reaction, aconitase protonates citrate at the C3 position prior to deprotonation at the C2 position to form the intermediate *cis*-aconitate. In the second reaction, *cis*-aconitate is flipped 180^o to allow the dehydration step to occur on the opposite face of the intermediate. This ensures that the stereochemistry (2R, 3S) of the reaction is correct. Following rotation, *cis*-aconitate is rehydrated to form isocitrate, with the overall result an interchange of a H^+ and an OH^-. The third step of the cycle is catalysed by isocitrate dehydrogenase (IDH) and constitutes the first of four oxidation-reduction reactions (32). The oxidative decarboxylation of isocitrate to α-ketoglutarate occurs via an oxalosuccinate intermediate and yields the first molecule of NADH and loses one carbon unit in the form of CO_2. The formation of α-ketoglutarate is

an important rate-determining step of the cycle as Isocitrate dehydrogenase can be allosterically activated (citrate, ADP) or inhibited (ATP), a form of regulation determined by the energy status of the cell. In the fourth step of the cycle, the conversion of isocitrate to α-ketoglutarate is followed by a second oxidative decarboxylation reaction, the formation of succinyl-CoA from α-ketoglutarate (33). This reaction is catalysed by the α-ketoglutarate dehydrogenase complex (OGDC) and yields the second molecule of NADH and loses another carbon unit as CO_2 (33). In the citrate synthase reaction, the cleavage of the thioester bond powers the generation of citrate and indeed succinyl-CoA is an energy-rich thioester compound with a free energy value comparable to ATP. In the fifth reaction, catalysed by succinyl-CoA synthetase, cleavage of the thioester bond of succinyl-CoA is coupled to the phosphorylation of a purine nucleoside diphosphate (usually GDP but also ADP) and the formation of succinate (34). This is the only reaction in the Krebs cycle that directly yields a compound with high phosphoryl-transfer potential.

Reactions of four-carbon compounds constitute the final stage (comprised of 3 reactions) of the citric acid cycle: the regeneration of oxaloacetate. The first step in the regeneration of oxaloacetate (and the sixth of the cycle) is the oxidation of succinate to fumarate by succinate dehydrogenase (SDH), also referred to as Complex II of the ETC (35). In SDH, the hydrogen acceptor is FAD, as the free energy change is insufficient to reduce NAD^+. The isoalloxazine ring of FAD is covalently attached to SDH via a histidine side chain of the enzyme and so does not dissociate from the enzyme. Rather, two electrons are transferred directly from $FADH_2$ to iron-sulphur clusters of the enzyme to Coenzyme Q (CoQ). The seventh step of the cycle is the hydration of fumarate

to form L-malate (36). This stereospecific *trans* addition of H^+ and OH^- is catalysed by fumarate hydratase (Fh). Finally, the eight (and last) step of the Krebs cycle, catalysed by malate dehydrogenase (MDH), is the oxidation of malate to oxaloacetate and the reduction of NAD^+ to form the third and final molecule of NADH (37). The standard free energy of this reaction is positive and is only driven forward by use of the products -oxaloacetate by citrate synthase and NADH by the ETC. And so, one full turn of the cycle is complete. The key outputs of the Krebs cycle from a biochemical point of view are the 3 NADH molecules and the $FADH_2$ that will feed the ETC (Fig. 1.2 & 1.6). As we shall see however, these intermediates in the Krebs cycle are also used as signals during macrophage activation.

1.2.2 – Oxidative phosphorylation

The main purpose of the ETC is to generate ATP, which then serves as the principal immediate donor of free energy in biological systems. In a typical cell, a molecule of ATP is consumed within a minute of its formation, whilst a typical human consumes the equivalent of 65 kg of ATP at rest over a period of 24 hours (38). However, the total quantity of ATP in the body is limited to approximately 100 g, thus the turnover of this small quantity of ATP is very high. Strikingly, each molecule of ATP is recycled between 1000 to 1500 times per day. To achieve this high degree of turnover, a sophisticated combination of enzyme and coenzyme complexes (ETC) work in tandem to synthesise ATP from ADP and Pi, in a process termed oxidative phosphorylation (OXPHOS) (27, 28) (Fig. 1.2 & 1.6). The transfer of electrons from NADH and $FADH_2$ to O_2 occurs at the inner mitochondrial membrane (IMM), the location of the ETC, and leads to the pumping of protons (H^+) out of the mitochondrial matrix into the intermembrane

space (27, 28). This unequal distribution of protons generates a pH gradient and transmembrane electrical potential (electrochemical gradient) that creates a proton-motive force. ATP is synthesised when protons flow back to the mitochondrial matrix. As such, the electron motive force generated by the Krebs cycle, is converted to a proton motive force and then into phosphoryl transfer potential (27, 28). The conversion of the electron motive force to the proton motive force is achieved by the respiratory chain, which consists of three electron-driven proton pumps – NADH-Q oxidoreductase (Complex I), Q-cytochrome *c* oxidoreductase (Complex III) and cytochrome *c* oxidase (Complex IV) (27, 28). Special electron carriers are also involved in ferrying the electrons from one complex to the next. The first of these is CoQ, also referred to as ubiquinone because it is a hydrophobic ubiquitous quinone, which diffuses rapidly within the IMM and shuttles electrons between Complex I and Complex III (27, 28). SDH (Complex II) also interacts and reduces CoQ to generate the proton motive force although it is not a proton pump itself, and unlike other Krebs cycle enzymes, directly associates with the IMM and the ETC (35). SDH therefore provides an integral physical link between the Krebs cycle and ATP formation. The second of the special electron carriers is cytochrome *c*, a small soluble protein that shuttles electrons from Complex III to Complex IV, the final proton pump of the chain and the site of O_2 reduction to H_2O (27, 28). The final phase of OXPHOS is carried out by the F_0F_1-ATP synthase, an ATP synthesising complex driven by the flow protons back into the mitochondrial matrix, thus converting the proton motive force to phosphoryl transfer potential (converting ADP to ATP) (28). Oxidative phosphorylation is a vivid demonstration that proton gradients are an incontrovertible currency of free energy in biological systems.

As we will see below, both the electrochemical proton gradient and the ETC can be also harnessed for signalling purposes during macrophage activation, largely via the generation of reactive oxygen species (ROS).

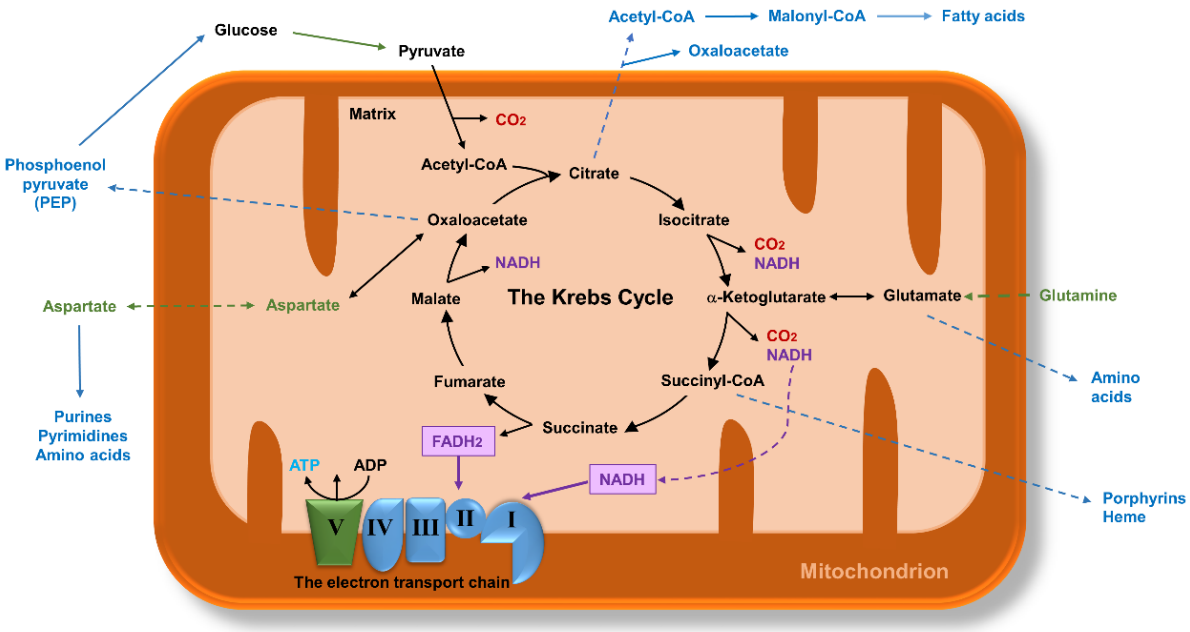

Figure 1.2 – The Krebs cycle and oxidative phosphorylation

The Krebs cycle is presented demonstrating the eight reactions required for one full turn and all five complexes required for oxidative phosphorylation (OXPHOS). Some anaplerotic (blue) and cataplerotic (green) sequences feeding the Krebs cycle are also shown. Key anaplerotic pathways indicated include the generation of phosphoenol pyruvate (PEP) from oxaloacetate, which can then feed gluconeogenesis to synthesise glucose and citrate export from the mitochondria, where it can be converted into acetyl-CoA and malonyl-CoA to feed fatty acid synthesis (*de novo* lipogenesis). The synthesis of porphyrins and heme from succinyl-CoA, purines and pyrimidines required for DNA synthesis from oxaloacetate and finally the synthesis of non-essential amino acids from oxaloacetate and α-ketoglutarate are also shown. Key cataplerotic pathways indicated include glucose feeding pyruvate (glycolysis), which can then enter the Krebs cycle as acetyl-CoA, aspartate feeding oxaloacetate and glutamine feeding α-ketoglutarate. One full turn of the Krebs cycle generates two molecules of CO_2 (red) and three molecules of NADH, which is used directly by complex I, and one molecule of $FADH_2$, which is used by complex II (purple).

1.2.3 – Krebs cycle rewiring

As the Krebs cycle is an amphibolic pathway, meaning it participates in anabolic and catabolic processes, the diversion of nutrients to replenish Krebs cycle intermediates, termed anaplerosis, or the removal of intermediates to feed biosynthetic pathways, termed cataplerosis, is necessary to ensure functionality of the cycle and to support important cellular processes (25) (Fig. 1.2). Anaplerosis and cataplerosis describe reciprocal and correlative reactions that can be dictated by changes in microenvironment of the cell, such as hypoxia, or in response to extracellular signals, such as hormones or inflammatory stimuli (39, 40). However, a concept first proposed in the 1970s (41, 42) has now re-emerged whereby the Krebs cycle can undergo remodelling to support the "non-metabolic" functions of its intermediates and their derivatives. This rewiring is often achieved through modulation of the expression and/or activity of specific Krebs cycle enzymes and both anaplerotic and cataplerotic sequences.

An early example of this concept comes from the study of prostate secretory epithelial cells, which have the specialized function and capability of accumulating extraordinarily high levels of citrate (40, 43, 44). The accumulated citrate is then secreted to form an important component of human prostatic fluid (semen) often reaching concentrations of up to 150 mM, an intriguing phenomenon first described way back in 1929 (44). This striking characteristic of prostate acinar epithelial cells is achieved by their unique ability to acquire high levels of zinc intracellularly via elevated expression of ZIP1 (SLC39A1), the major endogenous zinc uptake transporter (44). Increased mitochondrial zinc then acts as a competitive inhibitor of mitochondrial aconitase, which is not a typical rate-limiting enzyme in mammalian metabolism, by specifically targeting the citrate to

cis-aconitate reaction and truncating the Krebs cycle (44). Three key anaplerotic sequences are also employed and required to support citrate accumulation. These include an increase in the expression of pyruvate dehydrogenase (PDH), to increase acetyl-CoA synthesis from pyruvate, the aspartate transporter (EAAC1), to enhance aspartate uptake, and the aspartate aminotransferase (GOT2), to increase the synthesis of oxaloacetate from aspartate (43). These anaplerotic sequences ensure the replenishment of the 6-carbon units lost upon citrate secretion. Importantly, these enzymes and ZIP1 are positively regulated at the transcriptional level by the hormones testosterone and prolactin to optimise the operation of this metabolic pathway in prostate acinar epithelial cells (40). Therefore, a major reproductive function of these hormones is to rewire the Krebs cycle in order to promote citrate accumulation and secretion by the prostate. Given this example, it should not come as a huge surprise that a cell type as important and phenotypically plastic as the macrophage might require a rewiring of the Krebs cycle.

Hormonal regulation of zinc accumulation, citrate production and Krebs cycle remodelling is quite a rare example of how the Krebs cycle and its derivatives can be repurposed by environmental cues for non-metabolic roles. However, this concept has gained real traction in recent years with the discovery that classically-activated macrophages suppress OXPHOS and dramatically rewire the Krebs cycle, as identified primarily by the accumulation of succinate and itaconate (20, 45, 46) (Fig. 1.3). It has now been proposed that two metabolic ‘breakpoints’ occur in the Krebs cycle upon pro-inflammatory activation of macrophages.

The first breakpoint occurs at IDH, due to transcriptional repression of *Idh* mRNA levels, and was first suggested by TannahilI *et al* (2013) (20). In this landmark study, the authors generated a comprehensive metabolic map of LPS-activated macrophages by combining unbiased transcriptional and metabolic datasets, demonstrating that downregulation of many mitochondrial genes directly correlated with the expression profile of altered metabolites. This breakpoint was confirmed by Jha *et al* (2015) using an integrated high-throughput transcriptional and metabolic profiling analysis pipeline (CoMBI-T) (45). While the authors also observed transcriptional downregulation of *Idh* mRNA and an increase in the citrate:α-ketoglutarate ratio, they went one step further to validate this breakpoint by performing stable isotopic experiments using uniformly labelled glucose (U-^{13}C-glucose) and glutamine (U-^{13}C-glutamine) (45). Consistent with the CoMBI-T results, ~ 20% of the total citrate pool contained glucose-derived carbon, whereas α-ketoglutarate had none (45). Likewise, a loss of partially-labelled α-ketoglutarate from U-^{13}C-glutamine was also observed, indicative of interrupted Krebs cycle activity (45). Reverse flow through IDH was also undetectably low based on the absence of 5 carbon labelling in citrate from U-^{13}C-glutamine (45). Importantly, the authors of these studies also noted that in the context of *Idh* downregulation, *cis*-aconitate is redirected towards itaconate (45) and citrate toward lipid synthesis (20). A more recent study has found that downregulation of *Idh* mRNA does not result in the downregulation of IDH protein levels (47). However, IDH enzymatic activity is suppressed by NO-mediated cysteine nitrosation. As such, the induction of iNOS and NO synthesis is a crucial mediator of Krebs cycle rewiring and the first metabolic breakpoint in macrophages.

The second metabolic breakpoint in the Krebs cycle is proposed to occur at SDH (45, 46) (Fig. 1.3). While no change in the expression of SDH subunits was detected, U-^{13}C-glutamine tracing experiments suggested inefficient succinate-to-fumarate transition as ~35% of the total pool of succinate, but only 22% of the total pool of malate, contained glutamine-derived carbon (45). Importantly, succinate was previously shown to accumulate to high levels in response to LPS stimulation, a process that was largely-dependent on glutamine anaplerosis (20). Mechanistically, it was suggested that NO-based inhibition of SDH activity may account for impaired succinate oxidation (45), although more recent studies have identified itaconate-mediated SDH inhibition as the cause of this metabolic breakpoint, a discovery that will be discussed in detail below and in this thesis (48, 49). Importantly, these studies nicely demonstrated how the coordination of anaplerotic/cataplerotic sequences and Krebs cycle enzyme functionality act to remodel the Krebs cycle. Anaplerosis occurs via glutamine feeding the Krebs cycle at α-ketoglutarate, while cataplerosis includes withdrawal of citrate for lipid synthesis and *cis*-aconitate for itaconate production.

More recently, the Krebs cycle has been show to undergo two stages of remodelling highlighting the dynamic and temporal nature of this process. The first stage is characterised by the above metabolic breakpoints with succinate and itaconate transiently accumulating (50). The second later stage is marked by the subsistence of these metabolites, which is largely driven by the inhibition of the pyruvate dehydrogenase complex (PDHC) and the OGDC (50) (Fig. 1.4). PDHC is a large, highly integrated complex of three distinct enzymes that belongs to a family of homologous complexes, which includes the OGDC (33, 51-53). These complexes are giant with molecular masses ranging from 4 million to 10

million Daltons (51, 52). The three distinct enzymes are the pyruvate dehydrogenase component (E_1), Dihydrolipoyl transacetylase (E_2) and Dihydrolipoyl dehydrogenase (E_3). E_1 uses thiamine pyrophosphate (TPP) as a catalytic cofactor and catalyses the oxidative decarboxylation of pyruvate (or α-ketoglutarate in the case of OGDC) releasing CO_2 in the process (51, 52). E_2 uses lipoic acid as a catalytic cofactor (lipoamide as a prosthetic group) and catalyses the transfer of an acetyl group to CoA (stoichiometric cofactor) (51, 52). Finally, E_3 uses FAD as a catalytic cofactor and NAD^+ as stoichiometric cofactor and catalyses the regeneration of the oxidized form of lipoamide (51, 52). The core of the complex is formed by E_2 and consists of eight catalytic trimers (α_3) with a small domain at the amino terminus that contains the flexible lipoamide cofactor (51, 52). The lipoamide domain is followed by a domain that interacts with E_3 and a large transacetylase domain (51, 52). E_1 is an $\alpha_2\beta_2$ tetramer, of which there are 24 copies, while E_3 is an $\alpha\beta$ dimer, of which there are 12 copies (51, 52). E_1 and E_3 surround the E_2 core. The key to the efficient catalysis for both PDHC and OGDC is the flexible lipoamide arm of E_2 that carries substrate from active site to active site, thus the structural integration of three distinct enzymes and the lipoamide arm makes the coordinated catalysis of a complex reaction possible. In macrophages, inhibition of PDHC and OGDC in the second stage of remodelling is achieved by altering the lipoylation state of their E_2 subunits (50). PDHC activity is further inhibited by the phosphorylation of its E_1 subunit. As such, it can be proposed that a third metabolic breakpoint occurs in the Krebs cycle at OGDC. This study therefore elucidates a dynamic picture of Krebs cycle remodelling in pro-inflammatory macrophages, while uncovering key mechanistic insights into how this remodelling is achieved.

In a resting state, macrophages utilize an intact Krebs cycle and respire normally (4, 45, 54). Similarly, in an alternatively activated state, macrophages maintain robust oxidative TCA cycling while increasing OXPHOS and ATP levels (45, 54). A role for acetyl-CoA generated from glycolysis-derived pyruvate and β-oxidation has previously been suggested to facilitate enhanced mitochondrial respiration (55-58). However, the relative contribution of these pathways has been disputed in recent years as both seem to be dispensable for alternative activation (58, 59). These issues have largely arisen from the use of 2-deoxyglucose (2-DG), a glycolytic inhibitor that targets hexokinase, and etomoxir, a carnitine palmitoyl transferase 1 (Cpt1a) inhibitor that inhibits long chain fatty acid (LCFA) oxidation (58, 59). Specifically, Wang *et al* (2018) found that 2-DG impairs both glycolysis and OXPHOS, coinciding with reduced JAK-STAT6 pathway activity and alternative activation (58). However, effective suppression of glycolysis via glucose deprivation and substitution with galactose did not interfere with OXPHOS, JAK-STAT6 signalling or alternative activation (58). Similarly, high concentrations of etomoxir (> 10 μM) retained the ability to inhibit M[IL-4] polarisation in the absence of Cpt1a and Cpt2 expression (59). At concentrations of 200 μM etomoxir increased etomoxiryl-CoA levels and blocked alternative activation by perturbing intracellular CoA enzyme homeostasis (59). As such, the enhancement of Krebs cycle activity after IL-4 stimulation is now largely believed to be driven by anaplerotic rewiring of glutamine metabolism (45, 58, 60, 61). In fact, one third of all carbons in Krebs cycle metabolites in M[IL-4] macrophages originated from glutamine, as determined by U-^{13}C-glutamine. Interestingly, high concentrations of 2-DG inhibit glutamine anaplerosis in alternatively-activated macrophages, whereas it is further enhanced to

compensate for suppressed glycolytic activity achieved using galactose or glucose deprivation (58). Likewise, glutamine deprivation was associated with a distinctly downregulated Krebs cycle and M[IL-4] transcriptional signature in alternatively-activated macrophages (45). Furthermore, IL-4 induced PPARγ transcriptional activity is essential for alternative activation via modulation of Krebs cycle enzyme and RC gene expression and glutamine metabolism (61). Together these studies provide compelling support for a causal link between this anaplerotic sequence, Krebs cycle and OXPHOS functionality and alternative macrophage activation. How specific Krebs cycle metabolites co-ordinate pro- and anti-inflammatory macrophage gene expression programmes will now be discussed in turn and are summarised in Table.1.

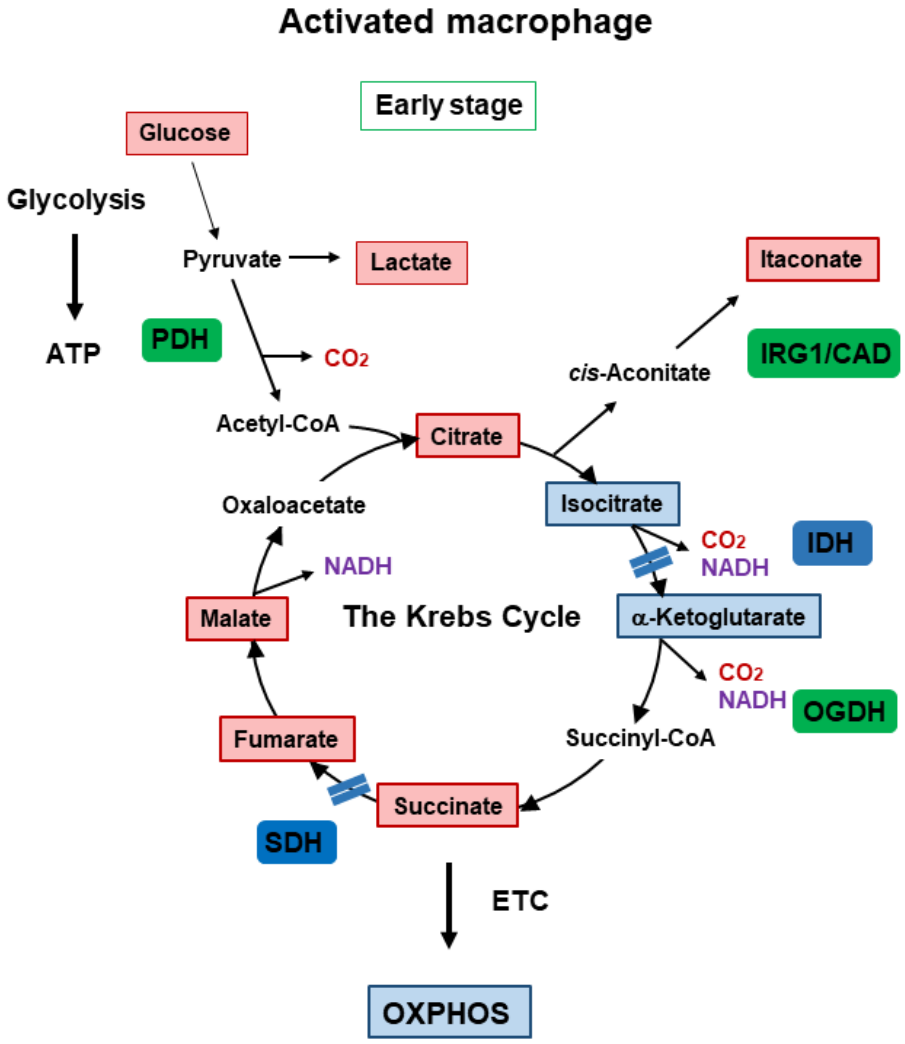

Figure 1.3 – Early stage Krebs cycle rewiring in macrophages

To meet their bioenergetic demands, quiescent macrophages utilise an intact Krebs cycle and oxidative phosphorylation (OXPHOS) to generate ATP. However, in response to lipopolysaccharide (LPS) and other pro-inflammatory stimuli, they undergo glycolytic reprogramming to generate ATP and lactate, whilst the Krebs cycle is rewired to facilitate the accumulation of Krebs cycle intermediates citrate, succinate, fumarate and malate. *cis*-Aconitate is also diverted away from the Krebs cycle to form itaconate. Accompanying this remodelling is a downregulation of OXPHOS and ATP production by the electron transport chain (ETC).

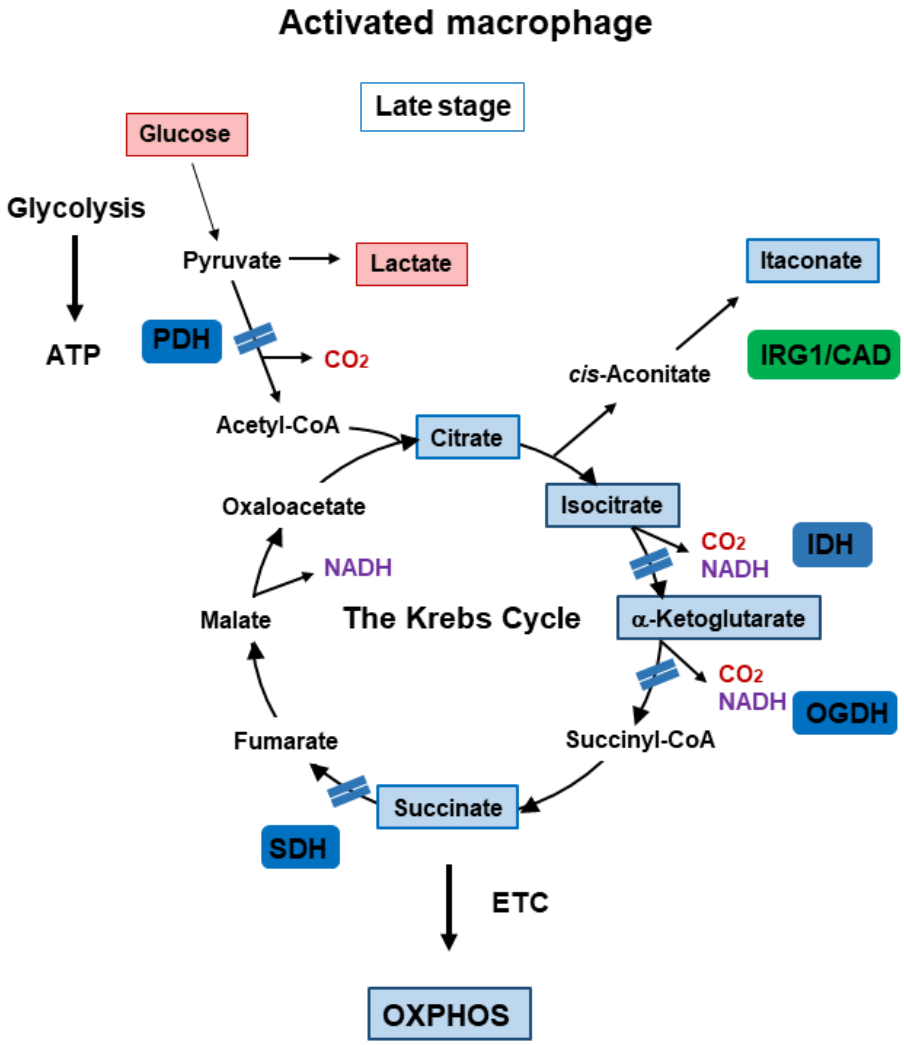

Figure 1.4 – Late stage Krebs cycle rewiring in macrophages

While early stage Krebs cycle remodelling supports the accumulation of itaconate and succinate, late stage remodelling results in a subsistence of these metabolites. The subsistence of these metabolites is achieved via inhibition of PDH and OGDH complexes, which prevents the flow of glucose-derived and glutamine-derived carbon into the Krebs cycle.

Table 1 – Overview of the Krebs cycle and Krebs cycle-derived metabolite signalling

Metabolite(s)	Synthesis (enzyme)	Cellular target(s) and/or PTM in macrophage	Signalling pathway(s) and/or processes	Inflammatory outcome(s)
Succinate	Succinyl-CoA synthetase	SUCNR1	G_i- and G_q-coupled	Increased IL-1β Chemotaxis Increased type 2 cytokine signalling
		α-KGDDs:	HIF-1α	Increased IL-1β)
		PHDs	Stabilisation	Increased
		JMJDs	Histone methylation	pro-inflammatory gene expression
α-Ketoglutarate	Isocitrate dehydrogenase	**α-KGDDs**:		
		PHDs	HIF-1α Inhibition	Decreased IL-1β
		JMJDs	Histone de-methylation	Increased
		TETs	DNA de-methylation	anti-inflammatory and M[IL-4] gene expression
Succinyl-CoA	α-ketoglutarate dehydrogenase complex	**Succinylation:** PKM2	HIF-1α activity	Increased IL-1β
Fumarate	Succinate dehydrogenase	**α-KGDDs:** JMJDs	Histone methylation	Increased TNF and IL-6
Citrate	Citrate Synthase	SLC25a1	Downstream citrate metabolism	Increased ROS, NO and prostaglandins
Acetyl-CoA	ATP-citrate lyase	**Acetylation:**		
		Histone H3	Transcription	Increased IL-6
		α-Tubulin	p38 kinase	Increased IL-10
Malonyl-CoA	Acetyl-CoA carboxylase	**Malonylation:**		
		GAPDH	Glycolysis, RNA binding	Increased TNF
Itaconate (and derivatives)	*cis*-Aconitate decarboxylase	SDH	Succinate oxidation	Inhibits pro-inflammatory cytokine production
		2,3-dicarboxypropylation:	NRF2	
		KEAP1	ATF3	Inhibits IL-1β
		GSH		Inhibits IL-6
		LDHA		
		Several others		Unknown
Itaconyl-CoA	Succinyl-CoA synthetase?	MUT	Mitochondrial B_{12} metabolism	Unknown

1.3 – The role of succinate and α-ketoglutarate as inflammatory signals

Succinate has recently emerged as a key player in macrophage activation (20, 62, 63). Mechanistically, succinate has been shown to act on several pathways to exert its immunomodulatory properties. Intracellularly, succinate can accumulate, undergo mitochondrial export and act to stabilise hypoxia-inducible factor-1α (HIF-1α) and/or undergo oxidation by SDH to drive mitochondrial reactive oxygen species (mtROS) generation from complex I (20, 62). Dysregulated succinate metabolism can also result in the accumulation of succinyl-CoA and lysine succinylation, a recently identified post-translational modification (PTM) (20, 64). Importantly, the balance between succinate and α-ketoglutarate levels intracellularly can also regulate members of the α-ketoglutarate-dependent dioxygenases (a-KGDDs) involved in epigenome remodelling and innate immune memory (60). A role for fumarate in this process will also be discussed here (65). Extracellularly, succinate can ligate the G-protein-coupled receptor (GPCR), succinate receptor 1 (SUCNR1), to elicit downstream signalling cascades and regulate macrophage effector functions (63, 66-68). This section will discuss in detail the current work carried out on both the intracellular and extracellular functions of succinate and α-ketoglutarate.

1.3.1 – Intracellular succinate signalling

A key discovery in the field of immunometabolism was the identification of succinate accumulation in macrophages treated with LPS and it's signalling via the transcription factor HIF-1α (20) (Fig. 1.5). HIF-1 is a highly conserved member of the basic helix-loop-helix (bHLH) family of transcriptional regulators,

central in directing the response to hypoxia (69, 70). HIF-1 was first discovered by Semenza and Wang in 1992 (71), where it was found to bind the human erythropoietin gene under hypoxic conditions. Since then, a crucial role for HIF-1 in the regulation of numerous cellular processes has emerged. Specifically, HIF-1 co-ordinates the expression of genes involved in cellular metabolism, angiogenesis, inflammation, erythropoiesis and proliferation by binding hypoxia response elements (HREs) in the promoters of its target genes (69, 70). A key outcome of its activation is the orchestrating of a transcriptional switch in the metabolic phenotype of the cell from the use of OXPHOS to glycolysis (glycolytic reprogramming), as previously discussed (69).

During hypoxia, HIF-1 forms a heterodimeric complex consisting of an oxygen-sensitive α subunit and a constitutively active β subunit (69). Under normoxic conditions (when O_2 levels are high), HIF-1α is tightly regulated by prolyl hydroxylases (PHDs), a family of α-KGDDs (72). Enzymatically, PHD1, 2 and 3 utilise α-ketoglutarate and molecular oxygen to hydroxylate conserved proline residues in HIF-1α, generating succinate in the process (72). Hydroxylation of HIF-1α provides a recognition site for the binding of an E3 ubiquitin ligase, the tumour suppressor protein Von Hippel-Lindau (VHL) (72, 73). The binding of VHL results in the ubiquitination of HIF-1α and its subsequent degradation via the 26S proteasome (73). Under hypoxic conditions, HIF-1α degradation is prevented enabling its translocation to the nucleus, dimerization with HIF-1β and the binding of target genes (69).

In 2005, Selak and colleagues identified a novel mitochondrion-to-cytosol signalling pathway linking the mitochondrial dysfunction observed in tumours with

SDH mutations and the activation of HIF-1α (74). Importantly, inefficient SDH activity enabled succinate to accumulate to high levels and competitively inhibit PHDs, even in the absence of VHL mutations, an important oncogenic event in tumour formation (74). As such, this represented the first identification of succinate as an 'oncometabolite'. Analogous to this, Tannahill *et al* (2013) demonstrated that under normoxic conditions LPS-induced succinate accumulation stabilised HIF-1α in macrophages (20). This study also suggested that succinate behaves as a danger signal or 'alarmin' to sustain the production of IL-1β via direct binding of succinate-induced HIF-1α to an HRE element in its promoter (20). As such, enhanced *Il1b* transcription was identified as a key inflammatory output from succinate accumulation. Furthermore, LPS-induced HIF1α activation is essential for the glycolytic reprogramming event observed in macrophages following stimulation (20). This study was the first to identify the importance of Krebs cycle rewiring in governing macrophage metabolic remodelling and emphasised the importance of Krebs cycle intermediates as inflammatory signalling molecules.

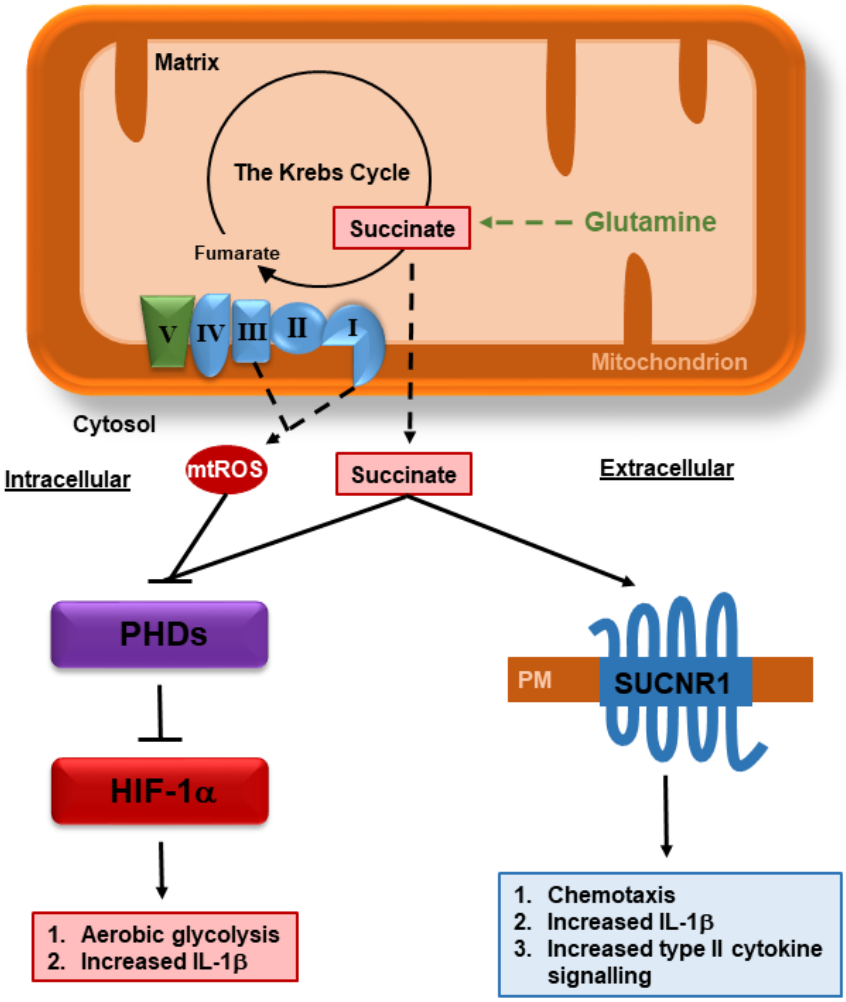

Figure 1.5 – Succinate as an inflammatory signal during inflammation

Succinate accumulation in pro-inflammatory macrophages can regulate IL-1β production. Succinate, derived in part from glutamine anaplerosis, can be exported from mitochondria into the cytosol where it directly inhibits PHD activity to stabilise HIF-1α. Mitochondrial ROS (mtROS) from complex I and complex III can also inhibit PHD activity to stabilise HIF-1α. Succinate can also be secreted from the cell where it can bind SUCNR1, which acts as an autocrine and paracrine sensor for succinate, as part of a positive feed forward loop to sustain IL-1β and promote chemotaxis. Extracellular succinate and SUCNR1 can also be anti-inflammatory in certain contexts by synergising with type II cytokine signaling to promote anti-inflammatory gene expression.

More recently, succinate oxidation by LPS-activated macrophages was shown to inhibit PHD activity indirectly via mtROS resulting in HIF-1α stabilisation and IL-1β production (62) (Fig. 1.5). Like succinate, ROS are critical regulators of PHD enzymatic activity under normoxic conditions (75, 76). Although the physiological relevance of mtROS in HIF-1α stabilisation is not without its controversy, normoxic mtROS production that arises from loss of SDHB from complex II has previously been suggested to inhibit PHDs by inducing non-enzymatic decarboxylation of α-ketoglutarate (75, 76). However, PHD activity is also highly dependent on iron (Fe^{2+}) as a cofactor and so ROS-mediated oxidation of Fe^{2+} to Fe^{3+} has also been proposed as a potential inhibitory mechanism (75). Interestingly, Mills *et al* (2016) found that limiting succinate oxidation in activated macrophages with the prodrug dimethyl malonate (DMM), which releases the potent complex II inhibitor malonate, potently blocked mtROS production from complex I while repressing LPS-induced HIF-1α and IL-1β (62). In a reciprocal manner, succinate oxidation limits the production of the anti-inflammatory cytokines IL-10 and IL-1RA, an impairment overcome by SDH inhibition with DMM (62). However, the precise role of HIF-1α in regulating IL-10 and IL-1RA remains to be explored. In line with this study, complex I-mediated mtROS generation in macrophages has previously been shown to promote IL-1β production while limiting IL-10, a process inhibited by the antidiabetic drug metformin (77). In addition to succinate oxidation by SDH, mtROS production by complex I was dependent on increased mitochondrial membrane potential (electrochemical gradient) (62). Hyperpolarisation of the IMM is thought to be driven by the hydrolysis of glycolytic ATP by the reverse activity of ATP synthase,

as inhibition of hexokinase 2-DG, or the F_0F_1-ATP synthase with oligomycin, is sufficient to lower membrane potential and impair LPS-induced IL-1β production (62). Treatment of macrophages with the proton ionophore uncoupling agent, carbonyl cyanide-4-(trifluoromethoxy) phenylhydrazone (FCCP), which dissipates mitochondrial membrane potential, was also sufficient to block mtROS, HIF-1α and IL-1β levels (62).

Mills *et al* (2016) argue that succinate-induced mtROS production from complex I in this setting is a result of reverse electron transport (RET) (62) (Fig. 1.6). This process was first observed in a model of ischaemia-reperfusion (IR) injury, whereby succinate accumulates during ischaemia due to a reversal in SDH directionality (78). Upon reperfusion however, SDH rapidly oxidises succinate resulting in excessive reduction of the CoQ pool (78). This forces electrons to flow backwards through complex I to generate superoxide (O_2^-), an event inhibited by DMM or the complex I inhibitor rotenone (62, 78). To further support a role for RET, macrophages expressing an alternative oxidase (AOX) from *Ciona intestinalis* were employed (62). Importantly, AOX enables the oxidation of excess electrons built up in the Q pool (62). In agreement with RET, AOX expression in macrophages impaired LPS-induced mtROS production, HIF-1α stabilisation and IL-1β production (62). Complex I-derived mtROS, caused by deletion of the essential subunit Ndufs4, has previously been shown to promote inflammation and potentiate macrophage activation even in the absence of stimulation, highlighting the relevance of this site in ROS production (79). The importance of complex II and succinate oxidation in innate immune signalling is also further exemplified by Garaude *et al* (2016) who nicely demonstrated the transient remodelling of complex I-containing supercomplexes in activated

macrophages, switching the relative contributions of complex I and complex II to respiration (80). Importantly, the authors demonstrated an impairment in the anti-bactericidal activity of macrophages and an inhibition of IL-1β in *Escherichia coli*-infected mice treated with DMM. While no direct evidence was presented, the authors suggested an impairment in RET may account for their observed phenotype. It is also important to note that a role for complex III-derived mtROS in regulating pro-inflammatory macrophage activation has recently been identified (81). As such, the dynamics of mtROS production and the relative contributions of RET, complex I and complex III to this process will require further investigation. Taken together, these observations highlight an essential role for the ETC and mtROS signalling in the regulation of macrophage activation and inflammation.

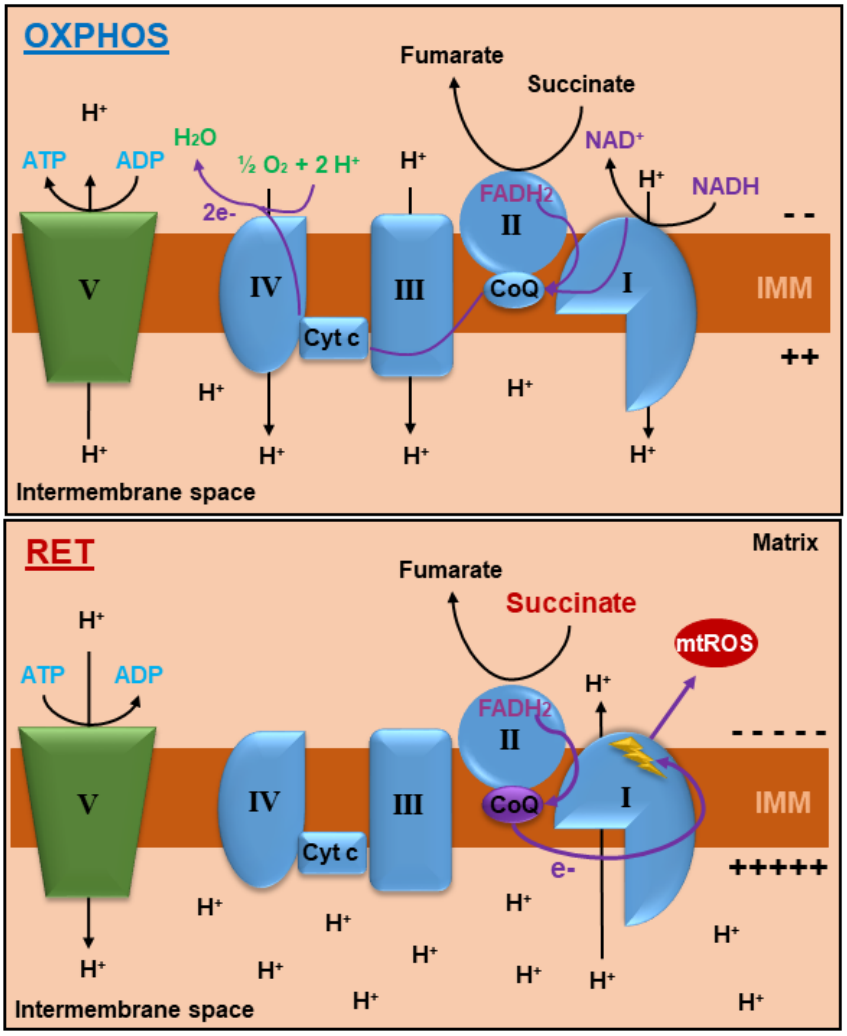

Figure 1.6 – Succinate oxidation and mtROS as an inflammatory signal

LPS reprograms oxidative phosphorylation (OXPHOS), which enables succinate oxidation by complex II to drive reverse electron transport (RET). RET promotes mitochondrial reactive oxygen species (mtROS) production from complex I, which inhibits PHD activity and stabilises HIF-1α. The repurposing of OXPHOS to RET is aided by glycolytic ATP, complex V and inner mitochondrial membrane (IMM) hyperpolarisation.

1.3.2 – Succinylation and inflammatory signalling

As mentioned, dysregulated succinate metabolism and succinyl-CoA accumulation can result in lysine succinylation, such as that observed in LPS-activated macrophages (20, 64). This modification induces a 100 Da change in mass and masks the positive charge of the lysine side chain, likely resulting in a significant conformational change in the target protein (82). Succinylation is largely thought to occur non-enzymatically, however, mitochondrial-localised SIRT5 is a known desuccinylase that can enzymatically remove succinyl groups and regulate signalling processes (83, 84). Interestingly, succinylation is known to regulate macrophage function in response to LPS (64). Specifically, hypersuccinylation of lysine 311 on pyruvate kinase M2 (PKM2), a key glycolytic enzyme previously known to interact with HIF-1α and regulate aerobic glycolysis in macrophages (21), inhibits its pyruvate kinase activity by promoting its tetramer-to-dimer transition (64). Importantly, Wang *et al* (2017) show that SIRT5 desuccinylates PKM2 to prevent its entry into the nucleus, the formation of a HIF-1α/PKM2 complex and IL-1β induction (64). Furthermore, the authors show that SIRT5-deficient mice are more susceptible to dextran sodium sulfate (DSS)-induced colitis and display elevated levels of IL-1β *in vivo* (64). This study, coupled with the identification of a plethora of substrates that constitute the 'succinylome', suggest this PTM could have far reaching consequences in altering protein function and as a signal in innate immunity.

1.3.3 – Succinate, α-ketoglutarate, fumarate and epigenetic reprogramming

In addition to the PHDs, α-ketoglutarate is an important cofactor for the α-KGDDs family of Jumonji-C-domain-containing histone demethylases (JMJDs), involved in histone demethylation, and the ten eleven translocation (TET) family of 5mC hydroxylases, which play a role in DNA demethylation (85). Like the PHDs, these enzymes can undergo competitive inhibition by succinate, and so the ratio of α-ketoglutarate to succinate can often be a key determinant of their enzymatic activity, thus enabling them to remodel the epigenome (60, 85). As previously mentioned, glutamine anaplerosis of the Krebs cycle represents an important metabolic module governing the alternative activation of macrophages in response to IL-4 (45, 60, 61). Liu *et al* (2017) took this observation further when they uncovered an important signalling role for glutamine-derived α-ketoglutarate, which facilitates an IL-4-induced gene expression programme via JMJD3-driven epigenetic changes (60) (Fig. 1.7). Furthermore, the authors found that α-ketoglutarate suppresses the classical activation of macrophages (as a low α-ketoglutarate/succinate ratio strengthens the pro-inflammatory phenotype) and supports endotoxin tolerance after classical activation (60). Recently, melatonin was shown to alleviate inflammation associated with obesity in part by increasing the ratio of anti- to pro-inflammatory adipose tissue macrophages (ATMs) (86). Mechanistically, this was achieved by the targeting of ATMs with adipocyte-derived exosomal α-ketoglutarate and TET-mediated DNA demethylation (86).

Epigenetic remodelling has also been implicated as an important mechanism governing innate immune memory (also known as trained immunity) (87, 88). Innate immune memory is an emerging concept in immunology describing a change in the reactivity of immune cells previously exposed to various inflammatory stimuli (87, 88). This change in reactivity allows macrophages to respond more robustly to subsequent, but potentially unrelated, insults. At the molecular level, stimuli, such as the fungal wall component β-glucan from *Candida albicans*, alter histone methylation patterns that persist after resolution of the infection and enhance cytokine production upon re-infection (88). Like LPS, β-glucan induces Krebs cycle rewiring and glutamine anaplerosis in human monocytes, which acts to increase intracellular fumarate levels (65). Fumarate, like succinate, is a competitive inhibitor of the JMJD and TET families of α-KGDDs that can modulate the epigenome (85). Importantly, Arts *et al* (2016) could show that glutamine-derived fumarate acted to inhibit the KDM5 family of histone demethylases after β-glucan training (65) (Fig. 1.7). Inhibition of these demethylases subsequently increased the levels of H3K4me3, a marker of active gene transcription, at the promoters of the pro-inflammatory cytokines TNF and IL-6, boosting their production upon re-stimulation with LPS (65). As such, the balancing of succinate, α-ketoglutarate and fumarate levels in macrophages can have profound functional consequences for macrophage polarization states and innate immune memory by altering the epigenetic landscape of the cell.

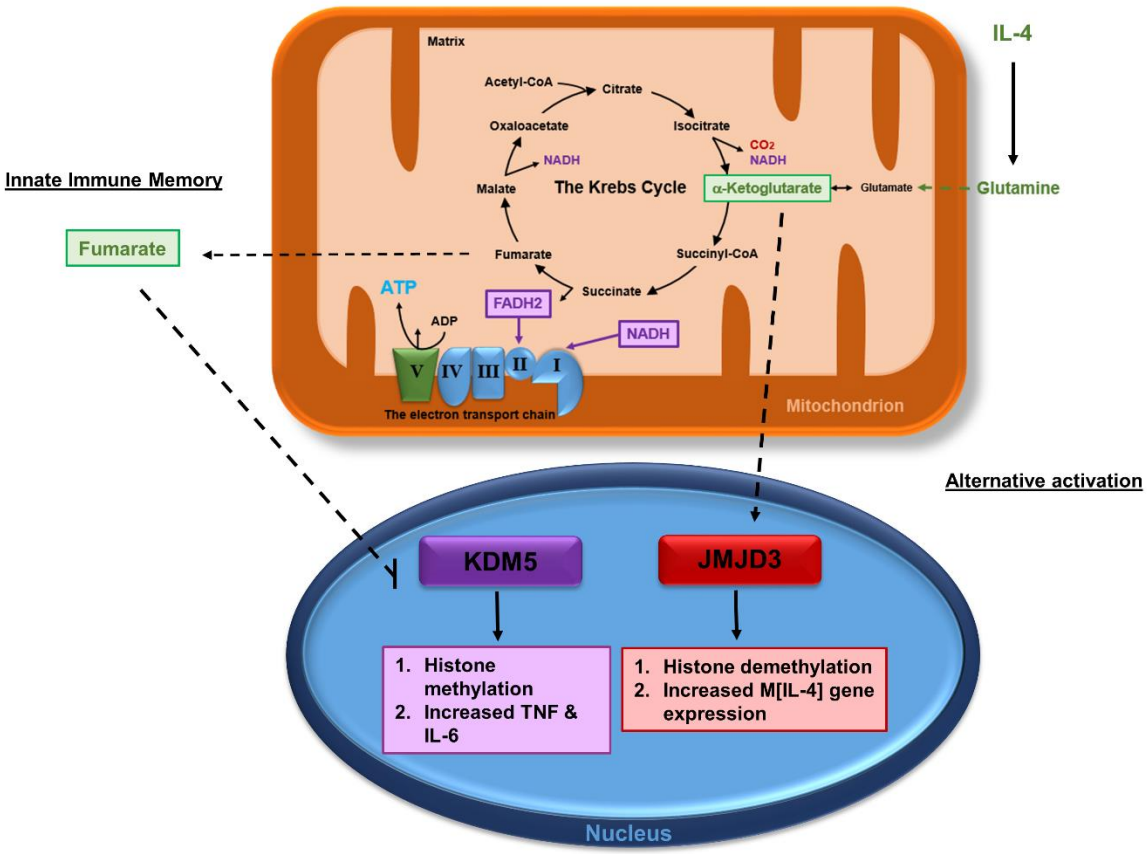

Figure 1.7 – α-Ketoglutarate and fumarate remodel the epigenetic landscape of macrophages

Glutamine-derived alpha-ketoglutarate and fumarate are required for epigenome remodelling in alternatively-activated macrophages and during innate immune memory, respectively. IL-4 induces glutamine anaplerosis during alternative activation to enhance oxidative phosphorylation (OXPHOS) and ATP production. This also increase alpha-ketoglutarate levels, which is then used as a cofactor by the histone demethylase JMJD3 to promote an anti-inflammatory M[IL-4] gene expression programme. Monocytes primed with β-glucan (used to induce innate immune memory) undergo Krebs cycle rewiring, which results in fumarate accumulation derived from glutamine anaplerosis. Fumarate then acts to inhibit the KDM5 family of histone demethylases, which alters histone methylation and results in increased TNF and IL-6 production upon re-challenge with other inflammatory stimuli, such as LPS.

1.3.4 – Extracellular succinate signalling

In 2004, He and colleagues discovered unexpectedly that the Krebs cycle intermediates succinate and α-ketoglutarate were the cognate ligands for the orphan GPCRs, GPR91 (also SUCNR1) and GPR99 (also OXGR1), respectively (89). Furthermore, SUCNR1 was found to be a G_i and G_q coupled GPCR highly expressed in the kidney, liver, spleen and small intestine. Importantly, the authors demonstrated that succinate acts as a hypertensive agent to increase blood pressure in animals, in part through SUCNR1 and the renin-angiotensin system (89). Thus, by acting as a ligand for SUCNR1, succinate was found to have an unexpected signalling function independent of its role in bioenergetics. Since this seminal discovery, subsequent studies have found SUCNR1 to be expressed on the plasma membrane of macrophages, with important consequences for their function during a variety of inflammatory contexts (63, 66-68) (Fig. 1.5).

Since the discovery of SUCNR1, the elucidation of the signalling cascades elicited by binding of succinate has begun to emerge (90, 91). Robben *et al* (2009) showed GPR91 to be a Gi- and Gq-coupled receptor using the inhibitors pertussis toxin (PTX) and YM254890 in kidney-derived MDCK cells (92). Sundström *et al* (2013) confirmed that GPR91 was a Gα(i)- and Gα(q)-coupled receptor resulting in the inhibition of 3'-5'-cyclic adenosine monophosphate (cAMP) inhibition and inositol triphosphate (IP3) formation (93). The agonist-mediated effects of SUCNR1 stably expressed in the human embryonic kidney (HEK) 293 cell line were detected using dynamic mass redistribution (DMR) and found to be sensitive to PTX (90, 91, 93). Inhibition of SUCNR1 signalling with PTX, edelfosine and U73122 also demonstrated the importance of SUCNR1 to elevate intracellular calcium (Ca^{2+}) via IP3 generated by phospholipase C β

(PLCβ) (90, 91, 93). Similar signalling pathways have also been uncovered in other SUCNR1-positive cell types including adipocytes treated with lipolytic hormones (94) and hematopoietic progenitors (95), which drove proliferation via activation of ERK1/2. Interestingly, succinate-induced responses in cardiac myocytes and platelets involved the induction of protein kinase A (PKA) through the Gs/cAMP pathway, suggesting cell-type specific coupling of G proteins to SUCNR1 (96, 97). Even more importantly, SUCNR1 stimulated with succinate was found to induce intracellular Ca^{2+} mobilisation and phosphorylation of ERK1/2 in DCs, highlighting its functionality in immune effector cells and inflammation (98).

In 2008, the first line of evidence that succinate signalling through SUCNR1 was an important inflammatory mechanism was proposed (98). Rubic *et al* (2008) demonstrated that succinate acted in synergy with TLR agonists to boost inflammatory cytokine expression in DCs (98). Specifically, succinate boosted TNF levels, in synergy with TLR3 agonist poly(I:C) and TLR7 agonist imiquimod, whilst it also potentiated IL-1β levels in conjunction with LPS (98). In addition, SUCNR1 was also found to be involved in DC chemotaxis, as monocyte-derived DCs (moDCs) exhibited enhanced migration to draining lymph nodes when treated with succinate (98). Furthermore, succinate was also found to enhance antigen presentation by DCs and antigen-specific activation of helper T cells, an effect abolished in SUCNR1 KO DCs (98).

In a recent study, Littlewood-Evans *et al* (2016) demonstrated that macrophages release succinate into the extracellular milieu when activated, while simultaneously upregulating SUCNR1 (66). Intriguingly, SUCNR1 then acts as an autocrine and paracrine sensor for extracellular succinate to augment IL-β

production, which in turn increases SUCNR1 levels fuelling this cycle of cytokine production (66). SUCNR1-deficient mice also show reduced macrophage activation and production of IL-1β in response to LPS and in a model of antigen-induced arthritis (66). Treatment of macrophages with synovial fluid from rheumatoid arthritis (RA) patients, which is abundant in succinate, elicits IL-1β release suggesting that chronically elevated succinate is pathological in this setting (66). Succinate levels are also elevated in other chronic inflammatory settings, such as in mouse adipose tissue during models of diet-induced obesity or in the plasma of patients with type 2 diabetes (68). Interestingly, SUCNR1-deficient mice were reported to have significantly reduced numbers of ATMs compared to adipocytes and improved glucose tolerance compared with wildtype (WT) mice fed a high-fat diet, owing in part to a reduction in macrophage chemotaxis (68). Succinate-induced chemotaxis has also been implicated in the pathogenesis of chronic neuroinflammation during experimental autoimmune encephalomyelitis, a mouse model of multiple sclerosis (MS) (67). Specifically, infiltration of damaging mononuclear phagocytes (MP) is decreased via the transplantation of neural stem cells (NSCs), which scavenge succinate from the cerebrospinal fluid (67). Mechanistically, inflammatory phagocytes release succinate that ligate SUCNR1 on the surface of NSCs to upregulate the expression of the dicarboxylate co-transporters SLC13a3 and SLC13a5, and induce the secretion of the anti-inflammatory lipid mediator prostaglandin E2 (PGE2) (67). Upregulation of solute carrier family 13 member 3 (SLC13a3) and SLC13a5 scavenges succinate away from inflammatory macrophages and microglial cells preventing further infiltration and secondary CNS damage (67). These findings suggest that SUCNR1-induced chemotaxis promotes the

infiltration of macrophages into various tissues during chronic inflammatory settings and presents itself as a promising target to combat inflammatory disease.

In contrast to these studies, Keiran *et al* (2019) have found that activation of SUCNR1 has a critical role in the anti-inflammatory response in macrophages during alternative activation and obesity (63). Specifically, SUCNR1 expression was increased in M[IL-4]-polarized macrophages and decreased in M[LPS]-polarized macrophages, in contrast to reports by Littlewood-Evans and colleagues, while succinate-SUCNR1 signalling promoted an anti-inflammatory phenotype by augmenting their response to type 2 cytokines (63). Transgenic mice which had SUCNR1 deleted specifically from the myeloid lineage also displayed signs of tissue inflammation and glucose intolerance when fed a normal chow diet, while the metabolic consequences of obesity, such as insulin insensitivity, were also exacerbated (63). Furthermore, myeloid-specific deletion of SUCNR1 impaired adipose-tissue browning in response to cold exposure (63). As such, an unexpected role for succinate in limiting inflammation during obesity was identified.

SUCNR1-deficient mice have also been shown to exhibit reduced arthritic disease in an ovalbumin-induced arthritis model, in line with previous findings (99). Interestingly however, these mice are also more susceptible to allergic contact dermatitis (ACD) attributed to increased mast cell activation (99). These results among others discussed have prompted the suggestion that SUCNR1 antagonism may constitute a promising therapeutic approach in RA patients and other inflammatory disorders, however, the observation of elevated ACD and metabolic disease during obesity suggests a possible anti-inflammatory role for

succinate and SUCNR1 under certain circumstances. Whether extracellular succinate is pro-inflammatory or anti-inflammatory during inflammation could therefore be context-dependent.

1.4 - The role of citrate and itaconate during inflammation

The last set of metabolites that will be considered within the context of Krebs cycle rewiring in macrophages are citrate and itaconate, which are synthesised in the mitochondrial matrix by citrate synthase and immunoresponsive gene 1 (IRG1), also known as *cis*-aconitate decarboxylase (CAD), respectively (30, 100). Intriguing roles for these metabolites have been reported in macrophage function and will be discussed below.

1.4.1 – Extra-mitochondrial citrate metabolism and inflammation

In a manner like that observed in prostate secretory epithelial cells, a key functional outcome of Krebs cycle rewiring in macrophages is to facilitate citrate synthesis and export from mitochondria (101-103). To achieve this, pro-inflammatory macrophages sustain pyruvate oxidation through pyruvate dehydrogenase (PDH) and increase glutamine uptake and anaplerosis, as demonstrated using stable-isotope-assisted metabolomics (101). This reprogramming event is quite surprising given that HIF-1α stabilisation can also result in the induction of pyruvate dehydrogenase kinase 1 (PDK1), which phosphorylates and inhibits PDH enzymatic activity in other contexts, such as during tumour hypoxia (101). In macrophages however, PDK1 expression is repressed by LPS stimulation via an as yet unidentified mechanism, thus enabling glucose-derived citrate synthesis (101). In addition to sustaining PDH activity, LPS increases the expression of the mitochondrial citrate carrier,

SLC25a1, in an NF-κB-dependent manner (102). SLC25a1 can then catalyse the exchange of mitochondrial citrate for cytosolic malate, leading to an efflux of citrate from the mitochondria and its accumulation in the cytosol (102) (Fig. 1.8). Functionally, inhibition of SLC25a1 in activated macrophages with the inhibitor 1,2,3-benzentricarboxylic acid (BTA) or through genetic silencing, leads to a marked reduction in ROS, NO and prostaglandin production (102). This suggests that the efflux of citrate from mitochondria is an essential pro-inflammatory signal during macrophage activation.

In the cytosol, citrate can be converted to acetyl-CoA and oxaloacetate by the ATP-citrate lyase (ACL) (103, 104) (Fig. 1.8). Like SLC25a1, ACL is transcriptionally upregulated in response to LPS and functionally required for ROS, NO and prostaglandin synthesis in activated macrophages (103). Although the precise mechanism by which citrate regulates these processes is unknown, acetyl-CoA produced in this manner is essential for *de novo* lipogenesis and as a cofactor for acetyltransferases, a family of enzymes that catalyse the transfer of acetyl groups to protein lysine residues (104-106). Acetyl-CoA can also be converted to malonyl-CoA via the acetyl-CoA carboxylase (ACC), which is then used by fatty acid synthase (FASN), along with acetyl-CoA, as the primary substrates for palmitate synthesis (105, 106). Importantly, FASN has recently been identified as a key regulator of classical macrophage activation (105, 106). Firstly, during diet-induced obesity deletion of FASN prevents macrophage adhesion, migration and activation *in vivo* by altering plasma membrane order and composition, primarily by reducing cholesterol retention, and impairing RHO GTPase trafficking (106). Secondly, FASN-derived acetoacetyl-CoA, synthesised from the condensation of acetyl-CoA and malonyl-CoA, was

unexpectedly required for endogenous cholesterol synthesis and enabled TLR4 recruitment to lipid rafts in response to LPS stimulation (105). TLR4 recruitment to lipid rafts is an important cellular event that facilitates signal transduction and pro-inflammatory macrophage activation during infection. Furthermore, C13*orf*31 (FAMIN), a recently identified protein that forms a complex with FASN on peroxisomes and promotes *de novo* lipogenesis, was also found to regulate ROS and cytokine production in LPS-activated macrophages (107). As such, inhibition of SLC25a1, ACL and downstream citrate metabolism may modulate ROS, cytokine and prostaglandin levels by impairing *de novo* lipogenesis, TLR4 receptor signalling and NF-κB activation.

1.4.2 – Acetylation and inflammatory signalling

Acetylation can also modulate macrophage function (108-112). ACL-derived acetyl-CoA has been shown to drive histone acetylation, a process that can have profound effects on cellular function (104). Importantly, histone acetyltransferases (HATs) can play a major role in the epigenetic regulation of gene expression by modifying chromatin structure (104, 113). Specifically, acetylation of lysine residues on H3 is associated with the expression of IL-6 in virus-infected (112) and paraquat (PQ)-treated (111) macrophages, MMP-1 and MMP-3 secretion in *Mycobacterium tuberculosis* (*Mtb*)-infected macrophages (110) and elevated IL-12p40 promoter activity (109). Despite this, there are only limited reports on the involvement of HATs in specific gene activation during macrophage activation and this remains an open area of investigation. Acetylation can also regulate the function of proteins outside of histone modifications. Specifically, acetylation of the cytoskeletal protein α-tubulin, by the tubulin acetyltransferase MEC17, was shown to regulate IL-10 induction in LPS-

activated macrophages (108) (Fig. 1.8). As such, acetylation can serve as an important signal to govern both pro- and anti-inflammatory cytokine production in activated macrophages.

1.4.3 – Malonylation and inflammatory signalling

Like succinyl-CoA and acetyl-CoA, malonyl-CoA can also modify protein lysine residues, in a process termed malonylation (82, 114, 115). Protein lysine malonylation is a highly-conserved protein modification, however it remains largely understudied. In two models of type 2 diabetes, proteomic analysis of liver tissue was used to identify 573 malonylated lysine sites from 268 proteins, many of which were metabolic enzymes involved in glycolysis, e.g. GAPDH, and lipid metabolism, e.g. ACLY (114). Recently, Galván-Peña *et al* (2019) showed an increase in the levels of malonyl-CoA and protein malonylation in activated macrophages (115). One of the targets identified also included GAPDH (115). In addition to its role in glycolysis, GAPDH also acts as an RNA binding protein to post-transcriptionally regulate mRNAs containing ARE elements in their 3'UTR, as previously mentioned (22, 115). In macrophages, GAPDH is known to post-transcriptionally repress TNF translation, however the signals that govern this process remain unclear. Interestingly, Galván-Peña and colleagues could show that upon LPS stimulation GAPDH undergoes malonylation on lysine 213, leading to its dissociation from *TNF* mRNA and promoting its translation (115) (Fig. 1.8). Furthermore, malonylation of GAPDH was also shown to increase its enzymatic activity and engagement in the glycolytic pathway (115). As such, malonylation was shown for the first time to be an important inflammatory signal in macrophages regulating both metabolic reprogramming and cytokine production.

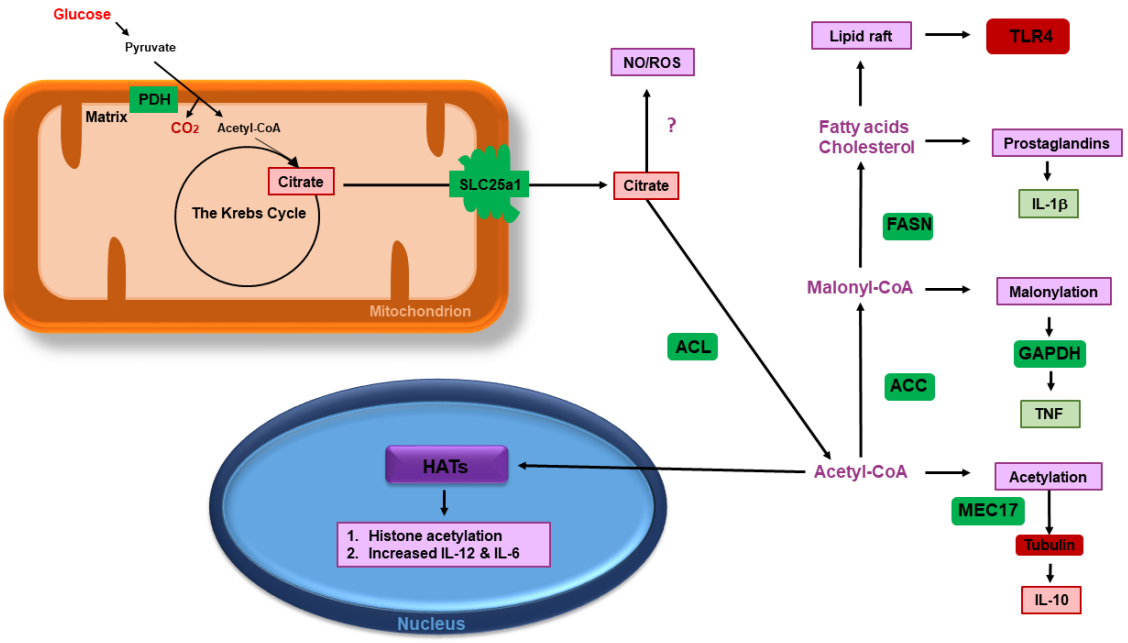

Figure 1.8 – Citrate as an inflammatory signal in macrophages

In macrophages, citrate synthesised from glucose-derived pyruvate and pyruvate dehydrogenase (PDH) can be exported from mitochondria via the mitochondrial citrate carrier SLC25a1. In the cytosol, citrate can be converted to acetyl-CoA and oxaloacetate by the ATP-citrate lyase (ACL). Increased cytosolic acetyl-CoA can then be used as a cofactor by acetyltransferases, such as MEC17, which acetylates tubulin during pro-inflammatory macrophage activation to increase the anti-inflammatory cytokine IL-10. Likewise, it can also be used by histone acetyltransferases (HATs) to regulate cytokine levels. Acetyl-CoA can also be converted to malonyl-CoA via the acetyl-CoA carboxylase (ACC). Similar to acetylation, malonyl-CoA can be used to malonylate protein lysine residues, such as observed with GAPDH, or it can feed into fatty acid and cholesterol synthesis through fatty acid synthase (FASN). Malonylation is an important pro-inflammatory signal that promotes TNF translation and secretion in response to LPS. Fatty acids and cholesterol from FASN are also essential for lipid raft formation, TLR4 signaling and the production/secretion of cytokines and prostaglandins

1.4.4 – Itaconate as an antimicrobial and immunomodulatory metabolite

In addition to citrate formation, a key functional outcome of IDH repression and PDH activity is the synthesis of the anti-bacterial metabolite itaconate (45, 49, 101, 116) (Fig. 1.9). Itaconate is synthesised from the Krebs cycle-intermediate *cis*-aconitate by *cis*-aconitate decarboxylase (CAD), an enzyme whose expression is induced in response to inflammatory macrophage activation and largely restricted to cells of the myeloid lineage (100). For decades, itaconic acid, also called methylenesuccinic acid, produced by the fungus *Aspergillus terreus* has been used in the industrial arena for the synthesis of various polymers and was not generally classified as a mammalian metabolite (117). However, in 2011 it was detected in primary murine macrophages that had been activated with LPS (117) and in the lungs of Mtb-infected mice (118). Following this discovery, Michelucci *et al* (2013) were able to demonstrate that immunoresponsive gene 1 (*Irg1*), now aconitate decarboxylase 1 (*Acod1*), which is highly expressed in mammalian macrophages during inflammation, was the sought after *cis*-aconitate decarboxylase (100). Furthermore, the authors observed a reduction in anti-microbial activity during bacterial infection upon loss of itaconate synthesis (100). The anti-bacterial function of itaconate had been first demonstrated in the 1970's, as it effectively inhibited isocitrate lyase (ICL) from *Pseudomonas indigofera* under low glucose conditions, however, this property of itaconate did not garner interest until its discovery as a naturally occurring immunometabolite (48, 119). In addition to *P. indigofera*, exogenous itaconate has since been shown to inhibit *in vitro* growth of numerous pathogenic bacteria including *M. tuberculosis, Staphylococcus aureus, S. enterica, Legionella pneumophillia* and *Acinetobacter baumannii* (100, 120). In another example, in *Yersinia pestis* and

Pseudomonas aeruginosa, itaconate degradation (mediated by 3 enzymes – itaconyl-CoA transferase, itaconyl-CoA hydratase and (S)-citramalyl-CoA lyase) is critical for bacterial survival and pathogenicity (121).

ICL itself is a key enzyme of the glyoxylate shunt, an anabolic variation of the Krebs cycle that circumvents the two decarboxylation reactions and is used as a mechanism for survival in glucose-poor conditions in some plants and microorganisms (122, 123). The importance of ICL as a virulence factor in microorganisms has been clearly demonstrated with the pathogenic fungus, *Candida albicans* (122). Upon infection, *C. albicans* undergoes phagocytosis by macrophages resulting in the upregulation of ICL1, however, *C. albicans* strains with a mutant ICL1 are significantly less virulent than wildtype strains. Similarly, deletion of both isoforms of ICL, ICL1 and ICL2, in *M. tuberculosis* resulted in complete impairment of intracellular replication in macrophages and its rapid elimination from the lungs of mice, whilst inhibition of ICL also inhibited growth in macrophages (124).

Despite the importance of ICL in infection and the evidence implicating itaconate as an antimicrobial agent, there has been some debate around the physiological relevance of studies using itaconate to inhibit bacterial cell growth (125). This has arisen from inconsistencies between the concentrations of itaconate used *in vitro*, ranging from 5 mM to 100 mM, and the intracellular concentrations identified in macrophages, ranging from 40 μM to 80 mM (125). However, many studies have used itaconate in the 10 mM range, a concentration close to some previous reports (100), whilst induction of IRG1 by both type I and type II interferons in *L. pneumophillia*-infected macrophages mediates itaconate production and restricts intravacuolar growth of the bacteria (120). A recent study

by Nair and colleagues found that Irg1-deficient mice succumbed rapidly to *M. tuberculosis* infection (126). This increase in mortality was accompanied by increased *Mtb* burden in the lungs and increased pro-inflammatory cytokine and chemokine production (126). Furthermore, the authors found that even when a strain of *M. tuberculosis* (Δcl1), which lacks a functional glyoxylate shunt, was used, *Irg1 -/-* mice still succumbed rapidly to infection with increases in cytokine and chemokine levels (126). The authors went further and demonstrated that this immunopathology was largely driven by increased infiltration of neutrophils into the lung (126). RNA seq analysis of *Mtb*-infected macrophages suggests this hyper-inflammatory phenotype was driven by the loss of itaconate and its ability to temper the immune response (126). As such, the role of itaconate as a physiologically relevant anti-bacterial metabolite remains an open question to be explored.

Despite the known bactericidal activity of itaconate, its role in regulating macrophage function remained unknown. Recent studies have brought to light the possibility that itaconate is an important immunomodulator (49, 116, 127). Importantly, LPS stimulated-BMDMs treated with methyl ester derivative of itaconate, dimethyl itaconate (DMI), exhibited potent inhibition of pro-inflammatory mediators including NO, ROS and the cytokines IL-1β, IL-12p70, and IL-6, however no effect on TNF levels was observed (49). Furthermore, LPS-activated *Irg1*-deficient BMDMs exhibited a boost in the production of IL-12, IL-6, NO, and under conditions that stimulate the NLRP3 inflammasome, increased IL-1β and IL-18 (49). An increase in *Hif1α* mRNA and HIF1α protein levels was also observed in *Irg1*-deficient BMDMs, a critical regulator of aerobic glycolysis and IL-1β production (49). The role of IRG1 and itaconate as negative regulators

of inflammation is further supported by the findings that IRG1 suppresses the production of TNF, IL-6 and IFN-β in LPS-tolerised macrophages (128). Additionally, IRG1 has also been found to mediate the immunosuppressive effects of CO releasing molecule 2 (CORM2)-induced heme oxygenase 1 (HO-1) on LPS-induced TNF production in macrophages and in a murine LPS sepsis model (129). Interestingly, IRG1 also appears to play a major role in embryo implantation in the womb, a process thought to require suppression of the immune system (130-132). These findings suggest that the production of itaconate by IRG1 in macrophages acts as a negative regulator of inflammation and crucially provides the first link between itaconate signalling and the modulation of pro-inflammatory cytokine production.

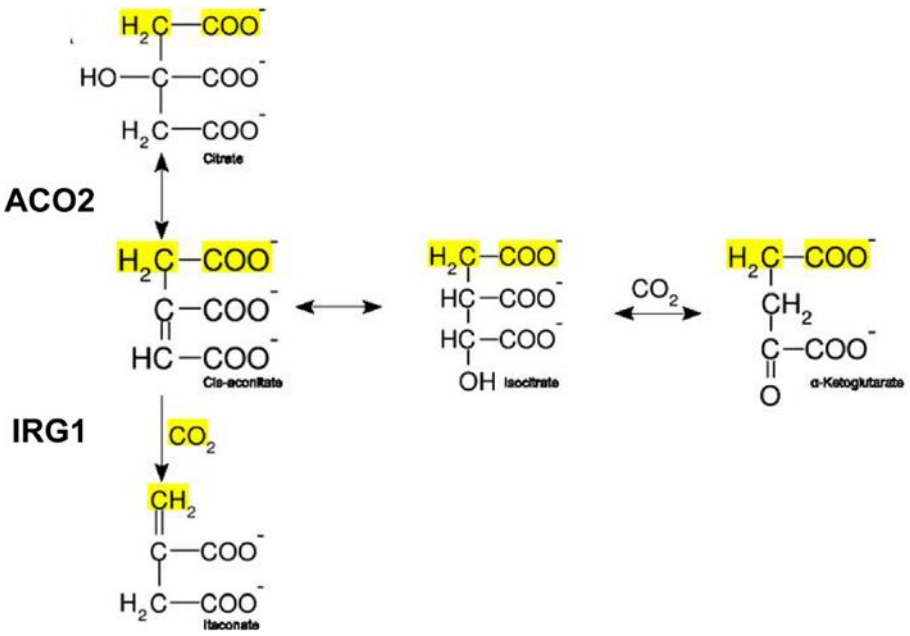

Figure 1.9 – Itaconate synthesis from *cis*-aconitate (100)

Chemical schematic showing itaconate synthesis via decarboxylation of citrate-derived cis-aconitate, a reaction catalysed by IRG1/CAD.

Mechanistically, itaconate is now known to mediate these effects via modulation of macrophage metabolism (48, 49, 116, 127) (Fig. 1.10). Firstly, itaconate can competitively inhibit complex II-mediated oxidation of succinate, which enables succinate accumulation in response to LPS and is thought to limit RET-induced inflammation (48, 49). Itaconate was first identified as a competitive SDH inhibitor in 1949 (133), which prompted the initial speculation that itaconate may modulate cellular metabolism in macrophages. In two independent studies, genetic deletion of *Acod1* and the exogenous addition of itaconate or itaconate derivatives was sufficient to decrease and increase succinate accumulation in macrophages, respectively (48, 49). Itaconate was also shown to competitively inhibit purified SDH (49). Furthermore, the suppression of OXPHOS is lost in *Acod1*-deficient macrophages treated with LPS and in fact an increase in oxygen consumption rates (OCR) is observed (49). This increase in OCR is likely due to increased fuelling of the Krebs cycle by glutamine in the absence of complex II inhibition. Together these papers provide compelling evidence that CAD-mediated itaconate synthesis promotes succinate accumulation and offers a molecular explanation for the second breakpoint in the TCA cycle.

Secondly, itaconate can bind and inactivate reactive thiol groups of proteins and glutathione, an irreversible non-enzymatic process termed 2, 3-dicarboxypropylation (116, 127). This novel function of itaconate, which was in part identified through work performed in this thesis, derives from its unsaturated dicarboxylic acid structure that makes it a mildly electrophilic alkylating agent when it accumulates to sufficient levels. Importantly, the alkylating potential of itaconate and its derivatives has important functional consequences during the inflammatory response (116). Specifically, it has been proposed that itaconate is

exported from mitochondria to the cytosol whereby it alkylates E3 ubiquitin ligase substrate adaptor, kelch-like ECH-associated protein 1 (KEAP1), and depletes intracellular GSH levels to drive the activation of the anti-inflammatory transcription factor Nrf2 (116). Evidence for KEAP1 targeting, the major Nrf2 repressor protein, comes primarily from the use of itaconate-derivatives, namely 4-octyl itaconate (4-OI), which has the same electrophilic properties of endogenous itaconate and has been shown to directly alkylate the key redox sensing cysteine, C151 (116). Importantly, mutation of C151 to serine (C151S) in KEAP1 impairs the ability of 4-OI to stabilise Nrf2 (116). In addition to Nrf2 regulation, GSH depletion by itaconate, and its more electrophilic derivatives, activates a novel NF-kB inhibitor zeta (Iκbζ)-ATF3 inflammatory axis that regulates IL-6 expression in LPS-tolerised macrophages and LPS-activated macrophages, respectively (127). Furthermore, several other targets of 2, 3-dicarboxypropylation were identified in a quantitative proteomic screen in LPS- and 4-OI-treated macrophages, including lactate dehydrogenase A (LDHA) (116). LDHA is an important regulator of aerobic glycolysis which suggests that this novel PTM may have far reaching consequences as an inflammatory signal during macrophage activation.

Itaconate accumulation has also been reported to increase itaconyl-CoA levels in macrophages. Intriguingly, two consequences of itaconyl-CoA accumulation are the inhibition of the mitochondrial B_{12}-dependent enzyme, methylmalonyl-CoA mutase (MUT) (134) and the abolition of substrate-level phosphorylation (SLP) (135). Inhibition of MUT by itaconyl-CoA results in B_{12} inactivation in LPS-activated macrophages and a reduction in circulating B_{12} levels in patients who present with the homozygous loss of the citramalyl-CoA ligase (CLYBL) (134).

However, the consequences of dysregulated B_{12} metabolism and indeed SLP inhibition with regard to macrophage activation and inflammation remains an open area of investigation. It is also tempting to speculate that increased itaconyl-CoA levels could result in the ‘itaconylation’ of protein lysine residues and thus act as an inflammatory signal akin to acetylation, malonylation and succinylation. Itaconate has also been shown to create an anti-viral metabolic niche in neurons infected with Zika virus (136). Whilst the exploration of itaconate signalling during macrophage activation (and indeed other inflammatory contexts) is still in its infancy, the profound levels to which it accumulates and the findings to date suggest it is a central regulator of macrophage metabolism and function.

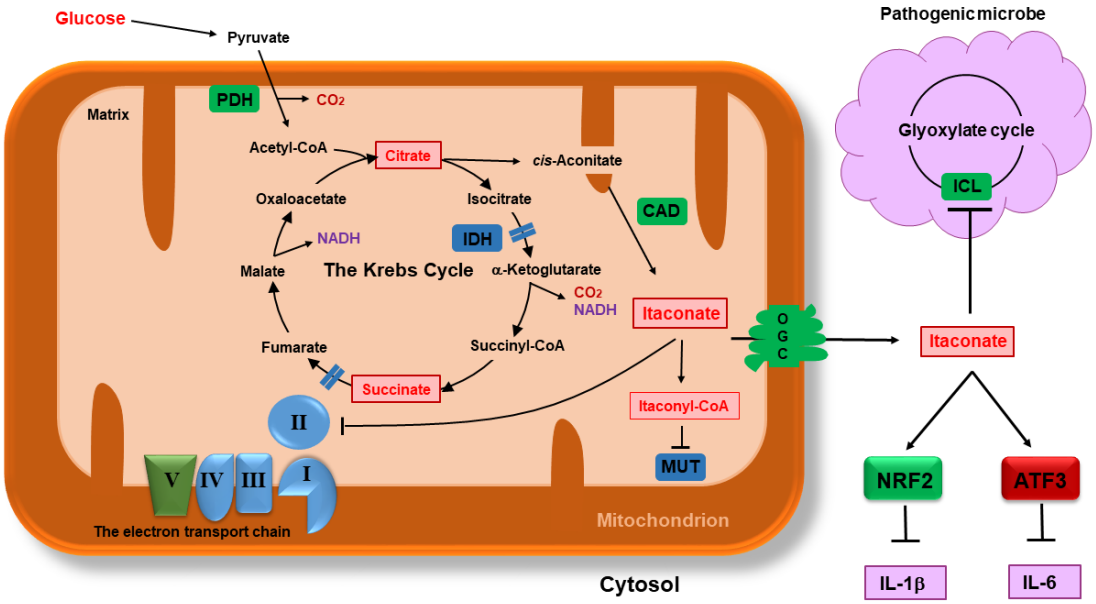

Figure 1.10 – Itaconate as an anti-microbial and anti-inflammatory metabolite

In the mitochondrial matrix, citrate can be converted to itaconate, via *cis*-aconitate by the enzyme immunoresponsive gene 1/*cis*-aconitate decarboxylase (IRG1/CAD). Increased itaconate levels result in the competitive inhibition of complex II, impaired succinate oxidation and a decrease in oxidative phosphorylation (OXPHOS). Increased itaconate also results in elevated itaconyl-CoA levels, which inhibits the vitamin B12-dependent enzyme, methylmalonyl-CoA mutase (MUT). Itaconate can also be exported from mitochondria by the oxoglutarate carrier (OGC), whereby it can stabilise the anti-oxidant and anti-inflammatory transcription factors Nrf2 and ATF3 to decrease the pro-inflammatory cytokines IL-1β and IL-6, respectively.

1.5 –The Nrf2 anti-oxidant defence system and inflammation

1.5.1 – Nrf2 discovery and structure

Nuclear factor-erythroid 2 p45-related factor 2 (Nrf2, also called Nfe2l2) is a key a focus of this project. It is a cap'n'collar (CNC) transcription factor that plays a major role in regulating cellular redox status and the expression of anti-oxidant proteins (137). Nrf2 was originally isolated as a homolog of the hematopoietic transcription factor NF-E2 p45 in 1994 with no known function (138). However, in 1997 it was identified as a *trans* regulator of *cis*-regulatory elements, designated anti-oxidant response elements (AREs), also referred to as electrophile response elements (EpREs), critical for the induction of phase II gene expression (139, 140). Specifically, Itoh *et al* (1997) observed a complete loss of the electrophile counterattack response and phase II gene expression in Nrf2-deficient mice challenged with the anti-oxidant 2 (3)-tert-butyl-4-hydroxyanisole (BHA) (140). It is now known that Nrf2 primarily functions as a guardian against cell intrinsic oxidative damage induced by ROS, environmental stressors, tissue injury and inflammation (137). Importantly, Nrf2 is widely and constitutively expressed in mouse and human tissues, including macrophages, and has a key role in limiting ROS-induced inflammation (137).

Nrf2 is composed of six functional domains Nrf2-ECH homology domain 1 (Neh1) to Neh6, identified by the phylogenetic comparison of Nrf2 across species (141). Neh1 contains the CNC and conserved basic region-leucine zipper (bZIP) motif that mediates DNA binding and heterodimerisation with small musculoaponeurotic fibrosarcoma (MAF) proteins (141). sMAF proteins are essential binding partners of the CNC family of transcription factors, including

Nrf2, and facilitate the efficient binding of Nrf2 to ARE motifs (140, 142). Neh3, Neh4 and Neh5 function as extremely important transactivation domains required for Nrf2s transcriptional activity (143, 144). Specifically, Neh4 and Neh5 work in concert to recruit the histone acetyl-transferase cAMP responsive element binding protein (CBP) and mediator complex (143, 144). Neh2 deletion markedly increases Nrf2 transcriptional activity, a key observation that led to the discovery of a unique de-repression mechanism governing Nrf2 activation, as detailed below. Finally, Neh6 is also an important domain regulating Nrf2 activity as it can be phosphorylated on a cluster of serine residues by glycogen synthase kinase 3 (GSK-3), which promotes Nrf2 degradation via β-transducin repeat-containing protein (βTrCP)-cullin-1 (Cul1)-mediated ubiquitination (145, 146).

1.5.2 – Nrf2 regulation by KEAP1 and the anti-oxidant response

Although Nrf2 had been identified as the primary transcription factor regulating the electrophile counterattack response in 1997, how it became activated in response to ROS and other intrinsic and extrinsic electrophiles remained a mystery. In 1999, Itoh and colleagues identified the thiol-rich protein KEAP1 as a novel interactor of Nrf2 using yeast two-hybrid screening (141). This was performed after an increase in Nrf2 transcriptional activity was observed in a truncated version of Nrf2 lacking the Neh2 domain (141). A highly important discovery that identified KEAP1 as a critical biosensor for electrophiles and ROS in mammalian cells.

The most important feature of Nrf2 is its inducible nature, which is created by its interaction with KEAP1 (Fig. 1.11). Under basal (unstressed) conditions, Nrf2 is negatively regulated KEAP1 located in the cytosol (141). KEAP1 itself is

a dimeric E3 ubiquitin ligase substrate adaptor that binds to high-affinity ETGE and low affinity DLG motifs in the Neh2 domain, a KEAP1-specific degron of Nrf2, both of which are required for Cullin (Cul)-3-RING (really interesting new gene)-box protein (Rbx)1 to ubiquitinate and target Nrf2 for degradation by the 26S proteasome (147-149). In contrast, the Neh6 domain of Nrf2 represents a KEAP1-independent degron of Nrf2 and is responsible for βTrCP-Cul1-dependent Nrf2 degradation in the nucleus (145).

Thus far, three domains have been identified in KEAP1, a broad complex-tramtrack-bric-a-brac (BTB) domain, an intervening region (IVR) and a double glycine repeat and COOH-terminal region (DC) domain (141). Structure-function and molecular dissection studies have shown that the DC domain of KEAP1 is responsible for the interaction of KEAP1 with both the ETGE and DLG motifs in the Neh2 domain of Nrf2 (148, 149). Furthermore, the stoichiometry of the interaction between Neh2 and KEAP1 is 1:2, highlighting the importance of KEAP1 homodimerisation (148). Indeed, an essential function of the BTB domain is to facilitate the homodimerisation of KEAP1 (150). Cul3 is also known to interact with a hydrophobic groove called the ‘3-box’ motif located between the BTB and IVR domains of KEAP1 (147, 151). As such, these interactions facilitate the formation of a CUL3-KEAP1-Nrf2 ternary complex permissive for Nrf2 ubiquitination. Live cell imaging has suggested that under basal conditions, the interaction between KEAP1 and Nrf2 follows a cycle whereby Nrf2 sequentially binds first one subunit of KEAP1 via its ETGE motif, to form an ‘open’ conformation, before the DLG motif is captured by the other Keap1 subunit to form the ‘closed’ conformation that enables Cul3–Rbx1 to ubiquitinate Nrf2 (152).

This subsequently allows free KEAP1 to be regenerated to bind newly synthesised Nrf2 (152).

Interestingly, KEAP1 is a thiol-rich protein containing many cysteine residues. Many KEAP1 cysteines are adjacent to the basic amino acids lysine and arginine creating an environment that promotes the reactive anionic form of the sulfhydryl group (153). Three major cysteine residues critical for the regulation of the ubiquitin E3 ligase activity of the KEAP1-CUL3 complex, and are covalently bound by electrophiles, have been identified (154). These three cysteines residues are cysteine 151 (C151), which is found in the BTB domain, and cysteine 273 (C273) and cysteine 288 (C288) found in the IVR domain (154). Upon initiation of oxidative stress, or when exposed to electrophilic agents, these critical cysteine residues in KEAP1 are oxidised or modified, preventing Cul3-Rbx1 assisted ubiquitination of Nrf2 (154). Modification of KEAP1 by electrophiles does not result in release of Nrf2, but rather blocks the Nrf2-KEAP1 cycle by causing conformational changes in KEAP1 (153). This ultimately leads to an uncoupling of the cycle. Consequently, free KEAP1 cannot be regenerated, and newly synthesized Nrf2 protein is therefore permitted to translocate directly to the nucleus. Following its modification, KEAP1 is targeted for degradation by the proteasome and autophagic degradation pathways (155, 156). Within the nucleus, Nrf2 forms heterodimers with sMAF proteins and binds to AREs upstream of several antioxidant genes, such as heme-oxygenase-1 (*Hmox1*) and NADPH:quinone oxidoreductase-1 (*Nqo1)*, thus inducing their expression (137).

In addition, Nrf2 is a crucial regulator of the master antioxidant, glutathione (GSH) and NADPH-regeneration enzymes. GSH is a tripeptide with a gamma peptide linkage between the carboxyl group of the glutamate side chain and

cysteine, while the carboxyl group of cysteine is attached by a normal peptide linkage to glycine (γ-glutamyl-cysteine-glycine) (137).GSH is a potent antioxidant, capable of acting as an electron donor, reducing disulphide bonds in cytoplasmic proteins. In return, GSH is oxidised to glutathione disulphide (GSSG) (137). Nrf2 induces expression of glutamate-cysteine ligase catalytic (*Gclc*) and glutamate-cysteine ligase modifier (*Gclm*), which form heterodimers catalysing the rate-limiting step of GSH synthesis (137). In addition to regulating GSH synthesis, Nrf2 is also capable of replenishing the GSH pool by inducing expression of glutathione reductase (*Gsr*), which converts GSSG to GSH, the ratio of which is crucial for maintaining the cellular redox state (137).

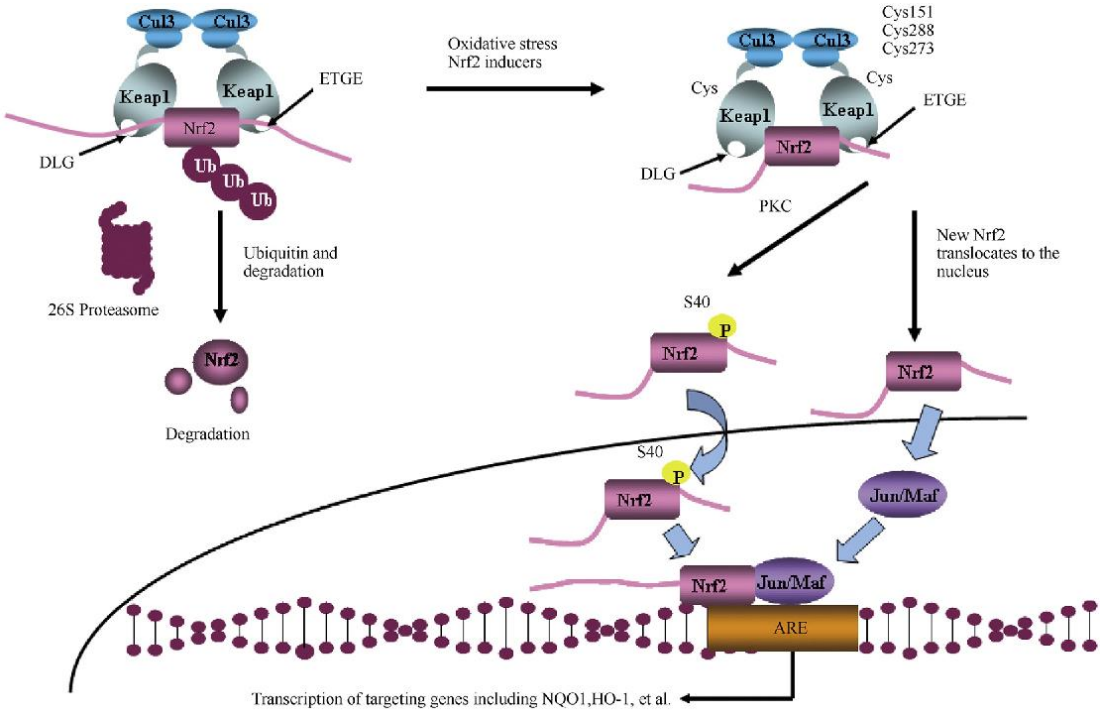

Figure 1.11 – Nrf2 regulation by KEAP1 (157)

Under homeostatic conditions, Nrf2 is polyubiquitinated by the Cul3-Rbx1-KEAP1 ternary complex and continually targeted for degradation by the 26S proteasome. In response to oxidative stress or Nrf2 inducers, key redox sensing cysteines are modified on KEAP1, which enables newly synthesised Nrf2 to translocate to the nucleus, dimerise with sMafs and bind AREs to induce anti-oxidant gene expression programmes.

1.5.3 – Nrf2 and inflammation

In addition to its role an anti-oxidant transcription factor, Nrf2 has also been found to act as a critical negative regulator of inflammation (137, 158, 159). Importantly, disruption of Nrf2 dramatically increased the mortality of mice in response to endotoxin- and caecal ligation and puncture-induced septic shock (158). LPS stimulus resulted in greater lung inflammation in Nrf2-deficient mice, whilst temporal analysis of pulmonary global gene expression after LPS challenge revealed augmented expression of large numbers of pro-inflammatory genes associated with the innate immune response, indicating severe immune dysregulation (158). In addition, Nrf2 has previously been linked to regulation of both IL-1β and IL-6, independent of its role as an anti-oxidant mediator (159). Nrf2 was found to bind to specific, non-antioxidant response elements, in the promoters of these cytokines, thus inhibiting RNA Polymerase II recruitment. Diethyl maleate (DEM), an Nrf2 activator, but not NAC, was able to decrease levels of *Il1b* and *Il6* transcription, demonstrating that this effect was outside of ROS regulation (159). However, this study was carried out after acute LPS activation of macrophages, at which ROS regulation is less critical. In later stages of macrophage activation, ROS levels accumulate, leading to a stabilization of HIF1α to drive IL-1β production (62, 160). It is likely that at later time points following LPS stimulation that both the anti-oxidant effect of Nrf2 and direct binding to the *Il1b* promoter regulate IL-1β production. Finally, several Nrf2 activators have been shown to have therapeutic efficacy in limiting inflammation in several inflammatory disorders, suggesting activation of Nrf2 may present a promising therapeutic approach in the treatment of inflammatory diseases (137, 161-164).

1.6 – Aims

The overall aim of this project is to further decipher the role of metabolic reprogramming and cell-intrinsic Krebs cycle-derived metabolite accumulation in governing pro-inflammatory cytokine production in LPS-activated macrophages. The specific aims are:

I. To determine the role of increased fumarate levels in macrophages
    a) What metabolic pathway(s) governs fumarate accumulation?
    b) Can this pathway(s) and fumarate act as immunomodulators to regulate cytokine levels?
    c) If so, by what mechanism?

II. To determine the role of IRG1 induction and itaconate production in macrophages
    a) What effect does itaconate have on macrophage metabolism?
    b) Can itaconate act as an immunomodulator and regulate cytokine levels?
    c) If so, by what mechanism?

A greater understanding of metabolic events arising from Krebs cycle rewiring could unearth novel biochemical signalling mechanisms that dictate cytokine status, thus opening-up the possibility of identifying new therapeutic targets for the treatment of inflammatory diseases.

Chapter 2:

Materials and Methods

2.1 – Materials

2.1.1 – General Buffers

Table 2.1 – Composition of most frequently used buffers in this study

Buffer Name	Buffer Composition
PBS (10X)	1.45 M NaCl, 39 mM NaH_2PO_4, 22.7 mM Na_2HPO_4
Sample Lysis Buffer (5X)	10% (w/v) glycerol, 2% (w/v) sodium dodecyl sulphate (SDS), 215 mM Tris pH 6.8, 200 µg/mL bromophenol blue. 50 µL of 1 M dithiothreitol (DTT) is added to 950 µL 5X sample buffer immediately before use.
SDS-PAGE Running Buffer (10X)	144 g 192 mM glycine, 30.3 g 25 mM Tris, 10 g 0.1% SDS. Diluted to 1 L with dH2O.
SDS-PAGE Transfer Buffer (10X)	1.9 M glycine, 35 mM SDS, 0.25 M Trizma base
Tris-buffered saline (TBS) Tween (TBST) (10X)	87.6 g NaCl, 10 mL Tween-20, 12.11 g Tris. Diluted to 1 L with dH_2O.
Low Stringency Lysis Buffer (500mL)	50mM HEPES, 100mM NaCl, 1 mM EDTA, 10% glycerol, 1% NP-40. pH to 7.5.
ELISA Wash Buffer	0.05% Tween in PBS, pH 7.2-7.4

Standard suppliers Sigma Aldrich or Fisher Scientific were used to obtain all other general laboratory chemicals unless otherwise stated.

2.1.2 – Cell culture media

DMEM (Dulbecco's Modified Eagle Medium) and Opti-MEM I reduced serum media were obtained from Gibco Biosciences. Foetal calf serum (FCS) was obtained from Biosera. Penicillin/Streptomycin (P/S) and Trypsin-ethylenediaminetetraacetic acid (EDTA) were sourced from Sigma Aldrich. DMEM (10% FCS, 1% P/S) was used for all *in vitro* experiments unless otherwise

stated. DMEM high glucose, no glutamine (11960044) and DMEM no glucose (11966025) were from Thermo Fisher Scientific.

2.1.3 – Cell types

The HEK293T cell line was from Invivogen. L929 cells were obtained from Sigma. COS1 cells were provided by Professor Albena T. Dinkova-Kostova (University of Dundee, UK). Bone-marrow-derived macrophages (BMDMs) were differentiated from murine bone marrow.

2.1.4 – Mouse strains

C57BL/6 mice obtained from Harlan UK were maintained under pathogen-free conditions in line with Irish and European Union regulations. Use of animals received ethical approval by the universities' ethics committees in accordance with the personal licence approved by the HPRA. Tamoxifen-CRE inducible *Fh* +/+, *Fh* +/- and *Fh* -/- mice were generated on the C57BL/6 genetic background and their hind legs were generously donated by Dr. Christian Frezza (University of Cambridge, UK). Hind legs from *Nrf2* +/+ and *Nrf2* -/- mice, both on the C57BL/6 genetic background, were generously donated by Professor Albena T. Dinkova-Kostova (University of Dundee, UK). Transgenic mice (Stock No: 029340) strain C57BL/6N-Acod1em1(IMPC)J/J and Wildtype controls C57BL/6NJ (Stock No. 005304) were obtained from The Jackson Laboratories.

2.1.5 – Reagents

LPS used in *in vitro* studies was from *Escherichia coli*, serotype EH100 (Alexis). Dimethyl malonate (DMM), dimethyl itaconate (DMI), dimethyl fumarate (DMF), monomethyl fumarate (MMF), aminooxyacetic acid (AOAA) and 4-hydroxytamoxifen and itaconic acid were from Sigma-Aldrich. 4-octyl itaconate

(4-OI), methyl-itaconate (4-MI), 4-octyl succinate (4-OS) and 4-octyl-2-methylsucinnate (4-OMS) were synthesised by Dr Stuart Caldwell and Professor Richard Hartley (University of Glasgow, UK). [U-13C] glucose (CLM-1822-SP_PK) and [U-13C] glutamine CLM-1396-MPT-PK were from Cambridge Isotope Laboratories.

Antibodies used were goat anti-mouse IL-1β (R&D Systems, AF401-NA), mouse anti-β-actin (Sigma-Aldrich, AC-74), rabbit anti-HIF-1α (D22U3T) (Cell Signalling Technology, 14179), rabbit anti-TNF (D2D4) XP® (Cell Signalling Technology, 11948) rabbit anti-Fumarase (D9C5) (Cell Signalling Technology, 4567), rabbit anti-Nrf2 (D179C) XP® (Cell Signalling Technology, 12721), rabbit anti-Hmox1 (P249) (Cell Signalling Technology, 5061) mouse, rabbit anti-IRG1 (Abcam, ab222411), rabbit anti-FLAG® (Sigma, F7425) and rabbit anti-2SC antibody was kindly provided by Dr. Norma Frizzell (University of South Carolina, US). Secondary horseradish peroxidase (HRP)-conjugated anti-mouse IgG, anti-rabbit IgG and anti-goat IgG were from Jackson ImmunoResearch Inc.

RNAimax and siRNAs were from Thermo Fisher Scientific, Nrf2 (Catalogue Number: 4390771, Assay ID: s70521 and s70522) and scrambled control (Catalogue Number: 4390843). MYC-DDK-tagged KEAP1 (Catalogue number: MR225865) was from Origene. GeneJuice was purchased from Novogen. Plasmid purification maxiprep kits were purchased from Qiagen. TNF, IL-6 and IL-10 ELISA Duoset kits were purchased from R&D Systems. Reverse transcription reagents were from Applied Biosystems (High capacity cDNA reverse transcription kit). The anchored oligo(dT) primer (TTTTTTTTTTTTTTTTTVN) was synthesised by Eurofins Genomics.

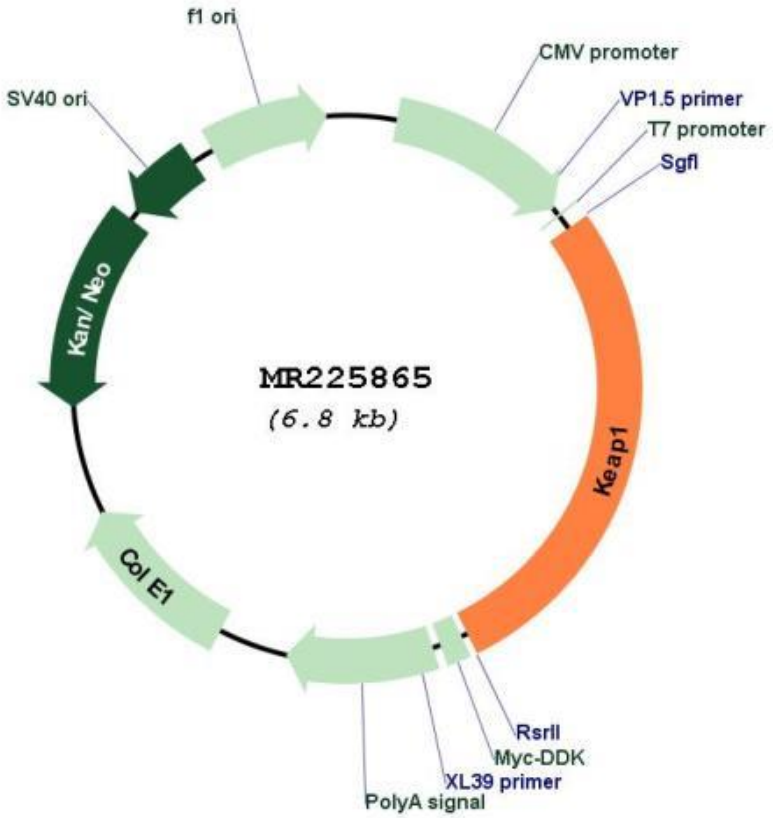

Figure 2.1 – MYC-DDK-tagged KEAP1 plasmid map

2.2 – Methods

2.2.1 – Cell culture

For optimal growth, all cell types were incubated in a humidified atmosphere at 37ºC with 5% CO_2. BMDMs, HEK293Ts and L929s were cultured in complete DMEM supplemented with 10% FCS and 1% P/S (v/v). HEK293Ts were removed from the T175 flask by incubation with 5 mL 1X trypsin-EDTA at 37ºC with 5% CO_2, and sub cultured 1:15-1:30 every 2-3 days. Cells were centrifuged at 1500 rpm for 5 mins before resuspending the pellet in fresh media. Cell viability and cell number were assessed using Trypan Blue dye, a haemocytometer and a bright light microscope before being plated for experiments. HEK293Ts were plated at 1 x 10^6 cells/mL in 10 cm dishes.

2.2.2 – Cell cryopreservation

To maintain stocks of HEK293T and L929 cell lines, cells were grown to ~70-80% confluency in T175 flasks and harvested as previously described. Cells were centrifuged at 1500 rpm for 5 mins and resuspended in 90% FCS and 10% dimethyl sulfoxide (DMSO) before being placed into 1.5 mL cryovials. Each cryovial was placed into a cryo-freezing container containing isopropanol at -80°C overnight before being transferred to liquid nitrogen for long-term storage.

2.2.3 – Generation of BMDMs

Mice were bred and maintained in WEHI animal facilities. Female mice were euthanized in a CO_2 chamber and death was confirmed by cervical dislocation. Bone marrow was then extracted from the from the femur, tibia and hip bones. Red blood cells were lysed using red blood cell lysis buffer (hypotonic solution). The remaining monocytic cell population was differentiated in complete DMEM

(containing 10% FCS, 1% P/S and 20% L929 supernatant) for 6-7 days at 37°C with 5% CO_2. After 6-7 days, the BMDM population was scraped, counted and re-plated for experiments. Unless otherwise stated, BMDMs were plated at 0.5 x 10^6 cells/mL in 12-well plates for *in vitro* experiments.

2.2.4 – Synthesis of octyl esters

Designed and performed by Dr Stuart Caldwell and Prof. Richard Hartley (University of Glasgow, UK) for this project.

4-octyl itaconate (4-OI)

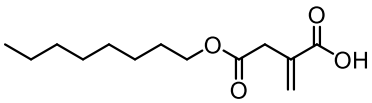

Itaconate anhydride (1.00 g, 8.92 mmol, 1.0 eq) and 1-octanol (1.22 g, 9.36 mmol, 1.05 eq) were heated to 110°C for 4h. After cooling to room temperature (RT) the solution was poured slowly into hexane (30 ml) and the resulting solid filtered off and washed with cold hexane (20 ml). The solid was recrystallised twice from hexane to give the acid as fine white needles (726 mg, 33%).

δ_H (400 MHz: $CDCl_3$): 0.88 (3H, t, *J* = 7.0 Hz, CH_3), 1.22-1.36 (10H, m, 5×CH_2), 1.69-1.56 (2H, m, OCH_2CH_2), 3.34 (2H, s, CH_2CO_2), 4.10 (2H, t, *J* = 6.7 Hz, OCH_2), 5.83 (1H, d, *J* = 0.8 Hz, C=CH_AH_B), 6.46 (1H, broad s, C=CH_AH_B), 11.68 (1H, broad s, OH).

δ_C (100 MHz: $CDCl_3$): 14.22 (CH_3), 22.78 (CH_2), 25.98 (CH_2), 28.66 (CH_2), 29.30 (CH_2), 29.32 (CH_2), 31.92 (CH_2), 37.47 (CH_2), 65.39 (CH_2), 130.79 (CH_2), 133.51 (C), 170.73 (C), 171.66 (C).

m/z (ESI): Found: 265.1410. $C_{13}H_{22}NaO_4$ requires $(M+Na)^+$, 265.1410.

ν_{max}(ATR)/cm^{-1}: 2918 (CH), 1722 (C=O of ester), 1683 (C=O of carboxylic acid), 1633 (C=C),

Regioisomer confirmed by NOE experiments. ^{1}H NMR data agree with literature (165).

4-octyl succinate (4-OS)

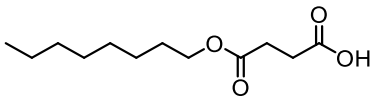

Succinic anhydride (1.40 g, 14.0 mmol, 1.0 eq) and 1-octanol (2.00 g, 15.4 mmol, 1.10 eq) were heated to 110 °C for 4h. After cooling to RT the solution was poured slowly into hexane (30 ml) then placed in an ice bath for 1h. The resulting solid was filtered off and washed with cold hexane (20 ml) to give the acid as fine white needles (2.02 g, 63%).

M.p. 36-38 °C.

δ_H (400 MHz: $CDCl_3$): 0.87 (3H, t, *J* = 6.7 Hz, CH_3), 1.26-1.34 (10H, m, 5×CH_2), 1.61 (2H, apparent quin, *J* = 6.8 Hz, OCH_2CH_2), 2.59-2.63 (2H, m, CH_2CH_2), 2.66-2.69 (2H, m, CH_2CH_2), 4.08 (2H, t, *J* = 6.7 Hz, OCH_2), 10.78 (1H, broad s, OH).

δ_C (100 MHz: $CDCl_3$): 14.21 (CH_3), 22.76 (CH_2), 25.99 (CH_2), 28.67 (CH_2), 29.01 (CH_2), 29.12 (CH_2), 29.29 (CH_2), 29.32 (CH_2), 31.90 (CH_2), 65.21 (CH_2), 172.35 (C), 178.55 (C).

m/z (ESI): Found: 253.1404. $C_{12}H_{22}NaO_4$ requires $(M+Na)^+$, 253.1410.

ν_{max}(ATR)/cm^{-1}: 2918 (CH), 1724 (CO_2R), 1705 (CO_2H).

^{1}H NMR data agree with literature (165).

4-octyl 2--methylsuccinate (4-OMS)

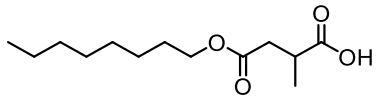

Palladium on carbon (5% Pd loading) (50 mg) was added to a solution of 4-octyl itaconate (500 mg, 2.06 mmol) in EtOAc (5 ml). The suspension was then stirred under an atmosphere of hydrogen (balloon) for 4 h. After this time the suspension was filtered through a plug of silica, which was then washed with EtOAc (20 ml). The combined organics were concentrated under vacuum to give the acid as colourless viscous oil (495 mg, 98%).

δ_H (400 MHz: $CDCl_3$): 0.85 (3H, t, *J* = 6.7 Hz, CH_3), 1.20-1.34 (13H, m, 5×CH_2 and C*H*$_3$CH), 1.58 (2H, apparent quin, *J* = 6.8 Hz, OCH_2*CH*$_2$), 2.39 (1H, dd, *J* = 16.6, 6.1 Hz, C*H*$_A$H$_B$), 2.71 (1H, dd, *J* = 16.6, 7.9 Hz, CH_A*H*$_B$), 2.92 (1H, m, CH), 4.05 (2H, t, *J* = 6.7 Hz, OCH_2), 11.15 (1H, broad s, OH).

δ_C (100 MHz: $CDCl_3$): 14.15 (CH_3), 16.86 (CH_3), 22.71 (CH_2), 25.95 (CH_2), 28.62 (CH_2), 29.24 (CH_2), 29.26 (CH_2), 31.86 (CH_2), 35.80 (CH), 37.45 (CH_2), 65.02 (CH_2), 171.91 (C), 181.68 (C).

m/z (ESI): Found: 267.1555. $C_{13}H_{24}NaO_4$ requires $(M+Na)^+$, 267.1567.

ν_{max}(ATR)/cm^{-1}: 2926 (CH), 1735 (CO_2R), 1705 (CO_2H).

Single product: the regioisomer unambiguous because it is derived from the 4-octyl ester of itaconate.

2.2.5 – Enzyme-linked immunosorbent assay (ELISA)

Cytokine concentrations in cell supernatants were measured using ELISA Duoset kits for mouse IL-10, IL-6 and TNF, according to the manufacturer's instructions. Optical density values were measured at a wavelength of 450 nm, using a FLUOstar Optima plate reader (BMG Labtech). Concentrations were calculated using a standard curve.

2.2.6 – Western blot

Protein samples from cultured cells were prepared by direct lysis of cells in 5X Laemmli sample buffer, followed by heating at 95°C for 5 min. Protein samples were resolved on 10 or 12% sodium dodecyl sulphate-polyacrylamide gel electrophoresis (SDS-PAGE) gels (Table 2.2) using a Bio-Rad Mini Protean III electrophoresis system. Samples were resolved alongside a pre-stained protein marker range (Spectra^{TM}, Thermo Fisher Scientific) for approximately 2-3 hours at 60V. Resolved proteins were then transferred onto a polyvinylidene difluoride (PVDF) or nitrocellulose membrane using a Bio-Rad wet transfer system at 40 mA overnight. Membranes were blocked in 5% (w/v) dried milk in TBST for 1 h at RT. Membranes were incubated with primary antibody (1:1000 - 1:10000) in 5% (w/v) milk or bovine serum albumin (BSA) in 1X TBST at 4^{o}C overnight or for 2 h at RT. Membranes were then washed 3 x 5 mins in 1X TBST, followed by incubation with the appropriate HRP-conjugated secondary antibody (1:2000) in 5% (w/v) milk in 1X TBST for 1 h at RT. The blots were then developed using enhanced chemiluminescent (ECL) substrate (Merck). Bands were visualized using the GelDoc system (Bio-Rad).

Table 2.2 – Composition of SDS-PAGE gels

Resolving gel	**10% (mL)**	**12% (mL)**	**Stacking gel**	**5% (mL)**
Sterile H_20	4	3.3	Sterile H_20	6.8
30% acrylamide mix	3.3	4	30% acrylamide mix	1.7
1.5 M Tris (pH 8.8)	2.5	2.5	1.0 M Tris (pH 6.8)	1.25
10% SDS	0.1	0.1	10% SDS	0.1
10% ammonium persulfate	0.1	0.1	10% ammonium persulfate	0.1
N,N,N,N-tetramethylethylenediamine (TEMED)	0.004	0.004	N,N,N,N-tetramethylethylenediamine (TEMED)	0.01

2.2.7 – Plasmid DNA preparation

Plasmid DNA was transformed into competent *E. coli* DH5α strain. 50ng of DNA was transformed into 20μL DH5α in a microcentrifuge tube and incubated on ice for 30 mins. Cells were then heat shocked at 42°C for 45 secs before immediately placing back on ice for 2 mins to allow for DH5α recovery. Cells were resuspended in 200μL S.O.C medium and plated on ampicillin agar plates. Agar plates were incubated at 37°C overnight.

After transformation on agar plates, a single colony was selected using a sterile micropipette tip and added to 5mL lysogeny broth (LB) medium without antibiotics for 4-6 h at 37°C and 250 rpm shaking. 100μL of this starter culture was transferred into 100mL of pre-warmed LB broth containing ampicillin and left shaking at 250 rpm overnight at 37°C. The bacterial cell culture was harvested the next day by centrifugation at 4000 rpm for 30 min at 4°C. LB broth was

removed, and cell pellets were used to extract plasmid DNA using a maxiprep kit according to the manufacturer's instructions, or frozen for future extraction.

2.2.8 – Transfection

Plasmid transfection of HEK293Ts was performed with GeneJuice (Novogen) according to manufacturer's instructions. Briefly, DNA and GeneJuice (3 μL per μg of DNA) were combined in Opti-MEM (250 μL per μg of DNA), incubated for 15 mins at RT and added dropwise to cells.

For siRNA transfection of BMDMs, cells were plated at 0.5 x 10^6 cells/ml in 12 well plates overnight and transfected using RNAimax the following day, as per the manufacturer's instructions. Briefly, on the day of transfection, the media was replaced with 500 µL DMEM without FCS or P/S. Two Eppendorfs/siRNA were prepared. Opti-MEM (250 µL/well) was added to each tube. RNAimax (add 5 µL/well) was added to one set of tubes and siRNA (50 nM/well) was added to the second set of tubes. The tubes containing the siRNA was added to the tube with RNAimax, mixed well by pipetting and incubated for 15 min. The mix (500 µL) was added to each well. 24 h post transfection cells were treated as required.

2.2.9 – KEAP1 Immunoprecipitation assay and liquid chromatography-mass spectrometry (LC-MS) analysis

HEK293Ts were transfected with a pCMV6-Keap1 vector (Myc-DDK-tagged mouse KEAP1) as previously described. 24 h post-transfection, cells were treated with OI (500 µM) or vehicle control (PBS) for 4 h. The cells were lysed in low stringency lysis buffer and vortexed at 1500 rpm for 15 mins at 4°C in a thermomixer. This was followed by centrifugation at 4°C at max rpm for 10 min. Tagged-Keap1 was then immunoprecipitated using an anti-FLAG™ antibody

(Sigma) and protein A/G beads (Santa Cruz). After immunoprecipitation, bound KEAP1 was eluted off the beads using FLAG™ peptide (500 µl; 200 µg/ml) (Sigma) diluted in 1X TBS pH 7.4. The samples were then concentrated, and the FLAG peptide removed using 10K centrifugation filter columns (Merck). The concentrated samples were then divided in half for downstream processing. One half of each sample was diluted 1 in 2 with 5X SDS sample buffer and separated using SDS-PAGE (Bio-Rad) as previously described.

Overexpressed KEAP1 was detected using Coomassie blue staining and the corresponding bands were excised from the gel and subjected to in-gel digest. Briefly, the gel slices were cut into smaller pieces (1-2 mm^3) prior to reduction with DTT (10 mM) and alkylation with IAA (50 mM). Half of the gel slices from each sample were then subjected to a trypsin (2 µg) digest, the other half were digested with elastase (1 µg) overnight at 37°C. Similarly, the remaining sample concentrates (in solution) were reduced with DTT and alkylated with IAA, prior to precipitation of the protein via the methanol-chloroform extraction method. The protein pellet was re-suspended in urea (6 M), which was then diluted to <1 M urea with ultrapure H_2O. The samples were then digested with trypsin (2 µg) overnight at 37°C.

Digested protein samples were analysed in an Orbitrap Fusion Lumos coupled to a UPLC ultimate 3000 RSLCnano System (both Thermo Fisher Scientific) by Dr. Roman Fischer in the lab of Professor Benedikt Kessler (University of Oxford, UK). The samples were loaded in 1% CH_3CN 0.1% TFA buffer and eluted using a gradient of 2 to 35% CH_3CN with 0.1% formic acid and 5% DMSO in 60 min at a flow rate of 250 nL/min. The survey scan was acquired within a 400-1500 m/z window at a resolution of 120.000 and AGC target of 4e5.

Precursor ions were fragmented by CID at 35% normalized collision energy after isolation in the quadrupole with a mass isolation window of 1.6Th. MS/MS data was acquired with an AGC target set to 4e3 in rapid mode for up to 300 mLs using full parallelization. The duty cycle time was fixed to 3 s and selected precursors were dynamically excluded for 7 secs.

MS data was analysed with PEAKS Studio 8 (Bioinformatics Solutions). Precursor mass tolerance was set to 10 ppm, while fragments were detected with a tolerance of 0.5 Da. We used Elastase cleavage specificity as previously reported (166). Oxidation (M), Deamidation (N, Q), Carbamidomethylation (C), modification of a cysteine by 4-octyl-Itaconate (C) and S-(2-monomethylsuccination) (C) were defined as variable modifications. The database used was the reviewed human proteome retrieved from UniProt on the 14/07/2017. Peptide FDR was set to 1%.

2.2.10 – KEAP1 cysteine target validation

COS1 cells (2.5 x 10^5 per well) in 6-well plates were co-transfected (Lipofectamine 2000) with 0.8 µg of V5-Nrf2 and 1.6 µg of wild-type or Cys151S mutant Keap1 14, or 1.6 µg of pcDNA. Cells were grown for 21 h prior to a 3 h treatment with 20 or 100 µM OI, 5 µM sulforaphane (SFN) or 0.1% acetonitrile (ACN, vehicle). Cell were washed in PBS and lysed in 200 µl of SDS-lysis buffer [50 mM Tris-HCl pH 6.8, 2% (w/v) SDS and 10% (v/v) Glycerol]. After sonication of the lysates (20 sec at 30% amplitude using Vibra-Cell ultrasonic processor, Sonic) and boiling of the samples (100°C for 3 min), DTT and Bromophenol blue were added up to 0.1M and 0.02% (w/v) final concentrations, respectively. Proteins (10 µg) were resolved on a gradient (4-12%) NuPAGE SDS gel, transferred onto nitrocellulose membranes, and immunoblotted with anti-Keap1

(rat monoclonal, Merk Millipore, clone 144), anti-Nrf2 (rabbit monoclonal, CST), and anti-β-actin (mouse monoclonal, Sigma) antibodies. HRP- or IRDye-labelled secondary antibodies were used interchangeably, followed by either ECL-detection or scanning using Odyssey imager (Li-COR).

2.2.11 – Assessment of cysteine alkylation by itaconate using iodoTMT

Following treatment cells were lysed in HEPES pH 7.5, EDTA, glycerol and NP40. 2 mM TCEP and 50 mM NEM were added in a buffer containing 50 mM HEPES, 2 % SDS, 125 mM NaCl, pH 7.2 and samples were incubated for 60 min at 37 °C in the dark to reduce and alkylate all unmodified protein cysteine residues. 20 % (v/v) TCA was added to stabilize thiols and incubated overnight at 4°C and then pelleted for 10 mins at 4000 g at 4 °C. The pellet was washed with 3 times with cold methanol (2 mL) and then resuspended in 2 mL 8 M urea containing 50 mM HEPES (pH 8.5). Protein concentrations were measured by BCA assay (Thermo Fisher Scientific) prior to protease digestion. Protein lysates were diluted to 4 M urea and digested with LysC (Wako, Japan) in a 1:100 enzyme/protein ratio and trypsin (Promega) at a final 1/200 enzyme/protein ratio for 4 hours at 37 °C. Protein extracts were diluted further to a 2.0 M urea and LysC (Wako, Japan) at 1/100 enzyme/protein ratio and trypsin (Promega) at a final 1/200 enzyme/protein ratio were added again and incubated overnight at 37 °C. Protein extracts were diluted further to a 1.0 M urea concentration, and trypsin (Promega) was added to a final 1/200 enzyme/protein ratio for 6 hours at 37 °C. Digests were acidified with 250 µL of 25% acetic acid to a pH ~2, and subjected to C18 solid-phase extraction (50 mg Sep-Pak, Waters). 6-7 M excess TMT label was added to each digest for 30 min at room temperature (repeated twice). The

reaction was quenched using 4 μL of 5% hydroxylamine. Samples were subjected to an additional C18 solid-phase extraction (50 mg Sep-Pak, Waters).

2.2.12 – LC-MS/MS parameters

Data was collected by Dr. Mark Jedrychowski (Harvard university, US) using an Orbitrap Fusion Lumos mass spectrometer (Thermo Fisher Scientific, San Jose, CA, USA) coupled with a Proxeon EASY-nLC 1200 LC pump (Thermo Fisher Scientific). Peptides were separated on a 100 μm inner diameter microcapillary column packed with 45 cm of Accucore C18 resin (2.6μm, 100 Å, Thermo Scientific Fisher). Peptides were separated using a 3 h gradient of 6–22 % acetonitrile in 0.125% formic acid with a flow rate of ~400 nL/min. Each analysis used an MS^3-based TMT method as described previously [100]. The data were acquired using a mass range of *m/z* 400 – 14000, resolution 120,000, AGC target 1×10^6, maximum injection time 100 ms, dynamic exclusion of 120 seconds for the peptide measurements in the Orbitrap. Data dependent MS^2 spectra were acquired in the ion trap with a normalized collision energy (NCE) set at 35%, AGC target set to 1.8×10^4 and a maximum injection time of 120 ms. MS^3 scans were acquired in the Orbitrap with a HCD collision energy set to 55%, AGC target set to 1.5×10^5, maximum injection time of 150 ms, resolution at 50,000 and with a maximum synchronous precursor selection (SPS) precursors set to 10.

2.2.13 – Data processing and MS2 spectra assignment

A compendium of in-house software was used to convert .raw files to mzXML format, as well as to adjust monoisotopic m/z measurements and correct erroneous peptide charge state assignments. Assignment of MS^2 spectra was performed using the SEQUEST algorithm (167). All experiments utilized the

Mouse UniProt database (downloaded 4/ 2016) where reversed protein sequences and known contaminants such as human keratins and bovine albumin were appended. SEQUEST searches were performed using a 20 ppm precursor ion tolerance, while requiring each peptide's N/C terminus to have trypsin protease specificity and allowing up to two missed cleavages. TMT tags on peptide N termini/lysine residues (+229.162932 Da) and cysteine (+ 125.047679 Da) were set as static modifications while methionine oxidation (+15.99492 Da) and cysteine alkylation (+4.978931 Da) was set as variable modifications.

2.2.14 – TMT reporter ion intensities and quantitative data analysis

For quantification, a 0.003 m/z window centered on the theoretical m/z value of each reporter ion was utilized for the nearest signal intensity. Reporter ion intensities were adjusted to correct for the isotopic impurities from the different TMT reagents as per manufacturer specifications. The signal to noise values for all peptides were summed within each TMT channel. For each peptide, a total minimum sum signal to noise value of 150 and an MS^1 and MS^2 isolation specificity of greater than 70% was required.

2.2.15 – Metabolomics analysis

Cells were treated as desired. For tracing studies, immediately prior to LPS stimulation the media was removed and replaced with DMEM media (1 ml) containing U-^{13}C-glucose (4.5 g/L) or U-^{13}C-glutamine (584 mg/mL) deplete of ^{12}C- glucose or ^{12}C-glutamine.

Cells were washed three times with ice-cold PBS, with all the PBS being removed after the last wash. Extraction solution (methanol/acetonitrile/water, 50:30:20 v/v/v) was added (1 mL per 1 x 10^6 cells) and samples were incubated

for 15 mins on dry-ice. The resultant suspension was transferred to ice-cold microcentrifuge tubes. Samples were agitated for 15 min at 4°C in a thermomixer and then incubated at -20°C for 1 h. Samples were centrifuged at maximum speed for 10 min at 4°C. The supernatant was transferred into a new tube and centrifuged again at maximum speed for 10 min at 4°C. The supernatant was transferred to autosampler vials and stored at −80°C prior to analysis by LC-MS.

LC-MS analysis was performed using a Q Exactive mass spectrometer coupled to a Dionex U3000 UHPLC system (Thermo) by Dr Sofia Costa and Efterpi Nikitopoulou in the lab of Dr. Christian Frezza (University of Cambridge, UK). The liquid chromatography system was fitted with a Sequant ZIC-pHILIC column (150 mm × 2.1 mm) and guard column (20 mm × 2.1 mm), both from Merck Millipore (Germany) and temperature maintained at 45°C. The mobile phase was composed of 20 mM ammonium carbonate with 0.1% ammonium hydroxide, and acetonitrile. The flow rate was set at 200 µL/min with the gradient described by Mackay and colleagues (2015) (168). The mass spectrometer was operated in full MS and polarity switching mode. Samples were randomised to avoid bias due to machine drift and processed blindly. The acquired spectra were analysed using XCalibur Qual Browser and XCalibur Quan Browser software (Thermo Scientific). Absolute quantification of selected metabolites was performed by interpolation of the corresponding standard curve obtained from serial dilutions of commercially available standards (Sigma Aldrich) running with the same batch of samples. Data was then further analysed using MetaboAnalyst 4.0 software.

2.2.16 – Assessing itaconate ester reactivity with glutathione

1- or 5-mM reduced glutathione and 5 mM itaconate esters or vehicle control were incubated in KCl buffer (pH 7.2 or 8) at 37°C for 2 h. The reaction was stopped by acidification with 5 % sulfosalicylic acid prior to assessing glutathione content by GSH recycling assay as described previously (169).

2.2.17 – Itaconate transport assays

Itaconate transport by mitochondrial carriers was assessed as described previously (170). Briefly, empty, *H. sapiens* citrate carrier (HsCTP), H. sapiens 2-oxoglutarate carrier (HsOGC), *H. sapiens* oxodicarboxylate carrier (HsODC), *S. cerevisiae* dicarboxylate carrier (ScDIC), *H. sapiens* ADP/ATP carrier (HsAAC1) and *S. cerevisiae* ADP/ATP carrier (ScAAC2) plasmid containing *L. lactis* pre-cultures were grown in M17 media containing 1% glucose (w/v) and 5 µg/ml chloramphenicol at 30°C before recombinant protein induction with 1:10,000 nisin A for a further 2 hours. Cells were disrupted (33,000 psi) in ice-cold PIPES buffer (pH 7), cell debris pelleted (10,800 x g, 20 min, 4°C) and supernatant ultracentrifuged to pellet membranes (138,000 x g, 1 h, 4°C).

To make membrane vesicle fusions, 1 mg lactis membranes was mixed with 5 mg liposomes (E. coli polar lipid and egg yolk phosphatidylcholine in a 3:1 ratio; Avanti Polar Lipids), diluted to a final volume of 900 µl with PIPES, and fused by six cycles of freezing in liquid nitrogen and thawing at room temperature before storage in liquid nitrogen. For HsAAC1, 3 mg lactis membranes were mixed with 3 mg liposomes and diluted to a final volume of 900 µl with PIPES. The membrane vesicle fusions were thawed, and 100 µl of 50 mM substrate was added (as indicated in the figures). Fused membranes were extruded 11 times

through a 1-µm polycarbonate filter, passed through a pre-equilibrated PD10 desalting column (GE Healthcare) to remove external substrate, and collected in 1.6 ml PIPES buffer.

Transport assays were carried out using a Hamilton MicroLab Star robot (Hamilton Robotics Ltd). Transport of [14C]-labeled malate (HsCTP, HsOGC and ScDIC), [14C]-labeled ADP (ScAAC2 and HsAAC1) and [14C]-labeled α-ketoglutarate (HsODC) (all from Perkin Elmer), and [3H]-labeled itaconate (American Radiolabeled Chemicals) was initiated by the addition of 100 µL PIPES buffer plus radioactivity (1 µM itaconate, 2.5 µM malate, 1.5 µM or 5 µM ADP and 1.5 µM α-ketoglutarate) to approximately 5 µg fusions in a MultiScreenHTS-HA 96-well filter plate (pore size = 0.45 µm; Millipore). The transport was stopped at 0, 10, 20, 30, 45, 60, 150 s and, 5, 7.5, 10 and 15 min by the addition of 200 µl ice-cold PIPES buffer and filtering using a vacuum manifold, followed by two additional wash steps with 200 µL ice-cold PIPES buffer. Levels of radioactivity in the vesicles were measured by the addition of 200 µL MicroScint-20 (Perkin Elmer) and by quantifying the amount of radioactivity with the TopCount scintillation counter (Perkin Elmer). Initial rates were determined using linear regression. For experiments using [3H]-labeled itaconate, filters were punched out, and radioactivity measured using Perkin Elmer TriCarb 2800 TR-liquid scintillation analyzer after addition of 3 ml UltimaGold (Perkin Elmer).

2.2.18 – RNA analysis, cDNA synthesis and qPCR

Total RNA was isolated using the RNeasy Plus Mini kit (Ambion) as per manufacturer's instructions and quantified using a Nanodrop 2000 UV-visible

spectrophotometer. After RNA extraction and quantification, reverse transcription polymerase chain reaction (RT-PCR) was used to convert RNA to complementary DNA (cDNA) using a high capacity cDNA reverse transcription kit. 10 μL of RNA (100 ng/μL) was added to 10 μL of reaction mix as described (Table 2.5). 20 μL RNA/RT-PCR mix was transferred to 200 μL microcentrifuge tubes and placed in a thermal cycler programmed to: 10 min 25°C, 120 min 37°C, 15 min 85°C and final holding stage of 4°C. Samples were diluted 1:4 to 80 μL and stored at -20°C.

Table 2.3 – RT-PCR of RNA to cDNA

Component	Volume (μL)
10X RT Buffer	2
10X Random Primers	2
100mM deoxyribonucleotide triphosphates (dNTPs)	1
MultiScribe Reverse Transcriptase	1
Nuclease-free water	3.5
RNA (50-100ng/μL)	10

Real-time quantitative PCR (qPCR) was performed on cDNA generated from RT-PCR. qPCR was used to examine the expression levels of mouse *TNF*, *IL1B*, *Hmox1*, *Nqo1*, *Taldo1*, *Pdg*, *Gclm*, *Gsr* and *Rps18* (Table 2.5). qPCR was performed using SYBR Green reagents (Table 2.4). Relative fold values were calculated using the comparative threshold cycle (C_t) method and normalized to *Rps18* housekeeping gene.

Table 2.4 – SYBR green qPCR reaction mix

Component	Volume (μL)
Kapa SYBR mix	5 μL
Primer Pair mixed (10 μM final)	0.6 μL (600 nM each)
Nuclease-free H_2O	0.4 μL
cDNA	4 μL

Table 2.5 – Primer sequences

Primer	Forward (5'-3')	Reverse (5'-3')
IL1B	TGGCAACTGTTCCTG	GGAAGCAGCCCTTCATCTTT
TNF	GCCTCTTCTCATTCCTGCTT	TGGGAACTTCTCATCCCTTTG
Hmox1	TCAGGCAGAGGGTGATAGAA	GCTCCTGCAACTCCTCAAA
Nqo1	GCTGCAGACCTGGTGATATT	ACTCTCTCAAACCAGCCTTT
Taldo1	GCTGTCATCAACCTGGGAAG	TGGGCGAAGGAGAAGAGTAA
Pdg	ACTGCCCTCTCCTTCTATGA	CTGTCCAGTTGGTGTGGATAA
Gclm	GACAAAACACAGTTGGAACAGC	CAGTCAAATCTGGTGGCATC
Gsr	CGGTGCCAGCTTAGGAATAA	GCCATCTCCACAGCAATGTA
Ass1	GGCTGAAGGAACAAGGCTA	CTTCCTGGCTTCCTCAAAGT
Fh	ATTGGAGGTGCTACGGAACG	ACCTTCAGCTACCTCATCTGC
PHD3	TGCTGAAGAAAGGGCAGAAG	GCACACCACAGTCAGTCTTTA
Rps18	GGATGTGAAGGATGGGAAGT	CCCTCTATGGGCTCGAATTT

2.2.19 – Fumarate assay

Analysis of fumarate levels were assessed using a fumarate colorimetric assay kit (Sigma) that uses an enzyme assay, which results in a colorimetric (450 nm) product proportional to the fumarate present, as per manufacturer's instructions.

2.2.20 – Cell volume analysis

Macrophage cell volume was assessed using acridine orange (AO), confocal microscopy and 3D reconstruction as previously described with some minor adjustments (171). Specifically, in this experiment BMDMs were plated and imaged directly in μ-Dish 35 mm and did not require transfer to a coverslip. In brief, a LEICA SP8 scanning confocal microscope with 40X oil objective NA 1.3 was used to detect AO signals at 506-590 nm. Z-series profiles in the range of 40-60 optical sections were collected. Using Bitplane imaris software, each optical section for each cell was combined to generate a 3D image of each cell and facilitated the assessment of volume based on the AO signal.

2.2.21 – Statistics

One-way ANOVA or two-tailed t-tests were used as reported in the figure legends.

Chapter 3:

Potential role for an inflammatory aspartate-argininosuccinate shunt and fumarate in the regulation of cytokine production

3.1 – Introduction

This chapter concerns the role of a newly identified metabolic pathway in inflammatory macrophages that links the Krebs cycle with the urea/NO cycle termed the aspartate-argininosuccinate shunt (45). The aspartate-argininosuccinate shunt, sometimes referred to as the 'Krebs bicycle', is generally a pathway describing the metabolic interaction between ureagenesis and the Krebs cycle (45, 172) (Fig. 3.1).

The three key enzymes involved in the shunt are the glutamic-oxaloacetate transaminase (GOT2), the argininosuccinate synthase (Ass1) and the argininosuccinate lyase (Asl) (172, 173). GOT2 is a mitochondrial localized enzyme, that catalyses the transamination of the Krebs cycle metabolite oxaloacetate to the amino acid aspartate (173). This is an essential step in the shunt as aspartate is one of the two fuel molecules of the urea/NO cycle (173). GOT2 also generates α-ketoglutarate, which can re-enter the Krebs cycle (173). Argininosuccinate synthase (Ass1) catalyses the formation of argininosuccinate from aspartate, citrulline and ATP, whilst the argininosuccinate lyase (Asl) catalyses the cleavage of argininosuccinate to produce fumarate and arginine (172, 173). Together with the argininosuccinate lyase (Asl), is responsible for the synthesis of the semi-essential amino acid arginine in most bodily tissues (173). Importantly, Ass1 also constitutes the rate-limiting step in the aspartate-argininosuccinate shunt and L-arginine biosynthesis (173). Subsequently, arginase can use arginine to produce urea and ornithine ensuring that arginine generated through the actions of GOT2, Ass1 and Asl are directed for the most part into ureagenesis (173). Alternatively, the arginine produced can be utilised

by NOS to generate NO, which is the case in inflammatory macrophages (45, 173).

Increased fumarate levels owing to the induction of an inflammatory aspartate-argininosuccinate shunt by LPS has previously been proposed (45). However, the role of this metabolic pathway in regulating fumarate accumulation has not been directly shown. Similarly, the link between the shunt, fumarate and cytokine production has yet to be investigated. Both aspects will be explored in this chapter.

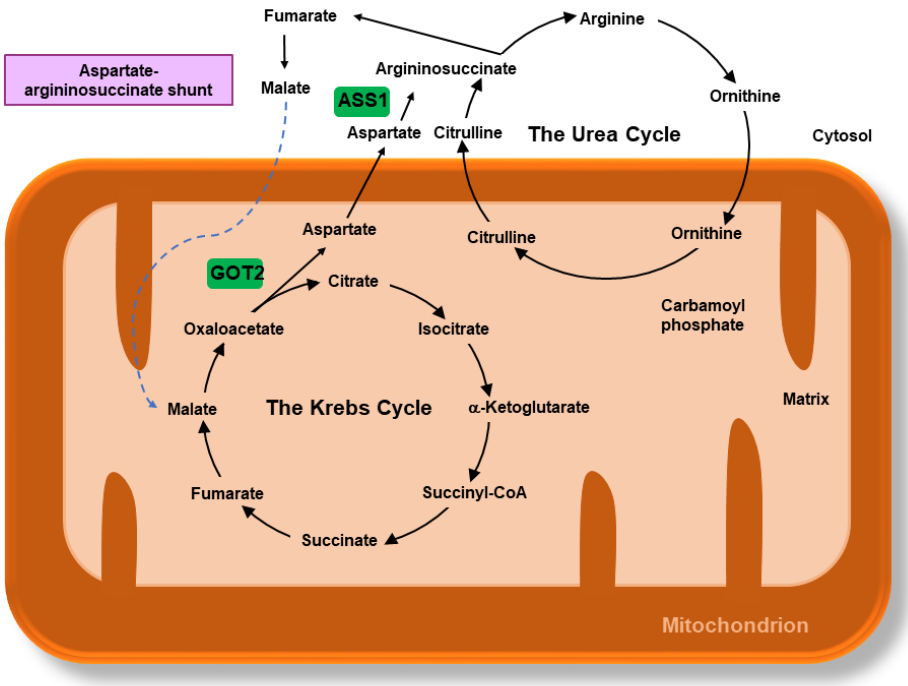

Figure 3.1 – Aspartate-argininosuccinate shunt of the Krebs cycle

The aspartate-argininosuccinate shunt also referred to as ‘Krebs bicycle’ is a metabolic pathway linking the Krebs cycle and the urea cycle. The rate-limiting enzyme of the shunt is Ass1, which synthesises argininosuccinate, a key intermediate of the urea cycle, from oxaloacetate- and GOT2-derived aspartate, in the cytosol. Asl cleaves argininosuccinate to form arginine and fumarate.

3.2 – Results

3.2.1 – LPS induces an inflammatory aspartate-argininosuccinate shunt and fumarate accumulation

The first aim was to determine the role of fumarate accumulation in LPS-activated BMDMs (20, 45). To this end, a semi-targeted metabolomics screen examining polar metabolites and utilising LC-MS was first used to confirm elevated fumarate levels in BMDMs stimulated with LPS (Fig. 3.2a, b). A full list of the significantly upregulated (red) or downregulated (blue) metabolites in LPS-activated BMDMs (Fig. 3.2a) can be found in Table 4.1. In addition to increased fumarate levels, significant increases in arginine (4.6 fold), argininosuccinate (31.4 fold) and a significant decrease in aspartate (0.28 fold) levels were also observed (Fig. 3.2a). Fumarate, aspartate, argininosuccinate and arginine are all known to participate in the aspartate-argininosuccinate shunt, a metabolic pathway that links the TCA cycle to the urea/NO cycle, as previously mentioned (45). Further analysis of the aspartate-argininosuccinate shunt demonstrated significant alterations in several metabolites linked to this pathway upon stimulation with LPS (Fig. 3.2a).

Utilising data generated from an unbiased quantitative proteomic screen, which used isobaric tandem mass tags (TMTs) coupled to LC-MS, a significant increase in the rate-limiting enzyme of the aspartate-argininosuccinate shunt, Ass1 (3.8 fold), was observed in LPS-activated BMDMs, whilst a small but significant decrease in fumarate hydratase (Fh) (0.81 fold), the enzyme responsible for fumarate catabolism (174-178), was also observed (Fig. 3.3b). To validate these findings, *Ass1* and *Fh* mRNA (Fig. 3.4a) expression was found to be significantly increased and decreased, respectively, over an LPS time-course.

a

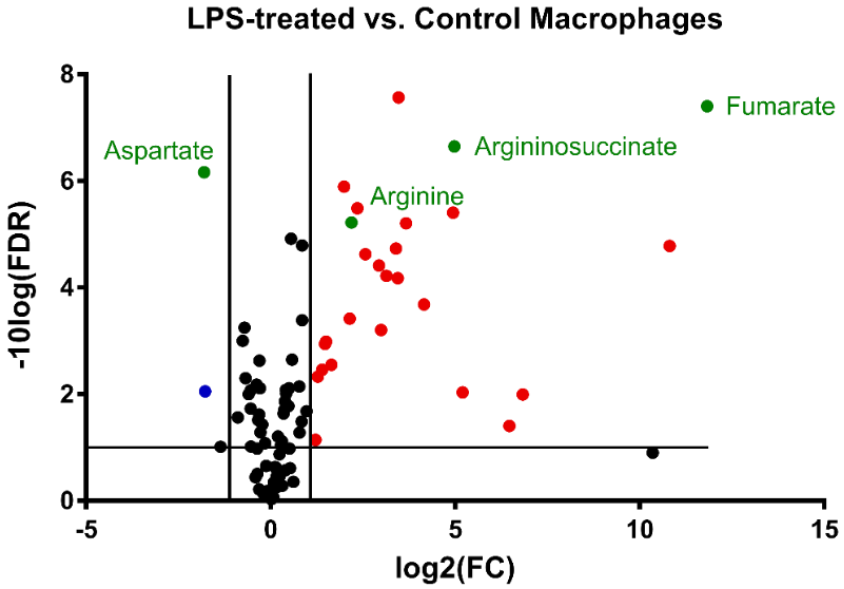

b

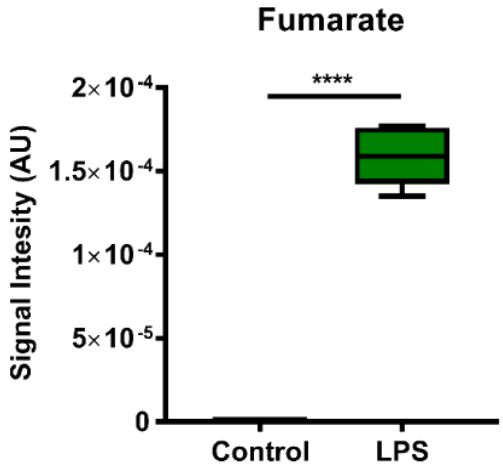

Figure 3.2 – LPS induces fumarate accumulation

Relative metabolite levels were determined by LC-MS in control or LPS-activated (100 ng/mL, 24 h) BMDMs. **(a)** Volcano plot indicating metabolites significantly up-regulated (red) or down-regulated (blue) upon treatment with LPS was generated using MetaboAnalyst 4.0 (*n*=5 biological replicates performed in technical duplicate). Aspartate, arginine, argininosuccinate and fumarate (green) are highlighted. FDR = false discovery rate. **(b)** Box and whiskers plot of relative fumarate levels (*n*=5 biological replicates performed in technical duplicate). *P*-values were calculated using an unpaired t-test. **P* <0.05, ***P* <0.01, ****P* <0.001, *****P* <0.0001.

a

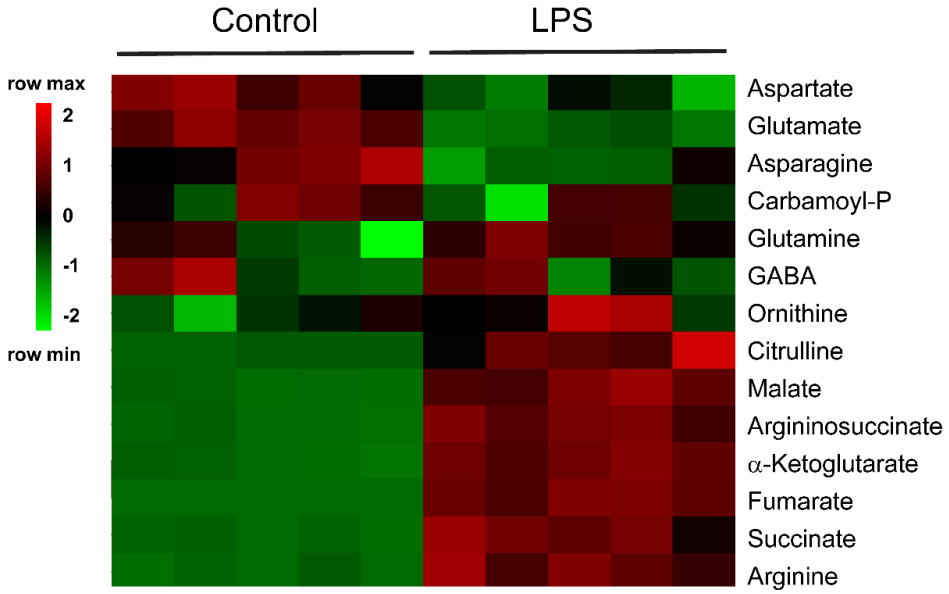

b

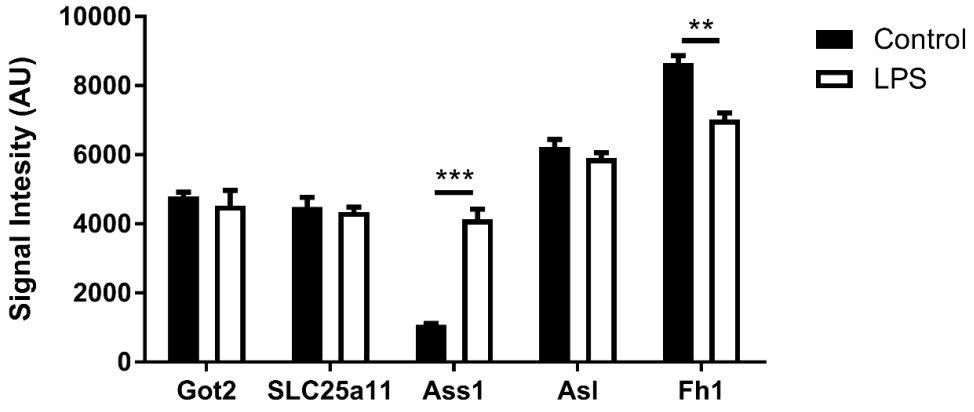

Figure 3.3 – LPS induces Ass1 & an inflammatory argininosuccinate shunt

(a) Heatmap of upregulated (red) and downregulated (green) metabolites involved in the argininosuccinate shunt generated using the Ward clustering algorithm and MetaboAnalyst 4.0 software (*n*=5 biological replicates performed in technical duplicate). **(b)** Relative changes in protein levels were quantified using TMT coupled to LC-MS in control and LPS-activated (100 ng/mL, 24 h) BMDMs. Relative changes in key enzymes of the argininosuccinate shunt are shown (*n*=4 biological replicates). Data is presented as mean ± SEM. *P*-values were calculated using an unpaired t-test. **P* <0.05, ***P* <0.01, ****P* <0.001, *****P* <0.0001.

a

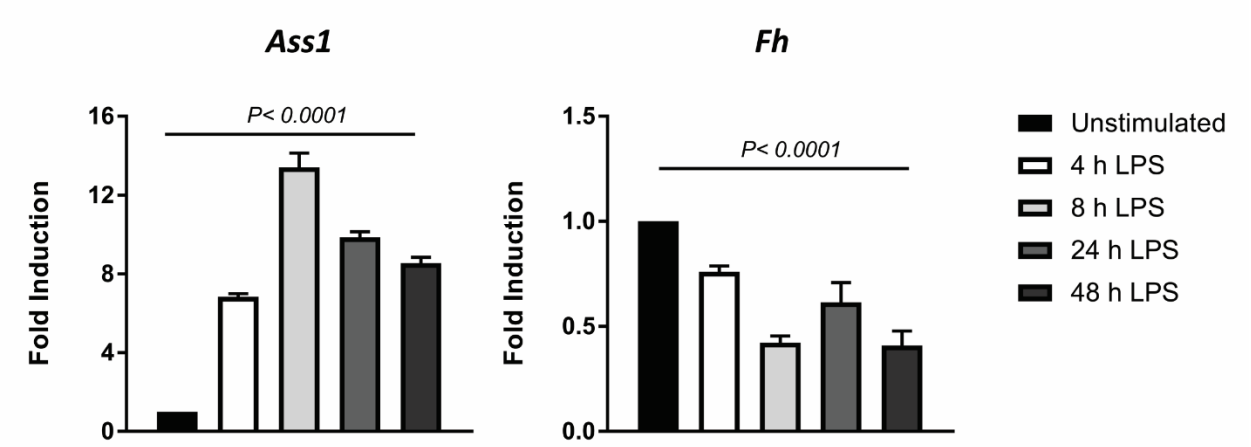

Figure 3.4 – LPS induces Ass1 & decreases Fh mRNA expression

(a) Relative fold change in mRNA levels of *Ass1* and *Fh* in response to LPS treatment (100 ng/mL) for indicated timepoints, as assessed by qPCR (*n*=3 biological replicates performed in technical duplicate). Data is presented as mean ± SEM. *P*-values were calculated using one-way ANOVA. **P* <0.05, ***P* <0.01, ****P* <0.001, *****P* <0.0001.

3.2.2 – The aspartate-argininosuccinate shunt regulates fumarate levels and cytokine production

Increased fumarate levels owing to the induction of an inflammatory aspartate-argininosuccinate shunt by LPS has previously been proposed (45). However, the role of this metabolic pathway in regulating fumarate accumulation has not been directly shown. Similarly, the link between the shunt, fumarate and cytokine production has yet to be investigated.

In addition to Ass1 and Asl, the mitochondrial aspartate aminotransferase GOT2, which catalyses the transamination of oxaloacetate to aspartate, constitutes an important enzyme for the functioning of the aspartate-argininosuccinate shunt, as discussed (45). As such, the GOT1/2 inhibitor aminooxyacetic acid (AOAA), which will inhibit aspartate synthesis from oxaloacetate, was employed as an experimental tool to assess the functional role of the shunt in LPS-activated BMDMs. Pre-treatment of BMDMs with AOAA resulted in potent inhibition of LPS-induced TNF protein expression (Fig. 3.5a; compare lanes 2-4 to lanes 8-10) and TNF secretion (Fig. 3.5c) but had no significant effect on *TNF* mRNA expression (Fig. 3.5d), over an LPS timecourse. Mouse and rat TNF are predicted to be glycosylated, which can influence the molecular weight of this cytokine, hence the three bands that appear on the western blot (Fig. 3.5a). Similarly, AOAA also inhibited LPS-induced pro-IL-1β levels (Fig. 3.6a; compare lane 7 to lane 8), and as previously reported [22], IL-6 secretion (Fig. 3.6b). Unlike TNF, the inhibition of IL-1β (Fig. 3.6c) and IL-6 (Fig. 3.6d) appears to occur at the transcript level. As expected, AOAA treatment on its own in unstimulated conditions (no LPS) had no effect on IL-6 (Fig. 3.6b) or TNF (Fig. 3.5c) secretion, or on TNF protein levels (Fig. 3.5a; compare lane 1 to

lanes 5-7) at 5 h (lane 6), 9 h (lane 7) and 25 h (lane 8) post treatment. AOAA treatment on its own also had no effect on pro-IL1β (Fig. 3.6a; compare lane 1 to lane 2), *IL1B* (Fig. 3.6c), *IL6* (Fig. 3.6d) or *TNF* (Fig. 3.5d) mRNA expression.

Furthermore, the specificity of GOT1/2 inhibition by AOAA was validated by loading BMDMs with aspartate or dimethyl aspartate (to overcome inhibition of GOT1/2) prior to AOAA treatment, which rescued the inhibitory effect of AOAA on TNF (Fig. 3.5b; compare lane 8 to lanes 11-12) and pro-IL-1β (Fig. 3.6b; compare lane 8 to lanes 11-12) levels, whilst pre-treatment of macrophages with aspartate or dimethyl aspartate on their own had no effect on LPS-induced TNF (Fig. 3.5b; compare lane 7 to lanes 9-10) and pro-IL-1β (Fig. 3.6b; compare lane 7 to lanes 9-10) levels or in unstimulated conditions (TNF; Fig. 3.5b, compare lane 1 to lanes 3-4, pro-IL1β; Fig. 3.6a; compare lane 1 to lanes 3-4).

In addition to affecting cytokine production, pre-treatment of BMDMs with AOAA also resulted in an inhibition of fumarate levels both in control and LPS-activated BMDMs (Fig. 3.7a). Furthermore, pre-treatment of BMDMs with the cell-permeable fumarate analogue, dimethyl fumarate (DMF), augmented LPS-induced *Ass1* mRNA expression suggesting a positive feedback loop may exist between fumarate and Ass1 (Fig. 3.7b).

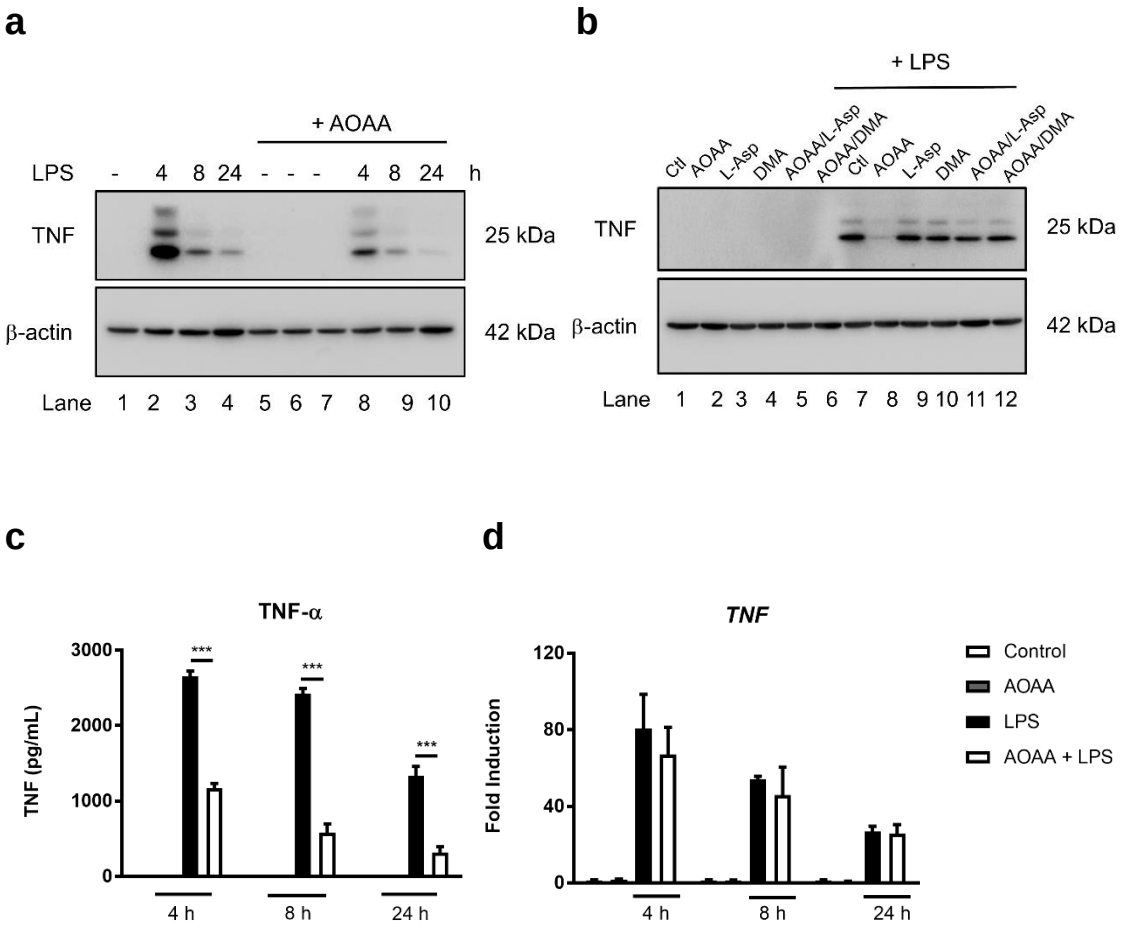

Figure 3.5 – Aminooxyacetic acid blunts LPS-induced TNF protein expression

(a) Protein expression of TNF and the loading control β-actin in response to LPS treatment (100 ng/mL) ± 1 h AOAA pre-treatment (5 mM) for indicated timepoints, as assessed by western blot. The results shown are representative of three independent experiments. **(b)** Protein expression of TNF and the loading control β-actin in response to LPS treatment (100 ng/mL, 4 h) ± 3 h L-Asp or DMA pre-treatment (10 mM and 2.5 mM, respectively) ± 1 h AOAA pre-treatment (5 mM), as assessed by western blot. The results shown are representative of three independent experiments. **(c)** TNF protein levels secreted into the CCM in response to LPS treatment (100 ng/mL) ± 1 h AOAA pre-treatment (5 mM) for indicated timepoints, as assessed by ELISA (*n*=3 biological replicates performed in technical duplicate). **(d)** Relative fold change in mRNA levels of *TNF* in response to LPS treatment (100 ng/mL) ± 1 h AOAA pre-treatment (5 mM) for indicated timepoints, as assessed by qPCR (*n*=3 biological replicates performed in technical duplicate). Data is presented as mean ± SEM. *P*-values were calculated using one-way ANOVA. **P* <0.05, ***P* <0.01, ****P* <0.001, *****P* <0.0001.

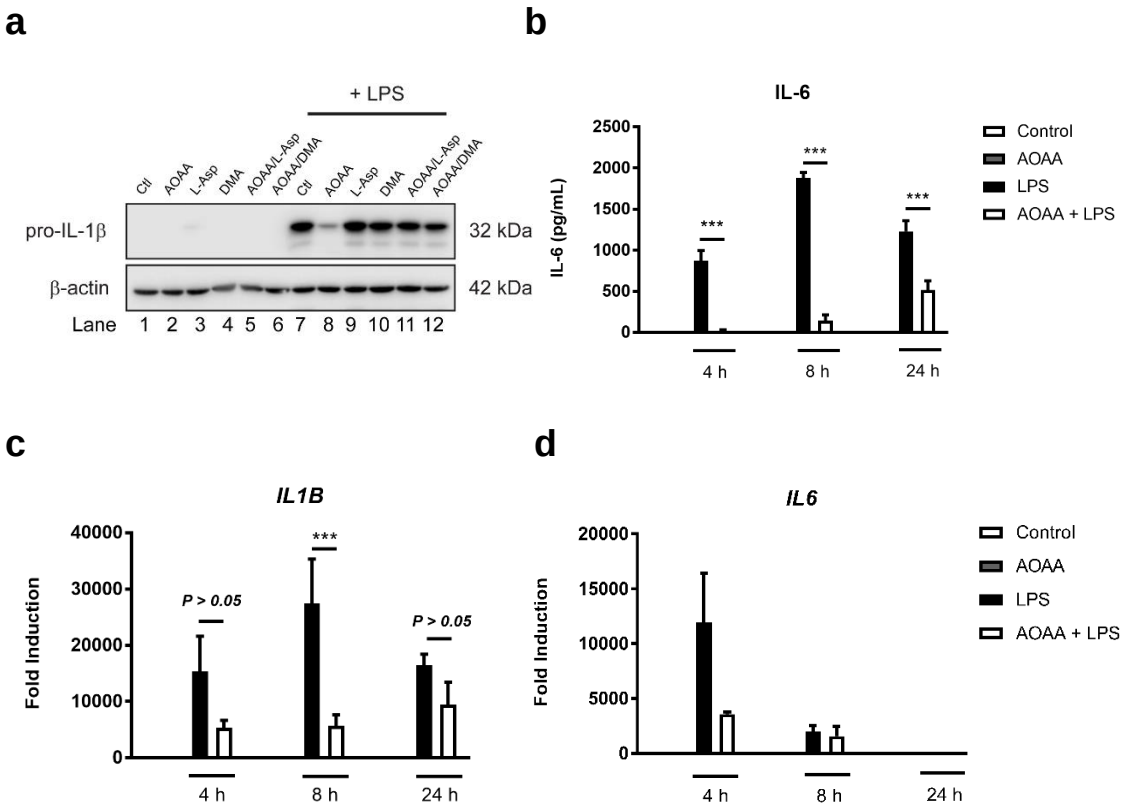

Figure 3.6 – Aminooxyacetic acid inhibits LPS-induced IL-1β & IL-6 levels

(a) Protein expression of pro-IL-1β and the loading control β-actin in response to LPS treatment (100 ng/mL) ± 1 h AOAA pre-treatment (5 mM) for indicated timepoints, as assessed by western blot. The results shown are representative of three independent experiments. **(b)** IL-6 protein levels secreted into the CCM in response to LPS treatment (100 ng/mL) ± 1 h AOAA pre-treatment (5 mM) for indicated timepoints, as assessed by ELISA (*n*=3 biological replicates performed in technical duplicate). Relative fold change in mRNA levels of **(c)** *IL1B* and **(d)** *IL6* in response to LPS treatment (100 ng/mL) ± 1 h AOAA pre-treatment (5 mM) for indicated timepoints, as assessed by qPCR (*n*=3 biological replicates performed in technical duplicate). Data is presented as mean ± SEM. *P*-values were calculated using one-way ANOVA. **P* <0.05, ***P* <0.01, ****P* <0.001, *****P* <0.0001.

a

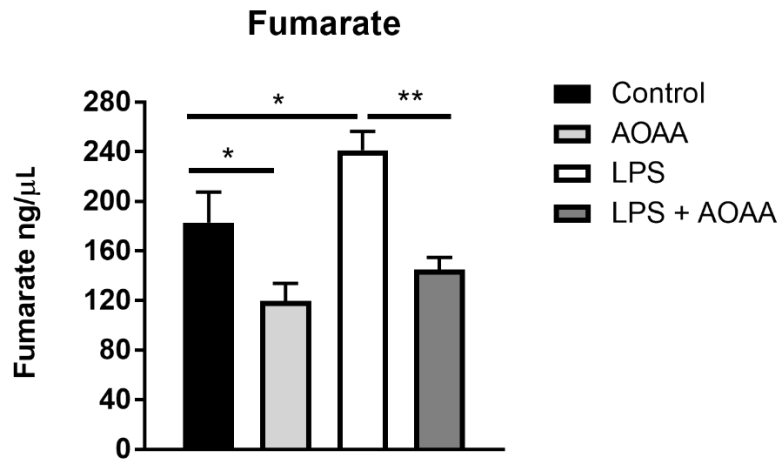

b

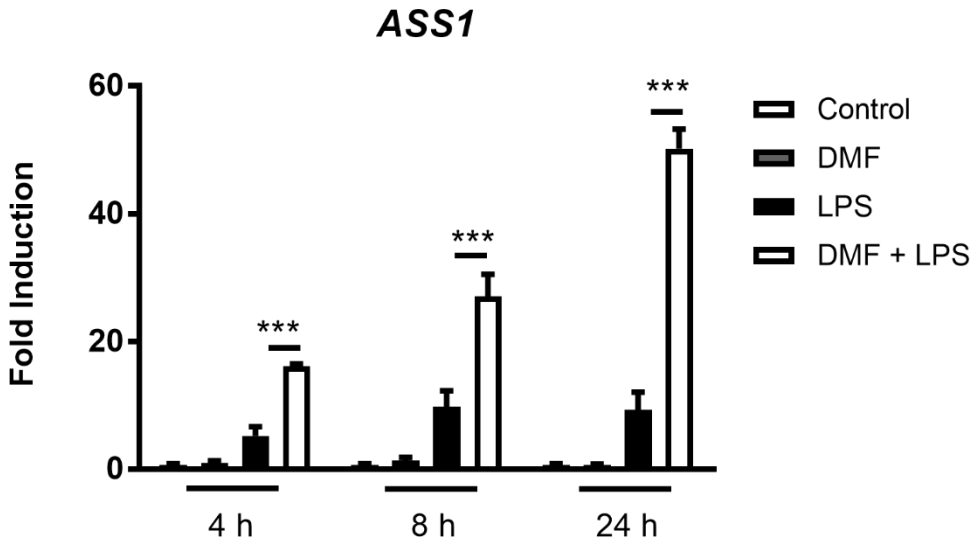

Figure 3.7 – Reciprocal regulation of *Ass1* & fumarate

(a) Fumarate levels in response to LPS treatment (100 ng/mL) ± 1 h AOAA pre-treatment (5 mM, 4 h), as assessed by a fumarate colorimetric assay (*n*=3 biological replicates performed in technical duplicate). **(b)** Relative fold change in mRNA levels of *Ass1* in response to LPS treatment (100 ng/mL) ± 1 h DMF pre-treatment (25 μM) for indicated timepoints, as assessed by qPCR (*n*=3 biological replicates performed in technical duplicate). Data is presented as mean ± SEM. *P*-values were calculated using one-way ANOVA. **P* <0.05, ***P* <0.01, ****P* <0.001, *****P* <0.0001.

3.2.3 – DMF modulates LPS-induced cytokine production

To determine the consequences of elevated fumarate levels on the inflammatory response in macrophages, a cell-permeable fumarate analogue, DMF, was employed as an experimental tool (179) (Fig. 3.8a). Pre-treatment of BMDMs with DMF resulted in potent inhibition of LPS-induced pro-IL1β levels (Fig. 3.8b; compare lanes 2-4 to lanes 9-11), IL-6 secretion (Fig 3.8c) and *IL1B* and *IL6* mRNA expression (Fig. 3.9a, b) over an LPS time-course. However, DMF pre-treatment also augmented LPS-induced TNF protein expression (Fig. 3.8b; compare lanes 3-4 to lanes 10-11) and TNF secretion (Fig. 3.8d) but had no significant effect on *TNF* mRNA expression (Fig. 3.9c). As expected, DMF treatment on its own in unstimulated conditions (no LPS) had no effect on IL-6 or TNF secretion (Fig 3.8c, d), or on TNF and pro-IL1β levels (Fig. 3.8b; compare lane 1 to lanes 6-8) at 5 h (lane 6), 9 h (lane 7) and 25 h (lane 8) post treatment. DMF treatment on its own in unstimulated conditions also had no effect on *IL1B*, *IL6* or *TNF* mRNA expression (Fig. 3.9a, b).

DMF is a key component of the anti-inflammatory drugs Fumaderm® and Tecfidera® used to treat psoriasis and multiple sclerosis (MS), respectively (161, 180). DMF is thought in part to mediate its anti-inflammatory mode of action via alkylation of key redox sensing cysteines on Keap1, a PTM termed succination, and subsequent activation of Nrf2 (174, 176). Pre-treatment of BMDMs with DMF augmented LPS-induced Nrf2 (Fig. 3.10a; compare lanes 2-4 to lanes 9-11) and Hmox1 (Fig. 3.10a; compare lanes 2-3 to lanes 9-10) protein and *Hmox1* mRNA (Fig. 3.9b) expression over an LPS time-course. DMF treatment on its own in unstimulated conditions also increased Nrf2 and Hmox1 protein (Fig. 3.10a; compare lane 1 to lanes 6-7) and *Hmox1* mRNA (Fig. 3.6b) levels at 5 (lane 6)

and 9 (lane 7) h post-treatment. However, 25 h post-treatment (lane 8), Nrf2 stabilisation and Hmox1 levels are no longer observed, likely due to negative regulation of the pathway by Nrf2 itself following acute activation.

As Nrf2 is a known regulator of inflammatory cytokine production (158), the ability of DMF to induce TNF, when Nrf2 levels are reduced using siRNA-mediated gene silencing, was investigated. DMF pre-treatment of BMDMs transfected with two independent siRNAs targeting *Nfe2l2* mRNA, or a scrambled control, resulted in a significant potentiation of TNF secretion (Fig. 3.10c).

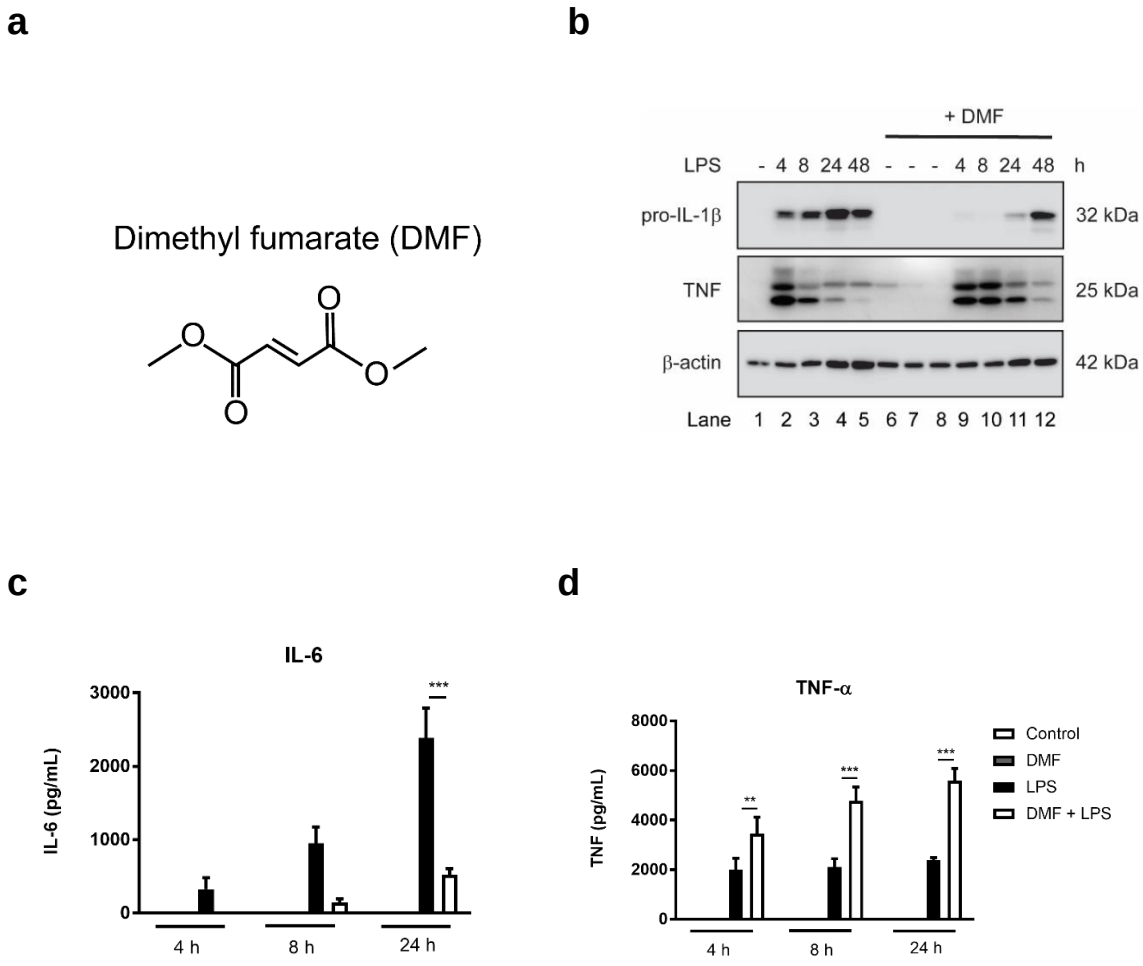

Figure 3.8 – DMF inhibits LPS-induced IL-1β & IL-6 but increases TNF levels

(a) Chemical structure of cell-permeable fumarate analogue DMF. **(b)** Protein expression of pro-IL-1β, TNF and the loading control β-actin in response to LPS treatment (100 ng/mL) ± 1 h DMF pre-treatment (25 μM) for indicated timepoints, as assessed by western blot. The results shown are representative of three independent experiments. **(c)** TNF and **(d)** IL-6 protein levels secreted into the CCM in response to LPS treatment (100 ng/mL) ± 1 h DMF pre-treatment (25 μM) for indicated timepoints, as assessed by ELISA (*n*=4 biological replicates performed in technical duplicate). Data is presented as mean ± SEM. *P*-values were calculated using one-way ANOVA. **P* <0.05, ***P* <0.01, ****P* <0.001, *****P* <0.0001.

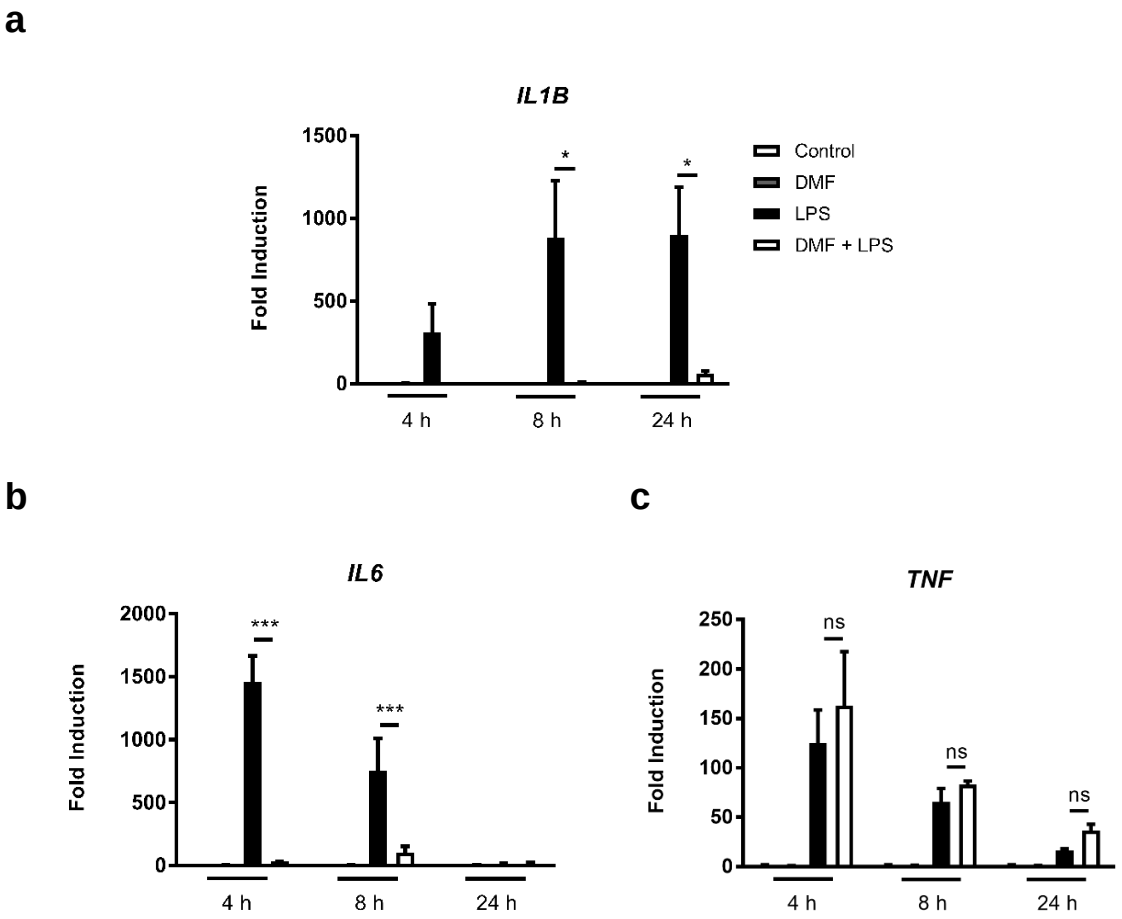

Figure 3.9 – DMF inhibits LPS-induced *IL1B* & *IL6* but not *TNF* mRNA levels

(a-c) Relative fold change in mRNA levels of *IL1B, IL6* and *TNF* in response to LPS treatment (100 ng/mL) ± 1 h DMF pre-treatment (25 μM) for indicated timepoints, as assessed by qPCR (*n*=3 biological replicates performed in technical duplicate). Data is presented as mean ± SEM. *P*-values were calculated using one-way ANOVA. **P* <0.05, ***P* <0.01, ****P* <0.001, *****P* <0.0001.

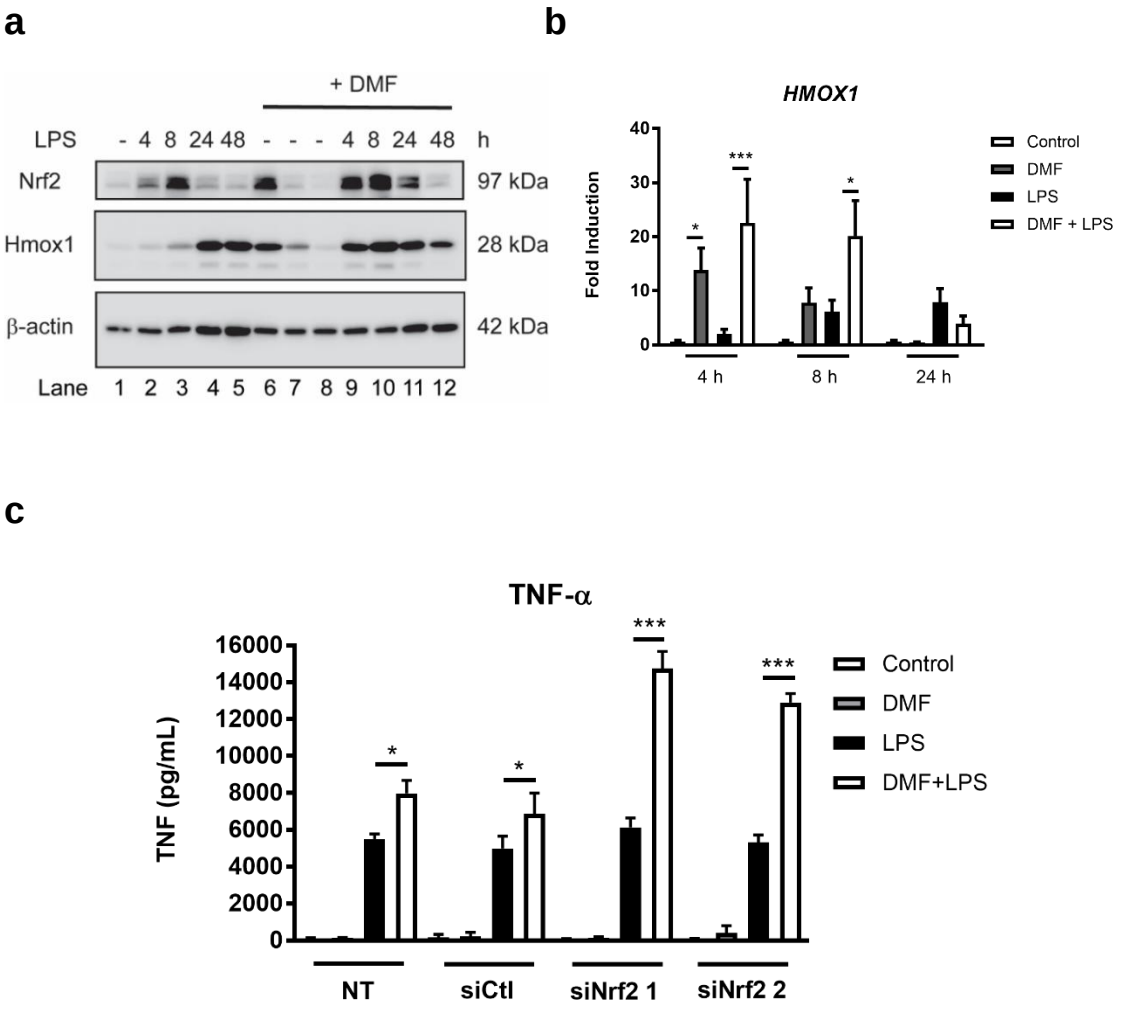

Figure 3.10 – LPS-induced TNF is further boosted by DMF upon Nrf2 silencing

(a) Protein expression of Nrf2, Hmox1 and the loading control β-actin in response to LPS treatment (100 ng/mL) ± 1 h DMF pre-treatment (25 μM) for indicated timepoints, as assessed by western blot. The results shown are representative of three independent experiments. **(b)** Relative fold change in mRNA levels of *Hmox1* in response to LPS treatment (100 ng/mL) ± 1 h DMF pre-treatment (25 μM) for indicated timepoints, as assessed by qPCR (*n*=3 biological replicates performed in technical duplicate). **(c)** TNF protein levels secreted into the CCM in response to LPS treatment (100 ng/mL, 24 h) ± 1 h DMF pre-treatment (25 μM) after transfection with two independent Nrf2 siRNAs or a scrambled siRNA control (24 h, 50 nM), as assessed by ELISA (*n*=3 biological replicates performed in technical duplicate). NT indicates non-transfected control. Data is presented as mean ± SEM. *P*-values were calculated using one-way ANOVA. **P* <0.05, ***P* <0.01, ****P* <0.001, *****P* <0.0001.

3.2.4 – MMF modulates LPS-induced cytokine production

DMF is metabolised to monomethyl fumarate (MMF) *in vivo* (Fig. 3.11a) and so it's thought that DMF itself is a prodrug and that the anti-inflammatory actions of Fumaderm® and Tecifidera® are mediated by MMF (181). MMF can also induce succination of target proteins, however, it is less electrophilic than DMF as only one carboxyl group is esterified (162) and is thus more likely to behave in a similar manner to endogenous fumarate. As such, the ability of MMF to modulate cytokine levels and Nrf2 was also investigated.

Pre-treatment of BMDMs with MMF differentially modulated LPS-induced pro-IL1β (Fig. 3.11b; compare lanes 2-5 to lanes 9-12) with a small inhibition after 24 h of LPS stimulation (compare lane 4 to lane 11) but a marked increase after 48 h of LPS stimulation (compare lane 5 to lane 12). The increase in pro-IL1β levels after 48 h of LPS stimulation in MMF pre-treated BMDMs is preceded by an increase in *IL1B* mRNA expression (Fig 3.12b) after 24 h of LPS stimulation in MMF pre-treated BMDMs. Like DMF, MMF pre-treatment also potentiated LPS-induced TNF protein expression (Fig. 3.11b; compare lanes 3-4 to lanes 10-11) and TNF secretion into the cell culture medium (Fig. 3.11d) but had no significant effect on *TNF* mRNA expression (Fig. 3.12d). Unlike DMF, MMF pre-treatment had no effect on IL-6 secretion (Fig 3.11c) or *IL6* mRNA expression (Fig 3.12c). As expected, MMF treatment on its own in unstimulated conditions (no LPS) had no effect on IL-6 or TNF secretion (Fig 3.11c, d), or on TNF and pro-IL1β levels (Fig. 3.11b; compare lane 1 to lanes 6-8) at 5 h (lane 6), 9 h (lane 7) and 25 h (lane 8) post treatment. MMF treatment on its own in unstimulated conditions also had no effect on *IL1B*, *IL6* or *TNF* mRNA expression (Fig. 3.12b-d).

Pre-treatment of BMDMs with MMF marginally augmented LPS-induced Nrf2 (Fig. 3.7b; compare lane 2 to lanes 9), but not Hmox1 (Fig. 3.12a; compare lane 2 to lane 9) protein levels, at an early LPS timepoint (4 h) but not at other timepoints. This early augmentation interfered with the kinetics of Nrf2 induction by LPS, as 24 h post LPS stimulation Nr2 was still stable in control conditions but not in the MMF-treated condition (Fig. 3.12a; compare lane 4 to lane 11). MMF treatment in unstimulated conditions (no LPS) marginally increased Nrf2 and Hmox1 protein levels (Fig. 3.12a; compare lane 1 to lanes 6-7), at 5 h (lane 6) and 9 h (lane 7) but not 25 h (lane 8) post-treatment. Again, these results implicate negative regulation of Nrf2 activation by itself. Induction of Nrf2 and Hmox1 was less potent than that observed with DMF (Fig. 3.10a; compare lane 1 to lanes 6-7), which is in line with MMF being less electrophilic than DMF.

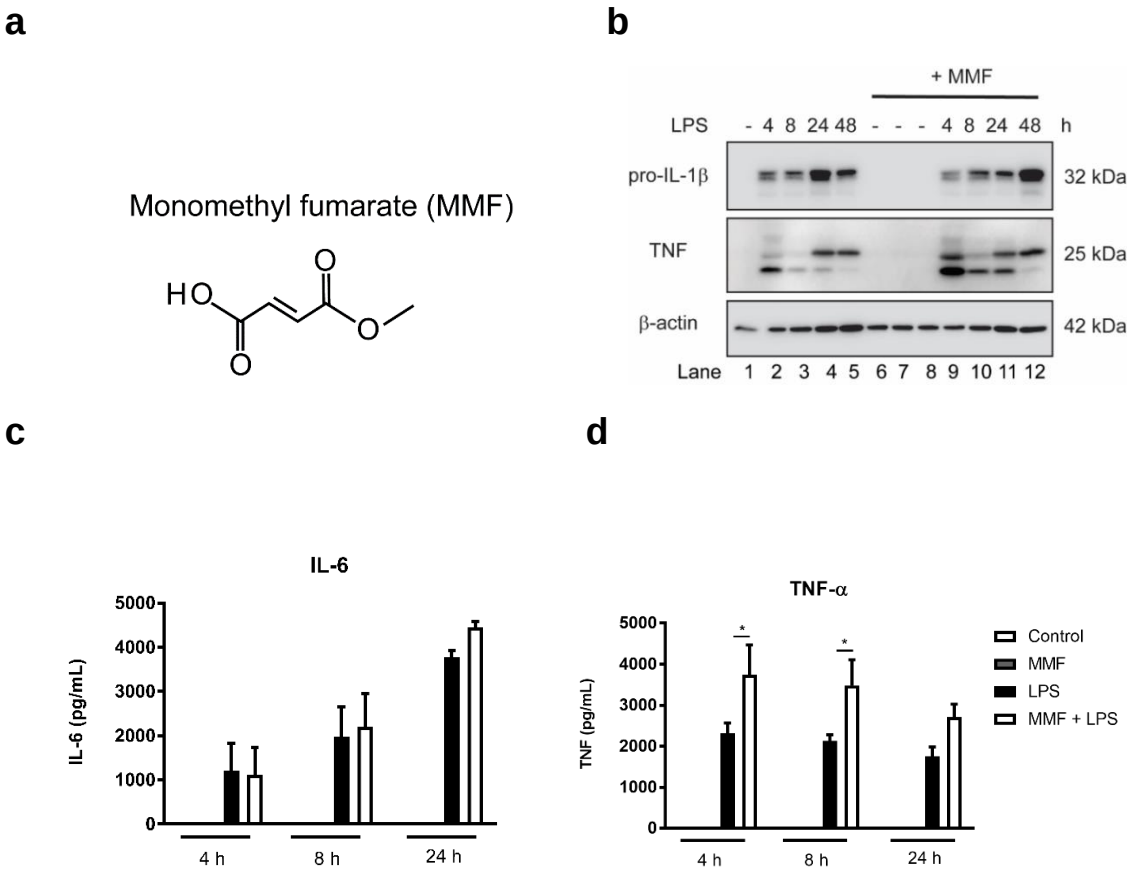

Figure 3.11 – MMF increases LPS-induced TNF production

(a) Chemical structure of cell-permeable fumarate analogue MMF. **(b)** Protein expression of pro-IL-1β, TNF and the loading control β-actin in response to LPS treatment (100 ng/mL) ± 1 h MMF pre-treatment (50 μM) for indicated timepoints, as assessed by western blot. The results shown are representative of three independent experiments. **(d-e)** IL-6 and TNF protein levels secreted into the CCM in response to LPS treatment (100 ng/mL) ± 1 h MMF pre-treatment (50 μM) for indicated timepoints, as assessed by ELISA (*n*=3 biological replicates performed in technical duplicate). Data is presented as mean ± SEM. *P*-values were calculated using one-way ANOVA. **P* <0.05, ***P* <0.01, ****P* <0.001, *****P* <0.0001

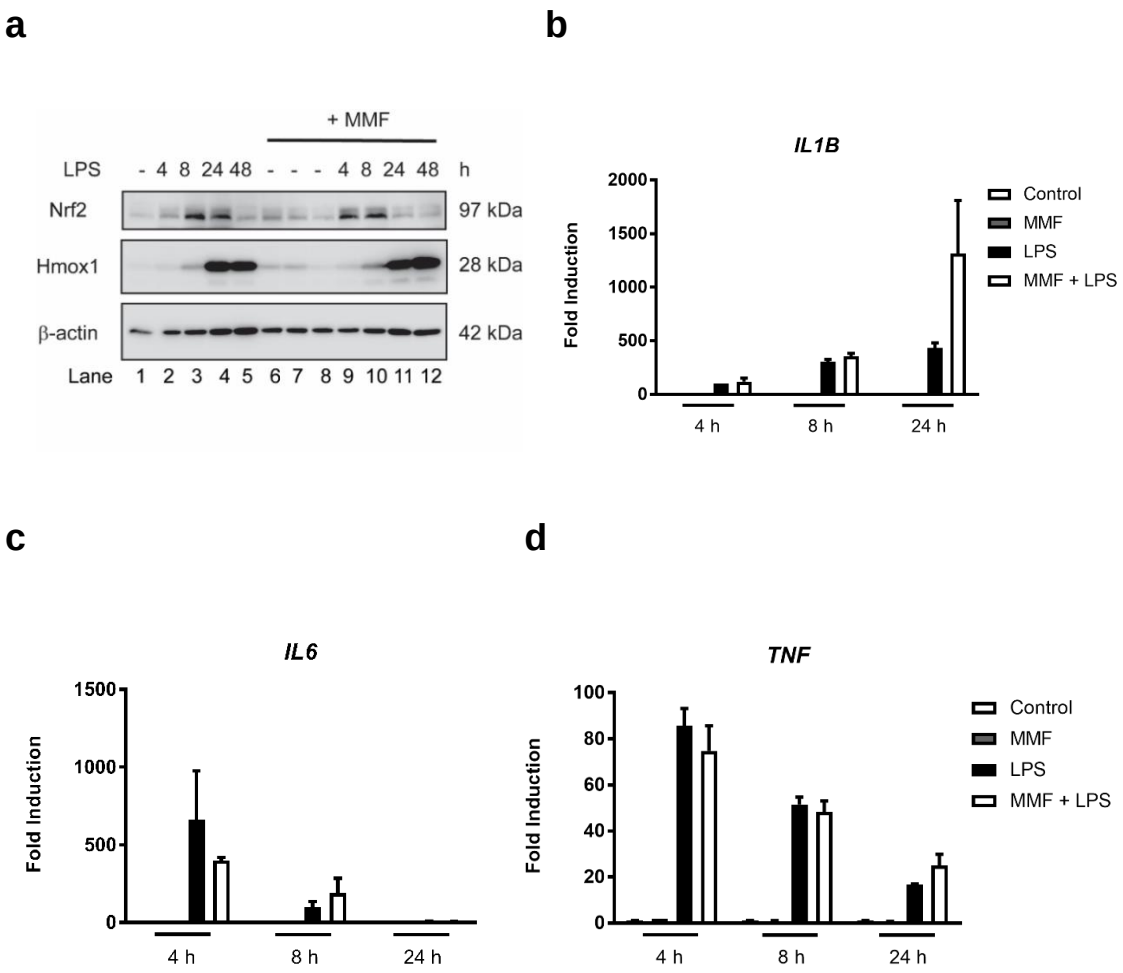

Figure 3.12 – MMF stabilises Nrf2 & differentially regulates cytokine levels

(a) Protein expression of Nrf2, Hmox1 and the loading control β-actin in response to LPS treatment (100 ng/mL) ± 1 h MMF pre-treatment (50 μM) for indicated timepoints, as assessed by western blot. The results shown are representative of three independent experiments. Relative fold change in mRNA levels of **(b)** *IL1B*, **(c)** *IL6* and **(d)** *TNF* in response to LPS treatment (100 ng/mL) ± 1 h MMF pre-treatment (50 μM) for indicated timepoints, as assessed by qPCR (*n*=2 biological replicates performed in technical duplicate). Data is presented as mean ± SEM.

3.2.5 – Fh deficiency modulates LPS-induced cytokine production

Endogenous fumarate is an electrophilic α, β-unsaturated carbonyl compound that can induce protein succination (176). However, esterification renders it an activated Michael acceptor as the thiol-reactive alkene component of fumarate is directly conjugated to both carboxyl groups. As such, the use of the cell-permeable fumarate surrogates DMF and MMF, whilst informative, are more chemically reactive than endogenous fumarate. MMF, whilst being less reactive than DMF and so more akin to fumarate, is also an agonist of the hydroxycarboxylic acid receptor HCA2 (182, 183), whereas fumarate itself is not. Although fumarate itself is cell impermeable, intracellular fumarate levels can also be elevated through genetic deletion of one or both alleles of the Krebs cycle enzyme Fh (174, 177, 178, 184).

To this end, the ability of LPS to modulate cytokine production in *Fh -/-* deficient BMDMs was investigated. Confirmation that these BMDMs lacked Fh protein expression (Fig. 3.13a; compare lanes 1-6 to lanes 7-12) and *Fh* mRNA expression (Fig. 3.14a) was assessed via western blot and qPCR, respectively. Downregulation of Fh protein levels (Fig. 3.13a; compare lane 1 to lanes 2-6) and *Fh* mRNA levels (Fig. 3.14a) by LPS was again observed in wildtype control *Fh* +/+ BMDMs. The ability of LPS to induce IL-6 secretion (Fig. 3.13b) and pro-IL-1β expression (Fig. 3.13a; compare lanes 2-6 to lanes 8-12) was relatively unaffected in *Fh -/-* BMDMs, with a small decrease in pro-IL-1β observed after 48 h LPS stimulation (Fig. 3.13a; compare lane 6 to lane 12). *IL6* mRNA expression was also no different between wildtype and knockout (Fig. 3.14a), however, *IL1B* mRNA expression appeared to increase after 24 h of LPS stimulation in *Fh -/-* BMDMs (Fig. 3.14d) similarly to that observed with MMF and

LPS (Fig. 3.12b). As with DMF and MMF, LPS-induced TNF protein levels (Fig. 3.12a; compare lanes 3-4 to lanes 8-9) and TNF secretion (Fig. 3.13c) were enhanced across an LPS timecourse (from 4 h), whilst no increase in *TNF* mRNA expression was observed at any timepoint (Fig. 3.14d).

As complete deletion of *Fh* truncates the Krebs cycle and drastically impairs OXPHOS (178), a less deleterious means to elevate endogenous fumarate was sought. To this end, the ability of LPS to modulate cytokine production in *Fh* +/- deficient BMDMs was examined, whereby there is only a partial loss of Fh and less severe impairment of OXPHOS, but fumarate can still accumulate (184). Confirmation that these BMDMs had reduced Fh protein levels (Fig. 3.15a; compare lanes 1-5 to lanes 6-10) and *Fh* mRNA levels (Fig. 3.16a) was assessed via western blot and qPCR, respectively. Downregulation of Fh protein levels (Fig. 3.15a; compare lane 1 to lanes 2-6) and *Fh* mRNA levels (Fig. 3.16a) by LPS was observed in both *Fh* +/- and *Fh* +/+ BMDMs. Unlike *Fh* -/- BMDMs, the ability of LPS to induce IL-6 secretion (Fig. 3.15b) and pro-IL-1β expression (Fig. 3.15a; compare lanes 2-6 to lanes 8-12) was increased in *Fh* +/- BMDMs but only evident at early timepoints for IL-6 and after 24 h LPS stimulation for pro-IL-1β (Fig. 3.15a; compare lane 4 to lane 9). These increases at the protein level in *Fh* +/- macrophages were mirrored at the transcript for both *IL6* (Fig. 3.16c) and *IL1B* (Fig 3.16d). Furthermore, LPS-induced TNF protein levels (Fig. 3.15a; compare lanes 2-3 to lanes 7-8) and TNF secretion (Fig. 3.15c) were augmented, whilst no increase in *TNF* mRNA expression was observed at any timepoint (Fig. 3.16b).

Elevated fumarate levels observed in mice genetically lacking Fh has previously been implicated in the succination and inhibition of Keap1 and

activation of Nrf2 (185). As such, it was investigated whether the induction of Nrf2 observed with LPS could be owed to increased fumarate accumulation in BMDMs. However, Nrf2 protein expression was surprisingly impaired in LPS-activated *Fh -/-* (Fig. 3.17a; compare lanes 2-6 to lanes 8-12) and *Fh +/-* (Fig. 3.17b; compare lanes 3-4 to lanes 8-9) BMDMs over an LPS time-course. Despite impairment of Nrf2 stabilisation, the Nrf2 target Hmox1 was still induced by LPS in both *Fh -/-* (Fig. 3.17a; compare lanes 5-6 to lanes 11-12) and *Fh +/-* (Fig. 3.17b; compare lanes 4-5 to lanes 9-10) BMDMs, suggesting it can be regulated independent of Nrf2 activation in response to LPS in macrophages.

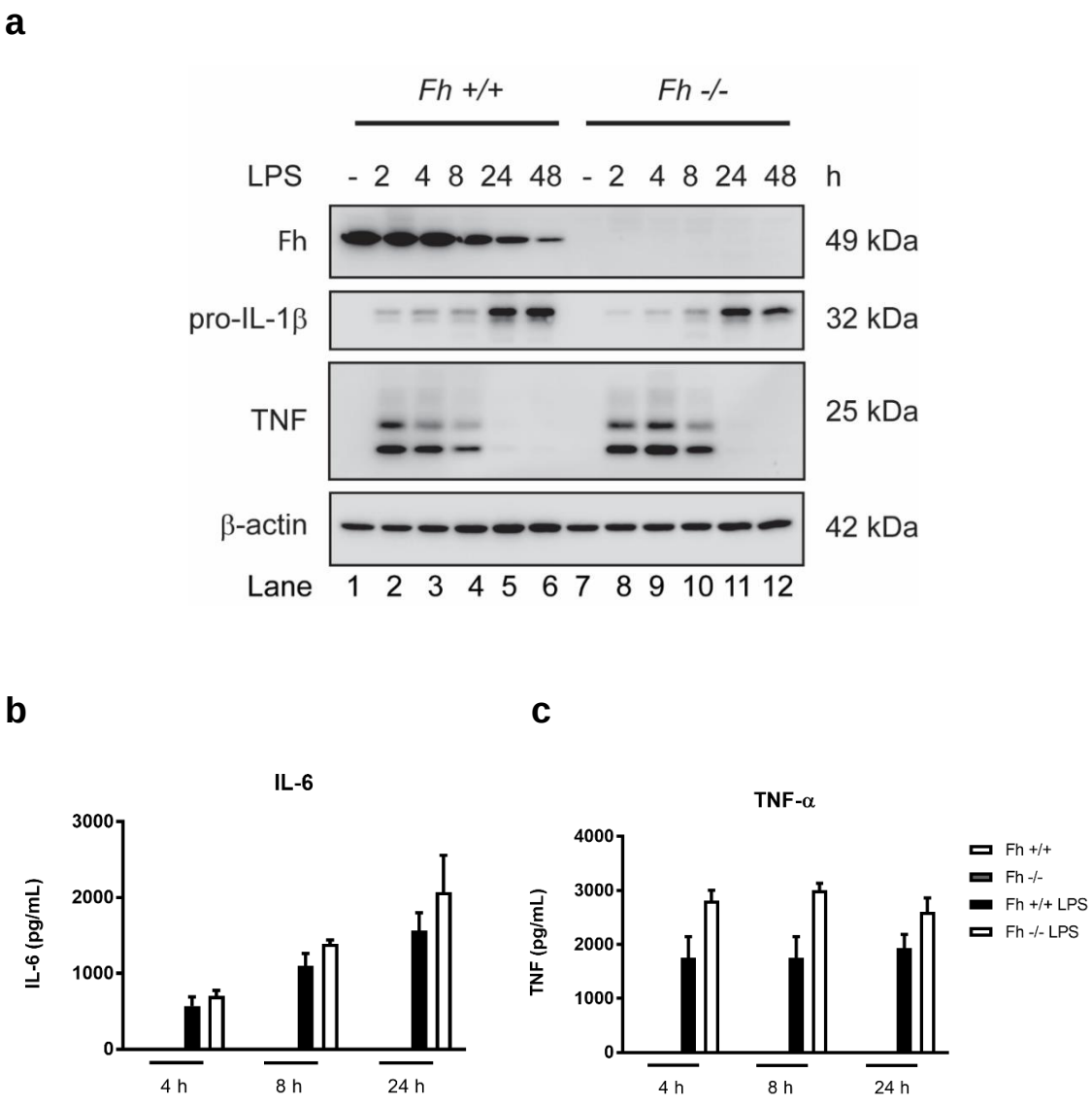

Figure 3.13 – *Fh* -/- deficiency increases LPS-induced TNF production

(a) Protein expression of Fh, pro-IL-1β, TNF and the loading control β-actin in Fh +/+ or Fh -/- BMDMs in response to LPS treatment (100 ng/mL) for indicated timepoints, as assessed by western blot. The results shown are representative of two independent experiments. IL-6 **(b)** and TNF **(c)** protein levels secreted into the CCM in response to LPS treatment (100 ng/mL) in *Fh* +/+ or *Fh* -/- BMDMs for indicated timepoints, as assessed by ELISA (*n*=2 biological replicates performed in technical duplicate). Data is presented as mean ± SEM.

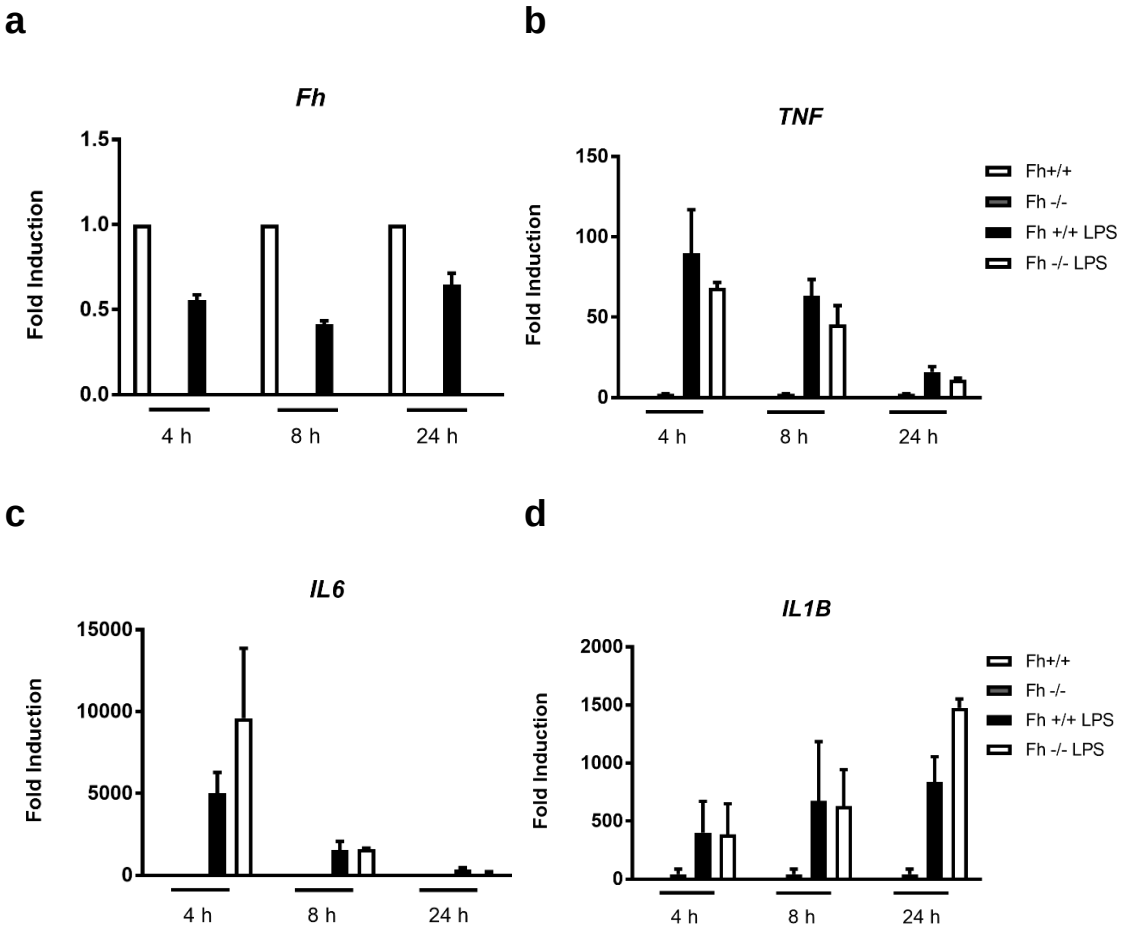

Figure 3.14 – *Fh* -/- deficiency has differential effects on cytokine mRNA levels

Relative fold change in mRNA levels of **(a)** *Fh*, **(b)** *TNF,* **(c)** *IL6* and **(d)** *IL1B* in response to LPS treatment (100 ng/mL) in *Fh* +/+ or *Fh* -/- BMDMs for indicated timepoints, as assessed by qPCR (*n*=2 biological replicates performed in technical duplicate). Data is presented as mean ± SEM.

a

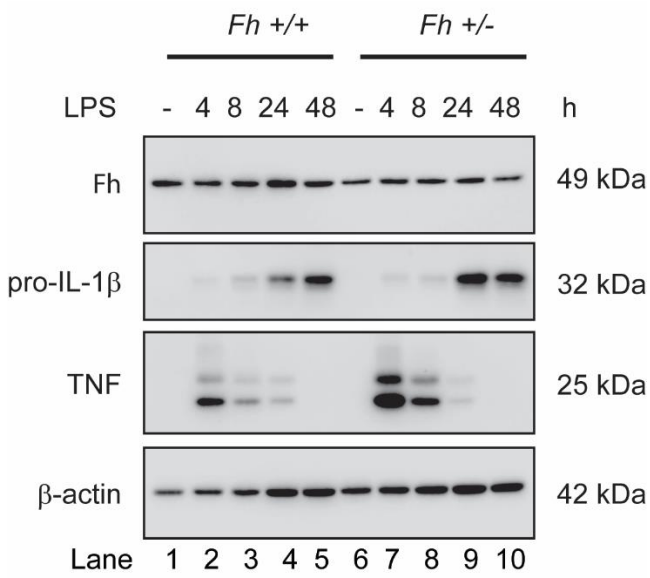

b

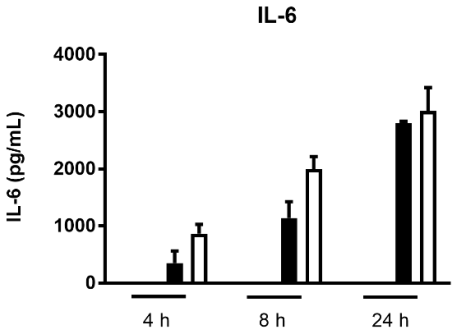

c

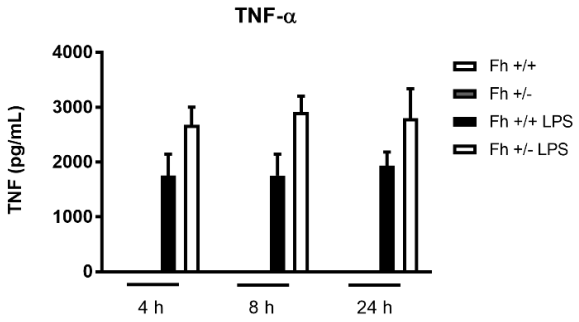

Figure 3.15 – *Fh* +/- deficiency increases pro-inflammatory cytokine production

(a) Protein expression of Fh, pro-IL-1β, TNF and the loading control β-actin in *Fh* +/+ or *Fh* +/- BMDMs in response to LPS treatment (100 ng/mL) for indicated timepoints, as assessed by western blot. The results shown are representative of two independent experiments. IL-6 **(b)** and **(c)** TNF protein levels secreted into the CCM in response to LPS treatment (100 ng/mL) in *Fh* +/+ or *Fh* +/- BMDMs for indicated timepoints, as assessed by ELISA (*n*=2 biological replicates performed in technical duplicate). Data is presented as mean ± SEM.

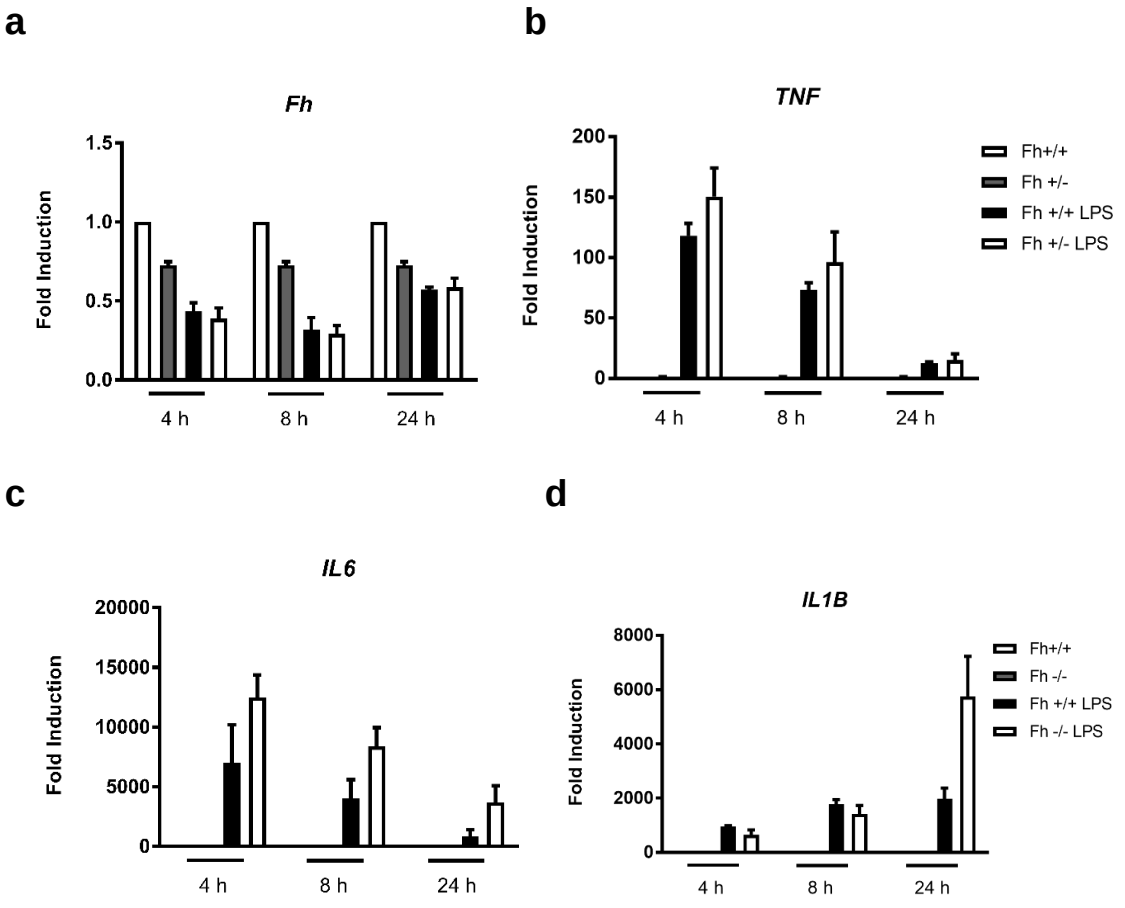

Figure 3.16 – *Fh* +/- deficiency has differential effects on cytokine mRNA levels

Relative fold change in mRNA levels of **(a)** *Fh*, **(b)** *TNF,* **(c)** *IL6* and **(d)** *IL1B* in response to LPS treatment (100 ng/mL) in *Fh* +/+ or *Fh* -/- BMDMs for indicated timepoints, as assessed by qPCR (*n*=2 biological replicates performed in technical duplicate). Data is presented as mean ± SEM.

a

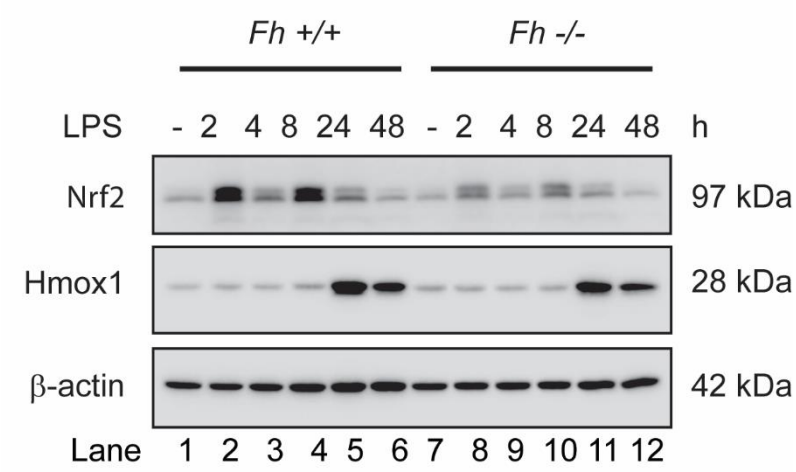

b

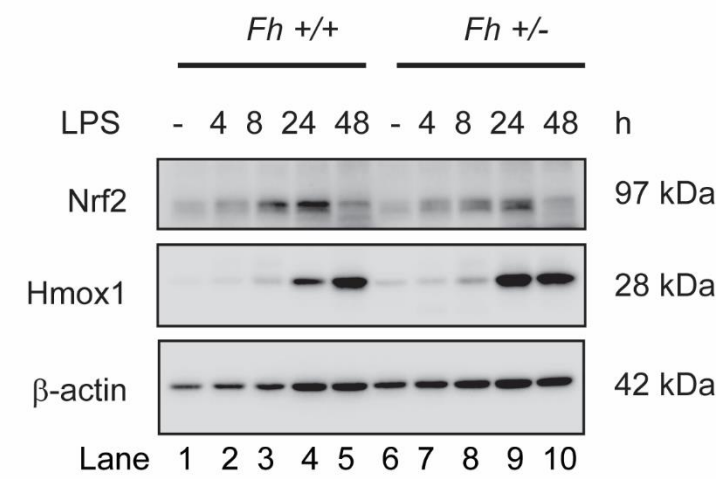

Figure 3.17 – *Fh* -/- and *Fh* +/- deficiency impairs induction of Nrf2 by LPS

Protein expression of Nrf2, Hmox1 and the loading control β-actin in **(a)** *Fh* +/+ or *Fh* -/- BMDMs and **(b)** *Fh* +/+ or *Fh* +/- BMDMs in response to LPS treatment (100 ng/mL) for indicated timepoints, as assessed by western blot. The results shown are representative of two independent experiments.

3.2.6 – LPS-induces fumarate-mediated protein succination

Whilst fumarate-mediated protein succination (Fig. 3.18a) is well documented under conditions of Fh deficiency and in mouse models of diabetes (176-178), whether this covalent modification occurs in LPS-activated macrophages has yet to be elucidated. To investigate protein succination in BMDMs a well validated antibody raised to a succinated peptide was employed (176).

Indeed, stimulation of BMDMs with LPS for 6 or 24 h resulted in an increase in protein succination (Fig. 3.18a), with a marked increase observable after 24 h (Fig. 3.18a; compare columns 1-3, 9-11 and 17-19 to lanes 7-8, 15-16 and 23-24). Protein extracts derived from *Fh -/-* MEFs, whereby fumarate is known to accumulate and induce succination, were used as a positive control demonstrating the specificity of the succination antibody (Fig. 3.18a; lane 25). Further to this, protein succination can also result in the accumulation of the metabolite, (S)-2-succinocysteine (2SC) (Fig. 3.19a), the final breakdown product arising from the degradation of succinated proteins and/or succinicGSH due to the irreversible nature of the thioether bond (175, 176). Utilising data generated from a semi-targeted metabolomics screen, 2SC was observed in both control and LPS-activated BMDMs (Fig. 3.19b) and largely appeared to be further increased in response to LPS stimulation reaching concentrations between 10 and 30 nM (Fig 3.19c).

a

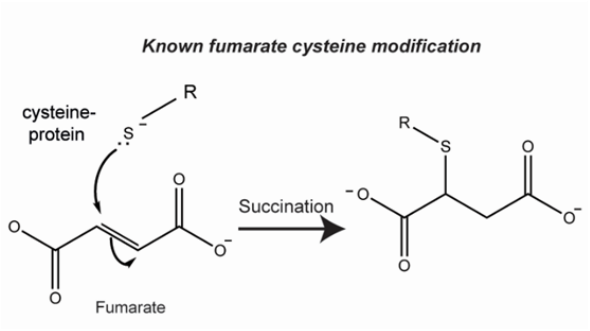

b

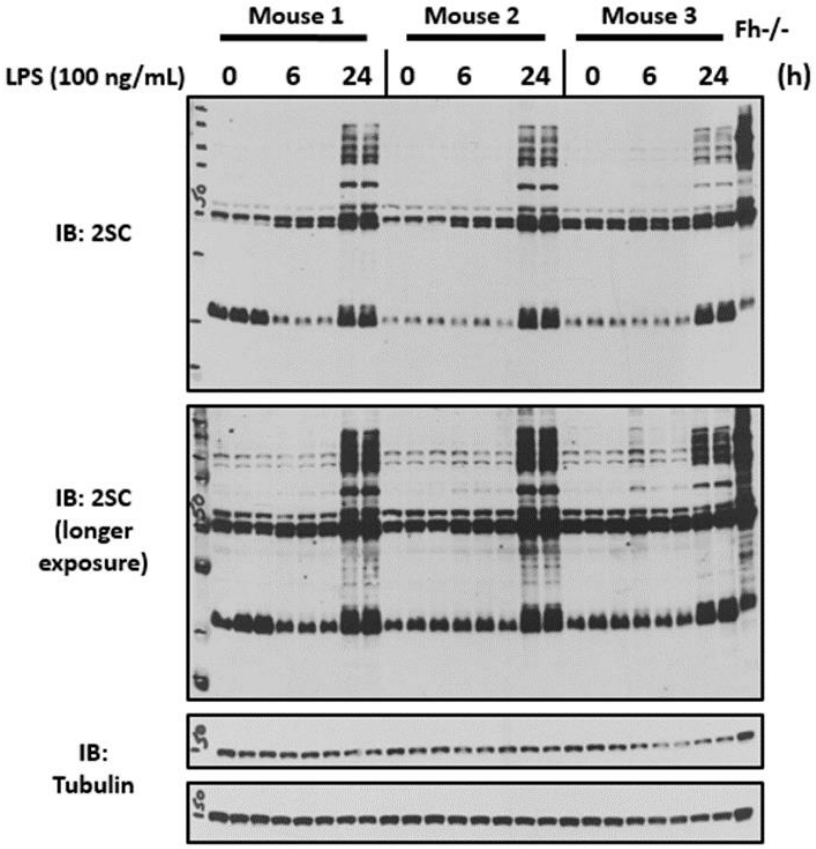

Figure 3.18 – LPS induces fumarate-mediated protein succination

(a) Schematic of fumarate-mediated cysteine modification termed succination. **(b)** Protein succination and the loading control tubulin in response to LPS treatment (100 ng/mL) for 6 and 24 h, as assessed by western blot (*n*=3). *Fh -/-* MEFs were used as a positive control.

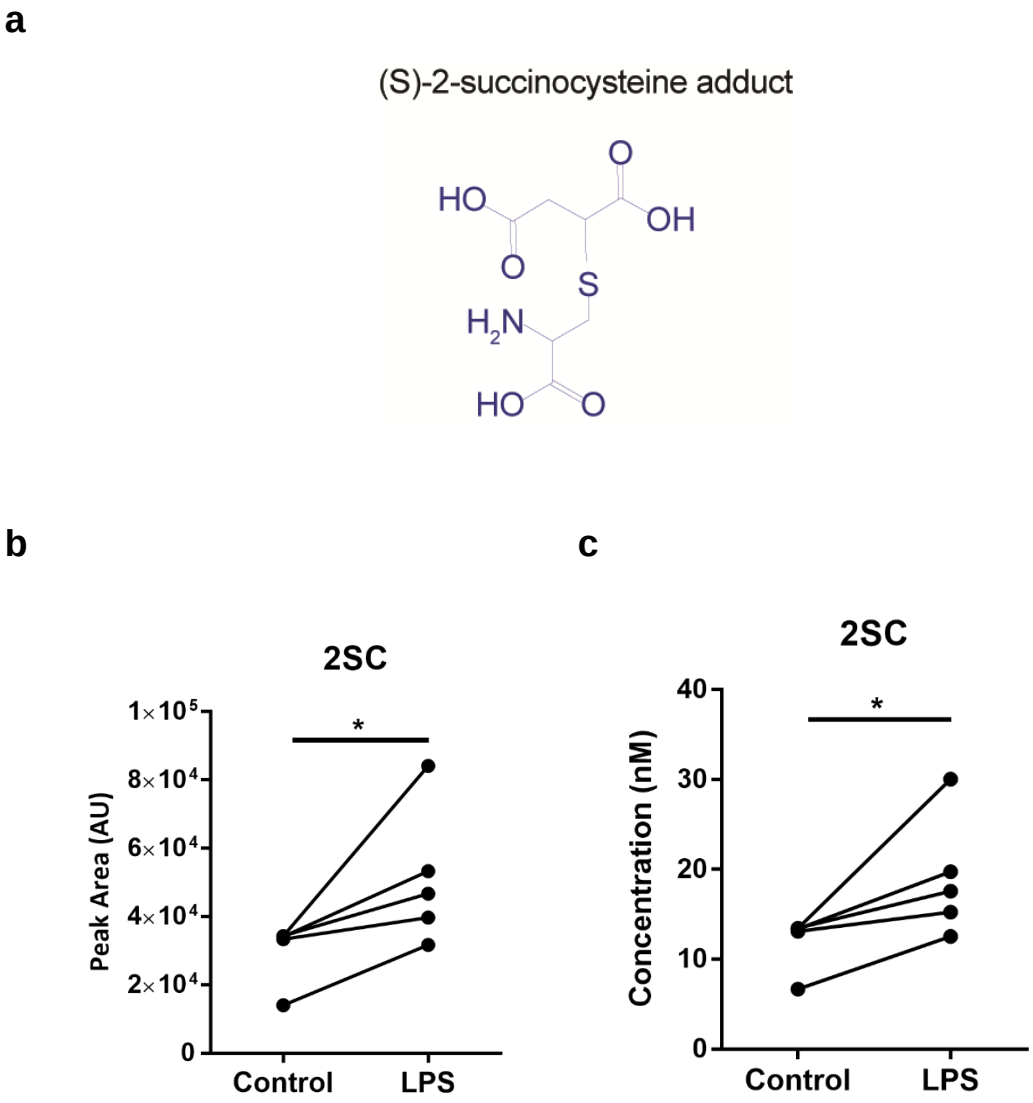

Figure 3.19 – LPS induces 2SC metabolite formation

(a) Chemical structure of the fumarate-cysteine metabolite 2SC. **(b)** Relative 2SC levels were determined by LC-MS in control or LPS-activated (100 ng/mL, 24 h) BMDMs (*n*=5 biological replicates performed in technical duplicate). Data is presented as mean. *P*-values were calculated using a paired t-test. **P* <0.05, ***P* <0.01, ****P* <0.001, *****P* <0.0001.

3.3 – Discussion

Recent findings on the role of Krebs cycle intermediates during inflammation have advanced our understanding of the complexity of immunometabolism. A precedent has now been set for metabolites generated by innate immune cells to have distinct functions as signalling entities and anti-bactericidal agents, beyond their role in bioenergetics. As such, the first aim of this project was to assess the previously uncharacterised role of fumarate accumulation in LPS-activated macrophages and to uncover the metabolic pathway(s) that govern its increase.

Evidence of increased fumarate levels in response to LPS was successfully confirmed, as previously reported (20, 45), whilst several metabolites involved in the aspartate-argininosuccinate shunt were also found to be significantly altered. Using CoMBI-T, Jha *et al* (2015) were the first to report the existence of an inflammatory aspartate-argininosuccinate shunt linking the Krebs cycle with NO production, noting increases in *Ass1* and argininosuccinate in response to LPS and IFN-γ (45). Furthermore, U-^{13}C-glutamine tracing revealed that carbon-labelling in malate was strikingly consistent with that found in argininosuccinate and aspartate, a common characteristic of metabolites partaking in common metabolic cycles (45). Jha *et al* (2015) went onto suggest that the increase observed in malate and fumarate were likely owed to this argininosuccinate shunt, however, a direct link between the shunt and fumarate was never shown (45). Consistent with this data, a significant increase in *Ass1* mRNA expression and protein levels was observed using qPCR and an unbiased quantitative proteomic screen, respectively, whilst inhibition of GOT1/2 and aspartate synthesis with AOAA lowered fumarate levels in both control and

activated macrophages, confirming a role for the aspartate-argininosuccinate shunt in regulating fumarate accumulation. Unfortunately, due to technical issues, U-^{13}C-glutamine tracing in LPS-activated macrophages and metabolic analysis by LC-MS failed to conclusively identify argininosuccinate and fumarate peaks, as they were below the limit of detection in that particular experiment. As such, confirmation of the aspartate-argininosuccinate shunt via U-^{13}C-glutamine tracing and/or tracing from U-^{13}C-aspartate into fumarate would need to be performed in future work. Furthermore, U-^{15}N-glutamine could be used to trace the fate of isotopically labelled nitrogen into argininosuccinate and arginine upon LPS stimulation. Pharmacological inhibition of Ass1 using α-Methyl-DL-aspartic acid (MDLA), in addition to genetic ablation, has recently been demonstrated to decrease intracellular fumarate levels in colorectal cancer cells thus impairing cancer pathogenicity, further supporting its role as a key regulator of fumarate production (186). Interestingly, DMF was also shown to induce *Ass1* mRNA expression suggesting a positive feedback loop may exist between fumarate and the shunt. In the same study, Ass1 itself was shown to be a cysteine-reactive metabolic enzyme (186), but how or if this affects its enzymatic activity or regulation remains to be explored.

In addition to increased Ass1, a small but significant decrease in both *Fh* mRNA expression and Fh protein levels was also observed upon LPS stimulation. As Fh catalyses the reversible hydration of fumarate to malate, *Fh* loss is well-reported to elevate intracellular fumarate (175, 178). Homozygous mutations of *Fh* lead to the lethal metabolic disorder fumaric aciduria, whilst heterozygous *Fh* mutations cause hereditary leiomyomatosis and renal cell carcinoma (HLRCC), a cancer syndrome characterised by cutaneous

leiomyoma, uterine fibroids and type 2 papillary renal cell cancer (178). As the oncogenic properties of *Fh* loss have mostly been ascribed to the intracellular accumulation of fumarate, LPS-mediated suppression of Fh is likely to synergise with increased Ass1 expression and the aspartate-argininosuccinate shunt to elevate fumarate in macrophages.

Prior to this study, little was known about the role of endogenous fumarate and cytokine production in macrophages. To elucidate this, three pharmacological agents and two genetic approaches were employed as experimental models to either lower or elevate intracellular fumarate levels. As mentioned, the first tool employed was AOAA an inhibitor of GOT1/2 and the aspartate-argininosuccinate shunt [22], which was verified to lower endogenous fumarate levels. Interestingly, inhibition of the aspartate-argininosuccinate shunt significantly attenuated LPS-induced pro-inflammatory cytokine production. Specifically, pre-treatment of LPS-activated macrophages with AOAA appeared to attenuate IL-6 expression and secretion, as previously demonstrated (45). Furthermore, AOAA was also found to significantly inhibit LPS-induced TNF and pro-IL1β levels, TNF secretion and *IL1B* mRNA expression, but not *TNF* mRNA expression. As AOAA is known to have off-target effects (187), the specificity of GOT2 inhibition in mediating these effects was confirmed by rescuing the decrease in either TNF or pro-IL1β expression by pre-loading macrophages with aspartate. However, GOT2 also participates in the malate-aspartate shuttle (MAS), a transport-transamination-redox cycle that enables the transfer of electrons from cytosolic NADH (which is impermeable to the IMM) into the mitochondrial matrix to enter the ETC (188, 189). The shuttle is also important for regenerating cytosolic NAD^+ to maintain glycolytic flux (188, 189). Indeed,

Jha *et al* (2015) also found that pre-treatment of LPS-activated BMDMs with AOAA attenuated the induction of aerobic glycolysis and prevented the inhibition of respiration, as assessed by extracellular acidification rates (ECAR) and oxygen consumption rates (OCR), respectively, using Seahorse technology (45). The authors attributed this result on respiration (and indeed IL-6) to the inhibition of NO production, which is known to suppress mitochondrial respiration in both murine dendritic cells and macrophages (190, 191). However, inhibition of the MAS could also explain the observed inhibition of aerobic glycolysis, which is an important regulator of IL1β, by preventing cytosolic NAD^+ regeneration (20). Hypothetically, Ass1 and the shunt would siphon off aspartate from the MAS, and so whether the MAS is functional in LPS-activated macrophages remains an open question. One way to assess this would be to evaluate NADH mitochondrial shuttling by tracing a deuterium from glucose (^{2}H-glucose) through glyceraldehyde 3-phosphate and NADH into malate, as previously done in alternatively activated macrophages (192). To further confirm and dissect the role of Ass1 and the aspartate-argininosuccinate shunt in the regulation of cytokine production (and fumarate production), the inhibitor, MDLA, or genetic ablation of Ass1 could be employed as experimental models (186). As such, these models would better enable the separation of the aspartate-argininosuccinate shunt from the malate-aspartate shuttle in future studies. However, with MAS functionality likely to be low, the use of AOAA supports a role for the shunt as an important metabolic module that regulates pro-inflammatory macrophage activation.

To assess whether fumarate itself is directly involved in regulating cytokine production, the first tool employed was DMF, a cell permeable fumarate analogue and a key component of the anti-inflammatory drugs Fumaderm® and Tecfidera®

used to treat psoriasis and relapse-remitting MS, as previously mentioned (180, 181). Furthermore, DMF has previously been shown to suppress the induction of pro-inflammatory cytokines, such as IL-1β, in LPS-activated microglia and astrocytes (163). These published findings would appear to exclude the possibility that fumarate would promote pro-inflammatory cytokine production because of an inflammatory argininosuccinate shunt, instead suggesting fumarate would be an anti-inflammatory metabolite that acted as a negative regulator of cytokine production.

Consistent with previous reports (163), pre-treatment of BMDMs with DMF was shown to potently inhibit LPS-induced *IL1B* and *IL6* mRNA levels, IL-6 secretion and pro-IL-1β expression, however, a significant increase in LPS-induced TNF protein levels and secretion was also observed. This suggested that fumarate may exert both pro- and anti-inflammatory effects. Mechanistically, it has been suggested that the anti-inflammatory action of DMF is mediated by alkylation of key redox sensing cysteines on KEAP1 (137, 162). Importantly, KEAP1 is a redox-sensitive E3 ubiquitin ligase substrate-adaptor essential for ubiquitin-mediated Nrf2 proteolysis (137). As such, KEAP1 modification and inhibition is an integral step in the stabilisation of Nrf2 (162). Nrf2 itself is an anti-oxidant transcription factor and a negative regulator of pro-inflammatory cytokine production in macrophages (159) and during experimental sepsis (158). Likewise, Nrf2 has been proposed to mediate the anti-inflammatory effect of DMF in experimental autoimmune encephalomyelitis (EAE), a mouse model of MS (164). Indeed, a marked increase in Nrf2 and its downstream target Hmox1 was observed in macrophages treated with DMF, suggesting it may play a role in the suppression of LPS-induced IL-6 and IL-1β in this context. Interestingly, induction

of TNF by DMF was further augmented upon genetic silencing of Nrf2, suggesting its acute activation partly masked DMFs ability to induce TNF.

More recently, the relevance of DMF-induced Nrf2 stabilisation in the treatment of EAE has been called into question (193). Furthermore, a chemical proteomic map of DMF sensitive cysteines also supported a Nrf2-independent role for the inhibition of primary T cell activation, which was in part owed to electrophilic inactivation of PKCθ thus blocking its interaction with CD28 (194). It must also be noted that DMF has previously been shown to impair NF-κB signalling in a Nrf2-independent manner, via inhibition of M1 and TLR-induced M1 and K63 ubiquitin chain formation in primary macrophages (195, 196). However, the concentration of DMF at which NF-κB signalling was inhibited was higher than the dose used in this study and indeed no inhibition was apparent at the lower dose (195). Furthermore, McGuire *et al* (2016) pre-treated BMDMs for 4 h in comparison to the 1 h pre-treatment used here, which is important as alkylation is a time-dependent process and essential in mediating the effects of DMF (195). Likewise, *TNF* mRNA levels were unaffected at this dose indicative of NF-κB signalling remaining intact. As such, inhibition of NF-κB signalling is unlikely to play a role in IL-6 and IL-1β inhibition here.

As previously mentioned, endogenous fumarate is an electrophilic α, β-unsaturated carbonyl compound that can induce protein succination (176). However, dimethyl esterification renders it an activated Michael acceptor as the thiol-reactive alkene component of fumarate is directly conjugated to both carboxyl groups (162, 197). Furthermore, DMF has been shown to chemically react with GSH rapidly, and at physiological pH, to yield a 1:1 mixture of both

diastereomeric 2-(S-glutathionyl)-succinic acid dimethyl esters *in vitro* and deplete intracellular GSH levels, which can result in acute and superfluous Nrf2 activation (162, 197). The lowest unoccupied molecular orbital (LUMO), which is the lowest energy orbital that has the scope to accept electrons thus characterising the susceptibility of a molecule to nucleophilic attack, of DMF is 1.5 eV. However, fumarate's LUMO, 12.2 eV, is far higher in energy than that of DMF, which increases the energetic barrier to covalent bond formation with nucleophilic cysteines (198). As such, DMFs increased reactivity may give rise to confounding variables, such as acute GSH depletion and electrophilic stress, when trying to use it as a tool to gauge the physiological functions of endogenous fumarate. More recently, depletion of intracellular GSH levels by DMF can also more broadly elicit an electrophilic stress response inducing activating transcription factor 3 (ATF3), which acts to inhibit IκBζ levels (127). Inhibition of IκBζ blocks secondary transcriptional responses in macrophages, such as *IL6* mRNA expression, but not primary transcriptional responses, such as *TNF* mRNA expression (127). This phenomenon likely explains the observed inhibition in *IL6* mRNA expression and IL-6 secretion by DMF in LPS-activated macrophages.

To counteract the issue of thiol reactivity, MMF was also employed to study the effects of increased fumarate levels. Unlike DMF, MMF was less able to inhibit LPS-induced pro-IL-1β, with some small inhibition observable after 24 h of LPS stimulation. This correlated with weaker induction of Nrf2 and Hmox1, consistent with previous reports on the differential effects of fumaric acid esters and Nrf2 stabilisation (162). It must also be noted that MMF has been identified as a potent agonist of the hydroxycarboxylic acid receptor (HCA2), a G-protein

coupled receptor highly expressed on macrophages (182, 183). Activation of HCA2 with niacin, in both bone marrow-derived and alveolar macrophages, has been reported to block LPS-induction of pro-inflammatory cytokines in an NF-κB-dependent manner, whilst it has also been suggested that HCA2 mediates the protective effect of DMF and MMF in EAE (182, 199). However, unlike DMF, MMF does not inhibit NF-κB signalling, which suggests inhibition of IL-1β occurs independently of HCA2 activation and NF-κB activity in this context (196). However, after 24 h MMF appeared to induce *IL1B* mRNA and after 48 h pro-IL1β levels. MMF can also induce HIF1α stabilisation via inhibition of the PHDs (65) and while that wasn't explored here it's likely the cause of this increase. Unlike DMF, MMF did not inhibit IL-6 secretion and indeed after 24 h there appeared to be a slight increase. This result also suggests that the inhibitory effect of DMF is due to its increased thiol reactivity, acute GSH depletion and electrophilic stress and as such is not representative of endogenous fumarate, as previously mentioned.

Intriguingly, MMF also potentiated LPS-induced TNF protein expression and secretion but had no effect on mRNA levels. This observation was in line with Asadullah *et al* (1997), whereby they observed increased TNF secretion from control and psoriatic peripheral blood mononuclear cells (PBMCs) (200). The authors further suggested that the well-documented adverse effects experienced by psoriatic patients after first initiating therapy could be owed in part to increased TNF production (200). More recently, Arts *et al* (2016) suggested that accumulation of fumarate in response to β-glucan was essential for trained immunity in macrophages (65). To discern the role of fumarate in this process, they also utilised MMF and showed that it increased H3K4me3 via

inhibition of the KDM5B family of histone demethylases. Furthermore, they also showed MMF could potentiate TNF secretion in their experimental system (65). However, it must be noted that the authors never showed whether MMF could induce *TNF* mRNA expression. In contrast to Arts *et al* (2016), results from this study suggest that MMF regulation of TNF occurs independently of its transcriptional regulation.

Although the reactivity of MMF more closely resembles that of fumarate, mono esterification may still render it more electrophilic as the thiol-reactive alkene component of fumarate is directly conjugated to both carboxyl groups, as aforementioned. MMF does not react as acutely with GSH as DMF, with theoretical calculations indicating this stems from MMF's higher lying LUMO of 6.4 eV, increasing the energy required for covalent bond formation (198). This higher lying LUMO would also enable it to react more readily with thiol groups on macromolecules (197). However, fumarate's LUMO is even higher than MMF at 12.2 eV, as previously mentioned. As such, to determine the role of endogenous fumarate on cytokine production, homo- and heterozygous Fh-deficient BMDMs were utilised, which are known to accumulate fumarate in other cell types (175, 177, 184). Like MMF, pro-IL-1β levels weren't increased in *Fh -/-* BMDMs, but an increase in mRNA expression was observed after 24 h of LPS stimulation. IL-6 mRNA levels and secretion were also unaffected in *Fh -/-* macrophages. However, LPS-induced TNF production was augmented in *Fh -/-* deficient BMDMs, comparably with that seen with MMF. As complete deletion of *Fh* truncates the Krebs cycle and drastically impairs OXPHOS (178), a less deleterious means to elevate endogenous fumarate was sought. To this end, the ability of LPS to modulate cytokine production in *Fh +/-* deficient BMDMs was

examined, whereby there is only a partial loss of Fh and less severe impairment of OXPHOS, but fumarate can still accumulate (184), as previously discussed. Indeed, *IL1B* mRNA expression and pro-IL-1β levels were increased in *Fh* +/- BMDMs after 24 h of LPS stimulation. IL-6 mRNA levels and secretion appeared to be increased at early timepoints. Interestingly, HIF overexpression and stabilisation, a key regulator of IL-1β in macrophages, correlates with genetic ablation of Fh and the accumulation of fumarate, which can act to competitively inhibit PHDs and promote evasion from von Hippel-Lindau-dependent degradation (201, 202). Fh loss can also promote ROS-dependent HIF stabilisation through glucose addiction (203). Fumarate has also been suggested to promote pseudohypoxia and increase HIF1α levels via non-canonical TBK1 activation, p65 phosphorylation and p65 accumulation at the HIF1α promoter (204). How both ROS levels and metabolite abundance, especially fumarate, are affected in Fh-deficient macrophages remain to be investigated, and how these regulate cytokine production will be an important component of future work. A more comprehensive investigation into other signalling pathways, such as the non-canonical NF-κB pathway, could also be explored. Furthermore, LPS-induced TNF protein levels and secretion, but not mRNA expression, were augmented in *Fh* +/- deficient BMDMs, comparably to MMF, DMF and *Fh* -/- BMDMs. Evidence from *Fh* +/- macrophages would suggest that endogenous fumarate can positively regulate IL-1β, IL-6 and TNF levels and therefore act as a pro-inflammatory signal to promote cytokine production. It also suggests that some of the effects observed by inhibiting the aspartate-argininosuccinate shunt may be due to inhibition of fumarate production.

Intriguingly, Fh can be localised to the cytosol, in addition to mitochondria (205), while a small but significant decrease in Fh is observed in LPS-activated macrophages. It would be interesting to examine whether the localisation and/or levels of Fh changes between cellular compartments in response to LPS in future studies. It could be possible that a decrease in *Fh* mRNA expression may preferentially decrease either the mitochondrial or extra-mitochondrial Fh levels if there is a difference in their half-life in the macrophage. Indeed, cytosolic Fh purified from rat liver has a much shorter half-life (4.7 days) than mitochondrial Fh (9.7 days) (206). This would suggest that decrease Fh mRNA expression would preferentially lower cytosolic Fh and increase extra-mitochondrial fumarate levels. Furthermore, Fh -/- kidney cells are known to synthesise argininosuccinate directly from fumarate via reversal of the argininosuccinate lyase (205). A phenomenon reversed by re-expression of cytosolic Fh (205). This demonstrates how closely interlinked Fh is with the Krebs bicycle and unearthing how this pathway operates in LPS-activated Fh -/- and Fh +/- macrophages would also be important to examine in future studies.

Genetic loss of Fh and subsequent accumulation of endogenous fumarate has previously been shown to activate Nrf2 in the kidney and found to be a contributing factor to cyst development and HLRCC (185). Adam *et al* (2011) also went on to show that Nrf2 stabilisation arose from fumarate-mediated succination and inactivation of KEAP1 (185). Furthermore, fumarate has also been shown to be cardioprotective via activation of Nrf2 in FH-deficient cardiomyocytes (174). In stark contrast, LPS-induced Nrf2 stabilisation was surprisingly decreased in both *Fh* +/- and *Fh* -/- BMDMs, which suggests endogenous fumarate is unlikely to play a major role in the induction of Nrf2 in macrophages and could also in part

explain the more pro-inflammatory phenotype observed in these macrophages. Interestingly, LPS maintained its ability to induce Hmox1 levels despite decreased Nrf2 stability, whilst Hmox1 levels were increased after 24 h in *Fh* +/- BMDMs. As well as a key Nrf2 target gene, *Hmox1* is also regulated at the transcriptional level by hypoxia and HIF1α stabilisation (207), as such, induction of Hmox1 in response to LPS is likely mediated (at least in part and in this context) by HIF1α.

Despite the individual caveats of each experimental model used to try and explore the role of fumarate accumulation in macrophages, as discussed, they all consistently point to a role for fumarate in the regulation of TNF (Fig. 3.20). To summarise, LPS-activated macrophages induce Ass1 and the aspartate-argininosuccinate shunt, which results in increased fumarate levels. Inhibition of the aspartate-argininosuccinate shunt (and fumarate accumulation) with AOAA inhibits TNF protein production, while treatment of macrophages with both cell permeable fumarate derivatives, MMF and DMF, elevate LPS-induced TNF protein levels. Furthermore, LPS-induced TNF protein levels are further elevated in Fh +/- and Fh -/- BMDMs, where endogenous fumarate levels will be high. The increase in TNF production by fumarate appears to occur at the post-transcriptional level.

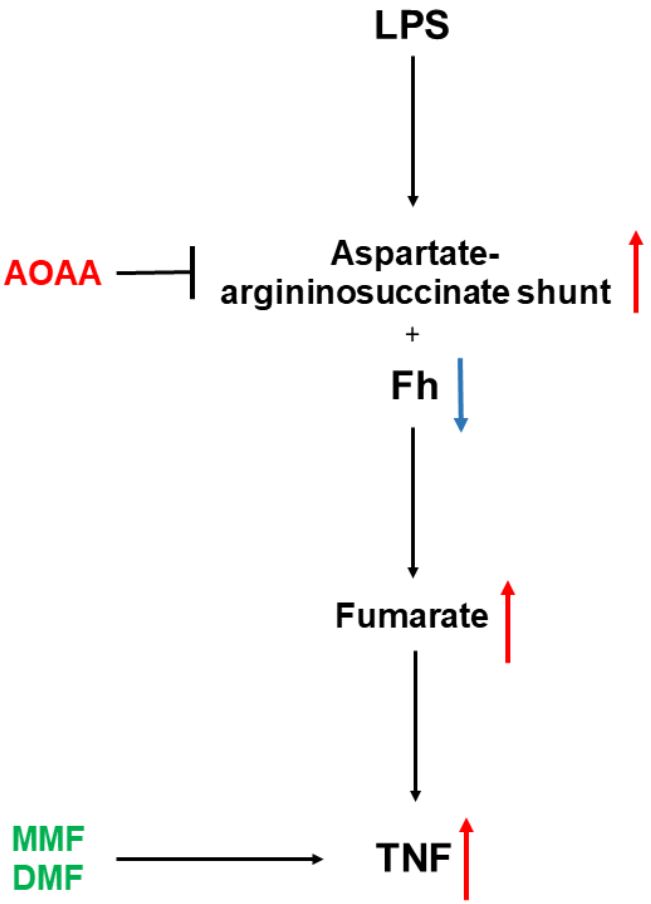

Figure 3.20 – Summary of experimental data on TNF production

Brief overview of how the different experimental tools employed influenced TNF protein production in LPS-activated macrophages.

Whilst these findings suggest that endogenous fumarate may play role in the post-transcriptional regulation of TNF in LPS-activated macrophages, the mechanism remains elusive. As aforementioned, Arts *et al* (2016) suggested fumarate-mediated epigenome remodelling was responsible for increased cytokine production during innate immune training (65), however, in this system no increase in *TNF* mRNA was observed, suggesting an alternative mechanism may also exist. Fumarate is known to non-enzymatically and irreversibly alkylate protein cysteine residues, a modification termed succination, in conditions in which fumarate levels are elevated, such as that observed in FH-deficient tumours (176), as previously mentioned. Based on these observations, it was hypothesised and experimentally confirmed that LPS could induce fumarate-mediated protein succination, the first report of this modification in macrophages. Furthermore, the breakdown product and established biomarker of succination, 2SC (175, 176), was also successfully detected in control and LPS-activated macrophages.

Interestingly, fumarate-mediated succination of key redox sensing cysteines on the glycolytic enzyme GAPDH is a well-reported phenomenon and known to inhibit its enzymatic activity (176, 177). DMF has also been reported to inhibit glycolysis in a mouse model of Parkinson's disease (208), whilst inhibition of glycolysis with 2-DG in LPS-activated macrophages has previously been shown to potently inhibit IL-1β (20). In addition to its role in glycolysis, GAPDH also acts as an RNA binding protein to post-transcriptionally regulate mRNAs containing ARE elements in their 3'UTR (22, 115). More specifically, GAPDH is known to post-transcriptionally repress TNF translation in macrophages (22, 115). Intriguingly, treatment of GAPDH with the oxidising agent diamide was

demonstrated to markedly decrease the binding of GAPDH to the 3'UTR of IFN-γ (209). This suggests that key cysteines of GAPDH may act as a "sulfhydryl switch" to regulate its RNA binding capacity. More recently and during this study, Kornberg *et al* (2018) suggested that a potential mechanism of elevated fumarate levels is to negatively regulate glycolysis via succination of the active site cysteine residue (C152) in GAPDH (179). This suggestion arose from the observation that the cell-permeable fumaric esters, dimethyl fumarate (DMF) and MMF, currently used to treat psoriasis and relapse-remitting multiple sclerosis (MS), modify and irreversibly inhibit GAPDH enzymatic activity and aerobic glycolysis in peripheral blood mononuclear cells (PBMCs) from mice and MS patients treated with DMF (179). Induction of aerobic glycolysis is a key marker of activated immune cells and represents an important phenotypic switch to facilitate proliferation and immune cell effector functions. Two pro-inflammatory T cell subsets implicated in the pathogenesis of MS, namely T_H1 and T_H17 cells, rely heavily on aerobic glycolysis and treatment with DMF or MMF inhibited their development *in vitro*, as previously reported. Importantly, inhibition of aerobic glycolysis by the specific GAPDH inhibitor heptelidic acid (HA) and 2-deoxyglucose (2-DG) recapitulated the immunomodulatory effects of DMF *in vitro*, whilst *in vivo* administration of HA inhibited the development of experimental autoimmune encephalomyelitis (EAE), a murine model of MS. As such, this represents an important proof-of-principle study supporting the concept that metabolically targeted therapies may be used successfully to treat inflammatory-driven diseases, whilst also providing mechanistic insight into the anti-inflammatory action of DMF.

Intriguingly, endogenous fumarate was also found to succinate GAPDH in both mouse and human macrophages, which suggests elevated fumarate levels and succination may act as a signal in inflammation. However, they provided no evidence that endogenous fumarate was itself anti-inflammatory and their potent anti-inflammatory effects could also be attributed to the higher lying LUMOs of DMF and MMF (and doses used). However, Kornberg *et al* (2018) also showed that DMF could inhibit the RNA binding capacity of GAPDH. From this and the accumulated data demonstrated here, it would be tempting to speculate that endogenous fumarate may succinate GAPDH on key cysteine residues to relieve its post-transcriptional repression of TNF (Fig. 3.21). Despite this, the precise role of the aspartate-argininosuccinate shunt and fumarate accumulation in macrophages and whether fumarate-mediated protein succination regulates IL-1β, IL-6 or TNF is not yet fully established.

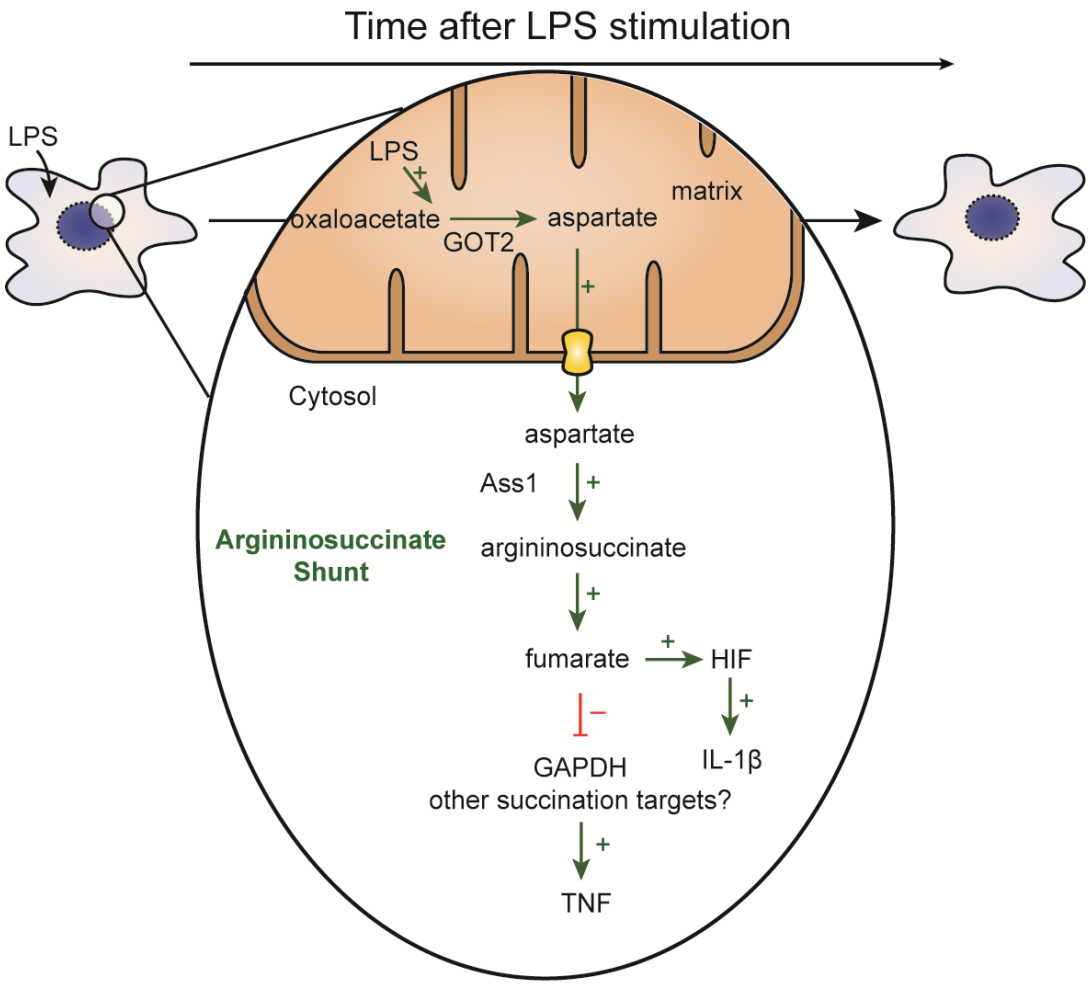

Figure 3.21 – Proposed model of fumarate-mediated cytokine regulation

Ligation of TLR4 by LPS results in the transcriptional upregulation of Ass1 and induction of the aspartate-argininosuccinate shunt. An increase in the shunt promotes fumarate accumulation, whereby it can positively regulate pro-inflammatory cytokine levels, namely IL-1β and TNF. Although the mechanism isn't clear, it's possible that fumarate can increase *IL1B* mRNA by inducing HIF1α stabilisation via inhibition of PHDs. Furthermore, fumarate can induce protein succination. As such, it is proposed that fumarate succinates GAPDH on key redox sensing cysteines, which inhibit its ability to post-transcriptionally repress *TNF* translation. Therefore, it is possible that the function of the aspartate-argininosuccinate shunt (in addition to supporting NO synthesis) is to generate fumarate in the cytosol as a pro-inflammatory signal to regulate cytokine production.

Chapter 4:

Itaconate is an anti-inflammatory metabolite that inhibits SDH and activates Nrf2

4.1 – Introduction

One of the most thought-provoking examples of an immunomodulatory metabolite that results from Krebs cycle rewiring is *cis*-aconitate-derived itaconate (100, 117). As mentioned, recent work by Cordes *et al* (2016) and Lampropoulou *et al* (2016) nicely demonstrated a role for itaconate as a competitive inhibitor of SDH that governed succinate accumulation in inflammatory macrophages (48, 49). Furthermore, Lampropoulou *et al* (2016) also demonstrated a key role for itaconate in the regulation of pro-inflammatory cytokine production, which is thought to arise from itaconate-mediated SDH inhibition (49).

Concerningly, a recent discovery found that DMI, the tool compound used in the study by Lampropoulou and colleagues, is not metabolised to itaconate intracellularly (210). It was also found that [^{13}C] itaconate in cell culture media was sufficient to increase intracellular levels of unlabelled succinate, with no evidence of cellular uptake (210). The authors posited this could be due to a receptor-mediated effect especially given the discovery of metabolites signalling via GPCRs, for example, the succinate receptor SUCNR1 (89). If an itaconate receptor did exist, the results of this study could indicate the *Irg1* -/- phenotype is in part due to a loss of autocrine or paracrine signalling by secreted itaconate. Importantly, esterification of both carboxyl groups is also predicted to increase the electrophilicity of itaconate and thus it may behave as a cysteine alkylating agent (210). This suggests the metabolic effects of DMI observed in macrophages do not appear to be due to intracellular itaconate accumulation but may instead be due to electrophilic inactivation of metabolic enzymes. This idea is partially supported since an RNA seq screen performed by Lampropoulou *et*

al (2016) reports an upregulation of genes involved in Phase II conjugation, glutathione conjugation and biological oxidations upon treatment with DMI (210). As such, improved methods of delivering itaconate to macrophages and other immune cells will be important to understand the metabomodulatory properties of this metabolite.

Furthermore, the role of IRG1 and itaconate production in regulating metabolism and cytokine production, beyond its role in SDH inhibition, has yet to be explored. Interestingly, itaconate is considered a relatively weak competitive inhibitor of SDH (135) and so it remains a possibility that some additional yet unidentified mechanism also exists that enables IRG1 and itaconate to modulate cytokine production.

4.2 – Results

4.2.1 - LPS promotes metabolic rewiring to facilitate itaconate and succinate production

An untargeted metabolomics screen utilising LC-MS was first used to confirm elevated itaconate levels (Fig. 4.1a, b) and the prototypical pro-inflammatory metabolite succinate (20) (Fig. 4.1a, c) in BMDMs stimulated with LPS. A full list of the significantly upregulated (red) or downregulated (blue) metabolites in LPS-activated BMDMs (Fig. 3.1a and Fig. 4.1a) can be found in Table 4.1. Itaconate, which was only recently found to be a mammalian metabolite, is synthesised from the Krebs cycle intermediate *cis*-aconitate by the mitochondrial decarboxylase Irg1 (also known as CAD) (100). Utilising data generated from an unbiased quantitative proteomic screen, which used isobaric tandem mass tags (TMTs) coupled to LC-MS, a significant increase in Irg1 (12.7-fold) was observed in LPS-activated BMDMs when compared to the unstimulated control (Fig. 4.2a, b).

In response to LPS, macrophages initiate rewiring of key metabolic pathways, such as the Krebs cycle, in addition to promoting flux through glycolysis and glutaminolysis (20, 45). This metabolic rewiring results in the accumulation of several Krebs cycle-derived metabolites, namely succinate, fumarate and itaconate, as previously mentioned (20, 45). As the role of itaconate in regulating macrophage function remains relatively unexplored, the intracellular volume of control (Fig. 4.3a) and LPS-activated (Fig. 4.3b) BMDMs was determined using AO, confocal microscopy and 3D reconstruction (171) to facilitate absolute quantification of itaconate and other metabolites in this experimental system. Interestingly, a clear change in morphology change was

observed in LPS-activated BMDMs (Fig. 4.3b), which became more heterogeneous in shape, but consistently flattened with observable projections, in comparison to the more columnar appearance of the unstimulated macrophages (Fig. 4.3a). Despite differences in morphology, the volume of unstimulated macrophages (4.55 x 10^{-12} L) and LPS-stimulated macrophages (4.68 x 10^{-12} L) was relatively unchanged.

Following this, a targeted metabolomics screen coupled with isotopic labelling, again using LC-MS, was utilised to assess the relative contribution of glucose and glutamine carbon to itaconate synthesis in control and LPS-activated BMDMs. Glucose (6-carbon compound) is converted to pyruvate (3-carbon compound), via glycolysis, which is subsequently converted to acetyl-CoA by the pyruvate dehydrogenase complex (PDHC), thus enabling the entry of 2 carbon units into the TCA cycle (Fig. 4.4a). As such, catabolism of U-^{13}C-glucose can result in the formation of differentially labelled isotopologues of Krebs cycle intermediates, such as citrate, and their derivatives, such as itaconate, as was observed in both control and LPS-activated BMDMs (Fig. 4.4a, b). Around 62% of the total pool of itaconate contained glucose-derived carbon (Fig. 4.4b). Of note, was a significant increase in the m+1 isotopologue of itaconate (~30 % of the total pool) upon LPS stimulation (Fig. 4.4c, d). Absolute quantification revealed itaconate reached concentrations of ~ 3.5 mM in LPS-activated macrophages (Fig. 4.4c). Catabolism of U-^{13}C-glucose can also result in the labelling of succinate, as such, tracing of glucose carbon into succinate was also examined to assess whether it was a major contributor to succinate accumulation. Whilst no glucose carbon was found to label succinate in resting macrophages, an increase in the m+2 isotopologue of succinate (~ 20% of the

total pool) was observed (Fig. 4.6a, c). Furthermore, absolute quantification revealed succinate reached concentrations of ~ 3 mM in LPS-activated macrophages (Fig. 4.6b).

Glutaminolysis, aka glutamine anaplerosis, represents an important mechanism for the replenishment of Krebs cycle intermediates (20). Glutamine anaplerosis has previously been shown to represent an important mechanism contributing to increased succinate levels in LPS-activated macrophages, as previously mentioned. Like U-^{13}C-glucose, U-^{13}C-glutamine can result in the formation of differentially labelled isotopologues of Krebs cycle intermediates with the m+4 isotopologue generally the most predominant (Fig. 4.5a). Similarly, ~ 60% of the total pool of itaconate contained glutamine-derived carbon (Fig. 4.5b). Of note, was a significant increase in the m+4 isotopologue of itaconate (~ 25% of the total pool) upon LPS stimulation (Fig. 4.5c, d), whilst absolute quantification revealed itaconate reached concentrations of ~ 5 mM in LPS-activated macrophages in this instance (Fig. 4.5c). Confirming previous reports, the labelling of succinate from U-^{13}C -glutamine increased from less than 10 % of the total pool in unstimulated control conditions to close to 50 % of the total pool in LPS stimulated conditions (Fig. 4.7b). Of note, was a significant increase in the m+4 isotopologue of succinate (~ 28% of the total pool) upon LPS stimulation (Fig. 4.7b, d). Absolute quantification of succinate again revealed it accumulated to ~ 3 mM in LPS-activated BMDMs (Fig. 4.7c).

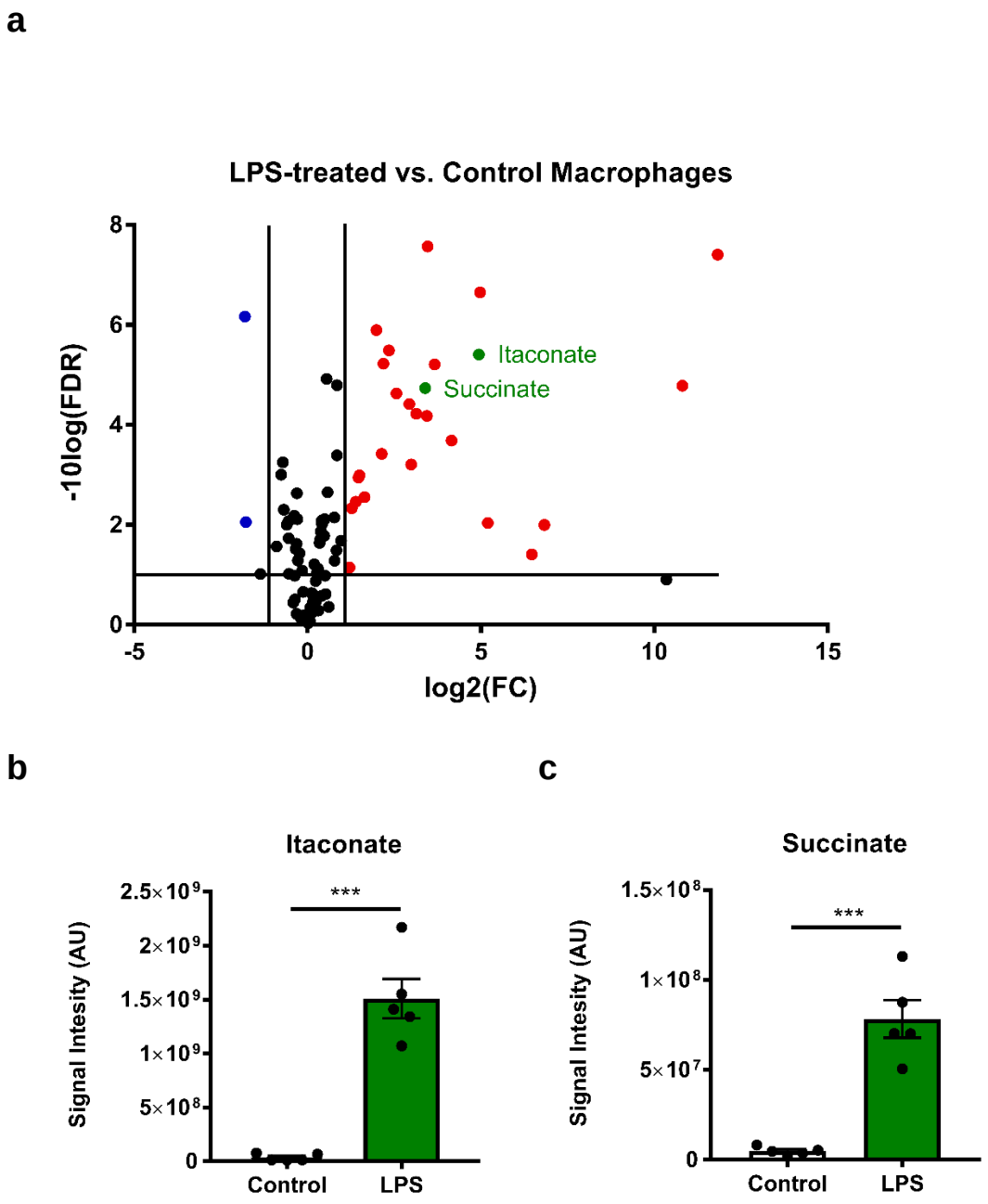

Figure 4.1 – LPS induces itaconate and succinate accumulation

Relative metabolite levels were determined by LC-MS in control or LPS-activated (100 ng/mL, 24 h) BMDMs. **(a)** Volcano plot indicating metabolites significantly up-regulated (red) or down-regulated (blue) upon treatment with LPS was generated using MetaboAnalyst 4.0 (*n*=5 biological replicates performed in technical duplicate). Itaconate and succinate (green) are highlighted. FDR = false discovery rate. Relative **(b)** itaconate and **(c)** succinate levels are shown (*n*=5). Data is presented as mean ± SEM. *P*-values were calculated using an unpaired t-test. **P* <0.05, ***P* <0.01, ****P* <0.001, *****P* <0.0001.

Table 4.1 – Detailed data table of LPS vs control volcano plot significant hits

Metabolite	FC	Log2(FC)	p.adjusted	-log10(p)
Fumarate	3632.9	11.827	1.8377E-6	5.7357
αKG	11.016	3.4615	1.8377E-6	5.7357
Argininosuccinate	31.423	4.9737	6.9657E-6	5.157
Aspartate	0.28594	-1.8062	1.5906E-5	4.7984
Malate	3.9621	1.9863	2.3827E-5	4.6229
Lysine	5.0894	2.3475	5.0664E-5	4.2953
Itaconate	30.657	4.9381	5.211E-5	4.2831
Fructose 6-Phosphate	12.701	3.6668	6.4279E-5	4.1919
Arginine	4.5635	2.1901	6.4279E-5	4.1919
Glyceraldehyde 3- phosphate	1795.6	10.81	1.2764E-4	3.894
Succinate	10.521	3.3952	1.3292E-4	3.8764
Lactate	5.9211	2.5659	1.5671E-4	3.8049
Carbamoyl_Aspartate	7.6379	2.9332	2.3949E-4	3.6207
Gluconate	8.8069	3.1386	3.5059E-4	3.4552
Uric_acid	10.867	3.4419	3.632E-4	3.4399
Pyruvate	17.829	4.1562	0.0010662	2.9722
Glucose_6-Phosphate	4.4142	2.1421	0.0018828	2.7252
Citrulline	7.9593	2.9926	0.002644	2.5777
2-HG	2.8222	1.4968	0.0039861	2.3994
Dihydrothymine	2.7676	1.4687	0.0042557	2.371
Hypoxanthine	3.1256	1.6441	0.0093033	2.0314
Cystathionine	2.6296	1.3948	0.011135	1.9533
UDP	2.4156	1.2724	0.014456	1.84
Propionylcarnitine	0.29157	-1.7781	0.021722	1.6631
CDP	36.768	5.2004	0.021943	1.6587
Fructose 1,6-bisphosphate	113.16	6.8273	0.022347	1.6508
UTP	88.55	6.4684	0.067767	1.169

a

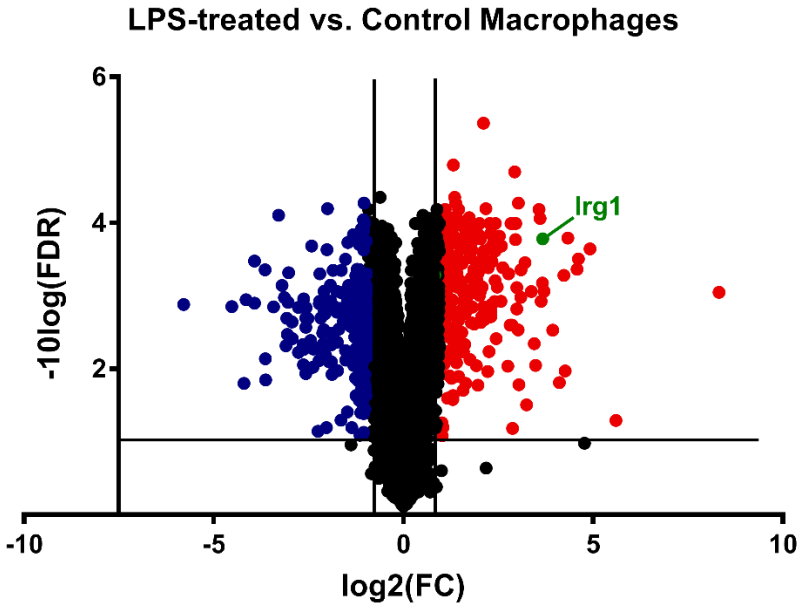

b

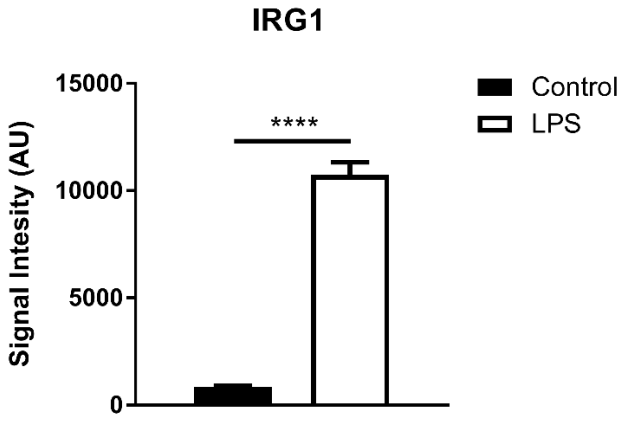

Figure 4.2 – LPS induces IRG1 expression

Relative changes in protein levels were quantified using tandem mass tag (TMT) LC-MS in control and LPS-activated (100 ng/mL, 24 h) BMDMs. **(a)** Volcano plot indicating metabolites significantly up-regulated (red) or down-regulated (blue) upon treatment with LPS (*n*=4 biological replicates). Irg1 (green) is highlighted. FDR = false discovery rate. **(b)** Relative change in Irg1 is shown (*n*=4). Data is presented as mean ± SEM. *P*-values were calculated using an unpaired t-test. **P* <0.05, ***P* <0.01, ****P* <0.001, *****P* <0.0001.

a

Control – 4.55 x 10^{-12} L

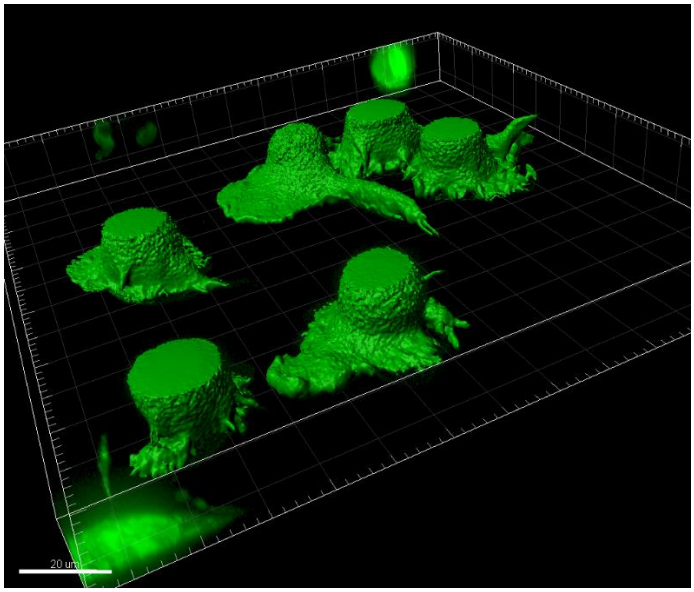

b

LPS – 4.68 x 10^{-12} L

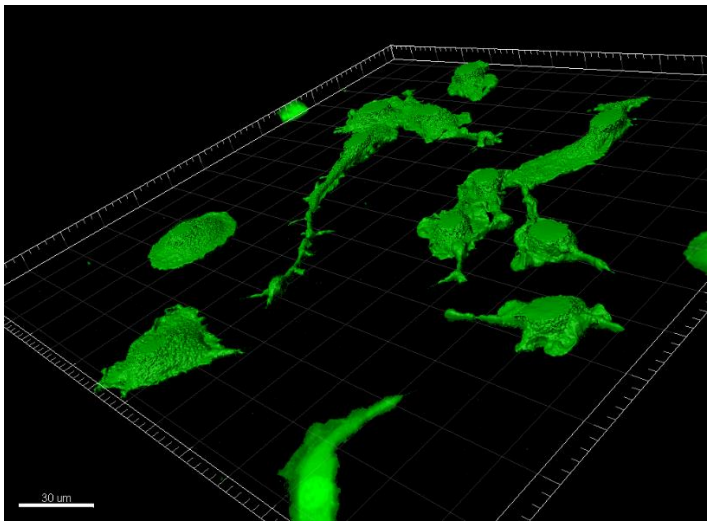

Figure 4.3 – Macrophage cell volume measurements

The cell volume of **(a)** control (*n*=83 individual cells) and **(b)** LPS-treated (100 ng/mL, 24 h) (*n*=190 individual cells) BMDMs was determined using acridine orange (AO, 1 μg/mL), confocal microscopy and 3D reconstruction of live cells.

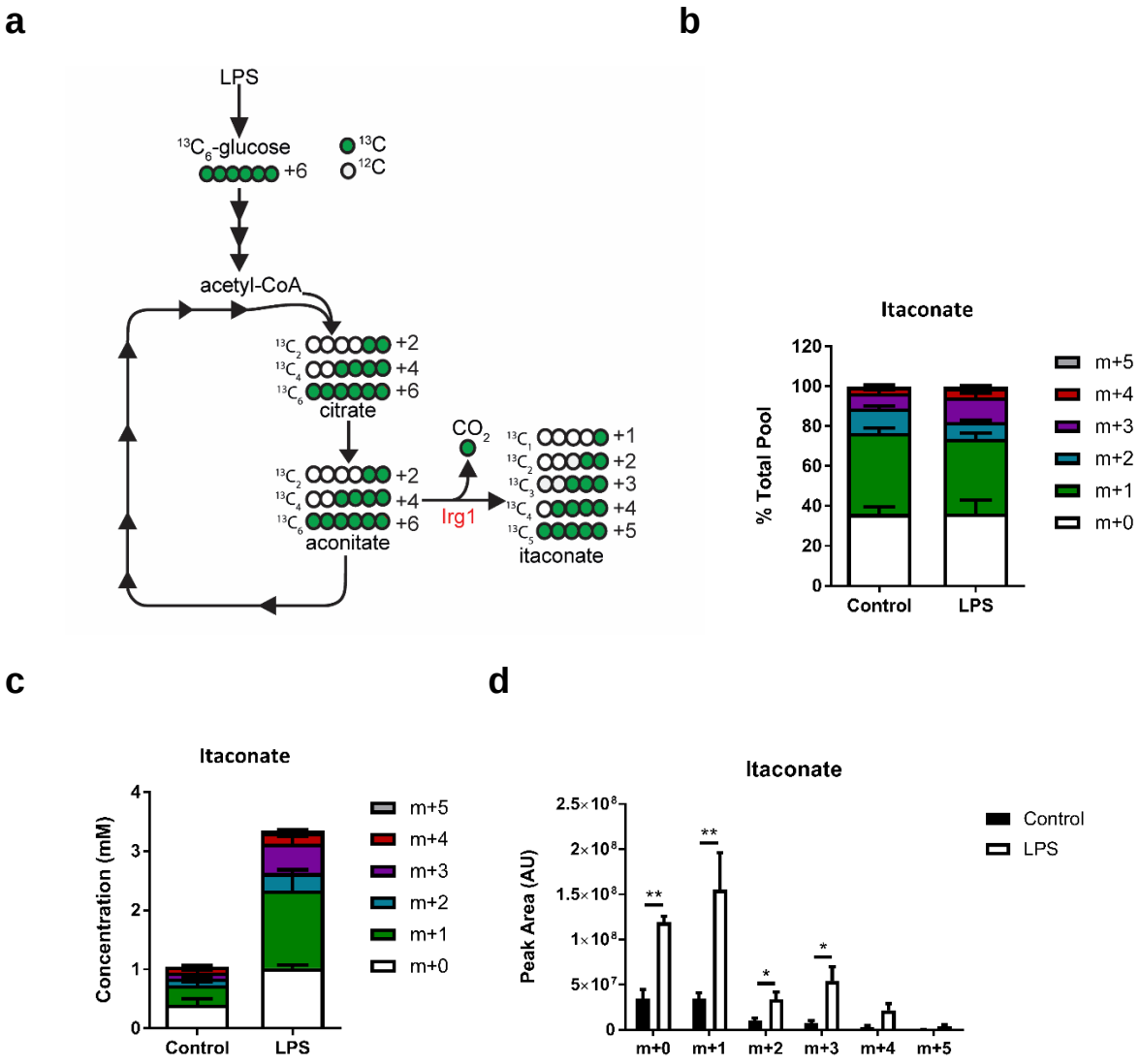

Figure 4.4 – LPS promotes increased flux of glucose into itaconate

Relative and absolute contribution of U-^{13}C-glucose to the itaconate pool was determined by LC-MS in control or LPS-activated (100 ng/mL, 24 h) BMDMs. **(a)** Schematic demonstrating all the possible isotopologue labelling patterns of citrate, *cis*-aconitate and itaconate derived from U-^{13}C-glucose. **(b)** Isotopologue labelling of itaconate presented in a stacked plot as % total pool (*n*=5 biological replicates performed in technical duplicate). **(c)** Absolute quantification of differentially-labelled itaconate isotopologues presented in a stacked plot (*n*=5). **(d)** Relative changes in different itaconate isotopologue levels (*n*=5). Data is presented as mean ± SEM. *P*-values were calculated using an unpaired t-test. **P* <0.05, ***P* <0.01, ****P* <0.001, *****P* <0.0001.

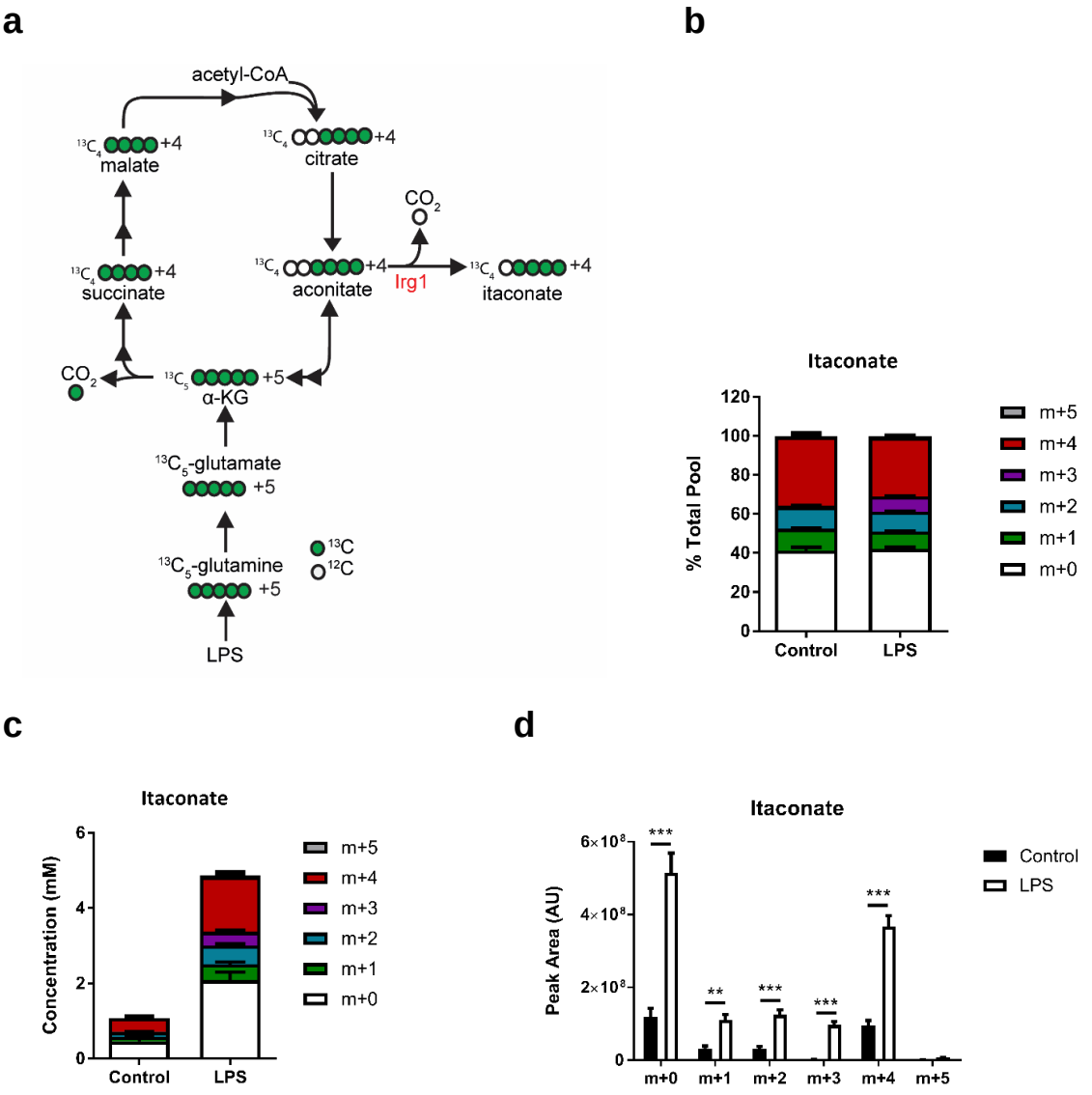

Figure 4.5 – LPS promotes increased flux of glutamine into itaconate

Relative and absolute contribution of U-^{13}C-glutamine to the itaconate pool was determined by LC-MS in control or LPS-activated (100 ng/mL, 24 h) BMDMs. **(a)** Schematic demonstrating most prominent isotopologue labelling pattern of glutamate, α-ketoglutarate, succinate, malate, citrate, *cis*-aconitate and itaconate derived from U-^{13}C-glutamine. **(b)** Isotopologue labelling of itaconate presented in a stacked plot as % total pool (*n*=5 biological replicates performed in technical duplicate). **(c)** Absolute quantification of differentially labelled itaconate isotopologues presented in a stacked plot (*n*=5). **(d)** Relative changes in different itaconate isotopologue levels (*n*=5). Data is presented as mean ± SEM. *P*-values were calculated using unpaired t-test. **P* <0.05, ***P* <0.01, ****P* <0.001, *****P* <0.0001.

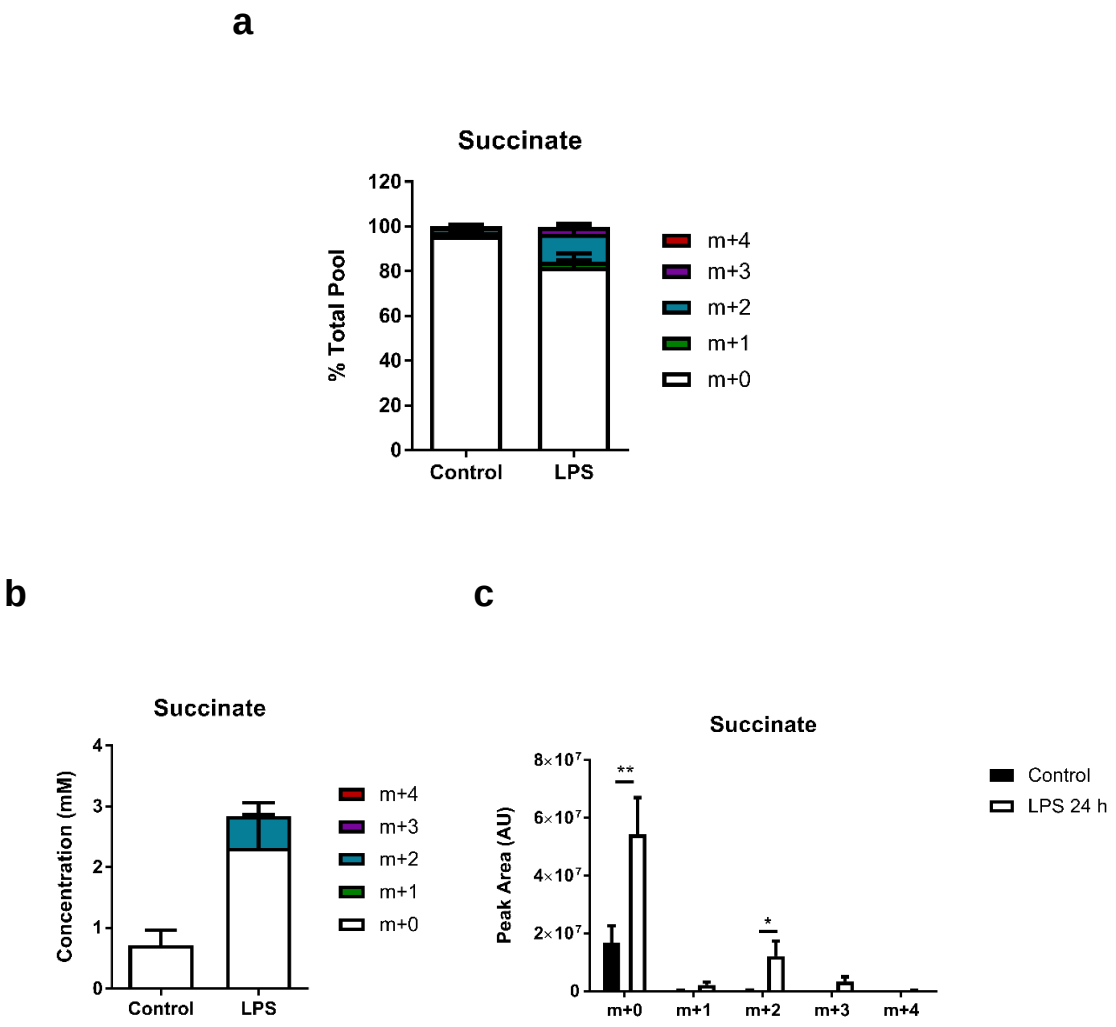

Figure 4.6 – LPS promotes increased flux of glucose into succinate

Relative and absolute contribution of U-^{13}C-glucose to the succinate pool was determined by LC-MS in control or LPS-activated (100 ng/mL, 24 h) BMDMs. **(a)** Isotopologue labelling of succinate presented in a stacked plot as % total pool (*n*=5 biological replicates performed in technical duplicate). **(b)** Absolute quantification of differentially labelled succinate isotopologues presented in a stacked plot (*n*=5). **(c)** Relative changes in different succinate isotopologue levels (*n*=5). Data is presented as mean ± SEM. *P*-values were calculated using an unpaired t-test. **P* <0.05, ***P* <0.01, ****P* <0.001, *****P* <0.0001.

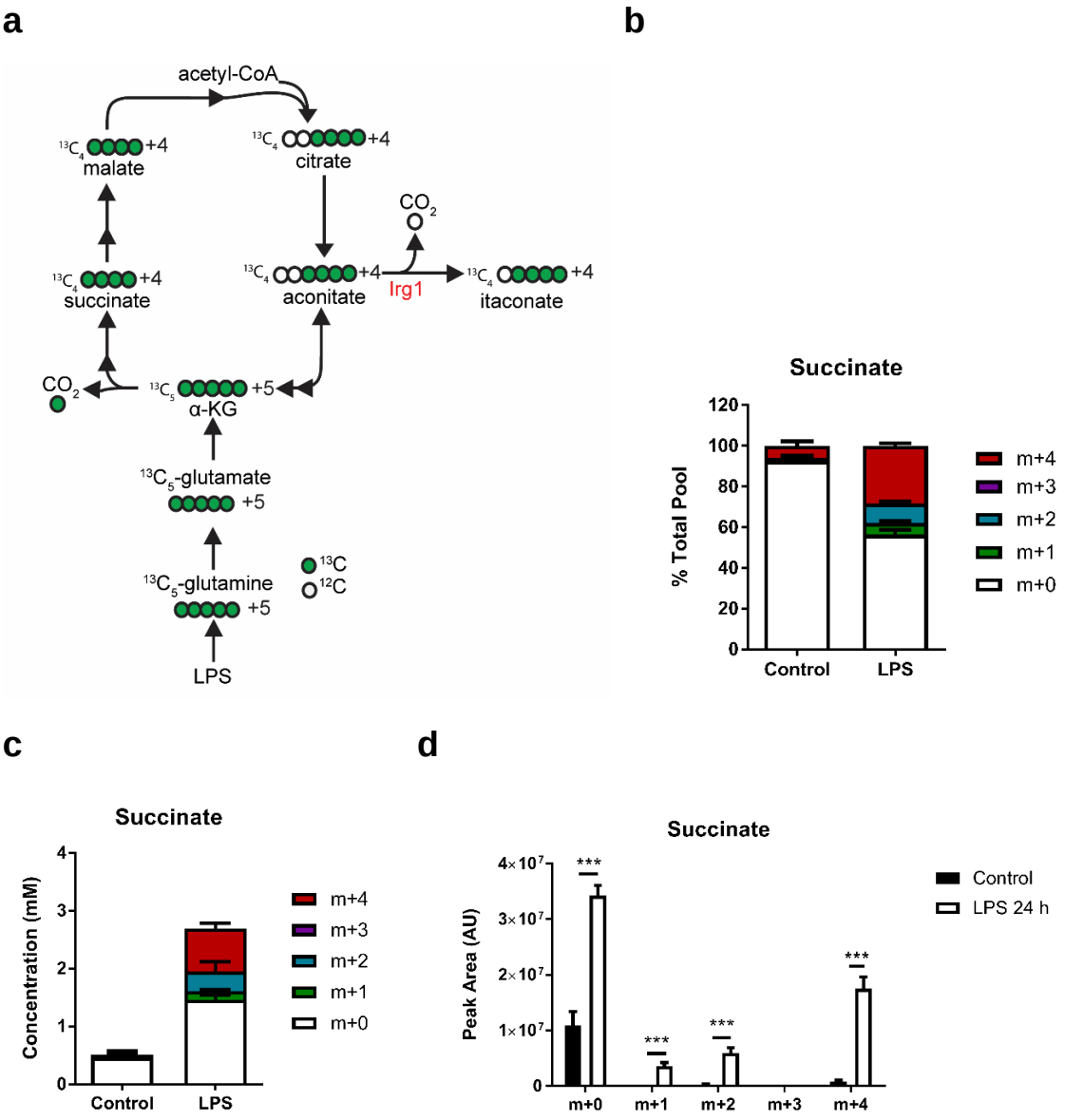

Figure 4.7 – LPS promotes increased flux of glutamine into succinate

Relative and absolute contribution of U-^{13}C-glutamine to the succinate pool was determined by LC-MS in control or LPS-activated (100 ng/mL, 24 h) BMDMs. **(a)** Schematic demonstrating most prominent isotopologue labelling pattern of glutamate, α-ketoglutarate, succinate, malate, citrate, *cis*-aconitate and itaconate derived from U-^{13}C-glutamine. **(b)** Isotopologue labelling of itaconate presented in a stacked plot as % total pool (*n*=5 biological replicates performed in technical duplicate). **(c)** Absolute quantification of differentially labelled succinate isotopologues presented in a stacked plot (*n*=5). **(d)** Relative changes in different succinate isotopologue levels (*n*=5). Data is presented as mean ± SEM. *P*-values were calculated using unpaired t-test. **P* <0.05, ***P* <0.01, ****P* <0.001, *****P* <0.0001.

4.2.2 – IRG1 and itaconate regulate succinate accumulation via competitive inhibition of SDH

As IRG1 is a mitochondrial enzyme that synthesises itaconate from the Krebs cycle intermediate *cis*-aconitate (100), an untargeted metabolomics screen utilising LC-MS was performed in *Irg1* +/+ and *Irg1* -/- BMDMs to determine whether loss of this enzyme and itaconate production affected the reprogramming of metabolism induced by LPS (Fig. 4.8a).

Stimulation of *Irg1* +/+ BMDMs with LPS induced the expected changes in many Krebs cycle metabolites, namely a significant increase succinate (Fig. 4.8a; Fig. 4.9b), fumarate (Fig. 4.8a; Fig. 4.10a), malate (Fig. 4.8a; Fig. 4.10b) and itaconate (Fig. 4.8a; Fig. 4.9a). As expected, itaconate production was completely lost in *Irg1* -/- BMDMs (Fig. 4.9a). Strikingly, the ability of LPS to induce succinate accumulation was also completely abolished in *Irg1* -/- BMDMs (Fig. 4.9b), whilst the metabolites fumarate (Fig. 4.10a), malate (Fig. 4.10b) and aspartate (Fig. 4.8a) downstream of succinate oxidation by SDH were further increased in LPS-activated *Irg1* -/- BMDMs. In addition to the observed changes in these important mitochondrial metabolites, there was also a significant increase in several fatty acids, such as palmitate, stearate, oleate and sphingosine and a significant decrease in some carnitine species, such as myristoylcarnitine (Fig. 4.8a) suggesting the loss of IRG1 and itaconate production has an impact on lipid metabolism.

To assess whether this reprogramming of metabolism was due to a direct consequence of signalling downstream of itaconate production, resting macrophages were pre-treated with itaconic acid (ITA) for 24 h and a semi-

targeted metabolomics screen was performed (Fig. 4.11a). A full list of the significantly upregulated (red) or downregulated (blue) metabolites in ITA-treated BMDMs (Fig. 4.11a) can be found in Table 4.2. Pre-treatment of BMDMs with itaconate resulted in a significant increase in the levels of both itaconate (Fig. 4.11b) and succinate (Fig. 4.11c) and a significant decrease in aspartate (Table 4.2). Pre-treatment of LPS-activated macrophages with an itaconic acid derivative 4-octyl itaconate (OI or 4-OI) also resulted in a significant increase in itaconate (Fig. 4.12a) and succinate (Fig. 4.12b), which suggests succinate accumulation occurs downstream of itaconate.

As metabolites downstream of succinate oxidation by SDH were increased in *Irg1 -/-* BMDMs and the accumulation of succinate appeared to be a direct consequence of signalling downstream of itaconate, this suggested that this metabomodulatory effect was occurring at the level of SDH inhibition. In agreement with this, itaconic acid was found to be a competitive inhibitor of SDH (Fig. 4.3a), as assessed by a complex II + III activity assay carried out in isolated bovine mitochondrial membranes, albeit less potent than the prototypical SDH inhibitor malonate (Fig. 4.3a). These findings suggest that competitive inhibition of SDH by itaconate, coupled to enhanced flux through succinate-producing pathways, such as glutaminolysis, contribute to succinate accumulation observed in response to LPS. These findings also support previous reports linking itaconate-mediated SDH inhibition to metabolic remodelling and succinate accumulation in macrophages (48, 49).

a

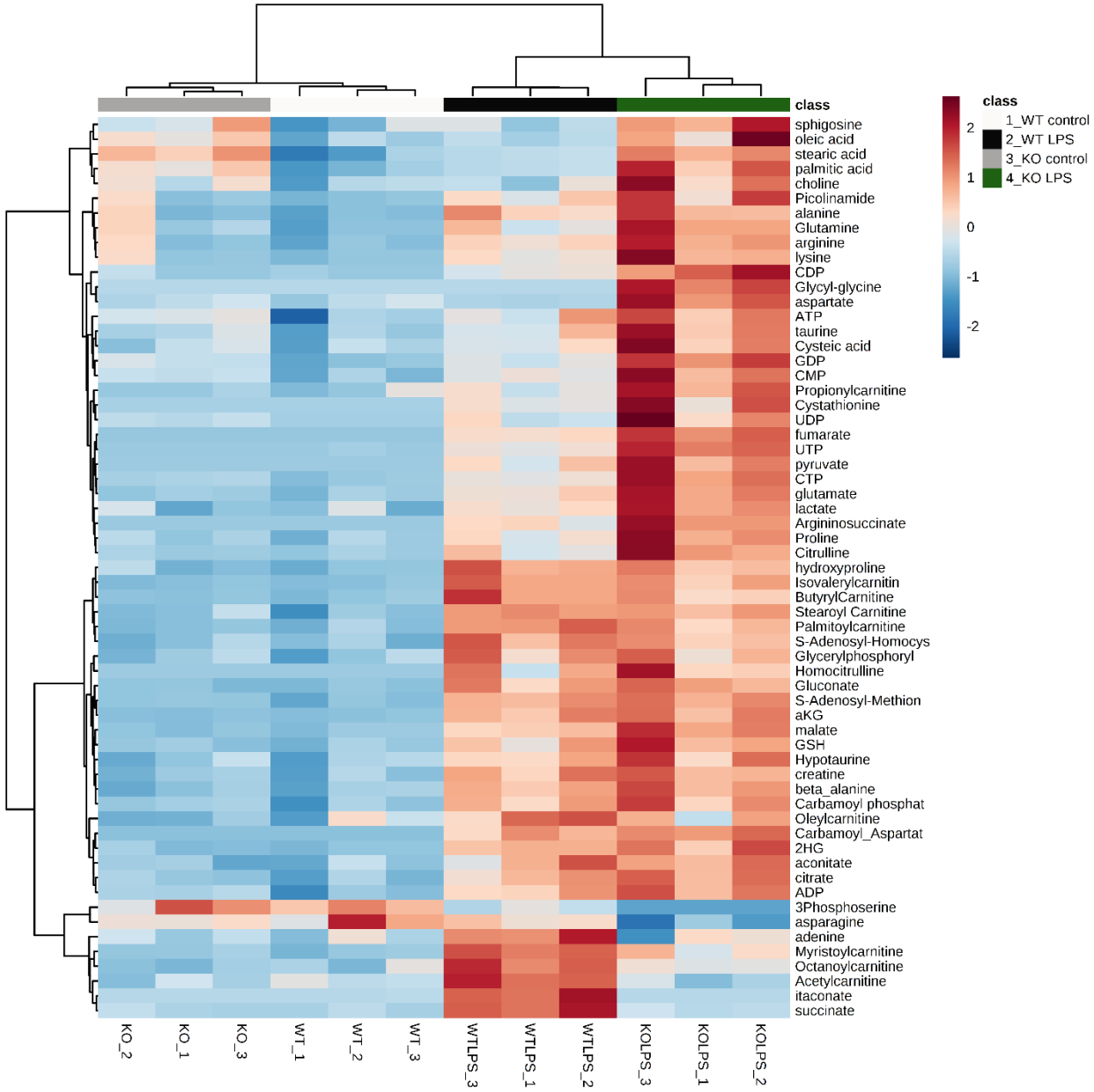

Figure 4.8 – LPS induction of IRG1 expression modulates metabolic remodelling

Relative metabolites levels were determined by LC-MS in control or LPS-activated (100 ng/mL, 24 h) *Irg1* +/+ and *Irg1* -/- BMDMs (*n*=3). **(a)** Heatmap of significantly upregulated (red) and downregulated (blue) metabolites generated using the Ward clustering algorithm in MetaboAnalyst 4.0. *P*-values were calculated using one-way ANOVA. **P* <0.05, ***P* <0.01, ****P* <0.001, *****P* <0.0001.

a

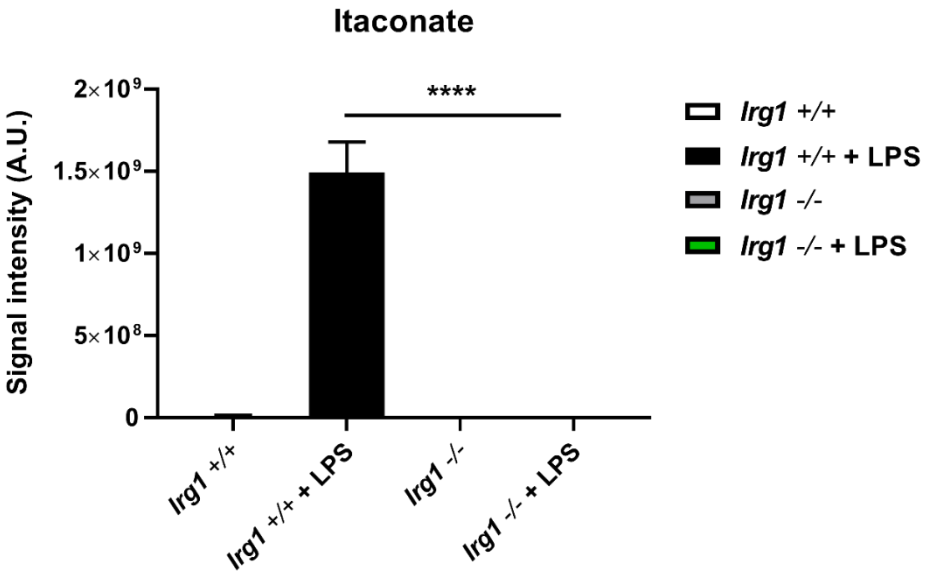

b

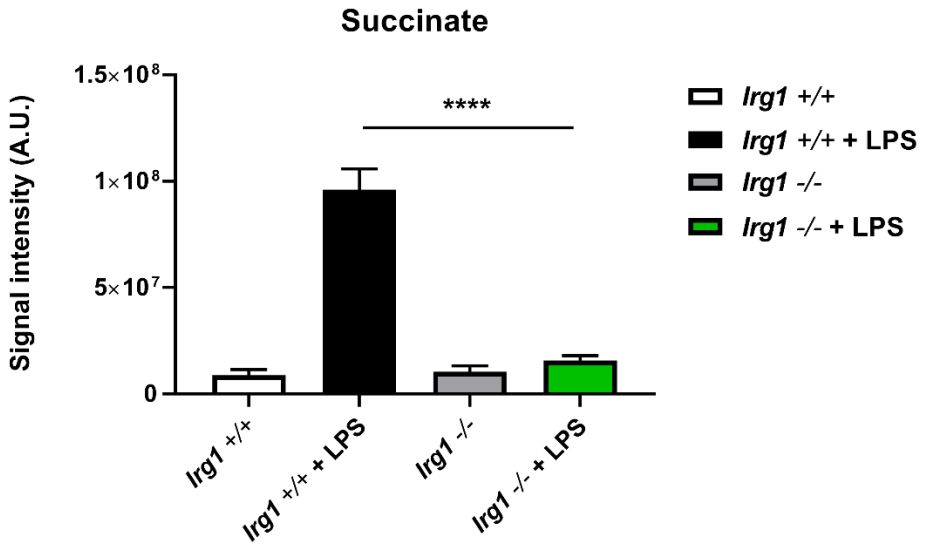

Figure 4.9 – LPS induction of itaconate and succinate is *Irg1*-dependent

Relative levels of **(a)** itaconate and **(b)** succinate were determined by LC-MS in control or LPS-activated (100 ng/mL, 24 h) *Irg1 +/+* and *Irg1 -/-* BMDMs (*n*=3). *P*-values were calculated using one-way ANOVA. **P* <0.05, ***P* <0.01, ****P* <0.001, *****P* <0.0001.

a

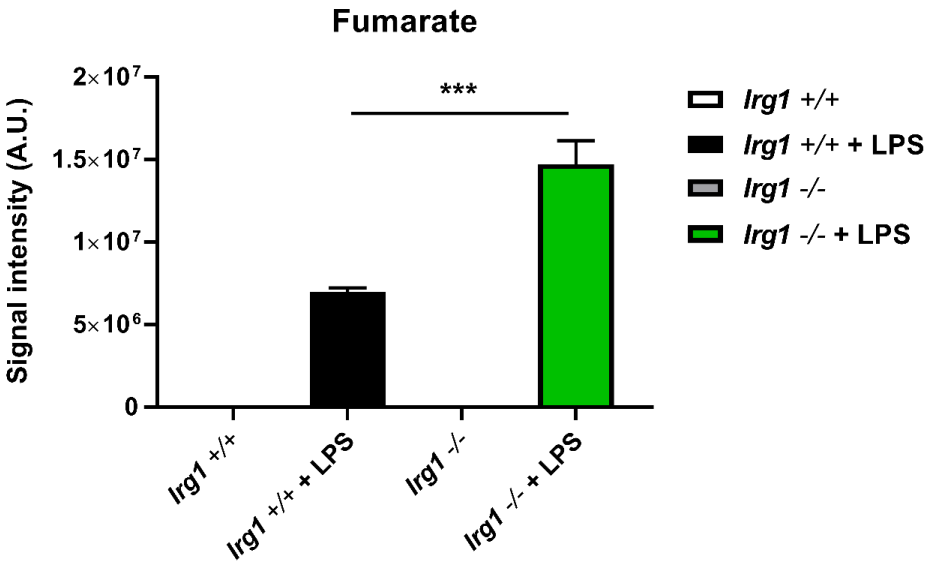

b

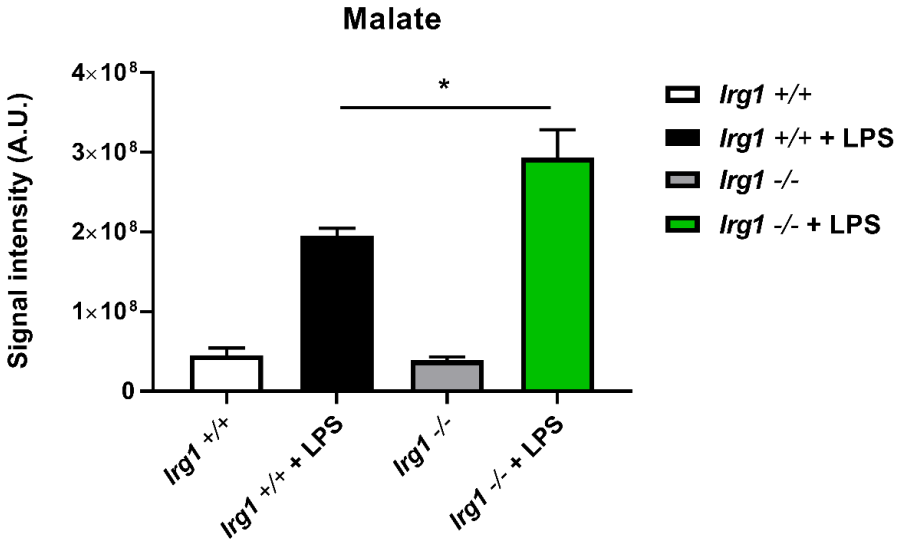

Figure 4.10 – LPS induction of fumarate and malate is increased in *Irg1 -/-* BMDMs

Relative levels of **(a)** fumarate and **(b)** malate were determined by LC-MS in control or LPS-activated (100 ng/mL, 24 h) *Irg1 +/+* and *Irg1 -/-* BMDMs (n=3). *P*-values were calculated using one-way ANOVA. **P* <0.05, ***P* <0.01, ****P* <0.001, *****P* <0.0001.

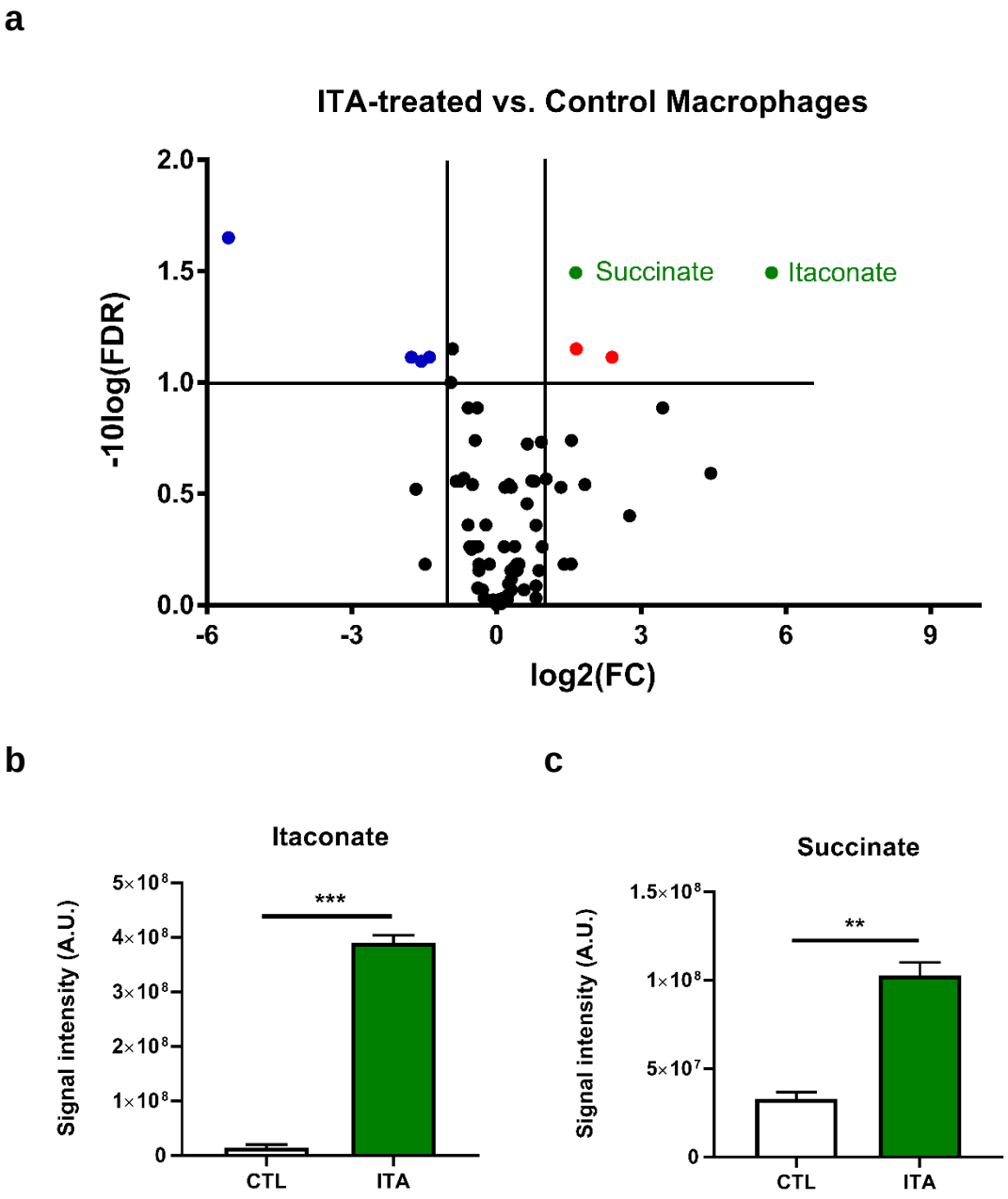

Figure 4.11 – Itaconate uptake in macrophages induces succinate accumulation

Relative metabolite levels were determined by LC-MS in control or itaconate-treated (pH 7.4, 5 mM, 24 h) BMDMs. **(a)** Volcano plot indicating metabolites significantly up-regulated (red) or down-regulated (blue) upon treatment with itaconate (*n*=3 biological replicates performed in technical duplicate). Succinate and itaconate (green) are highlighted. FDR = false discovery rate. Relative **(b)** itaconate and **(c)** succinate levels are shown (*n*=3). Data is presented as mean ± SEM. *P*-values were calculated using an unpaired t-test. **P* <0.05, ***P* <0.01, ****P* <0.001, *****P* <0.0001.

Table 4.2 – Detailed data table of ITA vs control volcano plot significant hits

Metabolite	FC	log2(FC)	p.ajusted	-log10(p)
Stearoyl Carnitine	0.021332	-5.5508	0.022375	1.6502
itaconate	52.073	5.7025	0.032119	1.4932
succinate	3.1349	1.6484	0.032119	1.4932
GSH	3.1543	1.6573	0.070797	1.15
aspartate	0.29543	-1.7591	0.076979	1.1136
ornithine	5.276	2.3994	0.076985	1.1136
Oleylcarnitine	0.38288	-1.3851	0.076985	1.1136
Propionylcamitine	0.33997	-1.5565	0.080343	1.0951

a

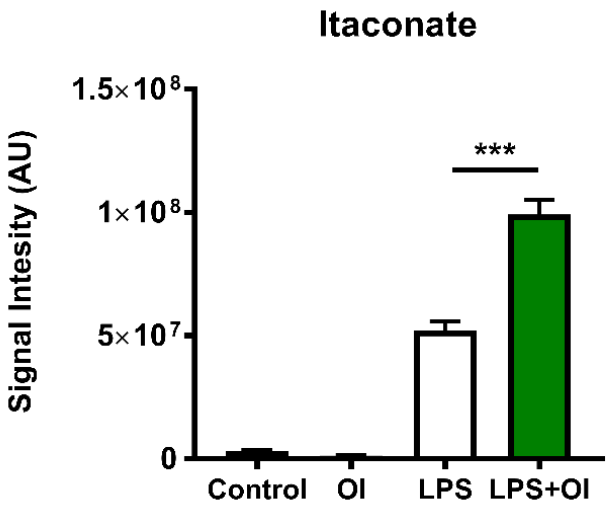

b

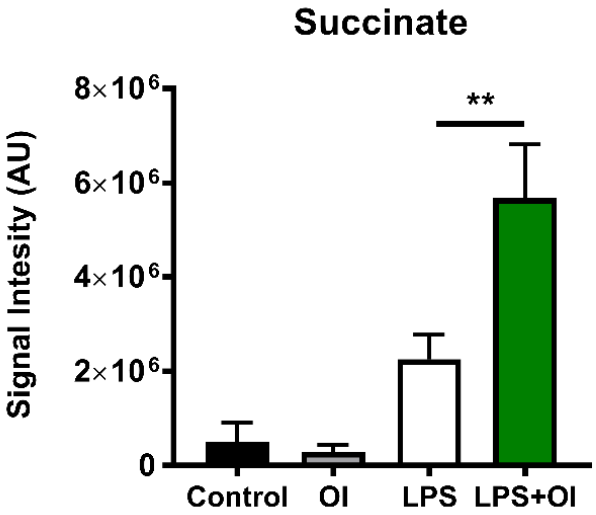

Figure 4.12 – 4-OI induces succinate accumulation in LPS-activated macrophages

Relative metabolite levels were determined by LC-MS in control or LPS-activated (100 ng/mL, 6 h) BMDMs ± 3 h 4-OI pre-treatment (250 μM). **(a)** Relative itaconate and succinate levels are shown (*n*=5 biological replicates performed in technical duplicate). Data is presented as mean ± SEM. *P*-values were calculated using an unpaired t-test. **P* <0.05, ***P* <0.01, ****P* <0.001, *****P* <0.0001.

a

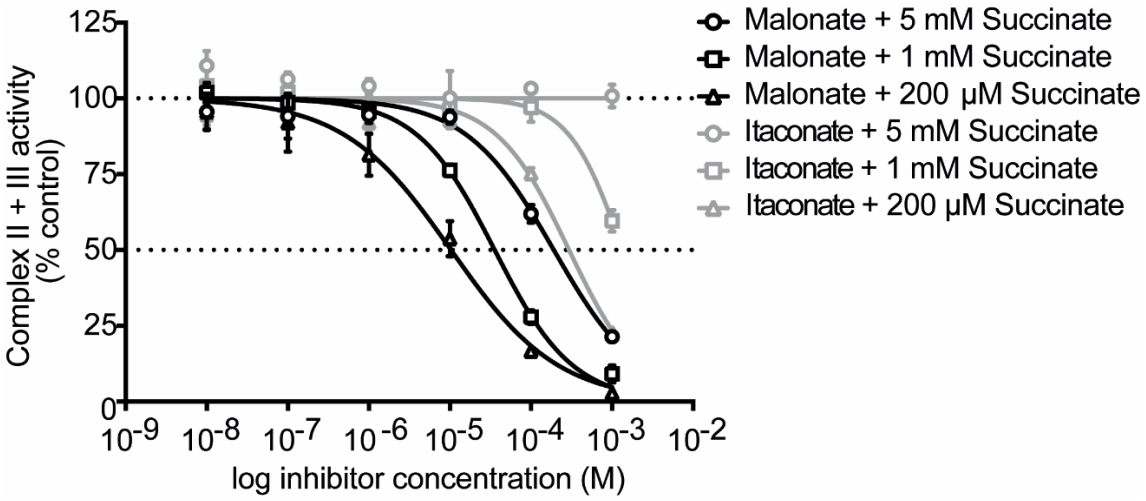

Figure 4.13 – Itaconate competitively inhibits SDH

(a) Complex II and III activity in bovine heart mitochondrial membranes incubated with succinate plus malonate (black) or itaconate (grey) at indicated concentrations for 10 min at 30ºC. Data is presented as % inhibition of control ± SEM. (*n* = 3).

4.2.3 – DMI induces Nrf2 and inhibits LPS-induced IL-1β

To determine the consequences of elevated itaconate levels on the inflammatory response in macrophages, a cell-permeable itaconate analogue, DMI (49), was employed initially as an experimental tool (Fig. 4.14a). Whilst previous reports suggested SDH inhibition was the mechanism by which itaconate exerted its anti-inflammatory effects, an RNA-seq screen in BMDMs treated with DMI revealed a distinct enrichment in genes known to be regulated by Nrf2 (49). As such, the potential link between itaconate and Nrf2 induction was investigated.

Pre-treatment of BMDMs with DMI resulted in potent inhibition of LPS-induced pro-IL1β levels at both an early (Fig. 4.14b; compare lane 3 to lane 4) and late (Fig. 4.14b; compare lane 5 to lane 6) LPS timepoint. Furthermore, pre-treatment of BMDMs with DMI augmented LPS-induced Nrf2 protein expression (Fig. 4.14b; compare lanes 3 & 5 to lanes 4 & 6). DMI treatment on its own in unstimulated conditions (no LPS) also promoted Nrf2 stabilisation post 25 h treatment (Fig. 4.14b; compare lane 1 to lane 2).

a

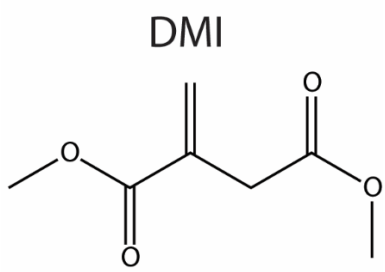

b

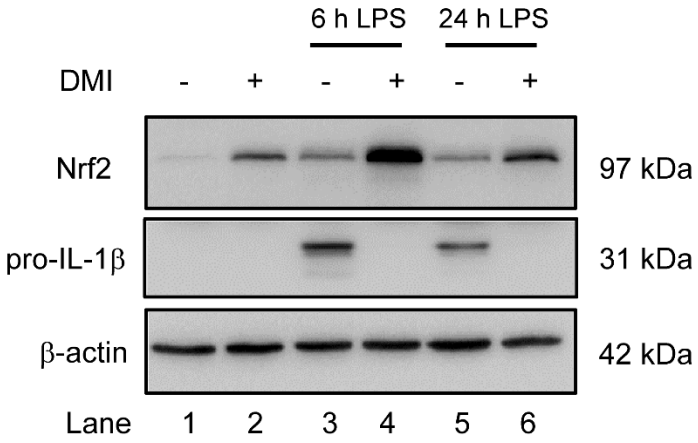

Figure 4.14 – DMI induces Nrf2 and inhibits LPS-induced IL-1β

(a) Chemical structure of cell-permeable itaconate analogue DMI. **(b)** Protein expression of Nrf2, pro-IL-1β and the loading control β-actin in response to LPS treatment (100 ng/mL) ± 1 h DMI pre-treatment (125 μM) for indicated timepoints, as assessed by western blot. The result shown is representative of three independent experiments.

4.2.4 – LPS-induces the formation of itaconate-cysteine adducts

Itaconate, like fumarate, is an α, β-unsaturated carbonyl compound. As DMI had the ability to induce Nrf2, it was hypothesised that the electrophilic alkene moiety of itaconate could undergo nucleophilic attack from cysteine thiolate ions. This would subsequently result in an irreversible covalent modification, more broadly termed an alkylation reaction, comparable to fumarate-mediated protein succination (Fig. 4.15a). As previously mentioned, the final breakdown product and established biomarker of protein succination is the metabolite 2SC (Fig. 4.16a). As such, it was speculated that if itaconate could modify the thiol group of cysteine residues it would also result in the formation of an itaconate-cysteine adduct akin to 2SC, chemically termed 2,3-dicarboxypropyl cysteine (Fig. 4.16b).

To investigate this, data generated from the U-^{13}C-glucose and U-^{13}C-glutamine isotopic tracing experiments was utilised. Like itaconate, a significant increase in 2,3-dicarboxypropyl cysteine was observed in LPS-activated BMDMs (Fig. 4.16c, d). Around 40% of the total pool of 2,3-dicarboxypropyl cysteine contained glucose-derived carbon (Fig. 4.16c). Of note, was a significant increase the m+1 isotopologue of 2,3-dicarboxypropyl cysteine upon LPS stimulation, reflecting isotopic labelling of itaconate (Fig. 4.4d). Similarly, ~ 25% of the total pool of itaconate contained glutamine-derived carbon (Fig. 4.16d). A significant increase in the m+4 isotopologue of itaconate upon LPS stimulation was also observed, again reflecting the discerned isotopologue distribution of itaconate (Fig. 4.5d). As such, LPS induced the formation of an itaconate-cysteine adduct, 2,3-dicarboxypropyl cysteine, akin to 2SC, which was in part derived from glucose and glutamine.

a

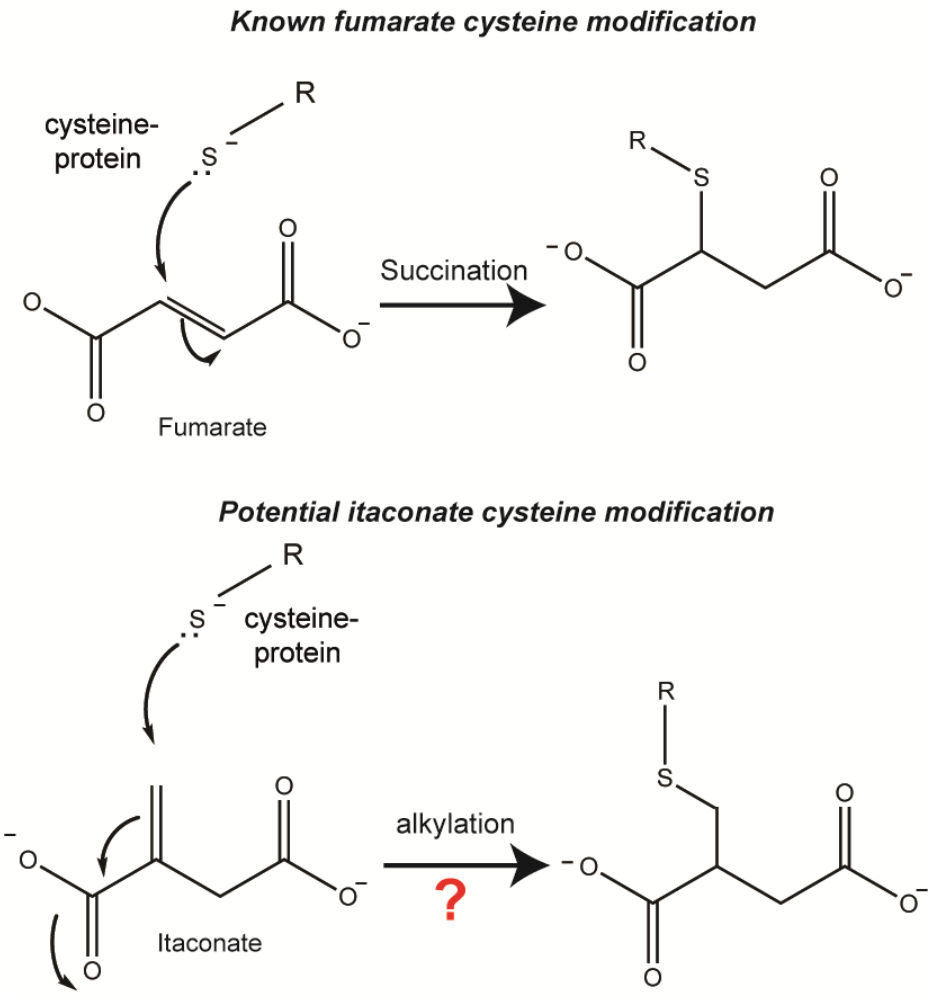

Figure 4.15 – Potential itaconate alkylation reaction

(a) Schematic of fumarate-mediated protein succination and potential cysteine modification mediated by itaconate to form a 2,3-dicarboxypropyl adduct.

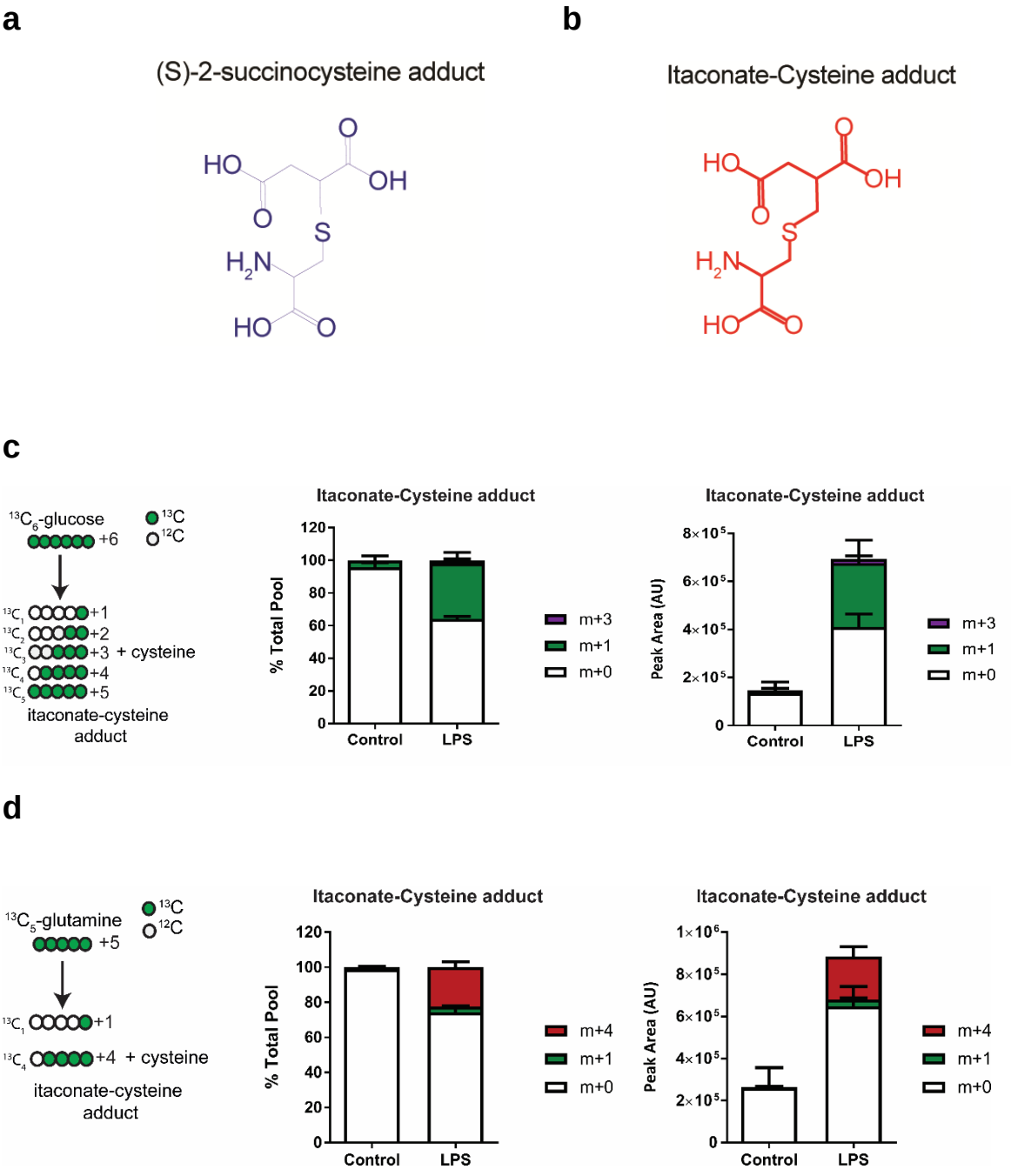

Figure 4.16 – LPS induces the formation of 2,3-dicarboxypropyl cysteine

Chemical structure of the fumarate-cysteine metabolite **(a)** 2SC and **(b)** potential itaconate-cysteine adduct 2,3-dicarboxypropyl cysteine. Relative contribution of U-^{13}C-glucose **(c)** and U-^{13}C-glutamine **(d)** to 2,3-dicarboxypropyl cysteine was determined by LC-MS in control or LPS-activated (100 ng/mL, 24 h) BMDMs (*n*=5 biological replicates in technical duplicate). Data is presented as % of total pool and mean ± SEM.

4.2.5 – 4-OI is a more suitable cell-permeable itaconate surrogate than DMI

Recently it was reported that DMI is not metabolised to itaconate intracellularly, whilst the uptake of itaconic acid into macrophages has also been called into question (210). This presented a potential problem regarding the use of DMI as a cell-permeable itaconate analogue due to the newly uncovered electrophilic nature of itaconate and indeed the use of exogenous itaconic acid to probe its intracellular function. Esterification of itaconate would hypothetically render itaconate an activated Michael acceptor, as observed with DMF, thus increasing its thiol reactivity. Unlike fumarate, the reactive alkene moiety of itaconate is only conjugated to one carboxyl group. To this end, selective esterification of the carboxyl group distal to the alkene would enable itaconate to cross the plasma membrane (PM) without altering its electrophilicity.

DMF rapidly depletes intracellular GSH levels resulting in acute and superfluous Nrf2 activation due to its enhanced thiol reactivity (162). As such, two novel itaconic acid esters were synthesised, 4-octyl itaconate (OI or 4-OI) and 4-methyl itaconate (MI or 4-MI), and their ability to deplete GSH, through alkylation of its cysteine thiol group, was compared with that of itaconate and DMI (Fig. 4.17a). Incubation of GSH with DMI resulted in its rapid depletion at pH 7.2, but neither itaconate, 4-MI nor 4-OI had any significant effect (Fig. 3.22b). Furthermore, DMI induced a larger decrease in GSH levels when incubated at pH 8, which is closer to the pKa of glutathione's thiol group and is more likely to be found in its reactive thiolate form, but again no significant effect was observed when GSH was incubated with itaconate, 4-MI or 4-OI after 2 hours of incubation (Fig. 4.17c).

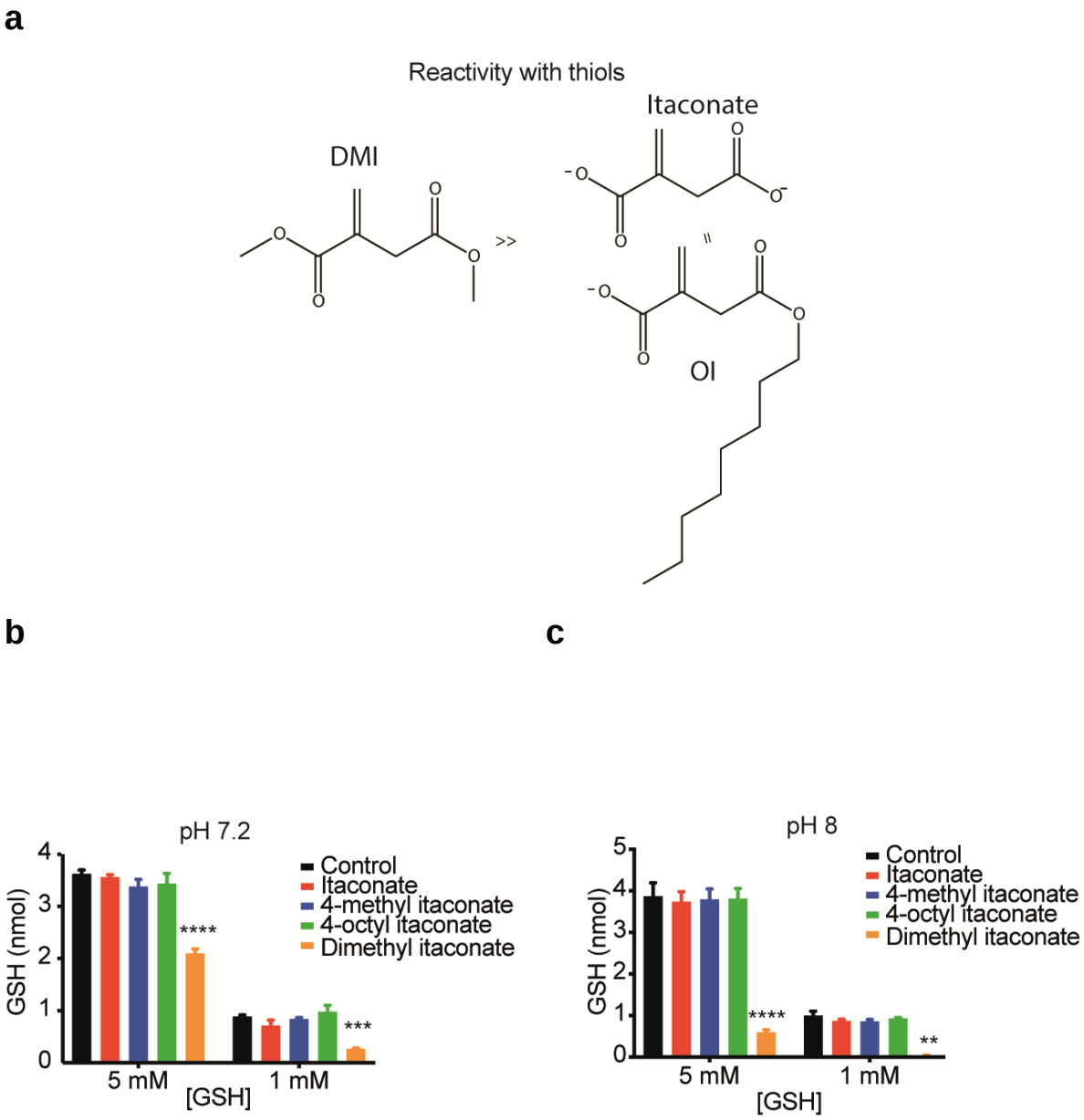

Figure 4.17 – 4-OI is a suitable cell-permeable itaconate surrogate

(a) Chemical structure of Itaconate, DMI and 4-OI. GSH (1 or 5 mM) was incubated with Itaconate, MI, 4-OI and DMI (5 mM) for 2 h at pH **(b)** 7.2 or **(c)** 8 prior to assessing GSH levels (n=3). Data is presented as mean ± SEM. P-values were calculated using one-way ANOVA. *P <0.05, **P <0.01, ***P <0.001, ****P <0.0001.

4.2.6 – IRG1, itaconate and 4-OI induce Nrf2 stabilisation

To ascertain the function of increased itaconate levels in macrophages, the new cell-permeable itaconate surrogate, 4-OI, was employed as an experimental tool. To this end, an unbiased quantitative proteomic screen, which used isobaric tandem mass tags (TMTs) coupled to LC-MS, was carried out in control and 4-OI-treated macrophages (Fig. 4.18a).

The most significant hit from the screen was an increase in Nrf2 (also known as Nfe2I2) protein levels (4.6 fold), whilst the downstream target proteins Hmox1 (2.5 fold) and Sqstm1 (2.3 fold) were also significantly increased (Fig. 4.18a, b). To validate these findings, Nrf2 and Hmox1 protein expression (Fig. 4.19a; compare lane 1 to lanes 2-5) was found to be dose-dependently increased in response to 4-OI both at 9 h (Fig. 4.19a; compare lane 1 to lanes 2-5) and 27 h (Fig. 4.20a; compare lane 1 to lanes 2-3) post treatment. Pre-treatment of BMDMs with 4-OI also augmented LPS-induced Nrf2 and Hmox1 protein levels after both 6 h (Fig. 4.19a; compare lane 6 to lanes 7-10) and 24 h (Fig. 4.20a; compare lane 4 to lanes 5-6). Furthermore, a significant increase in the Nrf2 target genes *Hmox1, Gsr, Nqo1, Gclm, Pdg* and *Taldo1* mRNA expression was observed in 4-OI-treated resting macrophages and further enhanced in LPS-stimulated macrophages (Fig. 4.19b).

Following this, the ability of 4-OI to induce Nrf2 stabilisation *in vivo* was also examined. Peritoneal exudate cells (PECs), which are largely composed of peritoneal resident macrophages, were derived from 4-OI-treated mice and exhibited a significant increase in Nrf2 protein stabilisation (~4.4 fold) when compared to control (Fig. 4.21a; compare lanes 1-3 to lanes 4-6; b), whilst Hmox1

protein expression (~2 fold) was also increased in response to 4-OI (Fig. 4.21a; compare lanes 1-3 to lanes 4-6; b).

Nrf2 is a key regulator of the GSH biosynthetic pathway (137) (Fig. 4.22a). As such, a targeted metabolomics screen was next used to assess changes in metabolite levels in BMDMs treated with 4-OI and LPS. Pre-treatment of BMDMs with 4-OI resulted in a significant increase in LPS-induced itaconate levels (Fig. 4.22b). Furthermore, analysis of this metabolic dataset demonstrated significant alterations in several metabolites linked to this pathway in LPS-activated BMDMs pre-treated with 4-OI (Fig. 4.22c). Of note, was a significant increase in serine and GSH levels, whilst a significant decrease in S-adenosyl methionine (SAM) was also observed (Fig. 4.22c).

To determine whether the itaconate moiety of 4-OI was responsible for the induction of Nrf2, two control octyl esters were synthesised, 4-octyl succinate (OS or 4-OS) and 4-octyl-2-methylsuccinate (OMS or 4-OMS), which contained the octyl group to enable cell permeability but lacked the electrophilic alkene functional group (Fig. 4.23a). Pre-treatment with 4-OI, but not 4-OS or 4-OMS, potentiated LPS-induced Nrf2 stabilisation and Hmox1 induction (Fig. 4.23b; compare lane 5 to lanes 6-8). Similarly, only 4-OI could induce Nrf2 and Hmox1 protein levels 9 h post treatment (Fig. 4.23b; compare lane 1 to lanes 2-4) and independent of LPS stimulation.

Although the cell permeability of itaconic acid has been called into question [63], an increase in intracellular itaconate was observed in ITA-treated macrophages (Fig. 4.11a, b), as previously mentioned. Treatment of resting macrophages with itaconate resulted in Nrf2 stabilisation and induction of Hmox1

(Fig. 4.24a), whilst GSH levels were also significantly increased in ITA-treated macrophages (Fig. 4.24b), likely via itaconate-mediated Nrf2 stabilisation. Furthermore, LPS-induced Nrf2 stabilisation was largely abrogated in *Irg1 -/-* BMDMs (Fig. 4.25a; compare lanes 7-9 to lanes 10-12), whereas a significant increase in oxidised glutathione (GSSG) levels (Fig. 4.25b) were also observed in LPS-activated *Irg1 -/-* BMDMs, suggesting an impairment of Nrf2-regulated glutathione metabolism.

a

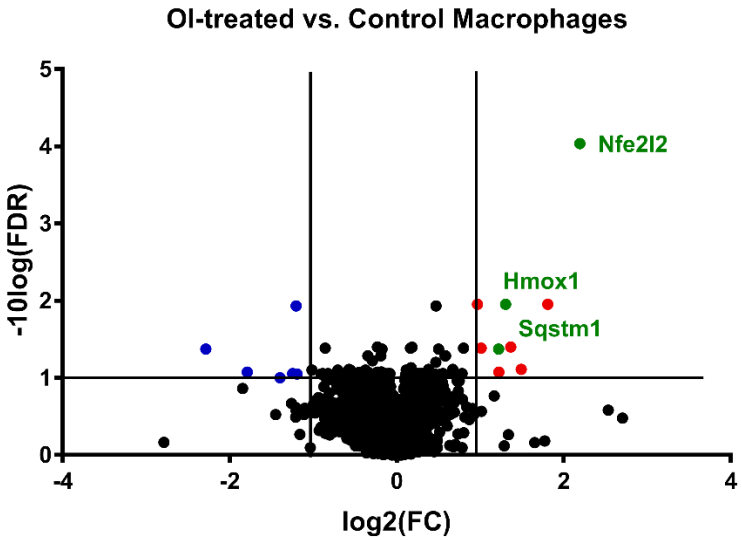

b

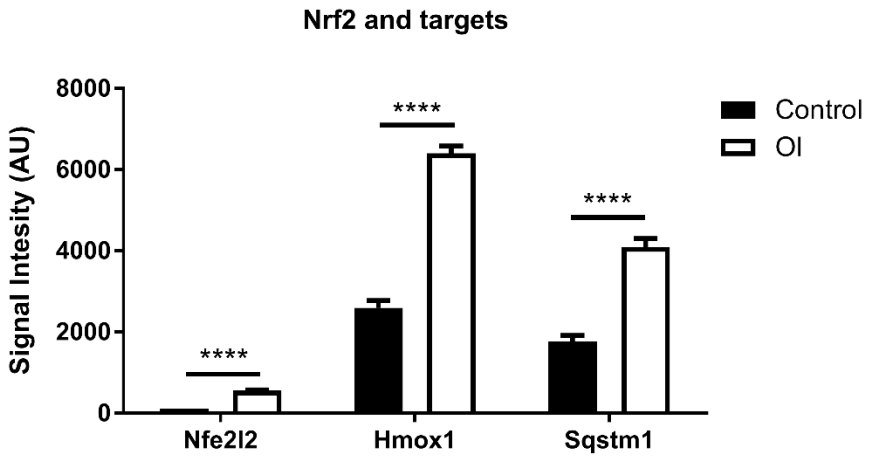

Figure 4.18 – 4-OI induces Nrf2 and Nrf2 target protein levels

Relative changes in protein levels were quantified using tandem mass tag (TMT) LC-MS in control and 4-OI-treated (250 μM, 6 h) BMDMs. **(a)** Volcano plot indicating metabolites significantly up-regulated (red) or down-regulated (blue) upon treatment with 4-OI (*n*=4 biological replicates). FDR = false discovery rate. **(b)** Relative changes in Nrf2, Hmox1 and Sqstm1 are shown (*n*=4). Data is presented as mean ± SEM. *P*-values were calculated using an unpaired t-test. **P* <0.05, ***P* <0.01, ****P* <0.001, *****P* <0.0001.

a

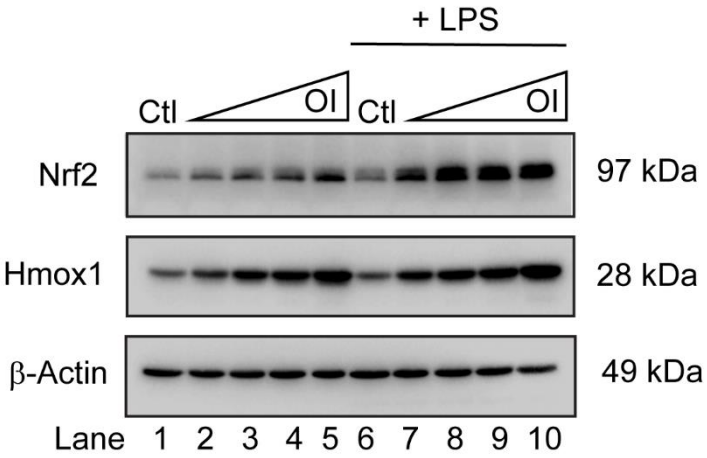

b

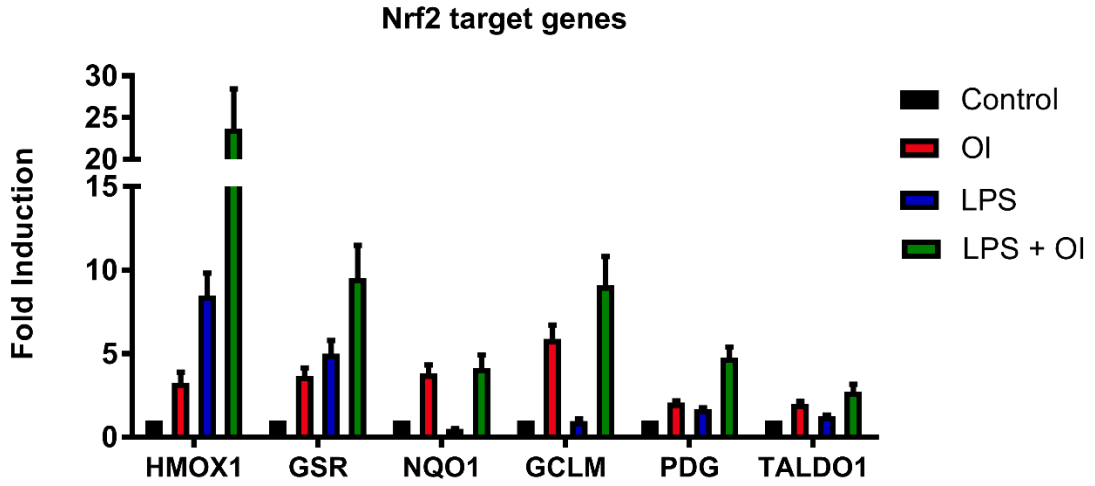

Figure 4.19 – 4-OI induces Nrf2 and Nrf2 target gene expression

(a) Protein expression of Nrf2, Hmox1 and the loading control β-actin in response to LPS treatment (100 ng/mL, 6 h) ± 3 h 4-OI pre-treatment (31.125, 62.5, 125 and 250 μM), as assessed by western blot. The result shown is representative of three independent experiments. **(b)** Relative fold change in mRNA levels of *Hmox1, Gsr, Nqo1, Gclm, Pdg* and *Taldo1* in response to LPS treatment (100 ng/mL, 6 h) ± 3 h 4-OI pre-treatment (125 μM), as assessed by qPCR (*n*=4 biological replicates performed in technical duplicate). Data is presented as mean ± SEM.

a

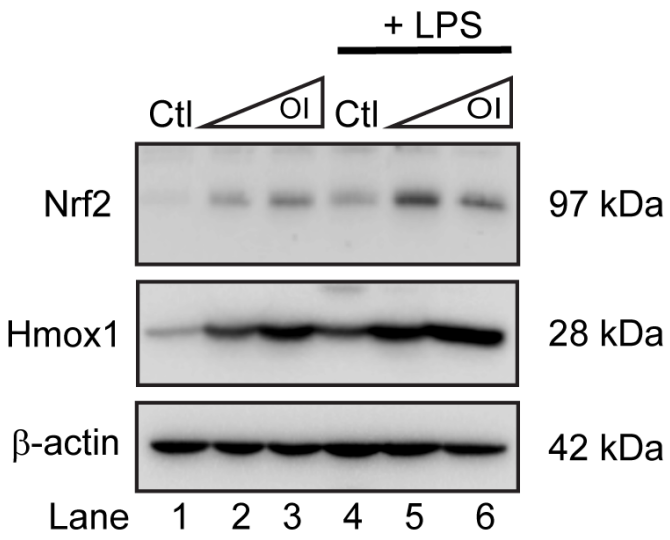

Figure 4.20 – 4-OI induces Nrf2 stabilisation and Hmox1 protein levels

(a) Protein expression of Nrf2, Hmox1 and the loading control β-actin in response to LPS treatment (100 ng/mL, 24 h) ± 3 h 4-OI pre-treatment (125 and 250 μM), as assessed by western blot. The result shown is representative of three independent experiments.

a

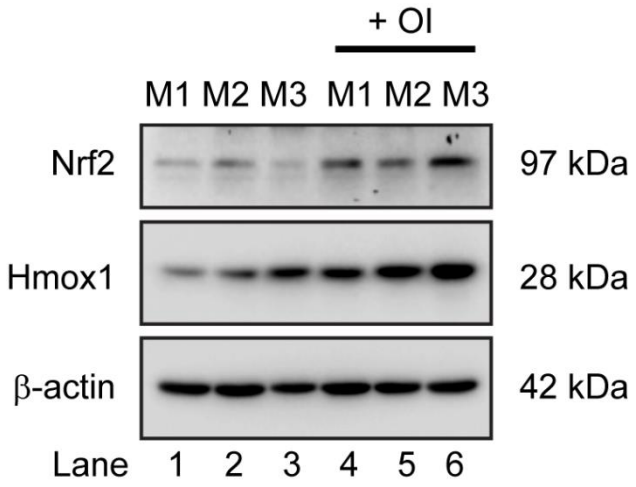

b

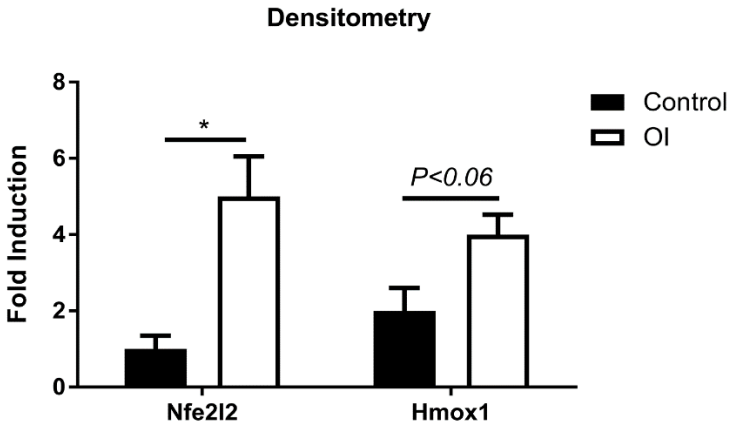

Figure 4.21 – 4-OI activates Nrf2 and Hmox1 in peritoneal macrophages *in vivo*

Protein expression **(a)** and densitometry analysis **(b)** of Nrf2, Hmox1 and the loading control β-actin in response to 4-OI treatment (50 mg/kg, 6 h) in PECs, as assessed by western blot (*n*=3 biological replicates). Data is presented as mean ± SEM. *P*-values were calculated using an unpaired t-test. **P* <0.05, ***P* <0.01, ****P* <0.001, *****P* <0.0001.

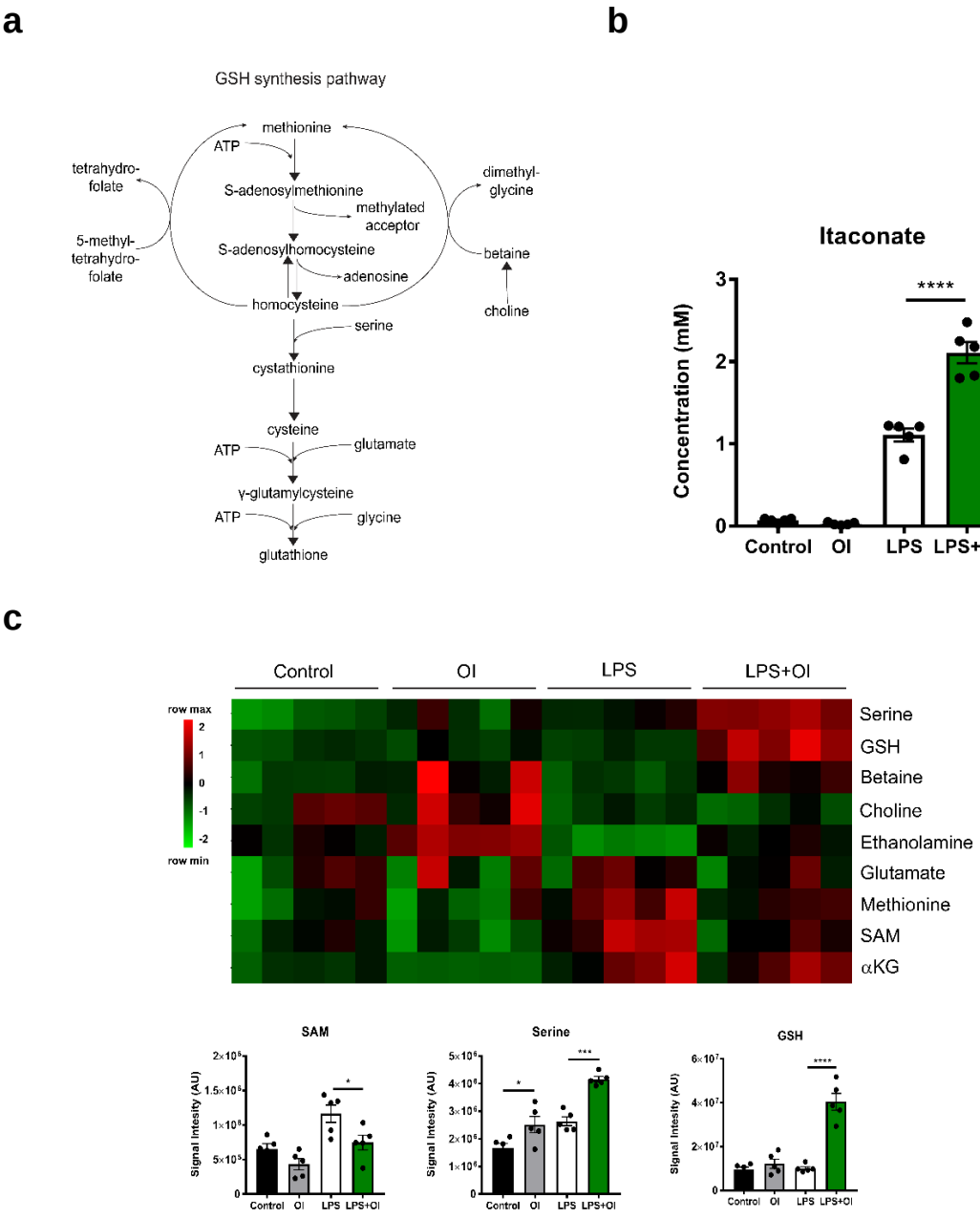

Figure 4.22 – 4-OI induces a Nrf2 metabolic signature in activated macrophages

Relative and absolute metabolite levels were determined by LC-MS in control or LPS-activated (100 ng/mL, 6 h) BMDMs ± 3 h 4-OI pre-treatment (250 μM). **(a)** Schematic of GSH synthesis pathway. **(b)** Absolute quantification of Itaconate (*n*=5). **(c)** Heatmap of upregulated (red) and downregulated (green) metabolites involved in GSH synthesis generated using the Ward clustering algorithm and MetaboAnalyst 4.0. Relative changes in SAM, serine and GSH are also shown (*n*=5 biological replicates performed in technical duplicate). Data is presented as mean ± SEM. *P*-values were calculated using unpaired t-test. **P* <0.05, ***P* <0.01, ****P* <0.001, *****P* <0.0001.

a

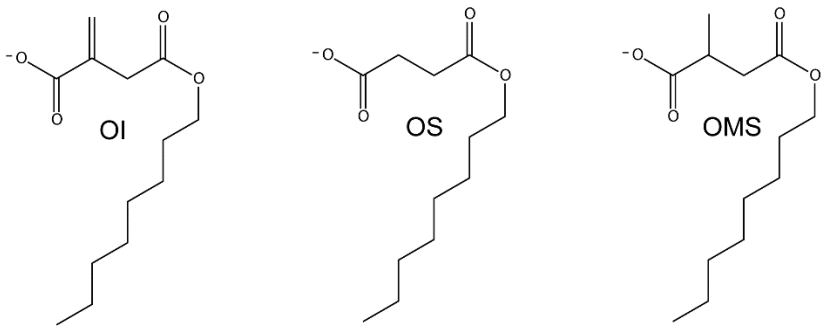

b

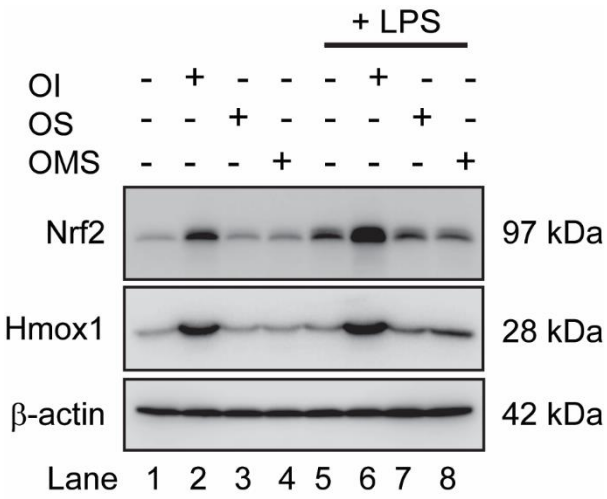

Figure 4.23 – 4-OI, but not 4-OS or 4-OMS, can induce Nrf2 and Hmox1

(a) Chemical structure of 4-octyl itaconate (OI), 4-octyl succinate (OS or 4-OS) and 4-octyl-2-methylsuccinate (OMS or 4-OMS). **(b)** Protein expression of Nrf2, Hmox1 and the loading control β-actin in control or LPS-activated BMDMs (100 ng/mL, 6 h) ± 3 h pre-treatment with 4-OI, 4-OS or 4-OMS (125 μM), as assessed by western blot. The result shown is representative of three independent experiments.

a

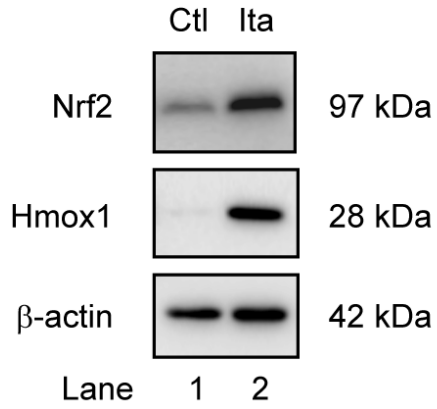

b

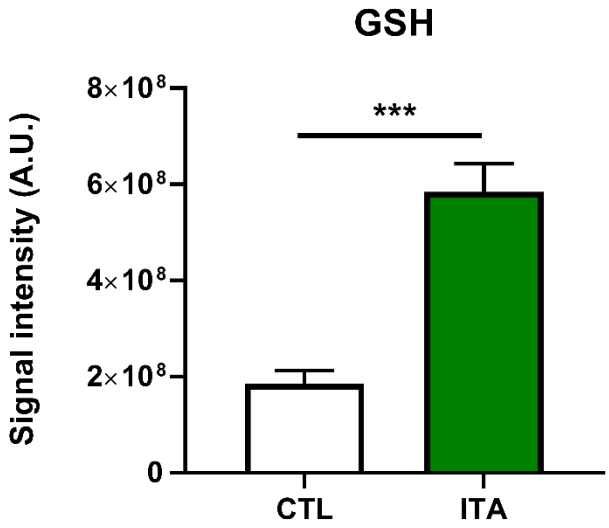

Figure 4.24 – Itaconic acid induces Nrf2 stabilisation and GSH synthesis

(a) Protein expression of Nrf2, Hmox1 and the loading control β-actin in response to Itaconate treatment (pH 7.4, 5 mM, 24 h), as assessed by western blot. The result shown is representative of two independent experiments. **(b)** Relative metabolite levels were determined by LC-MS in control or itaconate-treated (5 mM, 24 h) BMDMs. Relative GSH levels are shown (*n*=3 biological replicates performed in technical duplicate). Data is presented as mean ± SEM. *P*-values were calculated using an unpaired t-test. **P* <0.05, ***P* <0.01, ****P* <0.001, *****P* <0.0001.

a

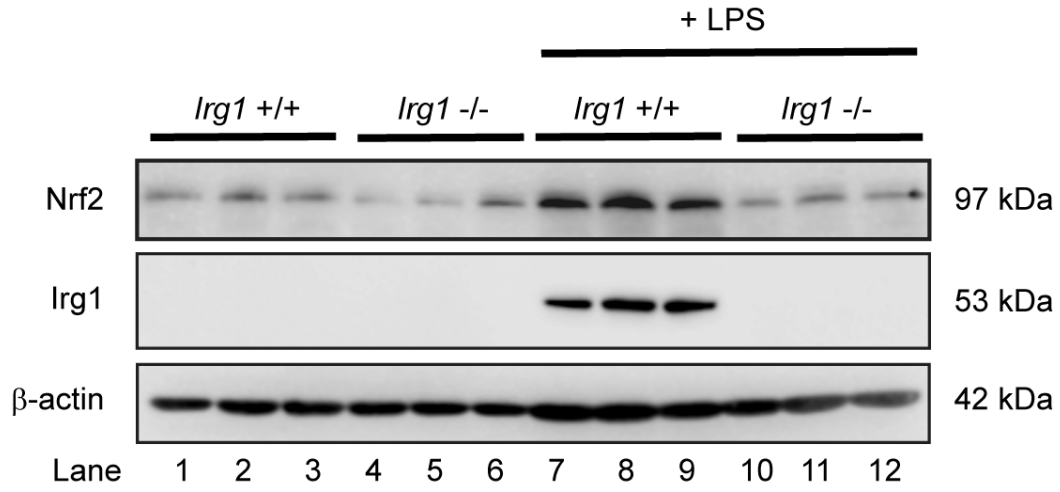

b

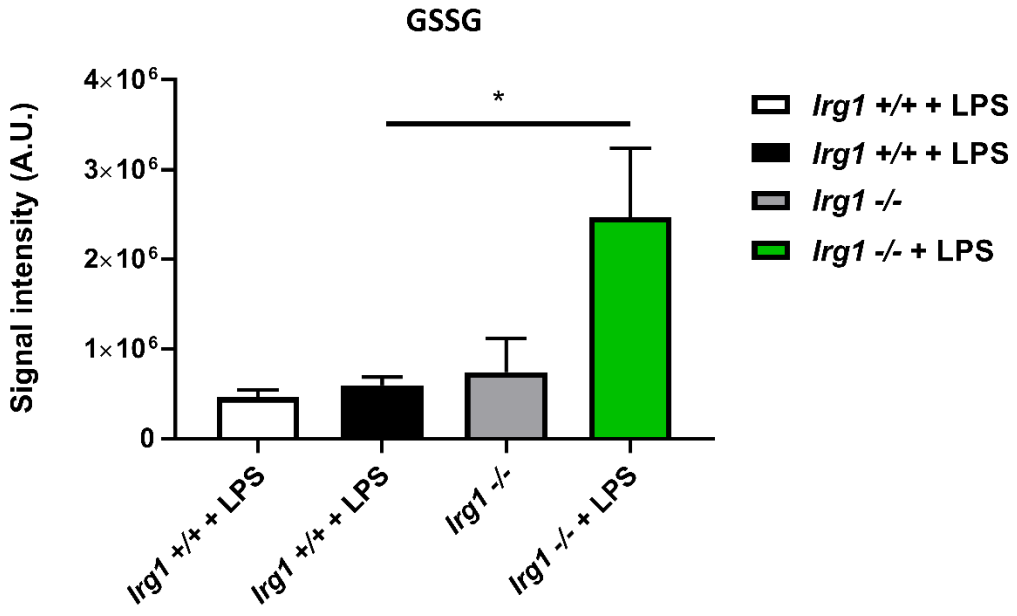

Figure 4.25 – LPS-induced Nrf2 stabilisation is lost in *Irg1 -/-* macrophages

(a) Protein expression of Nrf2, Irg1 and the loading control β-actin in response to LPS treatment (100 ng/mL, 24 h), as assessed by western blot (*n*=3) **(b)** Relative metabolite levels were determined by LC-MS in control or LPS-treated (100 ng/mL, 24 h) *Irg1* +/+ and *Irg1* -/- BMDMs. Relative GSSG levels are shown (*n*=3 biological replicates performed in technical duplicate). Data is presented as mean ± SEM. *P*-values were calculated using an unpaired t-test. **P* <0.05, ***P* <0.01, ****P* <0.001, *****P* <0.0001.

4.2.7 – 4-OI can alkylate cytosolic KEAP1 on key redox sensing cysteines

As itaconate had been found to competitively inhibit SDH and induce succinate accumulation, it was next examined whether inhibition of SDH with the cell permeable competitive inhibitor dimethyl malonate (DMM) could induce Nrf2. Pre-treatment of BMDMs with DMM resulted in a significant decrease in LPS-induced pro-IL1β (Fig. 4.26a; compare lanes 3, 7 & 11 to lanes 4, 8 & 12) and *IL1B* mRNA (Fig. 4.26b) levels but a significant increase in IL-10 secretion (Fig. 4.26c), as previously reported [68]. DMM had no effect on pro-IL1β levels (Fig. 4.26a; compare lanes 1, 5 & 9 to lanes 2, 6 & 10), *IL1B* mRNA (Fig. 4.26b) or IL-10 secretion (Fig. 4.26c) independent of LPS stimulation. DMM pre-treatment had no effect on LPS-induced Nrf2 stabilisation (Fig. 4.26a; compare lanes 3, 7 & 11 to lanes 4, 8 & 12). Equivalently, no induction of Nrf2 was observed in DMM-treated unstimulated BMDMs (Fig. 4.26a; compare lanes 1, 5 & 9 to lanes 2, 6 & 10) suggesting that inhibition of SDH does not play a role in Nrf2 stabilisation in this context.

As induction of Nrf2 by itaconate and 4-OI appeared to occur independently of SDH inhibition, it was hypothesised that covalent modification of key redox sensing cysteines on KEAP1, which is localised to the cytosol, may mediate this effect. Itaconate is generated by Irg1 in the mitochondrial matrix suggesting it must possess the potential to cross the inner mitochondrial membrane (IMM) to act on KEAP1 in the cytosol (141). Itaconate compares structurally to malate, which is transported across the IMM by the dicarboxylate (DIC), citrate (CTP) and oxoglutarate (OGC) carriers (170). As such, the ability of these transporters to traffic itaconate across the IMM was investigated. All three carriers could successfully transport itaconate, whereas the other tested

carriers, 2-oxodicarboxylate carrier (ODC), ADP/ATP carrier 1 (AAC1) and AAC2, could not (Fig. 4.27a, b). Of note, was the OGC carrier, which exhibited a marked ability to transport itaconate in comparison to the DIC and CTP transporters (Fig. 4.27a, b).

As KEAP1 is degraded by autophagy once modified (156) and due to its low copy number in the cell is extremely difficult to immunoprecipitate endogenously (185), direct alkylation of KEAP1 was assessed by overexpressing MYC-DDK-tagged KEAP1 in HEK293T cells and treating with 4-OI. Tandem mass spectrometry (MS) of immunoprecipitated KEAP1 (Fig. 4.28a) revealed that for the Cys 151-containing Keap1 peptide (144-152), generated by digesting KEAP1 with elastase, 4-OI treatment increased its mass by 242.15 Da, consistent with alkylation by 4-OI (Fig. 4.28b). To validate Cys 151 as a target of 4-OI, V5-Nrf2 was co-expressed with either wild-type or a C151S mutant KEAP1 in COS1 cells (Fig. 4.29a; compare lane 1 to lanes 2-3). 4-OI stabilised V5-Nrf2 in COS1 cells expressing wild-type KEAP1, but not the Cys151S mutant (Fig. 4.29a; 4-OI compare lanes 16-17 to lanes 18-19), comparably to known Nrf2 activator sulforaphane (SFN) (Fig. 4.29a; 4-OI compare lanes 8-9 to lanes 10-11). 4-OI also modified other known Keap1 regulatory cysteine residues (Cys 23, Cys 257, Cys 273, Cys 288 and Cys 297) (Fig. 4.30a; Table 4.3) all identified from digestion of KEAP1 with either trypsin (in gel and in solution digestion) or elastase (in gel digestion).

To further explore itaconate-mediated cysteine modification, the data generated from the untargeted quantitative proteomic screen was exploited. To this end, several additional targets were found in LPS-activated (Fig. 4.31a, Fig. 4.32a & Table 4.4) and 4-OI-treated (Fig. 4.33a, Fig. 4.34a & Table 4.5) BMDMs.

Notably, a significant increase in itaconate-mediated alkylation of Cys 84 in LDHA, following treatment with 4-OI itself (Fig. 4.33a) and in LPS-treated macrophages (Fig. 4.31a), was observed. This finding represents the identification of a wholly novel post-translational modification, hereafter defined as 2,3-dicarboxypropylation. Furthermore, these results coupled to the identification of the itaconate-cysteine adducts from LPS-activated macrophages (Fig. 4.16c, d) suggest that itaconate stabilises Nrf2 via alkylation of its key negative regulator KEAP1.

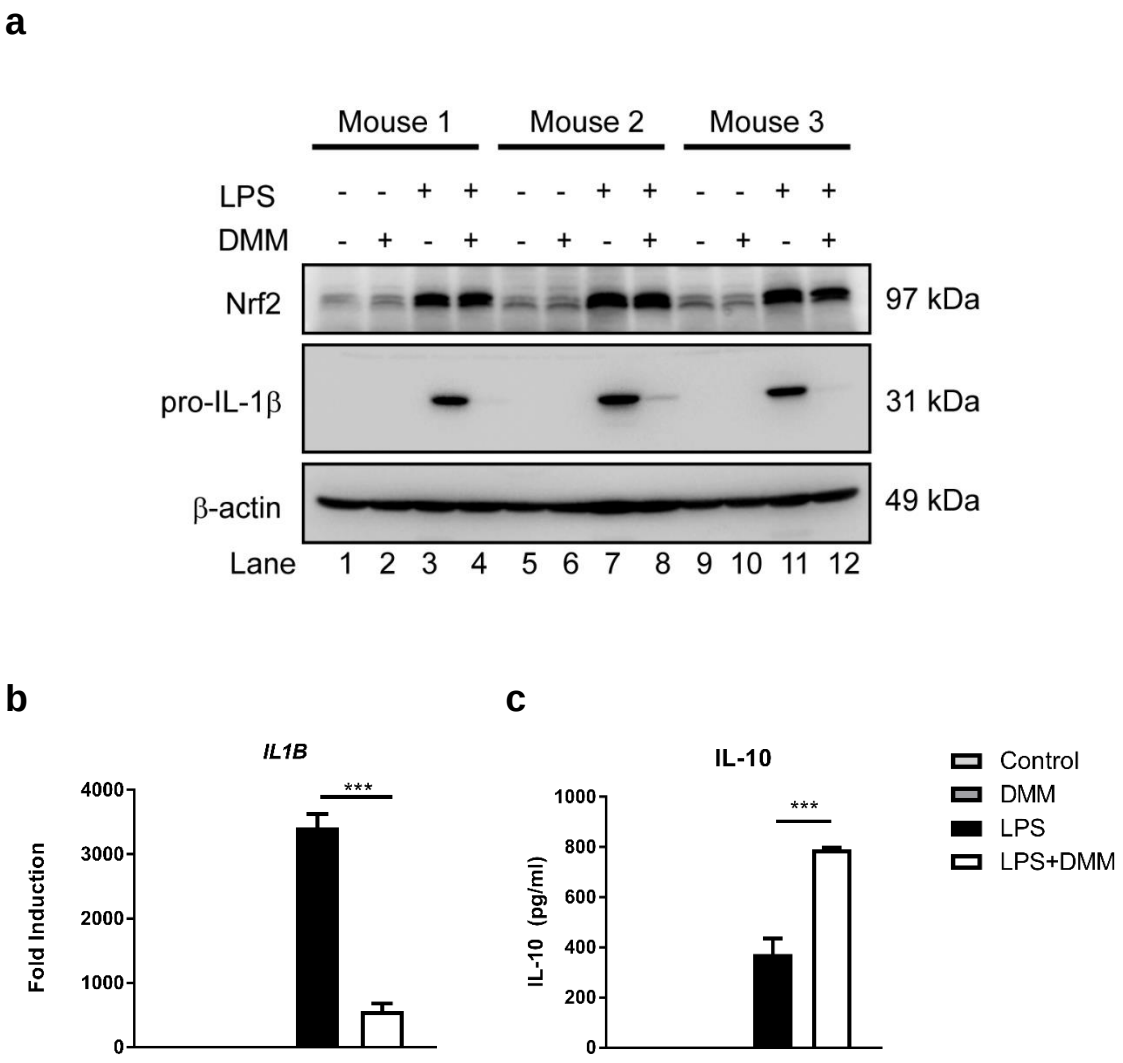

Figure 4.26 – DMM inhibits IL-1β and boosts IL-10, but has no effect on Nrf2

(a) Protein expression of Nrf2, Hmox1 and the loading control β-actin in control or LPS-activated BMDMs (100 ng/mL, 24 h) ± 3 h pre-treatment with DMM (10 mM), as assessed by western blot (*n*=3). **(b)** Relative fold change in *IL1B* mRNA levels in response to LPS treatment (100 ng/mL, 24 h) ± 3 h DMM pre-treatment (10 mM), as assessed by qPCR (*n*=3 biological replicates performed in technical duplicate). **(c)** IL-10 protein levels secreted into the CCM in response to LPS treatment (100 ng/mL, 24 h) ± 3 h DMM pre-treatment (10 mM), as assessed by ELISA (*n*=3 biological replicates performed in technical duplicate). Data is presented as mean ± SEM. *P*-values were calculated using an unpaired t-test. **P* <0.05, ***P* <0.01, ****P* <0.001, *****P* <0.0001.

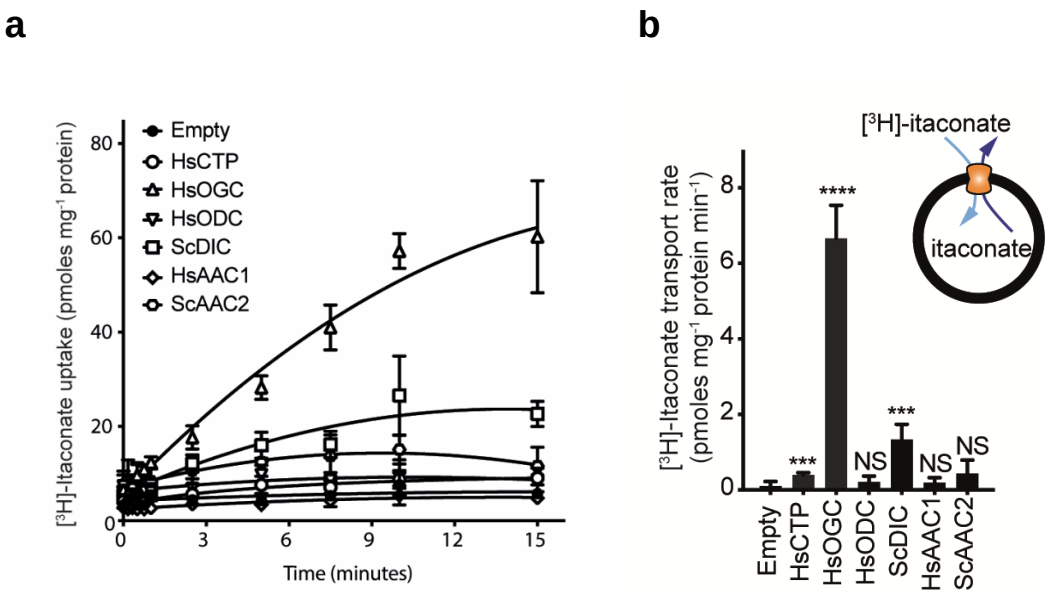

Figure 4.27 – Itaconate can be transported across the IMM

Liposomal-*Lactococcus lactis* membrane fusions expressing the indicated IMM transporters were loaded with itaconate (1 mM) and transport was initiated by the addition of [^{3}H]-itaconate (1 μM). **(a)** Data shows [^{3}H]-itaconate uptake (pmoles mg^{-1} protein) over indicated timecourse (*n*=4). **(b)** Initial transport rates (pmoles mg^{-1} protein min^{-1}) of each carrier for itaconate homoexchange (*n*=4). Empty vector control [^{3}H]-itaconate uptake and transport rates are also shown. Data is presented as mean ± SD. *P*-values were calculated using unpaired t-test. **P* <0.05, ***P* <0.01, ****P* <0.001, *****P* <0.0001.

a

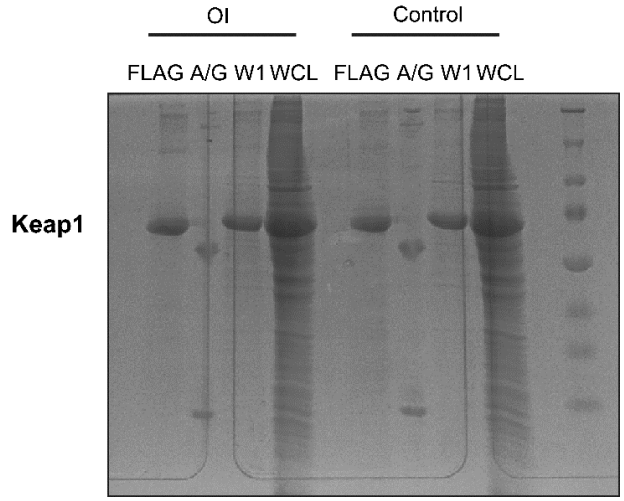

b

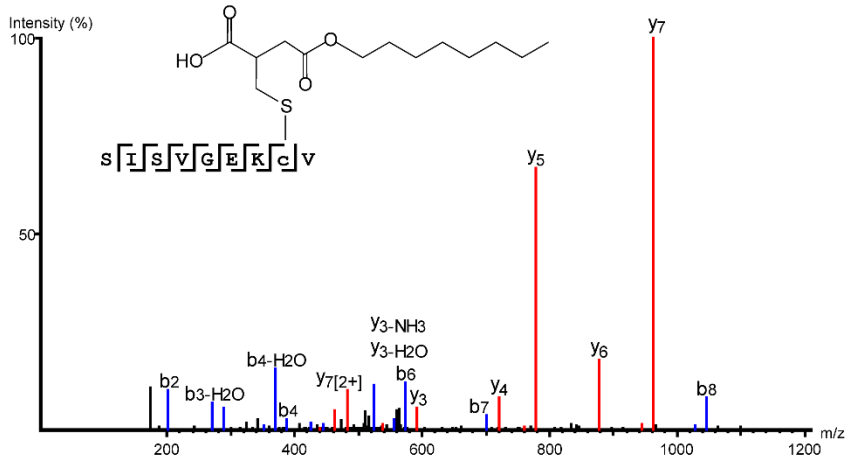

Cysteine 151 (C151)

	b-ions	Sequence	y-ions	
1	88.04	S		9
2	201.07	I	1076.77	8
3	288.20	S	963.45	7
4	378.29	V	876.41	6
5	444.22	G	777.30	5
6	573.25	E	720.28	4
7	701.28	K	591.26	3
8	1046.44	C(+242.15)	463.17	2
9		V	118.09	1

Figure 4.28 – 4-OI alkylates KEAP1 on key redox sensing cysteine C151

(a) MYC-DDK-tagged KEAP1 or empty vector control plasmids (10 μg) were transfected into HEK293Ts prior to treatment with OI (500 μM, 4 h). MYC-DDK-tagged KEAP1 was then immunoprecipitated using an anti-FLAG antibody (5 μg/mL), eluted with a FLAG peptide and ran on a 10% SDS-PAGE gel prior to Coomassie blue staining. Lanes are indicated as follows: FLAG – eluted KEAP1, A/G – protein A/G beads after FLAG elution, W1 – wash 1 and WCL – whole cell lysate. **(b)** MS/MS spectrum of Keap1 Cys151 peptide indicating alkylation with OI, as denoted by a mass shift of +242.15 Da. Detected N- and C-terminal fragments ions of the peptide are assigned in the spectrum and depicted as follows: b: N-terminal fragment ion; y: C-terminal fragment ion; *: fragment ion minus NH_3; ^{0}: fragment ion minus H_2O; and $^{2+}$: doubly charged fragment ion.

a

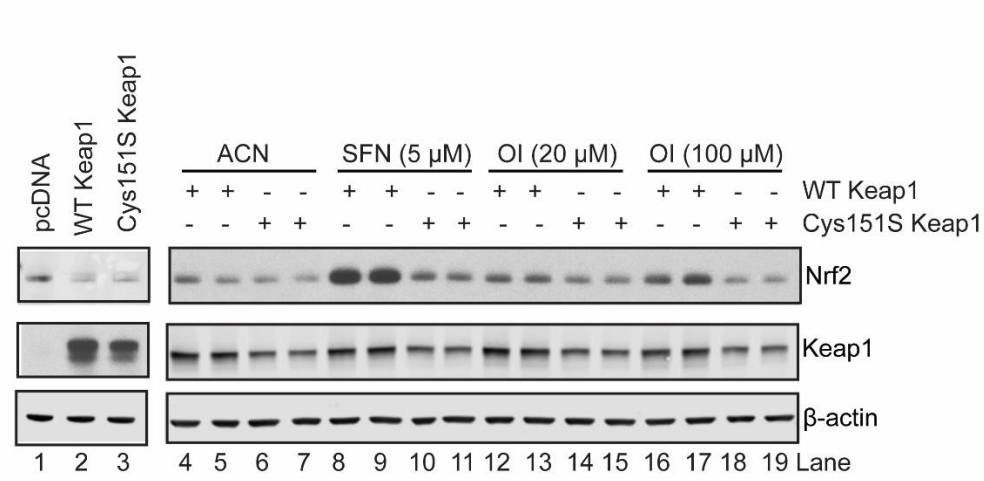

Figure 4.29 – Validation of C151 as a target of 4-OI

(a) Protein expression of Nrf2, KEAP1 and the loading control β-actin in COS1 cells co-transfected with V5-Nrf2 ± wild-type or C151S mutant KEAP1 plasmids and treated as indicated. For the right panel, two independent transfections for each condition is shown. The result is representative of three independent experiments, as assessed by western blot.

a

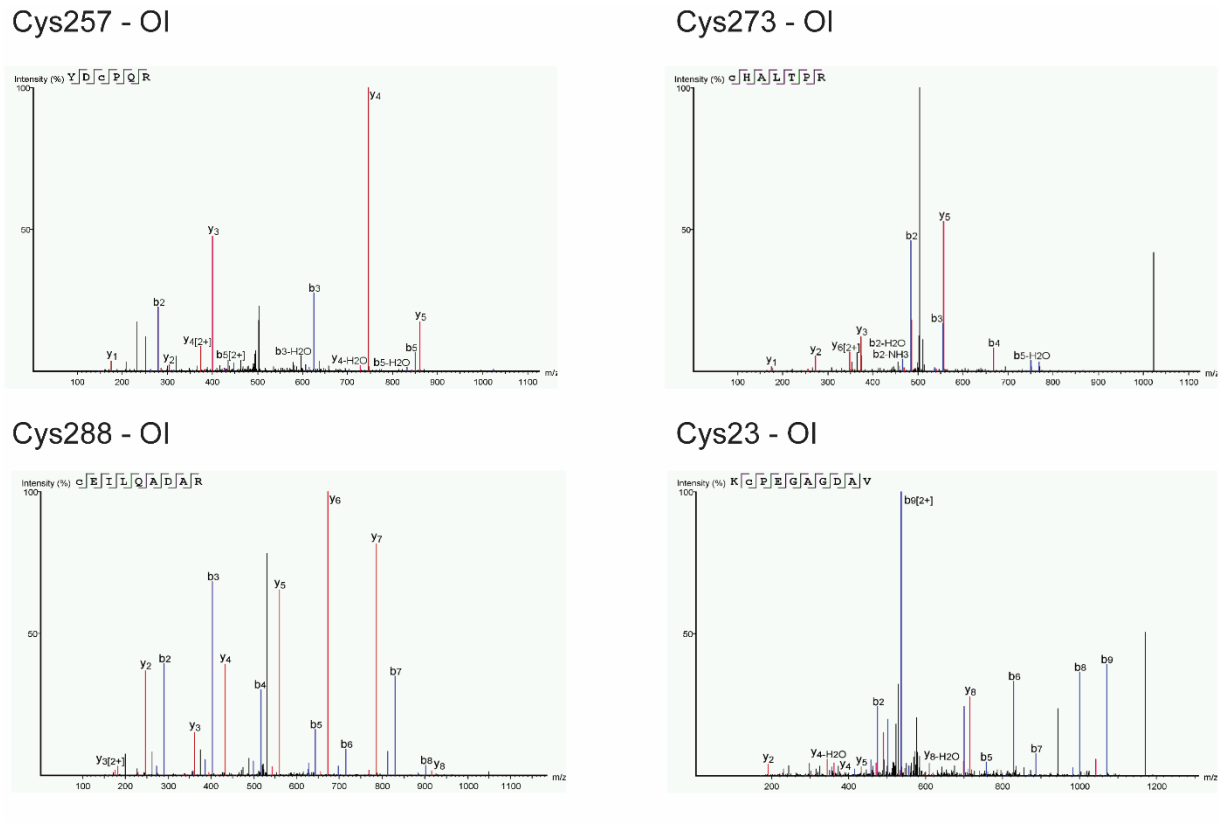

Figure 4.30 – 4-OI alkylates KEAP1 on other key cysteine residues

(a) MS/MS spectrum of KEAP1 Cys257, Cys273, Cys288 and Cys23 peptides indicating alkylation with 4-OI, as denoted by a mass shift of +242.15 Da. Detected N- and C-terminal fragments ions of the peptide are assigned in the spectrum and depicted as follows: b: N-terminal fragment ion; y: C-terminal fragment ion; *: fragment ion minus NH_3; ^{0}: fragment ion minus H_2O; and $^{2+}$: doubly charged fragment ion.

Table 4.3 – Cys residues in KEAP1 modified by OI as determined by tandem mass spectrometry

4-OI Residue	Peptide Amino Acid Position	Peptide Sequence	-10logP	Enzyme	Digest Type
Cys23	22-31	S.KC(+242.15)PEGAGDAV.M	31.47	Elastase	In Gel
Cys151	144-152	A.SISVGEKC(+242.15)V.L	44.11	Elastase	In Gel
	146-152	I.SVGEKC(+242.15)V.L	30.95		
	144-153	A.SISVGEKC(+242.15)VL.H	30.25		
	145-152	S.ISVGEKC(+242.15)V.L	29.32		
Cys257	254-260	V.KYDC(+242.15)PQR.R	35.44	Elastase	In Gel
	255-260	K.YDC(+242.15)PQR.R	40.13	Trypsin	In Gel
	255-260	K.YDC(+242.15)PQR.R	41.08	Trypsin	In Solution
Cys273	273-279	R.C(+242.15)HALTPR.F	35.93	Trypsin	In Gel
	273-279	R.C(+242.15)HALTPR.F	38.65	Trypsin	In Solution
Cys288	282-293	L.QTQLQKC(+242.15)EILQA.D	41.70	Elastase	In Gel
	282-290	L.QTQLQKC(+242.15)EI.L	36.70		
	284-293	T.QLQKC(+242.15)EILQA.D	33.47		
	280-296	R.FLQTQLQKC(+242.15)EILQADAR.C	55.81	Trypsin	In Gel
	288-296	K.C(+242.15)EILQADAR.C	50.84		
	288-296	K.C(+242.15)EILQADAR.C	48.80	Trypsin	In Solution
Cys297	294-304	A.DARC(+242.15)KDYLVQI.F	37.15	Elastase	In Gel
K615	602-615	R.SGVGVAVTMEPCRK(+242.15).Q	37.59	Trypsin	In Gel
	602-615	R.SGVGVAVTM(+15.99)EPCRK(+242.15).Q	36.40		

a

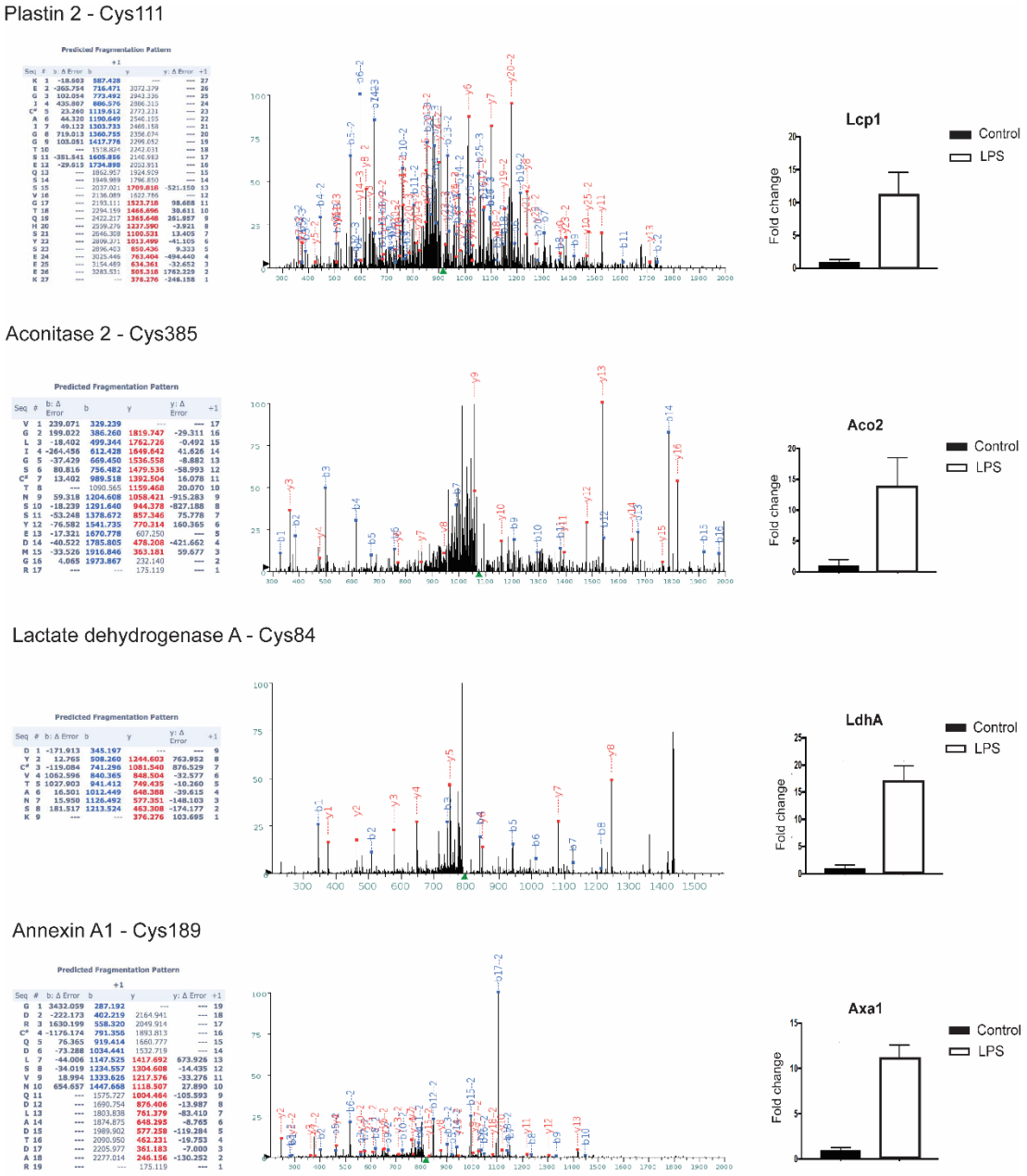

Figure 4.31 – LPS induces dicarboxypropylation of Lcp1, Aco2, LdhA and Axa1

(a) Relative changes in dicarboxypropyl cysteine peptides (right-hand side) were quantified using tandem mass tag (TMT) LC-MS in control and LPS-activated (100 ng/mL, 24 h) BMDMs (*n*=4 biological replicates). Data is presented as mean ± SEM. MS/MS spectrum of Lcp1 Cys111, Aco2 Cys385, LdhA Cys84 and Axa1 Cys189 peptides (left-hand side) indicating alkylation with itaconate.

a

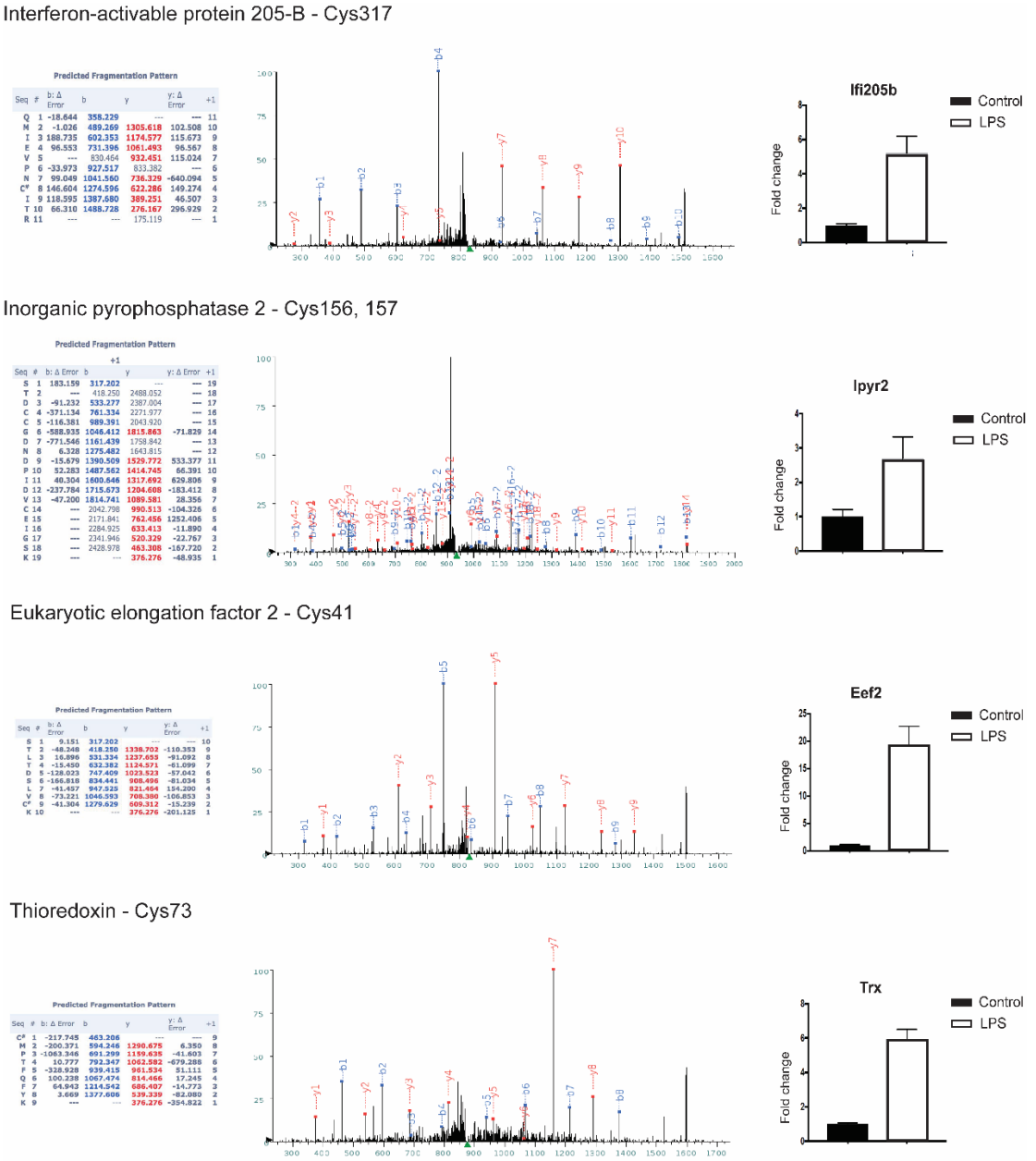

Figure 4.32 – LPS induces dicarboxypropylation of Ifi205b, Ipyr2, Eef2 and Trx

(a) Relative changes in dicarboxypropyl cysteine peptides (right-hand side) were quantified using TMT LC-MS in control and LPS-activated (100 ng/mL, 24 h) BMDMs (*n*=4 biological replicates). Data is presented as mean ± SEM. MS/MS spectrum of Ifi205b Cys317, Ipyr2 Cys157, Eef2 Cys41 and Trx Cys73 peptides (left-hand side) indicating alkylation with itaconate.

Table 4.4 – 2,3-dicarxypropyl cysteine residues identified using tandem mass spectrometry

Protein	Alkylated residue	Peptide amino acid position	Peptide sequence	X score	Ppm
Lcp1	Cys111	97-123	KEGIC(+4.98)AIGGTSEQSSVGTQHSYSEEEK	5.998	-2.22
Aco2	Cys385	378-395	VGLIGSC(+4.98)TNSSYEDMGR	4.212	4.17
Ldha	Cys84	82-90	DYC(4.98)VTANSK	3.474	-2.91
Anxa1	Cys189	186-204	GDRC(4.98)QDLSVNQDLADTDAR	3.514	-0.48
Ifi205b	Cys317	310-320	QMIEVPNC(+4.98)ITR	2.412	-4.16
Ipyr2	Cys156, 157	153-171	STDC(4.98)C(+4.98)GDNDPIDVCEIGSK	4.664	22.60
Ef2	Cys41	33-42	STLTDSLVC(+4.98)K	3.677	-1.41
Thio	Cys73	73-81	C(+4.98)MPTFQFYK	2.422	-2.22

a

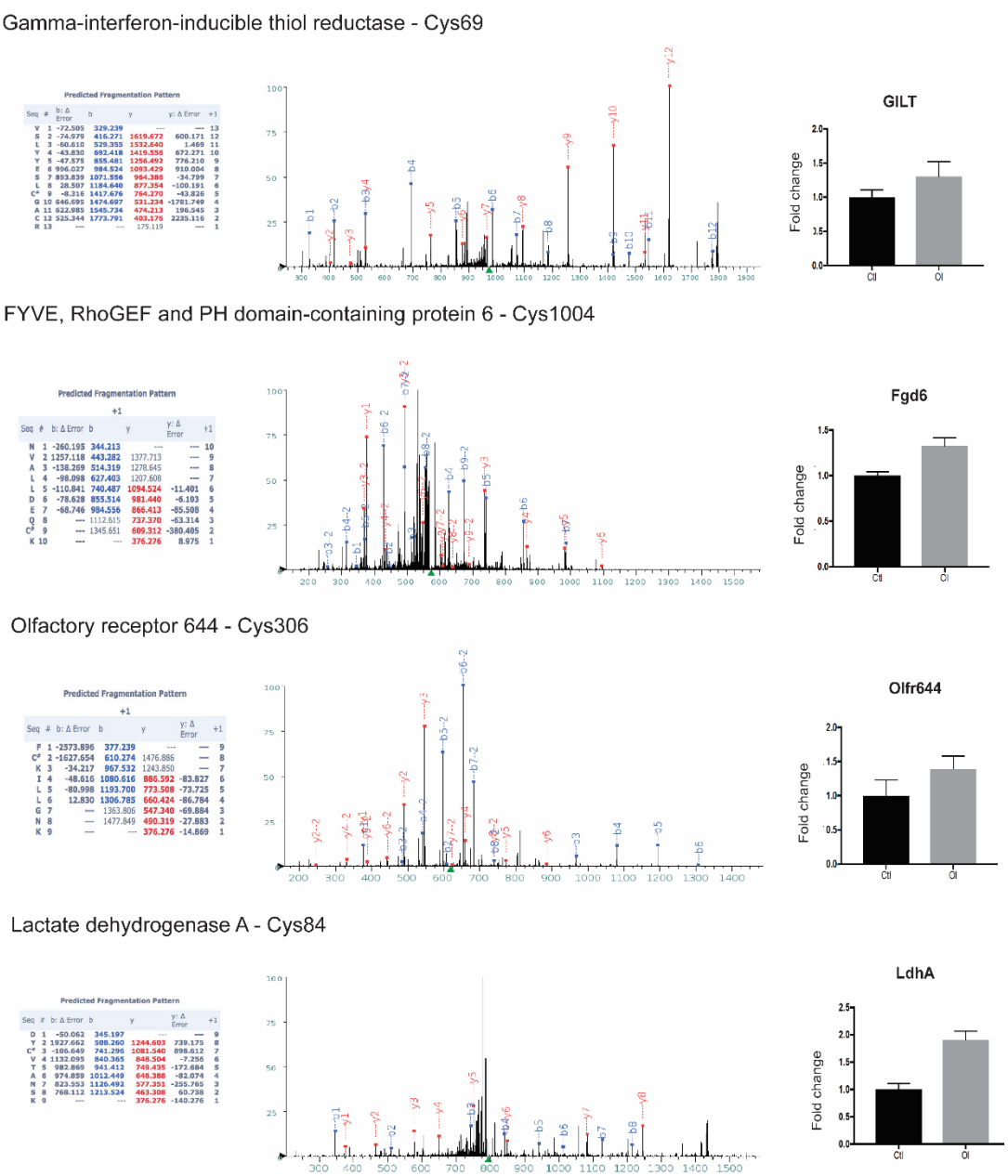

Figure 4.33 – 4-OI alkylates Gilt, Fgd6, Olfr644 and LdhA

(a) Relative changes in OI modified cysteine peptides (right-hand side) were quantified using TMT LC-MS in control and OI-treated (250 μM, 6 h) BMDMs (*n*=4 biological replicates). Data is presented as mean ± SEM. MS/MS spectrum of Gilt Cys69, Fgd6 Cys1004, Olfr644 Cys306 and LdhA Cys84 peptides (left-hand side) indicating alkylation with OI.

a

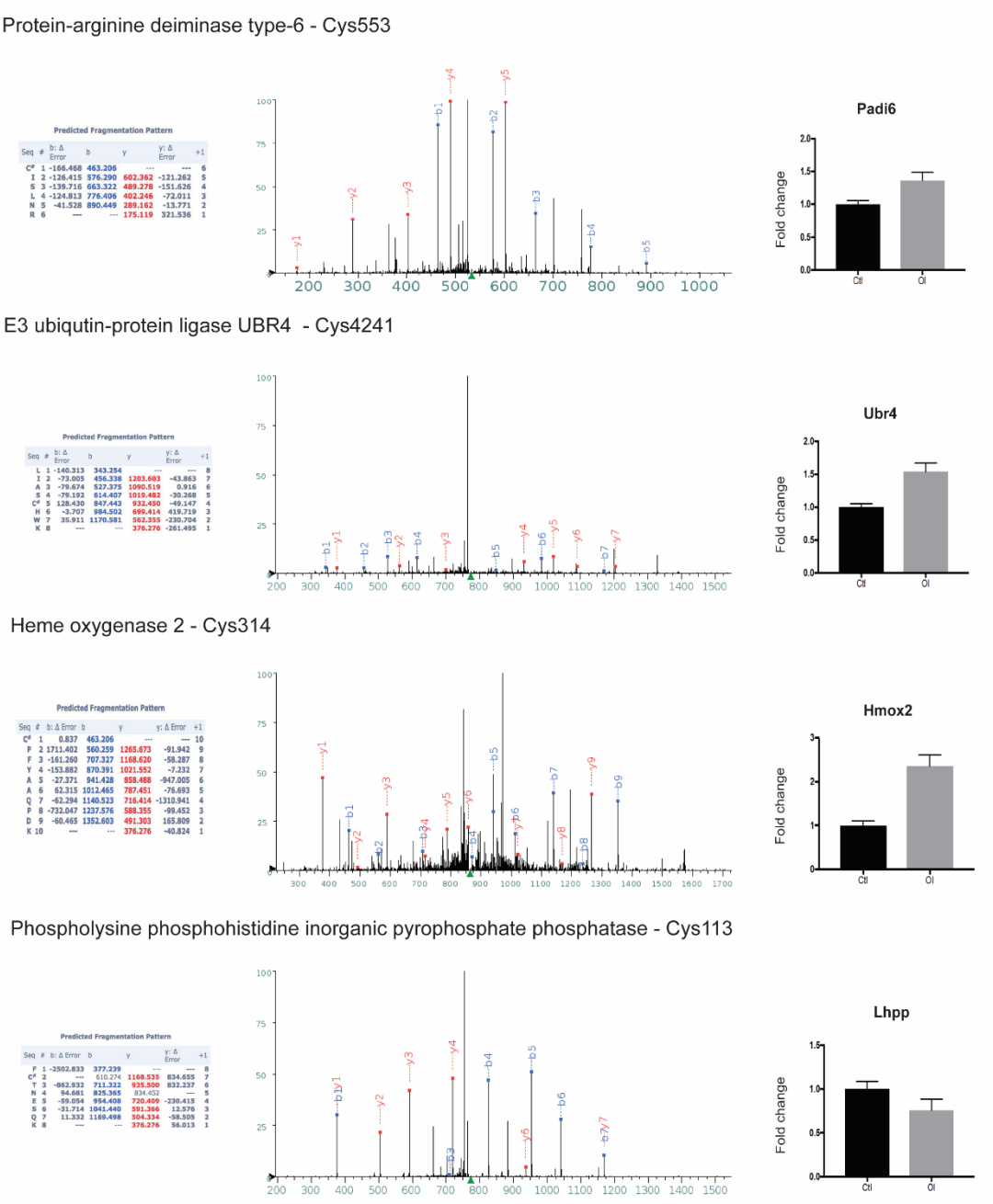

Figure 4.34 – 4-OI alkylates Padi6, Ubr4, Hmox2 and Lhpp

(a) Relative changes in OI modified cysteine peptides (right-hand side) were quantified using TMT LC-MS in control and OI-treated (250 μM, 6 h) BMDMs (*n*=4 biological replicates). Data is presented as mean ± SEM. MS/MS spectrum of Padi6 Cys553, Ubr4 Cys4241, Hmox2 Cys314 and Lhpp Cys113 peptides (left-hand side) indicating alkylation with OI.

Table 4.5 – 4-OI modified cysteine residues identified using tandem mass spectrometry

Protein	Alkylated residue	Peptide amino acid position	Peptide sequence	X score	Ppm
Gilt	Cys69	61-73	VSLYYESLC(+4.98)GACR	4.677	3.40
Fgd6	Cys1004	9996-1005	NVALLDEQC(+4.98)K	3.759	-7.98
Olfr644	Cys306	305-313	FC(+4.98)KILLGNK	3.155	-2.10
Ldha	Cys84	82-90	DYC(+4.98)VTANSK	2.832	3.88
Padi6	Cys553	553-558	C(+4.98)ISLNR	2.446	-18.58
Ubr4	Cys4241	4237-4244	LIASC(+4.98)HWK	2.421	-7.45
Hmox2	Cys314	314-323	C(+4.98)PFYAAQPDK	2.279	2.89
Lhpp	Cys113	112-118	FC(+4.98)TNESQK	2.169	-11.64

4.2.8 – Itaconate and 4-OI are anti-inflammatory metabolites that regulate IL1β

To determine the consequences of elevated itaconate levels on the inflammatory response in macrophages, 4-OI was again employed as an experimental tool. Pre-treatment of BMDMs with 4-OI dose-dependently inhibited LPS-induced pro-IL1β (Fig. 4.35a; compare lane 7 to lanes 8-12) and *IL1B* mRNA (Fig. 4.35b) levels but had no significant effect on *TNF* mRNA expression (Fig. 4.35c) after 6 h of LPS stimulation. In addition, 4-OI dose-dependently inhibited LPS-induced HIF1α stabilisation and pro-IL1β levels (Fig. 4.36a; compare lane 4 to lanes 5-6) after 24 h of LPS stimulation. 4-OI had no effect on pro-IL1β expression (6 h - Fig. 4.35a; compare lane 1 to lanes 2-5; 24 h - Fig. 4.36a; compare lane 1 to lanes 2-3) HIF1α stabilisation (Fig. 4.36a; compare lane 1 to lanes 2-3), *IL1B* (Fig. 4.35b) or *TNF* (Fig. 4.35c) mRNA levels independent of LPS stimulation. Furthermore, LPS-induced pro-IL1β levels were markedly elevated after both 6 h (Fig. 4.37a; compare lane 2 to lane 5) and 24 h (Fig. 4.37a; compare lane 3 to lane 6) LPS stimulation, whilst a significant increase in *IL1B* mRNA expression at both timepoints was also observed (Fig 4.37b). LPS-induced *PHD3* mRNA expression (Fig. 4.38a), pyruvate (Fig. 4.38b) and lactate (Fig. 4.38c) accumulation was also significantly higher in LPS-activated *Irg1 -/-* BMDMs after 24 h indicating elevated HIF1α activation. These data supported previously published reports [43] and indicated that itaconate and its derivatives were anti-inflammatory metabolites that acted to temper pro-inflammatory cytokine production.

Whilst induction of Nrf2 by itaconate and its derivatives had now been well-established, it was unknown whether this was an important mechanism by which it mediated its anti-inflammatory effect. To this end, the ability of 4-OI to modulate IL-1β production in LPS-activated Nrf2 -/- deficient BMDMs was investigated. Confirmation that these BMDMs lacked Nrf2 was first assessed via western blot in control and LPS-activated BMDMs (Fig. 4.39a, b; compare lanes 1-6 to lanes 7-12). Pre-treatment with 4-OI resulted in a dose-dependent inhibition of LPS-induced pro-IL1β protein levels in *Nrf2* +/+ BMDMs but not in *Nrf2 -/-* BMDMs (Fig. 4.39a; compare lane 5-6 to lanes 11-12) after 6 h of LPS stimulation. LPS-induced pro-IL1β expression was increased in *Nrf2 -/-* BMDMs after 24 h of LPS stimulation (Fig. 4.39b; compare lane 4 to lane 10), whilst 4-OI inhibition of pro-IL1β levels was in part abrogated in LPS-activated *Nrf2 -/-* BMDMs (Fig. 4.39b; compare lane 5-6 to lanes 11-12). This is likely due to other mechanisms also coming into play, such as SDH inhibition. Furthermore, 4-OI could no longer stabilise Hmox1 in unstimulated (Fig. 4.39a, b; compare lanes 2-3 to lanes 8-9) or LPS-stimulated (Fig. 4.39a, b; compare lanes 5-6 to lanes 11-12) *Nrf2 -/-* BMDMs. However, the ability of LPS to induce Hmox1 was not completely lost in *Nrf2 -/-* BMDMs (Fig. 4.39b; compare lane 4 to lane 10) suggesting other mechanisms can regulate its expression. All together this data indicates that itaconate and its derivatives are anti-inflammatory metabolites that temper the immune response through inhibition of SDH and stabilisation of Nrf2.

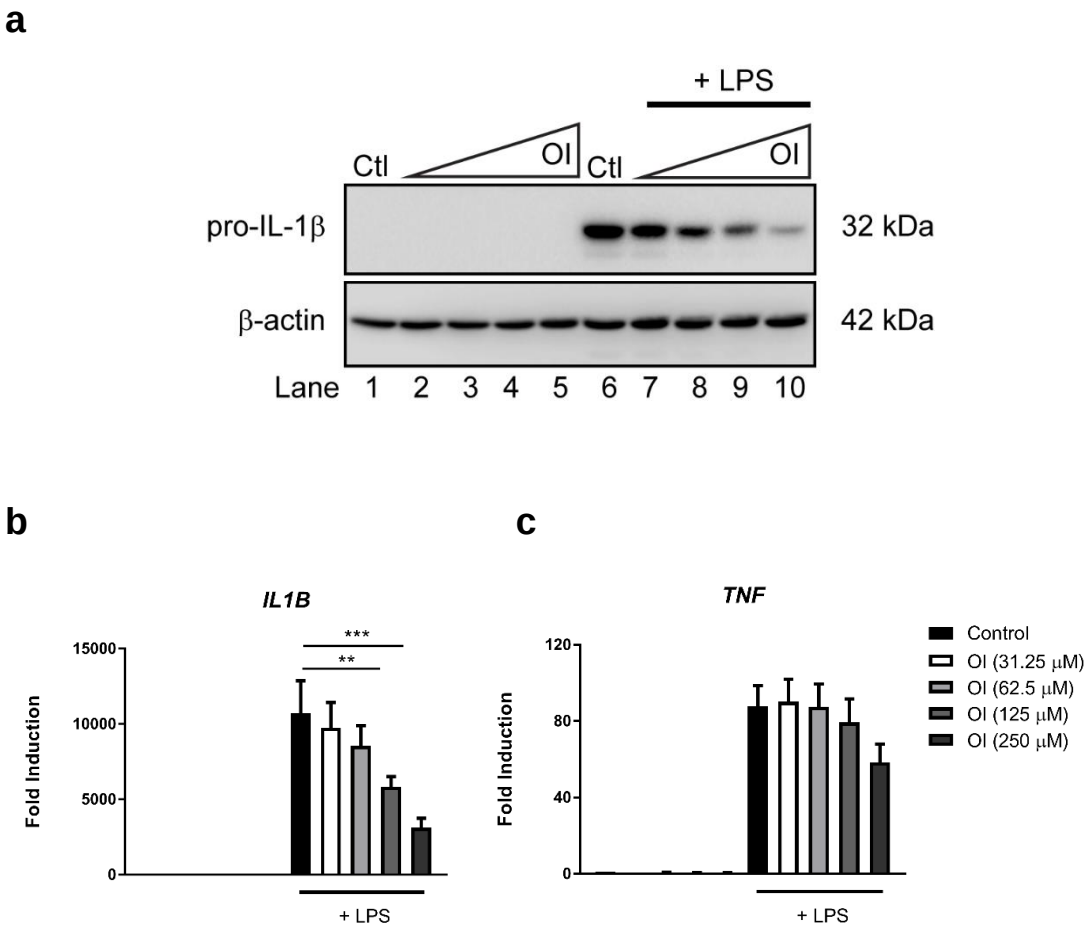

Figure 4.35 – 4-OI dose-dependently inhibits LPS-induced IL-1β production

(a) Protein expression of pro-IL-1β and the loading control β-actin in control or LPS-activated BMDMs (100 ng/mL, 6 h) ± 3 h pre-treatment with OI (31.25, 62.5, 125 and 250 μM), as assessed by western blot. The result shown is representative of three independent experiments. Relative fold change in mRNA levels of *IL1B* **(b)** and *TNF* **(c)** in response to LPS treatment (100 ng/mL, 6 h) ± 3 h OI pre-treatment (31.25, 62.5, 125 and 250 μM), as assessed by qPCR (*n*=4 biological replicates performed in technical duplicate). Data is presented as mean ± SEM. *P*-values were calculated using one-way ANOVA. **P* <0.05, ***P* <0.01, ****P* <0.001, *****P* <0.0001.

a

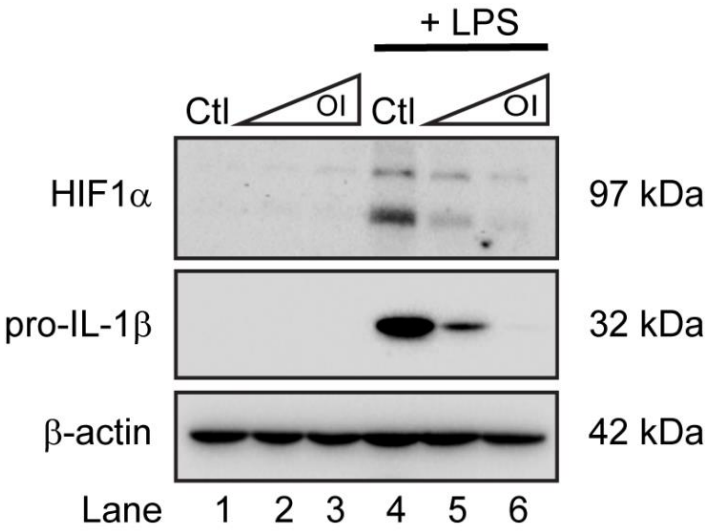

Figure 4.36 – 4-OI dose-dependently inhibits LPS-induced HIF & IL-1β levels

(a) Protein expression of HIF1α, pro-IL-1β and the loading control β-actin in control or LPS-activated BMDMs (100 ng/mL, 24 h) ± 3 h pre-treatment with OI (125 and 250 μM), as assessed by western blot. The result shown is representative of three independent experiments.

a

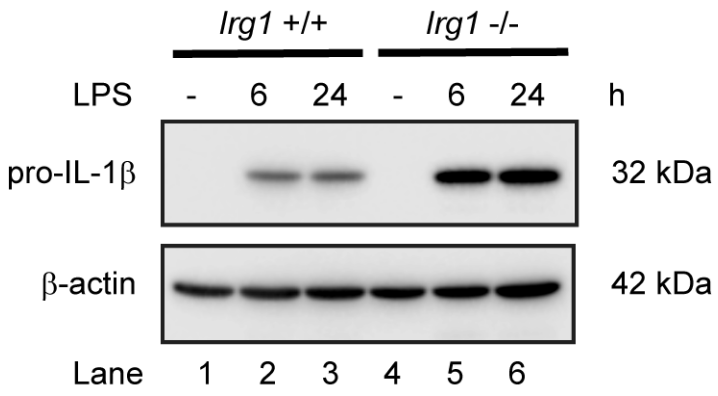

b

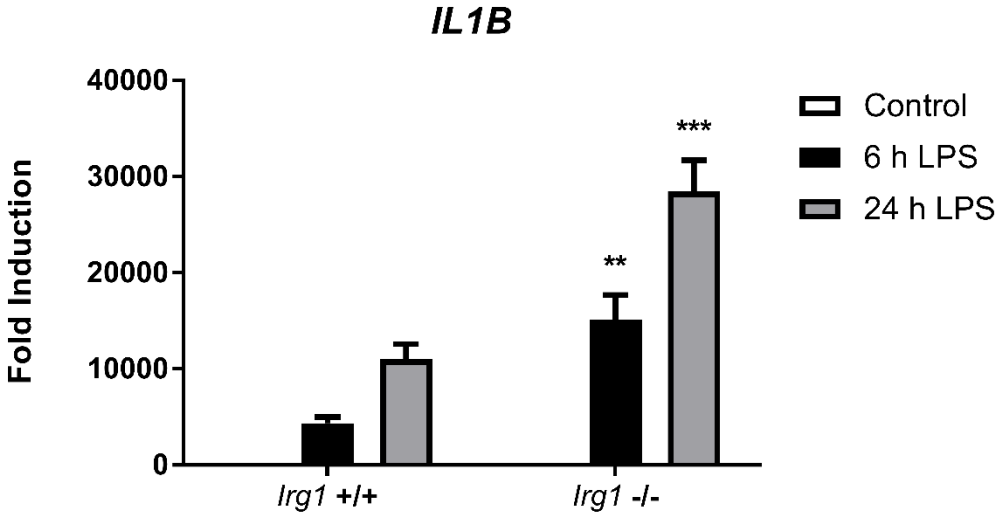

Figure 4.37 – LPS-induced IL-1β is elevated in *Irg1* -/- macrophages

(a) Protein expression of pro-IL-1β and the loading control β-actin in control or LPS-activated *Irg1* +/+ and *Irg1* -/- BMDMs (100 ng/mL, 6 & 24 h), as assessed by western blot. The result shown is representative of three independent experiments. **(b)** Relative fold change in mRNA levels of *IL1B* in response to LPS treatment actin in control or LPS-activated *Irg1* +/+ and *Irg1* -/- BMDMs (100 ng/mL, 6 & 24 h), as assessed by qPCR (*n*=3 biological replicates performed in technical duplicate). Data is presented as mean ± SEM. *P*-values were calculated using one-way ANOVA. **P* <0.05, ***P* <0.01, ****P* <0.001, *****P* <0.0001.

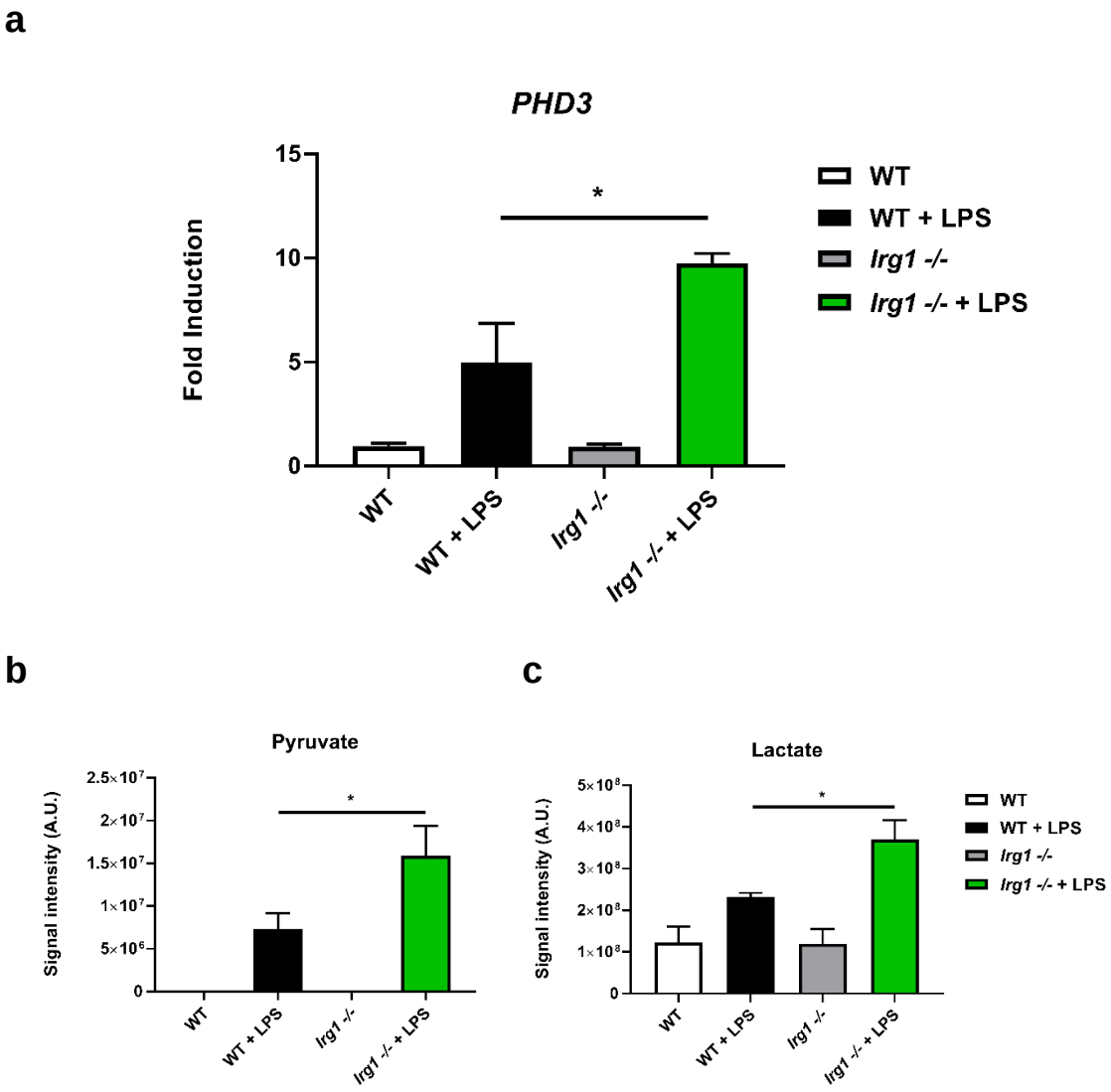

Figure 4.38 – HIF1α activity markers are increased in Irg1 -/- macrophages

(a) Relative fold change in mRNA levels of *PHD3* in response to LPS treatment in control or LPS-activated *Irg1* +/+ and *Irg1* -/- BMDMs (100 ng/mL, 24 h), as assessed by qPCR (*n*=3). **(b)** Relative metabolite levels were determined by LC-MS in control or LPS-treated (100 ng/mL, 24 h) *Irg1* +/+ and *Irg1* -/- BMDMs. Relative pyruvate and lactate levels are shown (*n*=3 biological replicates performed in technical duplicate). Data is presented as mean ± SEM. *P*-values were calculated using one-way ANOVA. **P* <0.05, ***P* <0.01, ****P* <0.001, *****P* <0.0001.

a

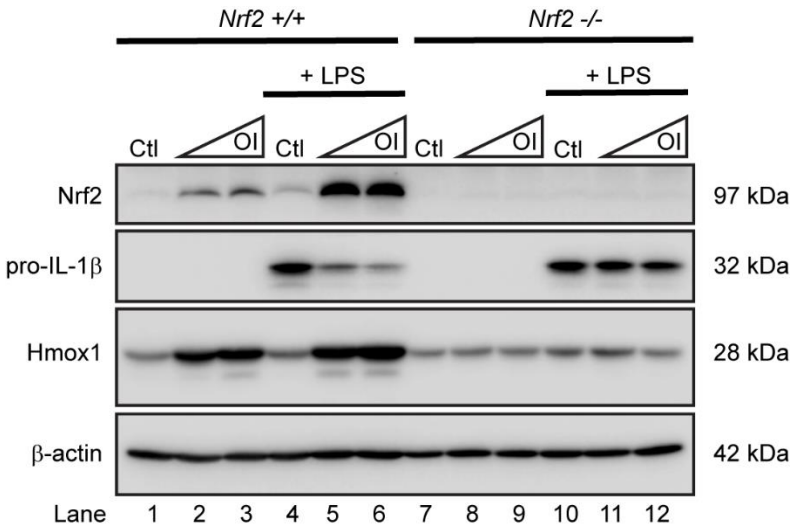

b

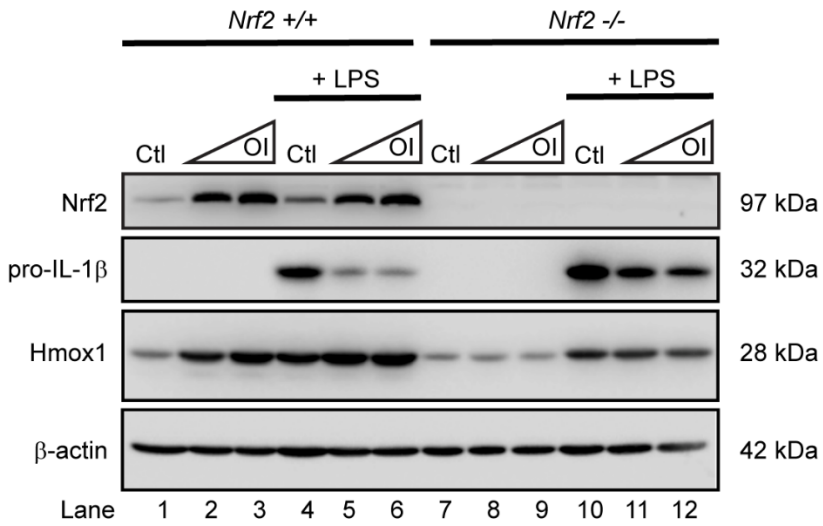

Figure 4.39 – 4-OI inhibition of IL-1β is blunted in *Nrf2 -/-* BMDMs

Protein expression of Nrf2, pro-IL-1β, Hmox1 and the loading control β-actin in *Nrf2 +/+* and *Nrf2 -/-* BMDMs in response to **(a)** LPS treatment (100 ng/mL, 6 h) or **(b)** LPS treatment (100 ng/mL, 24 h) ± 3 h pre-treatment with 4-OI (125 and 250 μM), as assessed by western blot (wildtype *n*=2 biological replicates, knockout *n*=4 biological replicates). The results shown are representative of four independent experiments.

4.3 – Discussion

As one of the most recent and thought-provoking examples of an immunomodulatory metabolite that results from Krebs cycle rewiring is itaconate (49). As such, the second aim of this project was to investigate the inflammatory outcome of elevated itaconate on macrophage function. Evidence of increased IRG1 and itaconate levels in response to LPS was successfully confirmed, as previously reported (45, 49, 100). Itaconate was also found to reach concentrations ranging from 3.5 to 5 mM in LPS-activated macrophages, while succinate was also shown to accumulate to just under 3 mM, again consistent with published observations (49).

In response to LPS, macrophages undergo profound metabolic remodelling, characterised by increased glucose uptake, glycolysis and glutaminolysis (20, 45). As such, the relative contribution of glucose and glutamine-derived carbon towards itaconate and succinate production was determined. Of note, was a significant increase in the m+1 isotopologue of itaconate derived from U-^{13}C-glucose in response to LPS. This shows that newly synthesised pyruvate enters the Krebs cycle to form m+2 labelled citrate, which is subsequently converted to m+2 labelled *cis*-aconitate. As IRG1 catalyses the decarboxylation of *cis*-aconitate, this results in the formation of m+1 labelled itaconate (101). As such, this result provides further evidence for the existence of a breakpoint at IDH in the Krebs cycle of LPS-activated macrophages (20, 45) and suggests that TLR4-induced glucose uptake, aerobic glycolysis and Krebs cycle rewiring occurs, at least in part, to support itaconate synthesis. This finding is also consistent with a study conducted by Meiser *et al* (2015), whereby the authors demonstrated the importance of pyruvate oxidation in supporting

itaconate synthesis in the macrophage-like RAW264.7 cell line (101). Unlike itaconate, where ~ 60 % of the total pool contained glucose-derived carbon, succinate had no glucose-derived carbon under resting conditions with this rising to ~ 20 % of the total pool upon LPS stimulation. This would suggest that other fuels primarily feed the Krebs cycle to facilitate succinate accumulation, although glucose does play a minor role.

Alternatively, when a U-^{13}C-glutamine tracer was used, a significant increase in the m+4 isotopologue of itaconate was found upon LPS stimulation, which suggests TLR4 activation also promotes the flux of glutamine into the Krebs cycle to support itaconate synthesis. Interestingly, glutamine anaplerosis and subsequent metabolism by either the oxidative arm or reductive arm (reversal through IDH) of the Krebs cycle can result in the generation of the m+4 itaconate isotopologue (48, 101). Using CoMBI-T, Jha *et al* (2015) failed to detect a reversal in the directionality of IDH, a strong indication that the reductive arm of the Krebs cycle was inactive in primary murine macrophages stimulated with LPS and IFN-γ (45). Data from this study also supports this finding as the presence of the m+4 isotopologue in succinate, malate, citrate and *cis*-aconitate (data not shown) implicates oxidative glutamine metabolism as the primary pathway feeding itaconate. Likewise, no m+5 labelling could be detected in the citrate pool. In contrast to this, Cordes *et al* (2016) demonstrated the importance of both the oxidative and reductive arm in generating glutamine-derived itaconate (48). This was accomplished by utilising a [1-^{13}C] glutamine tracer that can only label itaconate generated via reductive carboxylation (48). However, it is important to note that this study was performed in the RAW264.7, an immortalised cell line, known to demonstrate an appreciably different metabolic

profile upon LPS stimulation (135). Furthermore, the engagement of reductive glutamine metabolism (reductive carboxylation) is a hallmark of rapidly growing malignant cells with defective mitochondrial function, similar to that observed in an LPS-activated macrophage, suggesting the transformed nature of this macrophage-like cell line may not adequately mirror events in primary macrophages (211). As such, future tracing experiments in primary macrophages should utilise [1-^{13}C] glutamine to definitively determine the relative contribution of oxidative and reductive glutamine metabolism to itaconate synthesis. Consistent with previous reports (20), LPS-induced glutamine anaplerosis was shown to be a major pathway driving succinate accumulation.

During this project, two independent studies uncovered a novel role for itaconate as an important immunomodulator, whereby it acts as an endogenous inhibitor of SDH in LPS-activated macrophages (48, 49). Furthermore, the authors were able to demonstrate the importance of itaconate in dictating TLR4-induced metabolic rewiring, namely the suppression of OXPHOS and the accumulation of succinate (48, 49). Intriguingly, OCR levels significantly increased in *Irg1* -/- BMDMs stimulated with LPS (49). This increase is likely due to increased fuelling of the Krebs cycle by glutamine in the absence of SDH inhibition. Using the cell permeable itaconate derivative DMI and *Irg1*-deficient BMDMs, Lampropoulou *et al* (2016) went on to suggest that inhibition of SDH by itaconate acted as a negative regulator of several pro-inflammatory cytokines, such as IL-6 and IL-1β (49). That same year, Mills and Kelly *et al* (2016) convincingly demonstrated the importance of SDH and succinate oxidation in the regulation of pro-inflammatory cytokine production (62).

Outside of these studies, relatively little was known about the role of itaconate in metabolic reprogramming and cytokine production in macrophages. To elucidate this, three pharmacological agents and one genetic approach were employed as experimental models to either lower or elevate intracellular itaconate levels. As IRG1 is a mitochondrial enzyme that synthesises itaconate from the Krebs cycle intermediate *cis*-aconitate, an untargeted metabolomics screen utilising LC-MS was performed in *Irg1* +/+ and *Irg1* -/- BMDMs to determine whether loss of this enzyme and itaconate production affected the reprogramming of metabolism induced by LPS, as previously mentioned. Importantly, this screen again confirmed the requirement of IRG1/CAD for itaconate production in macrophages and that these were indeed *Irg1/Acod1* -/- mice. One of the most striking results from this metabolic screen was the complete loss of succinate accumulation in LPS-activated *Irg1* -/- BMDMs, which directly implicated itaconate in succinate accumulation. Furthermore, treatment of macrophages with either itaconic acid or the itaconate derivative, 4-OI, was sufficient to increase itaconate levels and induce succinate accumulation. Increased levels of fumarate, malate and aspartate, metabolites downstream of succinate oxidation and SDH, in *Irg1* -/- BMDMs and decreased aspartate levels in ITA-treated macrophages implied that itaconate modulated succinate levels via targeting of SDH, as previously reported (48, 49).

This result with itaconic acid also suggests that it can indeed cross the plasma membrane, as previously reported (48), and in agreement with a more recently published study that demonstrated uptake of itaconic acid into resting and IL-4 activated macrophages (212). However, it is important to note ElAzzouny *et al* (2017) also demonstrated appreciable adsorption of itaconic acid

to the plasma membrane surface. As such, the kinetics of itaconate uptake into macrophages needs to be further explored to determine how efficient this uptake is and how it occurs mechanistically. Current data indicates that uptake occurs down a concentration gradient as LPS-activated macrophages were less able to take up extracellular itaconate (212). As such, its use in exploring the function of activated macrophages may be limited where intracellular concentrations are high.

Interestingly, itaconic acid is secreted by LPS-activated macrophages (49, 117). It would be tempting to speculate that released itaconate may have paracrine or autocrine effects on local macrophage populations or indeed other inflammatory cell types, such as epithelial cells or T cells. Furthermore, there is also a possibility that some unknown dicarboxylate transporter exists on the plasma membrane mediating its uptake. However, published findings suggest that itaconate is not actively secreted from the cell but leaks out due to passive diffusion down its concentration gradient (213). The authors also failed to detect in urine or plasma from patients with sepsis or in bronchiolar lavage fluid (BALF) from patients with pulmonary inflammation (213). As such, it appears itaconate is a poor biomarker of systemic inflammation, and unlike lactate, is not actively secreted into major bodily fluids (213). It is important to note however, that these findings don't rule out the possibility of released itaconate acting more locally in certain tissues, such as in an arthritic joint, where it has been identified as an important biomarker (214) but does suggest that itaconate primarily acts in a cell intrinsic manner to modulate metabolism, inflammation and act as an anti-bacterial agent. These important questions and possibilities should be investigated in future studies.

More recently, itaconate, through its ability to inhibit SDH, has been found to be an important regulatory node linking innate immune tolerance and trained immunity (215). Specifically, Domínguez-Andrés *et al* (2019) demonstrated that itaconate production mediated tolerance in LPS activated human monocytes, whereas β-glucan induced trained immunity overcame this by inhibiting IRG1 and increasing SDH expression to maintain the integrity of the Krebs cycle (215). To further support the IRG1-itaconate-SDH axis in myeloid cells, the authors were able to identify polymorphisms in both IRG1 and SDH that modulate tolerance and innate immune training (215). In addition, a murine model of Zika virus (ZIKV) infection was recently used to identify a novel innate immune pathway in neurons (136). Intriguingly, ZIKV-infected neurons activated key components of the virus-induced necroptotic pathway (namely the nucleotide sensor ZBP1 and the kinase RIPK3), which induced IRG1 expression and itaconate synthesis, as opposed to cell death (136). Furthermore, itaconate was shown to inhibit SDH in neurons to suppress viral replication. As such, the findings from this project, along with published results, fully support the idea of itaconate as an endogenously produced SDH inhibitor that dictates rewiring of the Krebs cycle in macrophages, but now also extends this to neurons.

Itaconate is only regarded as a weak inhibitor of SDH (135) and is far less potent than the competitive inhibitor malonate, previously used as an experimental tool to assess the importance of SDH in regulating macrophage function (62). As such, it was hypothesised that itaconate may also mediate its anti-inflammatory effects via an additional yet unidentified mechanism. Interestingly, an RNA-seq screen conducted in DMI-treated BMDMs revealed a distinct enrichment in genes known to be regulated by Nrf2, notably those

involved in phase II detoxification and glutathione conjugation (49). This led to the hypothesis that itaconate may act as an endogenous activator of Nrf2, a critical anti-inflammatory and anti-oxidant transcription factor that regulates cytokine production in macrophages, as previously discussed (159). Indeed, the ability of DMI to induce Nrf2, augment LPS-induced Nrf2 and inhibit LPS-induced pro-IL-1β expression in macrophages was successfully confirmed. Furthermore, Itaconate, like fumarate, is an α, β-unsaturated carbonyl compound. As DMI had the ability to induce Nrf2, it was hypothesised that the electrophilic alkene moiety of itaconate could undergo nucleophilic attack from cysteine thiolate ions. This would subsequently result in an irreversible covalent modification comparable to the fumarate-mediated PTM succination, whilst it would also result in the formation of an itaconate-cysteine adduct, chemically termed 2,3-dicarboxypropyl cysteine, akin to 2SC (176). Interestingly, LPS was found to significantly induce formation of this novel metabolite, which like itaconate, was derived in part from glucose and glutamine. This provided strong evidence that endogenously produced itaconate is cysteine reactive and can modify protein thiol residues in LPS-activated macrophages, however, these itaconate-cysteine adducts could also represent breakdown products of Itaconate-GSH adducts, such as those observed by Bambouskova et al (2018) (127). As such this study along with Bambouskova *et al* (2018) provided the first evidence of itaconate as a thiol reactive metabolite.

During this study however, ElAzzouny *et al* (2017) convincingly found that DMI was not metabolised to itaconate intracellularly (210). This posed a problem as dimethyl esterification of itaconate would hypothetically render itaconate an activated Michael acceptor, as observed with DMF (162). Like DMF, DMI was

shown to rapidly deplete GSH levels, which suggested that DMI may also result in acute Nrf2 activation and electrophilic stress. Indeed, Bambouskova *et al* (2018) identified a novel ATF3-Iκbζ inflammatory axis activated by DMI in macrophages that regulated secondary transcriptional responses (127). This was based on its ability to deplete intracellular GSH by forming DMI-GSH adducts thus inducing an electrophilic stress response (127). Furthermore, stabilisation of Nrf2 was also confirmed in DMI-treated BMDMs, supporting the findings in this study.

Unlike fumarate, the reactive alkene moiety of itaconate is only conjugated to one carboxyl group. Under physiological conditions (pH 7.4) itaconate is preferentially found in its dicarboxylate form at a ratio of 90:1 (both carboxylic acid groups are deprotonated and negatively charged). As such, thiolate addition, which is the rate-determining step of the reaction, would result in the formation of a carboxylate dianion (high energy intermediate), but this only occurs at the carboxylate proximal to the electrophilic alkene (1 position) in itaconate. The formation of a carboxylate dianion is highly disfavoured due to electrostatic repulsion and so this reaction proceeds very slowly. Esterification of DMI at the 1 position lowers the energetic barrier (LUMO) required for the reaction to proceed. From this, itaconic acid is predicted to be 3600 times less reactive than DMI. It also predicts that the acidic pH increases the electrophilic properties of itaconate, such as that observed for fumarate (198). The chemical environment of the thiol group may also be important for 2,3-dicarboxypropylation as positively charged amino acids, such as arginine or lysine, could hypothetically donate a proton to the carboxyl group of itaconate proximal to the alkene thus stabilising the reaction. To counteract the increased thiol reactivity of DMI,

selective esterification of the carboxyl group distal to the alkene (4 position) was used to generate 4-OI. This selective esterification of the 4 position is important as it does not prevent the formation of the dianion at the 1 position after thiolate addition under physiological conditions (see Fig. 4.40 (216)). As such, 4-OI and itaconic acid should retain similar chemical reactivity, whilst the hydrophobic octyl group would enable 4-OI to cross the membrane. In contrast to DMI, 4-OI could not deplete GSH levels after 2 h indicating that 4-OI represented an appropriate cell-permeable itaconate surrogate.

Treatment of LPS-activated BMDMs with 4-OI also resulted in a significant increase in intracellular itaconate levels, however, no increase in intracellular itaconate was observed in control macrophages after 6 h. This was rather puzzling and so it was speculated that LPS could perhaps induce a carboxylic acid esterase that would be required for efficient hydrolysis of 4-OI. Interestingly, carboxylic acid esterase (CES1a) was found to be one of the most up-regulated proteins in LPS-activated macrophages in the proteomic screen, with very low expression in resting macrophages (data not shown). As such, LPS induction of CES1a provides a plausible explanation for this observation. Furthermore, a more comprehensive investigation into 4-OI hydrolysis in macrophages across a timecourse and using a U-^{13}C-4-OI tracer may be beneficial in future studies.

Using an unbiased quantitative proteomic screen, 4-OI was shown to significantly boost Nrf2, Hmox1 and SQSTM1 supporting a role for itaconate as an activator of Nrf2. SQSTM1 (also known as p62) is an autophagy cargo receptor known to interact and inhibit KEAP1 (155). 4-OI induction of Nrf2 and HMOX1 was further validated by western blot, an effect also observed in PECs derived from mice injected peritoneally with 4-OI. 4-OI also induced several Nrf2

target genes, including *Hmox1*, as well as increasing GSH and serine levels. Pre-treatment of BMDMs with itaconic acid also stabilised Nrf2, induced Hmox1 and increased intracellular GSH levels. Importantly, Nrf2 is a key regulator of serine and GSH biosynthesis (137, 217). Furthermore, LPS-induced Nrf2 stabilisation was lost in *Irg1 -/-* macrophages, consistent with findings from Bambouskova *et al* (2018) (127). Whilst a significant increase in GSSG was observed in LPS-activated *Irg1 -/-* macrophages, which can often occur under conditions where Nrf2 activation is defective (218). As such, this data provided strong evidence that itaconate is a key regulator of Nrf2 in macrophages.

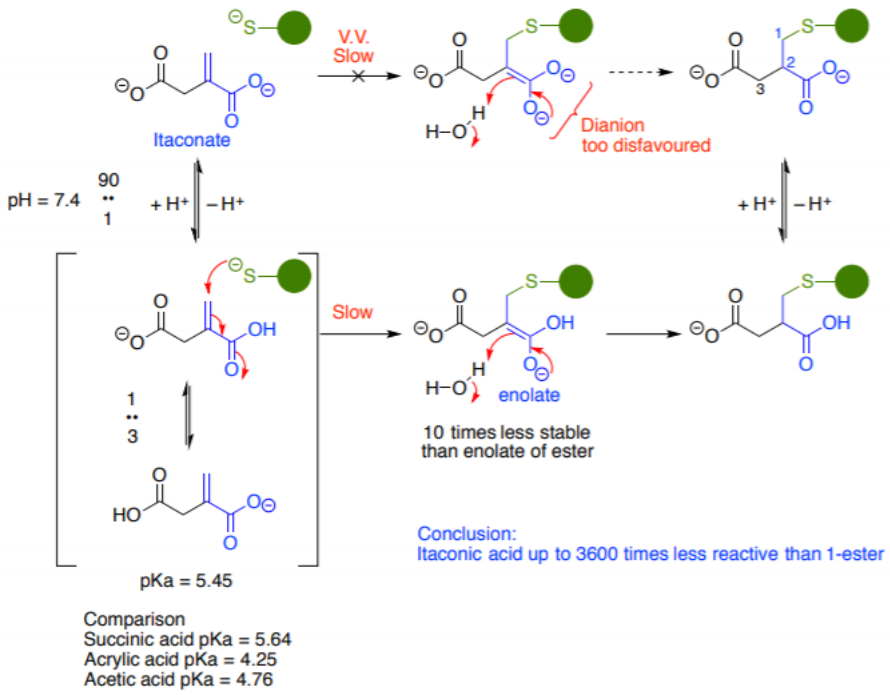

Figure 4.40 – Reaction mechanism of itaconate.

Overview of itaconate ionisation states at different pH and its reaction with thiolate ions of protein cysteine residues (216).

Nrf2 induction of p62 likely represents a means of eliminating thiol-modified and inactive KEAP1 from the cell (137), which coupled to the identification of 2,3-dicarboxypropyl cysteine and the necessity of the itaconate moiety of 4-OI to induce Nrf2 in an SDH-independent manner, suggested that itaconate may directly modify KEAP1. As KEAP1 is localised to the cytosol (141), itaconate would have to be exported from the mitochondrial matrix where it's produced by IRG1. Itaconate compares structurally to malate, which is transported across the IMM by the DIC, CTP and OGC carriers (170). Indeed, all three carriers were found to transport itaconate providing a means for itaconate to leave mitochondria and act on KEAP1 in the cytosol. As KEAP1 is degraded by autophagy once modified (156), direct alkylation of KEAP1 was assessed by overexpressing MYC-DDK-tagged Keap1 in HEK293T cells and treating with 4-OI. Using tandem mass spectrometry, 4-OI was found to modify several key redox sensing KEAP1 regulatory cysteine residues, including Cys151, Cys273 and Cys288. KEAP1 modifiers can be subdivided into four categories depending on the cysteine residues modified (154). Therefore, 4-OI can now be defined as a class III inducer as it was found to modify this key cysteine triad. This profile is also like that previously observed for fumarate and fumaric acid esters (162). One caveat of this approach is that itaconate-modified Keap1 itself was not detected, however, the totality of the evidence does strongly implicate this as the mechanism of Nrf2 activation. Bambouskova *et al* (2018) suggest Nrf2 activation by itaconate resulted from the depletion of intracellular GSH, and while this may contribute, it is far less likely as itaconate is not very reactive with GSH even at pH 8 (127). Itaconate would be predicted to react more readily with Cys151 of KEAP1, just like 4-OI, based on their shared reactivity profile. C151 is also a

more likely target because it exists entirely in its reactive thiolate form at physiological pH, as positively charged amino acid residues (H129, K131, R135, K150 and H154) in the surrounding environment act in concert to lower its pK_a (219). Cys151 is also the most frequently modified residue by Nrf2 activating agents.

Following this, pre-treatment of BMDMs with 4-OI was shown to potently inhibit LPS-induced *IL1B* mRNA, pro-IL-1β and HIF1α protein expression, however, no significant effect was observed on *TNF* mRNA levels. While LPS-induced *IL1B* mRNA, pro-IL-1β levels were also significantly elevated in *Irg1 -/-* BMDMs. Increased PHD3 mRNA expression and increases in the abundance of pyruvate and lactate (markers of aerobic glycolysis) suggested increased HIF1α activity in these cells, as previously reported (49). Although induction of Nrf2 by 4-OI had now been well-established, it was unknown whether this was an important mechanism by which it mediated its anti-inflammatory effects. Indeed, the ability of 4-OI to inhibit pro-IL1β expression in Nrf2-deficient macrophages was markedly impaired, confirming a role for itaconate-mediated Nrf2 stabilisation in the negative regulation of IL-1β. The ability of Nrf2 to regulate IL-1β in this context is likely two-fold. Firstly, by directly binding regulatory regions in the *IL1B* promoter thus interfering with the recruitment of RNA pol II, as previously shown (159). Secondly, Nrf2 activation is essential for ROS detoxification, whereas ROS are a key driver of HIF1α stabilisation and *IL1B* mRNA expression in LPS-activated macrophages (62). 4-OI was observed to potently lower ROS levels (data not shown) in addition to dose-dependently inhibiting LPS-induced HIF1α protein levels, strongly supporting this hypothesis.

Interestingly, Nrf2 has previously been shown to regulate type I interferons through the induction of autophagy, a process known to regulate IL-1β in macrophages (220, 221). It would be tempting to speculate that mechanistically an itaconate-Nrf2 axis may also drive this process in LPS-activated macrophages. It is also important to note that 4-OI still retained some capacity to inhibit pro-IL1β levels in Nrf2-deficient BMDMs post 24 h LPS stimulation, although this was evidently blunted. The decrease observed in this instance is likely owed (at least in part) to competitive inhibition of SDH by itaconate.

Since these findings have been published (116), several papers have demonstrated that 4-OI can induce Nrf2 stabilisation in variety of contexts to modulate immunity or act in a cytoprotective manner. 4-OI inhibits pro-inflammatory cytokine production in PBMCs derived from patients with systemic lupus erythematosus (SLE), in a Nrf2-depedent manner (222). Engagement of the Nrf2 pathway by 4-OI has also been demonstrated to suppress STING expression and type I IFN production in PBMCs derived from patients with STING-dependent interferonopathies (SAVI) (223), confirming a role for 4-OI in the regulation of IFNβ. Outside of immunity, 4-OI activation of KEAP1-Nrf2 signalling and the anti-oxidant response protects human umbilical vein endothelial cells from oxidative injury induced by high glucose (224). The authors also confirmed a key role for Cys151 in KEAP1 in the detection of 4-OI. Finally, 4-OI was found to be cytoprotective in hydrogen peroxide-treated SH-SY5Y cells and epigenetically de-repressed primary neurons, in a manner dependent on Cys151 in KEAP1 and Nrf2 stabilisation (225). As such, these results confirm the importance of KEAP1 alkylation and Nrf2 activation in governing the immunomodulatory and cytoprotective properties of 4-OI.

Since its discovery, the repertoire of succination targets has continued to grow (176). As such, it was speculated that targets of itaconate-mediated alkylation, other than KEAP1, may also exist. Using an unbiased proteomic screen, several additional targets were found in both LPS-activated and 4-OI-treated BMDMs. Excitingly, this represents the first identification of this novel PTM, herein defined as 2,3-dicarboxypropylation. Of note, was a significant increase in 2,3-dicarboxypropylation of Cys84 in LDHA and Cys385 in ACO2, key regulators of glycolysis and the TCA cycle, respectively. LDHA is an essential mediator of Warburg metabolism as it catalyses the regeneration of NAD^+ necessary to sustain flux through glycolysis (226). As there are no known enzymes or mechanisms to cleave the thioether bond of this modification the result is likely inhibitory, such as with succination. From this, it could be presumed that itaconate may also act as a negative regulator of aerobic glycolysis, a pathway known to be vitally important for the induction of IL-1β, as previously mentoned (20). Indeed, 4-OI has also been demonstrated to inhibit LPS-induced extracellular acidification rates (ECAR) (data not shown) indicating this may be the case. Whilst pyruvate and lactate levels were elevated in LPS-activated *Irg1* -/- BMDMs. Itaconate has previously been shown to inhibit glycolysis in the liver of mice (227). The authors suggest this stems from the ability of itaconate to inhibit fructose-6-phosphate 2-kinase (F6P2Kinase), an enzyme that synthesizes fructose 2,6-bisphosphate (F26BP), despite itaconate only weakly inhibiting F6P2Kinase *in vitro*. From this, it would be tempting to speculate that itaconate may regulate glycolysis at multiple levels, either through the regulation of HIF1α or by directly targeting glycolytic enzymes, such as demonstrated for fumarate and GAPDH.

Very recently, Qin *et al* (2019) have published a paper where they developed a specifc-thiol reactive probe, 1-OH-Az, for quantitative proteomic profiling of cysteine modifications by itaconate in macrophages (228). Using this technique, they generated a chemoproteomic portrait of itaconate-sensitive cystine residues and confirmed the modification of LDHA by itaconate, which inhibits it's enzymatic activity. Furthermore, the authors showed that itaconate alkylated several glycolytic enzymes, notably aldolase A (ALDOA) and GAPDH, resulting in an inhibition of glycolysis, mainly by targeting ALDOA. Inhibition of ALDOA and glycolysis by itaconate also contributes to the inhibition of LPS-induced IL-1β. As such, this study has confirmed that itaconate can alkylate protein cysteine residues and unearthed a novel anti-inflammatory feedback mechanism targeting glycolysis.

Interestingly, modification of Cys385 in ACO2 by superoxide is also known to inactivate this enzyme (229). As such, it would be tempting to speculate that a negative feedback loop exists between itaconate and ACO2, whereby itaconate dicarboxypropylates ACO2 to limit the synthesis of *cis*-aconitate, the substrate of IRG1, and thus its own synthesis. Furthermore, this would also explain the breakpoint observed in LPS-activated macrophages as no significant changes in the levels of IDH (data not shown) were observed in the proteomic screen, as previously suggested. As mentioned, the metabolic analyses of *Irg1* -/- BMDMs also showed significantly elevated fatty acid levels, and indeed fatty acid synthesis is important for the function of pro-inflammatory macrophages (105). This likely reflects the diversion of citrate away from fatty acid synthesis towards itaconate production. If true, this would put IRG1 and itaconate at the forefront of

TLR4-mediated metabolic remodelling and as a master regulator of Krebs cycle rewiring.

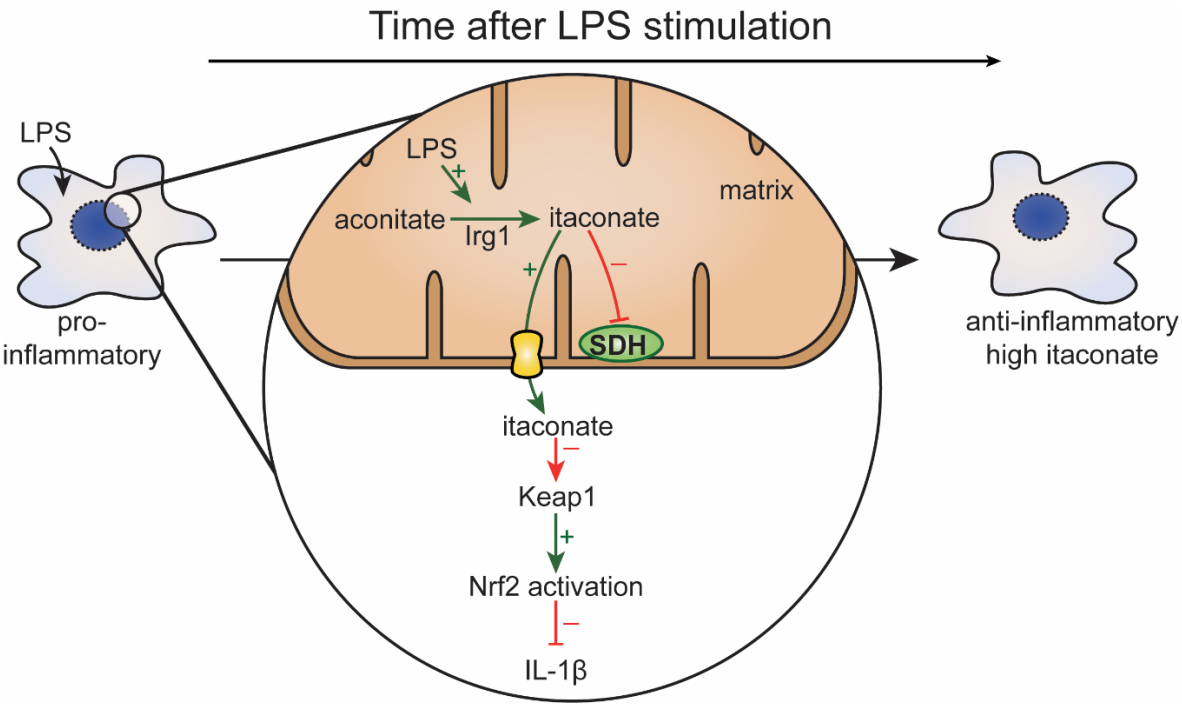

Figure 4.41 – Proposed model of Itaconate's anti-inflammatory mechanism of action

Ligation of TLR4 by LPS results in the transcriptional upregulation of *Irg1* and synthesis of itaconate from *cis*-aconitate. Accumulation of itaconate in the mitochondrial matrix competitively inhibits SDH and oxidative phosphorylation (OXPHOS). Itaconate is also exported from the mitochondria, primarily by the oxoglutarate carrier (OGC). In the cytosol, itaconate can alkylate key redox sensing cysteines on KEAP1 to activate Nrf2, which acts to negatively regulate IL-1β. As such, itaconate acts to temper the immune response and so itaconate derivatives, such as 4-octyl itaconate, are a new class of anti-inflammatory agents.

Chapter 5:

General Discussion

5.1 – Overview and summary of key findings

A striking change has been happening in the field of immunology whereby metabolic processes are now being considered as important a determinant of immune cell function as the activation of immune cells by cytokines and PRRs. This growing field of immunometabolism has benefitted greatly from technological advancements and improvements in instrumentation over the last 10 years, such as the use of mass spectrometric techniques and computational analysis (99, 100). In fact, this study has only been enabled through the use of these technologies and in doing so has identified additional signalling roles for the Krebs cycle in macrophages that would have not been possible otherwise. It is a testament to scientific progress that we can now dissect the fundamental questions of biology like never before using these newly available tools. Most importantly, this study also supports the evolving stance that mitochondria, the Krebs cycle and the ETC can no longer be viewed solely as a bioenergetic system whose purpose is to generate ATP, but is a central metabolic hub that can undergo dynamic remodelling in response to environmental cues. This dynamic remodelling generates signals that can participate in 'non-metabolic functions' and can act on a plethora of substrates and cellular signalling pathways to ultimately regulate nuclear gene expression programmes.

Here, we investigated the role of the Krebs cycle metabolite fumarate and the Krebs cycle-derived metabolite itaconate as regulators of cytokine production in LPS-activated macrophages. The data provides evidence for a role of an inflammatory argininosuccinate shunt, a metabolic pathway bridging the Krebs cycle and the urea cycle (Krebs bicycle), in generating fumarate in macrophages that can then act as a signal to increase pro-inflammatory cytokine production.

Furthermore, fumarate-mediated protein succination and the accumulation of (S)-2-succinocysteine (2SC) were identified for the first time in LPS-activated macrophages. This study has also confirmed a recently identified anti-inflammatory IRG1-itaconate-SDH signalling axis that occurs in macrophages, in addition to identifying a novel signalling pathway whereby itaconate is exported from mitochondria to activate the anti-oxidant and anti-inflammatory transcription factor Nrf2. Furthermore, a novel post-translational modification (PTM) termed 2,3-dicarboxypropylation and metabolite, 2-3-dicarboxypropyl cysteine, were identified akin to fumarate-mediated succination and 2SC.

5.2 – Evolutionary perspective on immunometabolism

The emergence of the field of immunometabolism and this newly identified role for mitochondria and Krebs cycle remodelling in macrophages, which repurposes Krebs cycle metabolites and the ETC for 'non-metabolic' signalling functions, raises many interesting evolutionary questions.

1) The first set of questions that come to mind are why and how have mitochondria been co-opted in evolutionary history to function as signalling organelles in eukaryotic organisms? More specifically, why has the Krebs cycle and its derivatives been repurposed for 'non-metabolic' signalling roles?
2) Secondly, from an evolutionary perspective, why does metabolism have such a profound influence on macrophage function in general and what are the governing principles?

5.2.1 – Mitochondria as signalling organelles

There is a growing list of evidence that now shows that mitochondria communicate with the cytosol to initiate key biological events, promote homeostasis and counteract stress conditions (230). Mitochondria are known to perform two major roles within the eukaryotic cell, the production of ATP via OXPHOS and the support of biosynthetic pathways. As such, mitochondria are essential for several biological processes in eukaryotic organisms, namely cellular proliferation, differentiation and stress adaptation. While classically it is thought that the nucleus is responsible for dictating and regulating mitochondrial function, rarely was it thought that mitochondria can in turn generate signals that influence nuclear function (230). However, as functioning mitochondria are required for such important cellular processes, feedback systems must exist to prevent a metabolic crisis and cell death. The existence of signalling mechanisms between mitochondria and the nucleus raises many important fundamental questions and suggests a third major role of the mitochondria is to operate as signalling organelles (230). Important fundamental questions include:

1) What are the primary mechanisms of communication?

2) How does this relate to the evolution of the eukaryotes?

3) How do the signals modulate cellular function?

In order to understand the role of mitochondria in regulating cellular function it is important to understand their origin and role in eukaryotic development. There are many competing views about the origin of eukaryotes and indeed the relative contribution of mitochondria to eukaryogenesis is weighted differently. There are two major theories on eukaryotic evolution, the gradualist theory and the

symbiogenic theory (231, 232). The gradualists' theory depict the origin of eukaryotic cell complexity and the origin of mitochondria as independent-unrelated processes that occurred in series. However, the symbiogenic theory depicts the origin of the eukaryotic cell complexity as emerging from the symbiosis that gave rise to mitochondria. The theory of symbiogenesis (endosymbiont theory) is considered the prevailing theory of eukaryotic origin. Specifically, a prokaryotic host (an archaeon) developed an endosymbiotic relationship with a facultative anaerobic α-proteobacteria (mitochondrion precursor) and that eukaryotic traits arose as a consequence of that symbiosis (231, 232). The benefit of this symbiotic relationship is a hotly debated topic but it's unlikely that ATP production itself was the benefit, at least initially. One speculative hypothesis is that this first endosymbiont relationship arose as the α-proteobacteria provided metabolites, namely hydrogen (H_2), CO_2 and acetate, which the archaeon could utilise to conduct methanogenesis (233). As these can be limiting, there was a strong selective pressure for the localization of the archaea and α-proteobacteria near each other that ultimately led to their fusion and dependence on each other. These then needed to develop mechanisms to communicate to each other giving rise to a eukaryotic cell and eukaryotic cellular processes.

In evolutionary history, mitochondria are thought to have contributed to the origin of eukaryotes by altering the bioenergetic configuration of the cell thus providing more energy, providing genes, as eukaryotes are genetic chimeras with more bacterial genes than archaeal genes, and finally as the origin of the eukaryotic endomembrane system (234). Intriguingly, the archaeal host is proposed to have brought preformed complexity to the eukaryotic lineage, such

as the ability to phagocytose and a primitive cytoskeleton (234). However, the largest known contribution of the archaeal host is informational genes and in informational processing, such as the RNA polymerase, the ribosome and aminoacyl tRNA synthetases (234). However, information processing does not set eukaryotes and prokaryotes apart, it is the amount of information they maintain, process and inherit that does.

There is far greater DNA content in eukaryotic cells than their prokaryotic progenitors, the majority of which is mobile DNA or 'selfish' DNA (234, 235). As such, the constraints that govern DNA content in prokaryotes is different to that in eukaryotes (236). It appears that the reason eukaryotes are better equipped to manipulate large levels of DNA is due to the organisation of DNA into nucleosomes. All organisms have proteins bound to their DNA, including archaea that have DNA-binding proteins with the histone-fold (Archaeal histones) (234, 237). Archaeal histones and DNA is more filamentous in nature than eukaryotic histones, which consist of slightly less than 150 bases of DNA wrapped around an octamer histone core made from two H2A/H2B dimers and a H3/H4 tetramer (238). As such, eukaryotic DNA and histone organisation resemble beads on a string. Histones contain about 55 % of the mass of nucleosomes, which are connected by short linker DNA segments, and comprise the primary structure of chromatin that leads to compaction of DNA up to 40-fold (234). In addition to compaction, nucleosomes permit a high degree of flexibility removing the constraint of DNA content and permitting complex manipulation and control of gene expression. Specifically, histone modifications on the N and C terminal 'tails' provides a powerful element for the control of gene expression (234). An example of Histone modifications that control gene expression is that of

acetylation and HATs, importantly, in eukaryotes acetylation is derived from the Krebs cycle intermediate citrate and ACL, both of which influence histone acetylation and gene expression (104, 239). In fact, the role of covalent modification of histones, termed the 'histone barcode', has become a central tenet of eukaryotic gene regulation and can affect distinct downstream cellular events by altering the structure of chromatin and/or through the recruitment of effector proteins (240). Acetylation of lysine residues located on N or C terminal histone tails by HATs, as well as other PTMs, such as phosphorylation and methylation, afford elaborate gene expression patterns in eukaryotes required by the increase in DNA content (234). Furthermore, this epigenetic regulation can persist over many cell generations, allowing the differentiation of stable gene expression patterns in various cell types, an essential process in complex multicellular organisms with different tissue types. As such, the bioenergetic configuration bestowed on eukaryotes by the mitochondrion enabled eukaryotes to take the first step towards true complexity via histone-dependent organisation of DNA into chromatin (234). Therefore the archaeal partner provided histones that would later evolve into eukaryotic histones and nucleosomes enabling epigenetic control of gene expression.

There are also very important connections between the energetic status of eukaryotic cells and histone modifications (234). As mentioned, acetylation covalently modifies histone lysine residues that neutralises their positive charge thereby decreasing their affinity for the negatively charged DNA backbone. This results in the opening up of chromatin for transcription. Mitochondrial proteins also tend to undergo spontaneous lysine acetylation and indeed one potential early messenger of α-proteobacteria is acetate, which can

be converted into acetyl-CoA in the cytosol and can control diverse cellular functions, such as metabolism and the cell cycle, through histone acetylation (241). As such, early in evolution, functioning mitochondria would make a lot of acetate, and thus acetyl-CoA, which could in turn promote open DNA, however, during an energy crisis acetate levels would lower leading to condensed transcriptionally inactive chromosomes (234, 242). As such, it's speculated that this simple reaction could have seeded eukaryotic gene regulation through histone regulation, which suggests that mitochondrial signalling was a key contributing event during eukaryogenesis (234). Indeed, histone modifications today are intricately linked to energy status, chromatin condensation and cell cycle decisions. The three main nutrient sensors of eukaryotes are AMPK, mTOR and GCN2 and these are conserved across eukaryotic groups and transmit signals to chromatin via histone modifications (234, 243). Furthermore, the CCAAT-box, which is found in 30% of eukaryotic promoters, can be traced back to archaeal histones (234). Specifically, the CCAAT-box binding protein (CBC), which promotes RNA pol II recruitment, is derived from archaeal histones, can be modified in the same manner as histones are, can bend DNA, and specifically regulates the cell cycle and helps to activate about 30% of eukaryotic genes. Through modifications, histones provide a simple mechanism of information transfer integrating the nutrient and energetic state of the cell into condensation of chromatin and the regulation of gene expression. In summary, archaea contain archaeal histones that pack DNA and so as a host during symbiosis provided an opportunity for complex eukaryotic nuclear structures to develop. However, no known archaea contain the complex nuclear structures of eukaryotes today.

Importantly, this could indicate that mitochondrial metabolite signalling was essential for the development of eukaryotic genome complexity.

5.2.2 – Coupling Krebs cycle remodelling to metabolite signalling

The Krebs cycle is perhaps the central biochemical pathway operating in eukaryotic cells and is responsible for the co-ordination of bioenergetic and biosynthetic processes. In fact, life builds its molecules form CO_2 and catabolises them through the intermediacy of just 5 universal metabolites, acetate, pyruvate, oxaloacetate, succinate and α-ketoglutarate, 3 of which are Krebs cycle intermediates (244). Intriguingly, a non-biological framework has now been proposed that could shed light on how core metabolism evolved and uses the pathways and intermediates that it does. Muchowska *et al* (2019) were able to demonstrate experimentally that a complex reaction network can develop from pyruvate and glyoxylate, two simple organic acids, in the presence of Fe^{2+} (245). Strikingly, this abiotic network produces 9 of the 11 Krebs cycle intermediates and the authors propose that this could have been an early route by which CO_2 dioxide was fixed into organic molecules. Furthermore, addition of hydroxylamine and metallic iron, which could have been available on early earth, extended this abiotic chemical network to produce 4 amino acids, namely glycine, alanine, glutamate and aspartate (245). Whilst it will never been known for sure it seems a realistic postulation that when life emerged on the planet it harnessed a pre-existing abiotic metabolic network before it developed genetically encoded catalysts, such as enzymes, to produce a more efficient system.

Therefore, it is not surprising that the Krebs cycle and its intermediates, within the context that a key contribution of mitochondria to eukaryotic evolution

was to facilitate complex DNA regulation, would be repurposed as signals to control gene expression. During evolutionary history, a metabolic crisis in mitochondrial precursors would have altered Krebs cycle metabolite abundance lending them the opportunity to act as an important feedback mechanism indicating impaired mitochondrial functioning (230). In fact, 5 Krebs cycle intermediates now have essential roles in modelling the epigenome to regulate gene expression. As mentioned, citrate-derived acetyl-CoA is essential for histone acetylation and gene expression. However, succinate, succinyl-CoA, α-ketoglutarate and fumarate are also immensely important regulators of covalent histone and DNA modifications (246, 247).

Importantly, the influence of these metabolites on dictating macrophage phenotype is now emerging. As previously discussed, α-ketoglutarate is an important cofactor for the α-KGDDs family of JMJDs, involved in histone demethylation, and TET family of 5mC hydroxylases, which play a role in DNA demethylation (85). These enzymes can undergo competitive inhibition by succinate and fumarate, and so the ratio of α-ketoglutarate to succinate or fumarate can often be a key determinant of their enzymatic activity (60, 85). Methylation marks on histones can positively or negatively influence gene expression, while DNA methylation is typically associated with open chromatin and active transcription. In this way, succinate, α-ketoglutarate and fumarate can remodel the epigenome. With this in mind, Liu *et al* (2017) uncovered an important signalling role for glutamine-derived α-ketoglutarate, which facilitates an IL-4-induced gene expression programme via JMJD3-driven epigenetic changes (60). The authors found that α-ketoglutarate suppresses the classical activation of macrophages (as a low α-ketoglutarate/succinate ratio strengthens

the pro-inflammatory phenotype) and supports endotoxin tolerance after classical activation (60). Likewise, fumarate can regulate pro-inflammatory cytokine production during trained immunity by inhibiting the KDM family of histone demethylases. Recently, melatonin was also shown to alleviate inflammation associated with obesity in part by increasing the ratio of anti- to pro-inflammatory adipose tissue macrophages (ATMs) (86). Mechanistically, this was achieved by the targeting of ATMs with adipocyte-derived exosomal α-ketoglutarate and TET-mediated DNA demethylation (86).

Given the importance of the IRG1-itaconate-SDH axis in regulating succinate accumulation in LPS-activated macrophages, a functional consequence of this axis could be to regulate the methylation status of histones and DNA. Likewise, genetic deletion of *Irg1* of macrophages resulted in an increase in lipids, such as palmitate and oleate, in response to LPS. It is therefore possible that loss of itaconate synthesis increases mitochondrial citrate export. In line with this finding, a recent study has found that iron depletion in human macrophages, which inhibits aconitase activity, limits itaconate synthesis and increases citrate levels, resulted in increased lipogenesis and the formation of lipid droplets. Hypothetically speaking, decreased itaconate synthesis and increased citrate export could elevate cytosolic acetyl-CoA levels, histone acetylation and thus regulate inflammatory gene expression. As such, a comprehensive investigation into the epigenetic landscape of *Irg1* -/- macrophages should performed to determine the role itaconate in governing these processes.

While a role for fumarate in regulating trained immunity has emerged, nothing is known about the role of the aspartate-argininosuccinate shunt and

fumarate in regulating the epigenome of classically-activated macrophages. Furthermore, Fh and fumarate are also implicated in the regulation of DNA damage repair (248, 249). Specifically, upon exposure to ionizing radiation DNA-PK phosphorylates nuclear Fh, which generates fumarate locally to inhibit the KDM2B enhance demethylation lysine 36 on histone H3. Enhanced dimethylation facilitates the recruitment of DNA-PK to double-stranded breaks (DSBs) and the initiation of non-homologous end-joining (NHEJ) DNA repair (248). Intriguingly, inflammatory macrophage activation induces complex III-mediated ROS production and DNA damage (81). It has also been reported that pro-NHEJ factors are more readily recruited to sites of damage in FH-deficient cells, when fumarate levels are high (249). It would be tempting to speculate, that induction of the inflammatory aspartate-argininosuccinate shunt and fumarate production acts as a mechanism to counter DNA damage induced by inflammatory stimuli. This process also demonstrates the importance of mitochondria and the Krebs cycle in evolutionary history as it provides a means to ensure DNA integrity in the face of damage and prevent genomic instability, in addition to the regulation of gene expression. As such, a comprehensive investigation into the role of Fh and fumarate in regulating the epigenetic landscape and DNA damage in LPS-activated macrophages could be an interesting area to explore.

In addition, Krebs cycle remodelling and the repurposing of Krebs cycle enzymes and their metabolites appears to be a common evolutionary strategy invoked by eukaryotes to adapt to a plethora of varying stress conditions and in regulating crucial biological processes. Phylogenetic analyses suggest that prior to symbiogenesis, the Krebs cycle seemed to operate as isolated steps in both

the archaeal host and the mitochondrial precursor (α-proteobacteria) (250). They seemed to be interconnected to other pathways during evolution, which may explain in part, the diversity of function of isoforms of Krebs cycle enzymes that can be found localised to different cellular compartments. In fact, a recent study has shown that Krebs cycle enzymes transiently localise to the nucleus during zygotic genome activation (ZGA) and regulate the epigenome (251). Impairment of Krebs cycle enzyme trafficking correlate with a loss of specific histone modifications and blocks ZGA. As such, the Krebs cycle and Krebs cycle metabolites are a crucial and conserved metabolic control mechanism underlying early pre-implantation development in mammals.

Krebs cycle metabolites act as key signals for the metabolic status of eukaryotic microorganisms, such as certain fungal species, but also prokaryotic microorganisms. An example of this is observed in the fungal species *Torula corallina* that produce high levels of fumarate from glucose and CO_2 (252). Elevated levels of fumarate then acts to inhibit erythrose reductase and erythritol synthesis. Likewise, metabolites of the glyoxylate shunt, such as succinate, are proposed to acts as 'nanosensors' to determine fumarate hydratase subcellular localisation in yeast (253). Even more intriguing is the signalling role Krebs cycle enzymes and metabolites play in prokaryotic organisms, which again makes a strong case for why Krebs cycle metabolites and mitochondria would have been co-opted as signals during eukaryotic development. For example, intracellular fumarate is a known regulator of alginate production in *Pseudomonas aeruginosa* and phosphorylation-independent flagellar motor switching *in Escherichia coli* (254). Likewise, fumarate and malate are modifiers of ruminal fermentation in *Selenomonas ruminantium* by increasing lactate uptake and the succinate-

propionate metabolic pathway (254). Perhaps the most striking example of this phenomenon is the discovery that fumarate hydratase in *Bacillus subtilis* is induced upon DNA damage, co-localized with bacterial DNA and is required for the DNA damage response (255). Specifically, fumarate hydratase produces L-malate, which promotes the translation of the DNA damage protein RecN. As such, Krebs cycle metabolites and enzymes likely adopted the role of 'non-metabolic' signals early in the evolution of prokaryotic life.

Plants also demonstrate clear molecular plasticity in the regulation of Krebs cycle enzymes, which in particular are dramatically altered in shoots in response to a range of stresses, such as osmotic, genotoxic, salt, heat, drought and oxidative stresses (250). For example, Fumarate hydratase is highly upregulated in response to drought and salt stresses in tomato plants, as it is an important regulator of stomatal function and photosynthesis (254). During salt stress, fumarate hydratase is also strongly co-expressed with malate dehydrogenase. Anti-sense inhibition of SDH in tomato plants also resulted in higher rates of photosynthesis. As such, modulation of the Krebs cycle acts to regulate photosynthesis and stomatal functioning (254). Furthermore, fumarate and malate are also used as pH regulators during nitrate assimilation in *Arabidopsis thaliana* (254). In contrast, UV-B radiation stress suppresses enzymes in the second half of the Krebs cycle, including fumarate hydratase and malate dehydrogenase, which enables intermediates to be siphoned off for the synthesis of phenylpropanoids (256). These results supports the idea that modulation of specific Krebs cycle enzymes and Krebs cycle metabolites is an evolutionary conserved phenomenon to adapt to various stress conditions. Intriguingly, the phenylpropanoid pathway is also essential for plant defence

against microbes (257). This suggests that the modular regulation of the Krebs cycle to generate Krebs-cycle-derived metabolites is important in the immune response and is conserved across diverse eukaryotic species. It is also very reminiscent of Krebs cycle-remodelling observed in macrophages, which suppresses IDH to facilitate the diversion of *cis*-aconitate away from the Krebs cycle to support the synthesis of the anti-bacterial and anti-inflammatory metabolite itaconate.

Interestingly, marine bivalves, such as the pacific oyster and molluscs, have recently been reported to synthesise itaconate during pathogen challenge (258). Itaconic acid was also shown to inhibit the growth of the *Vibrio* genus of gram-negative pathogenic bacteria (258). This suggests that remodelling of the Krebs cycle to generate itaconate is also an evolutionary conserved anti-microbial mechanism. Likewise, itaconic acid is produced in large quantities by the fungus, *Aspergillus terreus* while *Aspergillus sp*. are well known to produce a large range of anti-bacterial metabolites (259, 260). Furthermore, a range of pathogens, such as *Yersinia pestis* and *Pseudomonas aeruginosa*, express a distinct pathogenicity island that encodes three enzymes that facilitate itaconate degradation and thus enables virulence and survival in macrophages (121). This pathway ultimately converts itaconate into pyruvate and acetyl-CoA, which can then be used as an alternative fuel source for the Krebs cycle while at the same disarming itaconate's anti-bacterial properties. More recently, an itaconate resistance mechanism has been reported in *M. tuberculosis* with dissimilation mediated by a bifunctional enzyme, Rv2498c, which also participates in Leucine catabolism (261). Genetic deletion of Rv2498c resulted in the attenuation of *Mtb*-infection in a mouse model, suggesting the importance of this pathway in

promoting survival of *M. tuberculosis* in macrophages. Likewise, *Salmonella* have also acquired a genetic operon encoding itaconate degrading proteins, which is regulated by a neighbouring gene *ItaR* responsible for detecting itaconate produced by macrophages (262). Intriguingly, the existence of this pathway may explain why such high concentrations of itaconate are required to inhibit the growth of *M. tuberculosis, Salmonella* and other pathogens *in vitro* and suggests that over the course of evolutionary history mammalian pathogens have managed to circumvent this anti-microbial mechanism.

This then begs the question as to what point in evolutionary history did itaconate get co-opted to regulate the function of complex II, the Krebs cycle and other metabolic pathways? One speculation that could be made is that the emergence of itaconate-resistant bacteria led to exacerbated immune responses detrimental to the host. As such, itaconate may have acquired anti-inflammatory properties to curtail excessive inflammation induced by itaconate-resistant pathogens. Indeed, itaconate now has an important role in host survival by inhibiting neutrophil infiltration into the lung upon infection with *M. tuberculosis*. However, it's also possible that these two separate functions of itaconate evolved independent of one another. In neurons, Zika virus induces the necroptotic pathway to induce itaconate synthesis (136). This then inhibits complex II and neuronal respiration to restrict viral replication. Therefore, itaconate's metabomodulatory effects may have evolved as an anti-viral mechanism. Alternatively, itaconate-mediated metabolic regulation may have arisen due to the evolutionary and ecological theories of life history in tandem with its anti-microbial/anti-viral activity, which will be discussed below.

5.2.3 – Macrophage metabolism from a life history perspective

At the heart of macrophage metabolism is the regulated allocation of metabolic resources and metabolite signalling to support host defence and survival. Organisms use different strategies, referred to as 'life history traits', to optimise their reproductive success and survival in the face of environmental constraints (263, 264). Life history traits generally include lifespan, age and size at reproductive maturity, fertility, size at birth and temporal pattern of growth. Specifically, life history theory is an analytical framework that was formulated in the 1950s and aims to explain the diversity of lifestyles among different biological species given the diverse environmental constraints those species encounter (263). The three fundamental biological programs that organisms engage (according to life history theory) are growth, reproduction, and environment-specific survival strategies (maintenance programmes) and so they must effectively optimise the distribution of finite resources to these programmes (263). As such, restrictive unfavourable environments result in the reallocation of resources towards maintenance programmes, however, favourable conditions promote growth and reproduction.

There are two types of maintenance programmes identified, which include defence, initiated by the presence of factors that negatively impact fitness, such as pathogens, and dormancy, initiated by the absence of sufficient resources, such as limited nutrient availability (263). Both defence and dormancy occur at the expense of growth and reproduction but initiate different metabolic programs. Dormancy promotes energy conservation, engages catabolic metabolic programmes and are associated with high resistance to environmental stresses (263). Defence on the other hand promotes energy consumption and engages

anabolic metabolism to fuel protective responses against pathogens. A clear example of this is the use of glucose and glutamine by inflammatory macrophages to synthesise molecules associated with host defence (20, 116). Life history theory was originally developed as an organising framework for evolutionary ecology, however, it has been noted that the principles of life history theory can also be applied at the level of organisms and cells.

At the cellular level, life history programmes are reflected in the organization of cellular signalling pathways, which are dictated by the global state of the organism and by the sensing of the local microenvironment (263). Organismal signalling to cellular components is generally achieved by a multitude of endocrine signals, which in turn relay the environmental state in which the organism finds itself. For example, endocrine signals for ‘growth’ include growth factors, such as IGF-1, for ‘reproduction’ include oestrogens and androgens and for ‘maintenance’ include glucocorticoids and inflammatory cytokines. The local cellular environment is sensed by numerous nutrient sensors, such as the three key nutrient sensors of eukaryotes, AMPK, mTOR and GCN2, which are conserved across eukaryotic groups and transmit signals to chromatin via histone modifications, as previously discussed (243). Furthermore, numerous signalling pathways also exist in cells to sense oxygen levels (HIF pathway) and various negative microenvironmental factors, such as TLRs to detect pathogens, Nrf2 to detect oxidative stress and p53 to detect DNA damage (to name a few) and are generally termed cellular stress response pathways. As such, cells engage in their own version of life history programs in reaction to both the state of the whole organism and their local environment.

A fundamental aspect of a cell's life history programme choice is between quiescence and proliferation and differentiation. Quiescence (dormancy) generally relies on catabolic metabolism, such as an intact Krebs cycle and OXPHOS, whereas cell activation, proliferation and differentiation often require anabolic processes and depends on aerobic glycolysis and increased glucose and glutamine uptake. It is clear that metabolic reprogramming when viewed from a life history perspective engages specific metabolic pathways to support specific cellular functions. Both growth and reproduction use anabolic processes, whereas maintenance programmes use either catabolic processes (dormancy) or anabolic processes (defence).

It is also clear that macrophages engage specific metabolic pathways to execute their function in accordance with the principles of life history theory. As such they provide a great example of how the different life history programs have specific metabolic features governing them to effectively control the allocation of resources. Specifically, under normal homeostatic conditions macrophages proliferate using a c-Myc-controlled anabolic transcriptional program (growth) (265). However, in response to LPS, macrophages engage aerobic glycolysis through the induction of mTOR and HIF1α and the suppression of c-Myc (defence) (265). Macrophages also enhance *de novo* lipogenesis to support their effector functions and cytokine production (105). As such, alternative anabolic programs are engaged to support the different life history programmes.

Macrophages also suppress catabolic processes upon countering pathogens and PAMPs. In fact, the suppression of catabolic processes requires induction of the aspartate-argininosuccinate shunt, which supports NO synthesis from iNOS and nitrosylation of key components of the ETC, and the synthesis of

itaconate, which competitively inhibits complex II of the ETC (45, 49). Intriguingly, both NO and itaconate are also anti-microbial agents that help to combat infection, in addition to metabolic modulators that impair respiration and activate cellular stress response pathways, such as Nrf2. It is therefore possible that during evolutionary history these particular metabolic intermediates were preferentially selected for because they provided an effective means to perform two essential functions (anti-bacterial/anti-viral defence and suppression of catabolic pathways) when the defence programme is invoked and thus represent a highly effective way to optimise the use of finite resources. The application of a life-history theory derived framework to metabolic reprogramming in macrophages provides a clear explanation on why metabolism is such a critical determinant of macrophage (and other immune cell type) function and as such might explain why specific metabolic adaptations have emerged during evolution.

5.3 – Therapeutic and diagnostic opportunities

An exciting development that has emerged from the field of immunometabolism is that the identification of key metabolic events that govern immune cell function are also presenting new therapeutic opportunities for the treatment of autoimmune and inflammatory diseases. In particular, the emerging role of the Krebs cycle and Krebs cycle intermediates in inflammatory macrophages raises the possibility of a new class of anti-inflammatory therapies based on Krebs cycle metabolites themselves (and their derivatives) or focused on the targeting of Krebs cycle enzymes. This concept has already warranted investigation (78) in other pathophysiological contexts and indeed in relapsing remitting MS and psoriasis, which are both autoimmune disorders.

Specifically, the cell permeable fumarate derivative DMF is a key component of the anti-inflammatory drugs Fumaderm® and Tecfidera® used to treat psoriasis and relapse remitting MS, respectively (161, 180). Currently, a multiplicity of mechanisms have been suggested to mediate its anti-inflammatory effects and these include activation of the Nrf2 pathway and the HCA2 receptor, and inhibition of GAPDH and aerobic glycolysis (179). It appears that favoured mechanism currently stands as GAPDH and aerobic glycolysis. As such, the use of a modified version of this Krebs cycle intermediate revealed a metabolic module with clinical tractability. As shown in this study and others, the generation of itaconate from the Krebs cycle intermediate *cis*-aconitate contrasts with other metabolite signals emanating from the mitochondria in that it primarily acts a protective anti-inflammatory agent. This unique property of itaconate has created an interest in generating itaconate derivatives that can deliver it to the intracellular compartment of cells and enhance its anti-inflammatory capacity. The use of the cell permeable itaconate derivatives, 4-OI and DMI, were also shown to be protective *in vivo* in pre-clinical murine models of sepsis by decreasing pro-inflammatory cytokine production and increasing survival (116), and in psoriasis, which resulted in the amelioration of skin pathology (127), respectively. As Fumaderm® is already an FDA approved drug for the treatment of psoriasis, the development of small molecule drugs based on Krebs cycle intermediates and their derivatives, such as itaconate, may (and indeed do) represent promising therapeutics themselves. Furthermore, enhancing the electrophilicity of itaconate and fumarate through chemical modification, and the fine-tuning of cell delivery, represents an opportunity to develop novel and effective anti-inflammatory agents.

As well as acting within the cell, Krebs cycle metabolites can also be released into the circulation through poorly defined mechanisms and their exact roles in regulating biological processes in this situation is currently unknown. For example, a portion of the succinate that accumulates during ischaemia and inflammation is released from the cell into the extracellular environment. This phenomenon occurs in a variety of physiological contexts, such as IR injury, inflammation or cold exposure (67, 78, 266). The diverse consequences of succinate released into the circulatory system remain to be explored, but one likely role is as a pro-inflammatory and chemotactic signal, via ligation of SUCNR1. There is considerable interest in developing drugs that can counteract the effects of succinate on this receptor (267). Although SUCNR1 receptor inhibitors, such as compound '5g', are in their infancy, they may provide further understanding as to the signalling role of succinate and a method of blunting a cascade response during inflammation. The regulation of circulating Krebs cycle intermediates could represent a particularly interesting and underexplored therapeutic modality. As mentioned however, an unexpected role for succinate and the SUCNR1 in limiting inflammation during obesity was recently identified suggesting that extracellular succinate can be anti-inflammatory (63). It would be tempting to speculate that inhibition of complex II by itaconate is anti-inflammatory in certain contexts in part by promoting succinate accumulation and release into the extracellular milieu to activate SUCNR1. The role of itaconate in adipose tissue inflammation and obesity is therefore an interesting avenue of investigation. In addition, the use of potent synthetic SUCNR1 agonists, such as cis-epoxysuccinic acid and cis-1,2-cyclopropanedicarboxylic acid, may have utility as anti-inflammatory agents in certain contexts (268). The ability of

succinate SUCNR1 to initiate both pro-inflammatory and anti-inflammatory transcriptional programmes suggest great care must be taken when targeting this receptor in the clinic.

The specific targeting of Krebs cycle enzymes to treat pathophysiological processes with biomedical importance has also begun to emerge. This concept was first illustrated following the discovery that succinate accumulates during ischaemia and is then oxidised upon reperfusion (78). Oxidation of succinate by the Krebs cycle enzyme complex II drives mitochondrial superoxide formation, which contributes to ischaemia-reperfusion (IR) injury that can occur during myocardial infarction. Inhibiting complex II with DMM or malonate (and DMI) prevented succinate accumulation during ischaemia and protected against tissue damage upon reperfusion. This work indicates that simple inhibitors of Krebs cycle enzymes could be used to prevent pathological damage. The oxidation of succinate also generates mitochondrial ROS as a further pro-inflammatory redox signal during inflammatory macrophage activation (62). As the mechanism of mitochondrial superoxide generation by succinate oxidation during inflammation seems to be the same as that during IR injury (RET), it is perhaps unsurprising that DMM (in addition to itaconate derivatives) could also decrease inflammation in a mouse model of sepsis. Hence, simple molecules designed to inhibit complex II are emerging a novel class of anti-inflammatory and anti–IR injury compounds.

Finally, the use of Krebs cycle metabolites as diagnostic biomarkers of immune-related disease progression or status may also become integral in a clinical setting, with abnormal levels often observed in diseased tissue such as increased succinate and itaconate in the rheumatoid joint (66, 269). Interestingly, a significant decrease in 5 Krebs cycle metabolites, citrate, fumarate, isocitrate,

malate and succinate, has been observed in colonic biopsy samples from patients with ulcerative colitis, while fumarate, succinate and malate were significantly increased in the sera of patients with Crohn's disease (270). It is therefore inevitable that future therapeutic and diagnostic approaches based on Krebs cycle metabolites are likely to emerge.

5.4 – Improving the study of macrophage immunometabolism

Two areas that require improvement to better understand the immunomodulatory properties of the Krebs cycle and metabolic reprogramming in immune cells are organelle-specific metabolite analysis *in vitro* and metabolite profiling *in vivo*. Importantly, steps have been made in both directions. Although outside of an immune context these studies may have utility in the study of immunometabolism.

Firstly, Chen *et al* (2016) recently described a method for the rapid and specific isolation of mitochondria and its use in tandem with a database of predicted mitochondrial metabolites (MITObolome) (271). Intriguingly, they were able to utilise this method and compare it to the whole-cell metabolome across various states of respiratory chain function revealing extensive compartmentalization of mitochondrial metabolism and signatures unique to the inhibition of each RC complex (271).

Secondly, it is known that mammalian organs exchange metabolites via the circulation but a comprehensive investigation into this has only recently been carried. Jang *et al* (2019) compared metabolite concentrations in arterial blood versus draining venous blood from 11 organs in the pig, thus providing a quantitative atlas of inter-organ metabolite exchange that could prove fruitful in

understanding how organ-specific metabolism interacts with the immune system (272).

Thirdly, the use of stable-isotope tracing in humans has also been used to great effect in assessing metabolic heterogeneity and Krebs cycle functionality within tumours (273) and perhaps could be adapted for use in inflammatory diseases, whereby diseased tissue can be surgically excised. As such, these strategies may be adopted to encompass other tissue and cell types, cellular organelles and compartments in future studies. Specifically, these strategies may help us better understand the mechanics of Krebs cycle remodelling in macrophages and how this interacts with and influences cellular architecture and signalling, as well as revealing how this process unfolds in tissue-resident macrophage populations *in vivo* during inflammatory diseases.

5.5 – Final conclusion

It is now clear that the Krebs cycle and its intermediates go beyond their role in bioenergetics to influence cellular signalling and may serve as the ultimate determinant of macrophage function. The Krebs cycle has therefore been reborn in the macrophage as an immunometabolic signalling hub, the continuing study of which has great potential to deepen our understanding of the role of the macrophage in health and disease. Importantly, this thesis has made a major contribution to this emerging concept by identifying novel signalling pathways engaged by macrophages to direct inflammatory cytokine production.

Chapter 6:

References

1. Janeway CA, Jr., Medzhitov R. Innate immune recognition. Annu Rev Immunol. 2002;20:197-216.
2. Kelly B, O'Neill LA. Metabolic reprogramming in macrophages and dendritic cells in innate immunity. Cell Res. 2015;25(7):771-84.
3. Chen GY, Nunez G. Sterile inflammation: sensing and reacting to damage. Nat Rev Immunol. 2010;10(12):826-37.
4. Diskin C, Palsson-McDermott EM. Metabolic Modulation in Macrophage Effector Function. Front Immunol. 2018;9:270.
5. Lu YC, Yeh WC, Ohashi PS. LPS/TLR4 signal transduction pathway. Cytokine. 2008;42(2):145-51.
6. Ryu JK, Kim SJ, Rah SH, Kang JI, Jung HE, Lee D, et al. Reconstruction of LPS Transfer Cascade Reveals Structural Determinants within LBP, CD14, and TLR4-MD2 for Efficient LPS Recognition and Transfer. Immunity. 2017;46(1):38-50.
7. Chang L, Karin M. Mammalian MAP kinase signalling cascades. Nature. 2001;410(6824):37-40.
8. Yamamoto M, Sato S, Hemmi H, Hoshino K, Kaisho T, Sanjo H, et al. Role of adaptor TRIF in the MyD88-independent toll-like receptor signaling pathway. Science. 2003;301(5633):640-3.
9. Meylan E, Burns K, Hofmann K, Blancheteau V, Martinon F, Kelliher M, et al. RIP1 is an essential mediator of Toll-like receptor 3-induced NF-kappa B activation. Nat Immunol. 2004;5(5):503-7.
10. Oganesyan G, Saha SK, Guo B, He JQ, Shahangian A, Zarnegar B, et al. Critical role of TRAF3 in the Toll-like receptor-dependent and -independent antiviral response. Nature. 2006;439(7073):208-11.
11. Hacker H, Redecke V, Blagoev B, Kratchmarova I, Hsu LC, Wang GG, et al. Specificity in Toll-like receptor signalling through distinct effector functions of TRAF3 and TRAF6. Nature. 2006;439(7073):204-7.
12. Fitzgerald KA, McWhirter SM, Faia KL, Rowe DC, Latz E, Golenbock DT, et al. IKKepsilon and TBK1 are essential components of the IRF3 signaling pathway. Nat Immunol. 2003;4(5):491-6.
13. Essuman K, Summers DW, Sasaki Y, Mao X, Yim AKY, DiAntonio A, et al. TIR Domain Proteins Are an Ancient Family of NAD(+)-Consuming Enzymes. Curr Biol. 2018;28(3):421-30.e4.
14. Krawczyk CM, Holowka T, Sun J, Blagih J, Amiel E, DeBerardinis RJ, et al. Toll-like receptor-induced changes in glycolytic metabolism regulate dendritic cell activation. Blood. 2010;115(23):4742-9.
15. Rodriguez-Prados JC, Traves PG, Cuenca J, Rico D, Aragones J, Martin-Sanz P, et al. Substrate fate in activated macrophages: a comparison between innate, classic, and alternative activation. J Immunol. 2010;185(1):605-14.
16. Everts B, Amiel E, Huang SC, Smith AM, Chang CH, Lam WY, et al. TLR-driven early glycolytic reprogramming via the kinases TBK1-IKKvarepsilon supports the anabolic demands of dendritic cell activation. Nat Immunol. 2014;15(4):323-32.
17. Haschemi A, Kosma P, Gille L, Evans CR, Burant CF, Starkl P, et al. The sedoheptulose kinase CARKL directs macrophage polarization through control of glucose metabolism. Cell Metab. 2012;15(6):813-26.
18. Hard GC. Some biochemical aspects of the immune macrophage. Br J Exp Pathol. 1970;51(1):97-105.

19. Jantsch J, Chakravortty D, Turza N, Prechtel AT, Buchholz B, Gerlach RG, et al. Hypoxia and hypoxia-inducible factor-1 alpha modulate lipopolysaccharide-induced dendritic cell activation and function. J Immunol. 2008;180(7):4697-705.
20. Tannahill GM, Curtis AM, Adamik J, Palsson-McDermott EM, McGettrick AF, Goel G, et al. Succinate is an inflammatory signal that induces IL-1beta through HIF-1alpha. Nature. 2013;496(7444):238-42.
21. Palsson-McDermott EM, Curtis AM, Goel G, Lauterbach MA, Sheedy FJ, Gleeson LE, et al. Pyruvate kinase M2 regulates Hif-1alpha activity and IL-1beta induction and is a critical determinant of the warburg effect in LPS-activated macrophages. Cell Metab. 2015;21(1):65-80.
22. Millet P, Vachharajani V, McPhail L, Yoza B, McCall CE. GAPDH Binding to TNF-alpha mRNA Contributes to Posttranscriptional Repression in Monocytes: A Novel Mechanism of Communication between Inflammation and Metabolism. J Immunol. 2016;196(6):2541-51.
23. Krebs HA, Johnson WA. The role of citric acid in intermediate metabolism in animal tissues. FEBS Lett. 1980;117 Suppl:K1-10.
24. Kornberg H. Krebs and his trinity of cycles.
25. Owen OE, Kalhan SC, Hanson RW. The key role of anaplerosis and cataplerosis for citric acid cycle function. J Biol Chem. 2002;277(34):30409-12.
26. Buchanan BB, Arnon DI. A reverse KREBS cycle in photosynthesis: consensus at last. Photosynth Res. 1990;24:47-53.
27. Saraste M. Oxidative phosphorylation at the fin de siecle. Science. 1999;283(5407):1488-93.
28. Schultz BE, Chan SI. Structures and proton-pumping strategies of mitochondrial respiratory enzymes. Annu Rev Biophys Biomol Struct. 2001;30:23-65.
29. Mulkidjanian AY. On the origin of life in the zinc world: 1. Photosynthesizing, porous edifices built of hydrothermally precipitated zinc sulfide as cradles of life on Earth. Biol Direct. 2009;4:26.
30. Remington SJ. Structure and mechanism of citrate synthase. Curr Top Cell Regul. 1992;33:209-29.
31. Lloyd SJ, Lauble H, Prasad GS, Stout CD. The mechanism of aconitase: 1.8 A resolution crystal structure of the S642a:citrate complex. Protein Sci. 1999;8(12):2655-62.
32. Ma T, Peng Y, Huang W, Liu Y, Ding J. The beta and gamma subunits play distinct functional roles in the alpha2betagamma heterotetramer of human NAD-dependent isocitrate dehydrogenase. Sci Rep. 2017;7:41882.
33. Sheu KF, Blass JP. The alpha-ketoglutarate dehydrogenase complex. Ann N Y Acad Sci. 1999;893:61-78.
34. Johnson JD, Muhonen WW, Lambeth DO. Characterization of the ATP- and GTP-specific succinyl-CoA synthetases in pigeon. The enzymes incorporate the same alpha-subunit. J Biol Chem. 1998;273(42):27573-9.
35. Yankovskaya V, Horsefield R, Tornroth S, Luna-Chavez C, Miyoshi H, Leger C, et al. Architecture of succinate dehydrogenase and reactive oxygen species generation. Science. 2003;299(5607):700-4.
36. Rose IA. How fumarase recycles after the malate --> fumarate reaction. Insights into the reaction mechanism. Biochemistry. 1998;37(51):17651-8.
37. Chapman AD, Cortes A, Dafforn TR, Clarke AR, Brady RL. Structural basis of substrate specificity in malate dehydrogenases: crystal structure of a

ternary complex of porcine cytoplasmic malate dehydrogenase, alpha-ketomalonate and tetrahydoNAD. J Mol Biol. 1999;285(2):703-12.
38. Ruprecht JJ, Kunji ER. Structural changes in the transport cycle of the mitochondrial ADP/ATP carrier. Curr Opin Struct Biol. 2019;57:135-44.
39. Capitanio D, Fania C, Torretta E, Vigano A, Moriggi M, Bravata V, et al. TCA cycle rewiring fosters metabolic adaptation to oxygen restriction in skeletal muscle from rodents and humans. Sci Rep. 2017;7(1):9723.
40. Costello LC, Franklin RB. Testosterone and prolactin regulation of metabolic genes and citrate metabolism of prostate epithelial cells. Horm Metab Res. 2002;34(8):417-24.
41. Costello LC, Franklin R, Stacey R. Mitochondrial isocitrate dehydrogenase and isocitrate oxidation of rat ventral prostate. Enzyme. 1976;21(6):495-506.
42. Costello LC, Fadika G, Franklin R. Citrate and isocitrate utilization by rat ventral prostate mitochondria. Enzyme. 1978;23(3):176-81.
43. Costello LC, Franklin RB. A comprehensive review of the role of zinc in normal prostate function and metabolism; and its implications in prostate cancer. Arch Biochem Biophys. 2016;611:100-12.
44. Costello LC, Liu Y, Franklin RB, Kennedy MC. Zinc inhibition of mitochondrial aconitase and its importance in citrate metabolism of prostate epithelial cells. J Biol Chem. 1997;272(46):28875-81.
45. Jha AK, Huang SC, Sergushichev A, Lampropoulou V, Ivanova Y, Loginicheva E, et al. Network integration of parallel metabolic and transcriptional data reveals metabolic modules that regulate macrophage polarization. Immunity. 2015;42(3):419-30.
46. O'Neill LA. A broken krebs cycle in macrophages. Immunity. 2015;42(3):393-4.
47. Bailey JD, Diotallevi M, Nicol T, McNeill E, Shaw A, Chuaiphichai S, et al. Nitric Oxide Modulates Metabolic Remodeling in Inflammatory Macrophages through TCA Cycle Regulation and Itaconate Accumulation. Cell Rep. 2019;28(1):218-30.e7.
48. Cordes T, Wallace M, Michelucci A, Divakaruni AS, Sapcariu SC, Sousa C, et al. Immunoresponsive Gene 1 and Itaconate Inhibit Succinate Dehydrogenase to Modulate Intracellular Succinate Levels. J Biol Chem. 2016;291(27):14274-84.
49. Lampropoulou V, Sergushichev A, Bambouskova M, Nair S, Vincent EE, Loginicheva E, et al. Itaconate Links Inhibition of Succinate Dehydrogenase with Macrophage Metabolic Remodeling and Regulation of Inflammation. Cell Metab. 2016;24(1):158-66.
50. Seim GL, Britt EC, John SV, Yeo FJ, Johnson AR, Eisenstein RS, et al. Two-stage metabolic remodelling in macrophages in response to lipopolysaccharide and interferon-γ stimulation.
51. Hiromasa Y, Fujisawa T, Aso Y, Roche TE. Organization of the cores of the mammalian pyruvate dehydrogenase complex formed by E2 and E2 plus the E3-binding protein and their capacities to bind the E1 and E3 components. J Biol Chem. 2004;279(8):6921-33.
52. Izard T, Aevarsson A, Allen MD, Westphal AH, Perham RN, de Kok A, et al. Principles of quasi-equivalence and Euclidean geometry govern the assembly of cubic and dodecahedral cores of pyruvate dehydrogenase complexes. Proc Natl Acad Sci U S A. 1999;96(4):1240-5.

53. McCartney RG, Rice JE, Sanderson SJ, Bunik V, Lindsay H, Lindsay JG. Subunit interactions in the mammalian alpha-ketoglutarate dehydrogenase complex. Evidence for direct association of the alpha-ketoglutarate dehydrogenase and dihydrolipoamide dehydrogenase components. J Biol Chem. 1998;273(37):24158-64.
54. O'Neill LA, Kishton RJ, Rathmell J. A guide to immunometabolism for immunologists. Nat Rev Immunol. 2016;16(9):553-65.
55. Huang SC, Everts B, Ivanova Y, O'Sullivan D, Nascimento M, Smith AM, et al. Cell-intrinsic lysosomal lipolysis is essential for alternative activation of macrophages. Nat Immunol. 2014;15(9):846-55.
56. Huang SC, Smith AM, Everts B, Colonna M, Pearce EL, Schilling JD, et al. Metabolic Reprogramming Mediated by the mTORC2-IRF4 Signaling Axis Is Essential for Macrophage Alternative Activation. Immunity. 2016;45(4):817-30.
57. Nomura M, Liu J, Rovira, II, Gonzalez-Hurtado E, Lee J, Wolfgang MJ, et al. Fatty acid oxidation in macrophage polarization. Nat Immunol. 17. United States2016. p. 216-7.
58. Wang F, Zhang S, Vuckovic I, Jeon R, Lerman A, Folmes CD, et al. Glycolytic Stimulation Is Not a Requirement for M2 Macrophage Differentiation. Cell Metab. 2018;28(3):463-75.e4.
59. Divakaruni AS, Hsieh WY, Minarrieta L, Duong TN, Kim KKO, Desousa BR, et al. Etomoxir Inhibits Macrophage Polarization by Disrupting CoA Homeostasis. Cell Metab. 2018;28(3):490-503.e7.
60. Liu PS, Wang H, Li X, Chao T, Teav T, Christen S, et al. alpha-ketoglutarate orchestrates macrophage activation through metabolic and epigenetic reprogramming. Nat Immunol. 2017;18(9):985-94.
61. Nelson VL, Nguyen HCB, Garcia-Canaveras JC, Briggs ER, Ho WY, DiSpirito JR, et al. PPARgamma is a nexus controlling alternative activation of macrophages via glutamine metabolism. Genes Dev. 2018;32(15-16):1035-44.
62. Mills EL, Kelly B, Logan A, Costa ASH, Varma M, Bryant CE, et al. Succinate Dehydrogenase Supports Metabolic Repurposing of Mitochondria to Drive Inflammatory Macrophages. Cell. 2016;167(2):457-70.e13.
63. Keiran N, Ceperuelo-Mallafre V, Calvo E, Hernandez-Alvarez MI, Ejarque M, Nunez-Roa C, et al. SUCNR1 controls an anti-inflammatory program in macrophages to regulate the metabolic response to obesity. Nat Immunol. 2019;20(5):581-92.
64. Wang F, Wang K, Xu W, Zhao S, Ye D, Wang Y, et al. SIRT5 Desuccinylates and Activates Pyruvate Kinase M2 to Block Macrophage IL-1beta Production and to Prevent DSS-Induced Colitis in Mice. Cell Rep. 2017;19(11):2331-44.
65. Arts RJ, Novakovic B, Ter Horst R, Carvalho A, Bekkering S, Lachmandas E, et al. Glutaminolysis and Fumarate Accumulation Integrate Immunometabolic and Epigenetic Programs in Trained Immunity. Cell Metab. 2016;24(6):807-19.
66. Littlewood-Evans A, Sarret S, Apfel V, Loesle P, Dawson J, Zhang J, et al. GPR91 senses extracellular succinate released from inflammatory macrophages and exacerbates rheumatoid arthritis. J Exp Med. 2016;213(9):1655-62.
67. Peruzzotti-Jametti L, Bernstock JD, Vicario N, Costa ASH, Kwok CK, Leonardi T, et al. Macrophage-Derived Extracellular Succinate Licenses Neural Stem Cells to Suppress Chronic Neuroinflammation. Cell Stem Cell. 2018;22(3):355-68.e13.

68. van Diepen JA, Robben JH, Hooiveld GJ, Carmone C, Alsady M, Boutens L, et al. SUCNR1-mediated chemotaxis of macrophages aggravates obesity-induced inflammation and diabetes. Diabetologia. 2017;60(7):1304-13.
69. Corcoran SE, O'Neill LA. HIF1alpha and metabolic reprogramming in inflammation. J Clin Invest. 2016;126(10):3699-707.
70. Semenza GL. Regulation of oxygen homeostasis by hypoxia-inducible factor 1. Physiology (Bethesda). 2009;24:97-106.
71. Semenza GL, Wang GL. A nuclear factor induced by hypoxia via de novo protein synthesis binds to the human erythropoietin gene enhancer at a site required for transcriptional activation. Mol Cell Biol. 1992;12(12):5447-54.
72. Epstein AC, Gleadle JM, McNeill LA, Hewitson KS, O'Rourke J, Mole DR, et al. C. elegans EGL-9 and mammalian homologs define a family of dioxygenases that regulate HIF by prolyl hydroxylation. Cell. 2001;107(1):43-54.
73. Maxwell PH, Wiesener MS, Chang GW, Clifford SC, Vaux EC, Cockman ME, et al. The tumour suppressor protein VHL targets hypoxia-inducible factors for oxygen-dependent proteolysis. Nature. 1999;399(6733):271-5.
74. Selak MA, Armour SM, MacKenzie ED, Boulahbel H, Watson DG, Mansfield KD, et al. Succinate links TCA cycle dysfunction to oncogenesis by inhibiting HIF-alpha prolyl hydroxylase. Cancer Cell. 2005;7(1):77-85.
75. Kietzmann T, Gorlach A. Reactive oxygen species in the control of hypoxia-inducible factor-mediated gene expression. Semin Cell Dev Biol. 2005;16(4-5):474-86.
76. Guzy RD, Sharma B, Bell E, Chandel NS, Schumacker PT. Loss of the SdhB, but Not the SdhA, subunit of complex II triggers reactive oxygen species-dependent hypoxia-inducible factor activation and tumorigenesis. Mol Cell Biol. 2008;28(2):718-31.
77. Kelly B, Tannahill GM, Murphy MP, O'Neill LA. Metformin Inhibits the Production of Reactive Oxygen Species from NADH:Ubiquinone Oxidoreductase to Limit Induction of Interleukin-1beta (IL-1beta) and Boosts Interleukin-10 (IL-10) in Lipopolysaccharide (LPS)-activated Macrophages. J Biol Chem. 2015;290(33):20348-59.
78. Chouchani ET, Pell VR, Gaude E, Aksentijevic D, Sundier SY, Robb EL, et al. Ischaemic accumulation of succinate controls reperfusion injury through mitochondrial ROS. Nature. 2014;515(7527):431-5.
79. Jin Z, Wei W, Yang M, Du Y, Wan Y. Mitochondrial complex I activity suppresses inflammation and enhances bone resorption by shifting macrophage-osteoclast polarization. Cell Metab. 2014;20(3):483-98.
80. Garaude J, Acin-Perez R, Martinez-Cano S, Enamorado M, Ugolini M, Nistal-Villan E, et al. Mitochondrial respiratory-chain adaptations in macrophages contribute to antibacterial host defense. Nat Immunol. 2016;17(9):1037-45.
81. Cameron AM, Castoldi A, Sanin DE, Flachsmann LJ, Field CS, Puleston DJ, et al. Inflammatory macrophage dependence on NAD(+) salvage is a consequence of reactive oxygen species-mediated DNA damage. Nat Immunol. 2019;20(4):420-32.
82. Hirschey MD, Zhao Y. Metabolic Regulation by Lysine Malonylation, Succinylation, and Glutarylation. Mol Cell Proteomics. 2015;14(9):2308-15.
83. Du J, Zhou Y, Su X, Yu JJ, Khan S, Jiang H, et al. Sirt5 is a NAD-dependent protein lysine demalonylase and desuccinylase. Science. 2011;334(6057):806-9.

84. Park J, Chen Y, Tishkoff DX, Peng C, Tan M, Dai L, et al. SIRT5-mediated lysine desuccinylation impacts diverse metabolic pathways. Mol Cell. 2013;50(6):919-30.
85. Xiao M, Yang H, Xu W, Ma S, Lin H, Zhu H, et al. Inhibition of alpha-KG-dependent histone and DNA demethylases by fumarate and succinate that are accumulated in mutations of FH and SDH tumor suppressors. Genes Dev. 2012;26(12):1326-38.
86. Liu Z, Gan L, Zhang T, Ren Q, Sun C. Melatonin alleviates adipose inflammation through elevating alpha-ketoglutarate and diverting adipose-derived exosomes to macrophages in mice. J Pineal Res. 2018;64(1).
87. Cheng SC, Quintin J, Cramer RA, Shepardson KM, Saeed S, Kumar V, et al. mTOR- and HIF-1alpha-mediated aerobic glycolysis as metabolic basis for trained immunity. Science. 2014;345(6204):1250684.
88. Saeed S, Quintin J, Kerstens HH, Rao NA, Aghajanirefah A, Matarese F, et al. Epigenetic programming of monocyte-to-macrophage differentiation and trained innate immunity. Science. 2014;345(6204):1251086.
89. He W, Miao FJ, Lin DC, Schwandner RT, Wang Z, Gao J, et al. Citric acid cycle intermediates as ligands for orphan G-protein-coupled receptors. Nature. 2004;429(6988):188-93.
90. Gilissen J, Jouret F, Pirotte B, Hanson J. Insight into SUCNR1 (GPR91) structure and function. Pharmacol Ther. 2016;159:56-65.
91. Ariza AC, Deen PM, Robben JH. The succinate receptor as a novel therapeutic target for oxidative and metabolic stress-related conditions. Front Endocrinol (Lausanne). 2012;3:22.
92. Robben JH, Fenton RA, Vargas SL, Schweer H, Peti-Peterdi J, Deen PM, et al. Localization of the succinate receptor in the distal nephron and its signaling in polarized MDCK cells. Kidney Int. 2009;76(12):1258-67.
93. Sundstrom L, Greasley PJ, Engberg S, Wallander M, Ryberg E. Succinate receptor GPR91, a Galpha(i) coupled receptor that increases intracellular calcium concentrations through PLCbeta. FEBS Lett. 2013;587(15):2399-404.
94. Regard JB, Sato IT, Coughlin SR. Anatomical profiling of G protein-coupled receptor expression. Cell. 2008;135(3):561-71.
95. Hakak Y, Lehmann-Bruinsma K, Phillips S, Le T, Liaw C, Connolly DT, et al. The role of the GPR91 ligand succinate in hematopoiesis. J Leukoc Biol. 2009;85(5):837-43.
96. Aguiar CJ, Andrade VL, Gomes ER, Alves MN, Ladeira MS, Pinheiro AC, et al. Succinate modulates Ca(2+) transient and cardiomyocyte viability through PKA-dependent pathway. Cell Calcium. 2010;47(1):37-46.
97. Hogberg C, Gidlof O, Tan C, Svensson S, Nilsson-Ohman J, Erlinge D, et al. Succinate independently stimulates full platelet activation via cAMP and phosphoinositide 3-kinase-beta signaling. J Thromb Haemost. 2011;9(2):361-72.
98. Rubic T, Lametschwandtner G, Jost S, Hinteregger S, Kund J, Carballido-Perrig N, et al. Triggering the succinate receptor GPR91 on dendritic cells enhances immunity. Nat Immunol. 2008;9(11):1261-9.
99. Rubic-Schneider T, Carballido-Perrig N, Regairaz C, Raad L, Jost S, Rauld C, et al. GPR91 deficiency exacerbates allergic contact dermatitis while reducing arthritic disease in mice. Allergy. 2017;72(3):444-52.
100. Michelucci A, Cordes T, Ghelfi J, Pailot A, Reiling N, Goldmann O, et al. Immune-responsive gene 1 protein links metabolism to immunity by catalyzing itaconic acid production. Proc Natl Acad Sci U S A. 2013;110(19):7820-5.

101. Meiser J, Kramer L, Sapcariu SC, Battello N, Ghelfi J, D'Herouel AF, et al. Pro-inflammatory Macrophages Sustain Pyruvate Oxidation through Pyruvate Dehydrogenase for the Synthesis of Itaconate and to Enable Cytokine Expression. J Biol Chem. 2016;291(8):3932-46.
102. Infantino V, Convertini P, Cucci L, Panaro MA, Di Noia MA, Calvello R, et al. The mitochondrial citrate carrier: a new player in inflammation. Biochem J. 2011;438(3):433-6.
103. Infantino V, Iacobazzi V, Palmieri F, Menga A. ATP-citrate lyase is essential for macrophage inflammatory response. Biochem Biophys Res Commun. 2013;440(1):105-11.
104. Wellen KE, Hatzivassiliou G, Sachdeva UM, Bui TV, Cross JR, Thompson CB. ATP-citrate lyase links cellular metabolism to histone acetylation. Science. 2009;324(5930):1076-80.
105. Carroll RG, Zaslona Z, Galvan-Pena S, Koppe EL, Sevin DC, Angiari S, et al. An unexpected link between fatty acid synthase and cholesterol synthesis in proinflammatory macrophage activation. J Biol Chem. 2018;293(15):5509-21.
106. Wei X, Song H, Yin L, Rizzo MG, Sidhu R, Covey DF, et al. Fatty acid synthesis configures the plasma membrane for inflammation in diabetes. Nature. 2016;539(7628):294-8.
107. Cader MZ, Boroviak K, Zhang Q, Assadi G, Kempster SL, Sewell GW, et al. C13orf31 (FAMIN) is a central regulator of immunometabolic function. Nat Immunol. 2016;17(9):1046-56.
108. Wang B, Rao YH, Inoue M, Hao R, Lai CH, Chen D, et al. Microtubule acetylation amplifies p38 kinase signalling and anti-inflammatory IL-10 production. Nat Commun. 2014;5:3479.
109. Lu J, Sun H, Wang X, Liu C, Xu X, Li F, et al. Interleukin-12 p40 promoter activity is regulated by the reversible acetylation mediated by HDAC1 and p300. Cytokine. 2005;31(1):46-51.
110. Moores RC, Brilha S, Schutgens F, Elkington PT, Friedland JS. Epigenetic Regulation of Matrix Metalloproteinase-1 and -3 Expression in Mycobacterium tuberculosis Infection. Front Immunol. 2017;8:602.
111. Hu L, Yu Y, Huang H, Fan H, Yin C, Li K, et al. Epigenetic Regulation of Interleukin 6 by Histone Acetylation in Macrophages and Its Role in Paraquat-Induced Pulmonary Fibrosis. Front Immunol. 2016;7:696.
112. Feng D, Sangster-Guity N, Stone R, Korczeniewska J, Mancl ME, Fitzgerald-Bocarsly P, et al. Differential requirement of histone acetylase and deacetylase activities for IRF5-mediated proinflammatory cytokine expression. J Immunol. 2010;185(10):6003-12.
113. Kurdistani SK, Grunstein M. Histone acetylation and deacetylation in yeast. Nat Rev Mol Cell Biol. 2003;4(4):276-84.
114. Du Y, Cai T, Li T, Xue P, Zhou B, He X, et al. Lysine malonylation is elevated in type 2 diabetic mouse models and enriched in metabolic associated proteins. Mol Cell Proteomics. 2015;14(1):227-36.
115. Galvan-Pena S, Carroll RG, Newman C, Hinchy EC, Palsson-McDermott E, Robinson EK, et al. Malonylation of GAPDH is an inflammatory signal in macrophages. Nat Commun. 2019;10(1):338.
116. Mills EL, Ryan DG, Prag HA, Dikovskaya D, Menon D, Zaslona Z, et al. Itaconate is an anti-inflammatory metabolite that activates Nrf2 via alkylation of KEAP1. Nature. 2018;556(7699):113-7.

117. Strelko CL, Lu W, Dufort FJ, Seyfried TN, Chiles TC, Rabinowitz JD, et al. Itaconic acid is a mammalian metabolite induced during macrophage activation. J Am Chem Soc. 2011;133(41):16386-9.
118. Shin JH, Yang JY, Jeon BY, Yoon YJ, Cho SN, Kang YH, et al. (1)H NMR-based metabolomic profiling in mice infected with Mycobacterium tuberculosis. J Proteome Res. 2011;10(5):2238-47.
119. McFadden BA, Purohit S. Itaconate, an isocitrate lyase-directed inhibitor in Pseudomonas indigofera. J Bacteriol. 1977;131(1):136-44.
120. Naujoks J, Tabeling C, Dill BD, Hoffmann C, Brown AS, Kunze M, et al. IFNs Modify the Proteome of Legionella-Containing Vacuoles and Restrict Infection Via IRG1-Derived Itaconic Acid. PLoS Pathog. 2016;12(2):e1005408.
121. Sasikaran J, Ziemski M, Zadora PK, Fleig A, Berg IA. Bacterial itaconate degradation promotes pathogenicity. Nat Chem Biol. 2014;10(5):371-7.
122. Lorenz MC, Fink GR. The glyoxylate cycle is required for fungal virulence. Nature. 2001;412(6842):83-6.
123. Lorenz MC, Fink GR. Life and death in a macrophage: role of the glyoxylate cycle in virulence. Eukaryot Cell. 2002;1(5):657-62.
124. Munoz-Elias EJ, McKinney JD. Mycobacterium tuberculosis isocitrate lyases 1 and 2 are jointly required for in vivo growth and virulence. Nat Med. 2005;11(6):638-44.
125. Luan HH, Medzhitov R. Food Fight: Role of Itaconate and Other Metabolites in Antimicrobial Defense. Cell Metab. 2016;24(3):379-87.
126. Nair S, Huynh JP, Lampropoulou V, Loginicheva E, Esaulova E, Gounder AP, et al. Irg1 expression in myeloid cells prevents immunopathology during M. tuberculosis infection. J Exp Med. 2018;215(4):1035-45.
127. Bambouskova M, Gorvel L, Lampropoulou V, Sergushichev A, Loginicheva E, Johnson K, et al. Electrophilic properties of itaconate and derivatives regulate the IkappaBzeta-ATF3 inflammatory axis. Nature. 2018;556(7702):501-4.
128. Li Y, Zhang P, Wang C, Han C, Meng J, Liu X, et al. Immune responsive gene 1 (IRG1) promotes endotoxin tolerance by increasing A20 expression in macrophages through reactive oxygen species. J Biol Chem. 2013;288(23):16225-34.
129. Jamal Uddin M, Joe Y, Kim SK, Oh Jeong S, Ryter SW, Pae HO, et al. IRG1 induced by heme oxygenase-1/carbon monoxide inhibits LPS-mediated sepsis and pro-inflammatory cytokine production. Cell Mol Immunol. 2016;13(2):170-9.
130. Cheon YP, Xu X, Bagchi MK, Bagchi IC. Immune-responsive gene 1 is a novel target of progesterone receptor and plays a critical role during implantation in the mouse. Endocrinology. 2003;144(12):5623-30.
131. Sherwin JR, Freeman TC, Stephens RJ, Kimber S, Smith AG, Chambers I, et al. Identification of genes regulated by leukemia-inhibitory factor in the mouse uterus at the time of implantation. Mol Endocrinol. 2004;18(9):2185-95.
132. Chen B, Zhang D, Pollard JW. Progesterone regulation of the mammalian ortholog of methylcitrate dehydratase (immune response gene 1) in the uterine epithelium during implantation through the protein kinase C pathway. Mol Endocrinol. 2003;17(11):2340-54.
133. Ackermann WW, Potter VR. Enzyme inhibition in relation to chemotherapy. Proc Soc Exp Biol Med. 1949;72(1):1-9.

134. Shen H, Campanello GC, Flicker D, Grabarek Z, Hu J, Luo C, et al. The Human Knockout Gene CLYBL Connects Itaconate to Vitamin B12. Cell. 2017;171(4):771-82.e11.
135. Nemeth B, Doczi J, Csete D, Kacso G, Ravasz D, Adams D, et al. Abolition of mitochondrial substrate-level phosphorylation by itaconic acid produced by LPS-induced Irg1 expression in cells of murine macrophage lineage. Faseb j. 2016;30(1):286-300.
136. Daniels BP, Kofman SB, Smith JR, Norris GT, Snyder AG, Kolb JP, et al. The Nucleotide Sensor ZBP1 and Kinase RIPK3 Induce the Enzyme IRG1 to Promote an Antiviral Metabolic State in Neurons. Immunity. 2019;50(1):64-76.e4.
137. Hayes JD, Dinkova-Kostova AT. The Nrf2 regulatory network provides an interface between redox and intermediary metabolism. Trends Biochem Sci. 2014;39(4):199-218.
138. Moi P, Chan K, Asunis I, Cao A, Kan YW. Isolation of NF-E2-related factor 2 (Nrf2), a NF-E2-like basic leucine zipper transcriptional activator that binds to the tandem NF-E2/AP1 repeat of the beta-globin locus control region. Proc Natl Acad Sci U S A. 1994;91(21):9926-30.
139. Friling RS, Bensimon A, Tichauer Y, Daniel V. Xenobiotic-inducible expression of murine glutathione S-transferase Ya subunit gene is controlled by an electrophile-responsive element. Proc Natl Acad Sci U S A. 1990;87(16):6258-62.
140. Itoh K, Chiba T, Takahashi S, Ishii T, Igarashi K, Katoh Y, et al. An Nrf2/small Maf heterodimer mediates the induction of phase II detoxifying enzyme genes through antioxidant response elements. Biochem Biophys Res Commun. 1997;236(2):313-22.
141. Itoh K, Wakabayashi N, Katoh Y, Ishii T, Igarashi K, Engel JD, et al. Keap1 represses nuclear activation of antioxidant responsive elements by Nrf2 through binding to the amino-terminal Neh2 domain. Genes Dev. 1999;13(1):76-86.
142. Igarashi K, Kataoka K, Itoh K, Hayashi N, Nishizawa M, Yamamoto M. Regulation of transcription by dimerization of erythroid factor NF-E2 p45 with small Maf proteins. Nature. 1994;367(6463):568-72.
143. Katoh Y, Itoh K, Yoshida E, Miyagishi M, Fukamizu A, Yamamoto M. Two domains of Nrf2 cooperatively bind CBP, a CREB binding protein, and synergistically activate transcription. Genes Cells. 2001;6(10):857-68.
144. Sekine H, Okazaki K, Ota N, Shima H, Katoh Y, Suzuki N, et al. The Mediator Subunit MED16 Transduces NRF2-Activating Signals into Antioxidant Gene Expression. Mol Cell Biol. 2016;36(3):407-20.
145. Rada P, Rojo AI, Chowdhry S, McMahon M, Hayes JD, Cuadrado A. SCF/{beta}-TrCP promotes glycogen synthase kinase 3-dependent degradation of the Nrf2 transcription factor in a Keap1-independent manner. Mol Cell Biol. 2011;31(6):1121-33.
146. Chowdhry S, Zhang Y, McMahon M, Sutherland C, Cuadrado A, Hayes JD. Nrf2 is controlled by two distinct beta-TrCP recognition motifs in its Neh6 domain, one of which can be modulated by GSK-3 activity. Oncogene. 2013;32(32):3765-81.
147. Kobayashi A, Kang MI, Okawa H, Ohtsuji M, Zenke Y, Chiba T, et al. Oxidative stress sensor Keap1 functions as an adaptor for Cul3-based E3 ligase to regulate proteasomal degradation of Nrf2. Mol Cell Biol. 2004;24(16):7130-9.

148. Tong KI, Katoh Y, Kusunoki H, Itoh K, Tanaka T, Yamamoto M. Keap1 recruits Neh2 through binding to ETGE and DLG motifs: characterization of the two-site molecular recognition model. Mol Cell Biol. 2006;26(8):2887-900.
149. Tong KI, Padmanabhan B, Kobayashi A, Shang C, Hirotsu Y, Yokoyama S, et al. Different electrostatic potentials define ETGE and DLG motifs as hinge and latch in oxidative stress response. Mol Cell Biol. 2007;27(21):7511-21.
150. Suzuki T, Maher J, Yamamoto M. Select heterozygous Keap1 mutations have a dominant-negative effect on wild-type Keap1 in vivo. Cancer Res. 2011;71(5):1700-9.
151. Canning P, Cooper CD, Krojer T, Murray JW, Pike AC, Chaikuad A, et al. Structural basis for Cul3 protein assembly with the BTB-Kelch family of E3 ubiquitin ligases. J Biol Chem. 2013;288(11):7803-14.
152. Baird L, Lleres D, Swift S, Dinkova-Kostova AT. Regulatory flexibility in the Nrf2-mediated stress response is conferred by conformational cycling of the Keap1-Nrf2 protein complex. Proc Natl Acad Sci U S A. 2013;110(38):15259-64.
153. Dinkova-Kostova AT, Holtzclaw WD, Cole RN, Itoh K, Wakabayashi N, Katoh Y, et al. Direct evidence that sulfhydryl groups of Keap1 are the sensors regulating induction of phase 2 enzymes that protect against carcinogens and oxidants. Proc Natl Acad Sci U S A. 2002;99(18):11908-13.
154. Saito R, Suzuki T, Hiramoto K, Asami S, Naganuma E, Suda H, et al. Characterizations of Three Major Cysteine Sensors of Keap1 in Stress Response. Mol Cell Biol. 2016;36(2):271-84.
155. Komatsu M, Kurokawa H, Waguri S, Taguchi K, Kobayashi A, Ichimura Y, et al. The selective autophagy substrate p62 activates the stress responsive transcription factor Nrf2 through inactivation of Keap1. Nat Cell Biol. 2010;12(3):213-23.
156. Taguchi K, Fujikawa N, Komatsu M, Ishii T, Unno M, Akaike T, et al. Keap1 degradation by autophagy for the maintenance of redox homeostasis. Proc Natl Acad Sci U S A. 2012;109(34):13561-6.
157. Tong YH, Zhang B, Fan Y, Lin NM. Keap1-Nrf2 pathway: A promising target towards lung cancer prevention and therapeutics. Chronic Dis Transl Med. 2015;1(3):175-86.
158. Thimmulappa RK, Lee H, Rangasamy T, Reddy SP, Yamamoto M, Kensler TW, et al. Nrf2 is a critical regulator of the innate immune response and survival during experimental sepsis. J Clin Invest. 2006;116(4):984-95.
159. Kobayashi EH, Suzuki T, Funayama R, Nagashima T, Hayashi M, Sekine H, et al. Nrf2 suppresses macrophage inflammatory response by blocking proinflammatory cytokine transcription. Nat Commun. 2016;7:11624.
160. Early JO, Menon D, Wyse CA, Cervantes-Silva MP, Zaslona Z, Carroll RG, et al. Circadian clock protein BMAL1 regulates IL-1beta in macrophages via NRF2. Proc Natl Acad Sci U S A. 2018;115(36):E8460-e8.
161. Bomprezzi R. Dimethyl fumarate in the treatment of relapsing-remitting multiple sclerosis: an overview. Ther Adv Neurol Disord. 2015;8(1):20-30.
162. Brennan MS, Matos MF, Li B, Hronowski X, Gao B, Juhasz P, et al. Dimethyl fumarate and monoethyl fumarate exhibit differential effects on KEAP1, NRF2 activation, and glutathione depletion in vitro. PLoS One. 2015;10(3):e0120254.
163. Wilms H, Sievers J, Rickert U, Rostami-Yazdi M, Mrowietz U, Lucius R. Dimethylfumarate inhibits microglial and astrocytic inflammation by suppressing

the synthesis of nitric oxide, IL-1beta, TNF-alpha and IL-6 in an in-vitro model of brain inflammation. J Neuroinflammation. 2010;7:30.
164. Linker RA, Lee DH, Ryan S, van Dam AM, Conrad R, Bista P, et al. Fumaric acid esters exert neuroprotective effects in neuroinflammation via activation of the Nrf2 antioxidant pathway. Brain. 2011;134(Pt 3):678-92.
165. Richard J-V, Delaite C, Reiss G, Anne-Sophie S. A comparative study of the thermal properties of homologous series of crystallisable n-alkyl maleate and itaconate monoesters. 2016;623:136-43.
166. Davis S, Charles PD, He L, Mowlds P, Kessler BM, Fischer R. Expanding Proteome Coverage with CHarge Ordered Parallel Ion aNalysis (CHOPIN) Combined with Broad Specificity Proteolysis. J Proteome Res. 2017;16(3):1288-99.
167. Eng JK, McCormack AL, Yates JR. An approach to correlate tandem mass spectral data of peptides with amino acid sequences in a protein database. J Am Soc Mass Spectrom. 1994;5(11):976-89.
168. Mackay GM, Zheng L, van den Broek NJ, Gottlieb E. Analysis of Cell Metabolism Using LC-MS and Isotope Tracers. Methods Enzymol. 2015;561:171-96.
169. Akerboom TP, Sies H. Assay of glutathione, glutathione disulfide, and glutathione mixed disulfides in biological samples. Methods Enzymol. 1981;77:373-82.
170. Booty LM, King MS, Thangaratnarajah C, Majd H, James AM, Kunji ER, et al. The mitochondrial dicarboxylate and 2-oxoglutarate carriers do not transport glutathione. FEBS Lett. 2015;589(5):621-8.
171. Hevia D, Mayo JC, Rodriguez-Garcia A, Alonso-Guervos M, Quiros-Gonzales I, Cimadevilla H, et al. Cell volume and geometric parameters determination in living cells using confocal microscopy and 3D reconstruction Protocol exhange. 2011.
172. Pesi R, Balestri F, Ipata PL. Metabolic interaction between urea cycle and citric acid cycle shunt: A guided approach. Biochem Mol Biol Educ. 2018;46(2):182-5.
173. Haines RJ, Pendleton LC, Eichler DC. Argininosuccinate synthase: at the center of arginine metabolism. Int J Biochem Mol Biol. 2011;2(1):8-23.
174. Ashrafian H, Czibik G, Bellahcene M, Aksentijevic D, Smith AC, Mitchell SJ, et al. Fumarate is cardioprotective via activation of the Nrf2 antioxidant pathway. Cell Metab. 2012;15(3):361-71.
175. Zheng L, Cardaci S, Jerby L, MacKenzie ED, Sciacovelli M, Johnson TI, et al. Fumarate induces redox-dependent senescence by modifying glutathione metabolism. Nat Commun. 2015;6:6001.
176. Merkley ED, Metz TO, Smith RD, Baynes JW, Frizzell N. The succinated proteome. Mass Spectrom Rev. 2014;33(2):98-109.
177. Adam J, Ramracheya R, Chibalina MV, Ternette N, Hamilton A, Tarasov AI, et al. Fumarate Hydratase Deletion in Pancreatic beta Cells Leads to Progressive Diabetes. Cell Rep. 2017;20(13):3135-48.
178. Tyrakis PA, Yurkovich ME, Sciacovelli M, Papachristou EK, Bridges HR, Gaude E, et al. Fumarate Hydratase Loss Causes Combined Respiratory Chain Defects. Cell Rep. 2017;21(4):1036-47.
179. Kornberg MD, Bhargava P, Kim PM, Putluri V, Snowman AM, Putluri N, et al. Dimethyl fumarate targets GAPDH and aerobic glycolysis to modulate immunity. Science. 2018;360(6387):449-53.

180. Blair HA. Dimethyl Fumarate: A Review in Moderate to Severe Plaque Psoriasis. Drugs. 2018;78(1):123-30.
181. Linker RA, Haghikia A. Dimethyl fumarate in multiple sclerosis: latest developments, evidence and place in therapy. Ther Adv Chronic Dis. 2016;7(4):198-207.
182. Chen H, Assmann JC, Krenz A, Rahman M, Grimm M, Karsten CM, et al. Hydroxycarboxylic acid receptor 2 mediates dimethyl fumarate's protective effect in EAE. J Clin Invest. 2014;124(5):2188-92.
183. Tang H, Lu JY, Zheng X, Yang Y, Reagan JD. The psoriasis drug monomethylfumarate is a potent nicotinic acid receptor agonist. Biochem Biophys Res Commun. 2008;375(4):562-5.
184. Fan Z, Li L, Li X, Zhang M, Dou M, Zhao J, et al. Anti-senescence role of heterozygous fumarate hydratase gene knockout in rat lung fibroblasts in vitro. Aging (Albany NY). 2019;11(2):573-89.
185. Adam J, Hatipoglu E, O'Flaherty L, Ternette N, Sahgal N, Lockstone H, et al. Renal cyst formation in Fh1-deficient mice is independent of the Hif/Phd pathway: roles for fumarate in KEAP1 succination and Nrf2 signaling. Cancer Cell. 2011;20(4):524-37.
186. Bateman LA, Ku WM, Heslin MJ, Contreras CM, Skibola CF, Nomura DK. Argininosuccinate Synthase 1 is a Metabolic Regulator of Colorectal Cancer Pathogenicity. ACS Chem Biol. 2017;12(4):905-11.
187. Churchich JE, Bieler J. Reactivity of pyridoxal 5-phosphate residues of cystathionase. Biochim Biophys Acta. 1971;229(3):813-23.
188. McKenna MC, Waagepetersen HS, Schousboe A, Sonnewald U. Neuronal and astrocytic shuttle mechanisms for cytosolic-mitochondrial transfer of reducing equivalents: current evidence and pharmacological tools. Biochem Pharmacol. 2006;71(4):399-407.
189. Lu M, Zhou L, Stanley WC, Cabrera ME, Saidel GM, Yu X. Role of the malate-aspartate shuttle on the metabolic response to myocardial ischemia. J Theor Biol. 2008;254(2):466-75.
190. Everts B, Amiel E, van der Windt GJ, Freitas TC, Chott R, Yarasheski KE, et al. Commitment to glycolysis sustains survival of NO-producing inflammatory dendritic cells. Blood. 2012;120(7):1422-31.
191. Van den Bossche J, Baardman J, Otto NA, van der Velden S, Neele AE, van den Berg SM, et al. Mitochondrial Dysfunction Prevents Repolarization of Inflammatory Macrophages. Cell Rep. 2016;17(3):684-96.
192. Sanin DE, Matsushita M, Klein Geltink RI, Grzes KM, van Teijlingen Bakker N, Corrado M, et al. Mitochondrial Membrane Potential Regulates Nuclear Gene Expression in Macrophages Exposed to Prostaglandin E2. Immunity. 2018;49(6):1021-33.e6.
193. Schulze-Topphoff U, Varrin-Doyer M, Pekarek K, Spencer CM, Shetty A, Sagan SA, et al. Dimethyl fumarate treatment induces adaptive and innate immune modulation independent of Nrf2. Proc Natl Acad Sci U S A. 2016;113(17):4777-82.
194. Blewett MM, Xie J, Zaro BW, Backus KM, Altman A, Teijaro JR, et al. Chemical proteomic map of dimethyl fumarate-sensitive cysteines in primary human T cells. Sci Signal. 2016;9(445):rs10.
195. McGuire VA, Ruiz-Zorrilla Diez T, Emmerich CH, Strickson S, Ritorto MS, Sutavani RV, et al. Dimethyl fumarate blocks pro-inflammatory cytokine

production via inhibition of TLR induced M1 and K63 ubiquitin chain formation. Sci Rep. 2016;6:31159.
196. Gillard GO, Collette B, Anderson J, Chao J, Scannevin RH, Huss DJ, et al. DMF, but not other fumarates, inhibits NF-kappaB activity in vitro in an Nrf2-independent manner. J Neuroimmunol. 2015;283:74-85.
197. Schmidt TJ, Ak M, Mrowietz U. Reactivity of dimethyl fumarate and methylhydrogen fumarate towards glutathione and N-acetyl-L-cysteine--preparation of S-substituted thiosuccinic acid esters. Bioorg Med Chem. 2007;15(1):333-42.
198. Kulkarni RA, Bak DW, Wei D, Bergholtz SE, Briney CA, Shrimp JH, et al. A chemoproteomic portrait of the oncometabolite fumarate. Nat Chem Biol. 2019;15(4):391-400.
199. Zandi-Nejad K, Takakura A, Jurewicz M, Chandraker AK, Offermanns S, Mount D, et al. The role of HCA2 (GPR109A) in regulating macrophage function. Faseb j. 2013;27(11):4366-74.
200. Asadullah K, Schmid H, Friedrich M, Randow F, Volk HD, Sterry W, et al. Influence of monomethylfumarate on monocytic cytokine formation--explanation for adverse and therapeutic effects in psoriasis? Arch Dermatol Res. 1997;289(11):623-30.
201. Pollard PJ, Briere JJ, Alam NA, Barwell J, Barclay E, Wortham NC, et al. Accumulation of Krebs cycle intermediates and over-expression of HIF1alpha in tumours which result from germline FH and SDH mutations. Hum Mol Genet. 2005;14(15):2231-9.
202. Isaacs JS, Jung YJ, Mole DR, Lee S, Torres-Cabala C, Chung YL, et al. HIF overexpression correlates with biallelic loss of fumarate hydratase in renal cancer: novel role of fumarate in regulation of HIF stability. Cancer Cell. 2005;8(2):143-53.
203. Sudarshan S, Sourbier C, Kong HS, Block K, Valera Romero VA, Yang Y, et al. Fumarate hydratase deficiency in renal cancer induces glycolytic addiction and hypoxia-inducible transcription factor 1alpha stabilization by glucose-dependent generation of reactive oxygen species. Mol Cell Biol. 2009;29(15):4080-90.
204. Shanmugasundaram K, Nayak B, Shim EH, Livi CB, Block K, Sudarshan S. The oncometabolite fumarate promotes pseudohypoxia through noncanonical activation of NF-kappaB signaling. J Biol Chem. 2014;289(35):24691-9.
205. Adam J, Yang M, Bauerschmidt C, Kitagawa M, O'Flaherty L, Maheswaran P, et al. A role for cytosolic fumarate hydratase in urea cycle metabolism and renal neoplasia. Cell Rep. 2013;3(5):1440-8.
206. Tuboi S, Sato M, Ono H, Kobayashi K, Hiraga K. Mechanism of synthesis and localization of mitochondrial and cytosolic fumarases in rat liver. Adv Enzyme Regul. 1986;25:461-84.
207. Lee PJ, Jiang BH, Chin BY, Iyer NV, Alam J, Semenza GL, et al. Hypoxia-inducible factor-1 mediates transcriptional activation of the heme oxygenase-1 gene in response to hypoxia. J Biol Chem. 1997;272(9):5375-81.
208. Ahuja M, Ammal Kaidery N, Yang L, Calingasan N, Smirnova N, Gaisin A, et al. Distinct Nrf2 Signaling Mechanisms of Fumaric Acid Esters and Their Role in Neuroprotection against 1-Methyl-4-Phenyl-1,2,3,6-Tetrahydropyridine-Induced Experimental Parkinson's-Like Disease. J Neurosci. 2016;36(23):6332-51.

209. Nagy E, Rigby WF. Glyceraldehyde-3-phosphate dehydrogenase selectively binds AU-rich RNA in the NAD(+)-binding region (Rossmann fold). J Biol Chem. 1995;270(6):2755-63.
210. ElAzzouny M, Tom CT, Evans CR, Olson LL, Tanga MJ, Gallagher KA, et al. Dimethyl Itaconate Is Not Metabolized into Itaconate Intracellularly. J Biol Chem. 2017;292(12):4766-9.
211. Mullen AR, Wheaton WW, Jin ES, Chen PH, Sullivan LB, Cheng T, et al. Reductive carboxylation supports growth in tumour cells with defective mitochondria. Nature. 2011;481(7381):385-8.
212. Puchalska P, Huang X, Martin SE, Han X, Patti GJ, Crawford PA. Isotope Tracing Untargeted Metabolomics Reveals Macrophage Polarization-State-Specific Metabolic Coordination across Intracellular Compartments. iScience. 2018;9:298-313.
213. Meiser J, Kraemer L, Jaeger C, Madry H, Link A, Lepper PM, et al. Itaconic acid indicates cellular but not systemic immune system activation. Oncotarget. 2018;9(63):32098-107.
214. Michopoulos F, Karagianni N, Whalley NM, Firth MA, Nikolaou C, Wilson ID, et al. Targeted Metabolic Profiling of the Tg197 Mouse Model Reveals Itaconic Acid as a Marker of Rheumatoid Arthritis. J Proteome Res. 2016;15(12):4579-90.
215. Dominguez-Andres J, Novakovic B, Li Y, Scicluna BP, Gresnigt MS, Arts RJW, et al. The Itaconate Pathway Is a Central Regulatory Node Linking Innate Immune Tolerance and Trained Immunity. Cell Metab. 2019;29(1):211-20.e5.
216. Hartley R. The future of electrophiles in biology. 2018.
217. DeNicola GM, Chen PH, Mullarky E, Sudderth JA, Hu Z, Wu D, et al. NRF2 regulates serine biosynthesis in non-small cell lung cancer. Nat Genet. 2015;47(12):1475-81.
218. Harvey CJ, Thimmulappa RK, Singh A, Blake DJ, Ling G, Wakabayashi N, et al. Nrf2-regulated glutathione recycling independent of biosynthesis is critical for cell survival during oxidative stress. Free Radic Biol Med. 2009;46(4):443-53.
219. Dinkova-Kostova AT, Kostov RV, Canning P. Keap1, the cysteine-based mammalian intracellular sensor for electrophiles and oxidants. Arch Biochem Biophys. 2017;617:84-93.
220. Harris J, Hartman M, Roche C, Zeng SG, O'Shea A, Sharp FA, et al. Autophagy controls IL-1beta secretion by targeting pro-IL-1beta for degradation. J Biol Chem. 2011;286(11):9587-97.
221. Olagnier D, Lababidi RR, Hadj SB, Sze A, Liu Y, Naidu SD, et al. Activation of Nrf2 Signaling Augments Vesicular Stomatitis Virus Oncolysis via Autophagy-Driven Suppression of Antiviral Immunity. Mol Ther. 2017;25(8):1900-16.
222. Tang C, Wang X, Xie Y, Cai X, Yu N, Hu Y, et al. 4-Octyl Itaconate Activates Nrf2 Signaling to Inhibit Pro-Inflammatory Cytokine Production in Peripheral Blood Mononuclear Cells of Systemic Lupus Erythematosus Patients. Cell Physiol Biochem. 2018;51(2):979-90.
223. Olagnier D, Brandtoft AM, Gunderstofte C, Villadsen NL, Krapp C, Thielke AL, et al. Nrf2 negatively regulates STING indicating a link between antiviral sensing and metabolic reprogramming. Nat Commun. 2018;9(1):3506.
224. Tang C, Tan S, Zhang Y, Dong L, Xu Y. Activation of Keap1-Nrf2 signaling by 4-octyl itaconate protects human umbilical vein endothelial cells from high glucose. Biochem Biophys Res Commun. 2019;508(3):921-7.

225. Liu H, Feng Y, Xu M, Yang J, Wang Z, Di G. Four-octyl itaconate activates Keap1-Nrf2 signaling to protect neuronal cells from hydrogen peroxide. Cell Commun Signal. 2018;16(1):81.
226. Fan J, Hitosugi T, Chung TW, Xie J, Ge Q, Gu TL, et al. Tyrosine phosphorylation of lactate dehydrogenase A is important for NADH/NAD(+) redox homeostasis in cancer cells. Mol Cell Biol. 2011;31(24):4938-50.
227. Sakai A, Kusumoto A, Kiso Y, Furuya E. Itaconate reduces visceral fat by inhibiting fructose 2,6-bisphosphate synthesis in rat liver. Nutrition. 2004;20(11-12):997-1002.
228. Qin W, Qin K, Zhang Y, Jia W, Chen Y, Cheng B, et al. S-glycosylation-based cysteine profiling reveals regulation of glycolysis by itaconate. Nat Chem Biol. 2019.
229. Gardner PR, Raineri I, Epstein LB, White CW. Superoxide radical and iron modulate aconitase activity in mammalian cells. J Biol Chem. 1995;270(22):13399-405.
230. Chandel NS. Evolution of Mitochondria as Signaling Organelles. Cell Metab. 2015;22(2):204-6.
231. Martin WF. Symbiogenesis, gradualism, and mitochondrial energy in eukaryote evolution. Periodicum Biologorum. 2017;119(3):141-58.
232. Gray MW. Mitochondrial evolution. Cold Spring Harb Perspect Biol. 2012;4(9):a011403.
233. Martin W, Muller M. The hydrogen hypothesis for the first eukaryote. Nature. 1998;392(6671):37-41.
234. Brunk CF, Martin WF. Archaeal Histone Contributions to the Origin of Eukaryotes. Trends Microbiol. 2019;27(8):703-14.
235. Orgel LE, Crick FH. Selfish DNA: the ultimate parasite. Nature. 1980;284(5757):604-7.
236. Martin W, Koonin EV. Introns and the origin of nucleus-cytosol compartmentalization. Nature. 2006;440(7080):41-5.
237. Sandman K, Reeve JN. Archaeal histones and the origin of the histone fold. Curr Opin Microbiol. 2006;9(5):520-5.
238. Luger K, Dechassa ML, Tremethick DJ. New insights into nucleosome and chromatin structure: an ordered state or a disordered affair? Nat Rev Mol Cell Biol. 2012;13(7):436-47.
239. Grunstein M. Histone acetylation in chromatin structure and transcription. Nature. 1997;389(6649):349-52.
240. Strahl BD, Allis CD. The language of covalent histone modifications. Nature. 2000;403(6765):41-5.
241. Trub AG, Hirschey MD. Reactive Acyl-CoA Species Modify Proteins and Induce Carbon Stress. Trends Biochem Sci. 2018;43(5):369-79.
242. Eberharter A, Becker PB. Histone acetylation: a switch between repressive and permissive chromatin. Second in review series on chromatin dynamics. EMBO Rep. 2002;3(3):224-9.
243. Chantranupong L, Wolfson RL, Sabatini DM. Nutrient-sensing mechanisms across evolution. Cell. 2015;161(1):67-83.
244. Braakman R, Smith E. The compositional and evolutionary logic of metabolism. Phys Biol. 2013;10(1):011001.
245. Muchowska KB, Varma SJ, Moran J. Synthesis and breakdown of universal metabolic precursors promoted by iron. Nature. 2019;569(7754):104-7.

246. Salminen A, Kaarniranta K, Hiltunen M, Kauppinen A. Krebs cycle dysfunction shapes epigenetic landscape of chromatin: novel insights into mitochondrial regulation of aging process. Cell Signal. 2014;26(7):1598-603.
247. Wang Y, Guo YR, Liu K, Yin Z, Liu R, Xia Y, et al. KAT2A coupled with the alpha-KGDH complex acts as a histone H3 succinyltransferase. Nature. 2017;552(7684):273-7.
248. Jiang Y, Qian X, Shen J, Wang Y, Li X, Liu R, et al. Local generation of fumarate promotes DNA repair through inhibition of histone H3 demethylation. Nat Cell Biol. 2015;17(9):1158-68.
249. Johnson TI, Costa ASH, Ferguson AN, Frezza C. Fumarate hydratase loss promotes mitotic entry in the presence of DNA damage after ionising radiation. Cell Death Dis. 2018;9(9):913.
250. Cavalcanti JH, Esteves-Ferreira AA, Quinhones CG, Pereira-Lima IA, Nunes-Nesi A, Fernie AR, et al. Evolution and functional implications of the tricarboxylic acid cycle as revealed by phylogenetic analysis. Genome Biol Evol. 2014;6(10):2830-48.
251. Nagaraj R, Sharpley MS, Chi F, Braas D, Zhou Y, Kim R, et al. Nuclear Localization of Mitochondrial TCA Cycle Enzymes as a Critical Step in Mammalian Zygotic Genome Activation. Cell. 2017;168(1-2):210-23.e11.
252. Lee JK, Koo BS, Kim SY. Fumarate-mediated inhibition of erythrose reductase, a key enzyme for erythritol production by Torula corallina. Appl Environ Microbiol. 2002;68(9):4534-8.
253. Regev-Rudzki N, Battat E, Goldberg I, Pines O. Dual localization of fumarase is dependent on the integrity of the glyoxylate shunt. Mol Microbiol. 2009;72(2):297-306.
254. Araujo WL, Nunes-Nesi A, Fernie AR. Fumarate: Multiple functions of a simple metabolite. Phytochemistry. 2011;72(9):838-43.
255. Singer E, Silas YB, Ben-Yehuda S, Pines O. Bacterial fumarase and L-malic acid are evolutionary ancient components of the DNA damage response. Elife. 2017;6.
256. Kusano M, Tohge T, Fukushima A, Kobayashi M, Hayashi N, Otsuki H, et al. Metabolomics reveals comprehensive reprogramming involving two independent metabolic responses of Arabidopsis to UV-B light. Plant J. 2011;67(2):354-69.
257. La Camera S, Gouzerh G, Dhondt S, Hoffmann L, Fritig B, Legrand M, et al. Metabolic reprogramming in plant innate immunity: the contributions of phenylpropanoid and oxylipin pathways. Immunol Rev. 2004;198:267-84.
258. Nguyen TV, Alfaro AC, Young T, Green S, Zarate E, Merien F. Itaconic acid inhibits growth of a pathogenic marine Vibrio strain: A metabolomics approach. Sci Rep. 2019;9(1):5937.
259. Bonnarme P, Gillet B, Sepulchre AM, Role C, Beloeil JC, Ducrocq C. Itaconate biosynthesis in Aspergillus terreus. J Bacteriol. 1995;177(12):3573-8.
260. Al-Fakih AA, Almaqtri WQA.
261. Wang H, Fedorov AA, Fedorov EV, Hunt DM, Rodgers A, Douglas HL, et al. An essential bifunctional enzyme in Mycobacterium tuberculosis for itaconate dissimilation and leucine catabolism. Proc Natl Acad Sci U S A. 2019.
262. Hersch SJ, Navarre WW.
263. Wang A, Luan HH, Medzhitov R. An evolutionary perspective on immunometabolism. Science. 2019;363(6423).

264. Brommer JE. The evolution of fitness in life-history theory. Biol Rev Camb Philos Soc. 2000;75(3):377-404.
265. Liu L, Lu Y, Martinez J, Bi Y, Lian G, Wang T, et al. Proinflammatory signal suppresses proliferation and shifts macrophage metabolism from Myc-dependent to HIF1alpha-dependent. Proc Natl Acad Sci U S A. 2016;113(6):1564-9.
266. Mills EL, Pierce KA, Jedrychowski MP, Garrity R, Winther S, Vidoni S, et al. Accumulation of succinate controls activation of adipose tissue thermogenesis. Nature. 2018;560(7716):102-6.
267. Bhuniya D, Umrani D, Dave B, Salunke D, Kukreja G, Gundu J, et al. Discovery of a potent and selective small molecule hGPR91 antagonist. Bioorg Med Chem Lett. 2011;21(12):3596-602.
268. Geubelle P, Gilissen J, Dilly S, Poma L, Dupuis N, Laschet C, et al. Identification and pharmacological characterization of succinate receptor agonists. Br J Pharmacol. 2017;174(9):796-808.
269. Kim S, Hwang J, Xuan J, Jung YH, Cha HS, Kim KH. Global metabolite profiling of synovial fluid for the specific diagnosis of rheumatoid arthritis from other inflammatory arthritis. PLoS One. 2014;9(6):e97501.
270. Ooi M, Nishiumi S, Yoshie T, Shiomi Y, Kohashi M, Fukunaga K, et al. GC/MS-based profiling of amino acids and TCA cycle-related molecules in ulcerative colitis. Inflamm Res. 2011;60(9):831-40.
271. Chen WW, Freinkman E, Wang T, Birsoy K, Sabatini DM. Absolute Quantification of Matrix Metabolites Reveals the Dynamics of Mitochondrial Metabolism. Cell. 2016;166(5):1324-37.e11.
272. Jang C, Hui S, Zeng X, Cowan AJ, Wang L, Chen L, et al. Metabolite Exchange between Mammalian Organs Quantified in Pigs. Cell Metab. 2019.
273. Hensley CT, Faubert B, Yuan Q, Lev-Cohain N, Jin E, Kim J, et al. Metabolic Heterogeneity in Human Lung Tumors. Cell. 2016;164(4):681-94.

Chapter 7:

Appendix

7.1 – Conference abstracts

European Congress of Immunology (ECI), Amsterdam, NLD. September 2018

Invited talk

Title: Itaconate is an anti-inflammatory metabolite that activates Nrf2 via alkylation of KEAP1

Abstract:

The endogenous metabolite itaconate has recently emerged as a regulator of macrophage function, but its precise mechanism of action remains poorly understood. Here we show that itaconate is required for the activation of the anti-inflammatory transcription factor Nrf2 (also known as NFE2L2) by lipopolysaccharide in macrophages. We find that itaconate directly modifies proteins via alkylation of cysteine residues, a novel post-translational modification we've termed 2,3-dicarboxypropylation. We describe the use of a new cell-permeable itaconate derivative, 4-octyl itaconate (4-OI), which alkylates the key redox-sensing cysteine residues 151, 257, 288, 273 and 297 on the protein KEAP1, enabling Nrf2 to increase the expression of downstream genes with anti-oxidant and anti-inflammatory capacities. The activation of Nrf2 is required for the anti-inflammatory action of 4-OI, while there is a loss of Nrf2-stabilisation and enhanced cytokine production in *Irg1-/-* macrophages, which can no longer produce itaconate. Furthermore, 4-OI is protective against lipopolysaccharide-induced lethality *in vivo* and decreases inflammatory cytokine production. Our findings demonstrate that itaconate is a crucial anti-inflammatory metabolite that acts via Nrf2 to limit inflammation.

Cell Symposia – Metabolites as signalling molecules, Seattle, US. December 2018

Poster presentation

Title: Itaconate is an anti-inflammatory metabolite that activates Nrf2 via alkylation of KEAP1

Abstract:

The endogenous metabolite itaconate has recently emerged as a regulator of macrophage function, but its precise mechanism of action remains poorly understood. Here we show that itaconate is required for the activation of the anti-inflammatory transcription factor Nrf2 (also known as NFE2L2) by lipopolysaccharide in macrophages. We find that itaconate directly modifies proteins via alkylation of cysteine residues, a novel post-translational modification we've termed 2,3-dicarboxypropylation. We describe the use of a new cell-permeable itaconate derivative, 4-octyl itaconate (4-OI), which alkylates the key redox-sensing cysteine residues 151, 257, 288, 273 and 297 on the protein KEAP1, enabling Nrf2 to increase the expression of downstream genes with anti-oxidant and anti-inflammatory capacities. The activation of Nrf2 is required for the anti-inflammatory action of 4-OI, while there is a loss of Nrf2-stabilisation and enhanced cytokine production in *Irg1-/-* macrophages, which can no longer produce itaconate. Furthermore, 4-OI is protective against lipopolysaccharide-induced lethality *in vivo* and decreases inflammatory cytokine production. Our findings demonstrate that itaconate is a crucial anti-inflammatory metabolite that acts via Nrf2 to limit inflammation.

7.2 – Record of publications

First author publications:

1. Ryan D, Murphy M, Frezza C, Prag H, Chouchani E, O'Neill L et al. Coupling Krebs cycle metabolites to signalling in immunity and cancer. Nature Metabolism. 2018;1(1):16-33.
2. Mills E*, Ryan D*, Prag H, Dikovskaya D, Menon D, Zaslona Z et al. Itaconate is an anti-inflammatory metabolite that activates Nrf2 via alkylation of KEAP1. Nature. 2018;556(7699):113-117.
   *Joint-first
3. Ryan D, O'Neill L. Krebs cycle rewired for macrophage and dendritic cell effector functions. FEBS Letters. 2017;591(19):2992-3006.

Other publications:

4. Mills E*, Kelly B*, Logan A, Costa A, Varma M, Bryant C et al. Succinate Dehydrogenase Supports Metabolic Repurposing of Mitochondria to Drive Inflammatory Macrophages. Cell. 2016;167(2):457-470.e13.
   *Joint-first
5. Hughes M*, Lavrencic P*, Coll R, Ve T, Ryan D, Williams N et al. Solution structure of the TLR adaptor MAL/TIRAP reveals an intact BB loop and supports MAL Cys91 glutathionylation for signaling. Proceedings of the National Academy of Sciences. 2017;114(32):E6480-E6489.
   *Joint-first
6. Early J, Menon D, Wyse C, Cervantes-Silva M, Zaslona Z, Carroll R et al. Circadian clock protein BMAL1 regulates IL-1β in macrophages via NRF2. Proceedings of the National Academy of Sciences. 2018;115(36):E8460-E8468.
7. Olagnier D, Brandtoft A, Gunderstofte C, Villadsen N, Krapp C, Thielke A et al. Nrf2 negatively regulates STING indicating a link between antiviral sensing and metabolic reprogramming. Nature Communications. 2018;9(1).
8. Baardman J, Verberk S, Prange K, van Weeghel M, van der Velden S, Ryan D et al. A Defective Pentose Phosphate Pathway Reduces Inflammatory Macrophage Responses during Hypercholesterolemia. Cell Reports. 2018;25(8):2044-2052.e5.

LETTER

doi:10.1038/nature25986

Itaconate is an anti-inflammatory metabolite that activates Nrf2 via alkylation of KEAP1

Evanna L. Mills[1,2,3,4]*, Dylan G. Ryan[1]*, Hiran A. Prag[5], Dina Dikovskaya[6], Deepthi Menon[1], Zbigniew Zaslona[1], Mark P. Jedrychowski[2,3], Ana S. H. Costa[7], Maureen Higgins[6], Emily Hams[8], John Szpyt[3], Marah C. Runtsch[1], Martin S. King[5], Joanna F. McGouran[9], Roman Fischer[10], Benedikt M. Kessler[10], Anne F. McGettrick[1], Mark M. Hughes[1], Richard G. Carroll[1,4], Lee M. Booty[4,5], Elena V. Knatko[6], Paul J. Meakin[11], Michael L. J. Ashford[11], Louise K. Modis[4], Gino Brunori[12], Daniel C. Sévin[13], Padraic G. Fallon[8], Stuart T. Caldwell[14], Edmund R. S. Kunji[5], Edward T. Chouchani[2,3], Christian Frezza[7], Albena T. Dinkova-Kostova[6,15], Richard C. Hartley[14], Michael P. Murphy[5]§ & Luke A. O'Neill[1,4]§

The endogenous metabolite itaconate has recently emerged as a regulator of macrophage function, but its precise mechanism of action remains poorly understood[1–3]. Here we show that itaconate is required for the activation of the anti-inflammatory transcription factor Nrf2 (also known as NFE2L2) by lipopolysaccharide in mouse and human macrophages. We find that itaconate directly modifies proteins via alkylation of cysteine residues. Itaconate alkylates cysteine residues 151, 257, 288, 273 and 297 on the protein KEAP1, enabling Nrf2 to increase the expression of downstream genes with anti-oxidant and anti-inflammatory capacities. The activation of Nrf2 is required for the anti-inflammatory action of itaconate. We describe the use of a new cell-permeable itaconate derivative, 4-octyl itaconate, which is protective against lipopolysaccharide-induced lethality *in vivo* and decreases cytokine production. We show that type I interferons boost the expression of *Irg1* (also known as *Acod1*) and itaconate production. Furthermore, we find that itaconate production limits the type I interferon response, indicating a negative feedback loop that involves interferons and itaconate. Our findings demonstrate that itaconate is a crucial anti-inflammatory metabolite that acts via Nrf2 to limit inflammation and modulate type I interferons.

Macrophages have a key role in innate immunity. They respond rapidly to pathogens and subsequently promote an anti-inflammatory phenotype to limit damage and promote tissue repair. The factors driving these changes are incompletely understood. Itaconate, a metabolite synthesized by the enzyme encoded by *Irg1*[1], is increased in lipopolysaccharide (LPS)-activated macrophages[2] and has been suggested to limit inflammation by inhibiting succinate dehydrogenase (SDH), a crucial pro-inflammatory regulator[4]; however, the details remain unclear.

Itaconate was the most abundant metabolite in LPS-treated human macrophages (Fig. 1a) and reached 5 mM in mouse bone marrow-derived macrophages (BMDMs) after LPS stimulation (Fig. 1b, c). Itaconate can disrupt SDH activity, but is less potent than the classic SDH inhibitor malonate (Extended Data Fig. 1), suggesting that it may exert its anti-inflammatory effects via additional mechanisms.

Itaconate contains an electrophilic α,β-unsaturated carboxylic acid that could potentially alkylate protein cysteine residues by a Michael addition to form a 2,3-dicarboxypropyl adduct. An attractive candidate protein that undergoes cysteine alkylation is KEAP1, a central player in the anti-oxidant response (Fig. 1d). KEAP1 normally associates with and promotes the degradation of Nrf2, but alkylation of crucial KEAP1 cysteine residues allows newly synthesized Nrf2 to accumulate, migrate to the nucleus and activate a transcriptional anti-oxidant and anti-inflammatory program[5]. We therefore examined KEAP1 and Nrf2 as targets of itaconate.

The cell-permeable itaconate derivative dimethyl itaconate (DMI)[3] boosted levels of Nrf2 protein, expression of downstream target genes, including *Hmox1*, and glutathione (GSH) (Extended Data Fig. 2a–d). However, the lack of a negative charge on the conjugated ester group in DMI increases its reactivity towards Michael addition, making it a far superior Nrf2 activator than itaconate akin to the potent Nrf2 activator dimethylfumarate (DMF)[6]. DMI is rapidly degraded within cells without releasing itaconate[7], hence is unlikely to mimic endogenous itaconate. Even so, these data indicate that Nrf2 activation is anti-inflammatory[8] (Extended Data Fig. 2e, f).

To overcome the limitations of DMI, we synthesized 4-octyl itaconate (OI), a cell-permeable itaconate derivative (Extended Data Fig. 3a). Itaconate and OI had similar thiol reactivity that was far lower than that of DMI (Extended Data Fig. 3b, c, f), making it a suitable cell-permeable itaconate surrogate. Furthermore, OI was hydrolysed to itaconate by esterases in mouse myoblast C2C12 cells (Extended Data Fig. 3d) and LPS-activated mouse macrophages (Extended Data Fig. 3e). OI boosted Nrf2 levels (Fig. 1e, compare lane 5 to lane 1) and enhanced LPS-induced Nrf2 stabilization (Fig. 1e, compare lane 6 to lane 2), and increased the expression of downstream target genes[9], including the anti-inflammatory protein HMOX1[10] (Fig. 1f, g). We used a quantitative NAD(P)H:quinone oxidoreductase-1 (NQO1) inducer bioassay[11,12], to assess the potency of Nrf2 activation by the CD value (concentration required to double the specific enzyme activity) for NQO1, the prototypical Nrf2 target gene. OI (CD value of 2 μM), was more potent than the clinically used Nrf2 activator DMF (CD value of 6.5 μM) (Fig. 1h, Extended Data Fig. 3f). OI stimulated synthesis of the key anti-oxidant GSH (Extended Data Fig. 3g–i). OI also boosted canonical activation of Nrf2 by the pro-oxidant hydrogen peroxide (H_2O_2) (Extended Data Fig. 3j, k). Importantly, the related octyl esters 4-octyl 2-methylsuccinate and octyl succinate, which are not Michael acceptors, had no effect on Nrf2 activity, confirming the requirement

[1]School of Biochemistry and Immunology, Trinity Biomedical Sciences Institute, Trinity College Dublin, Dublin, Ireland. [2]Department of Cancer Biology, Dana-Farber Cancer Institute, Harvard Medical School, Boston, Massachusetts 02115, USA. [3]Department of Cell Biology, Harvard Medical School, Boston, Massachusetts 02115, USA. [4]GlaxoSmithKline, Gunnelswood Road, Stevenage, Hertfordshire, UK. [5]MRC Mitochondrial Biology Unit, University of Cambridge, Cambridge CB2 0XY, UK. [6]Jacqui Wood Cancer Centre, Division of Cancer Research, School of Medicine, University of Dundee, Dundee DD1 9SY, UK. [7]MRC Cancer Unit, University of Cambridge, Hutchison/MRC Research Centre, Box 197, Cambridge Biomedical Campus, Cambridge CB2 0XZ, UK. [8]School of Medicine, Trinity Biomedical Sciences Institute, Trinity College Dublin, Dublin, Ireland. [9]School of Chemistry, Trinity Biomedical Sciences Institute, Trinity College Dublin, Dublin, Ireland. [10]Nuffield Department of Medicine, Target Discovery Institute, University of Oxford, Oxford OX3 7FZ, UK. [11]Division of Molecular and Clinical Medicine, School of Medicine, University of Dundee, Dundee DD1 9SY, UK. [12]GlaxoSmithKline, Park Road, Ware, Hertfordshire, UK. [13]Cellzome, GlaxoSmithKline R&D, Heidelberg, Germany. [14]WestCHEM School of Chemistry, University of Glasgow, Glasgow G12 8QQ, UK. [15]Department of Pharmacology and Molecular Sciences, Johns Hopkins University School of Medicine, Baltimore, Maryland 21205, USA.
*These authors contributed equally to this work.
§These authors jointly supervised this work.

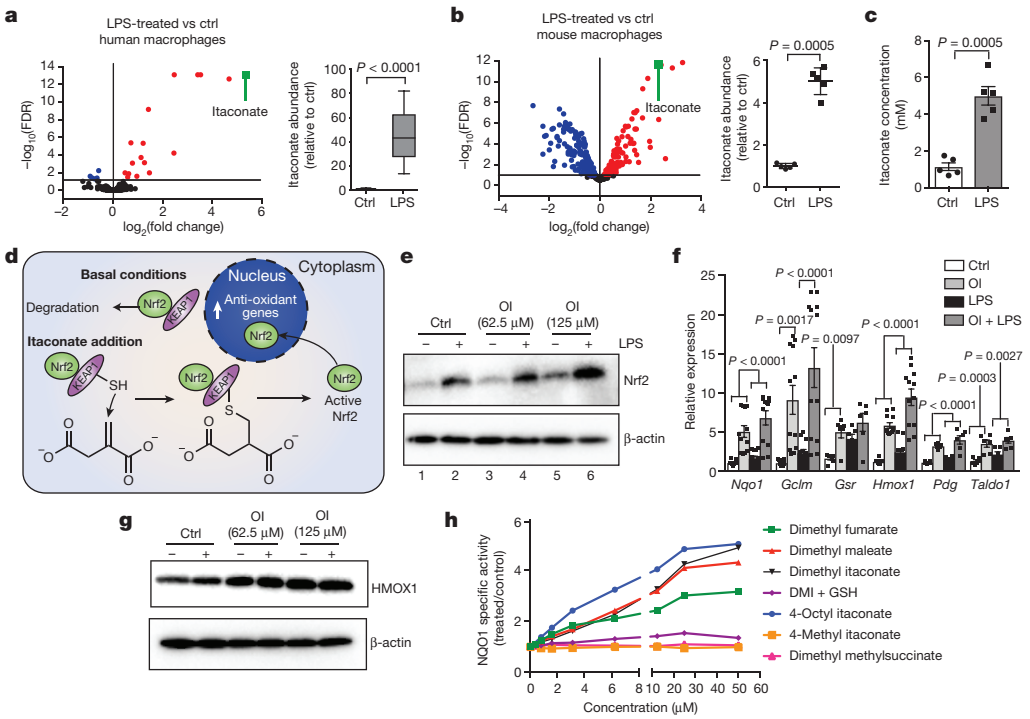

Figure 1 | Itaconate activates Nrf2. **a**–**c**, Metabolite levels and itaconate abundance in control (ctrl) versus LPS-induced (**a**, $n = 12$, 4 h; **b**, **c**, $n = 5$, 24 h) human (**a**) and mouse (**b**, **c**) macrophages. Red and blue dots represent metabolites significantly up- and downregulated by LPS, respectively. FDR, false discovery rate. **d**, Reactivity of itaconate with KEAP1 thiol group. **e**, **g**, LPS-induced Nrf2 (**e**, 24 h) and HMOX1 (**g**, 6 h) after treatment with OI as indicated. **f**, Nrf2 target gene expression in mouse macrophages with or without LPS (6 h) and OI (*Nqo1*, *Gclm*, *Hmox1*, $n = 12$; *Gsr*, *Pgd*, *Taldo1*, $n = 6$). **h**, NQO1 activity in mouse Hepa1c1c7 cells treated as indicated (48 h, $n = 8$). Data are mean ± s.e.m. *P* values calculated using one-way or two-tailed Student's *t*-test for paired comparisons. Blots are representative of three independent experiments. In the box plots, line shows mean. For gel source data, see Supplementary Fig. 1.

for the itaconate moiety (Extended Data Fig. 3l). Dimethyl malonate, a potent SDH inhibitor[4], did not activate Nrf2 (Extended Data Fig. 3m), confirming that Nrf2 activation by OI is independent of SDH inhibition.

Itaconate is generated by IRG1 in the mitochondrial matrix and must cross the mitochondrial inner membrane to act on Nrf2 in the cytosol. Itaconate is structurally similar to malate, which is transported across the mitochondrial inner membrane by the dicarboxylate, citrate and oxoglutarate carriers. All three carriers transported itaconate, whereas other tested carriers could not (Fig. 2a and Extended Data Fig. 4), suggesting that LPS-induced itaconate is generated in the mitochondrial matrix and is then exported to the cytosol to activate Nrf2.

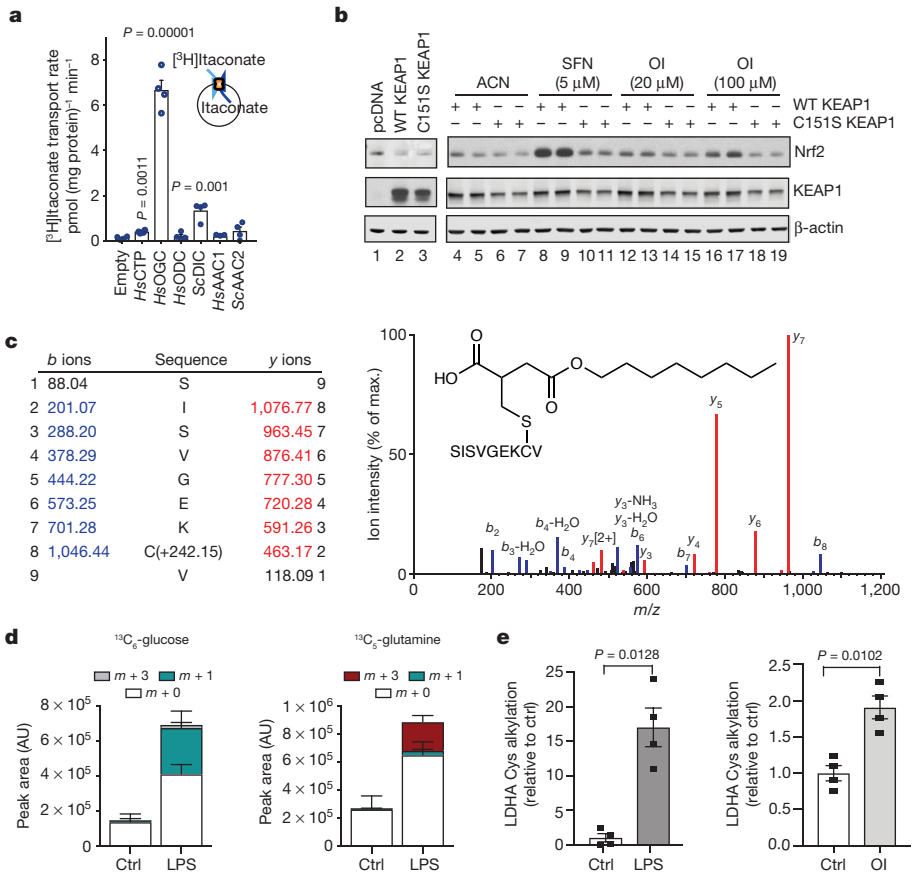

Figure 2 | Itaconate alkylates cysteines. **a**, Itaconate transport by the indicated carriers ($n = 4$). *Hs*AAC1, *Homo sapiens* ADP/ATP carrier; *Hs*CTP, *H. sapiens* citrate carrier; *Hs*ODC, *H. sapiens* oxodicarboxylate carrier; *Hs*OGC, *H. sapiens* 2-oxoglutarate carrier; *Sc*AAC2, *Saccharomyces cerevisiae* ADP/ATP carrier; *Sc*DIC, *S. cerevisiae* dicarboxylate carrier. **b**, Nrf2 and KEAP1 protein after co-transfection with Nrf2–V5, and the wild-type (WT) or Cys151Ser mutant KEAP1. **c**, Tandem mass spectrometry spectrum of Cys151-containing KEAP1 peptide after OI treatment. **d**, Metabolite ($^{13}C_6$-glucose (left), $^{13}C_5$-glutamine (right)) tracing to itaconate-cysteine adduct with or without LPS (24 h, $n = 5$). AU, arbitrary units. **e**, LDHA Cys84 alkylation plus LPS (24 h) or OI (250 μM, 4 h) ($n = 4$). Data are mean ± s.e.m. (in **d**, **e**) or s.d. (in **a**). *P* values calculated using one-way ANOVA for multiple comparisons or two-tailed Student's *t*-test for paired comparisons. Blots are representative of three independent experiments. For gel source data, see Supplementary Fig. 1.

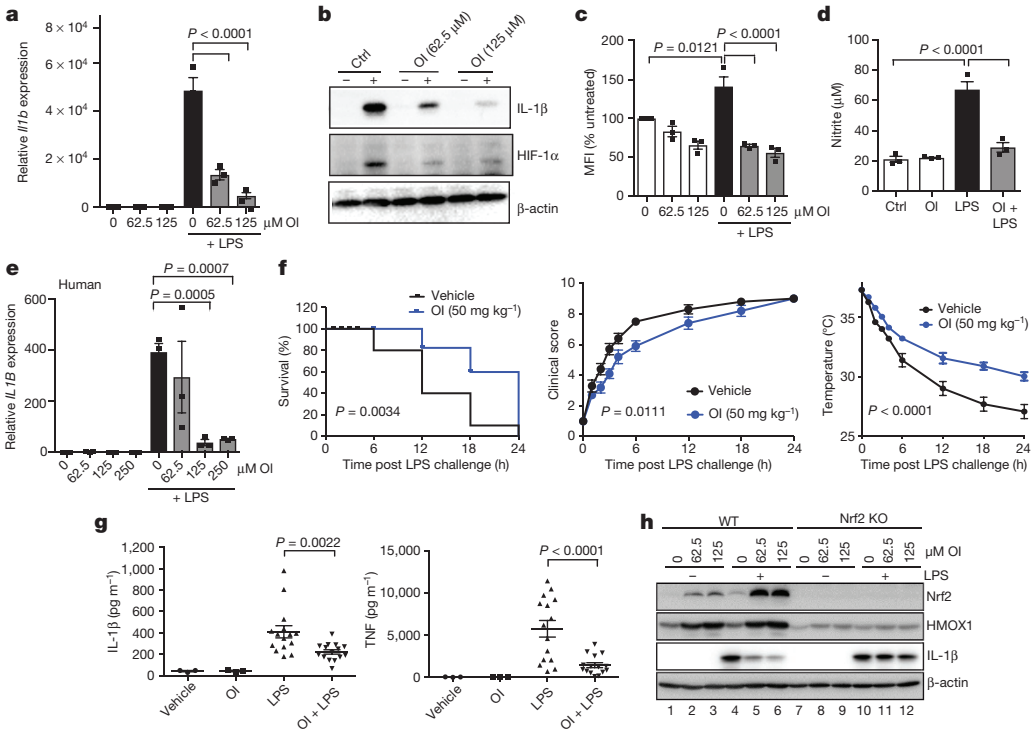

Figure 3 | OI limits IL-1β in an Nrf2-dependent manner and protects against LPS lethality. a–d, LPS (24 h) induced *Il1b* mRNA (**a**, $n = 3$), IL-1β and HIF-1α protein (**b**), ROS production (**c**, $n = 3$; measured as the percentage change in mean fluorescent intensity (MFI) relative to untreated control) and nitrite production (**d**, $n = 3$) ± OI. **e**, *IL1B* mRNA in human PBMCs treated as in **a–d** ($n = 3$). **f**, Survival (left), clinical score (middle) and body temperature (right) measurements in mice ($n = 10$) injected intraperitoneally with OI (50 mg kg^{-1}, 2 h) and LPS (15 mg kg^{-1}). **g**, Serum IL-1β and TNF levels from mice injected intraperitoneally with OI (50 mg kg^{-1}, 2 h) and/or LPS (2.5 mg kg^{-1}, 2 h, $n = 3$ vehicle, OI; $n = 15$ LPS, OI plus LPS). **h**, Nrf2, HMOX1 and IL-1β protein in wild-type and Nrf2 knockout (KO) mouse BMDMs treated with LPS (6 h) and OI as indicated. Data are mean ± s.e.m. *P* values calculated using one-way ANOVA. Blots are representative of three independent experiments. For gel source data, see Supplementary Fig. 1.

Our hypothesis is that itaconate activates Nrf2 by alkylation of KEAP1 cysteine residue(s)[13–15], similar to the modification of cysteines by fumarate (Extended Data Fig. 5a). Cysteine 151 (Cys151) is a principal sensor on KEAP1 for sulforaphane[16] and DMF[17]. OI stabilized V5-tagged Nrf2 (Nrf2–V5) in COS1 cells co-expressing wild-type KEAP1 but not a Cys151Ser mutant, similarly to sulforaphane (Fig. 2b, compare lanes 16 and 17 to lanes 18 and 19). To analyse KEAP1 alkylation directly, we overexpressed Myc-DDK-tagged KEAP1 in human HEK293T cells and treated the cells with OI. Tandem mass spectrometry of immunoprecipitated KEAP1 revealed that for the KEAP1 peptide (144–152), which contains Cys 151, OI treatment increased its mass by 242.15 Da, consistent with alkylation by OI (Fig. 2c). OI also modified other known KEAP1 regulatory cysteine residues (Cys257, Cys288 and Cys273) (Extended Data Fig. 5b–d, Extended Data Table 1a). Furthermore, itaconate-cysteine adducts, derived in part from glucose and glutamine (Fig. 2d and Extended Data Fig. 6), were detected in LPS-treated macrophages. These data suggest that itaconate activates Nrf2 by alkylating KEAP1 cysteine residues. We further explored cysteine alkylation induced by itaconate using an untargeted mass spectrometry approach in macrophages treated with OI, or with LPS, which increases itaconate levels. We identified several proteins that contain alkylated cysteine residues (Extended Data Table 1b, c). Notably LDHA, which has a crucial role in the regulation of glycolysis, was alkylated in OI- and LPS-treated macrophages (Fig. 2e and Extended Data Fig. 5e, f). This modification, here defined as 2,3-dicarboxypropylation, generates a stable thioether. As there are no known pathways for the removal of such post-translational modifications, modified proteins are probably degraded, suggesting that this modification will have profound effects on macrophage function.

We next assessed whether itaconate activation of Nrf2 could be anti-inflammatory. OI, used at concentrations that did not affect cellular viability, decreased LPS-induced *Il1b* mRNA, pro-IL-1β, HIF-1α and IL-10 protein levels, and decreased the extracellular acidification rate, yet had no effect on NF-κB activity or TNF (also known as TNFα) levels (Fig. 3a, b and Extended Data Fig. 7a–f). OI also decreased *Il1b* mRNA in BMDMs treated with the TLR2 and TLR3 ligands, Pam3CSK and polyinosinic:polycytidylic acid (poly(I:C)), respectively (Extended Data Fig. 7g). Levels of LPS-induced reactive oxygen species (ROS), nitrite and inducible nitric oxide synthase (iNOS) were limited by OI (Fig. 3c, d and Extended Data Fig. 7h, i). These effects are likely to be a consequence of ROS detoxification after Nrf2 induction by OI. IL-1β and TNF were decreased by OI in human peripheral blood mononuclear cell (PBMCs) (Fig. 3e, Extended Data Fig. 7j). OI also counteracted the pro-inflammatory response to LPS *in vivo*. OI, which activated Nrf2 (Extended Data Fig. 7k), prolonged survival, decreased clinical score and improved body temperature regulation, and decreased IL-1β and TNF levels but not IL-10 in an LPS model of sepsis (Fig. 3f, g and Extended Data Fig. 7l).

OI induction of HMOX1 was blocked in Nrf2-deficient macrophages (Fig. 3h (compare lanes 2 and 3 to lanes 8 and 9) and Extended Data Fig. 8a, d) or when Nrf2 was silenced (Extended Data Fig. 8a, d (compare lanes 7 and 8 to lanes 11 and 12)). Without Nrf2, the decrease in LPS-induced IL-1β with OI was significantly impaired (Fig. 3h (compare lane 6 to lane 12), Extended Data Fig. 8b–f (compare lanes 6 and 8 to 10 and 12 in c, d)). Furthermore, two Nrf2 activators, diethyl maleate and 15-deoxy-Δ12,14-prostaglandin J2 decreased LPS-induced IL-1β, IL-10, nitric oxide synthase (NOS2) and nitrite (Extended Data Fig. 8g–k). Thus, itaconate activates an anti-inflammatory program through Nrf2.

We next investigated how switching from a pro- to an anti-inflammatory state might affect itaconate production from aconitate by IRG1.

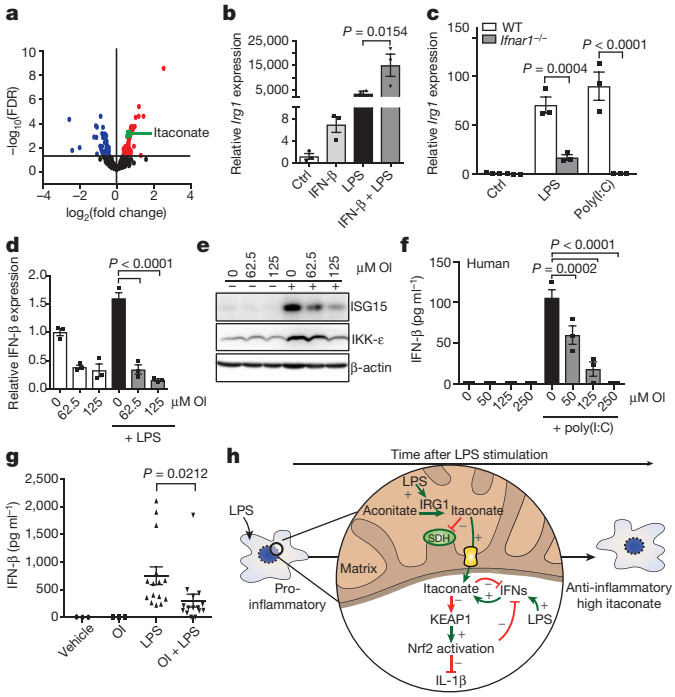

Figure 4 | A feedback loop exists between itaconate and IFN-β. **a**, Metabolite levels in control versus IFN-β-treated (1,000 U ml^{-1}; 27 h; $n = 5$) mouse macrophages. **b**, LPS-induced (24 h) *Irg1* expression ± IFN-β (1,000 U ml^{-1}; $n = 3$). **c**, *Irg1* expression in wild-type and IFN receptor-deficient (*Ifnar1*$^{-/-}$) BMDMs plus LPS or poly(I:C) (40 μg ml^{-1}) for 24 h ($n = 3$). **d**, IFN-β ($n = 3$) expression plus LPS (24 h) and OI as indicated. **e**, ISG15 and IKK-ε expression after treatment with LPS (24 h) and OI. **f**, IFN-β protein expression in PBMCs treated with poly(I:C) (20 μg ml^{-1}; 24 h) and OI ($n = 3$) as indicated. **g**, Serum IFN-β levels from mice injected intraperitoneally with OI (50 mg kg^{-1}, 2 h) with or without LPS (2.5 mg kg^{-1}; 2 h) ($n = 3$ vehicle, OI; $n = 15$ LPS, OI and LPS). **h**, The anti-inflammatory role of itaconate. Data are mean ± s.e.m. *P* values calculated using one-way ANOVA. Blots are representative of three independent experiments. Data in **f** are representative from one of two human donors. For gel source data, see Supplementary Fig. 1.

By modelling gene networks that control *Irg1* expression, the IFN response factor IRF1 was identified as a regulator[18]. We show here that itaconate levels are increased after IFN-β treatment (Fig. 4a), in agreement with others[19]. Levels of citrate and aconitate, the substrate for Irg1, were reduced by IFN-β as was the downstream metabolite α-ketoglutarate (Extended Data Fig. 9a). These data are consistent with an increase in aconitate conversion to itaconate rather than α-ketoglutarate. IFN-β enhanced basal and LPS-induced *Irg1* expression (Fig. 4b). LPS- and poly(I:C)-induced *Irg1* expression in BMDMs lacking type I IFN receptor was decreased (Fig. 4c), indicating that autocrine IFN facilitates IRG1 induction. OI limited the IFN response, decreasing the expression of IFN-β, IKK-ε, ISG20 and ISG15 protein, IFN-β production in poly(I:C)-treated PBMCs and LPS-induced IFN-β production *in vivo* (Fig. 4d–g and Extended Data Fig. 9b, c). IFN-β enhanced both the mRNA and protein expression of IL-10, with or without the addition LPS (Extended Data Fig. 9d), suggesting that the decrease in IL-10 after OI treatment is due to reduced type I IFN production[20]. Nrf2 knockout or knockdown attenuated the reduction of ISG20 expression by OI, whereas the Nrf2 activators diethyl maleate and 15-deoxy-Δ12,14-prostaglandin J2 reduced ISG20 expression (Extended Data Fig. 9e–g). This agrees with increased expression of IRF3-regulated genes in LPS-treated Nrf2-deficient mice[21].

These data suggest the operation of a negative-feedback loop: itaconate is generated in response to LPS, in part through type I IFNs, and promotes an anti-inflammatory program by Nrf2 activation (Fig. 4h), as well as SDH inhibition[3,22]. This limits further inflammatory gene expression and its own production by downregulating the IFN response. This helps to explain why Nrf2-deficient mice are more sensitive to septic shock[21], even though under certain circumstances these mice are protected from inflammation[23]. Our identification of itaconate as an inflammatory regulator, that directly modifies proteins through a newly identified post-translational modification, unveils therapeutic opportunities to use itaconate or OI to treat inflammatory diseases[24]. Furthermore, an intriguing link was recently made[25] from itaconate to vitamin B_{12}, and this warrants further investigation in the context of inflammation and immunity. Further understanding the role of itaconate as an anti-inflammatory metabolite and regulator of type I IFNs is likely to yield new insights into the pathogenesis of inflammatory diseases.

Online Content Methods, along with any additional Extended Data display items and Source Data, are available in the online version of the paper; references unique to these sections appear only in the online paper.

Received 28 July 2017; accepted 9 February 2018.
Published online 28 March 2018.

1. Michelucci, A. *et al.* Immune-responsive gene 1 protein links metabolism to immunity by catalyzing itaconic acid production. *Proc. Natl Acad. Sci. USA* **110,** 7820–7825 (2013).
2. Strelko, C. L. *et al.* Itaconic acid is a mammalian metabolite induced during macrophage activation. *J. Am. Chem. Soc.* **133,** 16386–16389 (2011).
3. Lampropoulou, V. *et al.* Itaconate links inhibition of succinate dehydrogenase with macrophage metabolic remodeling and regulation of inflammation. *Cell Metab.* **24,** 158–166 (2016).
4. Mills, E. L. *et al.* Succinate dehydrogenase supports metabolic repurposing of mitochondria to drive inflammatory macrophages. *Cell* **167,** 457–470 (2016).
5. Hayes, J. D. & Dinkova-Kostova, A. T. The Nrf2 regulatory network provides an interface between redox and intermediary metabolism. *Trends Biochem. Sci.* **39,** 199–218 (2014).
6. Brennan, M. S. *et al.* Dimethyl fumarate and monoethyl fumarate exhibit differential effects on KEAP1, NRF2 activation, and glutathione depletion *in vitro*. *PLoS One* **10,** e0120254 (2015).
7. ElAzzouny, M. *et al.* Dimethyl itaconate is not metabolized into itaconate intracellularly. *J. Biol. Chem.* **292,** 4766–4769 (2017).
8. Kobayashi, E. H. *et al.* Nrf2 suppresses macrophage inflammatory response by blocking proinflammatory cytokine transcription. *Nat. Commun.* **7,** 11624 (2016).
9. Lee, J. M., Calkins, M. J., Chan, K., Kan, Y. W. & Johnson, J. A. Identification of the NF-E2-related factor-2-dependent genes conferring protection against oxidative stress in primary cortical astrocytes using oligonucleotide microarray analysis. *J. Biol. Chem.* **278,** 12029–12038 (2003).
10. Piantadosi, C. A. *et al.* Heme oxygenase-1 couples activation of mitochondrial biogenesis to anti-inflammatory cytokine expression. *J. Biol. Chem.* **286,** 16374–16385 (2011).
11. Prochaska, H. J. & Santamaria, A. B. Direct measurement of NAD(P)H:quinone reductase from cells cultured in microtiter wells: a screening assay for anticarcinogenic enzyme inducers. *Anal. Biochem.* **169,** 328–336 (1988).
12. Fahey, J. W., Dinkova-Kostova, A. T., Stephenson, K. K. & Talalay, P. The "Prochaska" microtiter plate bioassay for inducers of NQO1. *Methods Enzymol.* **382,** 243–258 (2004).
13. Dinkova-Kostova, A. T. *et al.* Direct evidence that sulfhydryl groups of Keap1 are the sensors regulating induction of phase 2 enzymes that protect against carcinogens and oxidants. *Proc. Natl Acad. Sci. USA* **99,** 11908–11913 (2002).
14. McMahon, M., Lamont, D. J., Beattie, K. A. & Hayes, J. D. Keap1 perceives stress via three sensors for the endogenous signaling molecules nitric oxide, zinc, and alkenals. *Proc. Natl Acad. Sci. USA* **107,** 18838–18843 (2010).
15. Dinkova-Kostova, A. T., Kostov, R. V. & Canning, P. Keap1, the cysteine-based mammalian intracellular sensor for electrophiles and oxidants. *Arch. Biochem. Biophys.* **617,** 84–93 (2017).
16. Zhang, D. D. & Hannink, M. Distinct cysteine residues in Keap1 are required for Keap1-dependent ubiquitination of Nrf2 and for stabilization of Nrf2 by chemopreventive agents and oxidative stress. *Mol. Cell. Biol.* **23,** 8137–8151 (2003).
17. Linker, R. A. *et al.* Fumaric acid esters exert neuroprotective effects in neuroinflammation via activation of the Nrf2 antioxidant pathway. *Brain* **134,** 678–692 (2011).
18. Tallam, A. *et al.* Gene regulatory network inference of immunoresponsive gene 1 (*IRG1*) identifies interferon regulatory factor 1 (*IRF1*) as its transcriptional regulator in mammalian macrophages. *PLoS One* **11,** e0149050 (2016).
19. Naujoks, J. *et al.* IFNs modify the proteome of legionella-containing vacuoles and restrict infection via IRG1-derived itaconic acid. *PLoS Pathog.* **12,** e1005408 (2016).
20. Guarda, G. *et al.* Type I interferon inhibits interleukin-1 production and inflammasome activation. *Immunity* **34,** 213–223 (2011).

21. Thimmulappa, R. K. *et al.* Nrf2 is a critical regulator of the innate immune response and survival during experimental sepsis. *J. Clin. Invest.* **116,** 984–995 (2006).
22. Cordes, T. *et al.* Immunoresponsive gene 1 and itaconate inhibit succinate dehydrogenase to modulate intracellular succinate levels. *J. Biol. Chem.* **291,** 14274–14284 (2016).
23. Freigang, S. *et al.* Nrf2 is essential for cholesterol crystal-induced inflammasome activation and exacerbation of atherosclerosis. *Eur. J. Immunol.* **41,** 2040–2051 (2011).
24. Dinarello, C. A. Interleukin-1 in the pathogenesis and treatment of inflammatory diseases. *Blood* **117,** 3720–3732 (2011).
25. Shen, H. *et al.* The human knockout gene CLYBL connects itaconate to vitamin B_{12}. *Cell* **171,** 771–782 (2017).

Supplementary Information is available in the online version of the paper.

Acknowledgements We thank M. McMahon and J. D. Hayes for plasmids, and Cancer Research UK (C20953/A18644) and the BBSRC (BB/L01923X/1) for financial support for ATDK. This work was supported by a Wellcome Trust Investigator award to R.C.H. (110158/Z/15/Z), a grant to M.P.M. from the Medical Research Council UK (MC_U105663142), a Wellcome Trust Investigator award to MPM (110159/Z/15/Z), and a grant to E.R.S.K. and M.S.K. from the Medical Research Council UK (MC_U105663139). B.M.K. and R.F. are supported by the Kennedy Trust Fund. We acknowledge Metabolon for their assistance with the metabolic work and analysis. The O'Neill laboratory acknowledges the following grant support: European Research Council (ECFP7-ERC-MICROINNATE), Science Foundation Ireland Investigator Award (SFI 12/IA/1531), GlaxoSmithKline Visiting Scientist Programme and The Wellcome Trust (oneill-wellcometrust-metabolic, grant number 205455). E.T.C. is supported by the Claudia Adams Barr Program.

Author Contributions E.L.M. and D.G.R. designed and performed experiments and analysed the data. E.L.M. wrote the manuscript with assistance from all other authors. D.M., M.M.H., M.C.R. and A.F.M. performed *in vitro* experiments using OI. R.G.C., D.C.S., A.S.H.C. and C.F. assisted with the metabolomics analysis. Z.Z., P.G.F. and E.H. assisted with the *in vivo* mouse LPS trials. S.T.C. and R.C.H. were responsible for the design and synthesis of octyl esters. H.A.P., E.R.S.K., M.S.K. and L.M.B. assessed the effect of OI and itaconate on mitochondrial parameters and itaconate transport. D.D., M.H. and A.T.D.-K. performed the NQO1 assay and KEAP1 wild-type and Cys151Ser mutant experiments. J.F.M., R.F., B.M.K., E.T.C., M.P.J. and J.S. assisted with mass spectrometry experiments. L.K.M. and G.B. provided guidance and advice. E.V.K., P.J.M. and M.L.J.A. assisted with experiments in Nrf2-deficient mice. L.A.O'N. conceived ideas and oversaw the research programme. M.P.M. provided advice, reagents and oversaw a portion of the work.

Author Information Reprints and permissions information is available at www.nature.com/reprints. The authors declare no competing interests. Readers are welcome to comment on the online version of the paper. Publisher's note: Springer Nature remains neutral with regard to jurisdictional claims in published maps and institutional affiliations. Correspondence and requests for materials should be addressed to L.A.O'N. (laoneill@tcd.ie).

Reviewer Information *Nature* thanks N. S. Chandel, R. Rossignol, S. Werner and the other anonymous reviewer(s) for their contribution to the peer review of this work.

METHODS

Isolation of human PBMCs. Human PBMCs were isolated from human blood using Lymphoprep (Axis-Shield). Whole blood (30 ml) was layered on 20 ml lymphoprep and spun for 20 min at 2,000 r.p.m. with no brake on. The PBMCs were isolated from the middle layer. PBMCs were maintained in RPMI supplemented with 10% (v/v) FCS, 2 mM L-glutamine, and 1% penicillin/streptomycin solution.

Generation of human macrophages. Blood was layered on Histopaque and centrifuged at 800*g* for 20 min, acceleration 9, and deceleration at 4. The PBMC layer was isolated and the macrophages were sorted using magnetic-activated cell sorting (MACS) CD14 beads. Cells were plated at 0.5×10^6 cells ml^{-1} in media containing M-CSF (100 ng ml^{-1}) and maintained at 37 °C, 5% CO_2 for 5 days, to allow differentiation into macrophages. For further details, see Supplementary Methods.

Generation and treatment of BMDMs. Mice were euthanized in a CO_2 chamber and death was confirmed by cervical dislocation. Bone marrow cells were extracted from the leg bones and differentiated in DMEM (containing 10% fetal calf serum, 1% penicillin/streptomycin and 20% L929 supernatant) for 6 days, at which time they were counted and replated for experiments. Unless stated, 5×10^6 BMDMs per millilitre were used in *in vitro* experiments. Unless stated, the LPS concentration used was 100 ng ml^{-1}, the DMI and OI concentration was 125 μM, and in experiments where pre-treatments occurred before LPS stimulation this was for 3 h.

Synthesis of itaconate compounds. For details on synthesis and characterization of chemical compounds, see Supplementary Methods.

Metabolomic analysis with Metabolon. Macrophages were plated at 2×10^6 per well in 6-well plates and treated as required. BMDMs $n = 5$, human macrophages $n = 12$. Analysis was performed by Metabolon. For further details, see Supplementary Methods.

Metabolite measurements for absolute succinate and itaconate quantification and metabolite tracing. Cells were treated as desired. For tracing studies, immediately before LPS stimulation, the media was removed and replaced with DMEM media (1 ml) containing U-^{13}C-glucose (4.5 g l^{-1}) or U-^{13}C-glutamine (584 mg ml^{-1}) deplete of ^{12}C- glucose or ^{12}C-glutamine. Samples were extracted in methanol/acetonitrile/water, 50:30:20 (v/v/v) (1 ml per 1×10^6 cells) and agitated for 15 min at 4 °C in a Thermomixer and then incubated at −20 °C for 1 h. Samples were centrifuged at maximum speed for 10 min at 4 °C. The supernatant was transferred into a new tube and centrifuged again at maximum speed for 10 min at 4 °C. The supernatant was transferred autosampler vials. Liquid chromatograph–mass spectrometry (LC–MS) analysis was performed using a Q Exactive mass spectrometer coupled to a Dionex U3000 UHPLC system (Thermo). For further details, see Supplementary Methods.

Western blotting. Protein samples from cultured cells were prepared by direct lysis of cells in 5× Laemmli sample buffer, followed by heating at 95 °C for 5 min. For spleen samples, 30 mg of spleen was homogenized in RIPA buffer using the Qiagen TissueLyserII system. The resulting homogenate was centrifuged at 14,000 r.p.m. for 10 min at 4 °C, and supernatants were used for SDS–PAGE. Protein samples were resolved on 8% or 12% SDS–PAGE gels and were then transferred onto polyvinylidene difluoride (PVDF) membrane using either a wet or semi-dry transfer system. Membranes were blocked in 5% (w/v) dried milk in TBS-Tween (TBST) for at least 1 h at room temperature. Membranes were incubated with primary antibody, followed by the appropriate horseradish peroxidase-conjugated secondary antibody. They were developed using LumiGLO enhanced chemiluminescent (ECL) substrate (Cell Signalling). Bands were visualized using the GelDoc system (Biorad).

Quantitative PCR. Total RNA was isolated using the RNeasy Plus Mini kit (Qiagen) and quantified using a Nanodrop 2000 UV-visible spectrophotometer. cDNA was prepared using 20–100 ng μl^{-1} total RNA by a reverse transcription PCR (RT–PCR) using a high capacity cDNA reverse transcription kit (Applied Biosystems), according to the manufacturer's instructions. Quantitative PCR (qPCR) was performed on cDNA using SYBR Green probes. qPCR was performed on a 7900 HT Fast Real-Time PCR System (Applied Biosystems) using Kapa fast master mix high ROX (Kapa Biosystems, for SYBR probes) or 2× PCR fast master mix (Applied Biosystems, for Taqman probes). For SYBR primer pair sequences, see Supplementary Methods. Fold changes in expression were calculated by the $\Delta\Delta C_t$ method using mouse *Rps18* as an endogenous control for mRNA expression. All fold changes are expressed normalized to the untreated control.

NQO1 bioassay. Inducer potency was quantified by use of the NQO1 bioassay in Hepa1c1c7 mouse hepatoma cells[11,12]. Cells (10^4 per well of a 96-well plate) were grown for 24 h and exposed ($n = 8$) to serial dilutions of compounds for 48 h before lysis. NQO1 enzyme activity was quantified in cell lysates using menadione as a substrate. Protein concentrations were determined in aliquots from the same cell lysates by the bicinchoninic acid (BCA) assay (Thermo Scientific). The CD value was used as a measure of inducer potency. For assays examining the effect of GSH on inducer potency, 50 μM of each compound was incubated with 1 mM GSH in the cell culture medium at 37 °C for 30 min before treatment.

Preparation of rat liver mitochondria. Female Wistar rats aged between 10 and 12 weeks (Charles River) were culled by stunning and cervical dislocation before the liver being excised and stored in ice-cold buffer (STE buffer; 250 mM sucrose, 5 mM Tris-Cl, 1 mM EGTA (pH 7.4 at 4 °C)). Rat liver mitochondria were isolated by homogenization and differential centrifugation at 4 °C in STE buffer[26]. In brief, minced tissue was homogenized in STE buffer before centrifugation (1,000*g*, 3 min, 4 °C) and centrifuging the resulting supernatant (10,000*g*, 10 min, 4 °C). The mitochondrial pellet was resuspended in fresh STE before centrifuging (10,000*g*, 10 min, 4 °C). The resulting pellet was resuspended in STE and assayed for protein concentration via BCA assay (Thermo Scientific) against a BSA standard curve.

Preparation of bovine heart mitochondrial membranes. Bovine heart mitochondria were isolated by differential centrifugation in 250 mM sucrose, 10 mM Tris-Cl, 0.2 mM EDTA (pH 7.8 at 4 °C). To prepare membranes, bovine heart mitochondria were blended with MilliQ water at 4 °C before adding KCl to a final concentration of 150 mM and blending until homogenous. The suspension was centrifuged (13,500*g*, 40 min, 4 °C) and the pellet was resuspended in re-suspension buffer (20 mM Tris-Cl, 1 mM EDTA, 10% glycerol, pH 7.55 at 4 °C) before homogenization and assaying for protein by BCA assay (Thermo Scientific)[27].

Measuring complex II and III activity. Bovine heart mitochondrial membranes (80 μg protein per ml) were incubated in 50 mM potassium phosphate buffer (50 mM potassium phosphate, 1 mM EDTA, pH 7.4, 4 °C) supplemented with 3 mM KCN, 4 μM rotenone and succinate. In a 96-well microplate, inhibitor or vehicle control and membrane incubation were plated and incubated for 10 min at 30 °C. Alternatively, where indicated, itaconate was incubated with membranes and removed by twice centrifuging membranes and resuspending in non-itaconate containing buffer, before plating with 1 mM succinate. Oxidized cytochrome-*c* was added before measuring the respiratory chain activity by assessing the reduction of cytochrome-*c* spectrophotometrically at 550 nm at 20 s intervals for 5 min at 30 °C. Final concentrations were 10 μg protein per well bovine heart membranes and 30 μM ferricytochrome *c*.

Measuring rat liver mitochondrial respiration. Respiration of rat liver mitochondria was assessed with an Oxygraph-2K (OROBOROS instruments high resolution respirometry). Rat liver mitochondria (0.5 mg mitochondrial protein per ml) were added to KCl buffer (pH 7.2, 37 °C) and respiration assessed in the presence of 4 μg ml^{-1} rotenone, 1 mM succinate, 1 μM FCCP and inhibitors or buffer control.

Assessing itaconate ester reactivity with glutathione. GSH (1 or 5 mM) and 5 mM itaconate esters or vehicle control were incubated in KCl buffer (pH 7.2 or 8) at 37 °C for 2 h, where indicated, 10 μg recombinant GST was added to the incubation. The reaction was stopped by acidification with 5% sulfosalicylic acid before assessing glutathione content by the GSH recycling assay as described previously[28].

Itaconate transport assays. Itaconate transport by mitochondrial carriers was assessed as described previously[29]. For further details see Supplementary Methods.

Cell uptake of itaconate. C2C12 mouse myoblasts were plated at 300,000 cells per well in a 6-well plate in complete growth medium and adhered overnight in a humidified 5% CO_2, 37 °C incubator. The following day, media was replaced with serum-free DMEM containing itaconate esters and cells were treated for 30 min at 37 °C. Cells were extracted as described above (method for succinate quantification), with MS internal standard (100 pmol) added and stored at −80 °C before LC–MS/MS analysis. For further details, see Supplementary Methods.

LC–MS/MS analysis was performed using an LCMS-8060 mass spectrometer (Shimadzu) with a Nexera X2 UHPLC system (Shimadzu). For further details, see Supplementary Methods.

KEAP1 cysteine target validation. COS1 cells (2.5×10^5 per well) in 6-well plates were co-transfected (Lipofectamine 2000) with 0.8 μg of Nrf2-V5 and 1.6 μg of wild-type or Cys151S mutant KEAP1[14], or 1.6 μg of pcDNA. Cells were grown for 21 h then treated with 20 or 100 μM OI, 5 μM sulforaphane or 0.1% acetonitrile (vehicle) for 3 h. Cell were washed in PBS and lysed in 200 μl of SDS-lysis buffer (50 mM Tris-HCl, pH 6.8, 2% (w/v) sodium dodecyl sulfate (SDS) and 10% (v/v) glycerol). Lysates were sonicated (20 s at 30% amplitude using Vibra-Cell ultrasonic processor, Sonic) and boiled (3 min), and dithiothreitol (DTT) and Bromophenol blue were added up to 0.1 M and 0.02% (w/v) final concentrations, respectively. Proteins (10 μg) were resolved on a gradient (4–12%) NuPAGE SDS gel, transferred onto nitrocellulose membranes, and immunoblotted with anti-KEAP1 (rat monoclonal, Merk Millipore, clone 144), anti-Nrf2 (rabbit monoclonal, CST), and anti-β-actin (mouse monoclonal, Sigma) antibodies. Horseradish peroxidase (HRP)- or IRDye-labelled secondary antibodies were used interchangeably, followed by either ECL detection or scanning using Odyssey imager (Li-COR).

ELISA. Cytokine concentrations in cell supernatants were measured using ELISA Duoset kits for mouse IL-10 and TNF and human IFN-β and IL-1β, according to the manufacturer's instructions. Cytokine concentrations in serum samples isolated from whole blood were measured using Quantikine ELISA kits for mouse or human IL-1β, IFN-β, IL-10 and TNF. Duoset and Quantikine kits were from R&D Systems. Optical density values were measured at a wavelength of 450 nm, using a FLUOstar Optima plate reader (BMG Labtech). Concentrations were calculated using a four-parameter fit curve.

FACS analysis of ROS. BMDMs were seeded at 0.5×10^6 cells per ml and treated as normal. Then 2 h before staining, 100% ethanol was added to the dead cell control well. Thirty minutes before the end of the stimulation, CellROX (5 μM) was added directly into the cell culture medium. Supernatants of cells that were to be stained with Aqua Live/Dead were removed, and an Aqua Live/Dead dilution (1 ml; 1:1,000 in PBS) was added to each well. Cells were incubated in tinfoil at 37 °C for 30 min. Cells were washed with PSB, scraped in PBS (0.5 ml), and transferred to polypropylene FACS tubes. Samples were analysed using a DAKO CyAn flow cytometer, and data was analysed using FlowJo software. MFI was quantified as a measure of cellular ROS production.

Nitric oxide assay. Nitric oxide concentrations in cell supernatants were measured using Greiss reagent assay kit from Thermo Fischer Scientific according to the manufacturer's instructions. Optical density values were measured at a wavelength of 548 nm, using a SoftMax Pro plate reader. Concentrations were calculated using a linear standard curve.

GSH/GSSG measurements. BMDMs were plated at 0.1×10^6 cells per ml in opaque 96-well plates. Cells were pre-treated with OI (125 μM) for 2 h and then stimulated with hydrogen peroxide (100 μM) for 24 h. After 24 h, cell media was removed and the reduced glutathione to oxidized glutathione (GSH/GSSG) ratio was quantified using MyBio GSH/GSSG-Glo Assay (V6611) as per manufacturer's instructions. Luminescence was quantified using a FLUOstar Optima plate reader.

LDH assay. Cells were plated at 0.5×10^6 cells per ml in white 24-well plates (500 μl per well) and treated as required. Cytotoxicity, as determined by LDH release, was assayed using CytoTox96 Non-radioactive Cytotoxicity Assay kit (Promega) according to the manufacturer's instructions.

Seahorse analysis of lactate production. Cells were plated at 0.2×10^6 cells per well of a 24-well Seahorse plate. Cells were treated and stimulated as normal. A utility plate containing calibrant solution (1 ml per well) was placed in a CO_2-free incubator at 37 °C overnight. The next day, media was removed from cells and replaced with glucose-supplemented XF assay buffer (500 μl per well) was placed in a CO_2-free incubator for at least 0.5 h. Compounds (glucose, oligomycin and 2-deoxy-D-glucose (2DG); 70 μl) were added to the appropriate port of the injector plate. This plate together with the utility plate was run on the Seahorse for calibration. Once complete, the utility plate was replaced with the cell culture plate and run on the Seahorse XF-24.

Endotoxin-induced model of sepsis. For cytokine measurements, mice were treated intraperitoneally with OI (50 mg kg^{-1}) in 40% cyclodextrin in PBS or vehicle control for 2 h before stimulation with LPS (Sigma; 2.5 mg kg^{-1}) intraperitoneally for 2 h. Mice were euthanized in a CO_2 chamber, blood samples were collected and serum was isolated. Cytokines were measured using R&D ELISA kits according to manufacturer's protocol. For temperature recording, mice ($n = 10$ per group) were treated intraperitoneally with OI (50 mg kg^{-1}) in 40% cyclodextrin in PBS or vehicle control for 2 h before stimulation with LPS (5 mg kg^{-1}) and monitored for temperature at 1, 2, 3, 4, 6, 12, 18 and 24 h after LPS treatment. Temperature was monitored using subcutaneously implanted temperature transponder chips (Bio Medic Data Systems; IPTT 300) which were injected between the shoulder blades 48 h before experiment. At defined times, body temperature was measured by scanning the transponder with a corresponding BMDS Smart Probe. Animals were additionally monitored for clinical signs of endotoxic shock, based on temperature change, body condition, physical condition and unprovoked behaviour, with a combined score of 9 indicating the humane end point for the experiment.

siRNA transfection of BMDMs. Cells were plated at 1×10^6 cells per ml in 12-well plates overnight. On the day of transfection, the media was replaced with 500 μl DMEM without penicillin/streptomycin or FBS. For each target gene, two Eppendorfs were prepared. Optimem (250 μl per well) was added to each tube. RNAimax (add 5 μl per well) was added to one set of tubes and short interfering siRNA (siRNA; 50 nM per well) was added to the second set of tubes. The tube containing the siRNA was added to the tube with RNAimax, mixed well by pipetting and incubated for 15 min. The mix (500 μl) was added to each well. Twenty-four hours after transfection, cells were treated as required.

Analysis of KEAP1 modification by OI. Human embryonic kidney cells (HEK293T cells) were transfected with a pCMV6-KEAP1 vector (Myc-DDK-tagged mouse KEAP1) (OriGene). C2C12, Hepa1c1c7 cells and COS1 cells were from American Type Culture Collection (ATCC). The L929 cells are from Sigma (85011425). HEK293T cells were obtained from the Centre for Applied Microbiology and Research. Cell lines have not been tested for mycoplasma contamination. Twenty-four hours after transfection, cells were treated with OI (500 μM) or vehicle control (PBS) for 4 h. Tagged KEAP1 was immunoprecipitated using an anti-Flag antibody (Sigma) and protein A/G beads (Santa Cruz). After immunoprecipitation, bound KEAP1 was eluted off the beads using Flag peptide (500 μl; 200 μg ml^{-1}) (Sigma) diluted in 1× TBS pH 7.4. The samples were then concentrated and the Flag peptide was removed using 10K centrifugation filter columns (Merck). The concentrated samples were then divided in half for downstream processing. One-half of each sample was diluted 1:2 with 5× SDS sample buffer and separated using SDS–PAGE (Bio-Rad). Overexpressed KEAP1 was detected using Coomassie blue staining and the corresponding bands were excised from the gel and subjected to in-gel digest as described. In brief, the gel slices were cut into smaller pieces (1–2 mm^3) before reduction with DTT (10 mM) and alkylation with iodoacetamide (50 mM). Half of the gel slices from each sample were then subjected to a trypsin (2 μg) digest, the other half were digested with elastase (1 μg) overnight at 37 °C. Similarly, the remaining sample concentrates (in solution) were reduced with DTT and alkylated with iodoacetamide, before precipitation of the protein via the methanol–chloroform extraction method. The protein pellet was re-suspended in urea (6 M), which was then diluted to <1 M urea with ultrapure H_2O. The samples were then digested with trypsin (2 μg) overnight at 37 °C. Digested protein samples were analysed in an Orbitrap Fusion Lumos coupled to a UPLC ultimate 3000 RSLCnano System (both Thermo Fisher). For further details, see Supplementary Methods.

Assessment of cysteine alkylation by itaconate using Iodo-TMT. After treatment, cells were lysed in HEPES pH 7.5, EDTA, glycerol and NP40. 2 mM TCEP and 50 mM NEM were added in a buffer containing 50 mM HEPES, 2% SDS, 125 mM NaCl, pH 7.2, and samples were incubated for 60 min at 37 °C in the dark to reduce and alkylate all unmodified protein cysteine residues. 20% (v/v) TCA was added to stabilize thiols and incubated overnight at 4 °C and then pelleted for 10 min at 4,000*g* at 4 °C. The pellet was washed three times with cold methanol (2 ml) and then resuspended in 2 ml 8 M urea containing 50 mM HEPES, pH 8.5. Protein concentrations were measured by BCA assay (Thermo Scientific) before protease digestion. Protein lysates were diluted to 4 M urea and digested with LysC (Wako) in a 1:100 enzyme:protein ratio and trypsin (Promega) at a final 1:200 enzyme:protein ratio for 4 h at 37 °C. Protein extracts were diluted further to a 2.0 M urea and LysC (Wako) at 1:100 enzyme:protein ratio and trypsin (Promega) at a final 1:200 enzyme:protein ratio were added again and incubated overnight at 37 °C. Protein extracts were diluted further to a 1.0 M urea concentration, and trypsin (Promega) was added to a final 1:200 enzyme:protein ratio for 6 h at 37 °C. Digests were acidified with 250 μl of 25% acetic acid to a pH value of ~2, and subjected to C18 solid-phase extraction (50 mg Sep-Pak, Waters). Excess TMT label (6–7 M) was added to each digest for 30 min at room temperature (repeated twice). The reaction was quenched using 4 μl 5% hydroxylamine. Samples were subjected to an additional C18 solid-phase extraction (50 mg Sep-Pak). For LC–MS/MS parameters, data processing and MS2 spectra assignment, TMT reporter ion intensities and quantitative data analysis, see Supplementary Methods.

Reagents. For a complete list of reagents, see Supplementary Methods.

Mouse strains. Wild-type C57BL/6 mice were from Harlan UK and Harlan Netherlands. Animals were maintained under specific pathogen-free conditions in line with Irish and European Union regulations. Experiments were approved by local ethical review and were carried out under the authority of Ireland's project license. All animal studies performed in GSK were ethically reviewed and carried out in accordance with Animals (Scientific Procedures) Act 1986 and the GSK Policy on the Care, Welfare and Treatment of Animals. Nrf2-deficient mice and their wild-type counterparts, both on the C57BL/6 genetic background (used for isolation of BMDM cells), were bred and maintained in the Medical School Resource Unit of the University of Dundee.

Statistical analysis. Data were expressed as mean ± s.e.m. and *P* values were calculated using two-tailed Student's *t*-test for pairwise comparison of variables, one-way ANOVA for multiple comparison of variables, and two-way ANOVA involving two independent variables. A Sidak's multiple comparisons test was used. A confidence interval of 95% was used for all statistical tests. Sample sizes were determined on the basis of previous experiments using similar methodologies. For all experiments, all stated replicates are biological replicates. For *in vivo* studies, mice were randomly assigned to treatment groups. For mass spectrometry analyses, samples were processed in random order and experimenters were blinded to experimental conditions.

Data availability. Full scans for all western blots are provided in Supplementary Fig 1. Source Data for all mouse experiments have been provided. All other data are available from the corresponding author on reasonable request.

26. Chappell, J. B. & Hansford, R. V. A. *Subcellular Components: Preparation and Fractionation* 2nd edn (Butterworth, 1972).
27. Bridges, H. R., Mohammed, K., Harbour, M. E. & Hirst, J. Subunit NDUFV3 is present in two distinct isoforms in mammalian complex I. *Biochim. Biophys. Acta* **1858,** 197–207 (2017).
28. Akerboom, T. P. & Sies, H. Assay of glutathione, glutathione disulfide, and glutathione mixed disulfides in biological samples. *Methods Enzymol.* **77,** 373–382 (1981).
29. Booty, L. M. *et al.* The mitochondrial dicarboxylate and 2-oxoglutarate carriers do not transport glutathione. *FEBS Lett.* **589,** 621–628 (2015).

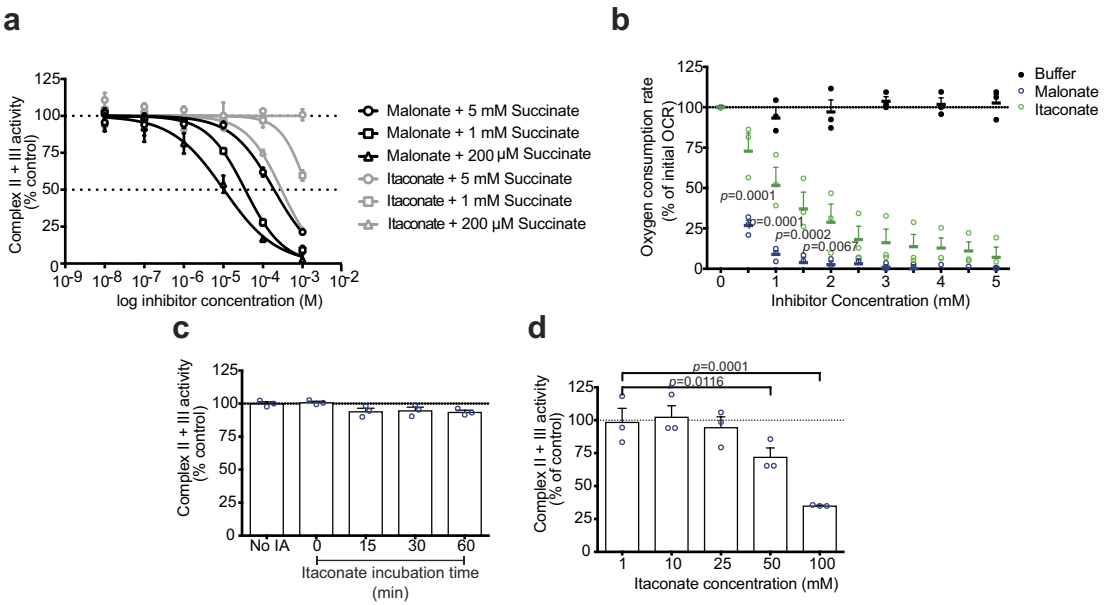

Extended Data Figure 1 | The effect of itaconate on complex II activity. a, Complex II and III activity in bovine heart mitochondrial membranes incubated with succinate plus malonate or itaconate ($n = 3$ independent experiments). **b**, Effect of malonate or itaconate on the oxygen consumption rate (OCR) of rat liver mitochondria in the presence of succinate (1 mM) and FCCP (1 μM; $n = 3$ independent experiments). **c**, **d**, Complex II and III activity in bovine heart mitochondrial membranes incubated with itaconate (IA; 1 mM unless indicated), with subsequent removal and addition of succinate (1 mM; $n = 3$ independent experiments) (see Methods for further details). Data are mean ± s.e.m. *P* values calculated using one or two-way ANOVA.

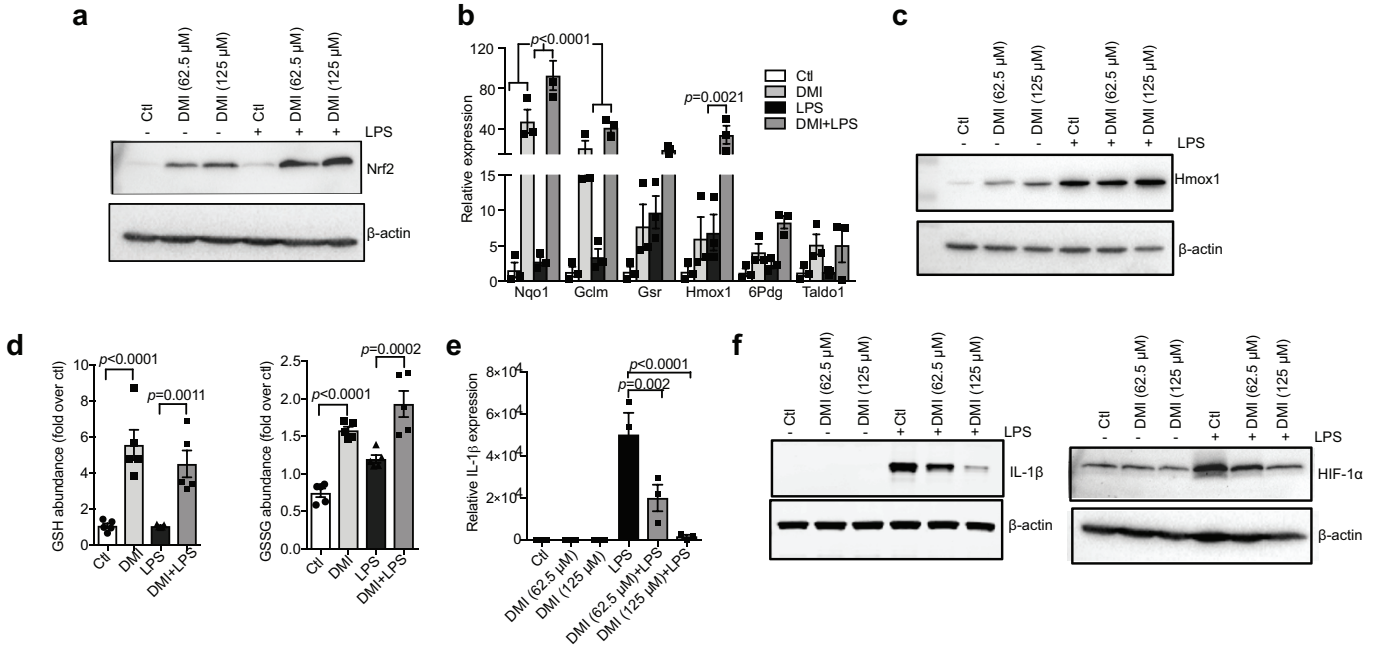

Extended Data Figure 2 | DMI activates Nrf2 and limits cytokine production. a, **c**, LPS (100 ng ml^{-1})-induced Nrf2 (**a**, 24 h) and HMOX1 (**c**, 6 h) protein expression with or without the itaconate derivative DMI. **b**, Nrf2-dependent mRNA expression after treatment with LPS (6 h) and DMI where indicated ($n = 3$). **d**, Reduced glutathione (GSH) and oxidized glutathione (GSSG) levels after treatment with LPS and DMI ($n = 5$). **e**, **f**, LPS (24 h)-induced *Il1b* mRNA (**e**), IL-1β and HIF-1α protein (**f**) expression in mouse macrophages with or without DMI ($n = 3$). Data are mean ± s.e.m. *P* values calculated using one-way ANOVA. Blots are representative of three independent experiments. For gel source data, see Supplementary Fig. 1.

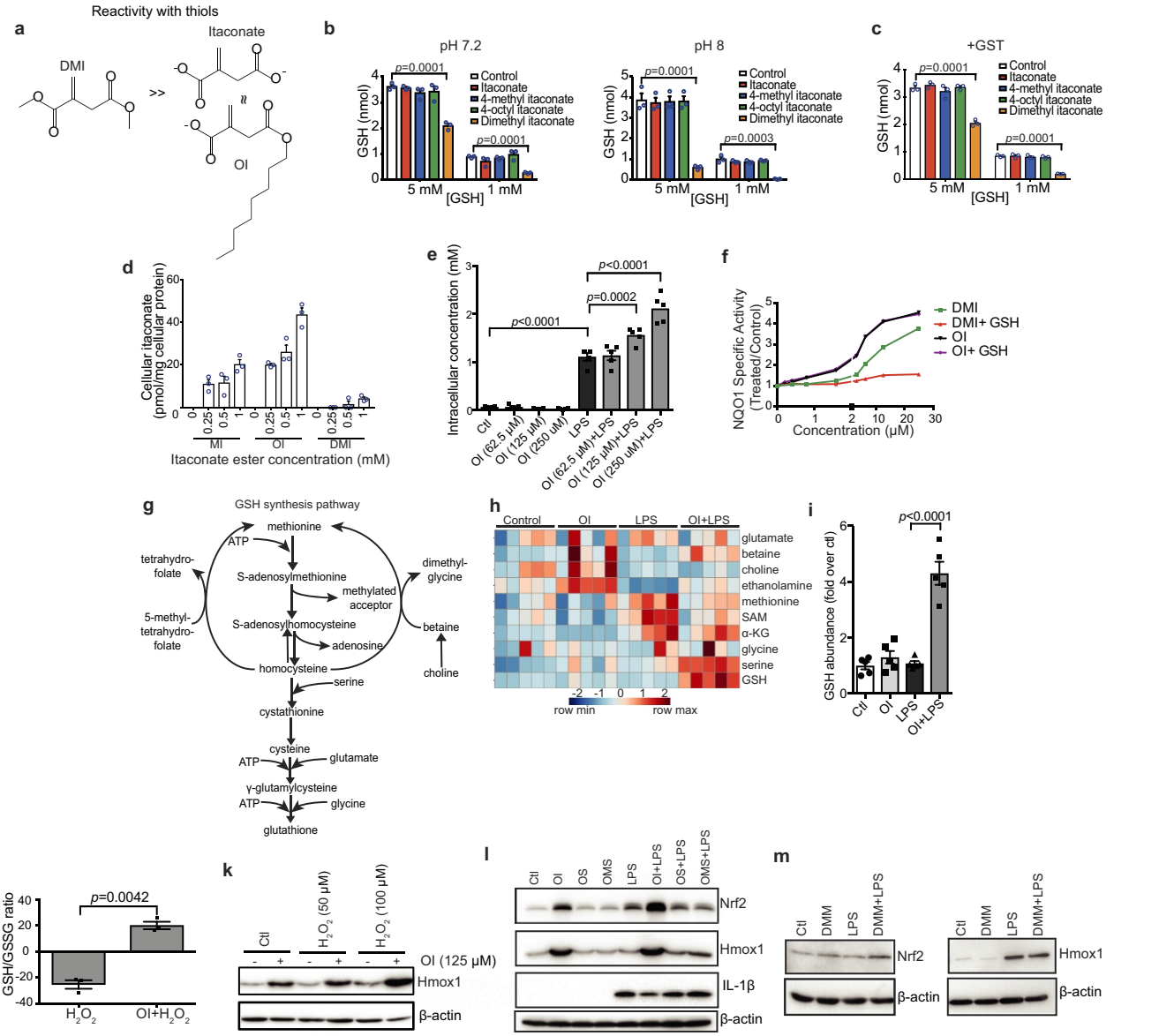

Extended Data Figure 3 | OI is the best tool to assess itaconate-dependent Nrf2 activity. a, Reactivity of DMI, itaconate and OI with thiols. **b**, **c**, Itaconate ester reactivity with GSH and glutathione-*S*-transferase (GST) as detailed in the Methods ($n = 3$). **d**, Itaconate levels in mouse C2C12 cells plus itaconate esters ($n = 3$). MI, 4-methyl itaconate. **e**, **i**, Itaconate (**e**) or GSH (**i**) levels plus LPS (6 h) and OI as indicated ($n = 5$). **f**, NQO1 activity in mouse Hepa1c1c7 cells treated with DMI or OI (48 h) and GSH ($n = 8$). **g**, **h**, Metabolic intermediates in GSH synthesis (**h**, average of five biological replicates). **i**, GSH levels after treatment with LPS (6 h) and/or OI ($n = 5$). **j**, GSH/GSSG ratio after treatment with OI (2 h) and H_2O_2 (100 μM, 24 h; $n = 3$) as indicated. **k**, HMOX1 protein levels after treatment with OI and/or H_2O_2 (24 h). **l**, Nrf2, HMOX1 and IL-1β protein levels in BMDMs pre-treated with OI, 4-octyl 2-methylsuccinate (OMS) or octyl succinate (OS), all 125 μM for 3 h with or without LPS (6 h). **m**, LPS-induced Nrf2 (24 h) and HMOX1 (6 h) protein expression with or without dimethyl malonate (DMM). Data are mean ± s.e.m. *P* values calculated using one- or two-way ANOVA. Blots are representative of three independent experiments. For gel source data, see Supplementary Fig. 1.

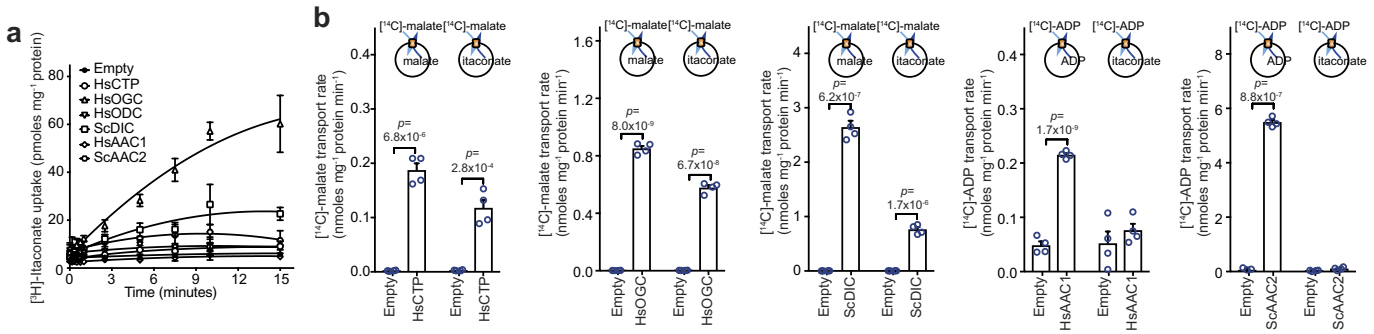

Extended Data Figure 4 | Itaconate is transported by the mitochondrial oxoglutarate, dicarboxylate and citrate carriers. a, Itaconate uptake into vesicles of *Lactococcus lactis* membranes expressing the indicated carriers loaded with itaconate (1 mM), and transport initiated by the addition of [^{3}H]itaconate (1 μM). **b**, Initial transport rates of each carrier with either canonical substrate (homo-exchange) or canonical substrate/itaconate (hetero-exchange). $n = 4$ independent experiments; data are mean ± s.d. *P* values calculated using two-tailed Student's *t*-test.

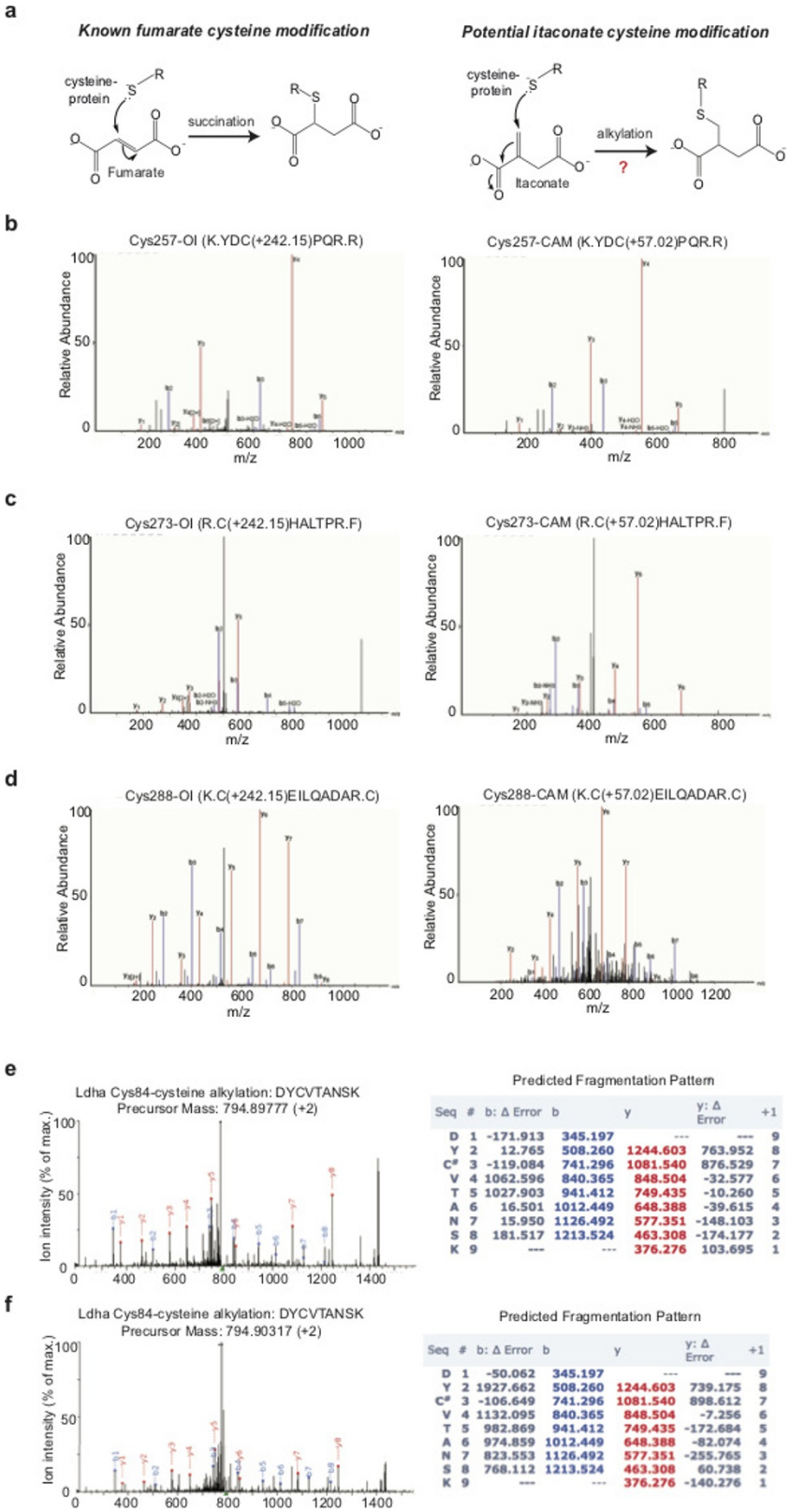

Extended Data Figure 5 | KEAP1 is alkylated by OI on major redox sensing cysteine residues. a, Modification of cysteine by fumarate or itaconate. Tandem mass spectrometry spectrum of KEAP1 Cys257 (**b**), Cys257 (**c**) and Cys288 (**d**) peptides, indicating alkylation of these sites after OI treatment (left) but not in the corresponding carbamidomethylated (CAM) peptides (right). **e**, **f**, LDHA Cys84 alkylation after treatment with LPS (**e**, 24 h) or OI (**f**, 250 μM, 4 h) ($n = 4$). Detected N- and C-terminal fragment ions of both peptides are assigned in the spectrum and depicted as follows: *b*: N-terminal fragment ion; *y*: C-terminal fragment ion; asterisk: fragment ion minus NH_3; 0 or asterisk: fragment ion minus H_2O; and 2+: doubly charged fragment ion. Representative of one independent experiment.

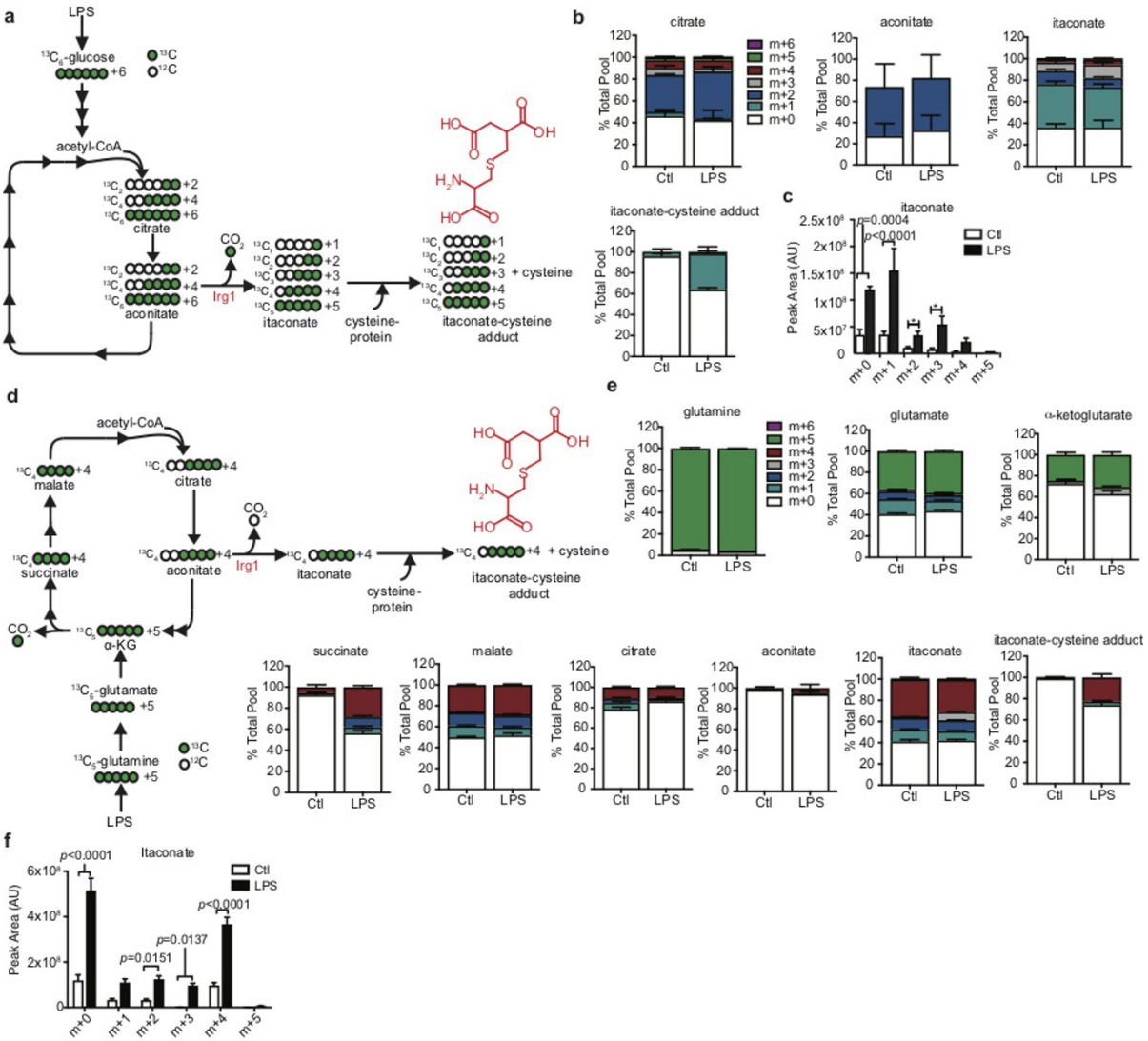

Extended Data Figure 6 | Identification of an itaconate-cysteine adduct. **a**–**e**, $^{13}C_6$-glucose (**a**–**c**) or $^{13}C_5$-glutamine (**d**, **e**) labelling experiment tracking itaconate-cysteine adduct formation in BMDMs treated with LPS ($n = 5$; 24 h). Data in **b** and **e** are expressed as the percentage isotopologue of the total pool. Data in **c** and **f** represent changes in the total pool after LPS treatment. Data are mean ± s.e.m., for five replicates. *P* values calculated using two-way ANOVA.

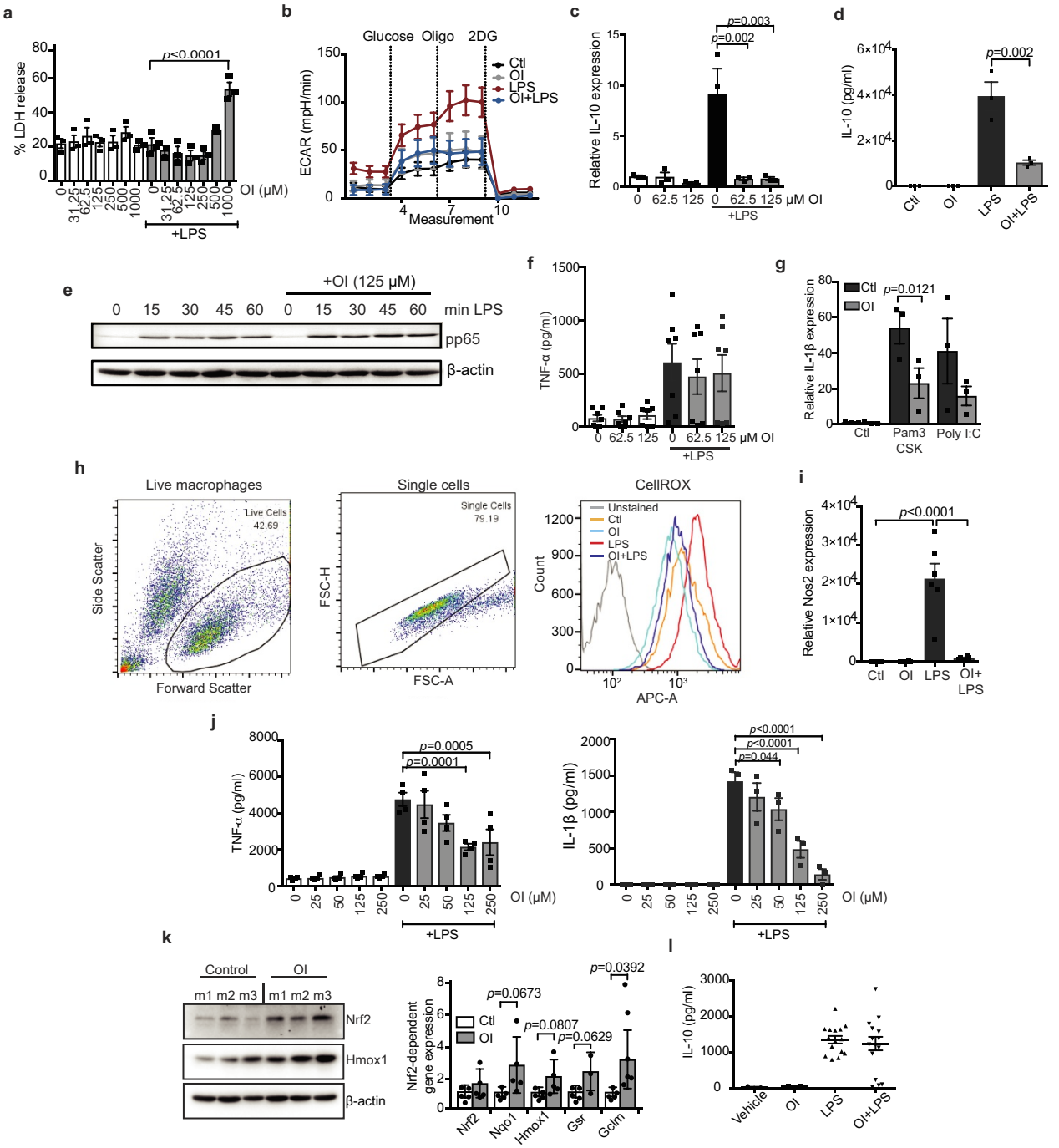

Extended Data Figure 7 | OI decreases LPS-induced cytokine production, extracellular acidification rate, ROS and nitric oxide. **a**, Percentage cytotoxicity (LDH release) in BMDMs after treatment with LPS and OI as indicated ($n = 3$). **b**, LPS-induced extracellular acidification rate (ECAR) after treatment with OI and/or LPS as indicated, analysed on the Seahorse XF-24 in BMDMs (trace representative of three independent experiments). **c**, **d**, LPS-induced *Il10* mRNA (**c**, 4 h) and protein (**d**, 24 h) and TNF protein (**f**; $n = 7$) after OI treatment as indicated ($n = 3$). **e**, Phosphorylated p65 (pp65) protein levels (a measure of NF-κB activity) after treatment with LPS and OI as indicated. **h**, Representative gating strategy for FACS analysis of ROS production in cells as treated in **d** (image representative of three independent experiments). **i**, LPS-induced NOS2 expression ($n = 6$), with or without OI treatment. **j**, LPS-induced TNF ($n = 4$) and IL-1β ($n = 3$) protein levels after OI treatment in PBMCs. **k**, Nrf2 and HMOX1 protein levels or Nrf2-dependent gene expression ($n = 5$) in peritoneal macrophages from mice (m) injected intraperitoneally with OI (50 mg kg^{-1}, 6 h) or vehicle control. **l**, Serum IL-10 from mice injected intraperitoneally with vehicle control or OI (50 mg kg^{-1}, 2 h) and LPS (2.5 mg kg^{-1}, 2 h, $n = 3$ vehicle, OI; $n = 15$ LPS, OI plus LPS). Data are mean ± s.e.m. *P* values calculated using one-way ANOVA. Blots are representative of three independent experiments. For gel source data, see Supplementary Fig. 1.

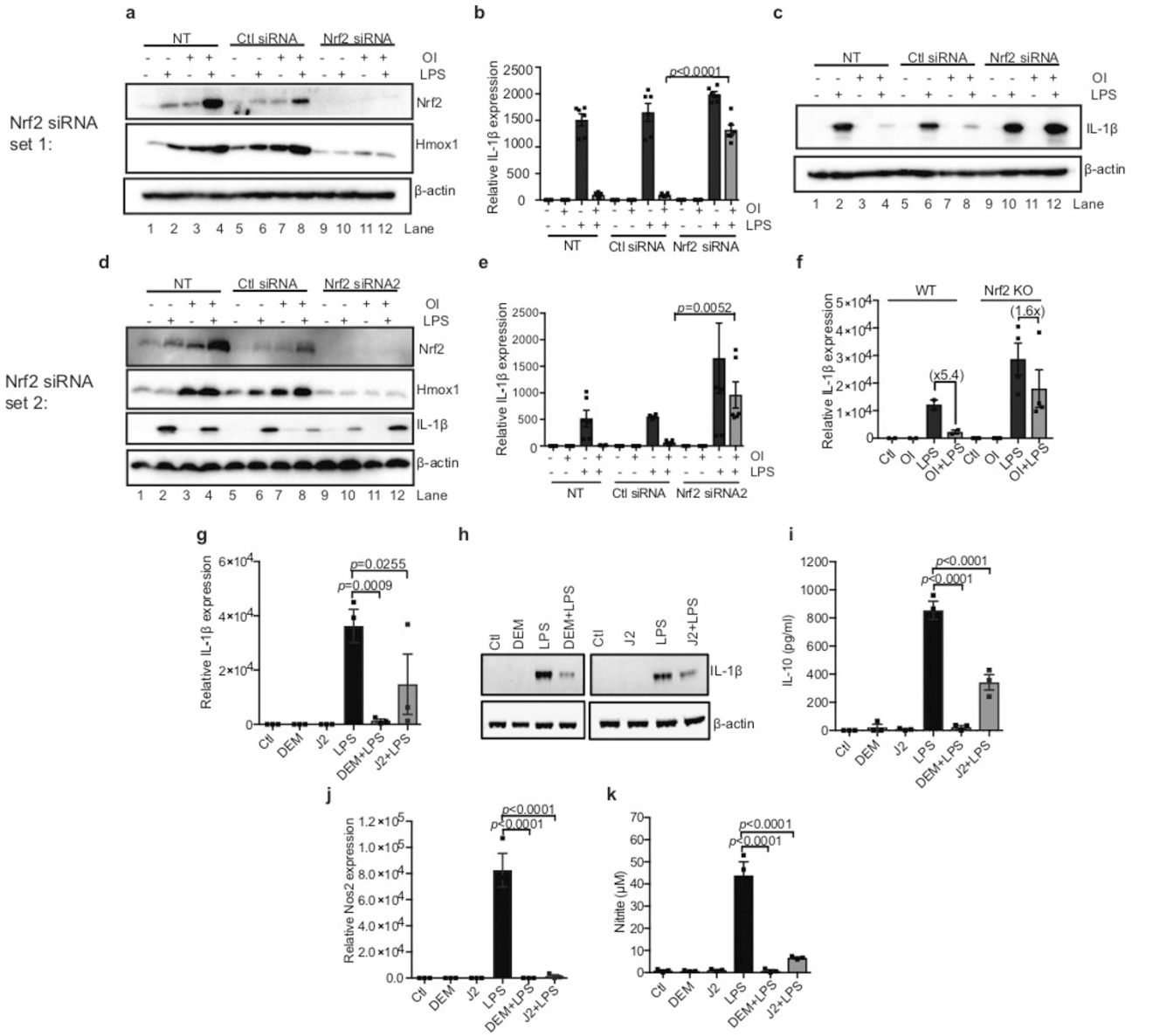

Extended Data Figure 8 | The effects of OI on cytokine production are Nrf2-dependent. a–**e**, Nrf2, HMOX1 and IL-1β protein levels (**a**, **c**, **d**) and *Il1b* mRNA expression (**b**, **e**) in mouse BMDMs transfected with two different *Nrf2* siRNAs (50 nM) compared with a non-silencing scrambled control siRNA plus LPS (6 h; **a**–**c**, **e**; 24 h; **d**) and/or OI ($n = 6$). NT, non-transfected. **f**, *Il1b* mRNA expression in wild-type and Nrf2-knockout BMDMs treated with LPS (24 h; WT $n = 2$, Nrf2 KO $n = 4$) and/or OI. **g**–**k**, *Il1b* (**g**) and *Nos2* (**j**) mRNA, and IL-1β (**h**), IL-10 (**i**), TNF and nitrite (**k**) production with or without LPS (24 h), diethyl maleate (DEM; 100 μM) or 15-deoxy-Δ12,14-prostaglandin J2 (J2; 5 μM) pre-treatment for 3 h ($n = 3$). Data are mean ± s.e.m. *P* values calculated using one-way ANOVA. Blots are representative of three independent experiments. For gel source data, see Supplementary Fig. 1.

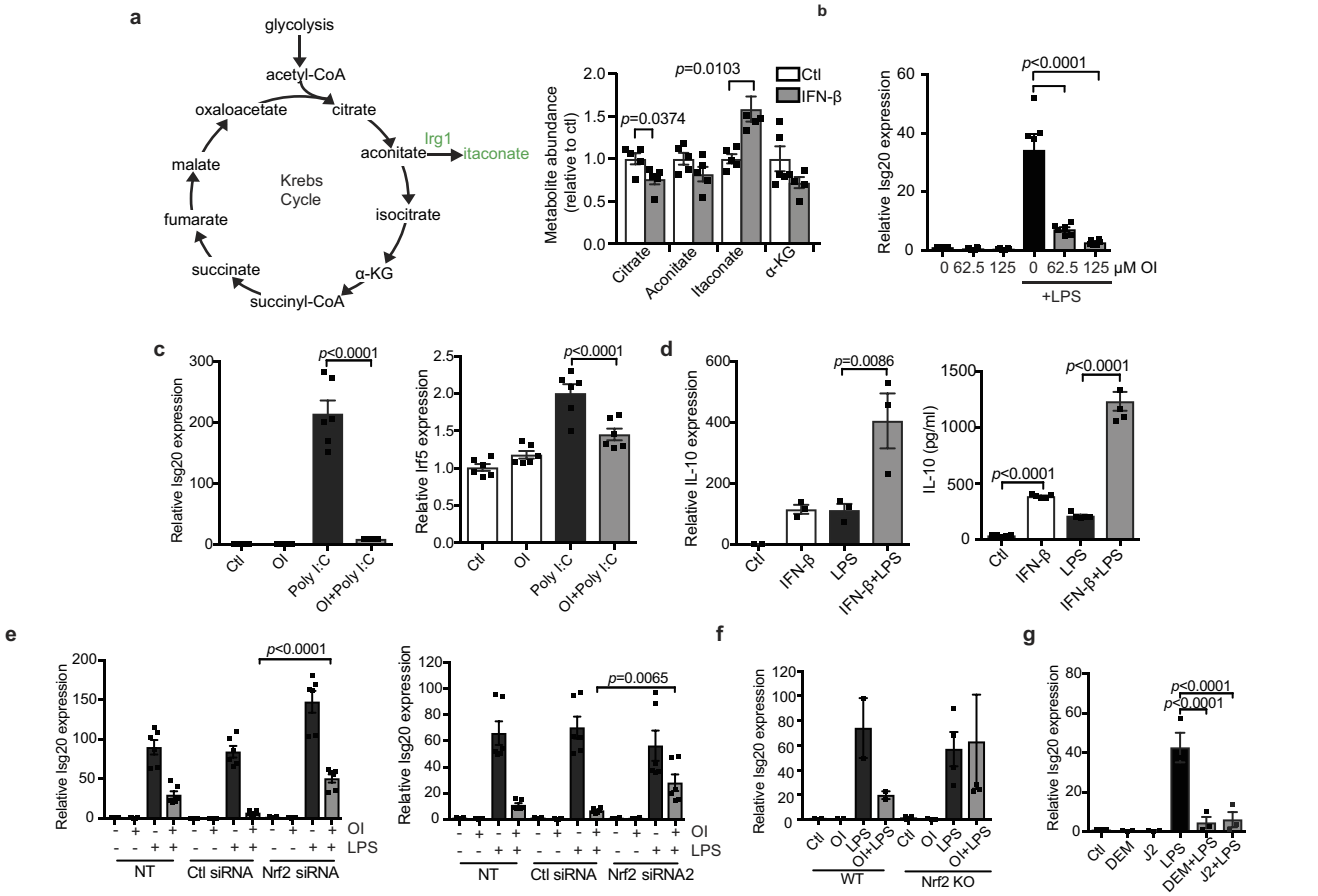

Extended Data Figure 9 | An Nrf2-dependent feedback loop exists between itaconate and IFN-β. a, Metabolite levels after treatment with IFN-β (1,000 U ml^{-1}; 27 h; $n = 5$). **b**, **c**, *Isg20* and *Irf5* mRNA expression in BMDMs treated with LPS (**b**) or poly(I:C) (**c**, 40 μg ml^{-1}; 24 h) and/or OI ($n = 6$). **d**, *Il10* mRNA ($n = 3$) and IL-10 protein ($n = 5$) expression after treatment with LPS for 4 h (left) or 24 h (right) and/or IFN-β treatment (1,000 U ml^{-1}) for 3 h. **e**, *Isg20* expression in BMDMs transfected with two different *Nrf2* siRNAs (50 nM) compared with non-silencing control plus LPS (6 h) and/or OI ($n = 6$). **f**, *Isg20* mRNA expression in wild-type ($n = 2$) and Nrf2-knockout ($n = 4$) BMDMs plus LPS (6 h) and/or OI. **g**, *Isg20* mRNA expression after pre-treatment with LPS (24 h) and/or diethyl maleate (100 μM) or 15-deoxy-Δ12,14-prostaglandin J2 (5 μM) for 3 h ($n = 3$). Data are mean ± s.e.m. *P* values calculated using one-way ANOVA.

Extended Data Table 1 | Mass spectrometry analysis of itaconate-induced cysteine alkylation

a

4-OI Residue	Peptide Amino Acid Position	Peptide Sequence	-10logP	Enzyme	Digest Type
Cys23	22-31	S.KC(+242.15)PEGAGDAV.M	31.47	Elastase	In Gel
Cys151	144-152	A.SISVGEKC(+242.15)V.L	44.11	Elastase	In Gel
	146-152	I.SVGEKC(+242.15)V.L	30.95		
	144-153	A.SISVGEKC(+242.15)VL.H	30.25		
	145-152	S.ISVGEKC(+242.15)V.L	29.32		
Cys257	254-260	V.KYDC(+242.15)PQR.R	35.44	Elastase	In Gel
	255-260	K.YDC(+242.15)PQR.R	40.13	Trypsin	In Gel
	255-260	K.YDC(+242.15)PQR.R	41.08	Trypsin	In Solution
Cys273	273-279	R.C(+242.15)HALTPR.F	35.93	Trypsin	In Gel
	273-279	R.C(+242.15)HALTPR.F	38.65	Trypsin	In Solution
Cys288	282-293	L.QTQLQKC(+242.15)EILQA.D	41.70	Elastase	In Gel
	282-290	L.QTQLQKC(+242.15)EI.L	36.70		
	284-293	T.QLQKC(+242.15)EILQA.D	33.47		
	280-296	R.FLQTQLQKC(+242.15)EILQADAR.C	55.81	Trypsin	In Gel
	288-296	K.C(+242.15)EILQADAR.C	50.84		
	288-296	K.C(+242.15)EILQADAR.C	48.80	Trypsin	In Solution
Cys297	294-304	A.DARC(+242.15)KDYLVQI.F	37.15	Elastase	In Gel
K615	602-615	R.SGVGVAVTMEPCRK(+242.15).Q	37.59	Trypsin	In Gel
	602-615	R.SGVGVAVTM(+15.99)EPCRK(+242.15).Q	36.40		

b

Protein	Alkylated residue	Peptide amino acid position	Peptide sequence	X score	Ppm
Plsl	Cys111	97-123	KEGIC(+4.98)AIGGTSEQSSVGTQHSYSEEEK	5.998	-2.22
Acon	Cys385	378-395	VGLIGSC(+4.98)TNSSYEDMGR	4.212	4.17
Ldha	Cys84	82-90	DYC(4.98)VTANSK	3.474	-2.91
Anxa1	Cys189	186-204	GDRC(4.98)QDLSVNQDLADTDAR	3.514	-0.48
Ifi5b	Cys317	310-320	QMIEVPNC(+4.98)ITR	2.412	-4.16
Ipyr2	Cys156, 157	153-171	STDC(4.98)C(+4.98)GDNDPIDVCEIGSK	4.664	22.60
Ef2	Cys41	33-42	STLTDSLVC(+4.98)K	3.677	-1.41
Thio	Cys73	73-81	C(+4.98)MPTFQFYK	2.422	-2.22

c

Protein	Alkylated residue	Peptide amino acid position	Peptide sequence	X score	Ppm
Gilt	Cys69	61-73	VSLYYESLC(+4.98)GACR	4.677	3.40
Fgd6	Cys1004	9996-1005	NVALLDEQC(+4.98)K	3.759	-7.98
Olfr644	Cys306	305-313	FC(+4.98)KILLGNK	3.155	-2.10
Ldha	Cys84	82-90	DYC(+4.98)VTANSK	2.832	3.88
Padi6	Cys553	553-558	C(+4.98)ISLNR	2.446	-18.58
Ubr4	Cys4241	4237-4244	LIASC(+4.98)HWK	2.421	-7.45
Hmox2	Cys314	314-323	C(+4.98)PFYAAQPDK	2.279	2.89
Lhpp	Cys113	112-118	FC(+4.98)TNESQK	2.169	-11.64

a, Cysteine/lysine residue(s) in KEAP1 modified by OI as determined by tandem mass spectrometry. **b**, Cysteine residues modified by itaconate in BMDMs treated with LPS identified using tandem mass spectrometry. **c**, Cysteine residues modified by itaconate in BMDMs treated with OI identified using tandem mass spectrometry.

nature research

Corresponding author(s): Luke O'Neill

☐ Initial submission ☐ Revised version ☒ Final submission

Life Sciences Reporting Summary

Nature Research wishes to improve the reproducibility of the work that we publish. This form is intended for publication with all accepted life science papers and provides structure for consistency and transparency in reporting. Every life science submission will use this form; some list items might not apply to an individual manuscript, but all fields must be completed for clarity.

For further information on the points included in this form, see Reporting Life Sciences Research. For further information on Nature Research policies, including our data availability policy, see Authors & Referees and the Editorial Policy Checklist.

Experimental design

1. Sample size

Describe how sample size was determined.

We have used at least 3 biological replicates for each experiment. This is designed to account for biological variability taking into account that the majority of experiments were performed in murine macrophages from inbred mice. See statistical analyses section of methods for full details.

2. Data exclusions

Describe any data exclusions.

Any exclusions from in vitro data were deemed outliers in GraphPad Prism. From the LPS in vivo cytokine data one LPS-treated sample has been removed as it appears that I did stimulate in response to LPS, most like an injection error.

3. Replication

Describe whether the experimental findings were reliably reproduced.

The in vivo trial required some optimization with various doses of compound as this was the first time it had been used in vivo. In vitro experiments were highly reproducible. All experimental findings were reproduced as biological replicates at the value stated in figure legends, unless otherwise indicated.

4. Randomization

Describe how samples/organisms/participants were allocated into experimental groups.

See statistical analyses section of methods. For in vivo studies, mice were randomly assigned to treatment groups. For MS analyses, samples were processed in random order and experimenters were blinded to experimental conditions.

5. Blinding

Describe whether the investigators were blinded to group allocation during data collection and/or analysis.

The in vivo trials were blinded. For MS analyses, samples were processed in random order and experimenters were blinded to experimental conditions.

Note: all studies involving animals and/or human research participants must disclose whether blinding and randomization were used.

6. Statistical parameters

For all figures and tables that use statistical methods, confirm that the following items are present in relevant figure legends (or in the Methods section if additional space is needed).

n/a	Confirmed
☐	☒ The exact sample size (*n*) for each experimental group/condition, given as a discrete number and unit of measurement (animals, litters, cultures, etc.)
☐	☒ A description of how samples were collected, noting whether measurements were taken from distinct samples or whether the same sample was measured repeatedly
☐	☒ A statement indicating how many times each experiment was replicated
☐	☒ The statistical test(s) used and whether they are one- or two-sided (note: only common tests should be described solely by name; more complex techniques should be described in the Methods section)
☐	☒ A description of any assumptions or corrections, such as an adjustment for multiple comparisons
☐	☒ The test results (e.g. *P* values) given as exact values whenever possible and with confidence intervals noted
☐	☒ A clear description of statistics including central tendency (e.g. median, mean) and variation (e.g. standard deviation, interquartile range)
☐	☒ Clearly defined error bars

See the web collection on statistics for biologists for further resources and guidance.

Software

Policy information about availability of computer code

7. Software

Describe the software used to analyze the data in this study.

Flowjo was used to flow cytometry analysis. Metabolite spectra were analysed using XCalibur Qual Browser and XCalibur Quan Browser software (Thermo Scientific). Labsolutions software (Shimadzu) was used to assess itaconate uptake. SoftMax Pro software was used for ELISAs. MS data was analysed with PEAKS Studio 8 (Bioinformatics Solutions). GraphPad Prism was used for all graphing and statistical tests.

For manuscripts utilizing custom algorithms or software that are central to the paper but not yet described in the published literature, software must be made available to editors and reviewers upon request. We strongly encourage code deposition in a community repository (e.g. GitHub). *Nature Methods* guidance for providing algorithms and software for publication provides further information on this topic.

Materials and reagents

Policy information about availability of materials

8. Materials availability

Indicate whether there are restrictions on availability of unique materials or if these materials are only available for distribution by a for-profit company.

4-octyl itaconate is available from the authors.

9. Antibodies

Describe the antibodies used and how they were validated for use in the system under study (i.e. assay and species).

Antibodies used were goat anti-mouse IL-1β (R&D Systems, AF401-NA), mouse anti-β-actin (Sigma-Aldrich, AC-74), rabbit anti-HIF-1α (Novus, NB100-449), rabbit anti-phospho-pIRF3 (Cell Signalling Technology, 4947) rabbit anti-total IRF3 (Cell Signalling Technology, 4302), rabbit anti-phospho-pTBK1 (Cell Signalling Technology, 5483) rabbit anti-total TBK1 (Cell Signalling Technology, 3013), rabbit anti-IKKε (Cell Signalling Technology, 3416), Nrf2 (Cell Signalling Technology, 12721), Hmox1 (Enzo Life Sciences, ADI-SPA-896-D), Ass1 (Abcam, SAB5300141). Secondary horseradish peroxidase-conjugated anti-mouse IgG, anti-rabbit IgG and anti-goat IgG were from Jackson ImmunoResearch Inc.

10. Eukaryotic cell lines

a. State the source of each eukaryotic cell line used.

C2C12, Hepa1c1c7 cells and COS1 cells were from American Type Culture Collection (ATCC). The L929 cells are from Sigma, cat no is 85011425.HEK293T cells were obtained from the Centre for Applied Microbiology and Research, Wiltshire, UK.

b. Describe the method of cell line authentication used.

No authentication was used

c. Report whether the cell lines were tested for mycoplasma contamination.

They were not tested.

d. If any of the cell lines used are listed in the database of commonly misidentified cell lines maintained by ICLAC, provide a scientific rationale for their use.

No commonly misidentified cell lines were used

Animals and human research participants

Policy information about studies involving animals; when reporting animal research, follow the ARRIVE guidelines

11. Description of research animals

Provide details on animals and/or animal-derived materials used in the study.

8 week old, C57BL/6JOlaHsd female mice were purchased from Envigo UK. The rats were 10-12 week old female Wistar Rats from Charles River Laboratories, Strain Code:003. Nrf2-deficient mice and their wild type counterparts, both on the C57Bl/6 genetic background (used for isolation of BMDM cells) were bred and maintained in the Medical School Resource Unit of the University of Dundee.

Policy information about studies involving human research participants

12. Description of human research participants

Describe the covariate-relevant population characteristics of the human research participants.

The blood was from anonymous donors so I do not have this information.

nature research

Corresponding author(s): Luke O'Neill

☐ Initial submission ☐ Revised version ☒ Final submission

Flow Cytometry Reporting Summary

Form fields will expand as needed. Please do not leave fields blank.

Data presentation

For all flow cytometry data, confirm that:

☒ 1. The axis labels state the marker and fluorochrome used (e.g. CD4-FITC).

☒ 2. The axis scales are clearly visible. Include numbers along axes only for bottom left plot of group (a 'group' is an analysis of identical markers).

☒ 3. All plots are contour plots with outliers or pseudocolor plots.

☒ 4. A numerical value for number of cells or percentage (with statistics) is provided.

Methodological details

5. Describe the sample preparation.	Murine bone marrow derived macrophages
6. Identify the instrument used for data collection.	Dako CyAn flow cytometer
7. Describe the software used to collect and analyze the flow cytometry data.	FlowJo
8. Describe the abundance of the relevant cell populations within post-sort fractions.	This was pure in vitro prepared bone marrow derived macrophages
9. Describe the gating strategy used.	Cells were gated first on side-scatter (area) versus forward scatter (area) (Population; P1; to determine the macrophage population) Then on forward-scatter (height) versus forward scatter (area) (P2; to eliminate doublets) Then on side-scater (area) versus pacific blue (to eliminate dead cells) Finally on counts versus APC (as a meaure of CellROX staining).

Tick this box to confirm that a figure exemplifying the gating strategy is provided in the Supplementary Information. ☒

REVIEW ARTICLE
https://doi.org/10.1038/s42255-018-0014-7

nature metabolism

Coupling Krebs cycle metabolites to signalling in immunity and cancer

Dylan G. Ryan[1], Michael P. Murphy[2], Christian Frezza[3], Hiran A. Prag[2], Edward T. Chouchani[4,5], Luke A. O'Neill[1]* and Evanna L. Mills[4,5]

Metabolic reprogramming has become a key focus for both immunologists and cancer biologists, with exciting advances providing new insights into the mechanisms underlying disease. There is now extensive evidence that intermediates and derivatives of the mitochondrial Krebs cycle—metabolites traditionally associated with bioenergetics or biosynthesis—also possess 'non-metabolic' signalling functions. In this review, we summarize the non-metabolic signalling mechanisms of succinate, fumarate, itaconate, 2-hydroxyglutarate isomers (D-2-hydroxyglutarate and L-2-hydroxyglutarate) and acetyl-CoA, with a specific focus on how such signalling pathways alter immune cell and transformed cell function. We believe that the insights gained from immune and cancer cells that are summarized here will also be useful for understanding and treating a range of other diseases.

In the past 5 years, there has been a remarkable increase in the knowledge of how intracellular metabolic changes in tumours and especially in immune cells are not only linked to energy demand and biosynthesis, but also to discrete effector mechanisms that alter cell behaviour in specific ways. An area of particular focus has been on the Krebs cycle (also known as the tricarboxylic acid (TCA) cycle or the citric acid cycle (CAC)), the primary oxidative pathway for acetyl-CoA and the pathway for generation of the reducing equivalents NADH and $FADH_2$ in aerobic organisms. Importantly, NADH and $FADH_2$ are required to transfer electrons to the mitochondrial respiratory chain, also known as the electron transport chain (ETC), a series of enzyme and coenzyme complexes found along the inner mitochondrial membrane (IMM). Transfer of electrons along the ETC occurs via several redox reactions to facilitate the generation of a proton (H^+) electrochemical potential gradient, which subsequently drives the maintenance of a high, energy-rich ATP (ATP) to adenosine diphosphate (ADP) ratio via F_oF_1-ATP synthase. This process is referred to as oxidative phosphorylation (OXPHOS) and requires oxygen (O_2).

The TCA cycle itself operates in the mitochondrial matrix and is an amphibolic pathway that acts as an important nexus for the integration of multiple catabolic and anabolic pathways, such as glycolysis and gluconeogenesis. As depicted in Fig. 1, the pathway consists of eight enzymes, namely citrate synthase (CS), aconitase (ACO2), isocitrate dehydrogenase (IDH), α-ketoglutarate dehydrogenase (α-KGDH), succinyl-CoA synthetase, succinate dehydrogenase (SDH), fumarate hydratase (FH) and malate dehydrogenase (MDH). The first reaction, an irreversible aldol condensation, is catalysed by CS and extends the four-carbon oxaloacetate to six-carbon citrate, with the additional two carbons derived from acetyl-CoA. In the second step, ACO2 catalyses the reversible stereo-specific isomerisation of citrate to isocitrate via cis-aconitate in a two-step reaction. To achieve this, ACO2 employs a dehydration–hydration mechanism. First, citrate is protonated at position C3 before deprotonation occurs at position C2 to form cis-aconitate (dehydration). Second, cis-aconitate flips 180° to allow the dehydration and hydration steps to occur on opposite faces of the intermediate, ensuring that the stereochemistry (2R, 3S) of the reaction is correct. Subsequently, cis-aconitate is converted to isocitrate (rehydration). The third step, catalysed by IDH, requires $NAD(P)^+$ and results in the oxidation of isocitrate to oxalosuccinate, generating NAD(P)H. Oxalosuccinate is subsequently decarboxylated to form the five-carbon α-ketoglutarate (α-KG) and CO_2. In the fourth step, α-KGDH catalyses the oxidative decarboxylation of α-KG to form succinyl-CoA, NADH and CO_2. Succinyl-CoA synthetase then catalyses the hydrolysis of succinyl-CoA, coupled to the condensation of GDP and inorganic phosphate (P_i) or of ADP and P_i to form succinate and either GTP or ATP, respectively, which are energetically equivalent. As such, the reaction catalysed by α-KGDH is referred to as substrate-level phosphorylation and constitutes the fifth step in the Krebs cycle. In the sixth step, SDH, also complex II of the ETC, catalyses the oxidation of succinate to fumarate. SDH, which uses FAD as a prosthetic group, generates $FADH_2$ from the oxidation of succinate. The two electrons carried by $FADH_2$ are subsequently used to reduce ubiquinone (Q) to ubiquinol (QH_2). In the seventh step, FH catalyses the hydration of the α,β-unsaturated carbonyl compound fumarate to form L-malate. The final step in the cycle is catalysed by MDH and results in the oxidation of malate to generate NADH. This step also regenerates oxaloacetate, which can then be re-used by CS to enable continuation of the cycle.

Intriguingly, Krebs cycle–derived metabolites have also been attributed both signalling functions and impact on multiple processes critical for immune cell activation and cellular transformation. The biological targets of succinate, itaconate, fumarate, 2-hydroxyglutarate (2-HG) and acetyl-CoA are of direct relevance to immunity and/or tumorigenesis, as they inhibit specific enzymes or drive covalent modifications of proteins to alter their functions. A common outcome of these processes is epigenome remodelling and altered expression of specific sets of genes that can govern both immune cell effector functions and tumour deveopment. The complexities of metabolic rewiring may ultimately lead to new therapeutic modalities that could have a major impact on the pathogenesis

[1]School of Biochemistry and Immunology, Trinity Biomedical Sciences Institute, Trinity College Dublin, Dublin, Ireland. [2]MRC Mitochondrial Biology Unit, University of Cambridge, Cambridge, UK. [3]MRC Cancer Unit, University of Cambridge, Hutchison/MRC Research Centre, Cambridge, UK. [4]Department of Cancer Biology, Dana-Farber Cancer Institute, Harvard Medical School, Boston, MA, USA. [5]Department of Cell Biology, Harvard Medical School, Boston, MA, USA. *e-mail: laoneill@tcd.ie

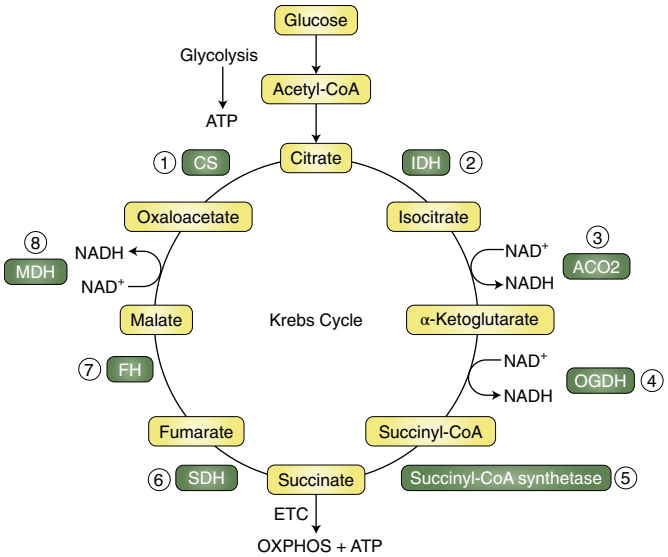

Fig. 1 | The Krebs cycle. The Krebs cycle is a metabolic pathway operating in the mitochondrial matrix of all aerobic organisms. Breakdown of nutrients, such as glucose, generates acetyl-CoA, which can then be funnelled into this pathway. For a full cycle to be completed, a series of ten enzymatic reactions are required. These reactions are catalysed by the mitochondrial enzymes CS (1), IDH (2), ACO2 (3), α-KG dehydrogenase (OGDH) (4), succinyl-CoA synthetase (5), SDH (6), FH (7) and MDH (8). The primary function of the TCA cycle is to generate reducing equivalents, such as NADH and $FADH_2$ (produced by SDH). NADH and $FADH_2$ can then transfer electrons to the ETC to drive OXPHOS and the production of ATP via F_oF_1-ATP synthase.

of multiple diseases previously linked to metabolic reprogramming. The field is on the cusp of a major paradigm shift in the understanding of how intracellular metabolic changes lead to disease, presenting the exciting prospect of new approaches to complement or even replace current therapeutic approaches for several diseases with an unmet therapeutic need. This review will discuss the extensive evidence for the non-metabolic functions of succinate, itaconate, fumarate, 2-HG and acetyl-CoA, focusing on immune cell signalling and carcinogenesis. Finally, the therapeutic opportunities that have arisen or that may arise from understanding these signalling pathways will also be examined.

Succinate as a signal in macrophages and tumour cells

As mentioned, succinate is generated in the mitochondrial matrix in a reversible three-step reaction catalysed by the TCA cycle enzyme succinyl-CoA synthetase, with concomitant production of a high-energy nucleoside triphosphate. Recent data indicate that succinate is a pro-inflammatory metabolite that accumulates in macrophages treated with lipopolysaccharide (LPS) and interferon-γ (IFN-γ)[1,2]. As depicted in Fig. 2, succinate has been shown to act through several pathways to exert its inflammatory effects: through generation of mitochondrial reactive oxygen species (mtROS), by activation of hypoxia-inducible factor-1α (HIF-1α; discussed below) and through ligation of the G-protein-coupled receptor succinate receptor 1 (SUCNR1).

Succinate and SUCNR1-mediated signalling in immunity. In 2004, He et al.[3] made an important discovery when they found that the Krebs cycle–derived metabolites succinate and α-KG acted as ligands for the orphan G-protein-coupled receptors GPR91 (now known as SUCNR1) and GPR99 (now known as OXRG1), respectively. The authors demonstrated that ligation of SUCNR1 by succinate acted as an important hypertensive agent by modulating the renin–angiotensin system, independently of its bioenergetic role[3]. Since this seminal discovery, important roles for SUCNR1 in regulating numerous physiological processes implicated in health and disease have emerged, notably in the prevention of age-related macular degeneration (AMD)[4] and immune cell function[5]. SUCNR1 is highly expressed in kidney, liver, spleen and small intestine[3], and on dendritic cells[5], and ligand binding induces G_i and G_q signalling cascades[3]. SUCNR1 ligation on dendritic cells or the U937 macrophage cell line induces cell migration, suggesting that succinate can act as a chemokine[5]. Extracellular succinate addition also acts in synergy with toll-like receptor (TLR) ligands to increase tumour necrosis factor-α (TNF-α) and interleukin-1β (IL-1β) expression[5] and increases the capacity of dendritic cells to act as antigen-presenting cells. Priming of dendritic cells with succinate and antigen simultaneously elevates antigen-specific T cell activation, increasing TNF-α and IFN-γ production from these cells[5]. SUCNR1 is also expressed on tuft cells in the intestine, where its signalling promotes type 2 immunity to certain infectious agents, such as tritrichomonad protists, and drives small intestine remodelling via a tuft cell–ILC2 circuit[6–8].

Littlewood-Evans et al.[9] have demonstrated that succinate can act in an autocrine and paracrine manner to increase IL-1β production in macrophages. Following LPS treatment, both intracellular succinate levels and the cell surface expression of SUCNR1 are increased. Interestingly, endogenously generated succinate is released through an undefined mechanism and binds to SUCNR1 on the same or nearby SUCNR1-expressing cells to amplify IL-1β production. IL-1β itself further enhances SUCNR1 expression, fuelling this cycle of cytokine production. Macrophage activation and IL-1β production are decreased in the absence of SUCNR1 both following LPS treatment and in a model of antigen-induced arthritis. This correlates with an observed increase in succinate in the synovial fluid from patients with rheumatoid arthritis (RA), suggesting that chronically elevated succinate is pathological in this setting[10]. Intriguingly, HIF-1α expression is also increased in synovial joints of patients with RA[11], suggesting that succinate may act through two routes to increase inflammation in RA: SUCNR1 and HIF-1α.

Tissue and circulating succinate are also elevated in other chronic inflammatory settings, such as models of diet-induced obesity[12]. It has been suggested that exposure of adipocytes to hypoxia and hyperglycaemia (for example, during obesity) induces succinate release from adipose tissue in mice[13], and this is associated with macrophage infiltration into the adipose tissue. The intracellular pathway driving succinate accumulation in these cells or its release from these cells is unclear. In the absence of SUCNR1, a reduction in absolute numbers of macrophages, but not inflammatory signalling, was observed, and this resulted in an improvement in adipose tissue inflammation and glucose tolerance in mice following high-fat diet feeding. In contrast to previous reports, the authors observed no effect of succinate alone on macrophage infiltration, suggesting that additional signals present in the hypoxic environment may also be required for succinate-induced chemotaxis. More recently, succinate has been implicated as a systemic signal for thermogenesis. It was demonstrated that brown adipocytes possess a unique capacity to sequester extracellular succinate, which serves to increase UCP1 activity as a consequence of elevated mtROS[14]. Interestingly, the authors demonstrate a role for shivering muscle in the generation of succinate following cold exposure. Succinate enters the circulation and is sequestered by the brown adipose tissue. Muscle has been demonstrated to produce succinate in other contexts too[15]. For example, it has been demonstrated that succinate is elevated in the plasma of marathon runners, and it is possible that muscle may act as a source tissue[15].

Succinate has also been implicated in the pathogenesis of neuroinflammation. In a mouse model of multiple sclerosis (MS), transplantation of neural stem cells (NSCs) reduced succinate levels in

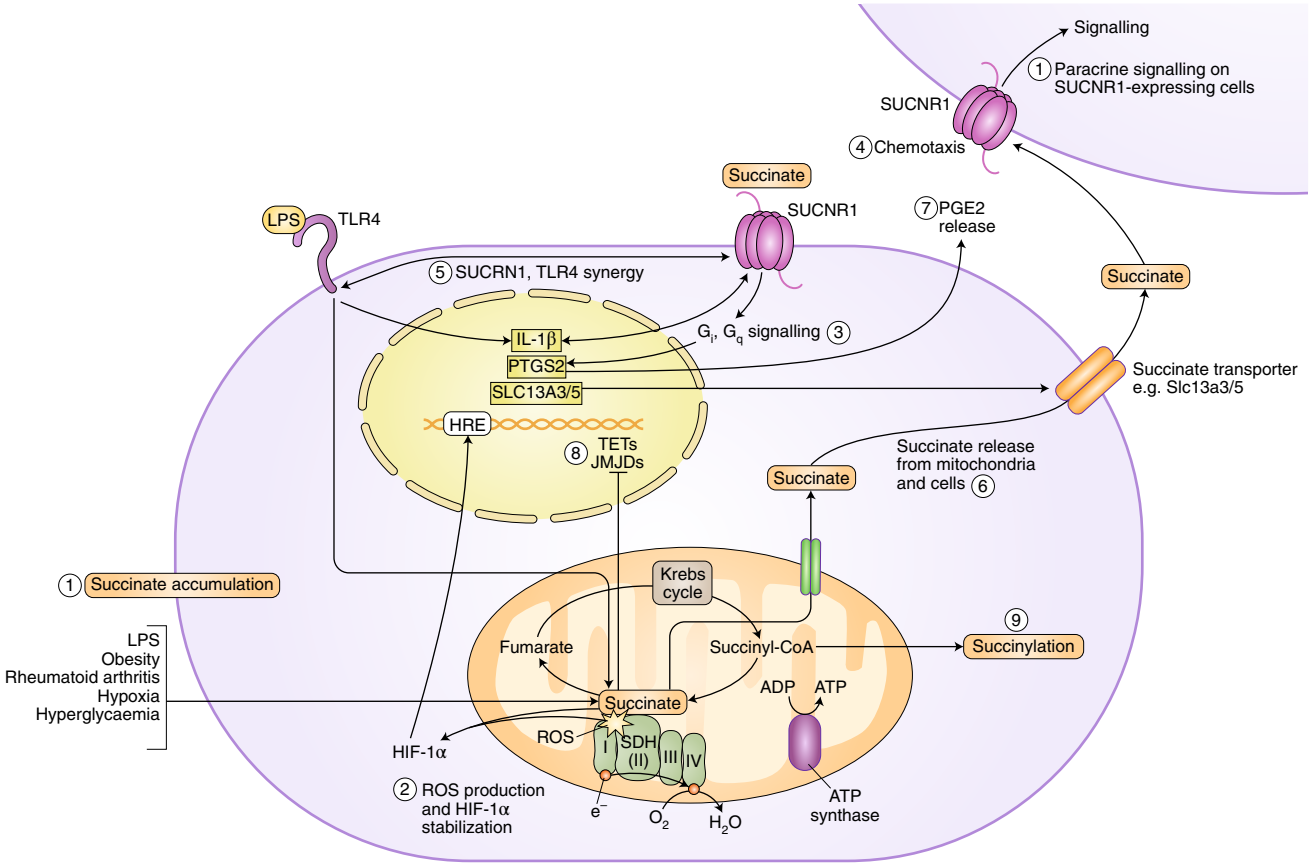

Fig. 2 | The diverse signalling roles of succinate. Succinate levels are elevated in response to LPS stimulation, in synovial fluids from patients with RA, in the circulation in models of diet-induced obesity and in adipose tissue in response to hypoxia and hyperglycaemia (1). Succinate oxidation (as well as direct product inhibition) and ROS HIF-1α, which binds to the HRE in the IL-1β promoter (2). Succinate is the ligand for the G-protein-coupled SUCNR1. Ligand binding induces G_i and G_q signalling cascades (3). SUCNR1 ligation on dendritic cells induces cell migration (4) and acts in synergy with TLR ligands to increase IL-1β expression, and IL-1β and LPS further enhance SUCNR1 expression (5). Endogenously generated succinate is released, for example via SLC13a3 and SLC13a5 (SLC13a3/5) in NSCs, and binds to SUCNR1 on the same or nearby SUCNR1-expressing cells (6). Activation of SUCNR1 on NSCs induces the secretion of anti-inflammatory prostaglandin E2 (7). Succinate regulates the activity of the JMJDs and the TET family of 5mC hydroxylases, which play a role in histone and DNA demethylation, respectively, and can thereby remodel the epigenome (8). Another consequence of succinate accumulation is the modification of proteins by lysine succinylation (9).

the cerebrospinal fluid and thereby decreased infiltration of damaging macrophages and microglial cells[16]. Mechanistically, ligation of SUCNR1 on the surface of NSCs upregulates the expression of the dicarboxylate co-transporter SLC13a3 and SLC13a5, correlating with increased uptake by the NSCs and thereby scavenging succinate away from pro-inflammatory immune cells. Activation of SUCNR1 on NSCs also induces the secretion of anti-inflammatory prostaglandin E2, further contributing to their anti-inflammatory phenotype.

On the basis of these data, it may be predicted that SUCNR1 antagonists will be protective in settings where inflammation is exacerbated, such as graft rejection or autoimmunity. A selective antagonist for human and rat SUCNR1 has been shown to be protective in hypertension[17]. Similarly, potent agonists have recently been synthesised, which will deepen our understanding of the signalling pathways affected by this important receptor[18]. Whether these compounds will have therapeutic potential remains to be explored.

HIF-1 and succinate in inflammation and tumorigenesis. Another mechanism by which succinate exerts its signalling properties involves the transcription factor HIF-1, as shown in Fig. 2. HIF-1 is a transcriptional regulator, central in the response to hypoxia[19]. HIF-1 was first discovered by Semenza and Wang[20] in 1992, and it was found to promote erythropoiesis by binding the erythropoietin gene enhancer. HIF-1 transcriptionally directs a switch in metabolism from oxidative phosphorylation to glycolysis, which allows rapid ATP production without the need for oxygen[21]. It is well-established that HIF-1 activity promotes tumour progression. Tumour environments are often oxygen-deprived, and such hypoxic conditions lead to activation of HIF-1. HIF-1 binds to hypoxia response elements (HREs) in target genes and increases the expression of numerous glycolytic enzymes and glucose transporter-1 (GLUT1) and GLUT3. It also targets genes involved in erythropoiesis, angiogenesis and proliferation.

HIF-1 is composed of a β-subunit that is constitutively active and an oxygen-sensitive α-subunit. HIF-1α is tightly regulated by prolyl hydroxylases (PHD), a class of α-KG-dependent dioxygenases (α-KGDDs) that convert α-KG to succinate and use molecular oxygen to hydroxylate HIF-1α. In the presence of oxygen, conserved proline residues in the HIF-1α subunit are hydroxylated by hypoxia-inducible factor prolyl hydroxylase 1 (PHD1)–PHD3 (ref. [22]). Hydroxylation provides a recognition site for the binding of Von Hippel-Lindau (VHL) E3 ubiquitin ligase, which ubiquitinates HIF-1α and subsequently targets it for proteasomal degradation[23]. This degradation is prevented in conditions of limited oxygen, allowing for HIF-1α translocation to the nucleus, dimerization with HIF-1β and binding of target genes[19].

HIF-1α is vital for the switch to glycolysis observed in M1 macrophages and dendritic cells following stimulation. It upregulates the expression of several glycolytic genes and aids in the switch to glycolysis by maintaining levels of nicotinamide adenine dinucleotide (NAD^+), a vital co-factor in the glycolytic pathway. It does so by increasing the expression of lactate dehydrogenase (LDH), which reduces pyruvate to lactate and consequently generates NAD^+ that will be reduced to NADH by an active glycolytic pathway. It also increases expression of pyruvate dehydrogenase kinase (PDK), which phosphorylates and inhibits pyruvate dehydrogenase (PDH); this limits production of acetyl CoA, which enters the Krebs cycle[24].

While the primary role of HIF-1α is to induce a switch to glycolysis, which is likely to be important at sites of inflammation where oxygen levels are low[19], hypoxia is not essential for HIF-1α activation in immune cells. Ligation of TLR4 by LPS can transcriptionally induce HIF-1α, as well as a range of HIF-1α target genes under hypoxic and also normoxic conditions[2], in a nuclear factor-kappa B (NF-κB)-dependent manner[25].

LPS can also stabilize HIF-1α indirectly by increasing succinate levels. Evidence for the role of succinate in HIF-1α stabilization first came from cancer studies. An elevation in succinate has been reported in rare hereditary tumours, such as paragangliomas (PGLs) and gastrointestinal stromal tumours (GISTs), that possess mutations in the genes encoding SDH[26]. The PHDs generate succinate from α-KG, and importantly succinate (acting via product inhibition) will inhibit the PHDs and stabilize HIF-1α (ref. [27]). An additional mechanism by which succinate accumulates in tumours involves the mitochondrial chaperone tumour necrosis factor receptor–associated protein 1 (TRAP1), which is highly expressed in many tumours[28]. TRAP1 decreases SDH activity, resulting in succinate accumulation. More recently, however, it has been demonstrated that succinate accumulation in tumours promotes angiogenesis via upregulation of vascular endothelial growth factor (VEGF) in a HIF-1α-independent manner. Succinate instead activates extracellular regulated kinase 1 (ERK1) and ERK2 and signal transducer and activator of transcription 3 (STAT3) in a SUCNR1-dependent manner[29].

Analogous to tumours, LPS-induced succinate was shown to both directly and indirectly (via ROS) inhibit PHD activity in macrophages, resulting in stabilization of HIF-1α (ref. [2]). Like succinate, ROS are critical regulators of HIF-1α activity. ROS can stabilize HIF-1α by inducing non-enzymatic decarboxylation of α-KG[30] and by oxidizing iron (Fe^{2+}) to Fe^{3+}, two required PHD co-factors[31]. ROS also impair the activity of factor inhibiting HIF (FIH), another member of the α-KGDD family[31], which hydroxylates an asparagine residue in the carboxy terminus of HIF-1α, resulting in a decrease in transcriptional activity. It should be noted that hypoxia and ischaemia, as well as decreased oxidative phosphorylation, drive succinate accumulation in the mitochondrial matrix[32,33]. As such, following ischaemia or hypoxia, or when SDH operation is affected by genetic aberrations (such as tumours harbouring SDH mutations), elevated succinate can potentiate the hypoxic phenotype by promoting further HIF-1α stabilization.

LPS-induced HIF-1α expression not only promotes glycolysis but is also directly pro-inflammatory. The finding that hypoxia was capable of inducing IL-1β production in astrocytes in an NF-κB-independent, HIF-1α-dependent manner[34] led to the discovery of an HRE in the IL-1β promoter[2]. The sustained induction of IL-1β in response to LPS was shown to require HIF-1α and to occur under normoxic conditions. The loss of HIF-1α in macrophages decreased TNF-α, IL-1β and IL-1α production but did not affect production of the anti-inflammatory cytokines IL-4 or IL-10 (ref. [35]). A critical consequence of succinate elevation in response to LPS is the potentiation of inflammatory signalling and, in particular, IL-1β, in a HIF-1α-dependent manner[2]. This requires both succinate oxidation by the enzyme SDH and an increase in mitochondrial membrane potential. These factors combine to drive pro-inflammatory ROS production, HIF-1α stabilization and increased IL-1β following LPS treatment[2,36]. Succinate reciprocally decreases anti-inflammatory cytokines, such as IL-10 and IL-1RA, but whether this is HIF-1α-dependent remains to be explored[36]. Limiting succinate oxidation with the prodrug dimethylmalonate (DMM), which releases malonate, a potent SDH inhibitor, profoundly represses LPS-induced HIF-1α, IL-1β and ROS and boosts IL-10 and IL-1RA. ROS production in this setting is believed to be a result of reverse electron transport (RET) at complex I of the ETC. Supporting this, the complex I inhibitor rotenone significantly decreased LPS-induced ROS. It should be noted that if the ETC was operating in the forward direction, then rotenone would boost RET-independent ROS production. To further investigate the potential role for RET in this process, the authors[36] examined macrophages from mice expressing an alternative oxidase (AOX) from *Ciona intestinalis*[37]. AOX provides a pathway to oxidise excess electrons that build up in the Q pool (as a result of succinate accumulation, for example) that would otherwise contribute to mtROS production. AOX expression in macrophages also impaired LPS-induced ROS production. These data suggest that complex I of the ETC is an important site of ROS production in macrophages and that such ROS production may depend on RET. In other conditions, complex I can generate significant ROS when operating in the forward direction (dependent on the NADH/NAD^+ ratio). Deletion of a subunit of complex I, NDUFS4, is sufficient to generate substantial ROS in macrophages, most likely as a result of impaired electron shuttling down the ETC and thereby enhanced ROS production, which will in turn promote inflammation[38]. This is unlikely to be RET-dependent ROS production as the membrane potential, which much be significantly elevated to drive ROS via RET, is decreased in NDUFS4-deficient macrophages[39]. Furthermore, these studies were performed in the absence of a stimulus like LPS, which is known to drive Q pool reduction (another requirement for RET). These data suggest that complex I can generate ROS through a variety of mechanisms in macrophages to promote inflammation.

The relationship between HIF-1α and succinate in macrophages has been extensively studied; however, this relationship is less well explored in other cell types, particularly adaptive immune cells, such as $CD4^+$ T cell subsets. The initial observation that LPS drives profound succinate accumulation in macrophages may account for the innate immune cell bias. Whether other stimuli are capable of driving a training phenotype similar to that of β-glucan warrants further investigation.

Succinate regulates the epigenome and innate immune memory. α-KG and succinate can regulate the activity of other members of the α-KGDD family of enzymes, in particular those involved in the regulation of histone and DNA demethylation, the α-KG-dependent Jumonji-C-domain-containing histone demethylases (JMJDs) and the ten eleven translocation (TET) family of 5mC hydroxylases, which play a role in DNA demethylation. Like the PHDs, these enzymes are subject to product inhibition by succinate, and therefore, their activity is dependent on the ratio of α-KG to succinate[40]. In this way, succinate and α-KG can remodel the epigenome. Methylation marks on histones can both positively and negatively influence gene expression, while DNA methylation is typically associated with an open chromatin state and active transcription; therefore, epigenetic changes can alter gene function, acting as on/off switches. Importantly, these changes in gene expression are heritable and appear to be intimately linked to the metabolic state of cells[41]. Succinate, fumarate and α-KG may also indirectly regulate the activity of histone demethylases through their effects on HIF-1α, which can bind to and induce the expression of certain histone demethylases, including JMJD1A, JMJD2C and JMJD2B, which are histone 3 lysine 9 (H3K9) demethylases[41].

Another critical consequence of altering the epigenome is the newly emerging concept of innate immune training. It has been recently revealed that innate immune cells demonstrate a form of immunological memory and have the ability to respond more robustly to a second potentially unrelated stimulation[42]. At a molecular level, this involves epigenetic modifications, leading to stronger gene transcription upon re-stimulation as opposed to gene recombination that occurs in the adaptive memory response. Epigenetic marks can persist after the stimulus that induced them has resolved and are therefore stable signals that can be sustained for days or even longer. Such innate immune training has been demonstrated to occur after training of human monocytes in vitro with β-glucan, a component of *Candida albicans*, and subsequent treatment with LPS; following this, elevated cytokine production was observed upon re-stimulation with LPS[43]. Interestingly, in addition to potentiating cytokine production in response to LPS, training with β-glucan has been shown to induce epigenetic upregulation of genes involved in glycolysis, such as HIF-1α, hexokinase (HK) and pyruvate kinase, and to increase succinate levels[44]. HIF-1α reciprocally enhanced trained immunity in response to β-glucan. Inhibition of HIF-1α with ascorbate impaired the training effect induced by β-glucan and decreased TNF-α production in these cells, demonstrating the importance of HIF-1α for enhanced immunity. Training with β-glucan was shown to be protective against *Staphylococcus aureus* infection, and this effect was abrogated in HIF-1α-deficient mice. As shown in Fig. 2, succinate and other metabolites may therefore be capable of influencing the epigenome through effects on HIF-1α and perhaps subsequently on IL-1β, which has also been demonstrated to induce trained immunity in monocytes[44]. Whether other stimuli are capable of driving a similar training phenotype as β-glucan does warrants further investigation.

Succinylation as a covalent modification. Another consequence of dysregulated succinate metabolism is the recently identified post-translational modification (PTM), lysine succinylation. This modification is caused by the accumulation of succinyl-CoA, which can result from SDH inhibition and succinate accumulation[39]. Treatment of mouse fibroblasts with the SDH inhibitor 3-nitropropionic acid increases succinylation[45]. This modification induces a 100-Da change in mass, comparable to that of two well-established lysine modifications: acetylation and dimethylation. Importantly, succinylation masks the positive charge on lysine, likely resulting in a significant conformational change in the protein. Western blot analysis of whole-cell lysates revealed that this modification is evolutionarily conserved and that substrates are numerous[46], including proteins involved in cellular metabolism[45]. Succinyl-proteome profiling in bacteria[47], plants[48,49] and HeLa cells all point toward metabolic pathways as key targets for this PTM. A study in yeast identifies histones as targets of this PTM; mutation of succinylation sites was found to reduce cell viability[50].

The enzyme responsible for succinylation is yet to be identified, and indeed it is possible that this reaction occurs non-enzymatically by direct reaction between succinyl CoA and the modified protein[48]. However, sirtuin 5 (SIRT5), which was previously thought to function primarily as a deacetylase, has been shown to have potent desuccinylase activity[51]. Interestingly, SDHA is a target of lysine succinylation. SIRT5-deficient mice had significantly increased SDH activity, suggesting that succinylation positively regulates its activity[45]. This PTM appears to be LPS-inducible. LPS decreases SIRT5 expression in macrophages and increases protein succinylation[2].

The α-ketoglutarate dehydrogenase complex (KGDHC) has also been suggested to mediate succinylation in an α-KG-dependent manner. Inhibition of KGDHC reduces succinylation of proteins in neuronal cells[52]. The authors identify the pyruvate dehydrogenase complex (PDHC), IDH and FH as targets of succinylation, with succinylation decreasing IDH activity and increasing FH activity[53].

Succinylation can also modulate macrophage function. Succinylation of Lys311 of pyruvate kinase M2 (PKM2), a key glycolytic enzyme required for the shift to glycolysis in activated macrophages, was shown to limit its activity by promoting its tetramer-to-dimer transition[54]. The authors demonstrate that SIRT5 desuccinylates and activates PKM2, which limits IL-1β production. Conversely, SIRT5-deficient mice exhibit hypersuccinylation and increased IL-1β. There are many aspects of this PTM that require further investigation. The breadth of the targets of succinylation and indeed the enzyme catalysing this PTM remain to be determined, as well as precisely how this PTM alters protein function.

These data demonstrate that succinate can have a profound impact on cellular function, acting both intracellularly via ROS, HIF-1α and succinylation and histone and DNA modification and extracellularly via SUCNR1.

Itaconate as a novel anti-inflammatory metabolite

One of the most striking examples of a Krebs cycle–derived metabolite acting as a signal in immunity is itaconate[1,55–58]. This previously unidentified dicarboxylic acid was first discovered in 1836 as a product of citric acid distillation by the Swiss chemist Samuel Baup[59]. In 1840, it was independently synthesised by the decarboxylation of cis-aconitate, resulting in the introduction of its current name, itaconic acid, an anagram of aconitic acid[59]. While itaconic acid has long been used in the industrial arena for the synthesis of various polymers, the first (unwittingly) relevant discovery regarding the role of itaconate in mammalian biology came in 1995 when Lee and colleagues[59,60] cloned immunoresponsive gene 1 (*Irg1*), a gene potently upregulated in LPS-activated peritoneal macrophages. However, it was not until 2011 that the production of itaconic acid in a mammalian system, and the first suggestion that it may play a role in cellular immunity, was uncovered[61]. Intriguingly, it was described in two separate immune contexts, both in the lungs of *Mycobacterium tuberculosis* (Mtb)-infected mice[61] and secreted into the supernatant of LPS-activated RAW264.7 cells (a macrophage cell line)[62]. A key discovery in the field of itaconate biology followed when Michelucci and colleagues[63] identified immunoresponsive gene 1 (IRG1) as the enzyme responsible for itaconate synthesis in both mouse and human macrophages. This subsequently led to the renaming of IRG1 to cis-aconitate decarboxylase (CAD). Although a role for itaconate as an anti-bactericidal agent has previously been suggested (see refs. [63–66]), more recently, itaconate has been found to be an important immunomodulatory metabolite[56,67–69].

Itaconate is an endogenous SDH inhibitor. Despite the known anti-bacterial function of itaconate, its role in regulating macrophage function remained virtually unexplored until 2016. Since 2016, several key studies have uncovered a role for itaconate as a crucial anti-inflammatory metabolite that negatively regulates the inflammatory response and cytokine production[56,67–69], as shown in Fig. 3. Importantly, Lampropoulou et al.[56] first demonstrated that bone-marrow derived macrophages (BMDMs) activated by LPS and pre-treated with a cell-permeable methyl ester derivative of itaconate, dimethyl itaconate (DI), exhibited potent inhibition of pro-inflammatory mediators, including nitric oxide (NO), ROS and the cytokines IL-6, IL-12p70 and IL-1β. Furthermore, *Irg1*-deficient BMDMs, in which genetic deletion of *Irg1* completely abolished itaconate synthesis, exhibited a significant increase in the production of IL-12, IL-6 and NO and, under conditions that activate the NLRP3 inflammasome, increased IL-1β and IL-18. An increase in HIF-1α, a critical regulator of aerobic glycolysis and IL-1β in macrophages, was also observed in *Irg1*-deficient BMDMs stimulated with LPS. As such, this study was the first to highlight a role for itaconate as an anti-inflammatory metabolite.

Mechanistically, Lampropoulou et al.[56] suggested that the ability of itaconate to modulate inflammation arose from its ability to

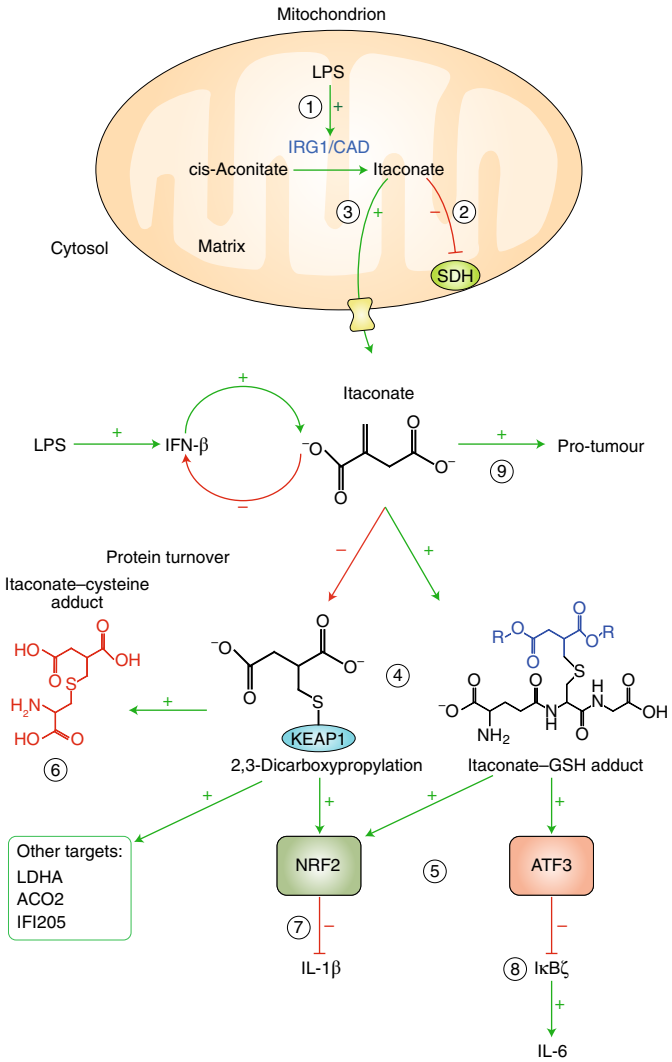

Fig. 3 | Itaconate is a thiol-reactive anti-inflammatory metabolite. In LPS-activated macrophages, mitochondrial IRG1/CAD (which requires autocrine/paracrine IFN-β signalling) synthesises itaconate from cis-aconitate (1), whereby it can inhibit SDH (2) or be exported out of the mitochondria via mitochondrial carrier proteins (3). In the cytosol, itaconate alkylates KEAP1, a novel PTM termed 2,3-dicarboxypropylation, and GSH to form an itaconate-GSH adduct, or 2,3-dicarboxypropyl-GSH (4). This in turn activates the anti-inflammatory and anti-oxidant transcription factors NRF2 and ATF3 (5). Levels of the metabolite 2,3-dicarboxypropyl cysteine (itaconate–cysteine adduct) increase, which is indicative of the turnover of 2,3-dicarboxypropylated targets (6). Activation of NRF2 acts to negatively regulate the pro-inflammatory cytokine IL-1β (7), while activation of ATF3 inhibits IκBξ and IL-6 (8). Itaconate has also been shown to boost ROS levels in certain contexts and promote tumour growth (9).

competitively inhibit SDH and succinate oxidation[56]. Intriguingly, itaconate was first shown to act as a competitive SDH inhibitor more than 60 years ago[70], which prompted speculation that it was an endogenous SDH inhibitor, akin to malonate, in macrophages. Supporting this notion, exogenous treatment of macrophages with DI and of RAW264.7 cells and A549 cells (a lung adenocarcinoma cell line) with itaconic acid were found to induce succinate accumulation, indicative of SDH inhibition[55,58]. Likewise, itaconic acid was found to competitively inhibit purified SDH[56]. Crucially, LPS-stimulated *Irg1*-deficient BMDMs displayed significantly attenuated succinate accumulation and an increased oxygen consumption rate (OCR), further supporting the role of itaconate in SDH inhibition and metabolic rewiring in macrophages[55,56]. As such, itaconate inhibition of SDH was proposed to limit inflammation by blocking the generation of ROS derived from RET at complex I, as previously discussed. Together these papers offer a molecular explanation for succinate accumulation[1], and the breakpoint observed in the TCA cycle by Jha et al.[1], whereby isotopic tracing using U-^{13}C-glutamine showed that approximately 35% of the pool of succinate, but only 22% of malate, could be attributed to glutamine anaplerosis in BMDMs treated with LPS, suggesting inefficient succinate-to-fumarate transition at SDH.

However, it must also be noted that, compared with malonate, itaconate is a relatively weak competitive inhibitor of SDH[55,57], which raises the question as to whether any additional mechanisms could contribute to the anti-inflammatory effects of itaconate. Furthermore, DI, the itaconate derivative used in these studies, is not metabolised to itaconate intracellularly. It has also been shown that exogenous addition of ^{13}C-itaconate to RAW264.7 cells was sufficient to increase intracellular levels of unlabeled succinate (suggestive of SDH inhibition), with no evidence of cellular uptake[71]. It is possible that the observed effect of itaconic acid on succinate levels could be receptor-mediated, as posited by El Azzouny and colleagues[71], especially considering that the discovery of Krebs cycle intermediate signalling via GPCRs, such as that observed for succinate and SUCNR1 (refs. [3,71]). It is also important to note that itaconate is an α,β-unsaturated carbonyl compound, making it a potential Michael acceptor that could undergo nucleophilic attack by the thiolate ion of protein cysteine residues; as such, the methyl esterification of the proximal carboxyl group conjugated to the alkene is predicted to increase the electrophilicity of itaconate. In this way, the effects of DI could possibly be attributed to electrophilic inactivation of metabolic enzymes, as opposed to an increase in intracellular itaconate[71]. Supporting this, Lampropoulou et al.[56] reported an upregulation of genes involved in phase II conjugation, glutathione conjugation and biological oxidations from an RNA sequencing (RNA-seq) screen performed in DI-treated BMDMs.

Itaconate alkylates redox-sensitive cysteine residues. Independently, Mills et al.[68] also noted that itaconate could potentially alkylate cysteine residues to form a 2,3-dicarboxypropyl adduct, as shown in Fig. 3. As such, it was hypothesised that the anti-inflammatory effects of itaconate could be due to alkylation of the key redox-sensing protein kelch-like ECH-associated protein 1 (KEAP1) and activation of the anti-inflammatory and anti-oxidant transcription factor nuclear factor, erythroid 2 like 2 (NFE2L2, also known as NRF2)[68,72]. DI was first employed as an experimental tool and was shown to potently induce NRF2 and several NRF2 target genes in unstimulated and LPS-activated BMDMs. This strongly suggested that DI was indeed a thiol-reactive metabolite; however, esterification on the 1-position would render it an activated Michael acceptor, akin to dimethyl fumarate (DMF), and this could result in rapid activation of NRF2 along with many other reactive intracellular thiols[68,73]. To overcome the limitations of DI, a new itaconate derivative, 4-octyl itaconate (4-OI), was synthesised in which the octyl ester group was located on the carboxyl group distal to the alkene. Importantly, itaconate and 4-OI were shown to have similar thiol-reactivity profiles, whereas DI was shown to significantly and acutely deplete glutathione (GSH) levels, confirming that it was indeed an activated Michael acceptor. Furthermore, the ability of DI to induce NQO1 activity (encoded by a prototypical NRF2 target gene) was diminished when pre-incubated with GSH; however, the ability of 4-OI to induce NQO1 activity remained unaffected. These findings suggest that 4-OI represents a suitable cell-permeable itaconate surrogate for probing the physiological function of itaconate[68]. Importantly, pre-treatment of unstimulated and LPS-activated

macrophages with 4-OI still resulted in a significant increase expression of in NRF2 and NRF2 target genes, namely Heme oxygenase 1 (*Hmox1*), suggesting that itaconate is an endogenous signal governing NRF2 activation. This finding was corroborated by Bambouskova et al.[67], who demonstrated a decrease in LPS-induced NRF2 stabilization in *Irg1*-deficient BMDMs, confirming that endogenous itaconate stabilises NRF2.

Further supporting the hypothesis that itaconate is a thiol-reactive metabolite, a significant increase in the levels of the metabolite 2,3-dicarboxypropyl cysteine (itaconate-cysteine adduct), akin to the breakdown product of fumarate-mediated protein succination *S*-(2-succino)cysteine (2SC), was observed in LPS-activated BMDMs[68]. Mechanistically, 4-OI has been shown to alkylate KEAP1 on several cysteine residues, including cysteine 151 (C151), a principal redox-sensing cysteine important for activation of NRF2 (refs. [68,74]). Furthermore, through a quantitative unbiased proteomic screen performed in both LPS- (which will drive intracellular itaconate accumulation) and 4-OI-treated macrophages, several metabolic and inflammatory proteins were found to be alkylated, representing the first demonstration of this novel post-translational modification (PTM) termed 2,3-dicarboxypropylation. Pre-treatment of LPS-activated BMDMs with 4-OI also resulted in a significant attenuation of IL-1β levels, an effect that was largely abrogated in *Nrf2*-deficent macrophages. It should also be noted that NRF2 can limit LPS-induced inflammatory gene transcription in a redox-independent manner through direct ligation of these genes and inhibition of RNA polymerase II recruitment[72]. Whether itaconate can mediate cytokine inhibition in this manner remains to be explored. 4-OI was also shown to be protective in an LPS lethality model in vivo, prolonging survival, improving body temperature regulation and decreasing pro-inflammatory cytokine production. In addition, a novel negative feedback loop between IRG1, itaconate and IFN-β was elucidated, whereby the induction of *Irg1* and itaconate were largely dependent on autocrine–paracrine type I IFN signalling[68]. Intriguingly, pre-treatment of LPS-activated macrophages with 4-OI resulted in a significant attenuation of IFN-β levels and IFN-stimulated genes (ISGs), such as *Isg20*, an effect that was at least partially dependent on NRF2. As such, this study confirmed itaconate as an anti-inflammatory metabolite and provided a unique insight into its mechanism of action with the discovery of a novel PTM. Further work is required to understand the scope of this PTM and its effect on protein function.

In addition to NRF2 regulation, a NF-κB inhibitor zeta-activating transcription factor 3 (IκBξ–ATF3) inflammatory axis has recently emerged as a target of itaconate and its more electrophilic derivatives[67]. Bambouskova and colleagues (2018) demonstrated that DI could induce electrophilic stress and NRF2 expression in macrophages via depletion of intracellular GSH to form a DI–GSH adduct, akin to 2,3-dicarboxypropylation, as previously discussed. Interestingly, DI is reported to selectively inhibit LPS-induced IL-6 while TNF-α levels remain unaffected, an effect shown to be mediated through inhibition of IκBξ the major transcription factor governing secondary transcriptional responses to TLR activation[67]. Mechanistically, inhibition of IκBξ by DI was shown to be mediated by activation of the transcription factor ATF3 and occurred at the level of *Nfkbiz* translation, as assessed by eIF2α phosphorylation, in a NRF2-independent manner.

The use of itaconate ester derivatives as endogenous itaconate mimics poses limitations due to varying electrophilicities, depending on whether the ester group lies on the carboxyl group proximal or distal to the methylene. To assess this, Bambouskova et al.[67] synthesised 1-ethyl itaconate (1EI) and 4-ethyl itaconate (4EI) and tested their effects on IκBξ. The authors demonstrate that 1EI (an activated Michael acceptor) could inhibit IκBξ; however, 4EI (which has similar reactivity to endogenous itaconate) could not inhibit IκBξ unless GSH synthesis was inhibited by buthionine sulfoximine (BSO). This highlights the importance of acute electrophilic stress that is required to induce this novel pathway. To determine the endogenous relevance of itaconate to the IκBξ–ATF3 inflammatory axis, the authors utilised *Irg1*-deficient macrophages; however, no differences were observed in IκBξ levels between *Irg1*$^{-/-}$ and wild-type macrophages stimulated with LPS. Even so, the authors posited that elevated itaconate levels may affect the induction of IκBξ in LPS-tolerised macrophages. Although the induction of IκBξ was much lower in LPS-tolerised macrophages, there was an increase in *Irg1*-deficient macrophages, suggesting that at later time points when itaconate has built up to sufficient levels (>18 h), it may induce low levels of electrophilic stress by modifying GSH, which subsequently regulates the tolerisation process[67]. As such, a unique link between electrophilic stress and the IκBξ–ATF3 inflammatory axis was uncovered that may be exploited for therapeutic gain.

A role for IRG1 and itaconate in the tolerisation process and as a negative regulator of inflammation is supported by the finding that IRG1 suppresses the production of the pro-inflammatory cytokines TNF-α, IL-6 and IFN-β in LPS-tolerised BMDMs[75]. Li et al.[75] attributed the effect of IRG1 on cytokine production to ROS-mediated induction of A20, a negative regulator of TLR signalling. Supplementation of ROS in *Irg1*-deficient BMDMs increased A20 expression and abolished the break of endotoxin tolerance. More recently, IRG1 was also found to be significantly increased in A20-deficient macrophages, which suggests an interesting feedback loop may exist between IRG1 and A20 expression[76]. Intriguingly, Li et al.[75] also observed increased IFN-β and IRF3 signalling in LPS-tolerised, *Irg1*-silenced macrophages, supporting the existence of a negative feedback loop between IRG1, itaconate and IFN-β, as previously mentioned. IRG1 has also been shown to mediate the immunomodulatory effects of CO-releasing molecule 2 (CORM2)-induced HMOX1 on TNF-α production in both LPS-activated macrophages and in a murine endotoxin shock model[77], and it also appears to play a major role in embryo implantation in the womb, a process thought to require immunosuppression[78–80]. More recently, an important role for myeloid-derived IRG1 (and presumably itaconate) in Mtb infection was uncovered. Nair et al.[69] convincingly demonstrated an increase in pro-inflammatory cytokine production, including IL-6 and IL-1β, in Mtb-infected *Irg1*-deficent mice; this effect was independent of its ability to act as an anti-bactericidal agent. Interestingly, IRG1 was shown to specifically impair neutrophil recruitment to the lungs, curtailing excessive lung inflammation and pathology—an effect thought to be a consequence of itaconate-mediated transcriptional regulation of the inflammatory response. These data suggest that itaconate may dampen the immune response of Mtb-infected mice to limit immunopathology.

Exploration of the role for itaconate in immune cell activation is still in its infancy, and the profound levels to which it is produced in macrophages suggest that it is likely to be central to macrophage function. Further work to decipher its potentially diverse roles and whether it has important signalling functions outside macrophage biology are ongoing

Itaconate in macrophage–tumour crosstalk. Most recently, an intriguing study in peritoneal tumours (B16 melanoma and ID8 ovarian carcinoma) has demonstrated that tumour-infiltrating macrophages release itaconate, which potentiates tumour growth[81]. Itaconate was shown to boost OXPHOS and mtROS generation and subsequent MAPK activation in tumour-infiltrating macrophages (Fig. 3). The effect of itaconate on ROS production is consistent with a previous study in zebrafish macrophages, which demonstrated that IRG1 was essential for OXPHOS-driven mtROS production and bactericidal killing[82]. Furthermore, Weiss et al.[81] demonstrated that ROS production in response to itaconate regulates NRF2, suggesting that there are two mechanisms for itaconate-induced NRF2

activation: directly via KEAP1 2,3-dicarboxypropylation and indirectly via ROS production (which would then modify KEAP1). NRF2 therefore appears to be an important target for itaconate. Furthermore, IRG1 (and presumably itaconate) levels were also shown to be markedly increased in glioma tissue. This was associated with a decrease in the microRNA miR-378, which targets *Irg1*, as well as poorer overall survival and clinicopathological parameters. Overexpression of miR-378 suppressed glioma tumour growth both in vitro and in vivo, the epithelial–mesenchymal transition (EMT) and metastasis[83]. These data are consistent with previous reports demonstrating that *Irg1* acts as an oncogene, driving glioma pathogenesis[84]. As such, itaconate serves as another example of crosstalk between macrophages and tumours in the context of metabolic reprogramming.

Fumarate as a signal of the immune system and tumours

Fumarate is a Krebs cycle intermediate generated through the oxidation of succinate by SDH. It is also produced as a breakdown product of tyrosine metabolism and from the urea and purine nucleotide cycles[85]. Fumarate is subsequently converted to malate by FH, which catalyses the reversible hydration of fumarate to malate both within the Krebs cycle and in the cytosol, as shown in Fig. 4.

Fumarate regulates the epigenome and immune cell function. Fumarate has recently emerged as an important inflammatory signal in innate immune training, as outlined above[44,86]. Importantly, Arts et al.[86] demonstrated that the accumulation of fumarate in β-glucan-treated monocytes was essential for trained immunity by enhancing cytokine production upon re-stimulation with LPS. Furthermore, increased fumarate levels were shown to be driven by enhanced shunting of glutamine into the TCA cycle, otherwise referred to as glutamine anaplerosis, as ascertained by a combination of biochemical techniques and the use of the glutaminase inhibitor BPTES[87]. Fumarate is a known epigenetic regulator that exerts its modulatory effects primarily through inhibition of α-KGDDs[86,88]. To determine the role of increased fumarate levels on the epigenetic landscape, Arts et al.[86] used the cell-permeable fumaric acid ester monomethyl fumarate (MMF), which was shown to alter histone methylation similarly to β-glucan training. Furthermore, treatment with MMF augmented TNF-α and IL-6 secretion in β-glucan-trained macrophages stimulated with LPS. The authors proposed that fumarate accumulation acted to inhibit the KDM5 family of histone demethylases, which subsequently increased the levels of H3K4me3, a marker of active gene transcription, at the promoters of both *Tnf* and *Il6*, thus providing the first link between Krebs cycle rewiring and epigenetic regulation in an inflammatory context[86].

Outside of trained immunity, fumarate has previously been reported to accumulate in LPS-activated macrophages[1,2]. Using an integrated high-throughput transcriptional metabolic profiling and analysis pipeline (CoMBI-T), Jha et al.[1] uncovered the induction of an inflammatory argininosuccinate shunt, a metabolic pathway that links the Krebs cycle to the urea cycle. Induction of this pathway occurred via an increase in the expression of argininosuccinate synthase (ASS1), which catalyses the formation of argininosuccinate from aspartate, citrulline and ATP[89]. Together with the argininosuccinate lyase (ASL), ASS1 is responsible for the synthesis of the semi-essential amino acid arginine in most bodily tissues. Importantly, ASS1 also constitutes the rate-limiting step in the aspartate–argininosuccinate shunt and L-arginine biosynthesis. Considering that ASL cleaves argininosuccinate into arginine and fumarate, the authors proposed that this metabolic pathway accounted for the elevated fumarate levels observed in macrophages.

The electrophilic properties of fumarate derivatives can also regulate T cell function. Blewett et al.[90] demonstrated that dimethyl fumarate (DMF), a potent electrophile currently used to treat psoriasis and relapsing-remitting MS, but not MMF inhibited the activation of human and mouse T cells. Using a proteomic approach, the authors discovered a range of proteins that regulate T cell function and are sensitive to covalent modification by DMF, including protein kinase C θ (PKCθ). Mechanistically, DMF blocked the association of PKCθ with the costimulatory receptor CD28 and T cell activation.

More recently, Kornberg and colleagues[91,92] suggested that a potential consequence of elevated fumarate levels is negative regulation of glycolysis via succination (see below) of the active site cysteine residue (C152) in GAPDH. This suggestion arose from the observation that the cell-permeable fumarate esters DMF and MMF modify and irreversibly inhibit GAPDH enzymatic activity and aerobic glycolysis in peripheral blood mononuclear cells (PBMCs) from mice and patients with MS treated with DMF[92]. Induction of aerobic glycolysis is a key marker of activated immune cells and represents an important phenotypic switch to facilitate proliferation and immune cell effector functions. Two pro-inflammatory T cell subsets implicated in the pathogenesis of multiple sclerosis (MS), T helper 1 (T_H1) and T_H17 cells, rely heavily on aerobic glycolysis, and treatment with DMF or MMF inhibited their development in vitro, as previously reported[92–95]. Importantly, inhibition

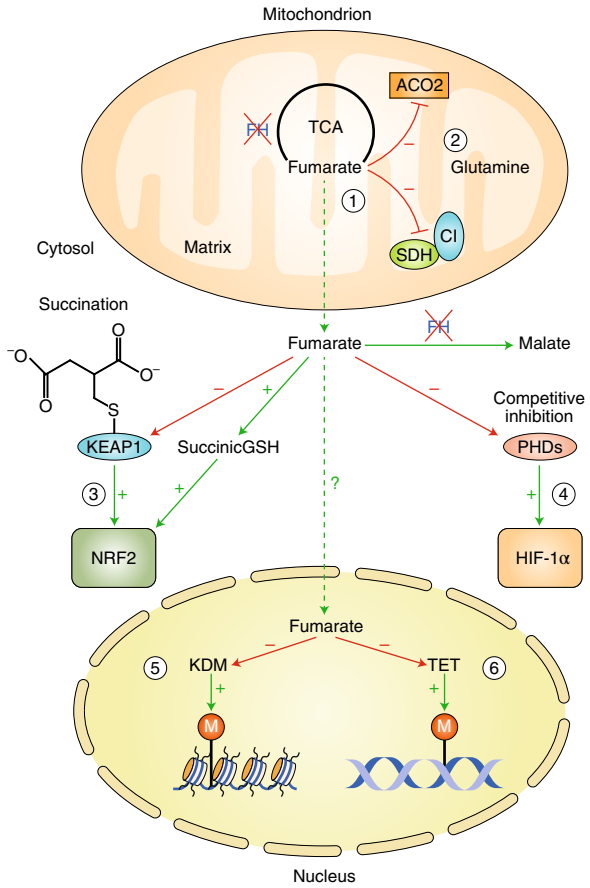

Fig. 4 | Fumarate is an oncometabolite and epigenetic modifier. Under conditions of FH deficiency, fumarate levels markedly increase, leading to perturbations in mitochondrial OXPHOS. Elevated fumarate acts as a competitive inhibitor of SDH, inhibits complex I via succination of key (Fe-S) cluster biogenesis proteins (1) and inhibits ACO2 via succination through redox-sensitive cysteine residues (2). In the cytosol, increased fumarate can succinate KEAP1 and GSH to activate NRF2 (3), while fumarate also acts to competitively inhibit PHDs and stabilise HIF-1α (4). In the nucleus, fumarate acts as an epigenetic modifier, whereby it can inhibit the KDM family of histone demethylases (5) and the TET family of DNA demethylases (6), which act as a signal to induce EMT.

of aerobic glycolysis by the specific GAPDH inhibitor heptelidic acid (HA) and 2-deoxyglucose (2-DG) recapitulated the immunomodulatory effects of DMF in vitro, while in vivo administration of HA inhibited the development of experimental autoimmune encephalomyelitis (EAE), a murine model of MS[92]. As such, this represents an important proof-of-principle study supporting the concept that metabolically targeted therapies may be successfully used to treat inflammatory-driven diseases and also providing mechanistic insight into the anti-inflammatory action of DMF and MMF. Intriguingly, endogenous fumarate was also found to succinate GAPDH in both mouse and human macrophages, suggesting that elevated fumarate levels may act as an endogenous anti-inflammatory signal to limit inflammation; however, the precise role of fumarate accumulation remains an open question to be explored. It is important to note that while HA and DMF have proven to be beneficial in the treatment of debilitating diseases such as MS, prolonged and/or systemic inhibition of glycolysis is likely detrimental to the host and will impair immune (both innate and adaptive) cell function, which in the context of infection would be unfavourable. Further work is required to fully understand the effect of prolonged glycolytic inhibition.

Fumarate and cellular transformation. In addition to its role as an inflammatory regulator, fumarate can also be viewed as an oncometabolite[96]. Given its central role in energy metabolism, FH was long considered a housekeeping enzyme[97]. Consistent with this view, homozygous FH loss in fumaric aciduria, an autosomal recessive metabolic disorder, leads to very severe neurological disorders and is fatal in early childhood[98]. However, in 2002 it was shown that mutations of FH are the cause of hereditary leiomyomatosis and renal cell cancer (HLRCC), a rare cancer predisposition syndrome characterized by benign tumours of the smooth muscle of skin and uterus, and a very aggressive form of renal cancer[87]. These findings indicate that not only do cells survive the loss of FH, but in specific tissues, they can also undergo transformation to tumour cells. How FH loss leads to cancer has been a long-standing question in the field.

The defining biochemical feature of FH loss is the accumulation of fumarate, which has been implicated in tumorigenesis[96]. To date, several biological functions have been ascribed to fumarate. For instance, accumulated fumarate can bind and inactivate reactive thiol residues of proteins and peptides in a process called succination. This protein modification was originally described in diabetes[99]. This function of fumarate derives from its unsaturated dicarboxylic acid structure, which makes it a mildly electrophilic molecule that can be involved in a Michael addition with nucleophiles, such as reactive thiol residues of proteins. The first insights into the relevance of succination in patients with HRLCC was proposed in 2011, when it was shown that fumarate could bind reactive thiol residues and inactivate KEAP1, the negative regulator of the master antioxidant transcription factor NRF2, leading to a powerful antioxidant response[100,101], as shown in Fig. 4. Later, it was also shown that fumarate binds glutathione (forming succinic-glutathione (succinicGSH)) and thereby depletes this antioxidant molecule, leading to unscheduled oxidative stress[95,102]. Of note, fumarate-dependent oxidative stress has also been shown to drive renal cells to senescence in an FH-deficient mouse model, and its bypass by the co-ablation of p21 increased malignant transformation in the kidneys[103]. Consistent with an important role of senescence bypass for the development of tumorigenesis, recent data in patients with HLRCC shows that *CDKN2A* (also known as *P16*), a key player in senescence, is hypermethylated and suppressed in tumours. Fumarate has been shown to cause succination of the mitochondrial aconitase ACO2, leading to an additional truncation of the TCA cycle[104], and also of iron-responsive element binding protein 2 (IRP2), promoting the transcription of transferrin[105]. Finally, it has been shown that fumarate can drive succination of several members of the family of iron sulfur (Fe-S) cluster biogenesis proteins, causing a depletion of the Fe-S clusters required for the activity of mitochondrial enzymes, including complex I[106]. All these reactions appear to be independent of enzymatic catalysis, driven by the high level of fumarate accumulation and irreversible. Succination is a hallmark of FH-deficient tumours, and an antibody against succinated proteins has been proposed as a diagnostic marker for HLRCC[107].

As mentioned, fumarate also inhibits a variety of α-KGDDs, enzymes involved in multiple cellular processes ranging from metabolism to signalling and epigenetics[88,108,109], as shown in Fig. 4. Examples of α-KGDDs inhibited by fumarate are the PHDs, which are negative regulators of HIFs[110]. Accordingly, fumarate causes HIF stabilization even under normoxic conditions, that is, pseudohypoxia, a hallmark of FH-deficient tumours[110]. α-KGDDs are also involved in the de-methylation of DNA, RNA and histones. Recent data have demonstrated that fumarate acts as a powerful inhibitor of the TET family of DNA demethylases and of a series of histone demethylases[88,108]. In this context, fumarate is considered an important epigenetic modifier (reviewed in ref. [111]). It has also been shown that fumarate accumulation leads to the inhibition of TET-dependent DNA demethylation of a class of anti-metastatic miRNAs, the miR200 family, promoting an EMT[112], a process involved in cancer initiation and metastasis[113]. Of note, FH-deficient renal cancers are characterized by a distinct DNA hypermethylation phenotype, which also affects the tumour suppressor *CDK2NA*[114], indicating that, by allowing senescence escape, this epigenetic activity of fumarate may have a critical role in tumour etiology.

Finally, fumarate and FH were recently proposed to be key players in the response to DNA damage. Originally described in yeast[115], FH has a 'moonlighting' role in the nucleus that capitalizes on the epigenetic-modifying function of fumarate. Upon DNA damage, FH localizes in the nucleus, where it is phosphorylated by the catalytic subunit of DNA-PK (DNA-PKcs)[116]. Here, via its reverse activity, FH generates fumarate that inhibits the histone lysine demethylase KDM2B, which in turn facilitates the binding of proteins involved in DNA repair. In support of this unexpected function of fumarate, it has recently been shown that the aberrant accumulation of this metabolite in HLRCC correlates with increased endogenous damage, lower DNA repair efficiency and increased sensitivity to poly-ADP ribose polymerase (PARP) inhibitors[117]. Of note, this biological function of fumarate is also shared with succinate and 2-HG (see below). It has also recently been shown that FH loss in renal cancer cells leads to increased DNA damage and ionising radiation (IR) resistance due to a fumarate-dependent inhibition of mitotic entry after IR, even in the presence of unrepaired damage[118]. Overall, these lines of evidence provide a potential model for how fumarate accumulation promotes genomic alterations that could give rise to cancer formation in patients with HLRCC, cooperating with the other above-described oncogenic signals it elicits.

2-hydroxyglutarate in immunity and cancer

The next intermediate we will consider is 2-HG, which exists in two enantiomeric forms, L-2-HG and D-2-HG[104], as shown in Fig. 5. Like itaconate, 2-HG was first discovered in the 1800s (in this instance by the German biochemist Karl Heinrich Ritthausen); however, it did not attract much attention until recently when its physiological function was uncovered[119]. Interest in these enantiomers heightened in the 1980s when they were linked to two rare but clinically related diseases, now termed L-2-hydroxyglutaric aciduria (L2-HGA) and D-2-hydroxyglutaric aciduria (D2-HGA), which manifest early in childhood and usually lead to severe disability and mental retardation in adulthood[120–122]. The cause of these so-called 2-hydroxyglutaric acidurias (2-HGAs) was attributed to germline mutations in L-2-HG dehydrogenase (*L2HGDH*) and D-2-HG dehydrogenase (*D2HGDH*), encoding the mitochondrial enzymes responsible for the conversion of 2-HG to α-KG and thus for the breakdown of 2-HG[123–125]. In the case of D2-HGA, about 50% of patients present

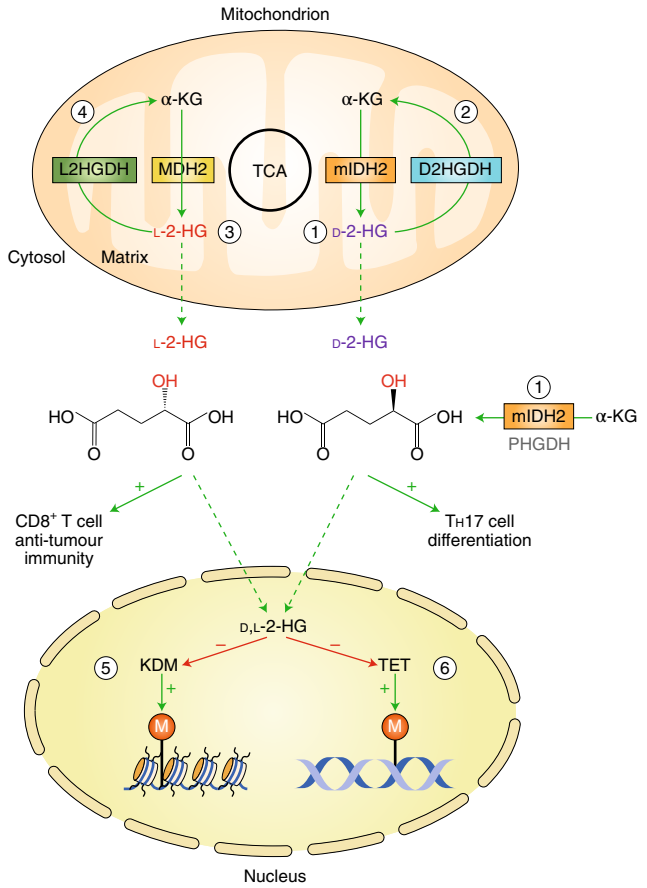

Fig. 5 | 2-HG is an oncometabolite and epigenetic modifier. 2-HG exists as two enantiomers, L-2-HG and D-2-HG. Under conditions whereby IDH1/2 are mutated (mIDH1/2), this mutant enzyme preferentially acts on α-KG, as opposed to isocitrate, to generate D-2-HG, and in this context, D-2-HG accumulates to high levels (1); however, under normal conditions, D-2-HG levels are maintained at low concentrations via D2HGDH (2). In response to hypoxia or acidic pH, LDHA and MDH2 can promiscuously generate L-2-HG from α-KG (3), whose levels are usually maintained at low concentrations via L2HGDH (4). Accumulation of D-2-HG and/or L-2-HG in the nucleus results in the competitive inhibition of the KDM family of histone demethylases (5) and the TET family of DNA demethylases (6), thus acting as an important epigenetic modifier driving tumorigenesis and as a regulator of T cell immunity.

with *D2HGDH* mutations, while the remaining half possess mutations in the gene encoding the Krebs cycle enzyme IDH2, which converts isocitrate to α-KG[126]. A third 2-HGA, in which both enantiomers accumulate, that arises from germline mutations in the mitochondrial citrate carrier *SLC25A1* has also been discovered. This provides an intriguing link between mitochondrial citrate metabolism and 2-HG production[127] that remains to be explored. In recent years, two landmark genomic studies carried out in human glioma and acute myeloid leukaemia (AML) found mutations in IDH1 and IDH2, and it is now appreciated that the genes encoding these enzymes (which drive elevated production of D-2-HG) are the most frequently mutated metabolic genes in human cancer[128–130]. Furthermore, the literature suggesting that these metabolites play a role in immune cell regulation is ever expanding.

2-HG governs T cell differentiation and anti-tumour immunity. While the role of 2-HG in tumorigenesis has been a heavy focus of research over the last several years, an unexpected role for this unusual metabolite has more recently begun to emerge as a regulator of T cell function and inflammation. It has become increasingly appreciated that different T cell subtypes undergo dramatic metabolic remodelling that governs their proliferation, differentiation and effector functions[131]. T_H17 cells, derived from naive $CD4^+$ T cells, are one such subset that rely heavily on a switch from OXPHOS to glycolysis, a process that requires the activation of HIF-1α and induction of RORγt[132,133]. On the other hand, induced regulatory T (iT_{reg}) cells, also derived from naive $CD4^+$ T cells, do not require HIF-1α (refs. [132,133]). Interestingly, Xu et al.[133]observed increased levels in of D-2-HG in T_H17 cells when compared to iT_{reg} cells. The elevated levels of D-2-HG were associated with increased DNA methylation levels at the *Foxp3* locus, the master transcription factor driving iT_{reg} differentiation, resulting in its repression[133]. Furthermore, T_H17 cell differentiation could be initiated by exogenous addition of D-2-HG to naive $CD4^+$ T cells or by genetic silencing of *TET1* and *TET2*, established targets of 2-HG[133–135]. Mechanistically, D-2-HG production was driven by the conversion of glutamate to α-KG by the aspartate aminotransferase GOT1. Inhibition of GOT1 by aminooxyacetic acid (AOAA), which decreases D-2-HG levels, promoted *Foxp3* expression and the differentiation of T_H17 cells to iT_{reg}s[133]. Lastly, AOAA ameliorated disease progression in EAE, a disease in which T_H17 cells mediate pathology. This study identified a crucial role for 2-HG as an epigenetic modifier governing T cell differentiation and suggests that therapeutic strategies aimed at lowering its levels may represent a promising approach for treatment of T_H17-mediated autoimmune disorders.

In addition to $CD4^+$ T cells, an unexpected role for L-2-HG in the promotion of tumour killing via $CD8^+$ T cells, which are cytotoxic T lymphocytes important for anti-tumour immunity, has emerged[136]. Like T_H17 cells, $CD8^+$ T cells are highly dependent on the activation of HIF-1α and glycolysis, which is responsible for mediating trafficking into hypoxic tumour environments and inflamed tissue[137,138]. Interestingly, Tyrakis et al.[136] observed a dramatic increase in L-2-HG levels, which reached up to 1.5 mM, in response to T cell receptor triggering in mouse $CD8^+$ T cells. This increase occurred under normoxic conditions and was dependent on HIF-1α stabilization. Mechanistically, HIF-1α stabilization induced LDHA expression and activity, which promiscuously converted glutamine-derived α-KG to L-2-HG[136]. Accumulation of L-2-HG altered $CD8^+$ T cell differentiation through modulation of both the histone and DNA methylation landscape of the cell and also through HIF stability. Furthermore, exogenous treatment of $CD8^+$ T cells with L-2-HG greatly enhanced the in vivo proliferation, persistence and anti-tumour capacity of adoptively transferred $CD8^+$ T cells[136]. 2-HG enantiomers are therefore beginning to emerge as important signalling moieties linking metabolic reprogramming, epigenetic alterations and effector functions of immune cells.

***IDH* mutations promote D-2-HG accumulation and tumorigenesis.** Genomic studies have established that somatic mutations in *IDH1* and *IDH2* are perhaps the first genetic events to occur during tumorigenesis in human glioma and AML, and these appear to initiate pathogenesis by a common mechanism[114,119,139,140]. The most commonly occurring cancers thought to arise from mutant IDH1 and IDH2 (mIDH1/2) include glioma, cartilaginous tumours, AML, angioimmunoblastic T cell lymphoma (AITL) and intrahepatic cholangiocarcinoma (ICC). Additionally, mutations in these genes have also been reported to sporadically arise in prostate cancer, melanoma, medulloblastoma and hepatocellular carcinoma (HCC)[119]. Remarkably, almost all IDH1/2 mutations occur in a few unique locations in the active site of the enzymes, which result in the acquirement of a neomorphic enzymatic activity converting α-KG to the oncometabolite D-2-HG[141–143]. As with succinate and fumarate, D-2-HG acts as a competitive inhibitor of α-KGDDs, including but not limited to the TET family and JMJD family of DNA

and histone demethylases, respectively[144,145]. D-2-HG, produced by mIDH1/2, has been shown to drive a CpG island methylator phenotype (G-CIMP) in both glioma and ICC tumours to promote tumorigenesis and has also been found to occupy the active site of histone demethylases, thereby increasing histone methylation in primary gliomas[144,146–148]. Furthermore, Flavahan et al.[149] demonstrated that the IDH-driven G-CIMP phenotype occurs at cohesion and CCCTC-binding factor (CTCF)-binding sites, compromising this methylation-sensitive insulator protein, and enables a constitutive enhancer to interact aberrantly with and activate the glioma oncogene *PDGFRA*.

Emphasis has often been placed on epigenetic alterations elicited by elevated D-2-HG as a driver of tumorigenesis in IDH-mutant cancers; however, it is also apparent that it can antagonise other α-KGDDs. Although the half-maximal inhibitory concentration (IC_{50}) of D-2-HG toward KDM family members is in the low micromolar range (24–106 μM), it can also inhibit FIH and PHD2, with IC_{50} values of 1.5 and 7.3 mM, respectively[144]. In IDH1/2-mutant gliomas, D-2-HG has been reported to accumulate to levels up to 35 mM; as such, D-2-HG could inhibit α-KGDDs to affect alternative cellular signalling pathways[141]. Indeed, D-2-HG accumulation in *IDH*-mutant glioma has been found to inhibit PHD hydroxylase and stabilise HIF-1α (ref. [150]), and HIF-1α stabilization has been shown to occur in IDH1-mutant brain tissue[128]. L-2-HG is also a potent inhibitor of α-KG-dependent enzymes. It has been reported that under conditions of hypoxia, L-2-HG is selectively produced by mammalian cells[151]. The authors demonstrate that this is independent of IDH1/2 and is primarily mediated by LDHA and malate dehydrogenase (MDH) via 'promiscuous' reduction of α-KG and is enhanced by an acidic pH[152]. Under acidic conditions, the protonation of α-KG promotes binding to LDHA and L-2-HG production. Functionally, L-2-HG is sufficient to drive histone methylation, in particular histone 3 lysine 9 (H3K9me3), and can also promote HIF-1α stabilization in normoxic conditions and therefore may assist with hypoxic adaptation. These data suggest that L-2-HG might represent a metabolic response to certain environmental stimuli, including hypoxia and acidosis, that drives changes in cellular signalling and function. Although it has been reported that D-2-HG is a less potent inhibitor of α-KGDDs than L -2-HG, the concentrations at which it accumulates under pathogenic conditions suggest HIF-1α stabilization and impaired collagen biogenesis may contribute to tumorigenicity[150,152–155]. Intriguingly, another possible mechanism by which D-2-HG drives tumorigenesis is through the promotion of genetic instability, predisposing cells to oncogenic transformation[119]. D-2-HG has been shown to inhibit α-KG-dependent alkylation repair homologs, ALKBH2 and ALKBH3, which are critical DNA damage repair enzymes that detoxify 1-methyladenine (1 mA) and 3-methylcytosine (3mC) lesions in DNA derived from alkylating agents[119,144,156]. Indeed, IDH-mutant cells display reduced DNA repair kinetics, accumulate DNA double-stranded breaks (DSBs) and are sensitised to alkylating agents[117,119,144,156]. Furthermore, D-2-HG has been proposed to promote DNA damage by altering the expression of genes involved in DNA repair, namely the DNA damage sensor *ATM* (ataxia-telangiectasia mutated), whereby an accumulation of repressive histone methylation markers, H3K9 and H3K27, were found at the ATM promoter in *Idh*-mutant mouse haematopoietic stem cells and human AML samples[157]. As such, these findings directly link mIDH-derived D-2-HG accumulation to DNA damage, genetic instability and carcinogenesis.

Alternative D-2-HG targets in cancer development. In addition to the role of α-KGDD inhibition by D-2-HG in the regulation of histone and DNA methylation and genomic instability, D-2-HG has been found to affect several other cellular pathways that may also contribute to cancer initiation and progression[119]. Of note, D-2-HG produced by mIDH1 in low-grade glioma was found to activate mechanistic target of rapamycin (mTOR) signalling[158]. Mechanistically, it was proposed that D-2-HG destabilised DEPTOR, a negative regulator of mTORC1 and mTORC2, partly through inhibition of the histone demethylase KDM4A[158]. Furthermore, metabolomic profiling of mIDH1/2 gliomas revealed significant alterations in cellular metabolism, an effect recapitulated with the exogenous addition of D-2-HG[159]. This metabolic rewiring resulted in a decrease in a common dipeptide found in the brain N-acetyl-aspartyl-glutamate (NAAG), and NAAG levels were found to be significantly lower in mIDH-mutant human glioma tissue[159]. Likewise, mutations in IDH were also found to reprogram pyruvate and Krebs cycle metabolism, lower dependence on oxidative mitochondrial metabolism and silence *LDHA* expression, all suggesting that cellular reprogramming elicited by D-2-HG may play a prominent role in the pathogenesis of IDH-mutant tumours[160–162]. However, the mechanism by which D-2-HG orchestrates these events remains to be explored. Furthermore, D-2-HG activates NF-κB in bone marrow stromal cells in an IκB kinase–independent fashion, thus generating a stromal niche for IDH-mutant AML development[163]. Intriguingly, D-2-HG has also been found to be a competitive inhibitor of SDH, a key metabolic enzyme and tumour suppressor as previously discussed, resulting in the accumulation of succinate, impaired mitochondrial oxygen consumption and increased protein succinylation[164]. As such, the initiation and pathogenesis of IDH-mutant tumours may share parallels with SDH-mutant tumours. D-2-HG has also been found to bind the DNA methyltransferase DNMT1, which subsequently represses receptor-interacting protein kinase 3 (RIP3). Finally, D-2-HG also impairs necroptosis and the small GTPase CDC42, leading to suppression of mixed lineage kinase 3 (MLK3)-mediated apoptosis[165,166]. These findings therefore suggest that both suppression of RIP3-mediated necroptosis and MLK3-mediated apoptosis by D-2-HG may contribute to IDH-mutant carcinogenesis[165,166].

Citrate as a source of acetyl-CoA for histone acetylation

One final metabolite to consider in the context of cellular signalling is acetyl-coenzyme A (acetyl-CoA), derived from citrate. Acetyl-CoA is an energy-rich intermediate that provides acetyl groups to the Krebs cycle through the generation of citrate, which is further oxidised for energy production. Acetyl-CoA is generated from the breakdown of carbohydrates, fatty acids and proteins though glycolysis, β-oxidation and the degradation of the amino acids leucine, isoleucine and tryptophan, respectively[85]. Acetyl-CoA serves as a building block for the synthesis of lipids, ketone bodies and amino acids. As fatty acid synthesis occurs in the cytosol, acetyl-CoA must exit the mitochondria to fulfil this function. To do so, following its conversion to citrate, it exits the mitochondria via the mitochondrial citrate carrier (CIC) and is then converted back to acetyl-CoA (and oxaloacetate) by the enzyme ATP-citrate lyase (ACL). It is this enzyme that endows acetyl-CoA with much of its signalling capacity in the context of tumour and immune cell biology.

Acetyl-CoA (derived from citrate) has been shown to drive histone acetylation, and this process can have a profound impact on both tumour and immune cell function, as shown in Fig. 6. Chromatin structure is regulated in part through modification of histones, including histone acetylation[167]. It has been demonstrated in mammalian cells that histone acetylation is dependent on ACL-induced production of acetyl-CoA[168], with ACL silencing decreasing the degree of histone acetylation. One of the earliest studies to identify a role for ACL in histone acetylation demonstrated a requirement for the *ACLY* gene (encoding ACL) in response to growth factor stimulation and during differentiation, for example, the differentiation of murine 3T3- L1 pre-adipocytes into adipocytes. Cells depleted of ACL contained visibly less lipid than control cells. This was linked to decreased expression of genes involved in glucose uptake and glycolysis, which are required for adipocytes to

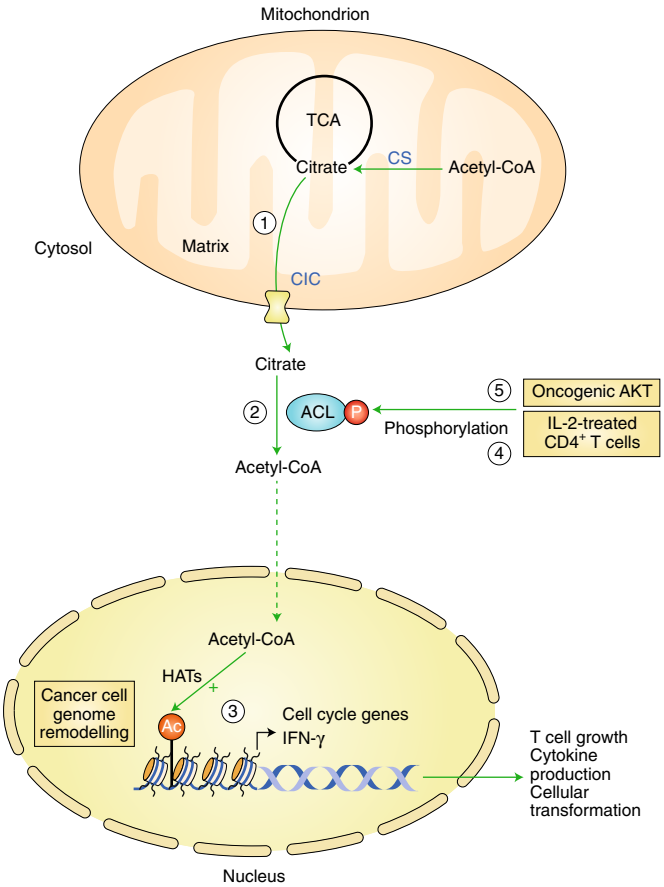

Fig. 6 | Acetyl-CoA as an epigenetic modifier in immunity and cancer. Acetyl-CoA, an energy-rich intermediate derived from citrate (and pyruvate), has been shown to drive histone acetylation, and this process can have a profound impact on both tumour and immune cell function. To facilitate this, citrate exits the mitochondria via the CIC (1) and is then converted back to acetyl-CoA by the enzyme ATP-citrate lyase (ACL) (2). In T cells, acetyl-CoA has been shown to enhance acetylation of histone H3 acetylation at lysine 9 (H3K9Ac) and to promote transcription of *IFNG* (3). In addition, IL-2 treatment of $CD4^+$ T cells promotes phosphorylation of ACL and acetylation of cell cycle genes to promote T cell growth (4). Oncogenic Akt has also been shown to phosphorylate ACL to promote acetylation and epigenomic remodelling of cancer cells, a hallmark of human glioma and prostate cancer (5).

engage in fat storage. It was shown that during adipocyte differentiation, global histone acetylation is determined by glucose availability through an ACL-dependent pathway[168]. These seminal findings highlight a clear link between nutrient sensing, metabolism and histone acetylation, which has now been extended to immune and tumour cell function.

Acetyl-CoA and histone acetylation regulate immunity. Acetyl-CoA levels and histone acetylation have been implicated in the regulation of immune cells. It is well-established that glycolysis is required for effector T cell function, and a recent study from Peng et al.[169] has provided mechanistic insight into this requirement. The authors demonstrate that LDHA, an enzyme that catalyses the reversible conversion of pyruvate and NADH to lactate and NAD^+, is induced in activated T cells and enhances histone acetylation of IFN-γ via the maintenance of acetyl-CoA levels to promote its expression. Mice with a T cell-specific LDHA deficiency produced less IFN-γ and were protected from immunopathology. Mechanistically, LDHA-deficient T cells showed decreased acetyl-CoA levels and decreased histone H3 acetylation at the lysine 9 residue (H3K9Ac), a histone mark associated with active transcription, on the IFN-γ promoter. Furthermore, artificial acetyl-CoA reduction, through inhibition of *ACLY*, decreased IFN-γ expression and acetate supplementation, which augmented acetyl-CoA production, and corrected H3K9Ac marks and IFN-γ expression in LDHA-deficient T cells.

The mechanism of IFN-γ regulation proposed by Peng et al.[169] differs from that proposed by Chang et al.[170], who suggest that aerobic glycolysis boosted IFN-γ production by engaging GAPDH and preventing its binding to the three prime untranslated region (3′-UTR) of *Ifng*, thereby enhancing IFN-γ translation. These assays are technically demanding to perform, and this discrepancy remains to be clarified. However, it should be noted that the study from Peng et al.[169] employed the use of an artificial construct—the bovine growth hormone 3′-UTR—rather than direct manipulation of the *Ifng* 3′-UTR itself. Multiple mechanisms involving acetyl-CoA may therefore exist to regulate *Ifng* expression. Activated T cells, which display elevated glycolysis, may remodel their chromatin, thereby generating *Ifng* mRNA that can be robustly translated, as GAPDH is engaged in glycolysis and no longer binds the *Ifng* mRNA. These data demonstrate the complex relationship between metabolism and gene regulation. It will be interesting to speculate whether acetyl-CoA can boost histone acetylation and transcription of other cytokines, or indeed other immune or tumour cells.

ACL and histone acetylation have also been implicated in T cell growth[171]. An unbiased mass spectrometry–based study of the nuclear phosphoproteome of resting and IL-2-treated $CD4^+$ T lymphocytes revealed that ACL is phosphorylated in response to IL-2 treatment[171]. Pharmacological or genetic ablation of ACL function impaired IL-2-promoted T cell growth. The authors demonstrate that ACL is required to enhance histone acetylation levels and induce the expression of cell cycle regulating genes in response to IL-2. They speculate that this is as a result of acetyl-CoA generation, but do not experimentally demonstrate this concept.

Acetyl-CoA alters the epigenome of tumour cells. In 2014, Lee et al.[172] demonstrated that acetyl-CoA levels and histone acetylation in tumours are regulated by oncogenic activation of protein kinase B (known as Akt) and subsequent ACL phosphorylation. This was one of the first reports to implicate metabolic reprogramming mediated by oncogenic activation in the regulation of the cancer cell epigenome. Importantly, histone acetylation and phosphorylated Akt levels correlate significantly in human glioma and human prostate cancer, and levels of histone acetylation have been shown to be predictive of which patients later exhibit biochemical failure, with lower levels predictive of a worse outcome. These data suggest that histone acetylation levels might be a valuable biomarker to predict tumour relapse. Histone acetylation has also been implicated in the development of human non-small cell lung carcinoma (NSCLC)[173,174]. Specifically, aberrant histone acetylation is reported to play an important role in EMT and metastasis in lung cancer[173]. More recently, Mi et al.[174] also identified an acetyllysine-binding protein, YEATS2, that is amplified in NSCLC and binds to acetylated histone H3 (H3K27Ac) to promote a transcriptional program required for cancer cell growth and survival. Further study is needed to understand how global histone acetylation levels impact tumour growth and progression, as well as response to treatment.

ACL and acetyl-CoA levels and histone acetylation have also been shown to play an important role in the DNA damage response in tumour cells[175]. ACL is phosphorylated downstream of Akt activation following DNA damage, and this facilitates histone acetylation at double-strand break (DSB) sites, enabling breast cancer early onset 1 (BRCA1) recruitment and DNA repair by homologous recombination. ACL deficiency results in impaired BRCA1 recruitment to sites of DSBs and suppressed homologous recombination.

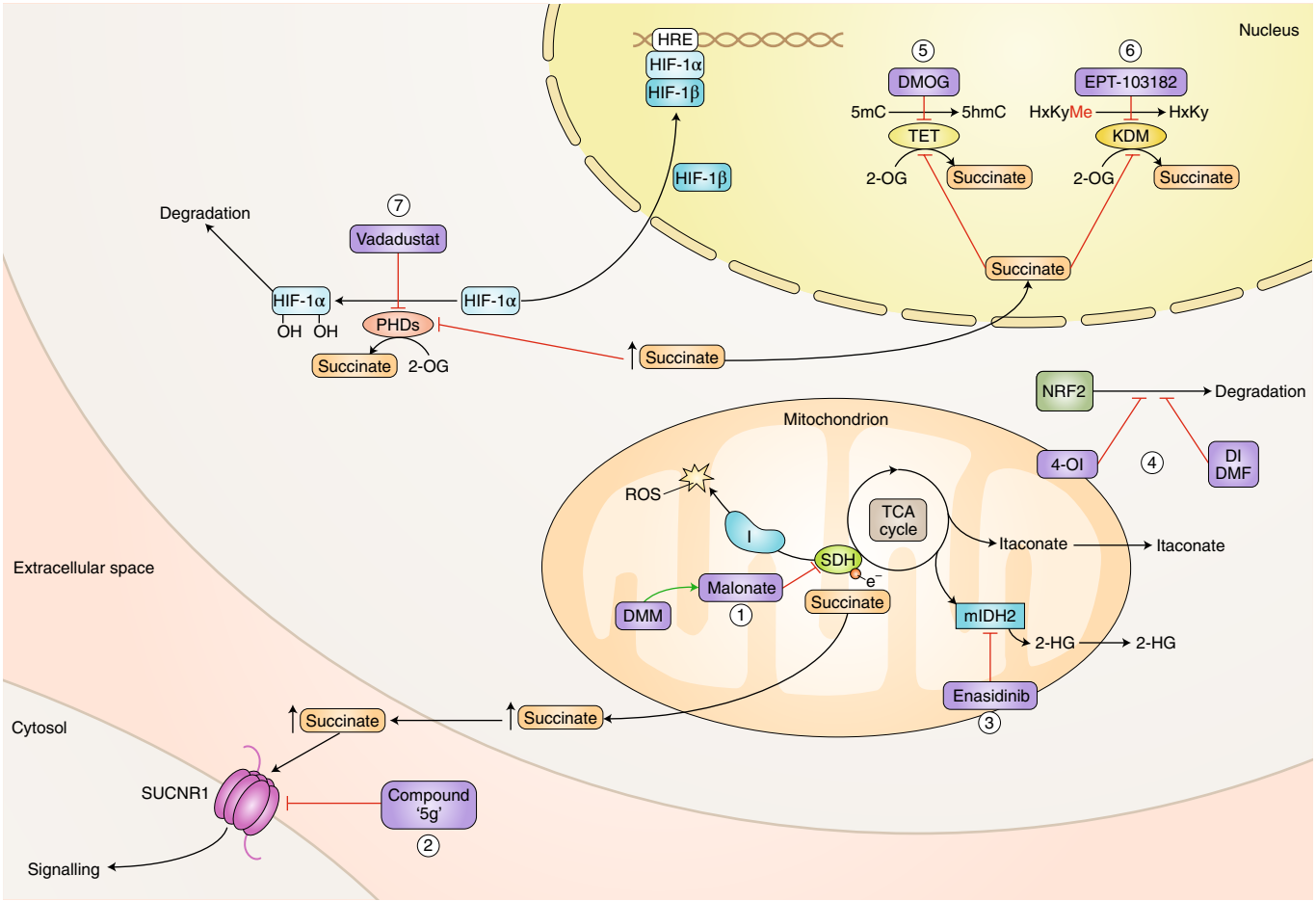

Fig. 7 | Therapeutic opportunities targeting metabolic signalling pathways. The SDH inhibitor malonate and the malonate prodrug DMM (hydrolysed to release malonate) ameliorate damage associated with succinate accumulation during ischaemia (1). SUCNR1 receptor inhibitors, such as compound 5g, are in development (2). Enasidinib, which targets mutated IDH2 to reduce 2-HG production, is leading to the treatment of AML (3). 4-OI, DI and DMF are anti-inflammatory and may have therapeutic potential (4). Inhibitors of α-KGDDs are an emerging target, but selectivity is an issue; for example, dimethyloxaloylglycine (DMOG) acts on TETs but also PHDs (5). Specific inhibition of KDMs has also been challenging, but EPT-103182 has shown promise in early pre-clinical work (6). The specific PHD inhibitor Vadadustat has shown promise in chronic kidney disease (7).

The mechanisms of Akt activation by DNA damage signalling and the mechanisms that regulate levels of nuclear ACL, which is critical for its role in regulating BRCA1 recruitment, are less clear.

Therapeutic opportunities

The emerging roles of Krebs cycle intermediates in the pathophysiology of biomedically important processes raises the possibility of the generation of a new class of therapies focused on these metabolites, as shown in Fig. 7. This concept has already warranted investigation and was first illustrated following the discovery that succinate is accumulated during ischaemia and is then oxidised upon reperfusion to drive the mitochondrial superoxide formation that contributes to ischaemia–reperfusion (IR) injury[33,174]. Inhibiting the mitochondrial enzyme SDH during ischaemia by preloading tissues with the SDH inhibitor DMM prevented succinate accumulation during ischaemia and protected against tissue damage upon reperfusion[33]. Malonate itself was also protective when added at reperfusion[176,177]. This work indicates that simple inhibitors of Krebs cycle enzymes could be used to prevent pathological damage. The production of succinate is also enhanced during inflammation[2], acting as a signal from mitochondria to the cytosol to activate pro-inflammatory gene expression while also generating ROS as a further pro-inflammatory redox signal[36]. As the mechanism of mitochondrial superoxide generation by succinate oxidation during inflammation seems to be the same as that during IR injury (RET)[36], it is perhaps unsurprising that DMM could also decrease inflammation in a mouse model of sepsis[36]. Hence, simple molecules designed to inhibit SDH are a novel class of anti-inflammatory and anti–IR injury compounds.

As well as acting within the cell, a portion of the succinate that accumulates during ischaemia and inflammation is released from the cell into the extracellular environment through poorly defined processes. This occurs following IR injury[178,179], inflammation[16] or cold exposure[14]. The diverse consequences of released succinate remains to be explored, but one likely role is as an inflammatory signal, acting via SUCNR1 (refs. [5,9,180,181]). There is considerable interest in developing drugs that can counteract the effects of succinate on this receptor[180]. Although SUCNR1 receptor inhibitors, such as compound '5g', are in their infancy, they may provide further understanding as to the signalling role of succinate and a method of blunting a cascade response during inflammation. Circulating Krebs cycle intermediates are particularly interesting potential drug targets.

As previously discussed, mitochondrial metabolites have an impact on metabolism following their export from the mitochondrial matrix to the cytosol and nucleus, and α-KGDDs are major targets for the action of mitochondrial metabolites, such as succinate and 2-HG[7,8,180,182]. High levels of succinate or 2-HG inhibit α-KGDDs. These include the PHDs, the TET DNA demethylases

and the JMJDs[109,183,184]. Inhibitors of α-KGDDs are often non-specific, either targeting multiple α-KGDD family members, such as dimethyloxaloylglycine (DMOG) acting on not only TETs but also PHDs[185]. Specific inhibition of histone lysine demethylases (KDMs) has also been challenging[186]. EPT-103182 has shown promise in early preclinical work in an osteosarcoma cell line; however, it has yet to be investigated in clinical trials[187]. However, specific PHD inhibitors have been developed, such as Vadadustat, and these have shown promise in chronic kidney disease, increasing erythropoiesis and providing a means of attenuating HIF in other pathologies[188]. The development of more effective drugs that affect the interactions of Krebs cycle intermediates with α-KGDDs is an area of considerable current interest[189].

A further therapeutic angle has revealed following the discovery of mutations in certain Krebs cycle enzymes that result in the generation of novel metabolites—the best example being mIDH2. Interestingly, the drug Enasidenib has been developed for AML, which binds to the mutated, but not the wild-type, form of IDH2 to prevent D-2-HG production[190].

The generation of itaconate from the Krebs cycle intermediate cis-aconitate contrasts with most other metabolite signals emanating from mitochondria in that it primarily acts as a protective, anti-inflammatory metabolite[63,67,68]. As itaconate acts as an endogenous protective and anti-inflammatory agent, there has been interest in developing drugs that enhance its levels within cells. 4-OI is an itaconate mimic that was protective in a mouse model of sepsis, decreasing cytokine production and increasing survival[68]. The therapeutic potential of DI was also demonstrated, as in vivo administration of DI resulted in an amelioration of skin pathology in a mouse model of psoriasis, a disease also currently treated by the related electrophile DMF[67,68,73]. Thus, the development of new therapies designed to fine-tune the cell delivery and activity of NRF2 activators is a promising therapeutic strategy.

In summary, the emerging role of Krebs cycle intermediates in many central biomedical pathways opens up the possibility of extending mitochondrial pharmacology[182,191–193] to manipulating the levels and impacts of mitochondrial metabolites both within the matrix and the rest of the cell, or following their release from the cell into the circulation.

Outstanding questions and concluding remarks

While the understanding of the role of metabolites as signalling molecules has come a long way, it is still in its infancy. The clear roles for succinate and HIF as pro-inflammatory signals, L-2-HG in driving anti-tumour immunity, fumarate as an anti-inflammatory and pro-tumorigenic signal and acetyl-CoA as an epigenetic regulator reveal some of the potential targets uncovered in this burgeoning field, yet many unanswered questions remain. One critical point to consider is the limited human and in vivo data that are available at present. These studies prove especially challenging owing to the rapid rate at which steady-state metabolism changes. Appropriate methods of euthanasia and tissue extrusion are paramount to obtain an accurate snapshot of the in vivo metabolic status of cells and tissues, making relevant and comparable analyses extremely challenging. Also, studies in human immune cells are currently very limited. Understanding the cellular location of metabolite accumulation as well as how these cells may signal in a paracrine manner remain to be explored. For example, the relevant ratios of the different metabolites, which may vary over time and in different compartments of the cell, will be informative. It is also likely that unidentified receptors and transporters exist, which are capable of recognising metabolites to initiate downstream signalling events or to facilitate cell entry from the extracellular milieu, respectively. Whether metabolites such as succinate, itaconate and acetyl-CoA serve as biomarkers or drivers of disease or tumour progression remains to be further explored. Of note, some of the major findings on the function of oncometabolites were obtained from rare cancer syndromes. However, many tumours appear to maintain a functional TCA cycle, as observed in human lung and brain tumours in vivo[194–197], while in some instances ETC dysfunction can act as a barrier to tumorigenesis[198]. As such, the intriguing role of these metabolites in driving rare cancer syndromes may represent an exception to the rule for tumorigenesis (if such a rule exists), and it will be crucial to understand whether some of the processes elicited by oncometabolites occur in other sporadic cancers and in the absence of inactivating mutations of FH, IDH, or SDH.

Interestingly, many of the metabolites discussed share converging molecular functions (including activation of HIF and NRF2 and alterations in chromatin structure), but we still do not know how specific outcomes emerge from these 'unspecific' functions in different cell types. It is possible that the function of these metabolites is highly context-dependent and the inherent chromatin landscape and biochemical set-up of a cell might be a key determinant of the response to the accumulation of these metabolites. On this note, it possible that the often-opposing roles of metabolites in the context of tumour progression and immune cell activation may be detrimental to the host. For example, succinate, which promotes a potentially tumour-fighting, pro-inflammatory state also drives HIF-1α activation in tumours, which is associated with cancer progression[2,26]. On the flip side, it would be interesting to explore if pathogens exploit or manipulate immunometabolism of the host for their own need or indeed if they produce metabolites that can either acts as pathogen- and damage-associated molecular patterns and/or impair immune cell function. It is likely that the field is only at the tip of the iceberg in terms of the breadth of both metabolites with signalling capacity and indeed the entire metabolome[152]. This field still remains in its infancy compared to proteomic and transcriptomic analysis, but liquid chromatography approaches to detect metabolites are constantly evolving, enabling both the detection of a broader range of metabolites and more unbiased analyses, which are likely to uncover novel metabolic signals. In the future, exciting new insights into how the Krebs cycle connects with signalling and perhaps how this cycle may serve as the ultimate determinant of cell function in health and disease will emerge.

Received: 9 August 2018; Accepted: 9 November 2018;
Published online: 30 December 2018

References

1. Jha, A. K. et al. Network integration of parallel metabolic and transcriptional data reveals metabolic modules that regulate macrophage polarization. *Immunity* **42**, 419–430 (2015).
2. Tannahill, G. M. et al. Succinate is an inflammatory signal that induces IL-1β through HIF-1α. *Nature* **496**, 238–242 (2013).
3. He, W. et al. Citric acid cycle intermediates as ligands for orphan G-protein-coupled receptors. *Nature* **429**, 188–193 (2004).
4. Chouchani, E. T. et al. A unifying mechanism for mitochondrial superoxide production during ischemia–reperfusion injury. *Cell. Metab.* **23**, 254–263 (2016).
5. Rubic, T. et al. Triggering the succinate receptor GPR91 on dendritic cells enhances immunity. *Nat. Immunol.* **9**, 1261–1269 (2008).
6. Lei, W. et al. Activation of intestinal tuft cell-expressed Sucnr1 triggers type 2 immunity in the mouse small intestine. *Proc. Natl Acad. Sci. USA.* **115**, 5552–5557 (2018).
7. Nadjsombati, M. S. et al. Detection of succinate by intestinal tuft cells triggers a type 2 innate immune circuit. *Immunity* 49, 33–41.e7 (2018).
8. Schneider, C. et al. A metabolite-triggered tuft cell–ILC2 circuit drives small intestinal remodeling. *Cell* **174**, 271–284.e14 (2018).
9. Littlewood-Evans, A. et al. GPR91 senses extracellular succinate released from inflammatory macrophages and exacerbates rheumatoid arthritis. *J. Exp. Med.* **213**, 1655–1662 (2016).
10. Kim, S. et al. Global metabolite profiling of synovial fluid for the specific diagnosis of rheumatoid arthritis from other inflammatory arthritis. *PLoS One* **9**, e97501 (2014).
11. Hollander, A. P., Corke, K. P., Freemont, A. J. & Lewis, C. E. Expression of hypoxia-inducible factor 1α by macrophages in the rheumatoid synovium: implications for targeting of therapeutic genes to the inflamed joint. *Arthritis Rheum.* **44**, 1540–1544 (2001).

12. Sadagopan, N. et al. Circulating succinate is elevated in rodent models of hypertension and metabolic disease. *Am. J. Hypertens.* **20**, 1209–1215 (2007).
13. van Diepen, J. A. et al. SUCNR1-mediated chemotaxis of macrophages aggravates obesity-induced inflammation and diabetes. *Diabetologia* **60**, 1304–1313 (2017).
14. Mills, E. L. et al. Accumulation of succinate controls activation of adipose tissue thermogenesis. *Nature* **560**, 102–106 (2018).
15. Lewis, G. D. et al. Metabolic signatures of exercise in human plasma. *Sci. Transl. Med.* **2**, 33ra37 (2010).
16. Peruzzotti-Jametti, L. et al. Macrophage-derived extracellular succinate licenses neural stem cells to suppress chronic neuroinflammation. *Cell Stem Cell* **22**, 355–368.e13 (2018).
17. Bhuniya, D. et al. Discovery of a potent and selective small molecule hGPR91 antagonist. *Bioorg. Med. Chem. Lett.* **21**, 3596–3602 (2011).
18. Geubelle, P. et al. Identification and pharmacological characterization of succinate receptor agonists. *Br. J. Pharmacol.* **174**, 796–808 (2017).
19. Tannahill, G. M. & O'Neill, L. A. The emerging role of metabolic regulation in the functioning of Toll-like receptors and the NOD-like receptor Nlrp3. *FEBS Lett.* **585**, 1568–1572 (2011).
20. Semenza, G. L. & Wang, G. L. A nuclear factor induced by hypoxia via de novo protein synthesis binds to the human erythropoietin gene enhancer at a site required for transcriptional activation. *Mol. Cell. Biol.* **12**, 5447–5454 (1992).
21. Semenza, G. L. Regulation of oxygen homeostasis by hypoxia-inducible factor 1. *Physiology (Bethesda)* **24**, 97–106 (2009).
22. Epstein, A. C. R. et al. *C. elegans* EGL-9 and mammalian homologs define a family of dioxygenases that regulate HIF by prolyl hydroxylation. *Cell* **107**, 43–54 (2001).
23. Maxwell, P. H. et al. The tumour suppressor protein VHL targets hypoxia-inducible factors for oxygen-dependent proteolysis. *Nature* **399**, 271–275 (1999).
24. Pearce, E. L. & Pearce, E. J. Metabolic pathways in immune cell activation and quiescence. *Immunity* **38**, 633–643 (2013).
25. Frede, S., Stockmann, C., Freitag, P. & Fandrey, J. Bacterial lipopolysaccharide induces HIF-1 activation in human monocytes via p44/42 MAPK and NF-κB. *Biochem. J.* **396**, 517–527 (2006).
26. Wu, W. & Zhao, S. Metabolic changes in cancer: beyond the Warburg effect. *Acta Biochim. Biophys. Sin. (Shanghai)* **45**, 18–26 (2013).
27. Selak, M. A. et al. Succinate links TCA cycle dysfunction to oncogenesis by inhibiting HIF-α prolyl hydroxylase. *Cancer Cell.* **7**, 77–85 (2005).
28. Rasola, A., Neckers, L. & Picard, D. Mitochondrial oxidative phosphorylation TRAP(1)ped in tumor cells. *Trends Cell Biol.* **24**, 455–463 (2014).
29. Mu, X. et al. Oncometabolite succinate promotes angiogenesis by upregulating VEGF expression through GPR91-mediated STAT3 and ERK activation. *Oncotarget* **8**, 13174–13185 (2017).
30. Guzy, R. D., Sharma, B., Bell, E., Chandel, N. S. & Schumacker, P. T. Loss of the SdhB, but not the SdhA, subunit of complex II triggers reactive oxygen species-dependent hypoxia-inducible factor activation and tumorigenesis. *Mol. Cell. Biol.* **28**, 718–731 (2008).
31. Hagen, T. Oxygen versus reactive oxygen in the regulation of HIF-1α: the balance tips. *Biochem. Res. Int.* **2012**, 436981 (2012).
32. Folbergrová, J., Ljunggren, B., Norberg, K. & Siesjö, B. K. Influence of complete ischemia on glycolytic metabolites, citric acid cycle intermediates, and associated amino acids in the rat cerebral cortex. *Brain Res.* **80**, 265–279 (1974).
33. Chouchani, E. T. et al. Ischaemic accumulation of succinate controls reperfusion injury through mitochondrial ROS. *Nature* **515**, 431–435 (2014).
34. Zhang, W. et al. Evidence that hypoxia-inducible factor-1 (HIF-1) mediates transcriptional activation of interleukin-1β (IL-1β) in astrocyte cultures. *J. Neuroimmunol.* **174**, 63–73 (2006).
35. Peyssonnaux, C. et al. Cutting edge: essential role of hypoxia inducible factor-1α in development of lipopolysaccharide-induced sepsis. *J. Immunol.* **178**, 7516–7519 (2007).
36. Mills, E. L. et al. Succinate dehydrogenase supports metabolic repurposing of mitochondria to drive inflammatory macrophages. *Cell* **167**, 457–470.e13 (2016).
37. El-Khoury, R. et al. Engineering the alternative oxidase gene to better understand and counteract mitochondrial defects: state of the art and perspectives. *Br. J. Pharmacol.* **171**, 2243–2249 (2014).
38. Jin, Z., Wei, W., Yang, M., Du, Y. & Wan, Y. Mitochondrial complex I activity suppresses inflammation and enhances bone resorption by shifting macrophage-osteoclast polarization. *Cell. Metab.* **20**, 483–498 (2014).
39. Murphy, M. P. How mitochondria produce reactive oxygen species. *Biochem. J.* **417**, 1–13 (2009).
40. Bénit, P. et al. Unsuspected task for an old team: succinate, fumarate and other Krebs cycle acids in metabolic remodeling. *Biochim. Biophys. Acta* **1837**, 1330–1337 (2014).
41. Brigati, C. et al. Inflammation, HIF-1, and the epigenetics that follows. *Mediators Inflamm.* **2010**, 263914 (2010).
42. Benn, C. S., Netea, M. G., Selin, L. K. & Aaby, P. A small jab—a big effect: nonspecific immunomodulation by vaccines. *Trends Immunol.* **34**, 431–439 (2013).
43. Saeed, S. et al. Epigenetic programming of monocyte-to-macrophage differentiation and trained innate immunity. *Science* **345**, 1251086 (2014).
44. Cheng, S. C. et al. mTOR- and HIF-1α-mediated aerobic glycolysis as metabolic basis for trained immunity. *Science* **345**, 1250684 (2014).
45. Park, J. et al. SIRT5-mediated lysine desuccinylation impacts diverse metabolic pathways. *Mol. Cell* **50**, 919–930 (2013).
46. Zhang, Z. et al. Identification of lysine succinylation as a new post-translational modification. *Nat. Chem. Biol.* **7**, 58–63 (2011).
47. Xie, L. et al. First succinyl-proteome profiling of extensively drug-resistant *Mycobacterium tuberculosis* revealed involvement of succinylation in cellular physiology. *J. Proteome Res.* **14**, 107–119 (2015).
48. Feng, S. et al. Succinyl-proteome profiling of *Dendrobium officinale*, an important traditional Chinese orchid herb, revealed involvement of succinylation in the glycolysis pathway. *BMC Genomics* **18**, 598 (2017).
49. He, D. et al. Global proteome analyses of lysine acetylation and succinylation reveal the widespread involvement of both modification in metabolism in the embryo of germinating rice seed. *J. Proteome Res.* **15**, 879–890 (2016).
50. Xie, Z. et al. Lysine succinylation and lysine malonylation in histones. *Mol. Cell. Proteomics* **11**, 100–107 (2012).
51. Du, J. et al. Sirt5 is a NAD-dependent protein lysine demalonylase and desuccinylase. *Science* **334**, 806–809 (2011).
52. Wang, Y. et al. KAT2A coupled with the α-KGDH complex acts as a histone H3 succinyltransferase. *Nature* **552**, 273–277 (2017).
53. Gibson, G. E. et al. α-ketoglutarate dehydrogenase complex–dependent succinylation of proteins in neurons and neuronal cell lines. *J. Neurochem.* **134**, 86–96 (2015).
54. Wang, F. et al. SIRT5 desuccinylates and activates pyruvate kinase M2 to block macrophage IL-1β production and to prevent dss-induced colitis in mice. *Cell Rep.* **19**, 2331–2344 (2017).
55. Cordes, T. et al. Immunoresponsive gene 1 and itaconate inhibit succinate dehydrogenase to modulate intracellular succinate levels. *J. Biol. Chem.* **291**, 14274–14284 (2016).
56. Lampropoulou, V. et al. Itaconate links inhibition of succinate dehydrogenase with macrophage metabolic remodeling and regulation of inflammation. *Cell Metab.* **24**, 158–166 (2016).
57. Meiser, J. et al. Pro-inflammatory macrophages sustain pyruvate oxidation through pyruvate dehydrogenase for the synthesis of itaconate and to enable cytokine expression. *J. Biol. Chem.* **291**, 3932–3946 (2016).
58. Németh, B. et al. Abolition of mitochondrial substrate-level phosphorylation by itaconic acid produced by LPS-induced Irg1 expression in cells of murine macrophage lineage. *FASEB J.* **30**, 286–300 (2016).
59. Okabe, M., Lies, D., Kanamasa, S. & Park, E. Y. Biotechnological production of itaconic acid and its biosynthesis in *Aspergillus terreus*. *Appl. Microbiol. Biotechnol.* **84**, 597–606 (2009).
60. Lee, C. G., Jenkins, N. A., Gilbert, D. J., Copeland, N. G. & O'Brien, W. E. Cloning and analysis of gene regulation of a novel LPS-inducible cDNA. *Immunogenetics* **41**, 263–270 (1995).
61. Shin, J. H. et al. ^{1}H NMR-based metabolomic profiling in mice infected with Mycobacterium tuberculosis. *J. Proteome Res.* **10**, 2238–2247 (2011).
62. Sugimoto, M. S. H. Y. et al. Non-targeted metabolite profiling in activated macrophage secretion. *Metabolomics* **8**, 624–633 (2011).
63. Michelucci, A. et al. Immune-responsive gene 1 protein links metabolism to immunity by catalyzing itaconic acid production. *Proc. Natl. Acad. Sci. USA.* **110**, 7820–7825 (2013).
64. McFadden, B. A. & Purohit, S. Itaconate, an isocitrate lyase-directed inhibitor in *Pseudomonas indigofera*. *J. Bacteriol.* **131**, 136–144 (1977).
65. Naujoks, J. et al. IFNs modify the proteome of *Legionella*-containing vacuoles and restrict infection via IRG1-derived itaconic acid. *PLoS Pathog.* **12**, e1005408 (2016).
66. Williams, J. O., Roche, T. E. & McFadden, B. A. Mechanism of action of isocitrate lyase from *Pseudomonas indigofera*. *Biochemistry* **10**, 1384–1390 (1971).
67. Bambouskova, M. et al. Electrophilic properties of itaconate and derivatives regulate the IκBξ–ATF3 inflammatory axis. *Nature* **556**, 501–504 (2018).
68. Mills, E. L. et al. Itaconate is an anti-inflammatory metabolite that activates Nrf2 via alkylation of KEAP1. *Nature* **556**, 113–117 (2018).
69. Nair, S. et al. *Irg1* expression in myeloid cells prevents immunopathology during *M. tuberculosis* infection. *J. Exp. Med.* **215**, 1035–1045 (2018).
70. Ackermann, W. W. & Potter, V. R. Enzyme inhibition in relation to chemotherapy. *Proc. Soc. Exp. Biol. Med.* **72**, 1–9 (1949).
71. El Azzouny, M. et al. Dimethyl itaconate is not metabolized into itaconate intracellularly. *J. Biol. Chem.* **292**, 4766–4769 (2017).

72. Kobayashi, E. H. et al. Nrf2 suppresses macrophage inflammatory response by blocking proinflammatory cytokine transcription. *Nat. Commun.* **7**, 11624 (2016).
73. Brennan, M. S. et al. Dimethyl fumarate and monoethyl fumarate exhibit differential effects on KEAP1, NRF2 activation, and glutathione depletion in vitro. *PLoS One* **10**, e0120254 (2015).
74. Saito, R. et al. Characterizations of three major cysteine sensors of Keap1 in stress response. *Mol. Cell Biol.* **36**, 271–284 (2015).
75. Li, Y. et al. Immune responsive gene 1 (IRG1) promotes endotoxin tolerance by increasing A20 expression in macrophages through reactive oxygen species. *J. Biol. Chem.* **288**, 16225–16234 (2013).
76. Van Quickelberghe, E. et al. Identification of immune-responsive gene 1 (IRG1) as a target of A20. *J. Proteome Res.* **17**, 2182–2191 (2018).
77. Jamal Uddin, M. et al. IRG1 induced by heme oxygenase-1/carbon monoxide inhibits LPS-mediated sepsis and pro-inflammatory cytokine production. *Cell Mol. Immunol.* **13**, 170–179 (2016).
78. Cheon, Y. P., Xu, X., Bagchi, M. K. & Bagchi, I. C. Immune-responsive gene 1 is a novel target of progesterone receptor and plays a critical role during implantation in the mouse. *Endocrinology* **144**, 5623–5630 (2003).
79. Luan, H. H. & Medzhitov, R. Food fight: role of itaconate and other metabolites in antimicrobial defense. *Cell. Metab.* **24**, 379–387 (2016).
80. Sherwin, J. R. et al. Identification of genes regulated by leukemia-inhibitory factor in the mouse uterus at the time of implantation. *Mol. Endocrinol.* **18**, 2185–2195 (2004).
81. Weiss, J. M. et al. Itaconic acid mediates crosstalk between macrophage metabolism and peritoneal tumors. *J. Clin. Invest.* **128**, 3794–3805 (2018).
82. Hall, C. J. et al. Immunoresponsive gene 1 augments bactericidal activity of macrophage-lineage cells by regulating β-oxidation-dependent mitochondrial ROS production. *Cell. Metab.* **18**, 265–278 (2013).
83. Shi, H. Z., Wang, D., Sun, X. N. & Sheng, L. MicroRNA-378 acts as a prognosis marker and inhibits cell migration, invasion and epithelial-mesenchymal transition in human glioma by targeting IRG1. *Eur. Rev. Med. Pharmacol. Sci.* **22**, 3837–3846 (2018).
84. Pan, J. et al. Immune responsive gene 1, a novel oncogene, increases the growth and tumorigenicity of glioma. *Oncol. Rep.* **32**, 1957–1966 (2014).
85. Frezza, C. Mitochondrial metabolites: undercover signalling molecules. *Interface Focus* **7**, 20160100 (2017).
86. Arts, R. J. et al. Glutaminolysis and fumarate accumulation integrate immunometabolic and epigenetic programs in trained immunity. *Cell. Metab.* **24**, 807–819 (2016).
87. Tomlinson, I. P. et al. Germline mutations in FH predispose to dominantly inherited uterine fibroids, skin leiomyomata and papillary renal cell cancer. *Nat. Genet.* **30**, 406–410 (2002).
88. Xiao, M. et al. Inhibition of α-KG-dependent histone and DNA demethylases by fumarate and succinate that are accumulated in mutations of FH and SDH tumor suppressors. *Genes Dev.* **26**, 1326–1338 (2012).
89. Delage, B. et al. Arginine deprivation and argininosuccinate synthetase expression in the treatment of cancer. *Int. J. Cancer* **126**, 2762–2772 (2010).
90. Blewett, M. M. et al. Chemical proteomic map of dimethyl fumarate-sensitive cysteines in primary human T cells. *Sci. Signal.* **9**, rs10 (2016).
91. Angiari, S. & O'Neill, L. A. Dimethyl fumarate: targeting glycolysis to treat MS. *Cell Res.* **28**, 613–615 (2018).
92. Kornberg, M. D. et al. Dimethyl fumarate targets GAPDH and aerobic glycolysis to modulate immunity. *Science* **360**, 449–453 (2018).
93. Brück, J., Dringen, R., Amasuno, A., Pau-Charles, I. & Ghoreschi, K. A review of the mechanisms of action of dimethylfumarate in the treatment of psoriasis. *Exp. Dermatol.* **27**, 611–624 (2018).
94. Mills, E. A., Ogrodnik, M. A., Plave, A. & Mao-Draayer, Y. Emerging understanding of the mechanism of action for dimethyl fumarate in the treatment of multiple sclerosis. *Front. Neurol.* **9**, 5 (2018).
95. Zheng, L. et al. Fumarate induces redox-dependent senescence by modifying glutathione metabolism. *Nat. Commun.* **6**, 6001 (2015).
96. Sciacovelli, M. & Frezza, C. Oncometabolites: unconventional triggers of oncogenic signalling cascades. *Free Radic. Biol. Med.* **100**, 175–181 (2016).
97. Rustin, P. et al. Inborn errors of the Krebs cycle: a group of unusual mitochondrial diseases in human. *Biochim. Biophys. Acta* **1361**, 185–197 (1997).
98. Allegri, G. et al. Fumaric aciduria: an overview and the first Brazilian case report. *J. Inherit. Metab. Dis.* **33**, 411–419 (2010).
99. Blatnik, M., Thorpe, S. R. & Baynes, J. W. Succination of proteins by fumarate: mechanism of inactivation of glyceraldehyde-3-phosphate dehydrogenase in diabetes. *Ann. NY Acad. Sci.* **1126**, 272–275 (2008).
100. Adam, J. et al. Renal cyst formation in Fh1-deficient mice is independent of the Hif/Phd pathway: roles for fumarate in KEAP1 succination and Nrf2 signaling. *Cancer Cell* **20**, 524–537 (2011).
101. Ooi, A. et al. An antioxidant response phenotype shared between hereditary and sporadic type 2 papillary renal cell carcinoma. *Cancer Cell* **20**, 511–523 (2011).
102. Sullivan, L. B. et al. The proto-oncometabolite fumarate binds glutathione to amplify ROS-dependent signaling. *Mol. Cell* **51**, 236–248 (2013).
103. Linehan, W. M. et al. Comprehensive molecular characterization of papillary renal-cell carcinoma. *N. Engl. J. Med.* **374**, 135–145 (2016).
104. Ternette, N. et al. Inhibition of mitochondrial aconitase by succination in fumarate hydratase deficiency. *Cell Rep.* **3**, 689–700 (2013).
105. Kerins, M. J. et al. Fumarate mediates a chronic proliferative signal in fumarate hydratase-inactivated cancer cells by increasing transcription and translation of ferritin genes. *Mol. Cell Biol.* **37**, e00079-17 (2017).
106. Tyrakis, P. A. et al. Fumarate hydratase loss causes combined respiratory chain defects. *Cell Rep.* **21**, 1036–1047 (2017).
107. Bardella, C. et al. Aberrant succination of proteins in fumarate hydratase-deficient mice and HLRCC patients is a robust biomarker of mutation status. *J. Pathol.* **225**, 4–11 (2011).
108. Laukka, T. et al. Fumarate and succinate regulate expression of hypoxia-inducible genes via TET enzymes. *J. Biol. Chem.* **291**, 4256–4265 (2016).
109. Salminen, A., Kauppinen, A. & Kaarniranta, K. 2-Oxoglutarate-dependent dioxygenases are sensors of energy metabolism, oxygen availability, and iron homeostasis: potential role in the regulation of aging process. *Cell. Mol. Life Sci.* **72**, 3897–3914 (2015).
110. Isaacs, J. S. et al. HIF overexpression correlates with biallelic loss of fumarate hydratase in renal cancer: novel role of fumarate in regulation of HIF stability. *Cancer Cell.* **8**, 143–153 (2005).
111. Yang, M., Soga, T., Pollard, P. J. & Adam, J. The emerging role of fumarate as an oncometabolite. *Front. Oncol.* **2**, 85 (2012).
112. Sciacovelli, M. et al. Fumarate is an epigenetic modifier that elicits epithelial-to-mesenchymal transition. *Nature* **537**, 544–547 (2016).
113. Brabletz, T., Kalluri, R., Nieto, M. A. & Weinberg, R. A. EMT in cancer. *Nat. Rev. Cancer* **18**, 128–134 (2018).
114. Brat, D. J. et al. Comprehensive, integrative genomic analysis of diffuse lower-grade gliomas. *N. Engl. J. Med.* **372**, 2481–2498 (2015).
115. Yogev, O. et al. Fumarase: a mitochondrial metabolic enzyme and a cytosolic/nuclear component of the DNA damage response. *PLoS Biol.* **8**, e1000328 (2010).
116. Jiang, Y. et al. Local generation of fumarate promotes DNA repair through inhibition of histone H3 demethylation. *Nat. Cell Biol.* **17**, 1158–1168 (2015).
117. Sulkowski, P. L. et al. Krebs-cycle-deficient hereditary cancer syndromes are defined by defects in homologous-recombination DNA repair. *Nat. Genet.* **50**, 1086–1092 (2018).
118. Johnson, T. I., Costa, A. S. H., Ferguson, A. N. & Frezza, C. Fumarate hydratase loss promotes mitotic entry in the presence of DNA damage after ionising radiation. *Cell Death Dis.* **9**, 913 (2018).
119. Ye, D., Guan, K. L. & Xiong, Y. Metabolism, activity, and targeting of d- and l-2-Hydroxyglutarates. *Trends Cancer* **4**, 151–165 (2018).
120. Chalmers, R. A. et al. d-2-hydroxyglutaric aciduria: case report and biochemical studies. *J. Inherit. Metab. Dis.* **3**, 11–15 (1980).
121. Duran, M., Kamerling, J. P., Bakker, H. D., van Gennip, A. H. & Wadman, S. K. l-2-Hydroxyglutaric aciduria: an inborn error of metabolism? *J. Inherit. Metab. Dis.* **3**, 109–112 (1980).
122. Kranendijk, M., Struys, E. A., Salomons, G. S., Van der Knaap, M. S. & Jakobs, C. Progress in understanding 2-hydroxyglutaric acidurias. *J. Inherit. Metab. Dis.* **35**, 571–587 (2012).
123. Rzem, R. et al. A gene encoding a putative FAD-dependent l-2-hydroxyglutarate dehydrogenase is mutated in l-2-hydroxyglutaric aciduria. *Proc. Natl. Acad. Sci. USA* **101**, 16849–16854 (2004).
124. Struys, E. A. et al. Mutations in the d-2-hydroxyglutarate dehydrogenase gene cause D-2-hydroxyglutaric aciduria. *Am. J. Hum. Genet.* **76**, 358–360 (2005).
125. Topçu, M. et al. l-2-Hydroxyglutaric aciduria: identification of a mutant gene C14orf160, localized on chromosome 14q22.1. *Hum. Mol. Genet.* **13**, 2803–2811 (2004).
126. Kranendijk, M. et al. IDH2 mutations in patients with d-2-hydroxyglutaric aciduria. *Science* **330**, 336 (2010).
127. Nota, B. et al. Deficiency in SLC25A1, encoding the mitochondrial citrate carrier, causes combined d-2- and l-2-hydroxyglutaric aciduria. *Am. J. Hum. Genet.* **92**, 627–631 (2013).
128. Dang, L. & Su, S. M. Isocitrate dehydrogenase mutation and *R*-2-hydroxyglutarate: from basic discovery to therapeutics development. *Annu. Rev. Biochem.* **86**, 305–331 (2017).
129. Mardis, E. R. et al. Recurring mutations found by sequencing an acute myeloid leukemia genome. *N. Engl. J. Med.* **361**, 1058–1066 (2009).
130. Parsons, D. W. et al. An integrated genomic analysis of human glioblastoma multiforme. *Science* **321**, 1807–1812 (2008).
131. MacIver, N. J., Michalek, R. D. & Rathmell, J. C. Metabolic regulation of T lymphocytes. *Annu. Rev. Immunol.* **31**, 259–283 (2013).
132. Dang, E. V. et al. Control of T_H17/T_{reg} balance by hypoxia-inducible factor 1. *Cell* **146**, 772–784 (2011).

133. Xu, T. et al. Metabolic control of T_H17 and induced T_{reg} cell balance by an epigenetic mechanism. *Nature* **548**, 228–233 (2017).
134. Figueroa, M. E. et al. Leukemic IDH1 and IDH2 mutations result in a hypermethylation phenotype, disrupt TET2 function, and impair hematopoietic differentiation. *Cancer Cell.* **18**, 553–567 (2010).
135. Losman, J. A. et al. *R*-2-hydroxyglutarate is sufficient to promote leukemogenesis and its effects are reversible. *Science* **339**, 1621–1625 (2013).
136. Tyrakis, P. A. et al. *S*-2-hydroxyglutarate regulates $CD8^+$ T-lymphocyte fate. *Nature* **540**, 236–241 (2016).
137. Doedens, A. L. et al. Hypoxia-inducible factors enhance the effector responses of $CD8^+$ T cells to persistent antigen. *Nat. Immunol.* **14**, 1173–1182 (2013).
138. Finlay, D. K. et al. PDK1 regulation of mTOR and hypoxia-inducible factor 1 integrate metabolism and migration of $CD8^+$ T cells. *J. Exp. Med.* **209**, 2441–2453 (2012).
139. Suzuki, H. et al. Mutational landscape and clonal architecture in grade II and III gliomas. *Nat. Genet.* **47**, 458–468 (2015).
140. Watanabe, T., Nobusawa, S., Kleihues, P. & Ohgaki, H. IDH1 mutations are early events in the development of astrocytomas and oligodendrogliomas. *Am. J. Pathol.* **174**, 1149–1153 (2009).
141. Dang, L. et al. Cancer-associated IDH1 mutations produce 2-hydroxyglutarate. *Nature* **462**, 739–744 (2009).
142. Ward, P. S. et al. The common feature of leukemia-associated IDH1 and IDH2 mutations is a neomorphic enzyme activity converting α -ketoglutarate to 2-hydroxyglutarate. *Cancer Cell* **17**, 225–234 (2010).
143. Yan, H. et al. IDH1 and IDH2 mutations in gliomas. *N. Engl. J. Med.* **360**, 765–773 (2009).
144. Chowdhury, R. et al. The oncometabolite 2-hydroxyglutarate inhibits histone lysine demethylases. *EMBO Rep.* **12**, 463 (2011).
145. Xu, W. et al. Oncometabolite 2-hydroxyglutarate is a competitive inhibitor of α-ketoglutarate-dependent dioxygenases. *Cancer Cell.* **19**, 17–30 (2011).
146. Noushmehr, H. et al. Identification of a CpG island methylator phenotype that defines a distinct subgroup of glioma. *Cancer Cell.* **17**, 510–522 (2010).
147. Turcan, S. et al. IDH1 mutation is sufficient to establish the glioma hypermethylator phenotype. *Nature* **483**, 479–483 (2012).
148. Wang, P. et al. Mutations in isocitrate dehydrogenase 1 and 2 occur frequently in intrahepatic cholangiocarcinomas and share hypermethylation targets with glioblastomas. *Oncogene* **32**, 3091–3100 (2013).
149. Flavahan, W. A. et al. Insulator dysfunction and oncogene activation in IDH mutant gliomas. *Nature* **529**, 110–114 (2016).
150. Zhao, S. et al. Glioma-derived mutations in IDH1 dominantly inhibit IDH1 catalytic activity and induce HIF-1α. *Science* **324**, 261–265 (2009).
151. Intlekofer, A. M. et al. Hypoxia induces production of l-2-hydroxyglutarate. *Cell Metab.* **22**, 304–311 (2015).
152. Intlekofer, A. M. et al. l-2-Hydroxyglutarate production arises from noncanonical enzyme function at acidic pH. *Nat. Chem. Biol.* **13**, 494–500 (2017).
153. Nadtochiy, S. M. et al. Acidic pH Is a metabolic switch for 2-hydroxyglutarate generation and signaling. *J. Biol. Chem.* **291**, 20188–20197 (2016).
154. Sasaki, M. et al. d-2-hydroxyglutarate produced by mutant IDH1 perturbs collagen maturation and basement membrane function. *Genes Dev.* **26**, 2038–2049 (2012).
155. Tarhonskaya, H. et al. Non-enzymatic chemistry enables 2-hydroxyglutarate-mediated activation of 2-oxoglutarate oxygenases. *Nat. Commun.* **5**, 3423 (2014).
156. Wang, P. et al. Oncometabolite d-2-hydroxyglutarate inhibits ALKBH DNA repair enzymes and sensitizes IDH mutant cells to alkylating agents. *Cell Rep.* **13**, 2353–2361 (2015).
157. Inoue, S. et al. Mutant IDH1 downregulates ATM and alters DNA repair and sensitivity to DNA damage independent of TET2. *Cancer Cell* **30**, 337–348 (2016).
158. Carbonneau, M. et al. The oncometabolite 2-hydroxyglutarate activates the mTOR signalling pathway. *Nat. Commun.* **7**, 12700 (2016).
159. Reitman, Z. J. et al. Profiling the effects of isocitrate dehydrogenase 1 and 2 mutations on the cellular metabolome. *Proc. Natl. Acad. Sci. USA* **108**, 3270–3275 (2011).
160. Chesnelong, C. et al. Lactate dehydrogenase A silencing in IDH mutant gliomas. *Neuro-Oncol.* **16**, 686–695 (2014).
161. Grassian, A. R. et al. IDH1 mutations alter citric acid cycle metabolism and increase dependence on oxidative mitochondrial metabolism. *Cancer Res.* **74**, 3317–3331 (2014).
162. Izquierdo-Garcia, J. L. et al. IDH1 mutation induces reprogramming of pyruvate metabolism. *Cancer Res.* **75**, 2999–3009 (2015).
163. Chen, J. Y. et al. The oncometabolite R-2-hydroxyglutarate activates NF-κ B-dependent tumor-promoting stromal niche for acute myeloid leukemia cells. *Sci. Rep.* **6**, 1 (2016).
164. Li, F. et al. $NADP^+$–IDH mutations promote hypersuccinylation that impairs mitochondria respiration and induces apoptosis resistance. *Mol. Cell* **60**, 661–675 (2015).
165. Jiang, B. et al. IDH1 mutation promotes tumorigenesis by inhibiting JNK activation and apoptosis induced by serum starvation. *Cell Rep.* **19**, 389–400 (2017).
166. Yang, Z. et al. 2-HG inhibits necroptosis by stimulating DNMT1-dependent hypermethylation of the RIP3 promoter. *Cell Rep.* **19**, 1846–1857 (2017).
167. Kurdistani, S. K. & Grunstein, M. Histone acetylation and deacetylation in yeast. *Nat. Rev. Mol. Cell Biol.* **4**, 276–284 (2003).
168. Wellen, K. E. et al. ATP-citrate lyase links cellular metabolism to histone acetylation. *Science* **324**, 1076–1080 (2009).
169. Peng, M. et al. Aerobic glycolysis promotes T helper 1 cell differentiation through an epigenetic mechanism. *Science* **354**, 481–484 (2016).
170. Chang, C. H. et al. Posttranscriptional control of T cell effector function by aerobic glycolysis. *Cell* **153**, 1239–1251 (2013).
171. Osinalde, N. et al. Nuclear phosphoproteomic screen uncovers ACLY as mediator of IL-2-induced proliferation of $CD4^+$ T lymphocytes. *Mol. Cell. Proteomics* **15**, 2076–2092 (2016).
172. Lee, J. V. et al. Akt-dependent metabolic reprogramming regulates tumor cell histone acetylation. *Cell. Metab.* **20**, 306–319 (2014).
173. Zhang, L., Liu, Z., Ma, W. & Wang, B. The landscape of histone acetylation involved in epithelial-mesenchymal transition in lung cancer. *J. Can. Res. Ther.* **9**, S86–S91 (2013).
174. Mi, W. et al. YEATS2 links histone acetylation to tumorigenesis of non-small cell lung cancer. *Nat. Commun.* **8**, 1088 (2017).
175. Sivanand, S. et al. Nuclear acetyl-CoA production by ACLY promotes homologous recombination. *Mol. Cell* **67**, 252–265.e56 (2017).
176. Valls-Lacalle, L. et al. Succinate dehydrogenase inhibition with malonate during reperfusion reduces infarct size by preventing mitochondrial permeability transition. *Cardiovasc. Res.* **109**, 374–384 (2016).
177. Valls-Lacalle, L. et al. Selective inhibition of succinate dehydrogenase in reperfused myocardium with intracoronary malonate reduces infarct size. *Sci. Rep.* **8**, 2442 (2018).
178. Kohlhauer, M. et al. Metabolomic profiling in acute ST-segment-elevation myocardial infarction identifies succinate as an early marker of human ischemia-reperfusion injury. *J. Am. Heart Assoc.* **7**, e007546 (2018).
179. Zhang, J. et al. accumulation of succinate in cardiac ischemia primarily occurs via canonical Krebs cycle activity. *Cell Rep.* **23**, 2617–2628 (2018).
180. Ariza, A. C., Deen, P. M. & Robben, J. H. The succinate receptor as a novel therapeutic target for oxidative and metabolic stress-related conditions. *Front. Endocrinol. (Lausanne)* **3**, 22 (2012).
181. Hamel, D. et al. G-protein-coupled receptor 91 and succinate are key contributors in neonatal postcerebral hypoxia-ischemia recovery. *Arterioscler. Thromb. Vasc. Biol.* **34**, 285–293 (2014).
182. Jean, S. R., Ahmed, M., Lei, E. K., Wisnovsky, S. P. & Kelley, S. O. Peptide-mediated delivery of chemical probes and therapeutics to mitochondria. *Acc. Chem. Res.* **49**, 1893–1902 (2016).
183. An, J., Rao, A. & Ko, M. TET family dioxygenases and DNA demethylation in stem cells and cancers. *Exp. Mol. Med.* **49**, e323 (2017).
184. Vissers, M. C., Kuiper, C. & Dachs, G. U. Regulation of the 2-oxoglutarate-dependent dioxygenases and implications for cancer. *Biochem. Soc. Trans.* **42**, 945–951 (2014).
185. Zhang, J. et al. Effect of TET inhibitor on bovine parthenogenetic embryo development. *PLoS One* **12**, e0189542 (2017).
186. Hatch, S. B. et al. Assessing histone demethylase inhibitors in cells: lessons learned. *Epigenetics Chromatin* **10**, 9 (2017).
187. Maes, T., Carceller, E., Salas, J., Ortega, A. & Buesa, C. Advances in the development of histone lysine demethylase inhibitors. *Curr. Opin. Pharmacol.* **23**, 52–60 (2015).
188. Pergola, P. E., Spinowitz, B. S., Hartman, C. S., Maroni, B. J. & Haase, V. H. Vadadustat, a novel oral HIF stabilizer, provides effective anemia treatment in nondialysis-dependent chronic kidney disease. *Kidney Int.* **90**, 1115–1122 (2016).
189. Yeh, T. L. et al. Molecular and cellular mechanisms of HIF prolyl hydroxylase inhibitors in clinical trials. *Chem. Sci.* **8**, 7651–7668 (2017).
190. Yen, K. et al. AG-221, a first-in-class therapy targeting acute myeloid leukemia harboring oncogenic *IDH2* mutations. *Cancer Discov.* **7**, 478–493 (2017).
191. Smith, R. A., Hartley, R. C., Cochemé, H. M. & Murphy, M. P. Mitochondrial pharmacology. *Trends Pharmacol. Sci.* **33**, 341–352 (2012).
192. Smith, R. A., Hartley, R. C. & Murphy, M. P. Mitochondria-targeted small molecule therapeutics and probes. *Antioxid. Redox Signal.* **15**, 3021–3038 (2011).
193. Yousif, L. F., Stewart, K. M. & Kelley, S. O. Targeting mitochondria with organelle-specific compounds: strategies and applications. *Chembiochem* **10**, 1939–1950 (2009).

194. Fan, T. W. et al. Altered regulation of metabolic pathways in human lung cancer discerned by ^{13}C stable isotope-resolved metabolomics (SIRM). *Mol. Cancer* **8**, 41 (2009).
195. Sellers, K. et al. Pyruvate carboxylase is critical for non-small-cell lung cancer proliferation. *J. Clin. Invest.* **125**, 687–698 (2015).
196. Maher, E. A. et al. Metabolism of [U-^{13}C]glucose in human brain tumors in vivo. *NMR Biomed.* **25**, 1234–1244 (2012).
197. Hensley, C. T. et al. Metabolic heterogeneity in human lung tumors. *Cell* **164**, 681–694 (2016).
198. Joshi, S. et al. The genomic landscape of renal oncocytoma identifies a metabolic barrier to tumorigenesis. *Cell Rep.* **13**, 1895–1908 (2015).

Acknowledgements

This work was supported by a grant to M.P.M. from the Medical Research Council UK (MC_U105663142) and a Wellcome Trust Investigator award to MPM (110159/Z/15/Z). The O'Neill laboratory acknowledges the following grant support: European Research Council (ECFP7-ERC-MICROINNATE), Science Foundation Ireland Investigator Award (SFI 12/IA/1531), GlaxoSmithKline Visiting Scientist Programme and The Wellcome Trust (oneill-wellcometrust-metabolic, grant number 205455).

Author contributions

All authors wrote, edited and approved final manuscript.

Competing interests

The authors declare no competing interests.

Additional information

Reprints and permissions information is available at www.nature.com/reprints.

Correspondence should be addressed to L.A.O.

FEBS Letters

FEBS PRESS science publishing by scientists

REVIEW ARTICLE

Krebs cycle rewired for macrophage and dendritic cell effector functions

Dylan Gerard Ryan and Luke A. J. O'Neill

School of Biochemistry and Immunology, Trinity College, Dublin, Ireland

Correspondence
D. G. Ryan, School of Biochemistry and Immunology, Trinity College, Dublin, Ireland
Fax: +353 1 677 2400
Tel: +353 1 896 2439
E-mail: ryand38@tcd.ie

(Received 22 May 2017, revised 28 June 2017, accepted 2 July 2017, available online 26 July 2017)

doi:10.1002/1873-3468.12744

Edited by László Nagy

The Krebs cycle is an amphibolic pathway operating in the mitochondrial matrix of all eukaryotic organisms. In response to proinflammatory stimuli, macrophages and dendritic cells undergo profound metabolic remodelling to support the biosynthetic and bioenergetic requirements of the cell. Recently, it has been discovered that this metabolic shift also involves the rewiring of the Krebs cycle to regulate cellular metabolic flux and the accumulation of Krebs cycle intermediates, notably, citrate, succinate and fumarate. Interestingly, a new role for Krebs cycle intermediates as signalling molecules and immunomodulators that dictate the inflammatory response has begun to emerge. This review will discuss the latest developments in Krebs cycle rewiring and immune cell effector functions, with a particular focus on the regulation of cytokine production.

Keywords: citrate; cytokines; dendritic cell; fumarate; inflammation; itaconate; Krebs cycle; macrophage; succinate

Metabolic reprogramming in macrophages and DCs

Macrophages and dendritic cells (DCs) constitute two major components of the innate immune system responsible for sensing microbial compounds and the products of damaged tissue [1,2]. The sensing of such products is achieved via the utilisation of multiple families of so-called pattern recognition receptors (PRRs), such as toll-like receptors (TLRs) [1,2]. Several recent studies have implicated the global rewiring of metabolic pathways, elicited during the transition from a resting to an activated state, in response to the TLR ligand lipopolysaccharide (LPS) and other proinflammatory stimuli [2]. A well-characterised response to LPS is the shift away from the use of oxidative phosphorylation (OXPHOS) towards a glycolytic phenotype, termed aerobic glycolysis or the Warburg effect, thus tailoring cellular metabolism to suit the bioenergetic and biosynthetic demands of the cell (Fig. 1) [2–4]. This metabolic switch also supports the diversion of glucose and glycolytic intermediates into the pentose phosphate pathway (PPP) [5,6]. The PPP is an anabolic pathway that runs parallel to glycolysis and is essential to produce NADPH, an important cofactor in lipid biosynthesis, antioxidant defence, and nitric oxide (NO) and reactive oxygen species (ROS) production [5,6]. The PPP also generates ribose 5-phosphate (R5P), an important precursor for nucleotide biosynthesis [5,6]. The very first observation of increased glycolysis and decreased OXPHOS in macrophages occurred in 1969 [7], and since then we have

Abbreviations
ACC, acetyl-CoA carboxylase; ACO, aconitase; BTA, 1,2,3-benzentricarboxylic acid; CIC, citrate carrier; COX2, cyclooxygenase 2; CS, citrate synthase; DCs, dendritic cells; ER, endoplasmic reticulum; ETC., electron transport chain; FH, fumarase; HAT, histone acetyltransferase; HDAC, histone deacetylase; IDH, isocitrate dehydrogenase; IFN-γ, interferon-gamma; IMM, inner mitochondrial membrane; LPS, lipopolysaccharide; MDH, malate dehydrogenase; NO, nitric oxide; OGDH, α-ketoglutarate dehydrogenase; OXPHOS, oxidative phosphorylation; PDK1, pyruvate dehydrogenase kinase 1; PPP, pentose phosphate pathway; PQ, paraquat; PRRs, pattern recognition receptors; R5P, ribose 5-phosphate; ROS, reactive oxygen species; SDH, succinate dehydrogenase; SLP, substrate-level phosphorylation; SNPs, single nucleotide polymorphisms; TLRs, toll-like receptors.

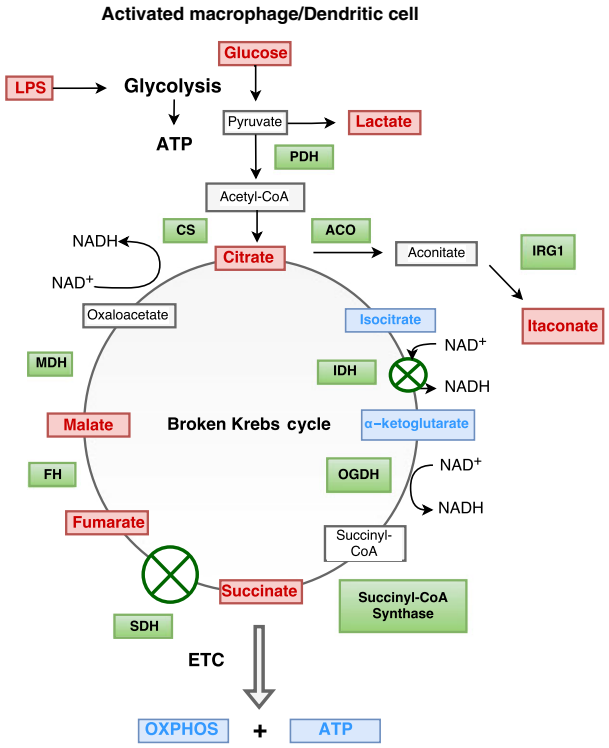

Fig. 1. Krebs cycle rewiring in macrophages and DCs. To meet their bioenergetic demands, quiescent macrophages and DCs utilise an intact Krebs cycle and oxidative phosphorylation (OXPHOS) to generate ATP. However, in response to lipopolysaccharide (LPS) and other proinflammatory stimuli, they undergo glycolytic reprogramming to generate ATP and lactate, while the Krebs cycle is rewired to facilitate the accumulation of the Krebs cycle intermediates citrate, succinate, fumarate and malate. Citrate is also diverted away from the Krebs cycle to form itaconate via aconitate. Accompanying this remodelling is a downregulation of OXPHOS and ATP production by the electron transport chain (ETC).

garnered important molecular insights into the signalling pathways that govern this switch during both macrophage and DC activation. Here we describe these recent findings, with a renewed focus on the role of Krebs cycle intermediates in these critical immune and inflammatory cells.

Krebs cycle rewiring

Accompanying the downregulation of OXPHOS and metabolic remodelling is a dramatic change in cell-intrinsic and -extrinsic metabolite levels, such as those that participate in the Krebs cycle (also known as the TCA or citric acid cycle), or those derived from Krebs cycle intermediates [8–10]. Elevated metabolite levels arise in large part due to a rewiring of the Krebs cycle upon immune cell activation (Fig. 1) [10]. The Krebs cycle was first proposed by Hans Adolf Krebs in 1937 and is the primary oxidative pathway for acetyl coenzyme A (acetyl-CoA) derived from carbohydrates, fats and amino acids in aerobic organisms [11,12]. The Krebs cycle is referred to as an amphibolic pathway, which is defined as a pathway that participates in both anabolic and catabolic processes. As such, it can be considered a nexus for integrating multiple anabolic and catabolic pathways, including glycolysis, gluconeogenesis, transamination, deamination, β-oxidation and lipogenesis [13].

The Krebs cycle occurs in the mitochondrial matrix and is comprised of several enzymes, namely, citrate synthase (CS), aconitase (ACO), isocitrate dehydrogenase (IDH), α-ketoglutarate dehydrogenase (OGDH), succinyl-CoA synthase, succinate dehydrogenase (SDH), fumarase (FH) and malate dehydrogenase (MDH) [14]. As mentioned, acetyl-CoA can be derived from many sources, including glucose [13]. Glucose is catabolised to pyruvate, via glycolysis, prior to decarboxylation by the pyruvate dehydrogenase complex (PDH) to form the two-carbon compound acetyl-CoA and the cofactor NADH [13]. Three major products of the Krebs cycle are NADH, GTP and $FADH_2$ (generated by SDH) [15]. NADH and $FADH_2$ are extremely important as they are reducing equivalents that can transfer electrons to the electron transport chain (ETC.), a series of protein complexes found along the inner mitochondrial membrane (IMM) [15]. Transfer of electrons along the ETC. occurs via a series of redox reactions that leads to the pumping of protons (H^+) across the inner membrane to generate the mitochondrial membrane potential ($M\Delta\psi$). Successful transfer of electrons is required to support formation of an electrochemical gradient that drives OXPHOS and highly efficient ATP production via ATP synthase [15].

For a full turn of the cycle to be completed, a series of eight enzymatic reactions are required (Fig. 1). The first step, catalysed by CS, is referred to as an aldol condensation reaction, whereby acetyl-CoA and oxaloacetate are converted to citrate [13]. Citrate is then converted to isocitrate by aconitase in a two-step reaction that first produces cis-aconitate via a dehydration reaction, which subsequently undergoes rehydration to form isocitrate [13]. The third reaction is catalysed by IDH, whereby isocitrate is decarboxylated to form α-ketoglutarate, CO_2 and NADH [13]. This step will be very important in future discussions of Krebs cycle rewiring. The next two reactions result in the conversion of α-ketoglutarate to succinate, via succinyl-CoA, which involves a second oxidative decarboxylation step followed by substrate-level phosphorylation (SLP), catalysed by α-ketoglutarate

dehydrogenase and succinyl-CoA synthase respectively [13]. Like the third reaction, the flavin-dependent dehydrogenation of succinate to fumarate by SDH is also of the utmost importance when discussing metabolic reprogramming of the Krebs cycle in activated macrophages [13]. The final two steps of the cycle involve the hydration of the α,β-unsaturated C=C double bond of fumarate to form malate, catalysed by FH, and regeneration of oxaloacetate from malate by MDH [13]. The conversion of malate to oxaloacetate also produces NADH and the regeneration of oxaloacetate completes the cycle as it can then react with newly generated acetyl-CoA to form citrate, hitherto starting another round of reactions [13].

As previously mentioned, the Krebs cycle is amphibolic and so diversion of nutrients towards the cycle (anaplerosis) or removal of intermediates to feed into biosynthetic pathways (cataplerosis) can be dictated by environmental cues, such as proinflammatory stimuli and nutrient availability, through modulation of the activity and expression of these TCA cycle enzymes. It is now appreciated that resting macrophages and DCs utilise OXPHOS and an intact TCA cycle to generate ATP and meet the bioenergetic demands of the cell [5,10,16]. However, in response to LPS (or LPS in combination with interferon-gamma (IFN-γ)), we see a dramatic rewiring of the Krebs cycle in macrophages, as identified by the accumulation of the Krebs cycle intermediates citrate, succinate and fumarate [8,10,17]. The importance of these metabolites in immune cell function will now be discussed in turn.

Citrate metabolism and inflammation

Citrate as a signal for ROS and NO production

It has been proposed that the accumulation of citrate in macrophages is in part caused by a break point in the TCA cycle at IDH (Table 1) [8,10,17]. Using an integrated high-throughput transcriptional metabolic profiling and analysis pipeline (CoMBI-T), Jha *et al.* [10,17] observed significant downregulation of *Idh* mRNA and a decreased pool of α-ketoglutarate. This suggested a reduction in isocitrate to α-ketoglutarate conversion constituting the first breakpoint in the cycle. To further examine metabolic flow through IDH, stable isotopic labelling experiments with U-^{13}C-glucose and U-^{13}C-glutamine was carried out [10,17]. This further validated the CoMBI-T results as 20% of citrate labelled after 4 h of stimulation was synthesised from glucose, whereas no glucose-derived carbons were found in α-ketoglutarate [10,17]. Reverse flow through IDH was also undetectably low based on the absence of glutamine-derived carbon labelling in citrate [10,17]. This breakpoint has also been observed in LPS-activated DCs utilising 1,2 ^{13}C-glucose tracing [5].

A key functional outcome of the switch to glycolysis and the repression of IDH is the channelling of pyruvate into the TCA cycle to form citrate [5,8,10,21]. In macrophages, glucose-derived pyruvate undergoes oxidation via PDH to form citrate in mitochondria, despite HIF1α induction, which is known to induce pyruvate dehydrogenase kinase 1 (PDK1), an inhibitor of PDH activity [21]. Notably, treatment of macrophages with LPS increases the expression of the mitochondrial citrate carrier (CIC), also known as solute carrier family 25 member 1 (Slc25a1), via activation of two NF-κB binding sites in the CIC promoter [18]. CIC catalyses the efflux of mitochondrial citrate in exchange for cytosolic malate, thus leading to accumulation of citrate in the cytosol (Table 1; Fig. 2) [18]. Genetic silencing of CIC or inhibition with the specific inhibitor, 1,2,3-benzentricarboxylic acid (BTA), leads to a marked reduction in NO and ROS production [18]. Although the mechanism by which citrate regulates NO and ROS is unknown, the authors propose that the observed effects can be explained based on the role of citrate in intermediary metabolism. In the cytosol, glucose-derived citrate can be converted to oxaloacetate and acetyl-CoA via ATP-citrate lyase (ACLY) [19]. In a follow-up study, Infantino *et al.* [32] found that ACLY was also induced in response to LPS and that genetic silencing and inhibition of ACLY activity similarly led to decreases in both NO and ROS levels (Table 1). The authors suggest that oxaloacetate itself may be converted to pyruvate in a two-step reaction involving cytosolic MDH and malic enzyme (ME), with NADPH being an important product [18]. However, evidence directly implicating citrate metabolism in regulating NO and ROS levels via NADPH has thus far been lacking. Another issue that must be noted is that no reverse or direct flow through ME has been detected in macrophages treated with LPS and IFN-γ [10].

Acetylation, *de novo* lipogenesis and prostaglandin synthesis

In addition to being an important signal for NO and ROS production, reprogramming of citrate metabolism is also essential to support acetyl-CoA production and *de novo* lipogenesis (lipid biosynthesis) in macrophages and DCs [5,8,10,20]. Cytosolic acetyl-CoA derived from citrate (Fig. 2) is an important cofactor for acetyltransferases, enzymes that catalyse the transfer of acetyl groups to lysine residues found on multiple proteins with distinct biological functions [19].

Table 1. Overview of metabolic enzyme/metabolite functions during Krebs cycle rewiring.

Protein name	Protein function in resting cell	Effect/Mechanism of TLR signalling	Effect of metabolic reprogramming	References
IDH	Converts isocitrate to α-ketoglutarate	Repressed in response to LPS and IFN-γ	Breakpoint in the Krebs cycle/ channelling of pyruvate to citrate	[8,10,17]
Slc25a1	Mitochondrial citrate transporter	TLR-activated NF-κB induces its expression via two binding sites in promoter	Accumulation of citrate in the cytosol/increased NO, ROS and PGE2 production	[18]
ACLY	Converts citrate to acetyl-CoA and oxaloacetate	Induced in response to LPS	Increased NO, ROS and PGE2 production	[19]
ACC	Converts acetyl-CoA to malonyl-CoA	Induced in response to LPS	*De novo* lipogenesis/membrane expansion of ER and Golgi/ increased cytokine and PGE2 production	[5]
FAMIN	Regulates *de novo* lipogenesis	Forms complex with FASN on peroxisome	Potentiates bactericidal activity/ ROS and cytokine production	[20]
IRG1/CAD	Converts *cis*-aconitate lo itaconate	Induced in response to LPS/ bacterial infection	Increased itaconate production/ inhibition of ICL and bactericidal activity/inhibits SDH and increases succinate/ inhibits ROS and cytokine production	[10,21–25]
SDH	Coverts succinate to fumarate/ complex II of the ETC.	Activity is decreased via inhibition with itaconate	RET-derived ROS regulates IL-1β production	[26]
HIF1α	Hypoxia-inducible transcription factor	Stabilised by ROS and succinate induced in response to LPS	Induces aerobic glycolysis/ boosts IL-1β production	[8,24,26,27]
SUCNR1/ GPR91	Gi- and Gq-coupled GPCR activated by succinate	Increased expression and PM localisation in response to TLR ligands	Acts as an autocrine and paracrine succinate sensor/ increases cytokine production/ enhanced chemotaxis and antigen presentation	[28–30]
KDM5	Histone demethylases	β-glucan-induced fumarate accumulation inhibits enzymatic activity	Enhanced cytokine production	[31]

Acetylation is an important post-translational modification known to be involved in sculpting the epigenome via modification of histones, a process regulated by ACLY [19]. Interestingly, genetic ablation of ACLY resulted in the suppression of genes involved in glycolysis and subsequently decreased glucose consumption [19]. These findings illustrate the crucial role of ACLY in linking cellular metabolism to the regulation of gene expression [19]. Citrate itself has also been shown to be an inhibitor HIF asparaginyl hydroxylase (FIH), an important regulator of HIF1α coactivator p300 acetyltransferase and HIF1α activity [33]. While no direct link between citrate/acetyl-CoA and glycolytic reprogramming has been shown in macrophages or DCs, work on other cell types suggest this may be an appealing avenue of investigation. However, acetylation has been shown to play an important role in the regulation of IL-6 and IL-10 in macrophages [34,35]. In paraquat (PQ)-treated macrophages, induction of IL-6 was found to be dependent on histone acetylation, as histone deacetylase (HDAC) inhibition enhanced expression of *Il6* mRNA, whereas histone acetyltransferase (HAT) inhibition blocked its induction [35]. Acetylation of α-tubulin in LPS-activated macrophages was also shown to regulate IL-10 induction [34]. Inactivation of the tubulin acetyltransferase MEC17 was found to inhibit IL-10, while inhibition of HDAC6 or stimulation of HDAC6-deficient macrophages with LPS led to IL-10 hyperinduction via p38 MAPK and Sp1-dependent *Il10* transcription [34].

Acetyl-CoA can also be funnelled into lipid biosynthesis via acetyl-CoA carboxylase (ACC), an enzyme that catalyses the conversion of acetyl-CoA to malonyl-CoA (Table 1; Fig. 2) [19,32]. Malonyl-CoA is then used as a substrate for fatty acid biosynthesis by fatty acid synthase (FASN), the rate-limiting enzyme responsible for synthesis of palmitate, the precursor to

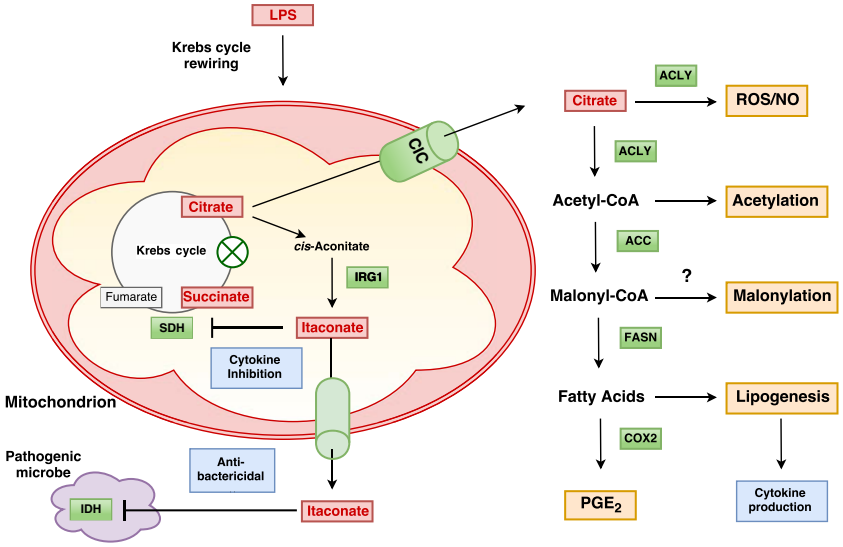

Fig. 2. Citrate metabolism and inflammation. In macrophages and DCs, citrate that accumulates due to Krebs cycle rewiring can be exported from mitochondria via CIC. In the cytosol, citrate can be converted to acetyl-CoA and oxaloacetate by ACLY leading to NO and ROS production by some unknown mechanism. Furthermore, acetyl-CoA can be used for acetylation by acetyltransferases or converted to malonyl-CoA via ACC. Similar to acetylation, malonly-CoA can be used to malonylate lysine residues or it can feed into fatty acid synthesis through FASN. Lipogenesis is essential for the production/secretion of cytokines and PGE_2. In the mitochondrial matrix, citrate can be converted to itaconate, via *cis*-aconitate, by IRG1. Itaconate may then act to inhibit SDH and cytokine production or be exported from mitochondria to inhibit microbial IDH and the glyoxylate shunt.

all lipids [12,36]. In DCs, citrate is funnelled from the Krebs cycle into *de novo* lipid biosynthesis that is subsequently required for membrane expansion of the endoplasmic reticulum (ER) and Golgi [5]. Inhibition of ACC with TOFA, or FASN with the inhibitor C75, blocked this process, which is essential for the synthesis, transport and secretion of TLR-induced cytokine production, e.g. IL-6, TNF-α and IL-12p40, and for LPS-induced surface expression of CD40, CD86 and MHC class I and class II proteins [5]. Inhibition of fatty acid synthesis in DCs also inhibited secretion of the inflammatory lipid-mediator prostaglandin E_2 (PGE_2), which is derived from arachidonic acid synthesis and induction of cyclooxygenase 2 (COX2) [5,18,32]. Similarly, genetic ablation or inhibition of CIC or ACLY also led to an inhibition of endogenous PGE_2 synthesis in LPS-activated macrophages, which has recently been shown to be essential for LPS induction of pro-IL-1β [18,32,37]. The requirement of citrate, FASN and fatty acid synthesis in macrophage activation has been further compounded by the discovery of C13*orf*31 (FAMIN), a protein that forms a complex with FASN on peroxisomes and promotes flux through *de novo* lipogenesis, although the precise mechanism by which it achieves this is still unknown (Table 1) [20]. Cader *et al.* [20] demonstrated that FAMIN association with FASN was an important regulator of macrophage ROS production, bactericidal activity and cytokine production in LPS-treated macrophages and in a murine *in vivo* endotoxin shock model. Intriguingly, FAMIN was identified through the study of consanguineous families that carried single nucleotide polymorphisms (SNPs) in the gene and is associated with an increased risk for the inflammatory diseases, systemic juvenile idiopathic arthritis, leprosy and Crohn's disease [20]. Malonyl-CoA like acetyl-CoA can also modify lysine residues, in a process termed malonylation (Fig. 2) [38,39]. Protein lysine malonylation is a highly conserved protein modification; however, it remains largely understudied [39]. In two models of type 2 diabetes, proteomic analysis of liver tissue was used to identify 573 malonylated lysine sites from 268 proteins, many of which were metabolic enzymes involved glycolysis, e.g. glyceraldehyde 6-phosphate dehydrogenase (GAPDH) and lipid metabolism, e.g. ACLY [39]. However, it remains to be seen if there is a role for malonylation in metabolic remodelling during inflammation.

Citrate-derived itaconate as an immunomodulator and antibacterial agent

One of the most thought-provoking examples of an immunomodulatory metabolite that results from Krebs cycle rewiring is citrate-derived itaconate [10,21–24]. While it has long been used in the industrial polymer

arena [40], the first relevant discovery regarding itaconate's role in cellular immunity came when Lee *et al*. [41] cloned IRG1, which was found to be significantly upregulated upon treatment of peritoneal macrophages with LPS. It was not until 2011 that the production of itaconate was described in two separate immune contexts, which included in the lungs of mice that had been infected with *Mycobacterium tuberculosis* [42] and its secretion into the supernatant of the macrophage-like cell line, RAW264.7, that had been stimulated with LPS [43]. Michelucci *et al*. [25] went on to demonstrate that IRG1 was the enzyme responsible for itaconate production in a gain-and-loss of function approach in both human and mouse macrophages. As IRG1 catalyses the decarboxylation of cis-aconitate to form itaconate (Table 1; Fig. 2), IRG1 was officially renamed cis-aconitate decarboxylase (CAD) [10,25]. Interestingly, Michelucci *et al*. [25] showed that genetic silencing of *Irg1*/*Acod1* in macrophages infected with *Salmonella enterica* decreased intracellular itaconate levels and reduced antibactericidal activity. The antibacterial function of itaconate had been first demonstrated in the 1970s, as it effectively inhibited isocitrate lyase (ICL) from *Pseudomonas indigofera* under low glucose conditions; however, this property of itaconate did not garner interest until its discovery as a naturally occurring immunometabolite [25,44,45]. In addition to *P. indigofera*, exogenous itaconate has since been shown to inhibit *in vitro* growth of numerous pathogenic bacteria including *M. tuberculosis, Staphylococcus aureus, S. enterica, Legionella pneumophillia* and *Acinetobacter baumannii* [25,42,46]. In another example in *Yersinia pestis* and *Pseudomonas aeruginosa*, itaconate degradation (mediated by three enzymes – itaconyl-CoA transferase, itaconyl-CoA hydratase and (S)-citramalyl-CoA lyase) is critical for bacterial survival and pathogenicity [47].

Isocitrate lyase itself is a key enzyme of the glyoxylate shunt, an anabolic variation of the Krebs cycle that circumvents the two decarboxylation reactions and is used as a mechanism for survival in glucose-poor conditions in some plants and microorganisms [48,49]. The importance of ICL as a virulence factor in microorganisms has been clearly demonstrated with the pathogenic fungus, *Candida albicans* [49]. Upon infection, *C. albicans* undergoes phagocytosis by macrophages resulting in the upregulation of ICL1; however, *C. albicans* strains with a mutant ICL1 are significantly less virulent than wild-type strains [49]. Similarly, deletion of both isoforms of ICL, ICL1 and ICL2, in *M. tuberculosis* resulted in complete impairment of intracellular replication in macrophages and its rapid elimination from the lungs of mice, while inhibition of ICL also inhibited growth in macrophages [50]. Despite the importance of ICL in infection and the evidence implicating itaconate as an antimicrobial agent, there has been some debate around the physiological relevance of studies using itaconate to inhibit bacterial cell growth [51]. This has arisen from inconsistencies between the concentrations of itaconate used *in vitro*, ranging from 5 mM to 100 mM, and the intracellular concentrations identified in macrophages, ranging from 40 μM to 80 mM [51]. However, many studies have used itaconate in the 10 mM range, a concentration close to some previous reports [43], while induction of IRG1 by both type I and type II interferons in *L. pneumophillia*-infected macrophages mediates itaconate production and restricts intravacuolar growth of the bacteria [46]. As such, the role of itaconate as a physiologically relevant antibacterial metabolite remains an open question to be explored.

Despite the known bactericidal activity of itaconate, its role in regulating macrophage function remained unknown. Recent studies have brought to light the possibility that itaconate is an important immunomodulator [21,24,52,53]. Importantly, LPS-stimulated BMDMs treated with methyl ester derivative of itaconate, dimethyl itaconate (DMI), exhibited potent inhibition of proinflammatory mediators including NO, ROS and the cytokines IL-1β, IL-12p70, and IL-6; however, no effect on TNF-α levels was observed [24]. Furthermore, LPS-activated *Irg1*-deficient BMDMs exhibited a boost in the production of IL-12, IL-6, NO and under conditions that stimulate the NLRP3 inflammasome, increased IL-1β and IL-18 [24]. An increase in *Hif1α* mRNA and HIF1α protein levels was also observed in *Irg1*-deficient BMDMs, a critical regulator of aerobic glycolysis and IL-1β production [8,24]. The role of IRG1 and itaconate as negative regulators of inflammation is further supported by the findings that IRG1 suppresses the production of ROS, TNF-α, IL-6 and IFN-β in LPS-tolerised macrophages [52]. Li *et al*. (2013) found that the effect of IRG1 on cytokine and interferon production was through ROS-mediated induction of A20, as supplementation of ROS levels in *Irg1*-knockdown macrophages boosted A20 levels and abrogated the breaking of endotoxin tolerance [52]. Additionally, IRG1 has also been found to mediate the immunosuppressive effects of CO-releasing molecule 2 (CORM2)-induced haem oxygenase 1 (HO-1) on LPS-induced TNF-α production in macrophages and in a murine LPS sepsis model [53]. Interestingly, IRG1 also appears to play a major role in embryo implantation in the womb, a

process thought to require suppression of the host immune system [51,54,55]. These findings suggest that the production of itaconate by IRG1 in macrophages acts as a negative regulator of inflammation and crucially provides the first link between itaconate signalling and the modulation of proinflammatory cytokine production. While the impact of itaconate on DCs has yet to be explored, it has been observed to accumulate in response to LPS [5], and future studies on how this regulates DC effector function and their interaction with adaptive immune cells could yield some fascinating discoveries.

In addition to the breakpoint at IDH, Jha *et al.* [10,17] described a second breakpoint in the TCA cycle using U-^{13}C-glutamine, as approximately 35% of the pool of succinate but only 22% of malate could be attributed to glutamine in LPS-activated macrophages, suggesting inefficient succinate-to-fumarate transition at SDH. Lampropoulou and coworkers argued that itaconate accumulation prevents succinate oxidation via SDH (Fig. 2), thus limiting inflammation by blocking the generation of ROS derived from reverse electron transport (RET) and complex 1, a process that will be discussed in detail later in the review [24]. Itaconate was first demonstrated to competitively inhibit SDH over 60 years ago [36] and this prompted speculation regarding its role in regulating cellular metabolism and decreased flux through SDH [24,56]. Exogenous addition of DMI, to both resting and activated macrophages and the lung adenocarcinoma cell line A549, was found to be sufficient to induce succinate accumulation [23,24]. Furthermore, itaconate was found to competitively inhibit purified SDH, while *Irg1* knockout BMDMs, which can no longer generate endogenous itaconate, had significantly decreased succinate levels and increased oxygen consumption rates (OCR) in response to LPS [24]. Together these papers offer a molecular explanation for the second breakpoint in the Krebs cycle and succinate accumulation.

However, it must also be noted that itaconate is only regarded as a weak competitive inhibitor of SDH [22] raising the question as to how physiologically relevant the findings are. Even more concerning is the recent discovery that DMI, the tool compound used in these studies, is not metabolised to itaconate intracellularly [57]. It was also found that [^{13}C] itaconate in cell culture media was sufficient to increase intracellular levels of unlabelled succinate, with no evidence of cellular uptake [57]. The authors posited that this could be due to a receptor-mediated effect especially given the discovery of metabolites signalling via G-protein-coupled receptors (GPCRs), for example the succinate receptor SUCNR1 (previously GPR91) [58]. If an itaconate receptor did exist, the results of this study could indicate the *Irg1* knockout phenotype is in part due to a loss of autocrine or paracrine signalling by secreted itaconate. Importantly, methyl esterification is also predicted to increase the electrophilicity of itaconate and thus it may behave as a cysteine alkylating agent [57]. This suggests the metabolic effects of DMI observed in macrophages do not appear to be due to intracellular itaconate accumulation, but may instead be due to electrophilic inactivation of metabolic enzymes. This idea is partially supported as Lampropoulou *et al.* [24] reported an upregulation of genes involved in Phase II conjugation, glutathione conjugation and biological oxidations upon treatment with DMI. As such, improved methods of delivering itaconate to macrophages and other immune cells will be important to understand the metabomodulatory properties of this metabolite.

Succinate as an inflammatory signal during inflammation

Succinate, HIF1α stabilisation and IL-1β production

An important advancement in the field of immunometabolism was the discovery of succinate accumulation in activated macrophages and its signalling through HIF1α (Table 1; Fig. 3) [8]. Tannahill *et al.* [8] showed that the principal source of succinate in LPS-activated macrophages was derived from glutamine-dependent anaplerosis, while a role for the γ-aminobutyric acid shunt was also identified. HIF itself is a highly conserved member of the basic helix-loop-helix (bHLH) family of transcription factors and considered the master transcriptional regulator of the cellular response to hypoxia [59–61]. Under hypoxic conditions, HIF forms a heterodimeric complex consisting of an α and β subunit [59–61]. When O_2 levels are high (normoxic), HIF is tightly regulated through hydroxylation of conserved proline residues in the HIF α subunit by prolyl hydroxylases (PHDs) [59–61]. Importantly, PHD enzymatic activity is highly dependent on the Krebs cycle intermediate α-ketoglutarate and O_2 [59,60]. Hydroxylation of HIF facilitates its ubiquitination, and subsequent degradation via the 26S proteasome, by the von Hippel–Lindau (VHL) E3 ubiquitin ligase [59–61]. In 2005, a breakthrough study on SDH-deficient tumours demonstrated that succinate acted as an oncometabolite to drive the Warburg effect and tumour formation [60]. This effect was credited to succinate's ability to stabilise HIF1α through product inhibition of PHDs, even in the absence VHL

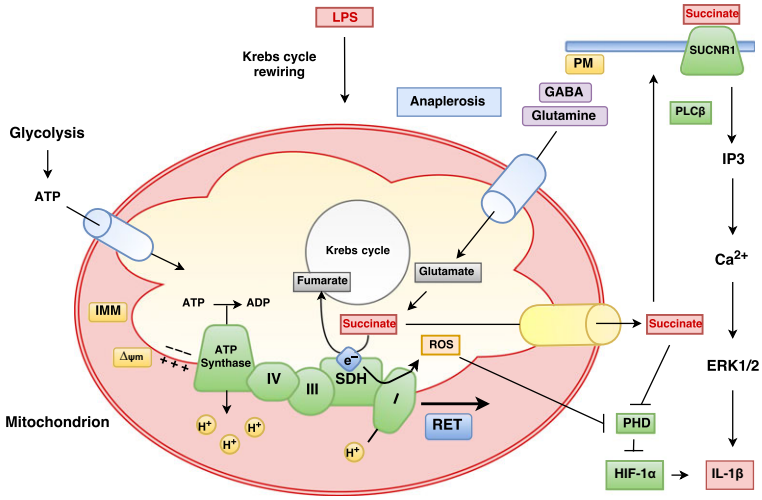

Fig. 3. Succinate as an inflammatory signal during inflammation. Succinate accumulation in response to LPS acts via three primary mechanisms to regulate IL-1β production. Firstly, succinate derived from glutamine anaplerosis and the γ-aminobutyric acid shunt can be oxidised by SDH to drive RET and ROS production from complex I, an effect aided by glycolytic ATP, ATP synthase and membrane hyperpolarisation. Succinate can also be exported from mitochondria into the cytosol, whereby it can synergise with ROS to directly inhibit PHD activity and stabilise HIF1-α. Succinate can also be secreted from the cell where it can bind SUCNR1, which acts as an autocrine and paracrine sensor for succinate, as part of a positive feed forward loop to sustain IL-1β, a process thought to be dependent on elevated Ca^{2+} and ERK1/2 activation.

mutations [60]. Analogous to SDH-deficient tumours, Tannahill *et al.* [8] showed that the accumulation of succinate in macrophages acts to stabilise HIF1α by direct inhibition of cytosolic PHD activity, even under normoxic conditions. It was demonstrated that the proinflammatory cytokine IL-1β contained HRE elements in its promoter and that succinate acted as a danger signal or alarmin to sustain production of IL-1β through induction of HIF1α [8]. Interestingly, a boost in protein succinylation, a modification akin to acetylation and malonylation, was also reported [8]. However, the functional importance of this modification and the role it may play in metabolic reprogramming has yet to be established. The findings by Tannahill *et al.* emphasised the importance of Krebs cycle rewiring in supporting glycolytic reprogramming, via HIF1α, and the crucial role of Krebs cycle intermediates as inflammatory signalling moieties.

Succinate dehydrogenase, ROS and IL-1β production

More recently, it has been suggested that succinate oxidation by SDH also plays an integral role in HIF1α stabilisation and IL-1β production, via ROS production (Table 1) [26]. Previously, it has been demonstrated that inhibition of the SDHB subunit of SDH, either by pharmacological inhibition or RNA interference, increases HIF1α in a ROS-dependent manner by inhibiting PHDs [62]. In addition to a-ketoglutarate and O_2, PHD activity is dependent on Fe^{2+} as a cofactor, as a result, ROS-mediated oxidation of Fe^{2+} to Fe^{3+} inhibits PHDs leading to HIF1α stabilisation [63]. Interestingly, Mills *et al.* [26] found that inhibition of SDH with the competitive inhibitor dimethyl malonate (DMM) potently blocked mitochondrial ROS (mtROS) production from complex I, HIF1α stabilisation and induction of IL1-β, while boosting the anti-inflammatory cytokine IL-10. Indeed, complex I had previously been shown to be a site of ROS production in LPS-treated macrophages, a process inhibited by the antidiabetic drug metformin [64]. DMM also exerted its anti-inflammatory effects in an LPS sepsis model by blocking IL-1β and boosting IL-10, indicating SDH activity plays an important role in the inflammatory response *in vivo* [26]. Furthermore, it was found that mtROS production was dependent on hyperpolarisation of the IMM, driven by increased glycolytic ATP, and treatment of LPS-stimulated macrophages with the proton ionophoric uncoupling agent, carbonyl cyanide-*4*-(trifluoromethoxy) phenylhydrazone (FCCP), was sufficient to block ROS, HIF1α and IL-1β [26].

Mills *et al.* [26,65] argued that inhibition of SDH by DMM blocks ROS generated by RET (Fig. 3), a process first observed in a model of ischaemia–reperfusion (IR) injury. During ischaemia, succinate accumulates due to reversal of SDH directionality, but upon

reperfusion, SDH rapidly oxidises accumulated succinate resulting in the overreduction of the coenzyme Q (CoQ) pool [65]. Excessive reduction of CoQ forces electrons to flow backwards through complex I to generate O_2^-, a process inhibited by DMM [65]. RET has also been implicated as a signalling mechanism in a variety of settings since it was first described in IR, such as in the ageing process in *Drosophila* [66] and oxygen sensing in the carotid body [67]. To support this model of ROS induction, Mills *et al.* [26] utilised BMDMs from mice expressing the enzyme alternative oxidase (AOX), which enables electrons to bypass the block at CoQ, thus limiting RET. Intriguingly, LPS-treated AOX-expressing macrophages limited IL-1β and HIF1α induction, an effect attributed to decreased RET-driven ROS production [26]. The role of SDH and the ETC. in regulating immune signalling and ROS production was further supported by the observation that macrophages infected with *Escherichia coli* and *S. enterica* remodelled complex I-containing supercomplexes [27]. Garaude *et al.* [27] reported that inhibition of SDH with DMM impaired the antibactericidal activity of macrophages infected with *E. coli*. While no direct evidence was provided, both Lampropoulou *et al.* and Garaude *et al.* [24,27] also suggested inhibition of RET, by DMM and itaconate respectively, as the molecular mechanism governing their observed phenotypes. Together these observations provide a striking role for SDH and succinate oxidation in regulating the inflammatory response and macrophage effector functions.

The succinate receptor (SUCNR1) and inflammation

It has also become apparent that another role for succinate accumulation during inflammation is as the cognate ligand for the G-protein-coupled receptor, GPR91, which has since been classified the succinate receptor SUCNR1 (Table 1) [28]. In 2004, He *et al.* [28] made the striking discovery that the Krebs cycle intermediates succinate and α-ketoglutarate, present extracellularly, acted as ligands for the previously orphan receptors, GPR91 and GPR99, respectively. GPR91 expression was found to be distributed in a plethora of mouse tissues including the kidney, the spleen, the liver and the small intestine [28]. The authors showed that succinate exhibited signalling functions beyond its conventional role in bioenergetics, acting as a hypertensive agent through GPR91 and modulation of the renin–angiotensin system [28]. Subsequent studies have also found SUCNR1 to be expressed on the plasma membrane (PM) in macrophages and DCs [29,30].

Since the discovery of SUCNR1, the elucidation of the signalling cascades elicited by binding of succinate has begun to emerge [58,68,69]. Robben *et al.* [70] showed GPR91 to be a Gi- and Gq-coupled receptor using the inhibitors pertussis toxin (PTX) and YM254890 in kidney-derived MDCK cells [71]. Sundström *et al.* confirmed that GPR91 was an Gα(i)- and Gα(q)-coupled receptor resulting in the inhibition of 3′-5′-cyclic adenosine monophosphate (cAMP) and inositol triphosphate (IP3) formation [58,68,69]. The agonist-mediated effects of SUCNR1 stably expressed in the human embryonic kidney (HEK) 293 cell line were detected using dynamic mass redistribution (DMR) and found to be sensitive to PTX [58,68,69]. Inhibition of SUCNR91 signalling with PTX, edelfosine and U73122 also demonstrated the importance of SUCNR1 to elevate intracellular calcium (Ca^{2+}) via IP3 generated by phospholipase C β (PLCβ) [58,68,69]. Similar signalling pathways have also been uncovered in other SUCNR1-positive cell types including adipocytes treated with lipolytic hormones [72] and hematopoietic progenitors [71], which drove proliferation via activation of ERK1/2. Interestingly, succinate-induced responses in cardiac myocytes and platelets involved the induction of protein kinase A (PKA) through the Gs/cAMP pathway, suggesting cell type-specific coupling of G proteins to SUCNR1 [73,74]. Even more importantly, SUCNR1 stimulated with succinate was found to induce intracellular Ca^{2+} mobilisation and phosphorylation of ERK1/2 in DCs, highlighting its functionality in immune effector cells and inflammation [30].

In 2008, the first line of evidence that succinate signalling through SUCNR1 was an important inflammatory mechanism (Fig. 3) was proposed [30]. Rubic *et al.* [30] demonstrated that succinate acted in synergy with TLR agonists to boost inflammatory cytokine expression in DCs [30]. Specifically, succinate boosted TNF-α levels, in synergy with TLR3 agonist poly(I:C) and TLR7 agonist imiquimod, while it also potentiated IL-1β levels in conjunction with LPS [30]. In addition, SUCNR1 was also found to be involved in DC chemotaxis, as monocyte-derived DCs (moDCs) exhibited enhanced migration to draining lymph nodes when treated with succinate [30]. Furthermore, succinate was also found to enhance antigen presentation by DCs and antigen-specific activation of helper T cells, an effect abolished in SUCNR1 KO DCs [30]. More recently, SUCNR1 has been shown to be an important regulator of macrophage activation [29]. In response to inflammatory insults, macrophages were shown to export succinate out of the cell into the extracellular milieu [29]. Importantly, LPS stimulation

upregulated expression of SUCNR1, which acted as an autocrine and paracrine sensor for succinate, and was required for the release of IL-1β, a process inhibited in SUCNR1-deficient macrophages [29]. Importantly, this positive feed forward loop was shown to be a driver of inflammation in an antigen-induced model of rheumatoid arthritis (RA), as succinate in the synovial fluid of RA joints acted through SUCNR1 to promote IL-1β production [29]. SUCNR1-deficient mice have also been shown to exhibit reduced arthritic disease in an ovalbumin-induced arthritis model [75]. Interestingly, these mice are also more susceptible to allergic contact dermatitis (ACD) attributed to increased mast cell activation [75]. These results among others have prompted the suggestion that GPR91 antagonism may constitute a promising therapeutic approach in RA patients and other inflammatory disorders; however, the observation of elevated ACD suggests a possible anti-inflammatory role for succinate and SUCNR1 in some allergic disorders, something that must be considered when moving forward to the clinic [29,75].

With these findings, the role of succinate and SUCNR1/GPR91 signalling in inflammation, under both physiological and pathophysiological settings, is slowly being unravelled. Coupled to its intracellular signalling capacity, succinate has placed itself as one of the most crucial mediators of inflammation in innate immunity and provides a startling example of how Krebs cycle rewiring and Krebs cycle intermediates dictate the effector functions of macrophages and DCs. This field is currently in its infancy and so these discoveries open up the possibility that other TCA cycle metabolites, and their derivatives, may act as receptor ligands to modulate important physiological processes, such as the inflammatory response.

Fumarate, the epigenome and trained immunity

Glutaminolysis, fumarate and cytokine production

Somewhat like LPS, another microbial product β-glucan, which occurs in the cell wall of fungi, will induce glycolytic reprogramming and rewiring of the Krebs cycle [31,76,77]. Similarly, β-glucan will cause the accumulation of the Krebs cycle intermediates succinate and fumarate (Fig. 4) [31]. Interestingly, α-ketoglutarate is an important cofactor for α-ketoglutarate-dependent dioxygenases, a family of enzymes involved in the regulation of DNA and histone demethylation [31,78–81]. Members of this family include the Jumonji C-domain-containing histone demethylases (JMJDs), involved in histone demethylation, and the ten-eleven translocation (TET) family of 5mC hydroxylases, which are involved in DNA demethylation [31,78–81]. These dioxygenases generate succinate from α-ketoglutarate as a product and so their activity is subject to feedback inhibition and dependent on the ratio of α-ketoglutarate to succinate in the cell [78–80]. Additionally, JMJD and TET enzymatic activity can also be competitively inhibited by fumarate [78,81]. As such, alterations in the levels of these Krebs cycle intermediates can alter the epigenetic landscape of a cell [78–80]. Arts *et al*. [31] showed that accumulation of fumarate in response to β-glucan was essential for trained immunity in macrophages. Mechanistically, it was proposed that glutamine anaplerosis was the source of elevated fumarate in these cells based on biochemical methods and the inhibition of glutaminolysis by the glutaminase inhibitor BPTES [31]. Treatment of cells with the cell permeable fumaric acid ester monomethyl fumarate (MMF) was shown to induce an epigenetic programme with similarities to β-glucan-induced training [31]. Monomethyl fumarate was also shown to boost TNF and IL-6 production upon LPS restimulation of β-glucan-trained macrophages [31]. The authors proposed that fumarate accumulation acted to inhibit KDM5 histone demethylases (Table 1), thus increasing the levels of H3K4 me3 at the promoters of *Tnf* and *Il6* [31]. As such, this study presented the first link between Krebs cycle rewiring and epigenetic reprogramming in trained immunity and inflammation. As previously mentioned, fumarate has also been reported to accumulate in LPS-activated macrophages and DCs; however, the consequences of this on inflammatory signalling and effector function have yet to be determined. One possibility is as an endogenous activator of Nrf2, a known negative regulator of inflammation and cytokine production in macrophages [82]. Ashrafian *et al*. [83] have previously shown fumarate to be cardioprotective in a model of heart ischaemia/reperfusion, acting to increase the antioxidant response via Nrf2. Whether fumarate has a similar effect in macrophages or DCs has yet to be determined.

Conclusions and perspectives

Recent findings on the role of Krebs cycle intermediates during inflammation have advanced our understanding of the complexity of immunometabolism. A precedent has now been set for metabolites generated by innate immune cells to have distinct functions as signalling entities and antibactericidal agents, beyond their role in bioenergetics. Our recent understanding of the integration of the immune system with cellular

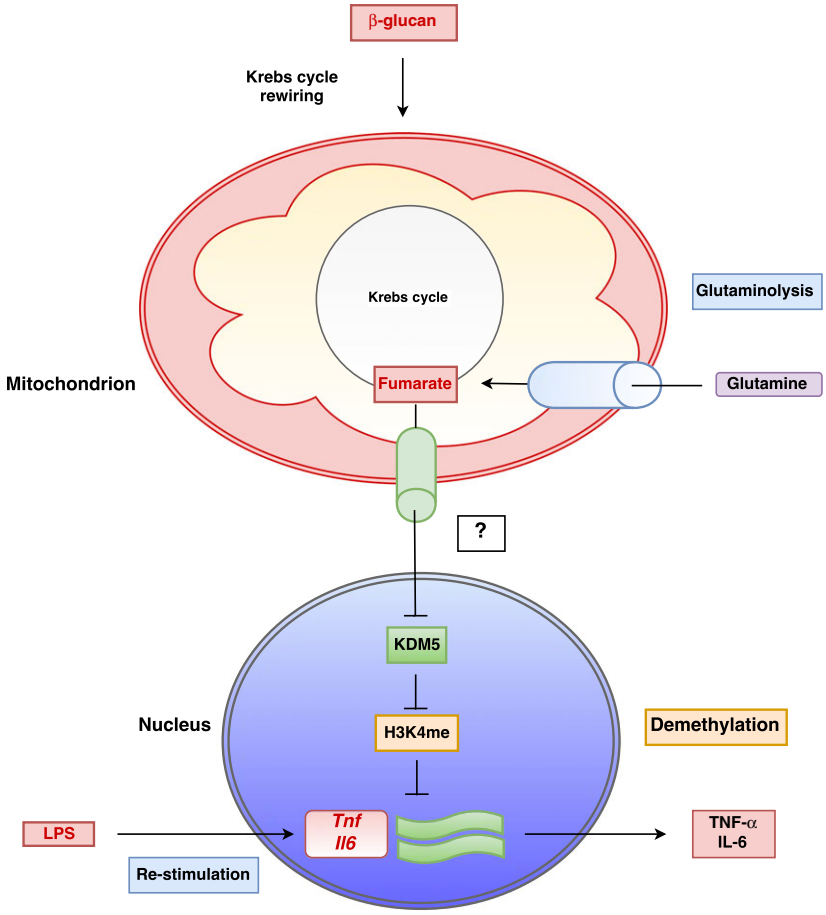

Fig. 4. Glutaminolysis and fumarate are required for epigenome reprogramming. Monocytes primed with β-glucan undergo Krebs cycle rewiring like LPS-treated macrophages. This results in fumarate accumulation derived from glutaminolysis, which then acts to inhibit KDM5 histone demethylases. Inhibition of KDM5 alters H3K4 methylation at the promoters of *Tnf* and *Il6*. When β-glucan primed monocytes are rechallenged with LPS, altered histone methylation results in elevated TNF-α and IL-6 production.

metabolism has in large part been owed to great technological advancements and improvements in instrumentation, such as those that have enabled systems level approaches to determine global gene and protein expression in response to inflammatory stimuli. Moreover, advancements in mass spectrometry and computational analysis now allows for detailed molecular modelling and determination of the metabolome in complex biological samples [8,10]. On a translational level, insight into the interface of metabolism and immunity could uncover new targets with promising therapeutic potential in transplantation, infection and inflammatory and autoimmune disorders. For example, succinate signalling through SUCNR1 has been implicated in the autoimmune disorder RA [29] with this discovery opening a new window of opportunity for the development of SUCNR1 antagonists in the treatment of this debilitating disease [29]. Furthermore, the use of metabolites as biomarkers for immune-related diseases may become integral in clinical settings due to the uncovering of abnormal metabolite levels in diseased tissues, such as the rheumatoid joint [29] and in the colon of ulcerative colitis patients [84].

On a basic level, a key discovery regarding Krebs cycle rewiring is the assumption of two breakpoints at IDH and SDH, as previously delineated. However, it is important to note that this view may be overly simplistic as itaconate has also been shown to abolish mitochondrial substrate-level phosphorylation (SLP) [22]. Nemeth *et al*. [22] postulated that the formation of itaconyl-CoA from itaconate creates a 'CoA trap' that negatively regulates the supply of succinyl-CoA, shifts equilibrium towards utilisation of ATP (or GTP) by succinyl-CoA synthase and depletes ATP (or GTP) levels, thus decreasing important cofactors for thioesterification. This suggests an additional impairment of the TCA cycle may also exist at succinyl-CoA synthase. Interestingly, Liu *et al*. [85] also demonstrated that LPS and IFN-γ stimulation of macrophages results in the downregulation of multiple TCA cycle genes in addition to *Idh*, including *SdhA, SdhaB* and *SdhC*, which suggests greater transcriptional regulation of the Krebs cycle is occurring. It is also important to note that while SDH activity appears to be reduced, it is still functionally active, unlike IDH, and so it could be argued that only one true breakpoint has thus far

been identified. Furthermore, SDH activity has been shown to be essential for mediating the immune response in macrophages, as previously discussed [26,27]. Evidently, the molecular mechanisms governing Krebs cycle remodelling are just beginning to be unearthed and warrant further investigation.

Despite technological advancements, there are still limits to our capabilities based on techniques currently applied in laboratories across the world. For example, one big advancement required to propel our understanding of immunometabolism to the next phase is moving away from whole-cell analysis of the metabolome towards looking at the dynamics of organelle-specific metabolites. Recently, steps have been made in this direction. In a remarkable study, Chen *et al*. [86] described a workflow that included a specific method for the rapid isolation of mitochondria and the absolute quantification of matrix metabolites. This technique enabled the authors to compare the dynamics of the whole-cell metabolome with the mitochondrial matrix metabolome (MITObolome) across various states of ETC. disruption [86]. Furthermore, adaptation of this technique may be applicable to other cellular organelles and cell types in the future. Employment of techniques such as this to study immunometabolism could lead to great discoveries in how the metabolite composition of organelles changes during inflammation. Such information could lead to new understandings of how metabolites are trafficked and secreted, unearth new cellular metabolic networks and discover novel targets and interactors in cell signalling pathways. The future is bright for the field of immunometabolism and we can be certain that hugely important discoveries shall be made in both basic and translational immunological research.

Author contributions

DGR wrote the manuscript, LAJO supervised and edited the manuscript.

References

1 Janeway CA Jr and Medzhitov R (2002) Innate immune recognition. *Ann Rev Immunol* **20**, 197–216.

2 Kelly B and O'Neill L (2015) Metabolic reprogramming in macrophages and dendritic cells in innate immunity. *Cell Res* **25**, 771–784.

3 Krawczyk CM, Holowka T, Sun J, Blagih J, Amiel E, DeBerardinis RJ, Cross JR, Jung E, Thompson CB, Jones RG *et al*. (2010) Toll-like receptor-induced changes in glycolytic metabolism regulate dendritic cell activation. *Blood* **115**, 4742–4749.

4 Rodríguez-Prados JC, Través PG, Cuenca J, Rico D, Aragonés J, Martín-Sanz P, Cascante M, Boscá L *et al*. (2010) Substrate fate in activated macrophages: a comparison between innate, classic, and alternative activation. *J Immunol* **185**, 605–614.

5 Everts B, Amiel E, Huang SC-C, Smith AM, Chang C-H, Lam WY, Redmann V, Freitas TC, Blagih J, van der Windt GJW *et al*. (2014) TLR-driven early glycolytic reprogramming via the kinases TBK1-IKKε supports the anabolic demands of dendritic cell activation. *Nat Immunol* **15**, 323–332.

6 Haschemi A, Kosma P, Gille L, Evans CR, Burant CF, Starkl P, Knapp B, Haas R, Schmid JA, Jandl C *et al*. (2012) The sedoheptulose kinase CARKL directs macrophage polarization through control of glucose metabolism. *Cell Metab* **15**, 813–826.

7 Hard GC (1970) Some biochemical aspects of the immune macrophage. *British J Exp Pathol* **51**, 97–105.

8 Tannahill GM, Curtis AM, Adamik J, Palsson-McDermott EM, McGettrick AF, Goel G, Frezza C, Bernard NJ, Kelly B, Foley NH *et al*. (2013) Succinate is an inflammatory signal that induces IL-1β through HIF-1α. *Nature* **496**, 238–242.

9 Palsson-McDermott EM, Curtis AM, Goel G, Lauterbach MA, Sheedy FJ, Gleeson LE, van den Bosch MW, Quinn SR, Domingo-Fernandez R, Johnston DG *et al*. (2015) Pyruvate kinase M2 regulates Hif-1α activity and IL-1β induction and is a critical determinant of the Warburg effect in LPS-activated macrophages. *Cell Metab* **21**, 347.

10 Jha AK, Huang SC, Sergushichev A, Lampropoulou V, Ivanova Y, Loginicheva E, Chmielewski K, Stewart KM, Ashall J, Everts B *et al*. (2015) Network integration of parallel metabolic and transcriptional data reveals metabolic modules that regulate macrophage polarization. *Immunity* **42**, 419–430.

11 Krebs H (1970) The history of the tricarboxylic acid cycle. *Perspect Biol Med* **14**, 154–172.

12 Krebs H and Johnson W (1980) The role of citric acid in intermediate metabolism in animal tissues. *FEBS Lett* **117**, K2–K10.

13 Akram M (2014) Citric acid cycle and role of its intermediates in metabolism. *Cell Biochem Biophys* **68**, 475–478.

14 Zatta P, Lain E and Cagnolini C (2000) Effects of aluminum on activity of Krebs cycle enzymes and glutamate dehydrogenase in rat brain homogenate. *Eur J Biochem* **267**, 3049–3055.

15 Nazaret C, Heiske M, Thurley K and Mazat J (2009) Mitochondrial energetic metabolism: a simplified model of TCA cycle with ATP production. *J Theor Biol* **258**, 455–464.

16 O'Neill L, Kishton R and Rathmell J (2016) A guide to immunometabolism for immunologists. *Nat Rev Immunol* **16**, 553–565.

17 O'Neill L (2015) A broken Krebs cycle in macrophages. *Immunity* **42**, 393–394.
18 Infantino V, Convertini P, Cucci L, Panaro MA, Di Noia MA, Calvello R, Palmieri F, Iacobazzi V *et al.* (2011) The mitochondrial citrate carrier: a new player in inflammation. *Biochem J* **438**, 433–436.
19 Wellen K, Hatzivassiliou G, Sachdeva U, Bui T, Cross J and Thompson C (2009) ATP-citrate lyase links cellular metabolism to histone acetylation. *Science* **324**, 1076–1080.
20 Cader MZ, Boroviak K, Zhang Q, Assadi G, Kempster SL, Sewell GW, Saveljeva S, Ashcroft JW, Clare S, Mukhopadhyay S *et al.* (2016) C13orf31 (FAMIN) is a central regulator of immunometabolic function. *Nat Immunol* **17**, 1046–1056.
21 Meiser J, Krämer L, Sapcariu SC, Battello N, Ghelfi J, D'Herouel AF, Skupin A, Hiller K *et al.* (2015) Pro-inflammatory macrophages sustain pyruvate oxidation through pyruvate dehydrogenase for the synthesis of Itaconate and to enable cytokine expression. *J Biol Chem* **291**, 3932–3946.
22 Németh B, Doczi J, Csete D, Kacso G, Ravasz D, Adams D, Kiss G, Nagy AM, Horvath G, Tretter L *et al.* (2015) Abolition of mitochondrial substrate-level phosphorylation by itaconic acid produced by LPS-induced Irg1 expression in cells of murine macrophage lineage. *FASEB J* **30**, 286–300.
23 Cordes T, Wallace M, Michelucci A, Divakaruni AS, Sapcariu SC, Sousa C, Koseki H, Cabrales P, Murphy AN, Hiller K *et al.* (2016) Immunoresponsive gene 1 and Itaconate inhibit succinate dehydrogenase to modulate intracellular succinate levels. *J Biol Chem* **291**, 14274–14284.
24 Lampropoulou V, Sergushichev A, Bambouskova M, Nair S, Vincent EE, Loginicheva E, Cervantes-Barragan L, Ma X, Huang SC, Griss T *et al.* (2016) Itaconate links inhibition of succinate dehydrogenase with macrophage metabolic remodeling and regulation of inflammation. *Cell Metab* **24**, 158–166.
25 Michelucci A, Cordes T, Ghelfi J, Pailot A, Reiling N, Goldmann O, Binz T, Wegner A, Tallam A, Rausell A *et al.* (2013) Immune-responsive gene 1 protein links metabolism to immunity by catalyzing itaconic acid production. *Proc Natl Acad Sci USA* **110**, 7820–7825.
26 Mills EL, Kelly B, Logan A, Costa AS, Varma M, Bryant CE, Tourlomousis P, Däbritz JH, Gottlieb E, Latorre I *et al.* (2016) Succinate dehydrogenase supports metabolic repurposing of mitochondria to drive inflammatory macrophages. *Cell* **167**, 457–470.e13.
27 Garaude J, Acín-Pérez R, Martínez-Cano S, Enamorado M, Ugolini M, Nistal-Villán E, Hervás-Stubbs S, Pelegrín P, Sander LE, Enríquez JA *et al.* (2016) Mitochondrial respiratory-chain adaptations in macrophages contribute to antibacterial host defense. *Nat Immunol* **17**, 1037–1045.
28 He W, Miao F, Lin D *et al.* (2004) Citric acid cycle intermediates as ligands for orphan G-protein-coupled receptors. *Nature* **429**, 188–193.
29 Littlewood-Evans A, Sarret S, Apfel V, Loesle P, Dawson J, Zhang J, Muller A, Tigani B, Kneuer R, Patel S *et al.* (2016) GPR91 senses extracellular succinate released from inflammatory macrophages and exacerbates rheumatoid arthritis. *J Exp Med* **213**, 1655–1662.
30 Rubic T, Lametschwandtner G, Jost S, Hinteregger S, Kund J, Carballido-Perrig N, Schwärzler C, Junt T, Voshol H, Meingassner JG *et al.* (2008) Triggering the succinate receptor GPR91 on dendritic cells enhances immunity. *Nat Immunol* **9**, 1261–1269.
31 Arts RJ, Novakovic B, Ter Horst R, Carvalho A, Bekkering S, Lachmandas E, Rodrigues F, Silvestre R, Cheng SC, Wang SY *et al.* (2016) Glutaminolysis and fumarate accumulation integrate immunometabolic and epigenetic programs in trained immunity. *Cell Metab* **24**, 807–819.
32 Infantino V, Iacobazzi V, Palmieri F and Menga A (2013) ATP-citrate lyase is essential for macrophage inflammatory response. *Biochem Biophys Res Comm* **440**, 105–111.
33 Koivunen P, Hirsila M, Remes A, Hassinen I, Kivirikko K and Myllyharju J (2006) Inhibition of hypoxia-inducible factor (HIF) hydroxylases by citric acid cycle intermediates: possible links between cell metabolism and stabilization of HIF. *J Biol Chem* **282**, 4524–4532.
34 Wang B, Rao YH, Inoue M, Hao R, Lai CH, Chen D, McDonald SL, Choi MC, Wang Q, Shinohara ML *et al.* (2014) Microtubule acetylation amplifies p38 kinase signalling and anti-inflammatory IL-10 production. *Nat Commun* **5**, 3479.
35 Hu L, Yu Y, Huang H, Fan H, Hu L, Yin C, Li K, Fulton DJ and Chen F *et al.* (2017) Epigenetic regulation of interleukin 6 by histone acetylation in macrophages and its role in Paraquat-induced pulmonary fibrosis. *Front Immunol* **7**. https://doi.org/10.3389/fimmu.2016.00696.
36 Ackermann W and Potter V (1949) Enzyme inhibition in relation to chemotherapy. *Exp Biol Med* **72**, 1–9.
37 Zasłona Z, Pålsson-McDermott EM, Menon D, Haneklaus M, Flis E, Prendeville H, Corcoran SE, Peters-Golden M and O'Neill LAJ (2017) The induction of Pro–IL-1β by lipopolysaccharide requires endogenous prostaglandin E 2 production. *J Immunol* **198**, 3558–3564.
38 Hirschey M and Zhao Y (2015) Metabolic regulation by lysine malonylation, succinylation, and glutarylation. *Mol Cell Proteomics* **14**, 2308–2315.

39 Du Y, Cai T, Li T, Xue P, Zhou B, He X, Wei P, Liu P, Yang F and Wei T (2014) Lysine malonylation is elevated in type 2 diabetic mouse models and enriched in metabolic associated proteins. *Mol Cell Proteomics* **14**, 227–236.
40 Okabe M, Lies D, Kanamasa S and Park E (2009) Biotechnological production of itaconic acid and its biosynthesis in Aspergillus terreus. *Appl Microbiol Biotechnol* **84**, 597–606.
41 Lee C, Jenkins N, Gilbert D, Copeland N and O'Brien W (1995) Cloning and analysis of gene regulation of a novel LPS-inducible cDNA. *Immunogenetics* **41**, 263–270.
42 Shin JH, Yang JY, Jeon BY, Yoon YJ, Cho SN, Kang YH, Ryu DH and Hwang GS (2011) 1H NMR-based metabolomic profiling in mice infected with *Mycobacterium tuberculosis*. *J Proteome Res* **10**, 2238–2247.
43 Sugimoto M, Sakagami H, Yokote Y, Onuma H, Kaneko M, Mori M, Sakaguchi Y, Soga T and Tomita M (2011) Non-targeted metabolite profiling in activated macrophage secretion. *Metabolomics* **8**, 624–633.
44 Williams JO, Roche TE and McFadden BA (1971) Mechanism of action of isocitrate lyase from *Pseudomonas indigofera*. *Biochemistry* **10**, 1384–1390.
45 McFadden BA and Purohit S (1977) Itaconate, an isocitrate lyase-directed inhibitor in *Pseudomonas indigofera*. *J Bacteriol* **131**, 136–144.
46 Naujoks J, Tabeling C, Dill BD, Hoffmann C, Brown AS, Kunze M, Kempa S, Peter A, Mollenkopf HJ, Dorhoi A *et al.* (2016) IFNs modify the proteome of Legionella-containing vacuoles and restrict infection via IRG1-derived itaconic acid. *PLoS Pathog* **12**, e1005408.
47 Sasikaran J, Ziemski M, Zadora P, Fleig A and Berg I (2014) Bacterial itaconate degradation promotes pathogenicity. *Nat Chem Biol* **10**, 371–377.
48 Lorenz M and Fink G (2002) Life and death in a macrophage: role of the glyoxylate cycle in virulence. *Eukaryot Cell* **1**, 657–662.
49 Lorenz M and Fink G (2001) The glyoxylate cycle is required for fungal virulence. *Nature* **412**, 83–86.
50 Muñoz-Elías E and McKinney J (2005) *Mycobacterium tuberculosis* isocitrate lyases 1 and 2 are jointly required for in vivo growth and virulence. *Nat Med* **11**, 638–644.
51 Luan H and Medzhitov R (2016) Food fight: role of itaconate and other metabolites in antimicrobial defense. *Cell Metab* **24**, 379–387.
52 Li Y, Zhang P, Wang C, Han C, Meng J, Liu X, Xu S, Li N, Wang Q, Shi X *et al.* (2013) Immune responsive gene 1 (IRG1) promotes endotoxin tolerance by increasing A20 expression in macrophages through reactive oxygen species. *J Biol Chem* **288**, 16225–16234.
53 Jamal Uddin M, Joe Y, Kim SK, Oh Jeong S, Ryter SW, Pae HO and Chung HT (2015) IRG1 induced by heme oxygenase-1/carbon monoxide inhibits LPS-mediated sepsis and pro-inflammatory cytokine production. *Cell Mol Immunol* **13**, 170–179.
54 Cheon Y, Xu X, Bagchi M and Bagchi I (2003) Immune-responsive gene 1 is a novel target of progesterone receptor and plays a critical role during implantation in the mouse. *Endocrinology* **144**, 5623–5630.
55 Sherwin J, Smith S and Sharkey A (2004) Identification of genes regulated by leukaemia inhibitory factor in the mouse uterus at the time of implantation. *Fertil Steril* **82**, S271.
56 Cordes T, Michelucci A and Hiller K (2015) Itaconic acid: the surprising role of an industrial compound as a mammalian antimicrobial metabolite. *Annu Rev Nutr* **35**, 451–473.
57 ElAzzouny M, Tom CT, Evans CR, Olson LL, Tanga MJ, Gallagher KA, Martin BR and Burant CF (2017) Dimethyl itaconate is not metabolized into itaconate intracellularly. *J Biol Chem* **292**, 4766–4769.
58 Sundström L, Greasley P, Engberg S, Wallander M and Ryberg E (2013) Succinate receptor GPR91, a Gαicoupled receptor that increases intracellular calcium concentrations through PLCβ. *FEBS Lett* **587**, 2399–2404.
59 Corcoran S and O'Neill L (2016) HIF1α and metabolic reprogramming in inflammation. *J Clin Invest* **126**, 3699–3707.
60 Selak MA, Armour SM, MacKenzie ED, Boulahbel H, Watson DG, Mansfield KD, Pan Y, Simon MC, Thompson CB, Gottlieb E (2005) Succinate links TCA cycle dysfunction to oncogenesis by inhibiting HIF-α prolyl hydroxylase. *Cancer Cell* **7**, 77–85.
61 Huang L, Arany Z, Livingston D and Bunn H (1996) Activation of hypoxia-inducible transcription factor depends primarily upon redox-sensitive stabilization of its subunit. *J Biol Chem* **271**, 32253–32259.
62 Guzy R, Sharma B, Bell E, Chandel N and Schumacker P (2007) Loss of the SdhB, but not the SdhA, subunit of complex II triggers reactive oxygen species-dependent hypoxia-inducible factor activation and tumorigenesis. *Mol Cell Biol* **28**, 718–731.
63 Kietzmann T and Görlach A (2005) Reactive oxygen species in the control of hypoxia-inducible factor-mediated gene expression. *Semin Cell Dev Biol* **16**, 474–486.
64 Kelly B, Tannahill G, Murphy M and O'Neill L (2015) Metformin inhibits the production of reactive oxygen species from NADH: ubiquinone oxidoreductase to limit induction of interleukin-1β (IL-1β) and boosts interleukin-10 (IL-10) in lipopolysaccharide (LPS)-activated macrophages. *J Biol Chem* **290**, 20348–20359.
65 Chouchani ET, Pell VR, Gaude E, Aksentijević D, Sundier SY, Robb EL, Logan A, Nadtochiy SM, Ord

EN, Smith AC *et al*. (2014) Ischaemic accumulation of succinate controls reperfusion injury through mitochondrial ROS. *Nature* **515**, 431–435.
66 Scialò F, Sriram A, Fernández-Ayala D, Gubina N, Lõhmus M, Nelson G, Logan A, Cooper HM, Navas P, Enríquez JA *et al*. (2016) Mitochondrial ROS produced via reverse electron transport extend animal lifespan. *Cell Metab* **23**, 725–734.
67 Fernández-Agüera M, Gao L, González-Rodríguez P *et al*. (2015) Oxygen sensing by arterial chemoreceptors depends on mitochondrial complex I signaling. *Cell Metab* **22**, 825–837.
68 Gilissen J, Jouret F, Pirotte B and Hanson J (2016) Insight into SUCNR1 (GPR91) structure and function. *Pharmacol Ther* **159**, 56–65.
69 Ariza A, Deen P and Robben J (2012) The succinate receptor as a novel therapeutic target for oxidative and metabolic stress-related conditions. *Front Endocrinol (Lausanne)* **3**, 22.
70 Robben J, Fenton R, Vargas S, Schweer H, Peti-Peterdi J, Deen PM and Milligan G (2009) Localization of the succinate receptor in the distal nephron and its signaling in polarized MDCK cells. *Kidney Int* **76**, 1258–1267.
71 Hakak Y, Lehmann-Bruinsma K, Phillips S *et al*. (2009) The role of the GPR91 ligand succinate in hematopoiesis. *J Leukoc Biol* **85**, 837–843.
72 Regard J, Sato I and Coughlin S (2008) Anatomical profiling of G protein-coupled receptor expression. *Cell* **135**, 561–571.
73 Aguiar CJ, Andrade VL, Gomes ER, Alves MN, Ladeira MS, Pinheiro AC, Gomes DA, Almeida AP, Goes AM, Resende RR *et al*. (2010) Succinate modulates Ca^{2+} transient and cardiomyocyte viability through PKA-dependent pathway. *Cell Calcium* **47**, 37–46.
74 Högberg C, Gidlöf O, Tan C, Svensson S, Nilsson-Öhman J, Erlinge D and Olde B. (2011) Succinate independently stimulates full platelet activation via cAMP and phosphoinositide 3-kinase-β signaling. *J Thromb Haemost* **9**, 361–372.
75 Rubić-Schneider T, Carballido-Perrig N, Regairaz C, Raad L, Jost S, Rauld C, Christen B, Wieczorek G, Kreutzer R, Dawson J *et al*. (2016) GPR91 deficiency exacerbates allergic contact dermatitis while reducing arthritic disease in mice. *Allergy* **72**, 444–452.
76 Cheng SC, Quintin J, Cramer RA, Shepardson KM, Saeed S, Kumar V, Giamarellos-Bourboulis EJ, Martens JH, Rao NA, Aghajanirefah A *et al*. (2014) mTOR- and HIF-1-mediated aerobic glycolysis as metabolic basis for trained immunity. *Science* **345**, 1250684.
77 Mills E, Kelly B and O'Neill L (2017) Mitochondria are the powerhouses of immunity. *Nat Immunol* **18**, 488–498.
78 Xiao M, Yang H, Xu W, Ma S, Lin H, Zhu H, Liu L, Liu Y, Yang C, Xu Y *et al*. (2012) Inhibition of α-KG-dependent histone and DNA demethylases by fumarate and succinate that are accumulated in mutations of FH and SDH tumor suppressors. *Genes Dev* **26**, 1326–1338.
79 Bénit P, Letouzé E, Rak M, Aubry L, Burnichon N, Favier J, Gimenez-Roqueplo AP and Rustin P (2014) Unsuspected task for an old team: Succinate, fumarate and other Krebs cycle acids in metabolic remodeling. *Biochim et Biophys Acta (BBA) -Bioenerget* **1837**, 1330–1337.
80 Kaelin W and McKnight S (2013) Influence of metabolism on epigenetics and disease. *Cell* **153**, 56–69.
81 Sciacovelli M, Gonçalves E, Johnson TI, Zecchini VR, da Costa AS, Gaude E, Drubbel AV, Theobald SJ, Abbo SR, Tran MG *et al*. (2016) Fumarate is an epigenetic modifier that elicits epithelial-to-mesenchymal transition. *Nature* **537**, 544–547.
82 Kobayashi EH, Suzuki T, Funayama R, Nagashima T, Hayashi M, Sekine H, Tanaka N, Moriguchi T, Motohashi H, Nakayama K *et al*. (2016) Nrf2 suppresses macrophage inflammatory response by blocking proinflammatory cytokine transcription. *Nat Commun* **7**, 11624.
83 Ashrafian H, Czibik G, Bellahcene M, Aksentijević D, Smith AC, Mitchell SJ, Dodd MS, Kirwan J, Byrne JJ, Ludwig C *et al*. (2012) Fumarate is cardioprotective via activation of the Nrf2 antioxidant pathway. *Cell Metab* **15**, 361–371.
84 Ooi M, Nishiumi S, Yoshie T, Shiomi Y, Kohashi M, Fukunaga K, Nakamura S, Matsumoto T, Hatano N, Shinohara M *et al*. (2011) GC/MS-based profiling of amino acids and TCA cycle-related molecules in ulcerative colitis. *Inflamm Res* **60**, 831–840.
85 Liu L, Lu Y, Martinez J, Bi Y, Lian G, Wang T, Milasta S, Wang J, Yang M, Liu G *et al*. (2016) Proinflammatory signal suppresses proliferation and shifts macrophage metabolism from Myc-dependent to HIF1α-dependent. *Proc Natl Acad Sci USA* **113**, 1564–1569.
86 Chen W, Freinkman E, Wang T, Birsoy K and Sabatini D (2016) Absolute quantification of matrix metabolites reveals the dynamics of mitochondrial metabolism. *Cell* **166**, 1324–1337.e11.